Fire and Environmental Change in Northern Australian Savannas during the Holocene

Emma Caitlin Rehn

Bachelor of Arts (Hons)

Submitted for the degree of Doctor of Philosophy

College of Science and Engineering

James Cook University

August 2020

Acknowledgements

"Ko hono ngata'anga e. Koia hono kotoa. Kuo osi. Kuo lava.

Leveleva e fatongia kau tatau atu."

This thesis is the culmination of four years of work supported, guided and made possible by a large network of amazing people.

I thank my JCU supervisors for their outstanding guidance, support and generosity. My thanks to Professor Michael Bird for sharing his knowledge as well as his calm and confident approach, including his confidence in me even when I wasn't sure of myself. Thanks to Dr Cassandra Rowe for helping me every step of the way, being generous with her feedback and her time, and always being happy to talk things through. I thank Professor Sean Ulm for his unwavering support since I began my undergraduate study, and keen editorial eye. I also thank everyone in the research group for their help in the field and the laboratory, and their friendship.

I would like to thank my family for their endless support, especially my parents; thanks for always listening and believing wholeheartedly in me. Thank you to my brother for showing me how it's done, and collaborating on the work that became my first publication (forming part of this thesis); thanks also to Aidan Possemiers for his contribution to that work. Thank you to Caitlin Fitzpatrick for always being there.

I thank my Australian Nuclear Science and Technology Organisation (ANSTO) co-supervisors Dr Craig Woodward and Dr Geraldine Jacobsen for their feedback and coordination of access

to ANSTO facilities. Huge thanks to all the ANSTO staff who helped me with laboratory work and made me feel welcome at Lucas Heights, including but not limited to Patricia Gadd, Sabika Maizma, Dr Atun Zawadzki, Dr Jay Chellappa, and everyone in Building 34. Thank you to the Australian Institute of Nuclear Science and Engineering (AINSE) for granting me a Postgraduate Research Award and International Conference Travel Scholarship, and to the friendly AINSE staff for all their help.

Thank you to the ARC Centre of Excellence for Australian Biodiversity and Heritage (CABAH) for professional development opportunities and for creating a welcoming research network.

Statement of the Contribution of Others

Nature of Assistance	**Contribution**	**Co-Contributors**
Intellectual support	Supervision (JCU)	Professor Michael Bird Dr Cassandra Rowe Professor Sean Ulm
	Supervision (ANSTO)	Dr Craig Woodward Dr Geraldine Jacobsen
	Data analysis	Professor Michael Bird Dr Cassandra Rowe
	Editorial assistance	Professor Michael Bird Dr Cassandra Rowe Professor Sean Ulm
Financial support	Research funding	Australian Research Council Laureate Fellowship (FL140100044, CI: M. Bird) Australian Research Council Centre of Excellence for Australian Biodiversity and Heritage (CE170100015)
	Scholarship/stipend	Australian Research Council (ARC) Laureate Postgraduate Research Scholarship (2016-2017)

		Australian Institute of Nuclear Science and Engineering Postgraduate Research Award (12143) (2017-2019) Australian Government Research Training Program Scholarship (2018-2020)
	Conference travel support	JCU College of Science and Engineering HDR Enhancement Scheme Conference Travel Support (2017) JCU Centre for Tropical Environmental and Sustainability Science Conference Travel Support Grant (2018) Australian Institute of Nuclear Science and Engineering International Conference Travel Scholarship (2019)
Data collection	Fieldwork team and sample collection (JCU)	Professor Michael Bird, Michael Brand, Rainy Comley, Maria Rivera Araya, Dr Cassandra Rowe, Dr Chris Wurster, Costijn Zwart
	Laboratory assistance (JCU)	Rainy Comley, Dr Jordahna Haig, Maria Rivera Araya, Dr Cassandra Rowe, Dr Jennifer Whan, Dr Chris Wurster
	Laboratory assistance (ANSTO)	Dr Jay Chellappa, Patricia Gadd, Sabika Maizma, Dr Craig Woodward, Dr Atun Zawadzki

Co-authored publications included in this thesis:

Chapter	**Details of publication**	**Nature and extent of intellectual input of each author, including the candidate**
Appendix 4	Rehn, E, Rehn, A & Possemiers, A 2019, 'Fossil charcoal particle identification and classification by two convolutional neural networks', *Quaternary Science Reviews*, vol. 226, p. 106038, DOI:10.1016/j.quascirev.2019.106038.	E. Rehn conceptualised the project and collected the data. A. Rehn developed the methodology, with software assistance from A. Possemiers. E. Rehn and A. Rehn trained the neural networks. All authors contributed to writing the paper. E. Rehn created the figures. E. Rehn and A. Rehn edited the paper and responded to reviewer comments.

I confirm the candidate's contribution to this paper and consent to the inclusion of the paper in this thesis:

Name: Adam Rehn **Name:** Aidan Possemiers

Signature: **Signature:**

Abstract

Fire has long had a pervasive importance in human lives and actively shapes many landscapes on Earth. Fire has a long history of interaction with Australian ecosystems but poses a growing risk as fire conditions become increasingly severe, due in part to anthropogenic climate change. Tropical savannas cover almost one quarter (1.9 million km^2) of the Australian land mass, and fire occurs in tropical savannas almost annually. A greater understanding of past fire regimes, and their environmental context, is essential for management and planning in an increasingly fire-prone landscape. Despite the central importance of fire in savanna ecosystems, the region remains understudied in Australian palaeofire research.

This thesis combines established visual/microscopic and emerging geochemical methods to create three new multiproxy palaeofire records for three wetland sites in northern Australian savannas. Charcoal from sedimentary records from these sites was separated into three size fractions (>250 μm, 250-125 μm and 125-63 μm) and quantified by stereomicroscope, with aspect ratios and morphotypes recorded to investigate changes in fuel composition over time. Pyrogenic carbon was chemically isolated using hydrogen pyrolysis, with percent carbon measured by elemental analysis with the $\delta^{13}C$ value of the pyrogenic carbon measured by isotope ratio monitoring mass spectrometry to determine changes in fuel composition over time. The novel combination of (optical) charcoal and (chemical) pyrogenic carbon measures enabled the identification of changes in relative fire intensities in the past, crucial to differentiating between anthropogenic and climatic influences within these palaeofire records. The palaeofire records were placed in a broader geochemical context using sediment elemental

composition (using μXRF) and placed in a temporal context through the development of ^{210}Pb and ^{14}C chronologies.

The three records are from (i) Marura Sinkhole (eastern Arnhem Land, 13.409°S, 135.774°E), (ii) Big Willum Swamp (Weipa, Cape York Peninsula, 12.657°S, 141.998°E), and (iii) Sanamere Lagoon (Cape York Peninsula, 11.117°S, 142.35°E).

The palaeofire record for Marura sinkhole covers approximately 4600 cal BP to present, with highest fire incidence 4600-2800 cal BP. Vegetation at Marura is of mixed tree-grass composition throughout the record, with variability in the fine (<63 μm) fraction. Variable relative fire intensities and divergence between local and regional fire and vegetation signals suggest increasing human influence on fire at Marura from ~2800 cal BP. Minimal charcoal and pyrogenic carbon transport into the site after ~900 cal BP is likely the result of the imposition of fine-scale patch mosaic burning. European arrival in Arnhem Land shows a delayed effect on fire at Marura, with increased fire incidence after ~1950 CE reaching levels not seen in the preceding 900 years.

The Big Willum Swamp palaeofire record covers ~3900 cal BP to present, with ephemeral conditions leading to minimal deposition early in the record prior to deepening of the site at ~2200 cal BP. Fire incidence at Big Willum Swamp is low until the last century, peaking at ~1970 CE with high relative fire intensities after the establishment of a bauxite mine around the site. Vegetation is a consistent tree-grass mix throughout the record comparable to modern vegetation across the Weipa Plateau.

The palaeofire record for Sanamere Lagoon spans ~8300-5500 cal BP. Fire incidence and sedimentation rate are highest from ~8300-8000 cal BP before an abrupt decline, possibly the result of deepening of the lagoon. Vegetation throughout the record is almost entirely C_3-derived with irregular pulses of grassy burnt material in the fine fraction, indicating that the

dwarf heathland currently present at the site has persisted for over 8000 years. High fire intensities that dominate throughout this record are consistent with the modern fire characteristics of heathlands. The absence of sediments dating from 160 to ~4000 years ago indicates sediment loss from one or more occurrences of scouring, likely triggered by cyclone or active monsoon events.

These records together demonstrate the heterogeneity of fire histories across the savannas of northern Australia. However, while Marura shows decreasing fire incidence through time and Big Willum Swamp contains minimal charcoal and pyrogenic carbon until the recent period, both sites present dramatic increases in fire incidence as a result of European land-use changes. The combination of methods in this thesis demonstrates the interpretive power of a multiproxy approach, with optical techniques such as charcoal morphology and chemical techniques such as the $\delta^{13}C$ values providing greater detail than these methods in isolation. The methods presented in this thesis for assessing changes in relative fire intensities will benefit future palaeofire research.

Table of Contents

List of Tables

List of Figures

Chapter 1 : Introduction

"Every day, somewhere in the world a fire burns." (Scott 2000, p.281)

1.1 Rationale

Palaeofire research provides insights into past interactions between fire, climate, humans and vegetation over decades to millennia. However, palaeofire data are limited for the tropical savannas of northern Australia. Minimal palaeofire records across the region are available, making the picture of the long history of fire in these savanna environments incomplete. This also affects attempts to model Australian palaeofire, with a small selection of available charcoal records assumed to be representative of the greater northern Australian savanna region (e.g. Reeves et al. 2013b). This spatial knowledge gap will be addressed in this thesis (see Research Objectives below). This study spans the Holocene with particular focus on the late Holocene as this period is shares climatic similarities with modern conditions (e.g. Shulmeister & Lees 1995; Donders et al. 2007, 2008; Reeves et al. 2013a) and includes major environmental and cultural changes such as Indigenous population growth and technological innovation (Williams 2013; Williams et al. 2015b) and sea-level stabilisation at modern levels after a mid-Holocene high-stand (Chappell 1983; Yu & Zhao 2010).

The late Holocene is a period worthy of detailed study as it is most climatically comparable to modern conditions (e.g. Shulmeister & Lees 1995; Donders et al. 2007, 2008; Reeves et al. 2013a)

Improving our understanding of palaeofire in Australia and globally requires not only additional records but also methodological improvements in how palaeofire data is created. Developments in other palaeoecological disciplines including automation (e.g. France et al. 2000; Maruyama et al. 2018) have outpaced comparable advances in palaeofire techniques. Emerging techniques for determining vegetation composition of burnt materials in sedimentary records (e.g. Bird & Ascough 2012; Enache and Cumming 2006; Umbanhowar & McGrath 1998) are promising but underutilised tools applicable to palaeofire research.

In addition to the identified spatial knowledge gap, existing palaeofire records for northern Australia are also methodologically limited. Existing records primarily utilise a single palaeofire proxy, commonly microscopic charcoal (e.g. Moss et al. 2015; Prebble et al. 2005; Rowe 2005; Shulmeister 1992). The only records in the region utilising multiple proxies are those of Big Willum Swamp (Stevenson et al. 2015), Lizard Island (Proske & Haberle 2012) and marine core ODP Site 820 (Moss & Kershaw 2000) that combine microscopic and macroscopic charcoal analysis. Fuel classification and chemical isolation fire proxies have not been conducted on sites in this region; these techniques are key to distinguishing relative fire intensities and better understanding connections between fire, vegetation, humans, and climate through time by disentangling human and climate influences on fire. This methodological knowledge gap will be addressed in this thesis.

1.2 Background

Fire is a "phenomenon, a problem, and a principle" (Pyne 2016, p.6) that occurs across vastly different scales – from local to global, minutes to millennia. Fire is both ancient and immediate; it is a chemical reaction, a domestic tool, a source of warmth, a transformer of landscapes (e.g. Yates, Edwards & Russell-Smith 2008), a symbol of the home, a power stolen from the gods

(Raggio 1958), accidental destruction brought to earth by spirits as falling stars (Norris & Hamacher 2009, p.44), and much more. Pyne (2016, p.6) describes fire in nature as "a shape-shifter, taking its character from its context"; any detailed consideration of fire is therefore shaped by context. This chapter establishes the context of this thesis and the fire examined therein.

Fire has existed on Earth since the Silurian (~420 million years ago; Glasspool, Edwards & Axe 2004). The earliest evidence of hominin fire use is dated to around one million years ago (by *Homo erectus*; Carbonell, Bermúdez de Castro & Sala 2018, p.111), and fire technology is often identified as a "defining trait of humanity" (Bowman et al. 2011, p.2224) with humans as the "planet's keystone species for fire" (Pyne 2016, p.7). However, there is "little understanding" of fire-human-environment interactions in the long term despite the significance of these relationships (Bowman et al. 2011).

Humans became an ignition source for fires in Australia over 60,000 years ago (Clarkson et al. 2017), although the effects of anthropogenic versus climatic influence on overall fire incidence in Australia through time is debated (Mooney et al. 2011). Unsurprisingly, across the vast array of ecoregions covering the Australian continent there have been, and continue to be, a large range of fire regimes, with fire return intervals of anywhere between one year to over 100 years (Cremer 2004, p.13). As described by Gammage (2012), the Australian landscapes encountered by British invaders in the eighteenth century were carefully managed, following thousands of years of fire management by Indigenous Australians for a wide range of purposes (see Gammage 2012; Pyne 1991, p.100). European invasion disrupted this ongoing fire management through displacement and decimation of Indigenous populations, and the introduction of grazing animals (see Horsfall & Morrison 2010, p.10; Ó Foghlú et al. 2016, p.2-3; Pyne 1991, p.132). Fire suppression policies and attitudes accompanied European colonisation in tropical savanna regions worldwide, including northern Australia (Moura et al.

2019). However, as modern fire conditions intensify with anthropogenic climate change, landscape fire is becoming an increasingly critical ecological, economic and political issue (e.g. Bradstock & Nolan 2019; Cox 2019; Kellett, Visontay & Gair 2019).

Fire is ever-present in the savannas of northern Australia that cover approximately one quarter of the continent (Fox et al. 2001). Of the estimated 50 million hectares that burn across Australia each year, 80 % occurs in northern Australian savannas (Commonwealth Scientific & Industrial Research Organisation [CSIRO] 2009; Figure 1.1). In the most frequently burned areas of this fire-prone region, fires can recur annually (see Northern Australian Fire Information [NAFI] 2019). Removal of Indigenous fire management from northern Australia has been associated with fires of higher intensities and greater sizes (Burrows et al. 2006). The introduction of European pastoral land management in northern Australia was also associated with changes in fire regime relating to timing and purpose (see Crowley 1995; Crowley & Garnett 2000). Active fire management in the savannas of northern Australia has gained recent economic importance with the introduction of international agreements on reductions of greenhouse gas emissions (Whitehead et al. 2008). Numerous ongoing prescribed burning programs have been established within the savannas of northern Australia, with Aboriginal ranger groups and scientists collaborating to control the timing and intensity of fires to reduce emissions (see Johnston 2016; Murphy 2013; Russell-Smith et al. 2013; Whitehead et al. 2008).

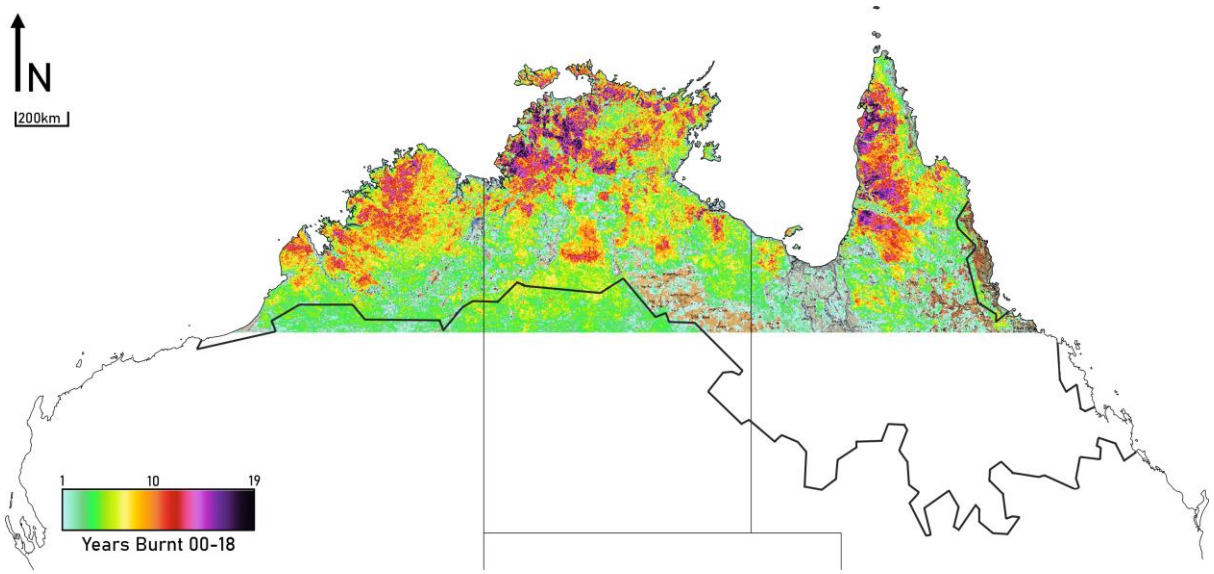

Figure 1.1: Extent of savanna vegetation in northern Australia (dark grey outline, after Fox et al. 2001) and years burnt from 2000-2018 (above 20 °S, after NAFI 2019). Base outline maps presented in this thesis are derived from the open data of OpenStreetMap Contributors (2019).

Palaeofire research is the study of fire in the past, and provides crucial context for understanding fire under changing climatic conditions in the present and into the future. Optical quantification of sedimentary charcoal particles to reconstruct fire histories began in the 1940s (see Iversen 1941) and has been widely applied since then, with later developments in chemical isolation techniques for pyrogenic carbon less commonly used (see Masiello 2004). While most palaeofire studies are not sufficiently resolved, temporally or spatially, to generate direct recommendations for future fire management, a comprehensive understanding of fire in Australian environments as climates shift requires data beyond the time-depth of the observational record. As described by Victor Steffensen:

> There is a common belief that climate change is to blame for an increase in wildfires. However, the climate has always changed and the people adapt the fire

> to whatever climate we get each year, hot, cold, wet, or dry. This makes the burning time different each year and is done by reading country (George et al. 2013, p.11).

Recent catastrophic fire conditions (e.g. in 2019) as well as high fire dangers occurring earlier in the year in eastern Australia have been described as "unprecedented" relative to the observational record (e.g. Bowman 2019; RMIT ABC Fact Check 2019) but this does not capture previous periods of significant climatic changes. Understanding fire characteristics during past shifts in climate provides the necessary context for modern and future fire.

1.3 Research Objectives

This study has two interrelated research aims:

1. The creation of new high resolution palaeofire records for northern Australian savannas in the late Holocene.
2. The evaluation of established and emerging palaeofire methods in the northern Australian savanna context.

By achieving these aims, this study intends to answer the following major research questions:

i) What are the fire histories of Cape York Peninsula and Arnhem Land during the late Holocene, and how has the vegetation burned changed (or not) over time? (to be addressed in Chapter 9).

ii) How can anthropogenic activity or influence be distinguished from climate in palaeofire records, in the context of existing archaeological and historical data? (to be addressed in Chapters 8 and 9).

iii) Can land use transitions such as European arrival, Indigenous Australian removal or displacement and the initiation of pastoral and/or mining activities be identified

in palaeofire records? If so, what are the characteristics of these transitions? (to be addressed in Chapter 9).

1.4 Thesis Structure

Chapter 1 introduced the study, its problem setting, rationale and objectives.

Chapter 2 reviews the existing palaeoenvironmental literature for northern Australia. The primary climate drivers in northern Australia are identified and briefly described, followed by palaeoclimate and palaeofire reconstructions for the late Holocene divided by region (northeastern Australia and central to western northern Australia).

Chapter 3 describes human activity in northern Australia by first reviewing existing archaeological data for the late Holocene by region (Cape York Peninsula and Arnhem Land) then discussing European arrival and influence via a historical timeline for each region. This is followed by a brief overview of fire dynamics and Indigenous Australian uses of fire recorded ethnographically.

Chapter 4 outlines the methodological approach of this study and critique of existing methods, including selection of fire proxies, site selection and sampling, and laboratory procedures.

Chapters 5, 6 and 7 present background information, site characteristics and results for Marura sinkhole (Northern Territory), Big Willum Swamp (Queensland) and Sanamere Lagoon (Queensland), respectively. This includes modern climate and vegetation, land use history, sediment descriptions and elemental composition, chronology and palaeofire proxy results. As Big Willum Swamp is the only site in this study that has been previously researched, Chapter 6 also presents a comparison of the results of this study to those of Stevenson et al. (2015).

Chapter 8 is a discussion and interpretation of results in terms of the palaeofire techniques used in this study. This chapter establishes the parameters to be used to interpret the palaeofire records of each site in Chapter 9.

Chapter 9 presents and discusses the palaeofire records for each site in this study, including interpretations supported by existing palaeoenvironmental, archaeological, historical and ethnographic data, where applicable.

Chapter 10 summarises the overall thesis including the main findings of this study, and proposes areas for future work.

Chapter 2 : Palaeoenvironmental Reconstructions of the Late Holocene in the Australian Tropics

2.1 Introduction

Palaeoenvironmental research across northern Australia presents a complex picture of climatic conditions and change through the mid-to-late Holocene and the late Holocene to the modern day. However, achieving a more holistic understanding of past conditions in this region is hindered by the scarcity of data relative to more southerly latitudes of Australia, with regions either being represented by a small selection of sites (north Queensland) or not represented at all (Arnhem Land in the Northern Territory and much of north Western Australia).

Existing records suggest that expressions of late Holocene climatic variability, including wet/dry phases and changes in vegetation communities, may be region-specific. While extensive work has been conducted in Australian palaeoenvironmental reconstructions, data are still very incomplete for the Australian tropics, and particularly lacking for Arnhem Land. Further investigation is required in northern Australia to create a nuanced reconstruction of past climate in the region, within the greater context of the continent.

This chapter reviews existing literature on palaeoenvironmental reconstructions for the late Holocene in northern Australia with a focus on the central and eastern tropics. Available palaeofire records are included in this review.

2.2 Climate Drivers in Northern Australia

While numerous interconnected climate systems affect the Australian tropics (Figure 2.1), the two major systems at play are the Indonesian-Australian Summer Monsoon and the El Niño-Southern Oscillation (Bureau of Meteorology [BOM] 2010; McRobie, Stemler & Wyrwoll 2015; Reeves et al. 2013a). Both of these systems greatly influence rainfall over northern Australia and have been identified as affecting past climate.

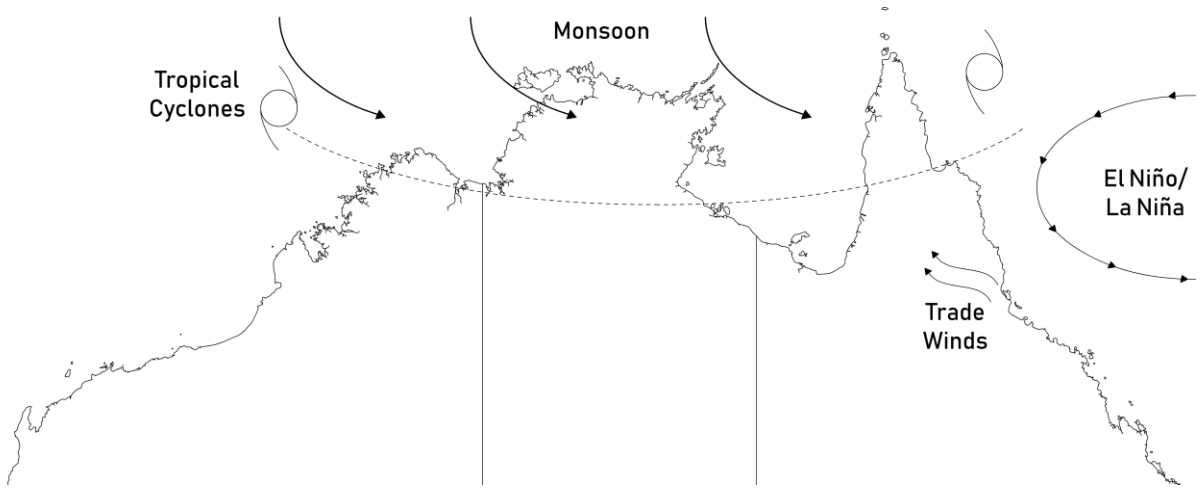

Figure 2.1: Map visualising the major systems affecting climate in northern Australia (adapted from Bureau of Meteorology [BOM] 2010).

2.2.1 Indonesian-Australian Summer Monsoon (IASM)

Alternatively called the 'Australian-Indonesian Summer Monsoon' or 'Australian summer monsoon', the IASM is a "seasonal reversal of winds" leading to high rainfall seasonality in the Australian tropics (BOM 2008). As the Intertropical Convergence Zone (ITCZ) moves south, northwesterly winds and a zone of low pressure (the monsoon trough) bring heavy rain

to northern Australia, resulting in the majority of rainfall in the region occurring between December and March (the wet season) (BOM 2008; Doyle 2019; Steinke et al. 2014; see also Bayon et al. 2017). The extent of the wet season is commonly longer (earlier onset and later retreat) in the Top End of the Northern Territory than in north Queensland (BOM 2008).

Wyrwoll and Miller (2001) identify ~14,000 BP as the point after the Last Glacial Maximum when the IASM became active, based on data from the Kimberley region. Fluctuations in monsoonal activity and strength since this activation have been recorded, including enhanced monsoon strength from 5-4 ka in central and eastern north Australia (Shulmeister 1999) and a weakening trend in the Australian tropics in the late Holocene (Reeves et al. 2013a). Field et al. (2017) report a series of wet/dry phases at Black Springs (WA) between 4700 and 550 BP, and Denniston et al. (2013, p.162) note a "weakening of monsoon rainfall" in the Kimberley region from 4.2-1.5 ka followed by an arid phase, then a "return to wetter conditions" with "smaller-scale variability" through the last millennium. Notaro, Wyrwoll and Chen (2011) investigate the possible influence anthropogenic burning may have had in the late Quaternary on the IASM, and conclude that humans did not have a major impact on the monsoon in northern Australia. However, this is a subject of debate (see Miller et al. 2005).

Late onset of the IASM and reduced rainfall is associated with El Niño phases of ENSO (BOM 2008).

2.2.2 El Niño-Southern Oscillation (ENSO)

The El Niño-Southern Oscillation has been described as "a coherent variation of barometric pressures at interannual intervals that is related to weather phenomena on a global scale, particularly in the tropics and subtropics" (Enfield 1989, p.161). An increased pressure gradient between the high pressure southeast Pacific region and low pressure Indonesian trough

strengthens Pacific trade winds during the ENSO "high phase" (La Niña) (Enfield 1989, p.161). The reverse occurs during the "low phase" (El Niño), weakening trade winds (Enfield 1989, p.61). Stronger trade winds in the La Niña phase are also associated with lower sea surface temperatures, while the El Niño phase is associated with higher sea surface temperatures along with the northward movement of the ITCZ. Subsequently, during the El Niño phase, a "significant decrease in summer precipitation (typically 150-300 mm below seasonal average) over much of Queensland" occurs (Turney & Hobbs 2006, p.1744; BOM 2019). While ENSO has pronounced effects on rainfall, it can also influence other environmental factors including temperature, cyclone activity and likelihood of bushfires (Diaz & Markgraf 1992, p.166).

ENSO has a strong influence on modern conditions, and is described by Diaz and Markgraf (1992, p.436) as having initiated at ~5000 BP and being "fully developed" by 3000 BP. Haug et al. (2001) identify the more persistent southerly movement of the Intertropical Convergence Zone (ITCZ) during the Holocene as a possible factor influencing increasing ENSO intensity in this period, while Field et al. (2017, p.15) and Reeves et al. (2013a) note indications of a mid-Holocene northward ITCZ shift. Numerous palaeoclimatic studies suggest the establishment of ENSO conditions comparable to modern as the cause of increased climatic variability in the mid-to-late Holocene (e.g. Donders et al. 2007; Donders, Wagner-Cremer & Visscher 2008; Field et al. 2017; Shulmeister & Lees 1995), as well as changes in fire regime (see Fletcher et al. 2015).

The expression of IASM and ENSO signals in palaeoenvironmental records vary depending on the type of proxy used, and their influence may be expressed in a number of ways such as a shift in vegetation communities (e.g. Donders et al. 2007), a change in fire activity (e.g. Rowe et al. 2019), or in wetland organic productivity (e.g. Field et al. 2017). Palaeoenvironmental reconstructions aim to not only pinpoint the timing of past climate events but also to investigate

the influence of these events on landscapes and better understand climate-human-environment interactions over time.

2.3 Northern Australia in the Late Holocene

A large body of literature is dedicated to elucidating the magnitude and trajectory of climate changes in both recent and deep time, integrating data from various sources; the combination of these data allow for the creation of broad climate reconstructions and trajectories of change, some continental and others regional. However, not all studies are in agreement on the nature of past climatic conditions and the timing of observed changes.

Reeves et al. (2013a) synthesise marine and terrestrial data obtained from sites across the Australian region to characterise changing climate from 35,000 years ago to the present. The authors present temperature and precipitation as increasing through the mid-Holocene, with "maximum temperature" occurring at different times between 8-5000 BP across the region, noting an unspecified "lag" in eastern sites compared to southerly sites (Reeves et al. 2013a, p.29). Donders et al. (2007, p.1631) identify differences of up to 1000 years between sites in the northern wet tropics for the "moisture maximum" of the mid-Holocene, although the region is represented by only four sites in this study (just one of which is in the Northern Territory: Four Mile Billabong). Shulmeister (1999, p.87) places the mid-Holocene precipitation maximum between 5-3.7 ka for the Northern Territory and north Queensland.

Reeves et al. (2013a, p.29) describe the late Holocene as increasingly variable and dry, supported by an agreement between various data derived from coral, speleothem, dune and fluvial proxies. However, sites in the southwest of Australia appear "relatively consistently warm and moist" during this period (Reeves et al. 2013a, p.29). Nanson et al. (2008) similarly note a period of drying in central Australia in the late Holocene, while Donders et al. (2007)

identify increasing aridity and variability in eastern Australian sites across multiple latitudes in this period. Quigley et al. (2010, p.1101) state that increasing aridity and variability began at ~5 ka in the Flinders Ranges, and that similar findings in other studies indicate that this climatic shift was "continental in scale". Diaz and Markgraf (1992, p.446) identify a period of "lowest levels of precipitation" in Australia from 3500 to 2500 BP, and note a general trend of increasing variability from 5000 BP.

Of particular relevance to this study are the climatic conditions across northern Australia during the comparatively recent past (~4000 BP). Reeves et al. (2013b, p.109) note that increasing variability and "localised aridity" characterise the late Holocene in the Australian tropics. However, studies across the region provide contradictory indications as to whether the mid-to-late Holocene can be described as wet/dry, warm/cool or variable at different sites. The following section investigates some of these regional patterns in northern Australia.

2.3.1 Northeastern Australia – Queensland

The mid-Holocene in north Queensland is commonly characterised as wet, relative to earlier periods (see Haberle 2005, p.354; Luly, Grindrod & Penny 2006; Reeves et al. 2013b). This phase is followed by a shift in the late Holocene to drier and increasingly variable conditions. Lees (1992) describes this climatic shift in dune field records in northern Queensland, while Kershaw (1983) notes an increase in warmth and seasonality at ~4.5-3 ka at Lynch's Crater (Figure 2.2). Haberle (2005, p.355) identifies "drier conditions and increased rainfall seasonality" as a potential explanation for increased rainforest disturbance at Lake Euramoo after ~4 ka. Stevenson et al. (2015, pp.26-27) note the end of a "warm and wet period" at ~5 ka at Big Willum Swamp, Weipa, and identify the period between 1000-400 BP as the period of "greatest variability" at the site. Burrows, Fenner and Haberle (2014, p.1716) investigated

late Holocene climate variability through the humification of peats at Quincan Crater and Bromfield Swamp, and identify a dry event in both records at 4060 BP as a possible indicator of "substantial climate change". Mackenzie et al. (2017) describe variable conditions over the last 1250 years in the South Wellesley Islands, including storm events, wet conditions at one site around 750 BP and a drying trend beginning in the last 150-50 years across three swamps.

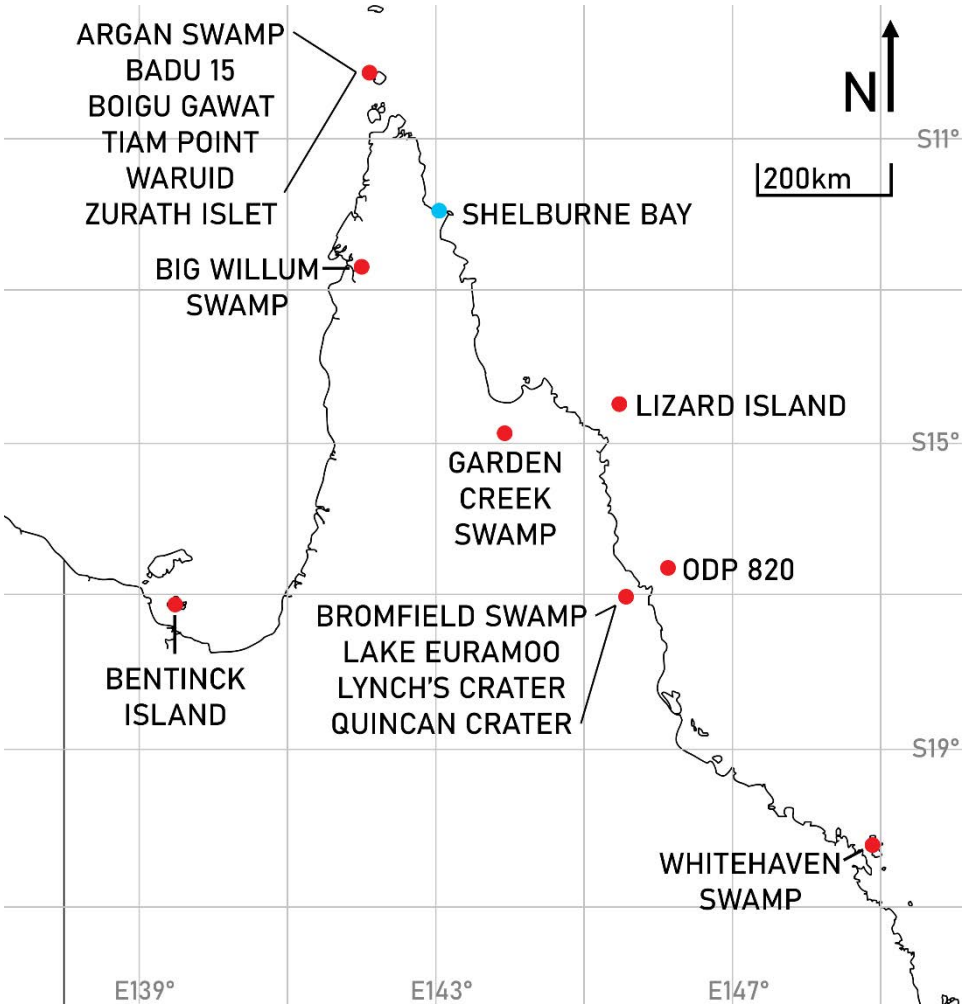

Figure 2.2: Map of palaeoenvironmental record sites for northern Queensland. Sites with charcoal records are marked in red.

In contrast, Kershaw (1971, p.678) refers to an increase in temperature and "possibly also of precipitation" from ~3 ka from a pollen record spanning ~7.2 ka from Quincan Crater, with a decrease in effective precipitation at ~2 ka marking the partial return of sclerophyll forest. The late onset of drier conditions coupled with higher temperatures at Quincan Crater may support the increasing variability suggested by other records, but not the decrease in rainfall seen in some other sites at the mid-to-late Holocene transition.

Charcoal data for northeastern Australia includes sites in Torres Strait (Rowe 2005, 2006, 2007), the Atherton Tablelands (Haberle 2005; Burrows, Fenner & Haberle 2014; Kershaw 1971, 1983; Kershaw, Bretherton & van der Kaars 2007), Lizard Island (Proske & Haberle 2012), the South Wellesley Islands (Moss et al. 2015, 2019), Weipa (Stevenson et al. 2015), the Whitsundays (Genever, Grindrod & Barker 2003), Garden Creek Swamp northwest of Cooktown (Stephens & Head 1995), and an offshore marine core adjacent to Cairns (Moss & Kershaw 2000). Many of these include microscopic charcoal counts (<125 μm) undertaken alongside pollen analysis, with some of these studies also including a macroscopic count (>125 μm for Badu 15 in Torres Strait, Big Willum Swamp in Weipa and Lake Euramoo on the Atherton Tablelands). The records for Quincan Crater and Bromfield Swamp (Atherton Tablelands) presented by Burrows, Fenner and Haberle (2014) are the only sites for which there is macroscopic charcoal data in two size classes (>250 μm and 250-125 μm) but no microscopic charcoal count, while Proske and Haberle (2012) present two sizes of macroscopic charcoal (>250 μm and 250-125 μm) as well as microscopic charcoal for Lizard Island.

These charcoal records vary significantly in time depth and resolution, with some spanning beyond the Holocene into the Pleistocene (>11 ka) (Lake Euramoo, Lynch's Crater, ODP Site 820). Microscopic charcoal peaks at ODP Site 820 outside of the Holocene (>43,000 BP) (Moss & Kershaw 2000). Peaks are present in three zones of the Holocene Lynch's Crater core (LC2, LC3 and LC5); however, few dates are provided for this core and Kershaw (1983, p.675)

notes multiple issues with these dates when attempting to compare the Holocene core to the original Lynch's Crater core (see Kershaw 1976). Macroscopic charcoal at Lake Euramoo peaks in the most recent period (~250 BP to present) (Haberle 2005).

For many of the Torres Strait records (except Talita Kupai and Waruid), charcoal concentration peaks in the most recent period, although many of these peaks are not independent of increasing pollen concentration and thus may be the result of changing sedimentation rate rather than changing fire (Rowe 2005, 2006, 2007). Microscopic charcoal concentration relative to pollen concentration at Badu 15 rises gradually from ~3000 BP to the present, with a similar trend in macroscopic charcoal (Rowe 2006, p.277). The highest charcoal peak independent of pollen accumulation for Big Willum occurs at ~1000 BP in both the micro- and macroscopic charcoal records, along with a macroscopic charcoal peak within the last century (Stevenson et al. 2015). Increasing microscopic charcoal and fire frequency is noted from ~1500 cal BP on Lizard Island by Proske and Haberle (2012, p.5, 10). Microscopic charcoal relative to pollen concentration at Whitehaven Swamp in the Whitsundays (Figure 2.2) also peaks within the most recent period (WHS1, not dated) (Genever, Grindrod & Barker 2003, p.147). Moss et al. (2019, p.518) describe charcoal peaking ~500 years ago, potentially linked to permanent occupation of the South Wellesley Islands and "increased burning associated with local occupation" of the site Thundiy. Moss et al. (2015, p.143) note that a significant increase in charcoal abundance at Marralda Swamp (South Wellesley Islands) coincides with the population of Bentinck Island relocating to Mornington Island following a cyclone in 1948.

Burrows, Fenner and Haberle (2014) identify numerous charcoal peaks for Bromfield Swamp and Quincan Crater as part of a high-resolution study of peat humification, although with some variations between the two sites. Both sites display a charcoal peak at ~4060 BP, coincident with peat initiation and the onset of drier conditions (Burrows, Fenner & Haberle 2014,

p.1713). Smaller isolated peaks occur at various times at both sites during both dry and wet phases (Burrows, Fenner & Haberle 2014, pp.1713-1714).

2.3.2 Central to Western Northern Australia – Northern Territory and Western Australia

The majority of climate reconstructions for the central and western regions of northern Australia are derived from non-lacustrine sedimentary records (e.g. May et al. 2017 for washover fans), dunes (e.g. Wende, Nanson & Price 1997; see Hesse, Magee & van der Kaars 2004 for a review), and speleothems (e.g. Denniston et al. 2013) as well as sea-level reconstructions based on mangrove studies (e.g. Woodroffe, Thom & Chappell 1985). Due to the lack of available records as well as the similarities in environments, north Western Australia and the Kimberley are often discussed collectively with the Top End of the Northern Territory. While a range of palaeoclimatic studies from various data sources are available for the region, few include palaeofire data. This section will focus primarily on palaeoenvironmental records from sediments for comparability to data for northern Queensland (Figure 2.3).

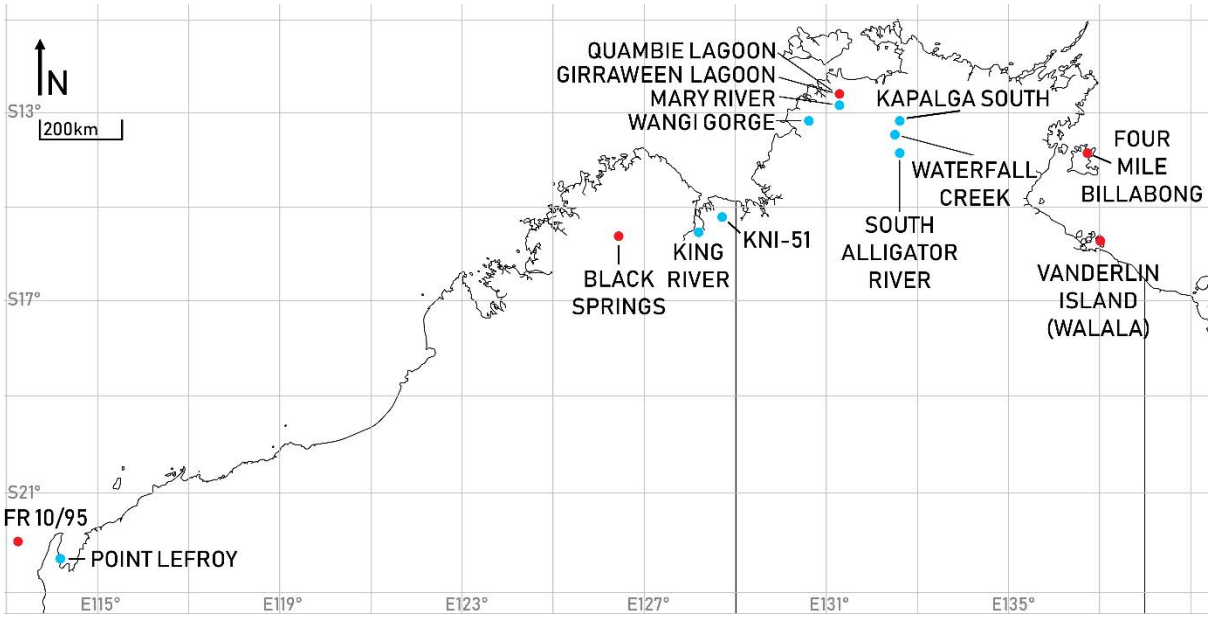

Figure 2.3: Map of palaeoenvironmental record sites for the Northern Territory and north Western Australia. Sites with charcoal records are marked in red.

Shulmeister (1992), using pollen data, identifies a precipitation maximum for Groote Eylandt at ~4 ka, declining at 3800 BP. Similarly, plunge pool sediment records analysed by Nott, Price and Bryant (1996) and Nott and Price (1999) display maximum levels of flooding in the early to mid-Holocene, with smaller scale flooding in the late Holocene suggesting decreased precipitation. Pollen data from Vanderlin Island suggest that the late Holocene was characterised by variable climate, with the appearance of vegetation typically associated with disturbed environments from ~3000 BP but charcoal/fire appearing as a "constant influence" throughout the Holocene (Prebble et al. 2005, p.368). Head and Fullager (1992, p.29) identify "increasing climatic variability" in the last 3000 years from dune instability in the East Kimberley. Similarly, McGowan et al. (2012) identify increasingly dry conditions from ~3 ka at Black Springs, also in the Kimberley region, with a transition to modern climate conditions at ~1300-1100 BP. Additional data provided by Field et al. (2017:14) for Black Springs display a series of wet and dry phases between 4.7 and 0.55 ka. Rowe et al. (2019, p.25) note

comparable short-lived drying phases at Girraween Lagoon between 3750-3500 cal BP and 1300-1250 cal BP "consistent with increasing late Holocene climatic variability". Proske (2016) notes a decrease in mangrove diversity at King River at some point after 6.3 ka, likely resulting from the "decrease in summer monsoon precipitation and peak dryness" between 4.2 and 1.5 ka reported by Denniston et al. (2013) in a speleothem record from the Kimberley. Shulmeister and Lees (1995, p.12) identify a dry period from ~4000 to 2100 BP followed by a "recovery" of effective precipitation from 2000 to 1600 BP at Kapalga South Billabong (based on unpublished data by Chappell & Guppy). The same authors note an arid phase at "roughly the same period" as Kapalga South Billabong followed by an increase in effective precipitation at 1400 BP at Kiina (based on data by Russell-Smith 1985).

Four of these sites include charcoal records, all microscopic: Black Springs, Groote Eylandt (Four Mile Billabong), Girraween Lagoon and Vanderlin Island. The Black Springs record covers ~6000 years, with charcoal concentration peaking at ~1300 BP coinciding with a "return to wetter conditions" indicated by changes in pollen (McGowan et al. 2012, p.2). The record from Groote Eylandt, which begins >9000 BP, features charcoal peaking in the top pollen zone (1000 BP to present) (Shulmeister 1992, p.110). As this is coupled with pollen indicative of wet conditions, the author suggests that this indicates an "increased frequency of 'cool' fires" (Shulmeister 1992, p.112). The Girraween Lagoon record, which begins >120,000 cal BP, shows peak charcoal abundances at ~3100 cal BP, declining thereafter (Rowe et al. 2019). Rowe et al. (2019, p.24) describe fire after this late Holocene peak as "milder burning", incorporating frequent smaller fire events along with an increase in woody cover potentially linked to anthropogenic fire regimes. The Vanderlin Island record begins at 10,000 BP with charcoal concentrations peaking at 5500 BP (Prebble et al. 2005). High charcoal concentration is maintained through to 3000 BP, with the authors noting that fire may have contributed to open woodland succession during this period (Prebble et al. 2005, p.367). The authors state

that “forest burning increases” in the most recent period from 1000 BP to present, and note that further work is needed to decouple climate and anthropogenic influences (Prebble et al. 2005, p.367).

2.3.3 Regional Comparison

Shulmeister (1999, p.82) summarises the Holocene climate in northern Australia as a gradual increase in temperature and effective precipitation through the early-to-mid-Holocene, followed by increased effective precipitation from ~5-3.7 ka, before a sharp decline in precipitation coupled with increasing variability. This general pattern appears to be supported at many sites, with the late Holocene commonly being described as a period of variable climate (see Denniston et al. 2013; Lees 1992; Prebble et al. 2005; Stevenson et al. 2015).

Multiple studies suggest the establishment of a climate comparable to modern conditions after ~3 ka, aligning with the onset of current ENSO conditions noted at this time by Diaz and Markgraf (1992, p.436) and Donders, Wagner-Cremer and Visscher (2008, pp.576-577). Donders et al. (2007, p.1634) identify the period since ~3 ka as showing conditions becoming “slightly drier and more variable (adapted to disturbance)” for most Australian sites.

The studies presenting a transition to modern climate at this point (~3 ka) include data from northeastern Australia (e.g. Shulmeister 1992), north Western Australia (e.g. van der Kaars & De Deckker 2002) and northern South Australia (e.g. Quigley et al. 2010), with a possible later onset by ~1200 BP in the Kimberley (McGowan et al. 2012). Stevenson et al. (2015, p.27) identify this as a broad east-west trend of increasing moisture and permanent water, but note exceptions from Witherspoon Swamp (Moss et al. 2012) and Three-Quarter Mile Lake (Luly, Grindrod & Penny 2006) with increasing dry conditions from ~2 ka and stable wet conditions

from ~5 ka, respectively. The latter contrasts with Shulmeister's (1999) characterisation of the late Holocene in northern Australia as a period of decreasing precipitation.

Charcoal records for northern Australia provide varying trajectories driven by climate and humans for the late Holocene, some of which can be explained by differences in the charcoal analysed (i.e. microscopic, macroscopic or both). Late Holocene variability is supported by many of the charcoal records, with various wet and dry phases (some coincident with charcoal peaks) identified at Bromfield Swamp and Quincan Crater (Burrows, Fenner & Haberle 2014) and a gradual increase in charcoal at Badu 15 from ~3000 BP to the present (Rowe 2006, p.277). Sites from across the Australian tropics display significant events at ~1000 BP, with a "return to wetter conditions" along with a charcoal peak at Black Springs (WA) (McGowan et al. 2012, p.2), an increase in the frequency of "cool" fires at Groote Eylandt (NT) (Shulmeister 1992, p.110), an increase in forest burning at Vanderlin Island (NT) (Prebble et al. 2005, p.367) and a charcoal peak in both the microscopic and macroscopic charcoal signals at Big Willum Swamp (QLD) (Stevenson et al. 2015). Multiple sites feature an increase in charcoal abundance in the most recent/modern period (Genever, Grindrod & Barker 2003; Moss et al. 2015; Rowe 2006, 2007; Stevenson et al. 2015). Fire is intrinsically linked to available biomass and as such these records may capture changes in biomass rather than directly reflect shifts in climate.

The addition of high-resolution charcoal records including both microscopic and macroscopic charcoal for northern Queensland and eastern Arnhem Land will provide valuable insights into local and regional fire patterns, along with investigating possible differences across the Gulf of Carpentaria. The presence or absence of increasingly variable conditions from ~3 ka and increasing fire activity since ~1 ka from these sites will determine whether these events visible elsewhere existed in Arnhem Land and Cape York Peninsula.

Chapter 3 : Late Holocene Human-Fire-Environment Interactions in the Australian Tropics

3.1 Introduction

Palaeoenvironmental, archaeological and historical data must be considered together to better understand human-fire-environment interactions. On the one hand, palaeoenvironmental and palaeoclimatic records can provide useful climatic and environmental contexts for interpreting archaeological data. Sim and Wallis (2008), for example, utilise records of ENSO and past sea level change to contextualize occupation phases of an offshore island (Vanderlin Island, Gulf of Carpentaria). On the other hand, archaeological and historical records provide a human context against which to interpret past environmental change. For example, an increase in fire incidence and vegetation thickening on Bentinck Island was dated to the 1940s onwards, when the last traditional owners of Bentinck Island were removed (Moss et al. 2015). Similarly, ethnographically recorded contact and post-contact period Indigenous Australian fire regimes assist investigations of human-fire-environment interactions in the past (e.g. Enright and Thomas 2008; Head 1994).

This study utilises history and archaeology to assist the interpretation of charcoal data, and this chapter presents an overview of these data for the Cape York Peninsula and Arnhem Land regions. This chapter also serves as an introduction to factors affecting and characterising fire regimes and Indigenous Australian uses of landscape fire.

3.2 Late Holocene Archaeology of Cape York Peninsula and Arnhem Land

Relationships between climate and human behaviour and disentangling human-climate-environment interactions are key themes of current archaeological research in late Holocene tropical Australia (e.g. Bourke et al. 2007; Haberle & David 2004; Shiner et al. 2013).

It is in the late Holocene that large-scale climatic and environmental variability increases likely due to the intensification of ENSO cyclicity (see Chapter 2). In an archaeological context, the late Holocene encompasses what is broadly referred to as a period of intensification. Archaeological signatures associated with intensification include increased site use such as higher site densities, rates of deposition, increased number of sites occupied, changes in rock art styles and techniques, and changes in resource exploitation including the introduction of toxic plants, all taken to indicate population growth (see summary by Lourandos & Ross 1994). Shell mounds are a significant example of one of the markers of intensification, and this chapter begins with a summary of this site type in the region.

Shell mounds are widespread across coastal northern Australia (see map in Morrison 2014, p.1 for example) and dominate the archaeological record of the region (Figure 3.1). These mounds have been subject to extensive investigation (see themes below) (e.g. Faulkner 2013; Hiscock & Faulkner 2006; Morrison 2014), and past debate on the potential cultural versus non-cultural (scrub fowl) origins of the mounds has settled on the former explanation (e.g. Bailey 1993; Bailey, Chappell & Cribb 1994; Mitchell 1993; cf. Stone 1989). Anthropogenic *Tegillarca granosa*-dominated shell mounds are predominant features of the mid-to-late Holocene, with Faulkner (2013, p.171) identifying 3000-500 BP as the "principal phase of mound formation" across northern Australia (Figure 3.2). Earth mounds are also found in this region during the late Holocene, with deposition periods similar to shell mounds, but are a less extensive site type (see Brockwell 2006).

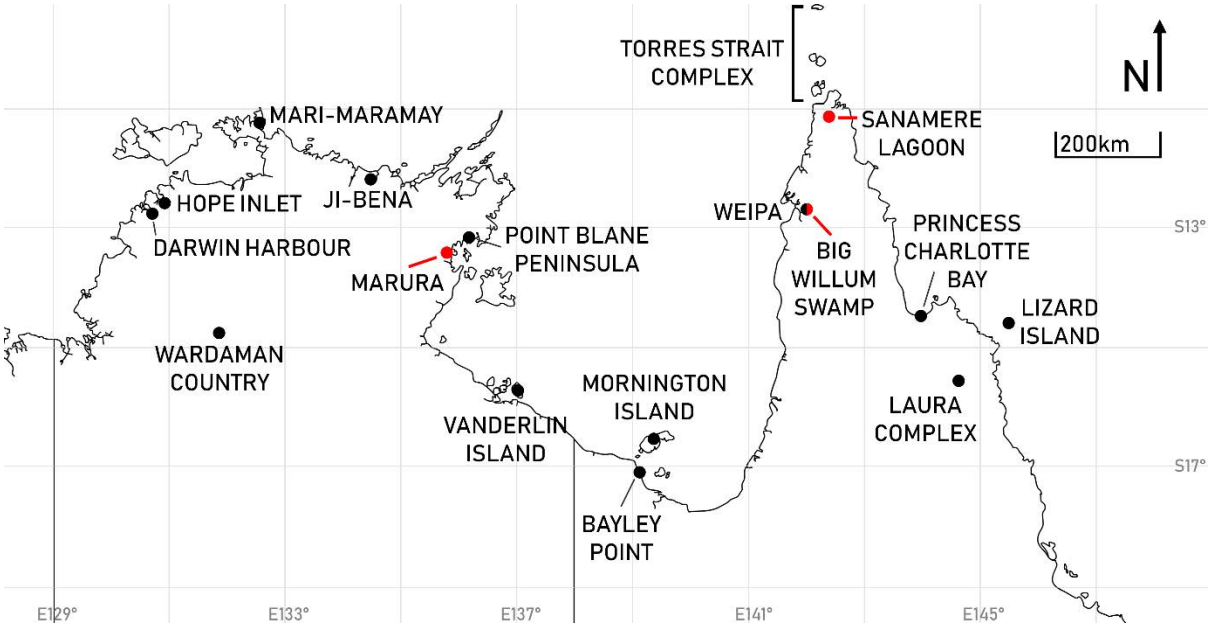

Figure 3.1: Archaeological sites in Cape York Peninsula, Arnhem Land and surrounding areas mentioned in the text. Palaeoenvironmental sites in this study are indicated in red (Marura, Big Willum Swamp and Sanamere Lagoon).

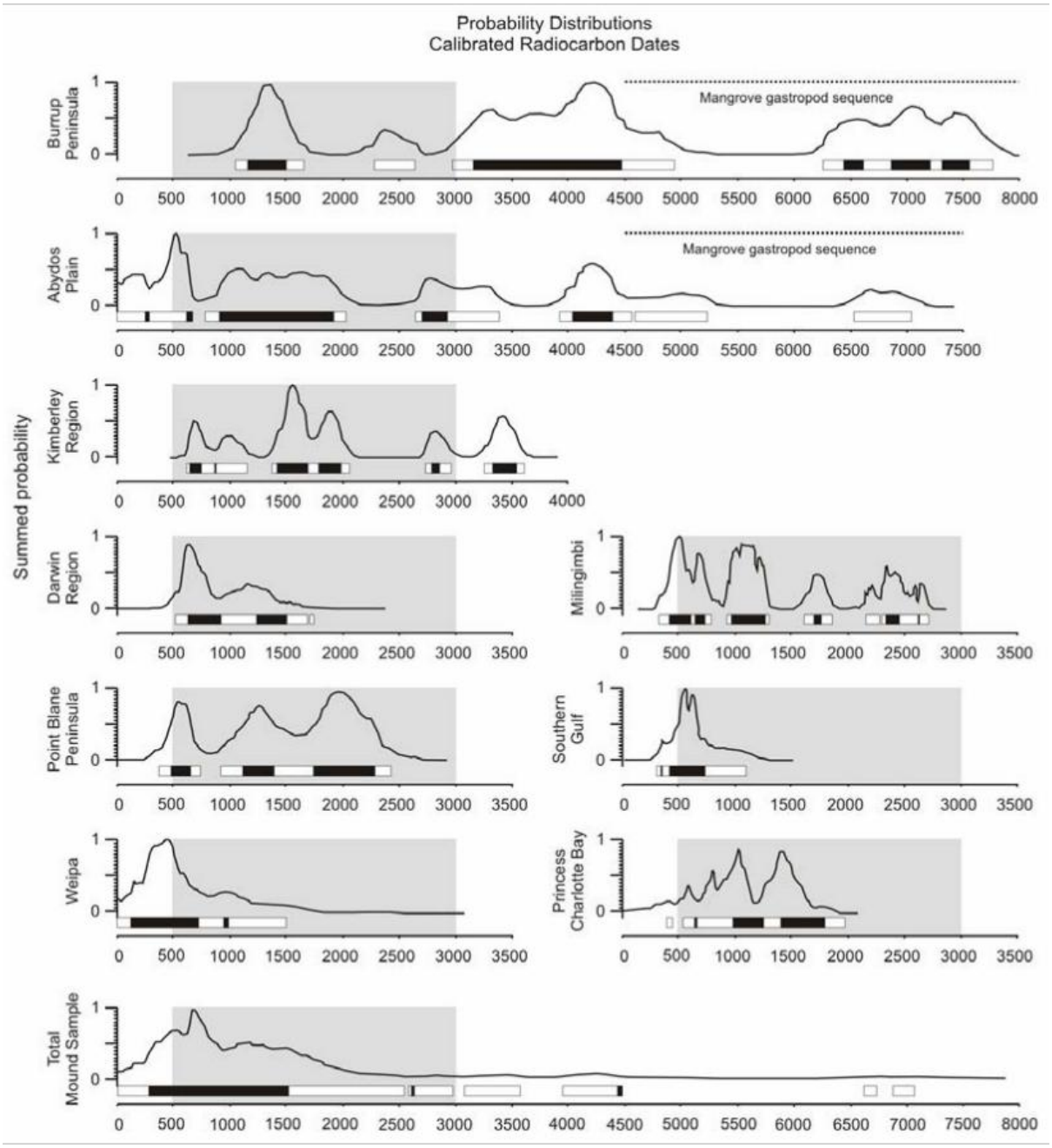

Figure 3.2: Comparison by Faulkner (2013, p.171) of the probability distributions of calibrated radiocarbon dates from coastal northern Australian *Tegillarca granosa*-dominated mounds. The principal mound formation phase is indicated in grey shading. In addition to Figure 3.1, refer to Faulkner (2013, p.171) for site locations and data references.

Shell mound-building has been linked to late Holocene environmental changes, "alterations in economy and land use" by Aboriginal Australians and potentially social and/or ideological changes as well (Hiscock & Faulkner 2006, p.213-219). While mound accumulation has previously been argued to have terminated by approximately 500 years ago (Hiscock & Faulkner 2006, p.211; see Hiscock 1997; Morrison 2013), shell mound-building has been demonstrated as continuous until European invasion (Ulm 2011). Of interest to this study is the documented change in land use and implied socioeconomic behaviour at the onset of shell mound construction. This behavioural shift may have included changes in fire management, such as an increase in fire activity, as people began using resources and landscapes differently.

Similarities are apparent in the late Holocene archaeological record across tropical Australia, particularly in shell mound sites. However, inter- and intra-regional variations can be found in the timing of broad-scale events as well as the ways in which different groups responded and adapted to environmental change.

3.2.1 Cape York Peninsula and Surrounds

The late Holocene archaeology of Cape York Peninsula and the surrounding region includes the occupation of islands in the Torres Strait, the emergence of regionalism in rock art styles in the southeast of the Peninsula (Haberle & David 2004), increased site use in rainforest areas, the introduction of toxic plants as a food resource (Lourandos & Ross 1994, p.57), and the appearance of deposition of *Tegillarca granosa*-dominated shell mounds.

Permanent occupation of islands in Torres Strait began between 3500 and 2500 BP, with horticulture established in the northern and eastern island groups by ~1200 BP (Barham, Rowland & Hitchcock 2004, p.29; Rowe 2005, p.132). While Indigenous communities on Cape York Peninsula are known to have had contact with Torres Strait Islanders (e.g. Loos 1982;

Moore 1979), the Straits area represents a distinct archaeological complex to that of the mainland (see Barham, Rowland & Hitchcock 2004; Rowe 2005) and therefore will not be discussed in detail here. Similarly, occupation of islands of the Great Barrier Reef east of Cape York Peninsula also occurred in the late Holocene, such as Lizard Island from ~4030 cal BP (Lentfer et al. 2013; Ulm et al. 2019). While human activity on offshore islands as well as rainforest occupation in the southeast contribute to the greater Cape York Peninsula cultural complex, they represent different environments and site types to those found in central and northern Cape York Peninsula (the focus of this study) and will not be discussed in detail.

While shell mounds are a common site type in the region, Morrison (2003, p.5) and Holdaway et al. (2017) describe variation in the shell mounds of Cape York Peninsula with differences in height, shape, location type, and cluster size, across both time and space, as the cumulative result of short-term social and environmental dynamics occurring over a long period. Site development, particularly of shell mounds, on Cape York Peninsula in the late Holocene peaks around ~1000 BP. While chenier (beach ridge) development initiated at ~4000 BP at Princess Charlotte Bay, occupation of these cheniers did not begin until 2000 years later, with deposition of shell mound material peaking at ~1000 BP (Beaton 1985). Similarly, shell mounds accumulated rapidly at Bayley Point in the southern Gulf of Carpentaria between ~1100-850 BP, followed by slower accumulation of smaller-mean-size *Tegillarca granosa* shells. The appearance of both terrestrial and marine vertebrate fauna followed from 850-400 BP, with mound deposition ceasing at ~400 BP (Robins, Stock & Trigger 1998, p.111). Accumulation of shell mounds on Mornington Island in the Gulf of Carpentaria had begun by ~2450 cal BP (Rosendahl et al. 2014). Deposition of *Tegillarca*-dominated shell mounds at Princess Charlotte Bay ceased between 600-500 BP (Beaton 1985). Stone artefact deposition at Early Man Rockshelter in southeast Cape York Peninsula, part of the Laura complex, peaked between 1700-900 cal BP (Haberle & David 2004, p.171). These trends in site occupation and

deposition may indicate a south-north pattern in late Holocene occupational and resource-use intensity, with resource use peaking earlier in southerly sites followed later by regions further north.

Extensive archaeological survey and excavation work has been conducted in the Weipa area (see Shiner & Morrison 2009 for an overview of survey data). Brockwell et al. (2016, p.5) record deposition beginning ~2200 cal BP at the oldest earth mound sites in the Wathayn area, with deposition at the majority of earth mound sites at Wathayn beginning around 500 cal BP. Deposition of earth mounds at the nearby Diingwulung area also began around 500 cal BP (Brockwell et al. 2016, p.5). Morrison (2013) presents a database of 477 shell matrix (scatter, midden and mound) sites in the Albatross Bay area, noting basal dates usually less than ~1600 cal BP for sites with dates available. Holdaway et al. (2017), however, present 212 radiocarbon determinations from shell matrix sites in the Wathayn region and note a "large number of mounds" with radiocarbon determinations between 2500 and 2000 cal BP, with the oldest mounds dating to ~4000 cal BP.

Unlike sites elsewhere in Cape York Peninsula and Arnhem Land (see next section), shell mound deposition at Weipa appears to have continued until the contact period (Shiner & Morrison 2009, pp.53-54; Ulm 2011; Table 3.1).

Table 3.1: Summary of archaeological data for Cape York Peninsula and surrounds. Refer to Figure 3.1 for site locations.

Approximate Age	Observations	Sites/Locations	References
4000 BP	Initiation of chenier ridge development at Princess Charlotte Bay	Princess Charlotte Bay	Beaton 1985
4000 BP	Accumulation of oldest shell mounds at Wathayn beings	Wathayn region, Weipa	Brockwell et al. 2016
3500 BP	Permanent occupation of Torres Strait islands	Torres Strait	Barham, Rowland & Hitchcock 2004; Rowe 2005
2200 BP	Accumulation of oldest earth mound sites at Wathayn begins	Wathayn region, Weipa	Brockwell et al. 2016
1700 BP	Peak deposition phase at Early Man Rockshelter begins	Laura region	Haberle & David 2004
1600 BP	Increased initiation of shell mounds at Albatross Bay	Weipa	Morrison 2013
1200 BP	Establishment of horticulture in Torres Strait	Torres Strait	Barham, Rowland & Hitchcock 2004; Rowe 2005

1100 BP	Rapid accumulation of shell mounds at Bayley Point	Bayley Point, southern Gulf of Carpentaria	Robins, Stock & Trigger 1998
1000 BP	Peak shell mound deposition, including on chenier ridges, at Princess Charlotte Bay	Princess Charlotte Bay	Beaton 1985
900 BP	Peak deposition phase at Early Man Rockshelter ends	Laura region	Haberle & David 2004
850 BP	Slower accumulation phase of shell mounds at Bayley Point begins, incorporating marine and terrestrial fauna	Bayley Point, southern Gulf of Carpentaria	Robins, Stock & Trigger 1998
600 BP	Cessation of shell mound accumulation at Princess Charlotte Bay	Princess Charlotte Bay	Beaton 1985
500 BP	Accumulation of majority of earth mounds at Wathayn begins, accumulation of oldest earth mounds at Diingwulung begins	Wathayn region and Diingwulung region, Weipa	Brockwell et al. 2016
400 BP	Cessation of shell mound accumulation at Bayley Point	Bayley Point, southern Gulf of Carpentaria	Robins, Stock & Trigger 1998

3.2.2 Arnhem Land and Surrounds

The archaeology of the far north of the Northern Territory (NT) is both spatially and temporally extensive, including rock shelters, rock art panels, earth mounds, artefact scatters, shell middens and shell mounds (Brockwell et al. 2011, pp.3-4). Brockwell et al. (2009, pp.61-62) review archaeological research undertaken in coastal plains of the "Top End" of the Northern Territory and provide a cultural chronology for the region. They identify three main occupational phases:

- *Transition Phase, ~4000 BP:* marked by the shift from favourable mid-Holocene climate to "climatic uncertainty and rapidly changing environments with increased resource patchiness". This phase features sites reflecting "flexible, varying and mobile foraging strategies", and an increasing abundance of earth mounds, shell mounds and shell middens.
- *Early Freshwater Phase, ~2000 BP:* identified as the "main period of *Tegillarca*-dominated mound building" and includes earth mounds and rock shelter deposits.
- *Late Freshwater Phase, ~500 BP:* characterised by continued climatic variability and "major cultural changes" resulting from Macassan, Chinese and European contact.

Brockwell et al.'s (2009) Transition Phase is visible in the occupation of new sites in the northern region of the NT and the appearance of diverse technology. Initial occupation of Vanderlin Island occurred from 4200-2500 BP (Sim & Wallis 2008), and Mari-maramay shell mound on Croker Island was deposited between ~3000-2000 BP (Mitchell 1993). The first appearance of bifacial points "in abundance" along with a "sudden increase in implement diversity" at ~3000 cal BP is reported by Clarkson (2007, pp.129-150) at rock shelter sites in Wardaman country, southwest of Katherine. Initial occupation of open coastal sites at Point

Blane Peninsula in Blue Mud Bay, eastern Arnhem Land has been dated to ~3000 BP (Faulkner & Clarke 2004, p.28).

The Early Freshwater Phase is evident across numerous shell mound sites in the region, with highest occupation intensities at ~1500-1200 BP. "Peak occupational intensity" occurred at a rock shelter in Wardaman country from ~1500 cal BP to present (Clarkson 2007, p.162). Peak site use at Bindjarran rockshelter, located in what is now Kakadu National Park, occurred around 1200 cal BP (Shine et al. 2015). Occupation of wetland sites at Point Blane Peninsula spans the last 1800 years and "fades out around 550 BP" (Faulkner & Clarke 2004, p.28). Bourke et al. (2007, p.95) notes that most sites in the Blyth River area of Arnhem Land date from 1200 cal BP to modern, with the exception of Maganbal midden at ~3400 cal BP. Continuous site occupation of Ji-bena earth mound (also in the Blyth River region) began at 1400 BP, with a "shift in subsistence strategies" at 800 BP as the adjacent Balpilja Swamp transitioned from estuarine to freshwater conditions (Brockwell, Meehan & Ngurrabangurraba 2005, pp.85-87). *Tegillarca*-dominated mound Bayview Haven 3 in Darwin Harbour formed between 1400-850 BP (Hiscock 1997), and shell mound accumulation at Haycock Reach, Darwin terminated ~1200-600 cal BP (Hiscock & Hughes 2001). Shell mounds at nearby Hope Inlet were deposited from 2000-500 cal BP, including a decrease in *Tegillarca granosa* coincident with an increase in mangrove gastropods at ~700 cal BP in mound HI80 (Bourke 2004). Vanderlin Island sites were either abandoned or occupied at lower intensities from 2500-1700 BP, followed by renewed occupation at ~1300 BP with "more intensive island use" than to the previous occupation period (Sim & Wallis 2008, p.103). The first phase of site occupation at Ingaanjalwurr rockshelter in western Arnhem Land occurred ~1900-1300 cal BP, but poor organic preservation makes it unclear if freshwater sources were exploited during this period (Shine, Hiscock & Denham 2016). Continuous occupation at Birriwilk rockshelter in

western Arnhem Land began at 750 BP, with a focus on freshwater sources for hunting and foraging (Shine et al. 2013).

The Late Freshwater Phase is marked by the termination of shell mound deposition at many sites, likely reflecting climatic and subsequent environmental changes (e.g. estuarine to freshwater transition at Bapilja Swamp and a general decline in habitats favoured by *Tegillarca granosa*). Sim and Wallis (2008, p.103) note "scant evidence for the use or manufacture of flaked stone implements" from ~500 BP at Vanderlin Island, suggesting technological changes as well (Table 3.2). The second, "primary" occupation phase at Ingaanjalwurr rockshelter commenced ~460 cal BP and was characterised by an emphasis on quartzite point manufacture (Shine, Hiscock & Denham 2016, p.73).

Table 3.2: Summary of archaeological data for Arnhem Land and surrounds. Refer to Figure 3.1 for site locations.

Time	Observations	Sites/Locations	References
4200 BP	Initial occupation of Vanderlin Island	Vanderlin Island, Gulf of Carpentaria	Sim & Wallis 2008
3400 BP	Accumulation of Maganbal midden begins	Blyth River region, Arnhem Land	Bourke et al. 2007
3000 BP	Deposition of Mari-maramay shell mound begins	Croker Island	Mitchell 1993

	First appearance of bifacial points in abundance, increase in implement diversity in Wardaman Country	Wardaman country, central NT	Clarkson 2007
	Initial occupation of open coastal sites at Point Blane Peninsula	Point Blane Peninsula, Blue Mud Bay	Faulkner & Clarke 2004
2500 BP	Abandonment, or decreased occupational intensity, of sites on Vanderlin Island	Vanderlin Island, Gulf of Carpentaria	Sim & Wallis 2008
2000 BP	Cessation of deposition of Mari-maramay shell mound	Croker Island	Mitchell 1993
	Accumulation of Hope Inlet shell mounds begins	Darwin	Bourke 2004
1900 BP	First occupation phase of Ingaanjalwurr rockshelter begins	Western Arnhem Land	Shine, Hiscock & Denham 2016
1800 BP	Occupation of wetland sites on Point Blane Peninsula begins	Point Blane Peninsula, Blue Mud Bay	Faulkner & Clarke 2004

1500 BP	Peak occupational intensity in Wardaman country, lasting until the present	Wardaman country	Clarkson 2007
1400 BP	Continuous occupation of Ji-bena earth mound begins	Blyth River region, Arnhem Land	Brockwell, Meehan & Ngurrabangurraba 2005
	Accumulation of Bayview Haven 3 shell mound begins	Darwin	Hiscock 1997
1300 BP	Renewed occupation and intensified land use at Vanderlin Island	Vanderlin Island, Gulf of Carpentaria	Sim & Wallis 2008
	End of first occupation phase of Ingaanjalwurr rockshelter	Western Arnhem Land	Shine, Hiscock & Denham 2016
1200 BP	Occupation of majority of sites in Blyth River region begins	Blyth River region, Arnhem Land	Bourke et al. 2007
	Cessation of deposition of Haycock Reach shell mounds	Darwin	Hiscock & Hughes 2001
	Peak site use at Bindjarran rockshelter	Kakadu National Park	Shine et al. 2015

800 BP	Change in subsistence strategies at Ji-bena earth mound as nearby swamp transitions from estuarine to freshwater	Blyth River region, Arnhem Land	Brockwell, Meehan & Ngurrabangurraba 2005
750 BP	Continuous occupation of Birriwilk rockshelter begins	Western Arnhem Land	Shine et al. 2013
700 BP	Increase in mangrove gastropods in Hope Inlet mound HI80, decrease in *Tegillarca granosa*	Darwin	Bourke 2004
550 BP	Occupation of wetland sites on Point Blane Peninsula ends	Point Blane Peninsula, Blue Mud Bay	Faulkner & Clarke 2004
500 BP	Cessation of deposition of Hope Inlet shell mounds	Darwin	Bourke 2004
	Disappearance of evidence of stone implement manufacture at Vanderlin Island	Vanderlin Island, Gulf of Carpentaria	Sim & Wallis 2008
460 BP	Second occupation phase of Ingaanjalwurr rockshelter begins	Western Arnhem Land	Shine, Hiscock & Denham 2016

The varied shifts in climate and environment identified in palaeoenvironmental records for northern Australia in the late Holocene (see Chapter 2) are evident in the archaeological record as people interacted with these changes. Major phases of environmental and cultural change are apparent across both the Cape York Peninsula and Arnhem Land regions, particularly at ~1500-1000 BP with intensification of site occupation and the cessation of *Tegillarca*-dominated shell mound building by ~500 BP (with the exception of sites in the Weipa area). However, links between regional environmental changes and the archaeological record are limited by the low number of palaeoenvironmental records for northern Australia. The last ~400 years also included dramatic changes associated with contact as voyagers reached Australia to initiate trade and to colonise the continent.

3.3 Europeans in Northern Australia

Direct comparison of palaeoenvironmental records to specific historical events is often not possible due to differences in chronological resolution. However, the historical record provides useful context, particularly focused on human activity, through which to interpret the most recent period (~400 years in northern Australia) of palaeoenvironmental records.

3.3.1 Cape York Historical Timeline

The earliest recorded European presence in Cape York Peninsula was in 1606 when the Dutch ship *Duyfken* sailed along the west coast of the peninsula, believing it to be a continuation of mainland New Guinea (Loos 1974, p.3; Palmer 1903, pp.21-22). One of the crew is recorded as having been fatally speared at Batavia (now Wenlock) River while onshore during the return journey northward (Heeres 1899, p.42; Loos 1974, p.3; Weipa Town Authority 2014).

The next Dutch exploration of the region was in 1623 with the ships *Pera* and *Arnhem*, again sailing along western Cape York Peninsula, and naming the Gulf of Carpentaria after the Governor-General of the Dutch East India Company (Australia On the Map 2006). People in northern Cape York Peninsula (between 13° and 11°S) were noted by Jan Carstenszoon of the *Pera* as being "acquainted with muskets, of which they would seem to have experienced the fatal effect" from the crew of the *Duyfken* coming ashore in 1606, and subsequently showing greater hostility to the crew of the *Pera* than Aboriginal groups further south (Heeres 1899, p.43).

European presence on the peninsula increased in the 19th century after British colonisation of Australia. The *bêche-de-mer* (trepang) industry in the Torres Strait region began at this time, with processing stations in northern Cape York Peninsula documented from 1862 (Horsfall & Morrison 2010, p.13). The first "large-scale commercial shipment" of pearl shell from Torres Strait occurred in 1869, and the pearling industry expanded rapidly thereafter (Horsfall & Morrison 2010, p.13). The first overland expedition across Cape York Peninsula, led by Edmund Kennedy, occurred in 1848 (Carron 1849; Palmer 1903, pp.61-62). After the separation of the Colony of Queensland from New South Wales in 1859, a government settlement was established at Somerset at the tip of Cape York Peninsula in 1864 (Queensland Government 2015c). The path of the Cape York Overland Telegraph Line was surveyed in 1883, and the line was completed in 1886, connecting Somerset with Laura (Horsfall & Morrison 2010, p.9). During this period, "Aboriginal people were often hunted and shot on sight" (Horsfall & Morrison 2010, p.10). The establishment of missions in Cape York Peninsula began with a short-lived Anglican mission at Somerset (1867-1870), followed by Mapoon (originally Batavia River) Mission on the Wenlock (Batavia) River in 1891 and Weipa (Embley River) Mission on the Embley River in 1896 (Horsfall & Morrison 2010, p.34; Queensland Government 2015b, 2017a; Weipa Town Authority 2014).

Crowley and Garnett (2000, pp.14-15) note that observations from Cape York Peninsula made in journals of European explorers prior to 1881 recorded fires primarily in the "mid-dry season (June to September)", and mention witnessing Aboriginal people burning grass. Fires in the subsequent pastoral period (post-1881) were typically lit between May and August by pastoralists to create firebreaks and encourage new growth for grazing (green-pick) (Crowley & Garnett 2000, pp.21-22; see Fire Dynamics and Indigenous Australian Uses of Fire sections below). Jardine and Jardine (1867) mention a scarcity of grass due to Indigenous burning in September and October during their overland journey through Cape York Peninsula.

Queensland's Indigenous population had decreased by over 90 % by the 20th century (Ó Foghlú et al. 2016, p.2). In 1897 the *Aboriginals Protection and Restriction of the Sale of Opium Act* (Queensland) was introduced, allowing for Indigenous inhabitants to be removed from their homes and relocated to missions and reserves (Ó Foghlú et al. 2016, p.3). By 1939, almost 7,000 people had been removed under the Act (Blake 1998, p.51).

Economic bauxite deposits were discovered near Weipa in 1955, and the first commercial bauxite shipments by Comalco commenced in 1963 with Weipa township officially opened in 1967 (Weipa Town Authority 2014). The Aboriginal reserves of Bamaga, Cowal Creek (Injinoo), Mapoon, New Mapoon, Seisia and Weipa South (Napranum) held by the Queensland government were transferred to the trusteeship of their respective councils under Deeds of Grant in Trust between 1986 and 1989 (Queensland Government 2015a, 2015b, 2015c, 2016, 2017b).

3.3.2 Arnhem Land Historical Timeline

While Macassan *bêche-de-mer* (trepang) fishers from Sulawesi are known to have visited the Arnhem Land coast since the seventeenth century (Taçon et al. 2010; see also Horsfall &

Morrison 2010, p.13), the earliest recorded European sighting of Arnhem Land was in 1623 by its namesake ship, the Dutch *Arnhem*, sailing westward after separating from its sister ship, the *Pera* (see Cape York Historical Timeline; Duyfken 1606 Replica Foundation 2016). Journals and charts from the expedition of the *Arnhem* have not survived (Heeres 1899, p.viii). In 1644 Abel Tasman sailed along the western coast of Cape York Peninsula and around the Gulf of Carpentaria, mistaking Mornington Island and Maria Island as parts of the mainland (Heeres 1899, p.vii). Tasman is recorded as having sailed between Groote Eylandt and the mainland (Arnhem Land) (Heeres 1899, p.vii).

Similarly to Cape York Peninsula, European exploration of Arnhem Land increased in the 19th century after British colonisation of Australia. Matthew Flinders reached, and named, Bickerton Island in January 1803, and proceeded to name numerous features including islands and capes, such as Blue Mud Bay after its sediment and Morgan Island after a crewmember killed by traditional owners of the island, during his voyage on the *HMS Investigator* (Figure 3.3; Flinders 1966).

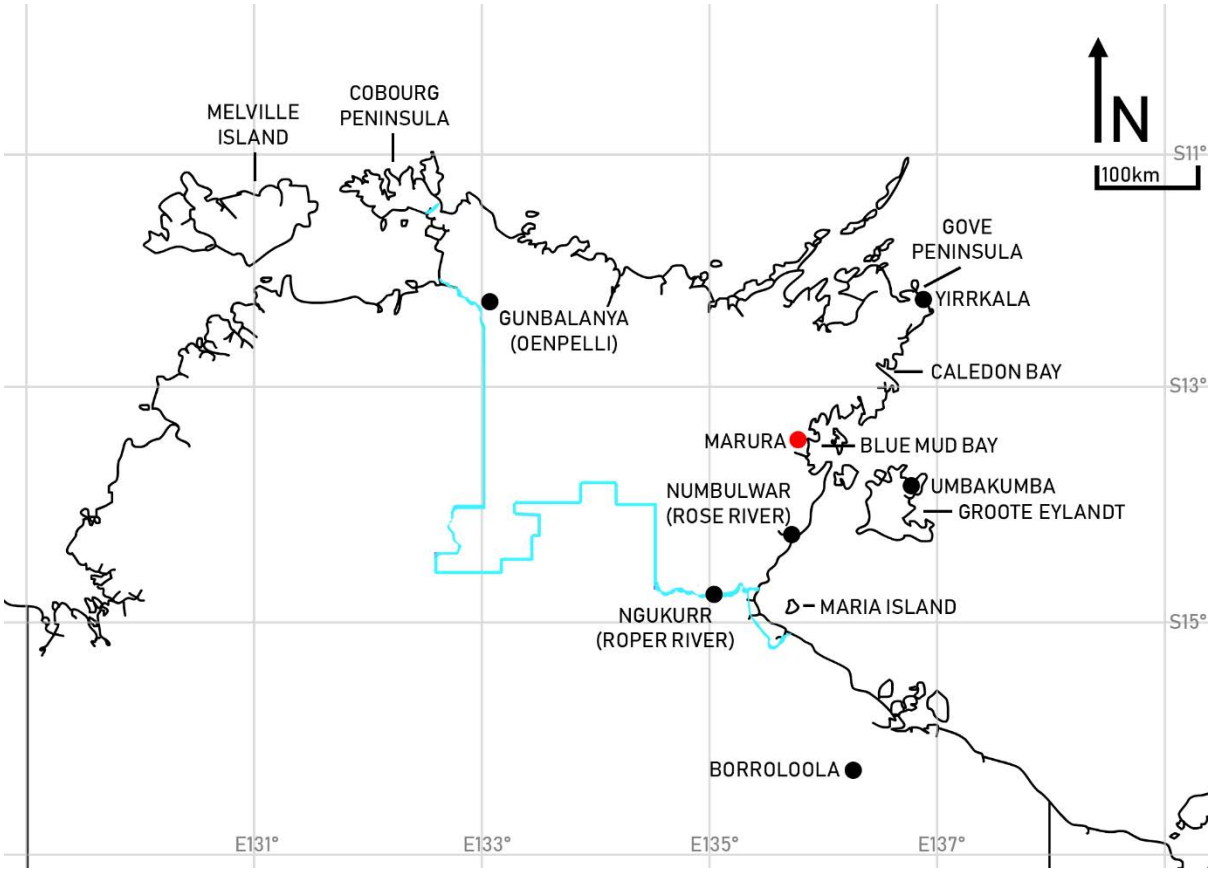

Figure 3.3: Locations mentioned in the text, as well as modern communities that began as missions (original mission names in brackets). Approximate boundary of Arnhem Land indicated in blue. Palaeoenvironmental site in this study (Marura) indicated in red.

Fort Dundas on Melville Island was the first of four failed European settlement attempts between 1824 and 1867 (South Australian History 2018). Water buffalo were introduced between 1825 and 1843 on Melville Island and the Cobourg Peninsula as a meat source for settlers; buffalo populations expanded after these settlements were abandoned and caused extensive damage to wetland ecosystems in the Top End over the next century (Department of Sustainability, Environment, Water, Population & Communities 2011). The first pastoral leases in the Northern Territory were granted in 1872 (National Archives of Australia 2018a), and in

1883 David Lindsay was commissioned by the South Australian government to explore central and eastern Arnhem Land "with a view to settlement" (State Library of South Australia 2007; Sydney Morning Herald 2004). The remote township of Borroloola was established in 1885 (South Australian Register 1885), and a mission was founded at Roper River (later relocated to Ngukurr) in 1908 – the first of six missions established in the region between 1908 and 1958 (Sydney Morning Herald 2004). In the late 19th and early 20th century, Arnhem Land was under pastoral lease; the Eastern and African Cold Storage Company held a lease covering ~50,000 km^2 in 1903 and:

> …the Company employed gangs of people to hunt out and shoot up the 'blacks' on sight. As the country of the Nunggubuyu clans lay within this leasehold a number of the ancestors of those living in Numbulwar today were killed in this way (Cole 1982, p.14).

Attempts at pastoralism were later abandoned (McMillan 2008, p.105), and Groote Eylandt and Arnhem Land were declared Aboriginal Reserves in 1920 and 1931, respectively (National Museum of Australia 2018; Barrier Miner 1931; Sydney Morning Herald 2004). A series of killings near Caledon Bay and Blue Mud Bay known as the Caledon Bay Crisis occurred from 1932-3, beginning with the deaths of five Japanese trepang fishermen killed by Yolngu men; to resolve the situation, anthropologist Donald Thomson was sent to eastern Arnhem Land and "facilitated the establishment of peaceful relations between the Yolngu people and the Commonwealth government" (Australian Dictionary of Biography 2018; National Archives of Australia 2018b).

Open-cut mining began on Groote Eylandt in 1964, and a Special Mineral Lease (SML 11) and Special Purpose Leases were granted to the Gove Joint Venture Participants in 1969 (Anindilyakwa Land Council 2016; Nhulunbuy Corporation n.d.). Bälma, near Blue Mud Bay,

was settled by Djarrwark people in 1970 (Laynhapuy Homelands Aboriginal Corporation 2017a).

Dhimurru (north-east Arnhem Land), Laynhapuy (east Arnhem Land) and Anindilyakwa (Groote Eylandt, surrounding islands and marine environment), and South East Arnhem Land Indigenous Protected Areas were declared in 2000, 2006, and 2016, respectively (Department of the Environment & Energy 2013; Laynhapuy Homelands Aboriginal Corporation 2017a; Anindilyakwa Land Council 2016; Northern Land Council 2019).

As with the archaeological record, historical events across Cape York Peninsula and Arnhem Land feature numerous similarities. Both regions were affected by European invasion later than areas to the south, and were initially explored for pastoral and later for mining uses. However, while pastoralism was short-lived Arnhem Land and officially ended by the 1931 declaration of the Arnhem Land Aboriginal Reserve, pastoralism is ongoing on Cape York Peninsula (e.g. Hardy, Nelson & Holmes 1995). Both regions experienced Indigenous depopulation of lands after permanent European settlement. Causes of depopulation included deaths from introduced diseases as well as massacres (e.g. Cole 1982, p.14; Ó Foghlú et al. 2016, pp.2-4), and the removal of Aboriginal people to reserves and missions (e.g. Blake 1998, p.51). The removal of people from these areas also removed the land management systems they maintained, including landscape fire management (e.g. Head 1994).

3.4 Fire Dynamics

Numerous interconnected factors characterise and control fires from the level of individual fires (e.g. ignition source, heat) through to long-term regional fire regimes (e.g. vegetation communities, large scale climate variability) (Figure 3.4). Palaeofire reconstructions, including this study, primarily focus on the fire regime to super fire regime scales due to the coarse

resolution of sedimentary records. However, understanding fire behaviour at any point along this spectrum requires acknowledgement of the interrelated nature of fire controls at different spatial and temporal scales. This section describes features at the flame and fire event scales that combine to form the fire regimes discussed later in this study.

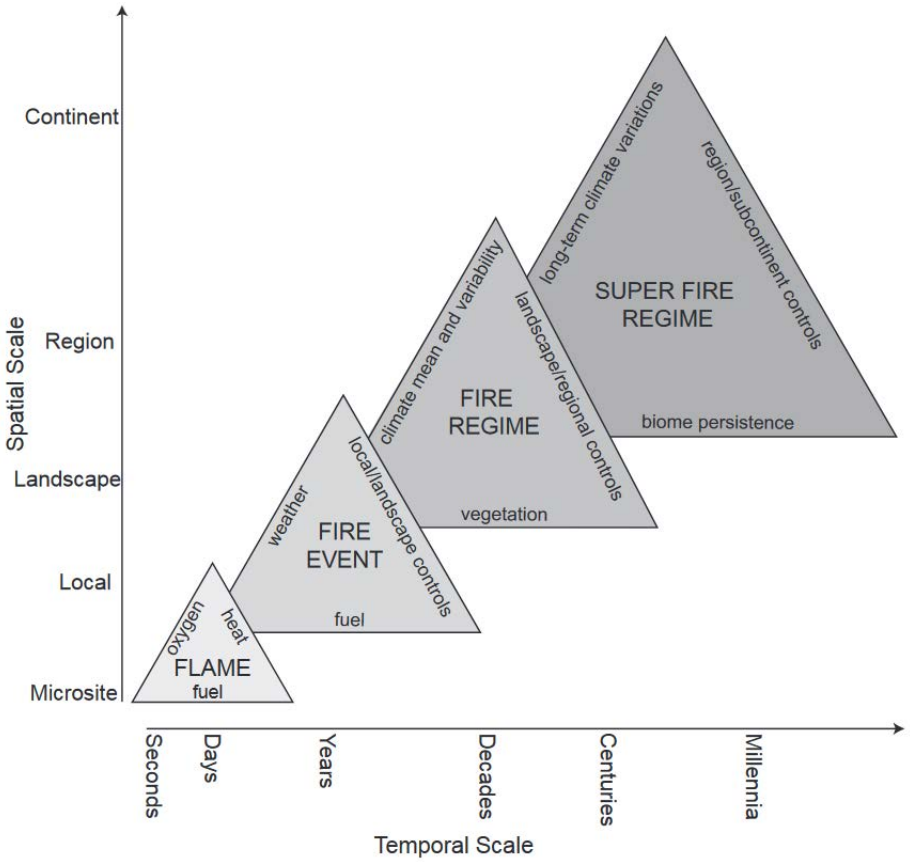

Figure 3.4: Diagrammatic representation of fire controls over space and time (from Whitlock et al. 2010, p.7).

Fires during the early dry season (April to July) in northern Australia are associated with smaller fuel loads, lower air temperatures, higher moisture content, burn smaller areas and may leave unburnt patches (Crowley 1995, p.6; Evans & Russell-Smith 2019, p.3), and are usually

targeted as part of prescribed burning programs (e.g. Russell-Smith et al. 2013). Late dry season fires, occurring between August and the onset of the wet season October-November, are typically high intensity, destructive to both woody and non-woody biomass, and burn large areas (Evans & Russell-Smith 2019, p.3). Natural lightning-triggered fires typically occur late in the dry season, when fuel loads are high and moisture content low, as lightning strikes increase at the onset of the wet season (Andersen, Cook & Williams 2003, p.3; Bureau of Meteorology [BOM] 2016a; Figure 3.5).

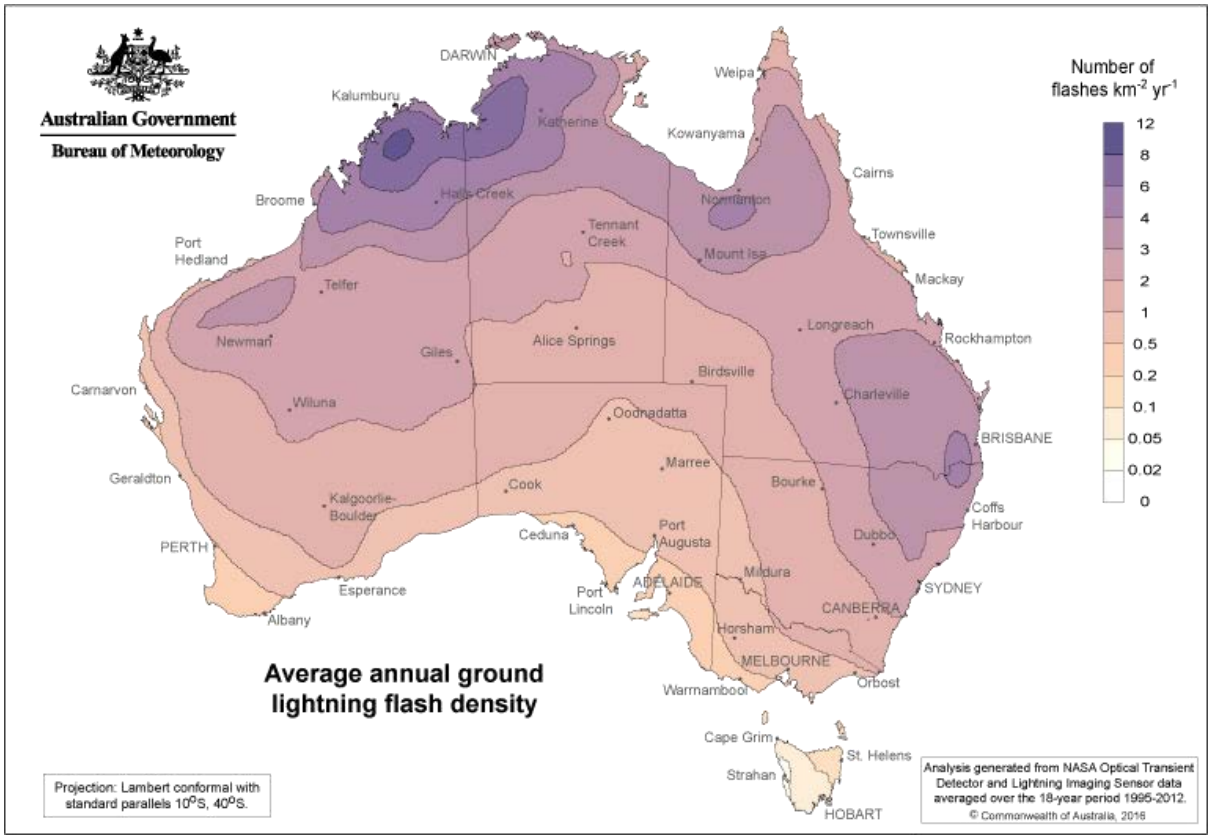

Figure 3.5: Average annual lightning cloud-to-ground flash density map for Australia (from BOM 2016a).

European “management” fires in Cape York Peninsula and the Top End of the NT typically occur in the early dry season and at the onset of the wet season (Crowley 1995, p.50; Crowley & Garnett 2000, p.18). Pastoral reasons for burning, both in the past and present, include the creation of fresh feed for cattle, assistance in cattle control, improvement of visibility and access, weed control, and control of cattle ticks (Crowley 1995, p.45; Crowley & Garnett 2000, p.18). Some of these uses of fire are shared by managers of National Parks, which include fires lit for “fuel reduction, infrastructure protection, habitat manipulation, feral animal control, weed control and boundary definition” (Crowley 1995, p.48).

Prescribed burning programs, such as the West Arnhem Land Fire Abatement Project (WALFA), aim to reduce large-scale high intensity late dry season fires, and thereby reduce carbon emissions, through the application of controlled early dry season burns (see Evans & Russell-Smith 2019; Fitzsimons et al. 2012; Russell-Smith et al. 2013). These programs manage fire by controlling the combination of fire frequency, intensity and timing (see also Andersen, Cook & Williams 2003, p.12). Prescribed burning has also been investigated as a tool for faunal and floral biodiversity conservation; the heterogeneous (patchy, mosaic) burning pattern created by small-scale early dry season controlled burns has been associated with increased biodiversity (Crowley 1995, p.21; see Bliege Bird et al. 2013; Fitzsimons et al. 2012; cf. Parr & Andersen 2006). The West Arnhem Fire Abatement Project, as well as other prescribed burning programs, aims to “re-establish customary Indigenous fire management regimes” (Fitzsimons et al. 2012, p.52).

3.5 Indigenous Australian Uses of Fire

Extensive ethnographic work in the contact and post-contact periods has recorded Aboriginal Australian applications of small- to large-scale landscape fire (e.g. Bird, Bliege Bird & Parker

2004; Bliege Bird et al. 2008; Burrows et al. 2006; Russell-Smith 2001; Yibarbuk et al. 2001). Uses of landscape fire in the past and present include hunting small animals fleeing the flames (Yanyuwa of the Northern Territory, Baker 1988, p.139), dazing animals with smoke and other "specialised forms of hunting with smoke" (groups of the Western Desert (Walpiri, Winanpa and Pintupi), Kimber 1988, p.123; Tiwi of the Northern Territory, Hart & Pilling 1960, p.42), enabling tracking of lizards through post-fire ash (Yanyuwa of the Northern Territory, Baker 1988, p.139), clearing "heavy growth" of vegetation and encouraging "certain vegetable growth" (groups of the Western Desert, Kimber 1988, pp.122-123) and attracting kangaroos and other animals with regrowth after fire (groups of the Western Desert, Kimber 1988, p.123; Yanyuwa of the Northern Territory, Baker 1988, p.139; groups of northern Cape York Peninsula, Moore 1979, p.127).

Indigenous seasonal calendars demonstrate land management similarities and differences across different regions and environments. The seasonal calendar of the Yolngu of eastern Arnhem Land features "bushfires lit in the dry grass" during May-August (Dharratharra/Wadut) as "Yolngu set bushfires (worrk) to burn off the undergrowth" to more easily locate animal holes (Faulkner 2013, p.38), while the Kunwinjku, of western Arnhem Land, calendar describes August to mid-November as the period for "kawurluwurlhme kunak (floodplain burning)" to clear grass (CSIRO 2016). The seasonal calendar of the Yirrganydji of southeast Cape York Peninsula includes "burn-offs" early in the dry season, beginning in May (BOM 2016b).

Indigenous fire regimes in northern Australia have a discontinuous history over the last ~200 years. Indigenous land management was disrupted by European invasion and settlement as regions were depopulated (see Gammage 2012 and Europeans in Northern Australia section above). Historical records, primarily in the form of journals of explorers or pastoralists, provide insight into Aboriginal fire regimes in tropical Australia during the contact period. Crowley

and Garnett (2000, p.16) note journal records of frequent late dry season fires on Cape York Peninsula in the 19th century, and Preece (2002) describes fires lit throughout the full length of the dry season across the Northern Territory in explorers' journals.

The establishment of Indigenous Protected Areas and ranger programs has reintroduced Indigenous fire management in some northern regions (e.g. Groote Eylandt, Anindilyakwa Land Council 2016; north-east Arnhem Land, Department of the Environment, Water, Heritage & the Arts 2008). Baker (1988, p.139) describes the Yanyuwa of the Borroloola region using fire for land management in the post-contact period:

> After the end of the wet season great attention is paid to when the tall, wet season grasses will burn. Once there is even the most remote chance some will burn, trips out bush become slow, stop-start affairs, during which literally hundreds of lighted matches are thrown out of the car windows (and hasty departures are made if the grass catches alight). As most of the grass is still too wet to burn, these early dry season burns produce the mosaic pattern of burning that other authors (Latz and Griffin 1978; Latz 1982) have commented on. This pattern of burnt and unburnt areas means that fires lit later in the dry season have fire breaks of already burnt ground around them (Baker 1988, p.139).

Bliege Bird, Bird and Codding (2016) demonstrate that both lightning-dominated and anthropogenic fire regimes are coupled to climate. Compared to a lightning-dominated regime of infrequent large-scale fires concentrated late in the year, Aboriginal Australian landscape burning features a higher number of small-scale fires spread throughout the year (Bliege Bird et al. 2008; Bliege Bird, Bird & Codding 2016; Table 3.3).

Table 3.3: Summary of general fire regimes in the Australian tropics explained in the text.

Fire Regime	Style of Fire	Outcomes/Impact
Indigenous Australian	Throughout dry season, may include wet season when possible Weak fire weather (fires not lit when aridity is high and winds are strong) Varied fuel loads	Controlled burns Small, low intensity fires Small areas burned Patchy, heterogeneous pattern of areas at different post-fire intervals
European pastoral	Early to mid-dry season Weak fire weather (aridity lower in the early dry season, fires not lit when winds are strong) Low fuel loads	Controlled burns Small-to-medium areas burned Creation of fire-breaks
Lightning-triggered	Late dry season, early wet season Strong fire weather (high aridity, strong winds) Large, dry fuel loads Increased lightning with onset of wet season	Uncontrolled burns Intense/severe fires Large areas burned Potential vegetation damage due to fire severity (e.g. canopy fires, combustion of woody biomass)

3.6 Conclusion

The late Holocene was a period of significant changes across Australia, including widespread intensification of site occupation and diversification of resource use. The Cape York Peninsula and Arnhem Land regions share a broadly similar human past through this period, including shell mounding as an adaptation to late Holocene climatic variability, Indigenous depopulation of lands in the 19th and early 20th centuries through massacres by European colonists and relocations to missions and reserves, and the introduction of pastoralism followed by mining. The impact of pastoralism was more pronounced in Cape York Peninsula and continues today, while pastoralism in Arnhem Land was abandoned before 1920. Therefore, while all sites in this study are expected to show evidence of changed fire regimes with Indigenous depopulation of the region, only sites on Cape York Peninsula would be expected to reflect the introduction and maintenance of a new prescribed burning pattern (European pastoral).

Differences such as the late construction period of shell mounds in the Weipa area highlight variation in human behaviour and demonstrate that not all broad trends identified for this region are accurate at smaller scales; this is an important consideration for palaeoecological interpretations. The combination of archaeological data, the historical record and ethnographic observations provides a strong starting point for interpreting human-fire-environment interactions in the palaeoenvironmental record. With the greater palaeoenvironmental and archaeological context of the region established in Chapters 2 and 3, the next step is to detail and critique the methodologies to be used in this study (Chapter 4).

Chapter 4 : Methodological Approach and Critique

4.1 Introduction

A range of techniques can be used to reconstruct fire histories, including optical or chemical analysis of charcoal, differentiating between local and regional fire signals, and distinguishing fuel types; however, many studies disagree on what thresholds to use (e.g. for microscopic/macroscopic charcoal; Stevenson & Haberle 2005; Mooney & Tinner 2011; for length-width ratios of grass; Umbanhowar & McGrath 1998; Jensen et al. 2007; Aleman et al. 2013; Crawford & Belcher 2014), few studies combine or compare these various methods, and many techniques have been developed using samples from the temperate northern hemisphere (e.g. Enache & Cumming 2006; Jensen et al. 2007; Courtney Mustaphi & Pisaric 2014). This study will utilise a range of existing methods to create fire records for Australian tropical savanna sites to test their applicability to this environmental context and investigate the potential interpretive power of a multiproxy approach.

The first part of this chapter will present a brief background and critique of existing methods for reconstructing fire abundance, local versus extra-local or regional fire signals, and fuel types. The later sections of this chapter outline the methodological approach of this study including site selection, sample collection in the field, subsampling and pretreatment in the laboratory, and laboratory analyses. Multiple techniques have been utilized not only to create a more robust record but also to compare, contrast and critique these methods and their usefulness in palaeofire research. Examples of this include charcoal abundance against pyrogenic carbon content isolated using hydrogen pyrolysis to determine fire abundance, and

charcoal length-width ratios against charcoal morphotypes against $\delta^{13}C$ values of pyrogenic carbon (isolated using hydrogen pyrolysis) to determine grass versus non-grass content.

4.2 Fossil Charcoal as a Fire Proxy

Charcoal is a powerful tool for reconstructing chronologies of fire and subsequently investigating factors that may have influenced fire abundance to change through time (e.g. rainfall, anthropogenic activity). Measures of charcoal developed from particle counts, such as accumulation and flux, are used as proxies for fire activity. Stated simply, higher amounts of charcoal are considered indicative of greater fire abundance. Unlike some palaeoenvironmental proxies such as pollen, charcoal is not produced and deposited continuously in the environment but appears as "discrete events" as fires occur (Clark 1983, p.34). Optical charcoal analysis has been applied to a vast number of sites worldwide (e.g. Aleman et al. 2013; Black & Mooney 2006; Black, Mooney & Haberle 2007; Breman, Gillson & Willis 2011; Buckman et al. 2009; Ekblom & Gillson 2010; Genever, Grindrod & Barker 2003; Haberle, Hope & van der Kaars 2001; Haberle et al. 2010; Higuera, Sprugel & Brubaker 2005; Laird & Campbell 2000; Luly, Grindrod & Penny 2006; MacDonald et al. 1991; Mooney et al. 2011; Rowe 2005, 2006, 2007; van der Kaars & De Deckker 2002; Williams et al. 2015a). The spatial and temporal coverage of fossil charcoal assemblages are determined by the characteristics of the depositional site (e.g. wetland) including watershed features and the date of site formation. Various methods (discussed below) have been proposed to obtain more data from charcoal analysis than a single measure of accumulation or flux.

The analytical tool CharAnalysis (Higuera et al. 2009) has been widely used in sedimentary charcoal studies for peak detection within continuously sampled records. However, this program and similar signal-to-noise index methods (e.g. Finsinger et al. 2014) were designed

for temperate and boreal environments where fire return intervals are long, such as forests (S. Mooney pers. comm.; e.g. Courtney Mustaphi & Pisaric 2013; Fletcher et al. 2015; Hawthorne & Mitchell 2016; Moos & Cumming 2012). Such methods are not widely applicable to environments where fire recurs frequently such as the tropical savannas of northern Australia, and therefore will not be applied in this study.

4.2.1 Local versus Extra-Local: Particle Size

Microscopic (<125 μm) charcoal (Mooney & Tinner 2011) is commonly presented as representative of regional or extra-local (outside the watershed being investigated) fire signals while macroscopic (>125 μm) charcoal represents local (within the watershed) fire signals, as models of charcoal dispersal illustrate that smaller particles are able to cover greater distances than large particles before deposition (see Clark 1988; Peters & Higuera 2007). This allows for the construction of a more nuanced fire history beyond identifying the presence or absence of fire, with both spatial and temporal analysis. The distance from a site and total area represented in the local (macroscopic) and extra-local (microscopic) signals differ for every site due to factors such as watershed size, topography and wind. This is why the terms "local" and "extra-local" are used, as these are subjective measures relative to a given site rather than representing a measurable distance.

4.2.2 Fuel Type: Particle Morphology and Aspect Ratio

Morphological analysis of charcoal particles provides more information about palaeofire and palaeoenvironments; numerous studies have investigated the possibility of identifying the fuel type (e.g. grass, leaves, wood or a specific plant species) of a particle using charcoal morphotypes (Figure 4.1; Courtney Mustaphi & Pisaric 2014; Enache & Cumming 2006) or

measurements such as length-width ratios (Jensen et al. 2007; Umbanhowar & McGrath 1998). This study will investigate the applicability of these systems to Australian tropical savanna contexts.

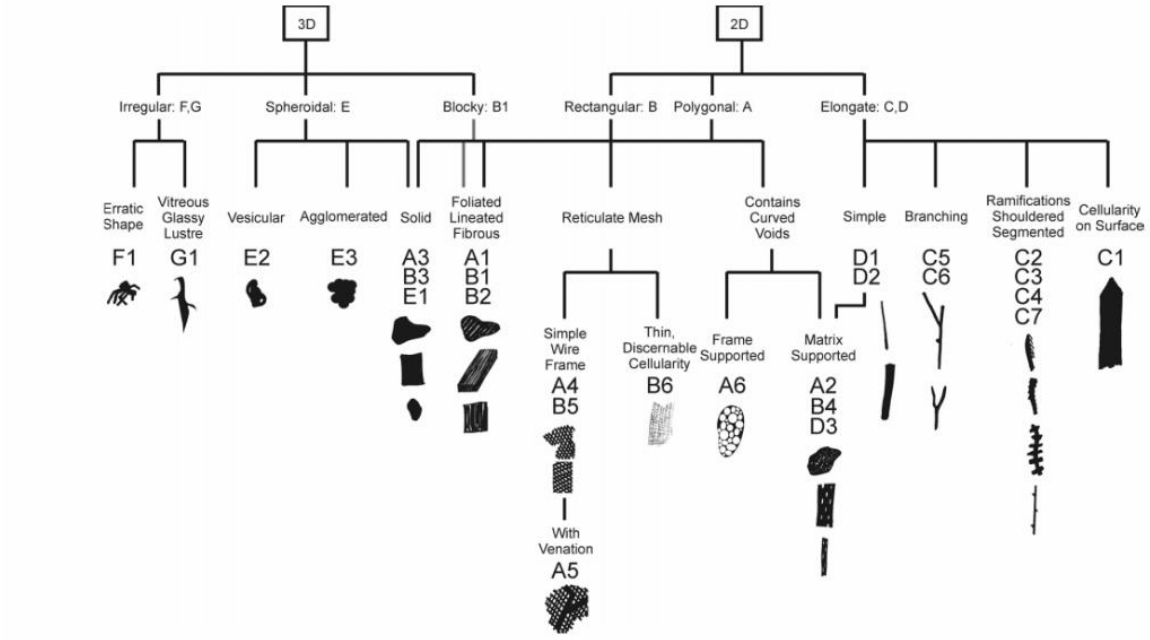

Figure 4.1: Charcoal morphotypes identified by Courtney Mustaphi and Pisaric (2014, p.744) for use in charcoal analysis. 25 of 27 morphotypes list, within the text, an associated fuel type.

Morphotype classifications can be based on laboratory-created reference collections linking identifiable physical characteristics of a particle, such as the presence of elliptical voids or a glassy surface, to a fuel type known to generate that morphology when burned (e.g. Courtney Mustaphi & Pisaric 2014). Alternatively, Enache and Cumming (2006) present a seven-type classification system generated from samples from a fossil charcoal record. The limitation of the former, laboratory-based, method is that the morphotypes are generated under laboratory

conditions and have not been affected by the depositional processes that fossil charcoal particles experience. The limitation of the latter, field-based, method is that the morphotypes cannot be definitively linked to known fuel types, as the fuel type of the fossil charcoal particles sampled is unknown. Both classification systems have not yet been applied to and tested in the southern hemisphere.

Aspect ratio has been proposed as a more simplistic system for classifying the fuel source of charcoal particles. Particles with a length-width ratio greater than or equal to a predetermined threshold are identified as elongate and therefore grass-derived. However, studies disagree on which ratio identifies each type. While in agreement that grass particles have an L:W ratio of approximately 3.6-3.7, Umbanhowar and McGrath (1998) identify a ratio of 1.97 as being a wood source and 2.23 a leaf source. Crawford and Belcher (2014) reverse this, labelling a ratio of approximately 1.91 as a leaf source and approximately 2.13 as wood. Aleman et al. (2013) use a different approach by analysing W:L ratios, with values closer to zero representing more elongate particles and a ratio of 1 indicating a perfect square, and identifying a ratio of <0.5 as representative of grass (equivalent to a L:W ratio of >2). Leys et al. (2017, p.9) also analyse particles using W:L ratios and identify a ratio of ≤0.5 as representative of vegetation "composed at least 40 % by grassland cover". No experimental studies to date have explored whether the relationship between L:W ratios and fuel types exist in microscopic charcoal particles.

It is possible that the morphotype classification of elongate particles is less accurate when determining the contribution of grass to the charcoal record than the use of length-width ratios. This is due to the distinction between an elongate type (e.g. D3, elongate with curved voids, see Figure 4.2) and its corresponding non-elongate type (e.g. B4, geometric with curved voids) being at the discretion of the analyst which can result in particles classified as grass-derived using length-width ratios being recorded as a non-elongate morphotype. However, the

correlation between length-width ratio and fuel type has only been demonstrated for macroscopic particles (>125 μm). Subsequently, morphotypes are a method applicable to all size classes to collect fuel source data.

Benefits of the length-width method over the morphotype system include the minimisation of user error (whether a particle is classified elongate is not user-determined but calculated) and simplicity for training and implementation. While many studies proposing this method use case studies and samples from the northern hemisphere (Aleman et al. 2013; Jensen et al. 2007; Umbanhowar & McGrath 1998), this technique is theoretically applicable globally and less dependent on species-specific morphologies than morphotype classifications developed in the temperate northern hemisphere (e.g. Enache & Cumming 2006; Courtney Mustaphi & Pisaric 2014). The combination of both length-width ratios and morphotype classifications may allow for the determination of the contribution of grass and non-grass vegetation to a record in all sizes with additional verification in the macroscopic sizes.

4.2.3 Fuel Type: Carbon Isotopic Value

Stable isotopes are a currently underutilized proxy in charcoal records and palaeofire chronologies (see Bird & Cali 1996) and have not been widely applied in Australia. The analysis of carbon isotopes (C_3 photosynthesis from trees leads to $\delta^{13}C$ values of ~-25‰ while C_4 photosynthesis from tropical grasses leads to distinctly different $\delta^{13}C$ values of ~-14‰) can allow for the proportion of wood- versus grass-derived burned material to be identified for savanna ecosystems (O'Leary 1988; Wurster et al. 2012; Saiz et al. 2018).

Pyrogenic carbon (carbon derived from combustion) can be chemically quantified (Wurster et al. 2012). This provides a useful complement to charcoal count data as chemical quantification

can be applied to the smallest size fractions (<63μm), which cannot be optically quantified, thereby alleviating some of the issues of particle fragmentation encountered in optical counts.

4.3 Site Selection

Potential coring sites were identified as freshwater bodies (wetlands) isolated from creeks or rivers with a high percentage of water permanence located in far northern Australia. Additional selection criteria included physical accessibility and permission to access the site.

Two sites in Cape York Peninsula, Queensland (Big Willum Swamp and Sanamere Lagoon) and one in Arnhem Land, Northern Territory (Marura) were selected for this study (Figure 4.2). While these sites are climatically similar (AW – Tropical/Equatorial Savannah with dry winter under the global Köppen-Geiger Climate Classification; Peel, Finlayson & McMahon 2007; Kottek et al. 2006), they diverge in vegetation, land-use histories and physical characteristics including wetland size, water depth and catchment area.

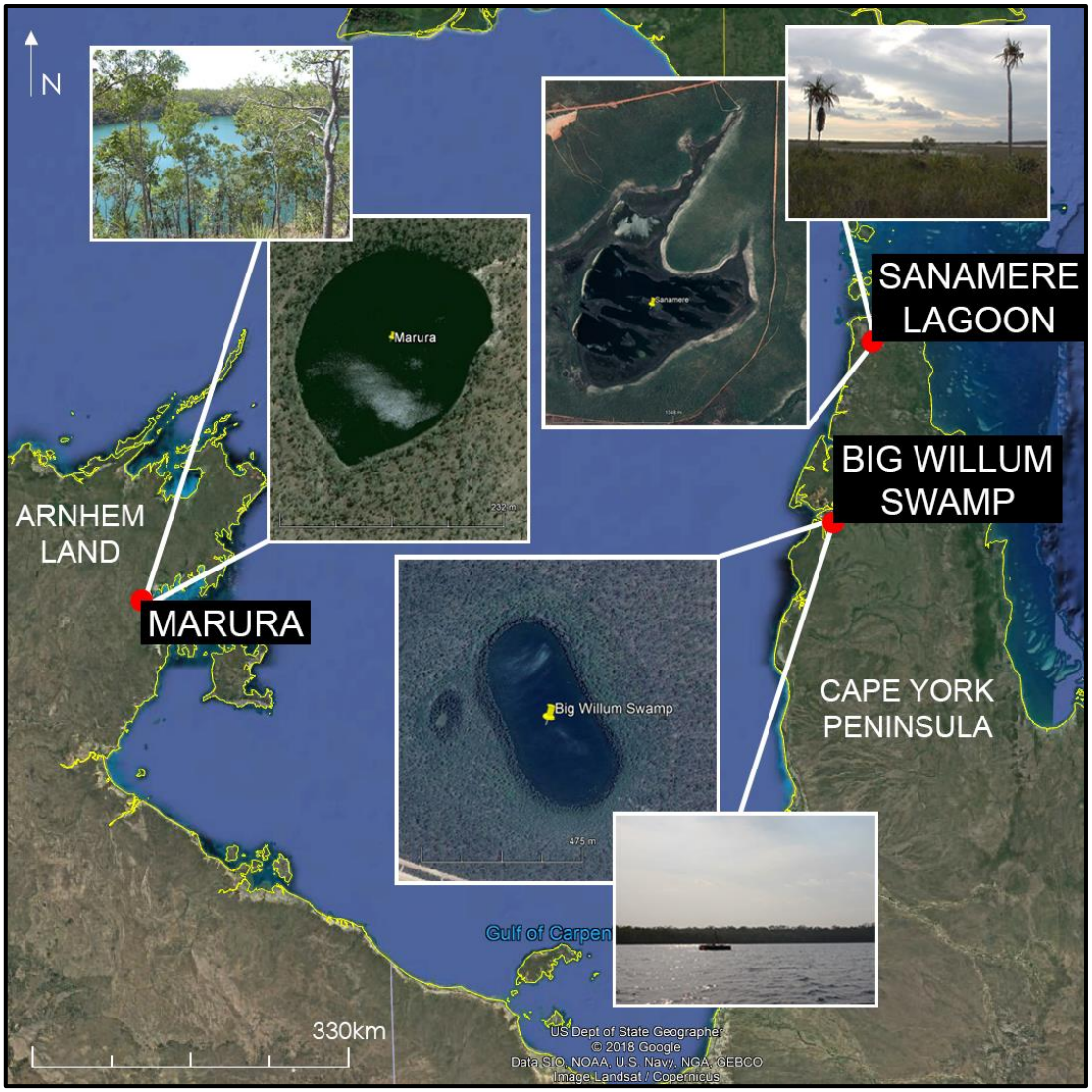

Figure 4.2: Location of study sites (after Google Earth 2018d).

4.4 Core Collection

Fieldwork was conducted in the Northern Territory in 2015 by other members of the research group prior to the commencement of this project. Cape York fieldwork was undertaken in April and June 2016 and July 2017.

One metre full cores and semi-circular (D-section) cores were collected using a raft-mounted Eijkelcamp percussion corer and by hand, respectively (Figure 4.3, Figure 4.4, Figure 4.5).

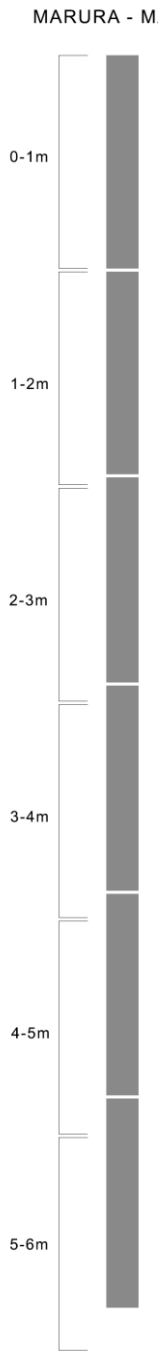

Figure 4.3: Representation of MAR2 cores collected from Marura.

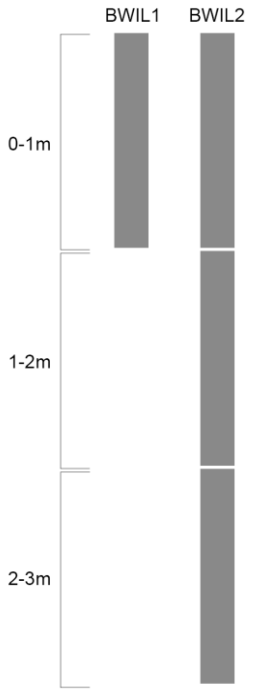

Figure 4.4: Representation of cores collected from Big Willum Swamp.

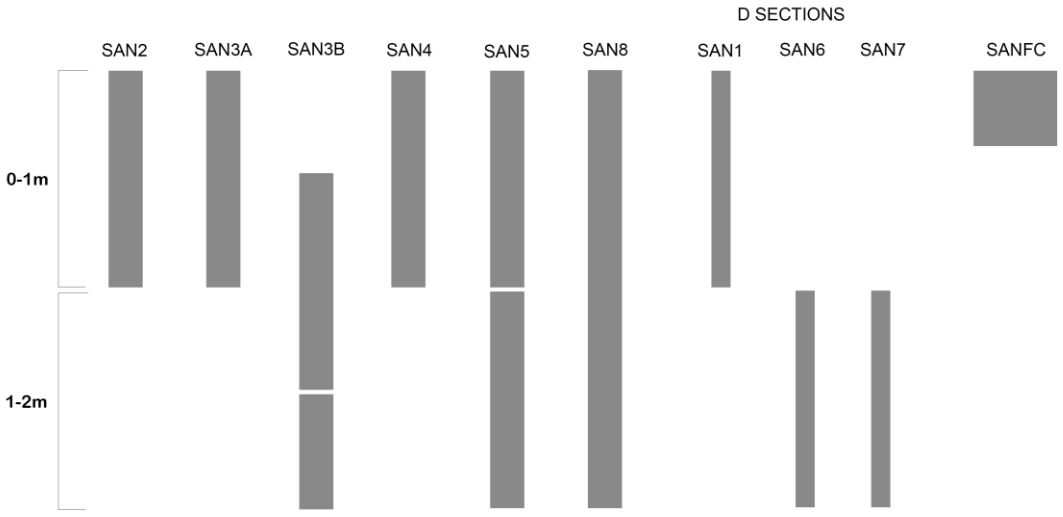

Figure 4.5: Representation of cores collected from Sanamere Lagoon. Core numbers indicate the order of collection and are not related to coring location.

4.5 Modern Sample Collection

Samples representative of modern conditions were collected via two methods: sediment grab samples and airborne charcoal traps. The sediment grab sampler consists of a metal container with hinged doors which are closed remotely after the sampler has been lowered underwater to the sediment surface. Grab samples provide a high volume sample of the uppermost sediment. Multiple grab samples were collected from Sanamere, including ten surface samples every ~50 metres along a transect from the central coring position to the shoreline. Grab sampling was not possible at Big Willum due to a large volume of aquatic plants preventing the sampler from reaching sediment, and not possible at Marura due to the water depth exceeding equipment reach.

Charcoal traps were deployed to collect modern airborne charcoal (Figure 4.6). Three charcoal traps were constructed, consisting of a funnel (~30 cm diameter) and bucket for maximum collection diameter, a pipe for sample collection, and an overflow valve containing two layers of mesh (125 μm and 63 μm) to prevent loss of accumulated particles. Charcoal traps were installed at three locations across Cape York during 2016 fieldwork: Sanamere, Kendall River and Coen (Figure 4.7). These locations cover various vegetation communities (dwarf heathland and open woodland) and current land use (Aboriginal Freehold land tenure, cattle farming and township, respectively). Charcoal traps remained on site for one year to capture cross-seasonal fire and eliminate seasonal bias. Charcoal trap samples were rinsed through a 2 mm and a 63 μm sieve, with the fraction between 2 mm and 63 μm processed for optical charcoal quantification. The 2 mm sieve was required to remove large organics including uncharred leaves and twigs. Unlike the fossil charcoal method, the <63 μm size fraction was not collected as this was potentially lost in the field through the overflow valve.

Figure 4.6: Kendall River charcoal trap on site after installation (2016).

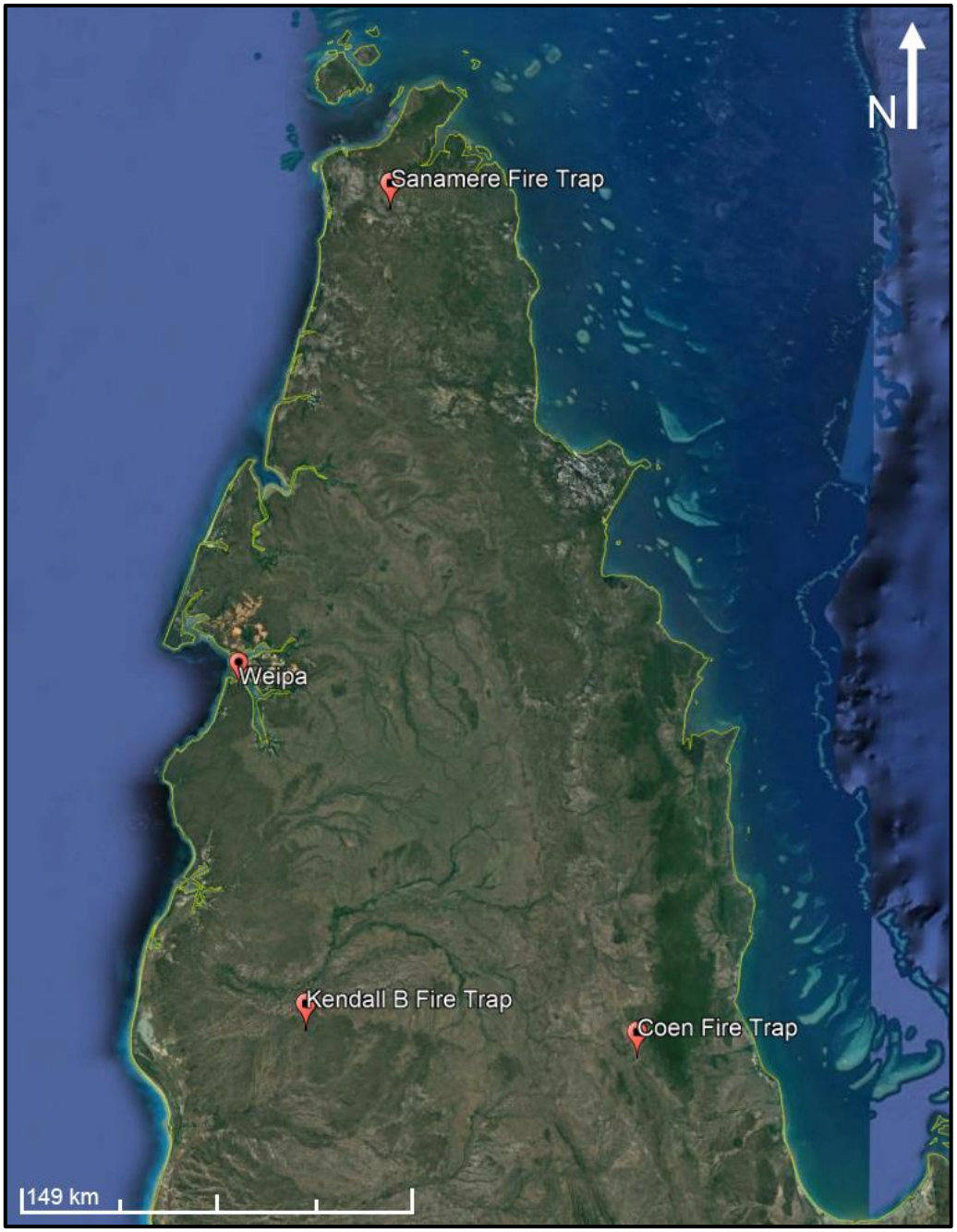

Figure 4.7: Location of installed Cape York charcoal traps (from Google Earth 2018b).

4.6 Core Subsampling

All full (non-D-section) cores were measured for magnetic susceptibility using a Bartington MS2C Core Logging Sensor at 0.5 cm (Sanamere and Big Willum) or 1 cm (Marura) intervals prior to subsampling. Magnetic susceptibility has been identified as a possible fire signal as

burning may trigger increased soil erosion or create the magnetic mineral maghemite (Millspaugh & Whitlock 1995; Mullins 1977). The presence or absence of a magnetic susceptibility peak coincident with a charcoal peak may also differentiate a local from an "extralocal" fire signal (matching signals for local, lack of magnetic susceptibility peak for extralocal; Millspaugh & Whitlock 1995).

D-section sediment cores were subsampled on site. Full cores were frozen in-tact in the field for storage before subsampling in the laboratory. Sediment descriptions were recorded during sampling, including Munsell colour classifications and any observable stratigraphy or compositional/textural changes.

4.7 Charcoal Analysis Preparation

4.7.1 Sample Preparation and Size Fractions

Sediment core, modern charcoal trap and modern surface samples were prepared for optical charcoal quantification following Stevenson and Haberle (2005). Sediments were found to be sufficiently disaggregated so the use of KOH for sample dispersal was not required. Samples were placed in approximately 10 mL of mid-strength bleach (~5 % concentration) to lighten organic matter. Preliminary tests determined that organics were sufficiently bleached when left in bleach for approximately 72 hours.

Bleached samples were rinsed using distilled water through three nested sieves of 250 µm, 125 µm and 63 µm mesh. Sieve contents were stored as >250 µm, 250-125 µm and 125-63 µm size fractions, respectively. Water and sediment that passed through the 63 µm sieve was retained, with approximately 5 mL 37 % HCl added to remove particles from suspension and excess liquid poured off; the remaining sediment was stored as the <63 µm size fraction for chemical quantification (hydrogen pyrolysis, see subsection later in this chapter).

Particles in size fractions >250 µm, 250-125 µm and 125-63 µm were optically quantified and categorised while suspended in water. Samples were placed in a petri dish and photographed on a lightbox to remove shadows before being placed under a dissecting microscope (x20 magnification).

4.7.2 Charcoal Measurements and Morphology

Length and width measurements were taken during optical charcoal counting using a microscope eyepiece scale. Measurements were recorded for the macroscopic size fractions (>250 µm and 250-125 µm). Length-width ratios greater than 3.6 were designated as elongate particles during analysis. Application of this measurement technique contrasted with the use of morphotypes (see below) to determine fuel types was undertaken to assess the analytical power of each method and determine if they produce comparable results.

Two morphotype classification systems were selected for use in this project: a basic system of seven categories outlined by Enache and Cumming (2006), and a comprehensive system of 27 categories described by Courtney Mustaphi and Pisaric (2014) as an extension of the simpler Enache and Cumming (2006) classification (Figure 4.8). The selection of two classification systems enabled the maximum amount of available data to be recorded (using the 27 type system) while also allowing for accurate classification when high levels of detail were not available (using the 7 type system). The simpler classification system was applied to the smallest size fraction to be counted manually (125-63 µm). The more complex system was applied to the two larger size fractions (250-125 µm and >250 µm), with the option of changing to the 7 type system if preservation degraded with increasing age/depth.

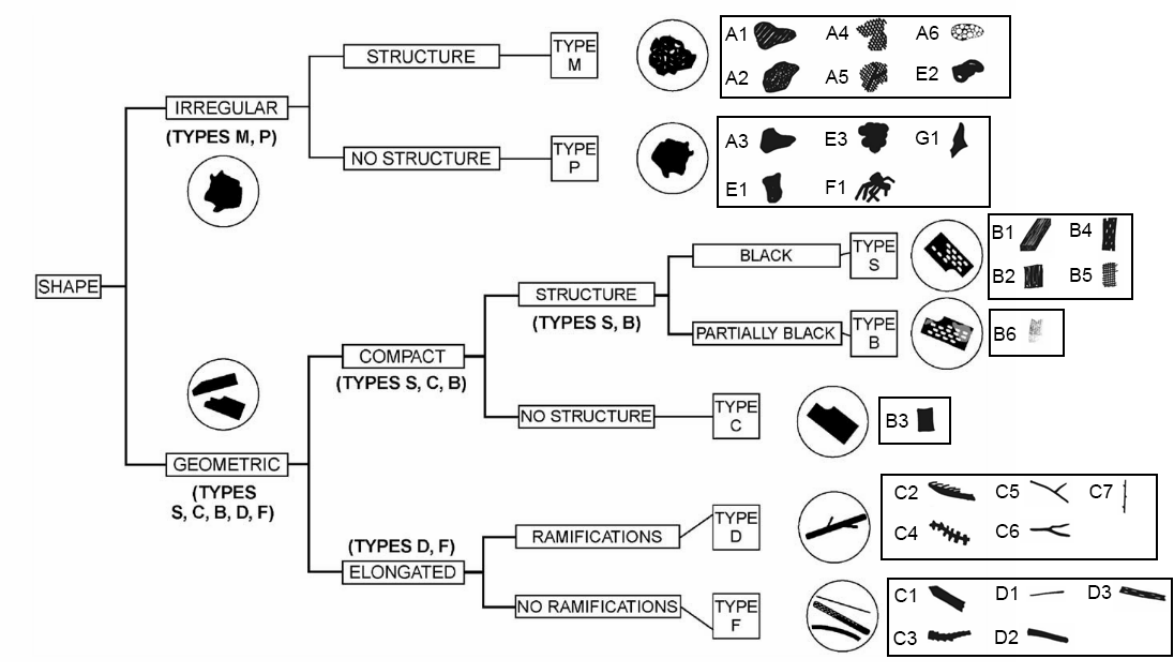

Figure 4.8: Morphotype classification systems of Enache and Cumming (2006) (left) and Courtney Mustaphi and Pisaric (2014) (right) displaying how the 27 types of the more detailed system are categorised under the 7 type system.

The application of these morphotype classification systems enabled the identification of fuel/vegetation source for each particle, with the minimum identification as either grass or tree derived. The use of both the simplified and complex systems allowed for comparison of the fuel type data generated to determine whether the additional detail from the Courtney Mustaphi and Pisaric (2014) classification system enabled more precise identification of fuel types in a charcoal sample than that provided by the Enache and Cumming (2006) system.

4.8 Hydrogen Pyrolysis and Elemental Analysis

Hydrogen pyrolysis (hypy) was used on bulk samples matched to those used for charcoal analysis, along with the <63 µm size fraction produced during charcoal preparation, following

the procedure outlined by Wurster et al. (2012). <63 µm samples were centrifuged and excess water poured off. All samples were freeze-dried, ground and weighed. Approximately 10 % sediment weight of molybdenum (Mo) catalyst was added to a weighed aliquot of sample. Methanol was added before samples were placed in a sonicator bath for 15 minutes then transferred to a hot plate at 75 °C to dry overnight.

Catalyst-loaded samples were then transferred to glass hypy inserts between filters, with sample weight and total insert weight recorded. Inserts were loaded into the hydrogen pyrolysis rig (approximately five samples per run) in the Advanced Analytical Centre at James Cook University Cairns, and the rig was set up following the JCU Hydrogen Pyrolysis Rig Standard Operating Procedures. Samples were heated to 550 °C over 40 minutes under 150 barG hydrogen flow, and held at this temperature for two minutes.

Sample carbon content and carbon isotope composition ($\delta^{13}C$) before and after hydrogen pyrolysis were measured using a Costech Elemental Analyser. Isotopic composition of the pyrogenic (black) carbon, of both the bulk and <63µm fraction, was calculated in RStudio using the equation given in Wurster et al. (2012, p.2692).

4.9 Itrax™ XRF Scanning

X-ray fluorescence (XRF) scanning of sediment cores is a non-destructive technique that provides high resolution semi-quantitative data on elemental composition which assists in identifying changes in sedimentation and landscape processes (for a review of applications of XRF scanning to lake sediments, see Davies, Lamb & Roberts 2015).

Sediment core segments were scanned using the Itrax™ core scanning facility at the Australian Nuclear Science and Technology Organisation (ANSTO) Lucas Heights facility. A thin slice of sediment (approximately one quarter of the full core) was removed from each core using a

lapidary saw and plastic-wrapped before being placed in a 50 cm PVC half-pipe surrounded by kinetic sand to support the core during transport and scanning. Core slices were transported to ANSTO Lucas Heights while frozen. Sediment core segments were scanned through the Itrax™ core scanner at 1000 µm intervals with 10 second exposure, using a molybdenum tube. Optical and radiographic images were also taken of each core using the Itrax™, prior to XRF scanning. Processing of Itrax™ data was completed by ANSTO Itrax™ Facility Officer Patricia Gadd. Itrax™ elemental counts were normalized using the procedure outlined by Weltje et al. (2015); elements of interest were isolated after selection from interpreted elements listed by Davies, Lamb and Roberts (2015) and counts were divided by the incoherent scatter for that depth. As described by Woodward and Gadd (2019), Mo ratio (Mo inc/Mo coh) can be used to represent organic content and Mo ratio is interpreted as such in this study.

4.10 Lead-210 (^{210}Pb) Dating

Sample dating using lead-210 (^{210}Pb) was undertaken to create a high resolution chronology for the previous approximately 160 years at each site. Sample preparation and analysis for ^{210}Pb dating were undertaken at the ANSTO Lucas Heights facility. Due to the large sediment volume required, only Sanamere samples were analysed for ^{210}Pb using gamma spectrometry, taken from a wide-diameter core (SAN FC) collected specifically for this purpose. Samples from all sites were analysed for ^{210}Pb using alpha spectrometry, including SANFC samples previously analysed by gamma spectrometry due to poor results (see Chapter 5). Prior to analysis, all sediment samples were ground either using a mill or mortar and pestle to achieve homogeneity.

4.10.1 Gamma Spectrometry

Samples were packed into 3 mL glass vials, sealed and then left for three weeks to collect emitted radon gas before being measured in a High Purity Geranium Well-detector gamma spectrometry system for at least two days. Gamma spectrometry analysis was completed by ANSTO staff member Jay Chellappa and a data report was compiled by ANSTO radiochemist Atun Zawadzki.

4.10.2 Alpha Spectrometry

Samples were prepared for analysis by alpha spectrometry in October 2017 and May 2018 following the ANSTO Environmental Radioactivity Measurement Centre (ERMC) Lead-210 dating sample preparation method (see also Eakins and Morrison 1978), ERMC Polonium chemical isolation method (see also De Oliceria Goday 1983) and ERMC Radium chemical isolation method (see also Golding 1961; Lim & Dave 1981; Lim, Dave & Cloutier 1989) (Figures 4.9, 4.10, 4.11, 4.12; see also Appendix 1).

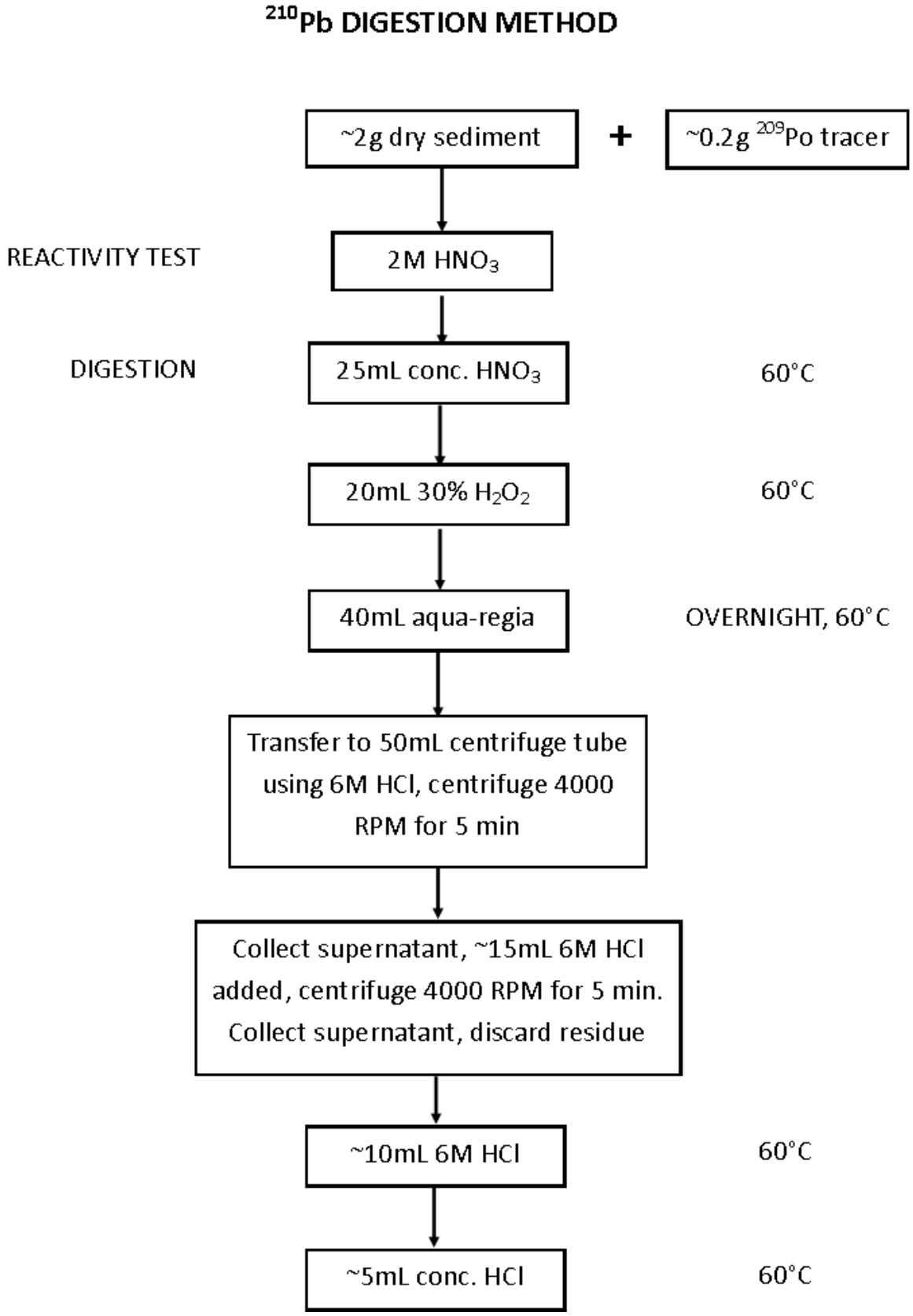

Figure 4.9: Flowchart of the ^{210}Pb analysis by alpha spectrometry sample preparation method, part one: digestion.

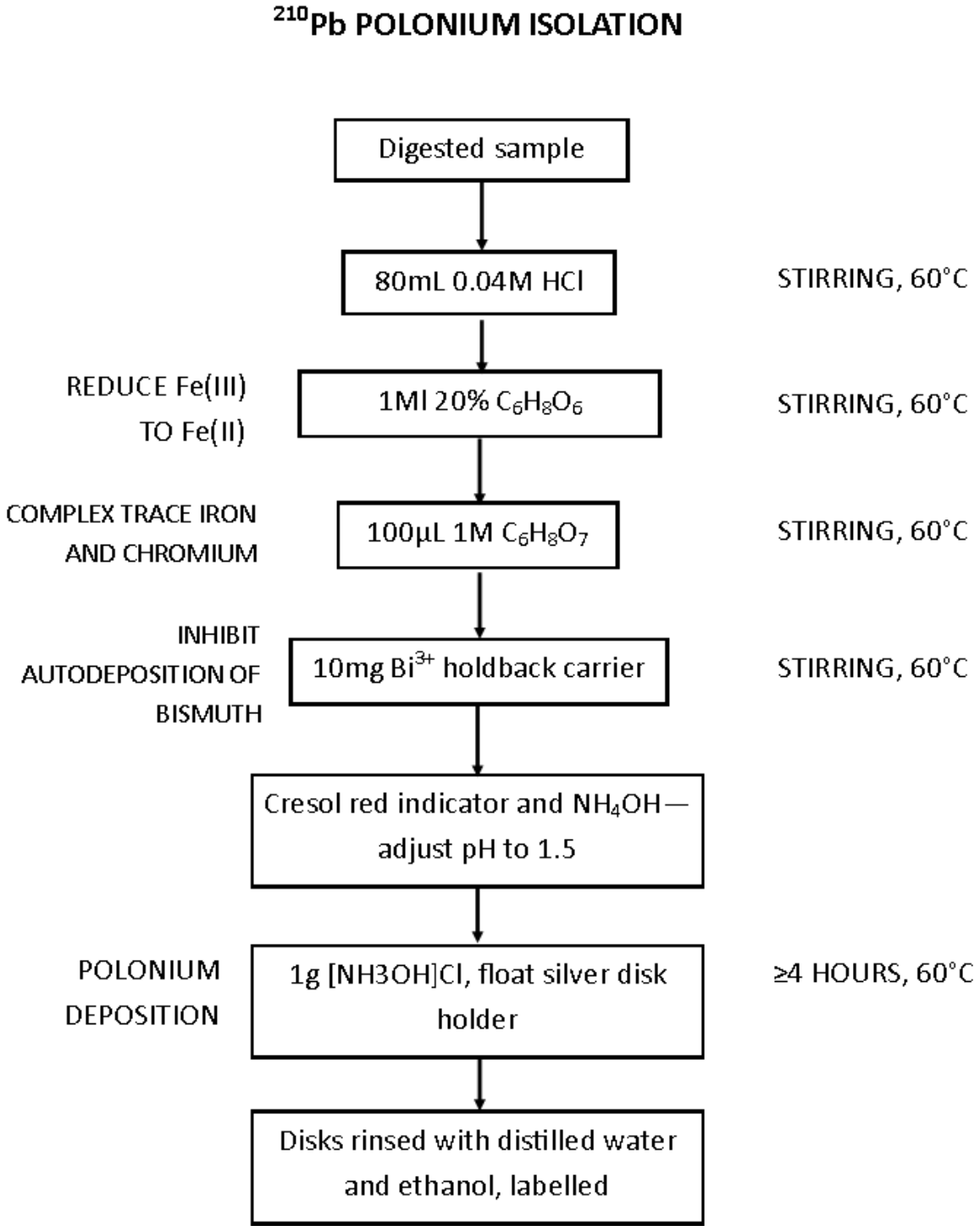

Figure 4.10: Flowchart of the ^{210}Pb analysis by alpha spectrometry sample preparation method, part two: polonium isolation.

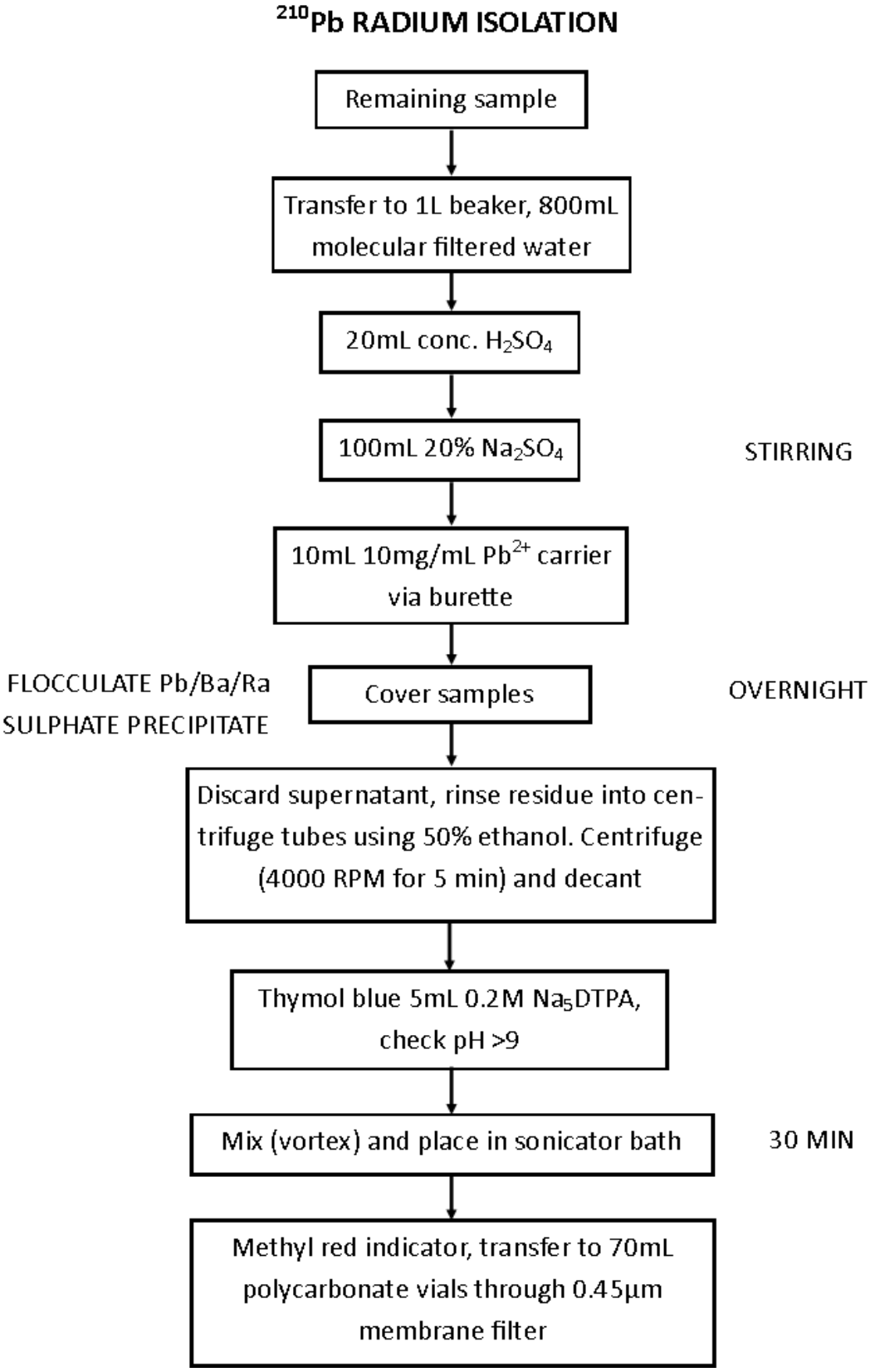

Figure 4.11: Flowchart of the ^{210}Pb analysis by alpha spectrometry sample preparation method, part three: radium isolation.

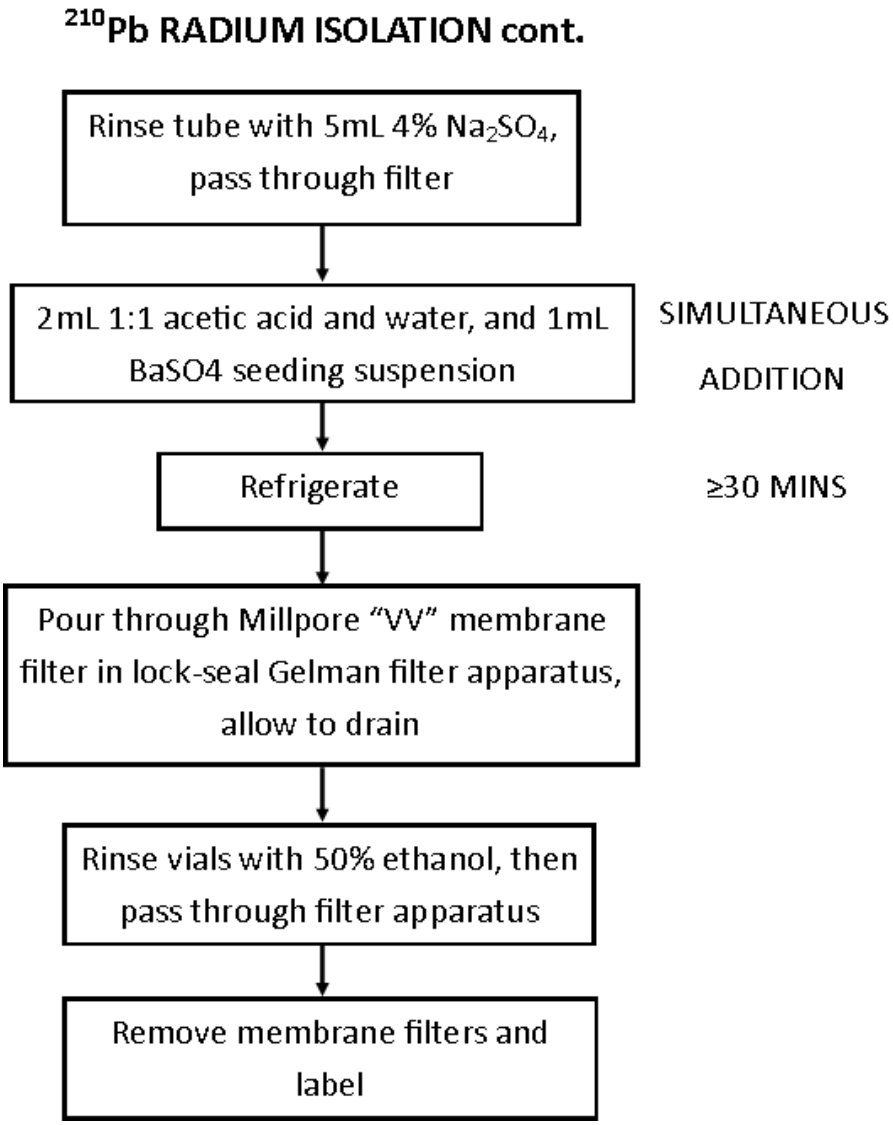

Figure 4.12: Figure 4.16: Flowchart of the ^{210}Pb analysis by alpha spectrometry sample preparation method, part four: final stages of radium isolation.

Alpha spectrometry analysis was undertaken by Sabika Maizma and data processing of alpha spectrometry results was completed by ANSTO radiochemist Atun Zawadzki, including application of CIC (Constant Initial Concentration) and CRS (Constant Rate of Supply) age models.

4.11 Carbon-14 (^{14}C) Dating

Sample dating using ^{14}C analysis by accelerator mass spectrometry allows for the construction of chronologies spanning thousands of years, and complements the application of ^{210}Pb dating (see previous).

Processing of samples for ^{14}C dating was undertaken in the ANSTO Centre for Accelerator Science in November 2017 and June 2018 (Figure 4.13, see also Appendix 2). Bulk sediments were freeze-dried and ground prior to pretreatment, while hydrogen pyrolysis residue was already homogenous as part of the hypy analytical process.

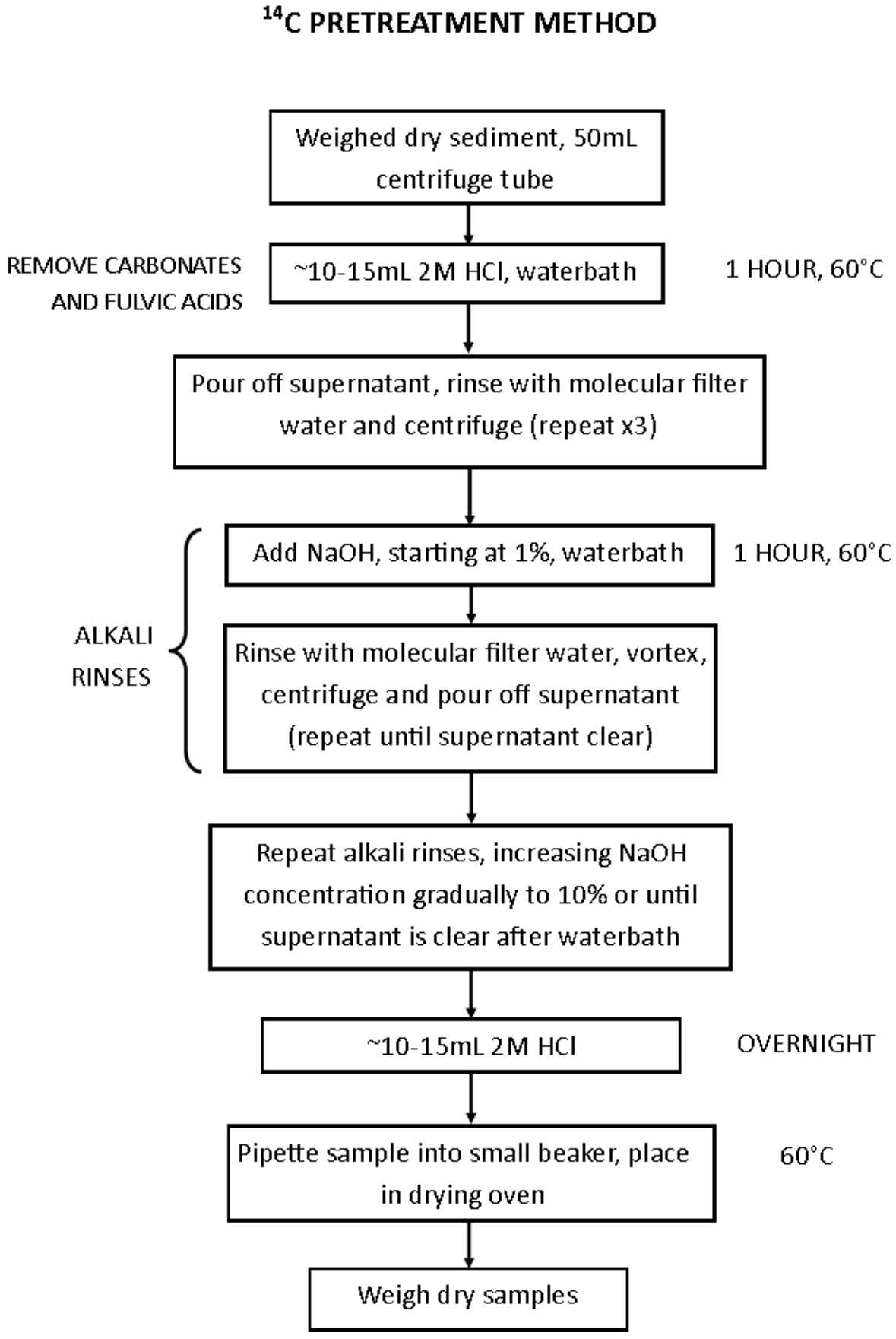

Figure 4.13: Flowchart of the ^{14}C analysis by AMS bulk sample pretreatment method.

Dried samples (not already in combustion tubes) were transferred to vials and weighed. Samples were then transferred to pre-cleaned, quartz combustion tubes (desired weights calculated prior based on approximate carbon content) along with cupric oxide, silver wire and copper wire. The pretreated samples were combusted at 900 °C in evacuated, sealed quartz tubes to convert the organic carbon to CO_2 (Vandeputte, Moens & Dams 1996). The CO_2 produced was dried and collected, the yield determined, and then it was converted to graphite by reduction with excess hydrogen over iron catalyst at 600 °C, to produce targets for AMS measurements (Hua et al. 2001). ^{14}C accelerator mass spectrometry (AMS) measurements were performed on the ANTARES 10 MV and STAR 2 MV particle accelerators at ANSTO Lucas Heights. Separate sub-samples of each fraction were combusted in a coupled elemental analyser-isotope ratio mass spectrometer system for measurement of $\delta^{13}C$, which were used to correct for fractionation during the results calculation (Fink et al. 2004).

Chapter 5 : Marura Sinkhole

5.1 Introduction

This chapter provides an overview of the land use history, geology, vegetation and current fire regime surrounding Marura, eastern Arnhem Land, Northern Territory. An overview of the methods applied is presented, followed by results for sedimentary analyses, chronology and fire proxies. Objectives of analysis for this site, linked to the overall research aims of this study presented in Chapter 1, are as follows:

1) The creation of a new high resolution late Holocene palaeofire record for Arnhem Land
2) Characterisation of vegetation burned in the Marura record, and how it has or has not changed through time
3) Investigation of potential European influence, through Indigenous depopulation and pastoral land use, on fire in the Marura record

Marura was selected for analysis as it is a perennially wet sinkhole in a region (Arnhem Land) that currently has no published palaeoenvironmental records.

5.2 Site Description

Marura (13.409°S, 135.774°E) is a sinkhole located approximately 9.5 km inland from Blue Mud Bay in eastern Arnhem Land, Northern Territory (Figure 5.1, Figure 5.2). The sinkhole is approximately 230 m wide north to south by 210 m east to west at its widest points.

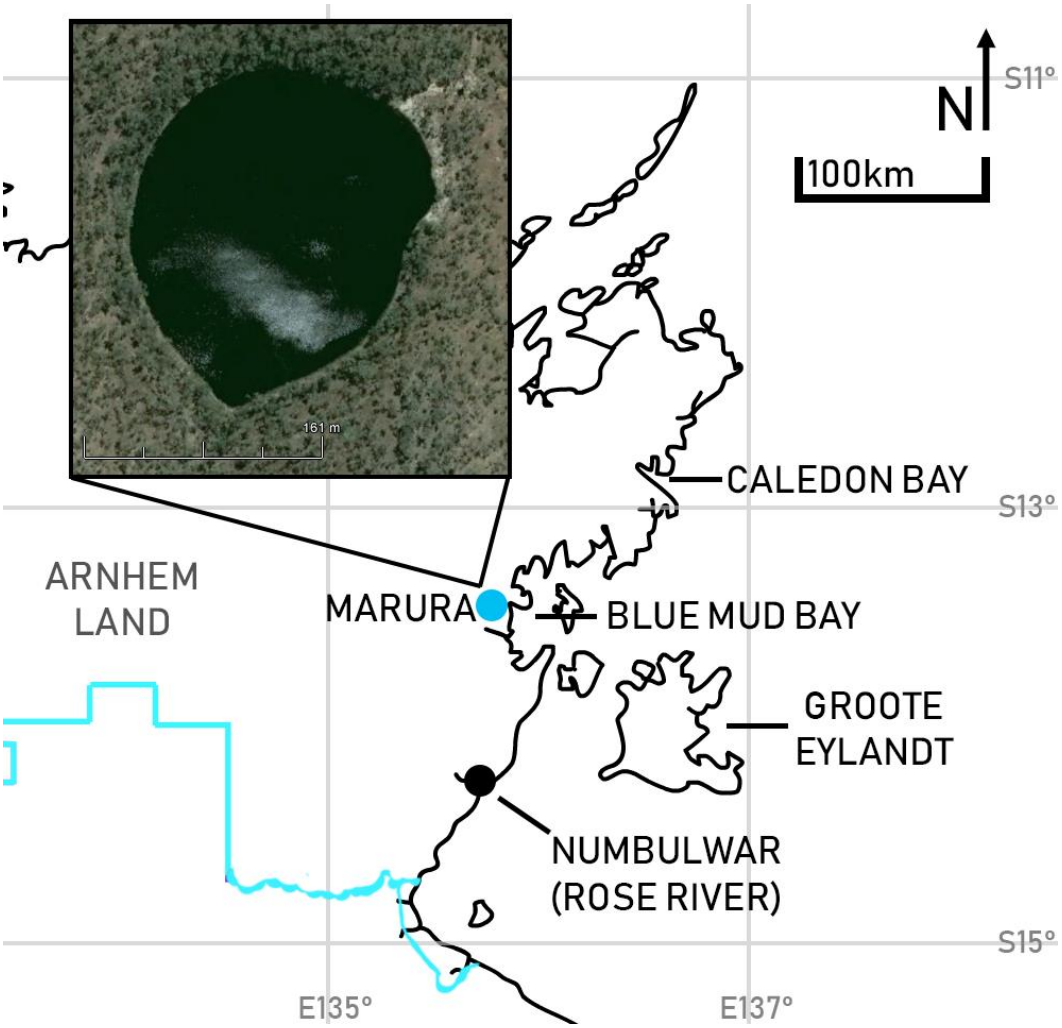

Figure 5.1: Location of Marura, with blue line representing the approximate boundary of Arnhem Land (inset after Google Earth 2018f).

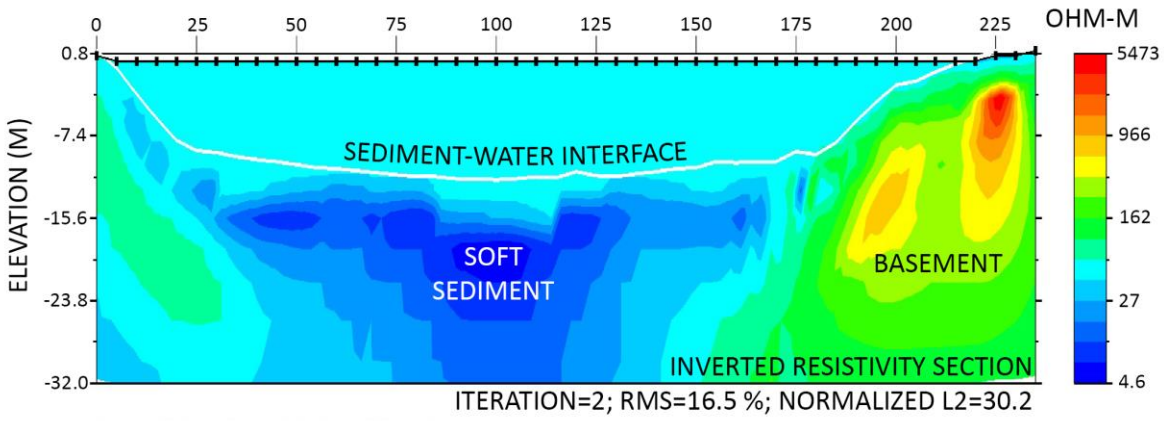

Figure 5.2: Marura inverted resistivity section.

Marura is at 50 m a.s.l., with a recorded maximum water depth of 11 m during fieldwork in September 2015. Marura is perennially wet (Figure 5.3) and has the smallest catchment area of the three sites in this study, of approximately 0.2 km^2 (Figure 5.4).

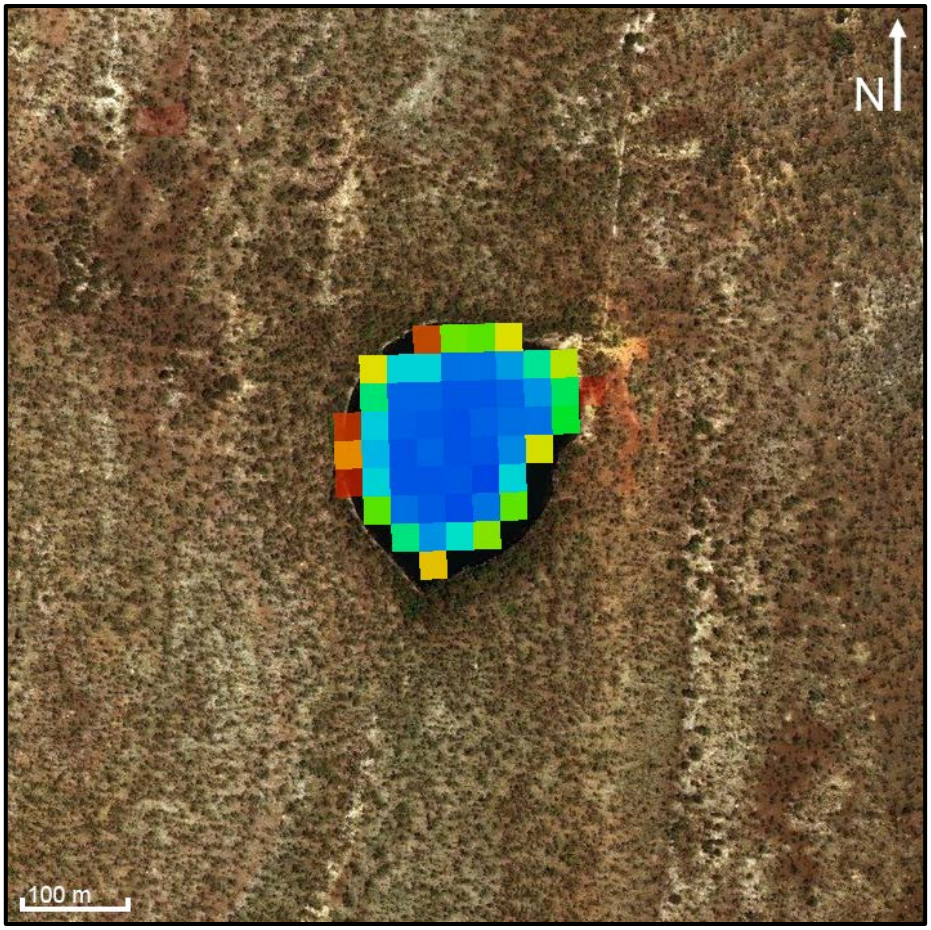

Figure 5.3: Marura water permanence derived from LANDSAT imagery for the period 1970-2018 (after Geoscience Australia 2018; Department of the Prime Minister & Cabinet 2019). Dark blue indicates >90 % water permanence over the observation period.

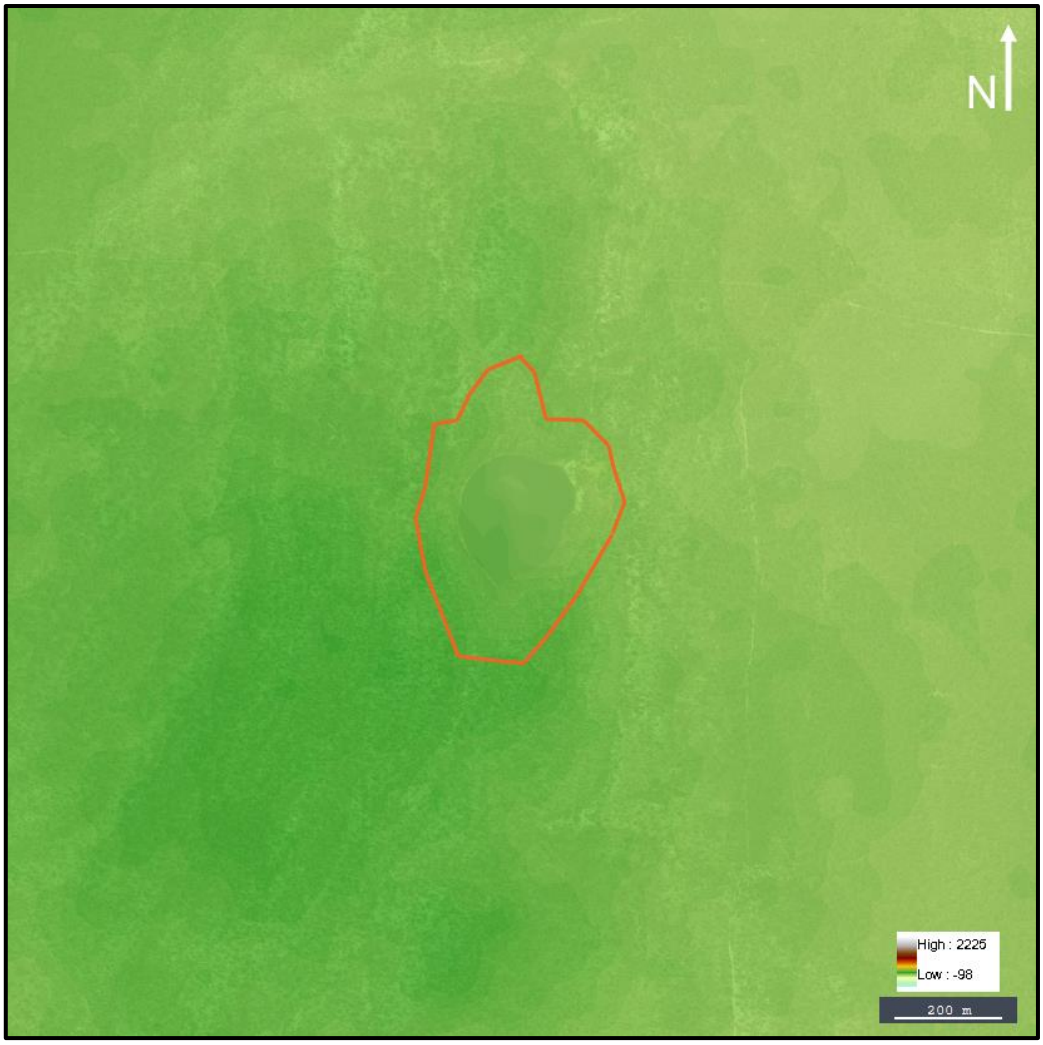

Figure 5.4: Digital elevation map of Marura and surrounds, with the approximate catchment area marked in orange (after Geoscience Australia 2015).

Data loggers placed at Marura recorded total water depth, water conductivity, air and water temperature and air pressure (Figure 5.5). Recorded water depth varied less than 1 metre (range of 11-11.9 m), demonstrating annual water permanence (see also Figure 5.3) and a maximum water depth of 11.9 m before water overflows the sinkhole via the north-eastern sill.

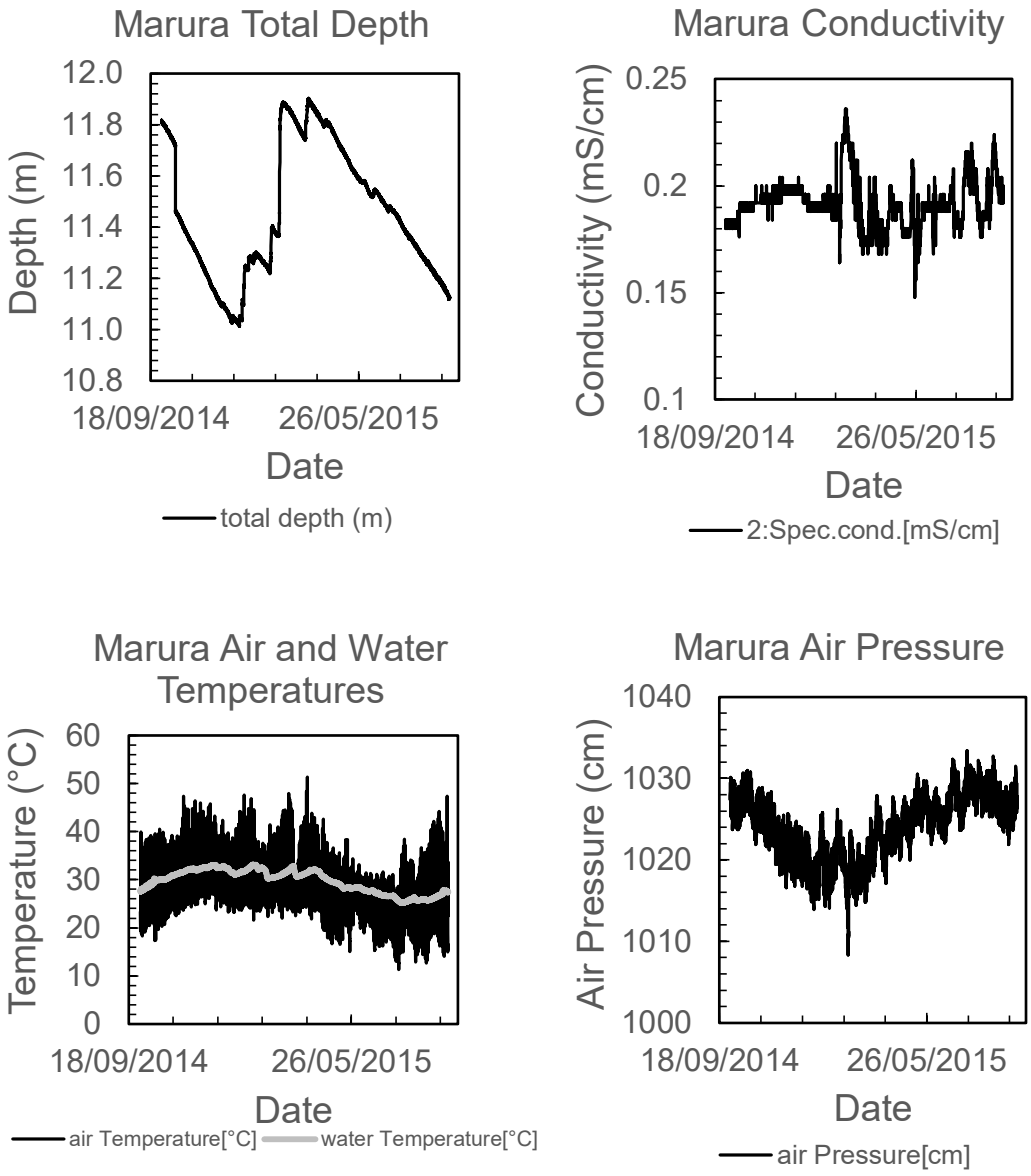

Figure 5.5: Logger data for Marura recorded October 2014 to September 2015.

Marura is a freshwater body, with a conductivity range of 0.15 to 0.24 mS/cm (well within the 0-1 mS/cm range expected for freshwater; Prajapati 2017). Variability within conductivity measurements independent of depth variations demonstrates the connection of a shallow aquifer to Marura, providing pulses of higher salinity groundwater which are diluted over time. Recorded air temperatures varied between ~11 and ~50 °C and reflect diurnal cycles, while water temperatures ranged from ~25 to ~33 °C.

Minimum air pressure during the recording period occurred on 20 February 2015, caused by Tropical Cyclone Lam (Department of Science, Information Technology & Innovation 2015). Water depth also peaked at this time, resulting from increased rainfall accompanying Tropical Cyclone Lam.

5.2.1 Land Use History

Historical aerial photographs of Marura from 1952 and 1982, and satellite imagery from 2006, show no visible changes to the sinkhole (Figure 5.6). The surrounding terrain is also unchanged with the exception of a road to the north, first visible faintly in the 1982 image. Due to the image resolution, it is unclear whether the 1982 photograph includes the track which branches from this road and runs to Marura's north-eastern edge, as seen in the 2006 satellite image. A southerly branch from the northern road was added between 1982 and 2006 passing approximately 300 m from Marura.

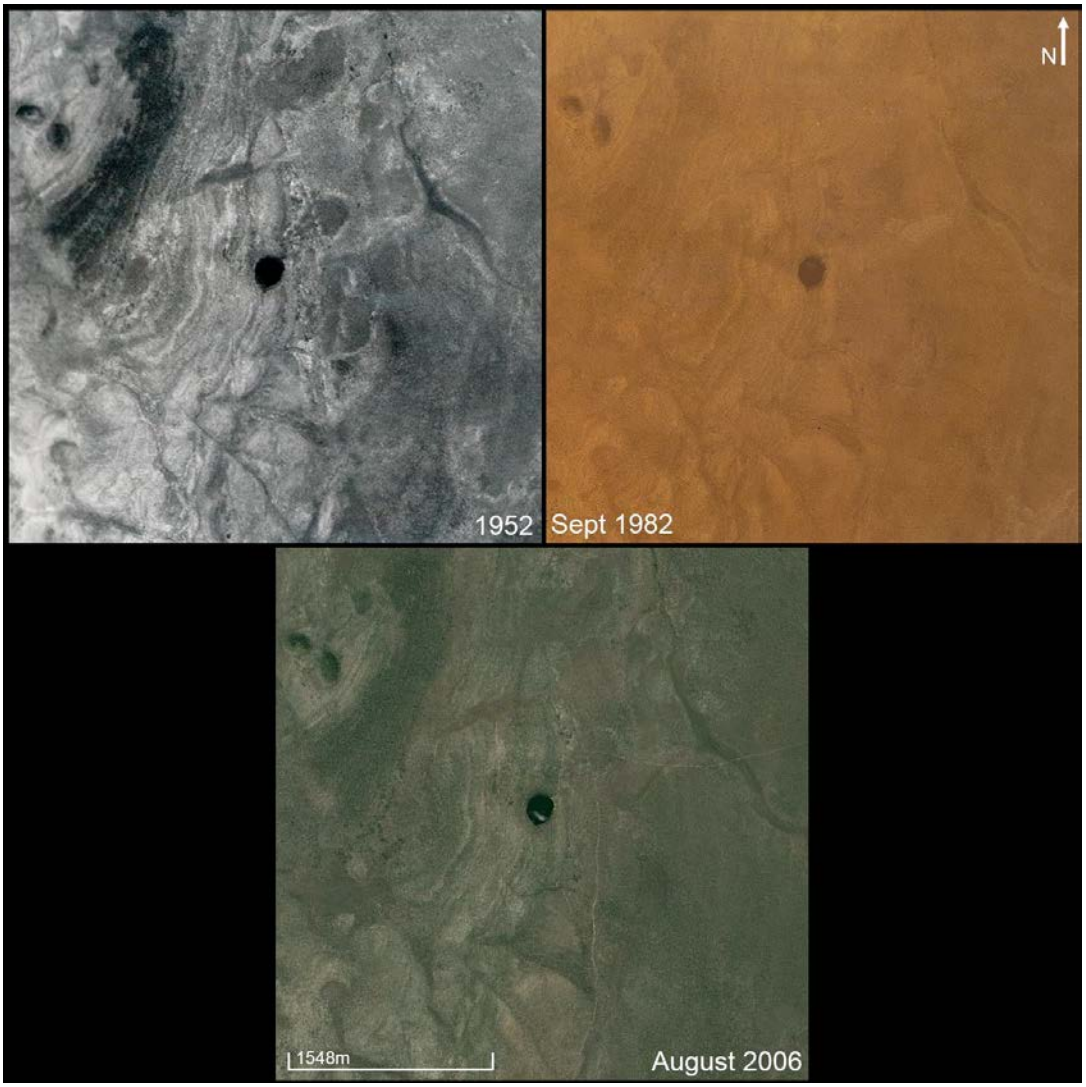

Figure 5.6: Aerial images of Marura (after Google Earth 2018f; National Library of Australia 1950-1952; Northern Territory Government 1982).

The closest small settlement to Marura is Markalawa Outstation (Laynhapuy Homelands Aboriginal Corporation 2017b). The nearest town to Marura is Numbulwar (~95 km to the south), with the largest population centre over 300 km away at Borroloola on the coast of the Gulf of Carpentaria.

5.2.2 Environment

5.2.2.1 Climate

The climate of Marura is classified as AW – Tropical/Equatorial Savanna with dry winter under the global Köppen-Geiger Climate Classification (Peel, Finlayson & McMahon 2007; Kottek et al. 2006). Mean annual rainfall is 1314.8 mm measured from the nearest weather station (Groote Eylandt Airport, approximately 98 km southeast of Marura), with rainfall primarily (~90 %) occurring between November and April (BOM 2018b). Winds are predominantly from the west-northwest and southeast in January and July, respectively (BOM 2018b) (Figure 5.7). Average minimum and maximum daily temperature ranges from 15.1 °C to 34.5 °C, in August and November respectively (BOM 2018b). Mean relative humidity measured at 9 am varies between 61 % (September-October) and 79 % (March) (BOM 2018b).

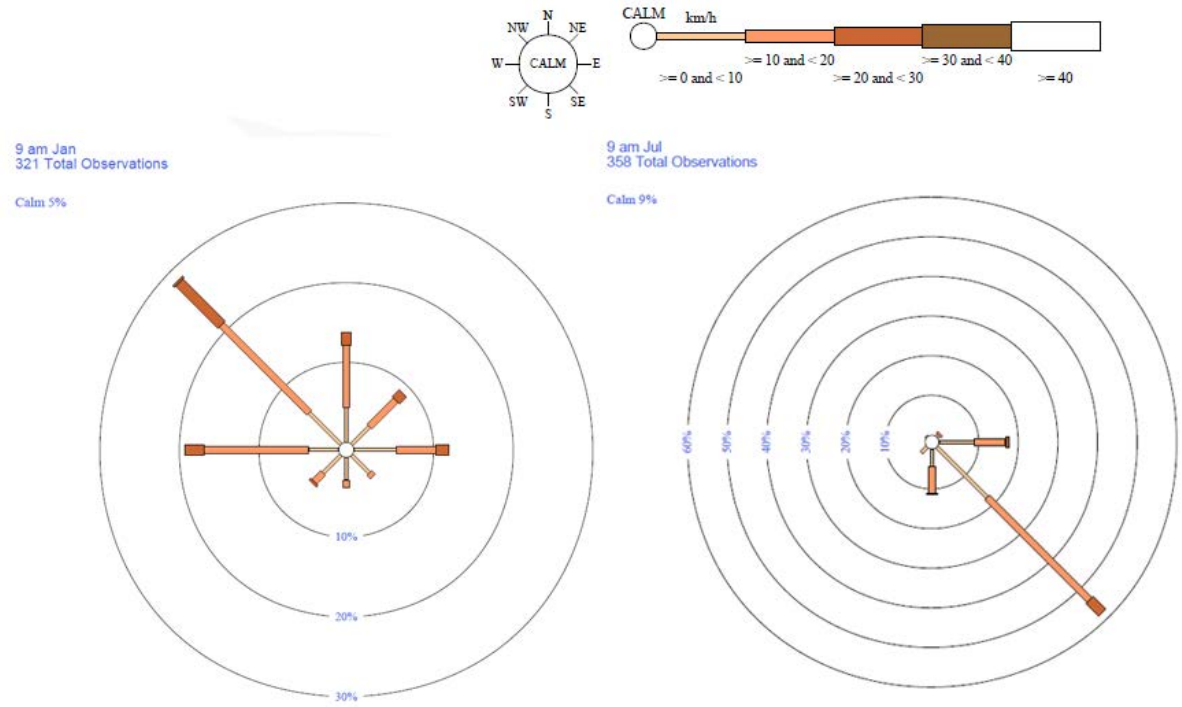

Figure 5.7: Average wind direction and speed 1999-2010, measured at 9 am in January (left) and July (right), from Groote Eylandt Airport (after BOM 2018b).

In the period 1969-2016, 14 cyclones passed within 50 km of Marura, and 22 within 100 km (BOM 2018a). Eastern Arnhem Land has an average annual lightning (cloud-to-ground) flash density of 2-3 flash/km^2/year, primarily occurring between November and April (see also Chapter 3; BOM 2016a; Dowdy & Kuleshov 2014).

5.2.2.2 Geology and Vegetation

Marura is within the Bath Range formation of the Balma Group comprised of "dolomitic siltstone, sandstone, dolarenite, certified evaporitic-stromatolitic dolostone" (Haines et al. 1999), an area of which dissolved to form Marura sinkhole. This is partly overlain by Cenozoic to Holocene unconsolidated sediments and laterite duricrust (Haines et al. 1999). Marura is located on the eastern edge of the Gulf Fall, a "dissected hilly" landscape with "moderate to strong relief" drained by streams into the Gulf of Carpentaria (Plumb & Roberts 1967, p.4); soils include shallow stony sands (Uc4.1, Uc1.4, Uc4.2) associated with slopes and plains of yellow earthy sands and soils (Uc5.22, Uc5.21, Gn2.1, Gn2.2, Gn2.6) (Northcote et al. 1960-1968).

Marura's small catchment area is due to the sinkhole's semi-encircled formation within the landscape. The terrain visibly slopes towards the sinkhole around the southern edge of the site, with an average elevation of ~43 m a.s.l. on the eastern side up to ~63 m a.s.l. on the southern side (Figure 5.8, see Figure 5.4 above). This slope, and its direct drop into the sinkhole pool, has meant *Melaleuca* fringes and/or swampy-sedge wetland edges (such as at Big Willum Swamp, see Chapter 6) are absent at Marura. Aquatics, including submerged floating plants, are also absent, likely due to water depth.

Figure 5.8: Slope on the south to southwest edge of Marura (left) and the southeast edge looking northwest (right).

Vegetation surrounding Marura is open eucalypt woodland, characterised by dominant *Eucalyptus tetrodonta* and *E. miniata*, with species of *Acacia*, *Calytrix* and *Callitris intratropica* in the subcanopy (Figure 5.9; Department of the Environment & Energy 2017). Canopy cover varies between 20 and 50 % in the upper tree layer (Department of the Environment & Energy 2017). Ground cover is dominated by grasses; these are variable in their distribution, and thinner to patchy to the north where soils are shallow. This same woodland extends downslope to the waterline at Marura, incorporating higher tree density and a more obvious shrub layer with species such as *Livistona humilis*.

Figure 5.9: Vegetation on the northeast edge (left) and southern side (right) of Marura.

5.2.2.3 Fire

In the 18 year period spanning 2000-2018 the area surrounding Marura burned on average every 2 to 4 years (every year at its most frequent, including area directly surrounding Marura between 2008 and 2010) (Figure 5.10; NAFI 2019). Fires in the period 2000-2018 were primarily between July and October, with three fire scars in November (2001, 2003, 2018) and one in December (2006) (NAFI 2019). No recent burning was evident at Marura during fieldwork, and the presence of *Callitris intratropica* also suggests a low-intensity fire regime and/or unburnt patches in the area as *C. intratropica* is known for its sensitivity to fire (see Bowman & Panton 1993; Trauernicht et al. 2015).

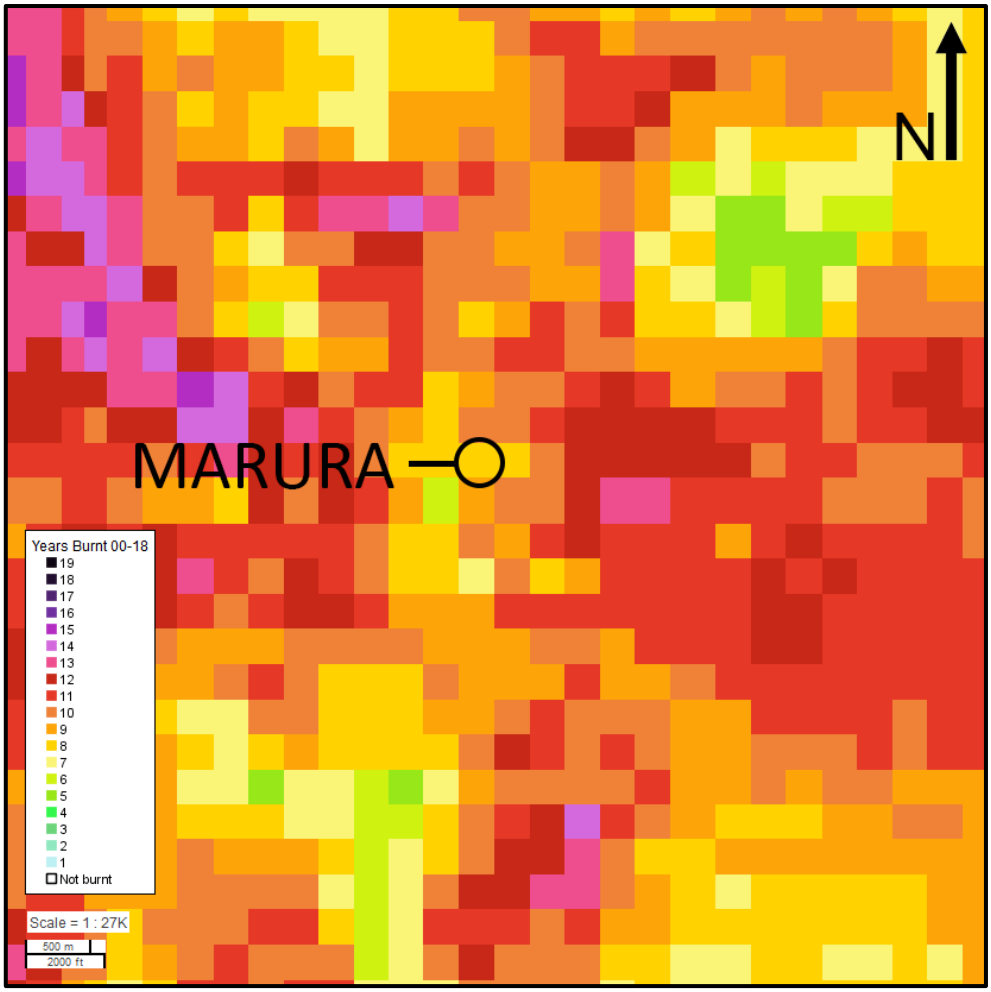

Figure 5.10: Number of years that the area surrounding Marura burned from 2000-2018 (after NAFI 2019).

5.3 Methods

5.3.1 Sample Collection

Samples were collected from Marura during 2015 fieldwork. Cores were collected from a single coring location using a raft-mounted hydraulic corer modified from Eijkelkamp equipment to a depth of 5.85 m.

5.3.2 Laboratory Analyses

As per Chapter 4, the core was divided for optical charcoal analysis (>250 µm, 250-125 µm and 125-63 µm; Courtney Mustaphi & Pisaric 2014; Enache & Cumming 2006; Stevenson & Haberle 2005) and chemical analysis (freeze-dried bulk and <63 µm samples; Wurster et al. 2012). Sediment slices from all MAR2 cores were analysed in an Itrax™ Elemental Core Scanner at the Australian Nuclear Science and Technology Organisation (ANSTO) Lucas Heights campus, as detailed in Chapter 4 (see Weltje et al. 2015 for elemental count normalisation procedure). ^{210}Pb sample preparation and analysis by alpha spectrometry and ^{14}C sample preparation and analysis by accelerator mass spectrometry were undertaken at ANSTO Lucas Heights on bulk sediment samples from MAR2 as per the procedures outlined in Chapter 4 (see also De Oliceria Goday 1983; Eakins & Morrison 1978; Golding 1961; Lim & Dave 1981; Lim, Dave & Cloutier 1989).

5.4 Results

5.4.1 Sediment Descriptions

Munsell colour descriptions were determined using slices after Itrax™ scanning and subsequently may have been affected by thawing, refreezing and drying. The top of MAR2 has a high moisture content, particularly from 0-12.5 cm, and is 7.5YR – 2.5/1 Black (Figure 5.11).

Figure 5.11: MAR2 0-0.5m slice optical image captured by Itrax™ showing dark, moisture-rich sediment characteristic of the top 2.9 m of MAR2 (top on left, bottom on right).

7.5YR – 2.5/1 Black continues with no visible stratigraphy for the remainder of the depth analysed here (2.9 m) with the exception of sediments from 1-1.45 m that are 2.5Y – 4/2 Dark greyish brown (Figure 5.12).

Figure 5.12: MAR2 1-1.45 m slice optical image captured by Itrax^{TM} showing lighter sediments than all other slices in the top 2.9 m of MAR2 (top on left, bottom on right).

Moisture content is high in the uppermost sections of MAR2, decreasing gradually with depth and measured as weight loss of a sample after drying as a percentage of wet sediment weight (Figure 5.13). The low moisture content of the topmost sample is a measurement error.

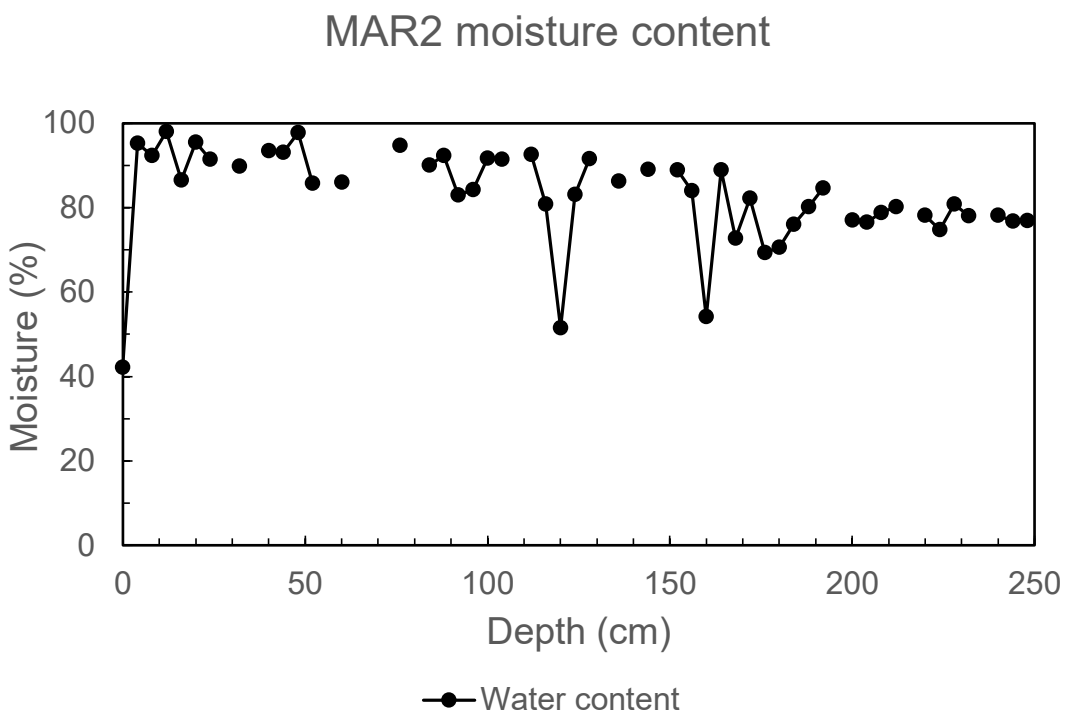

Figure 5.13: Moisture content for MAR2 0-2.9 m. Gaps indicate samples that were not accurately measured resulting in values >100 %, omitted in this figure.

5.4.2 Chronology

5.4.2.1 Lead-210 (^{210}Pb) Dating

Samples analysed by alpha spectrometry displayed a decreasing profile with depth of unsupported ^{210}Pb between 10 and 20 cm, with sediments above 10 cm displaying mixing and the sample below 20 cm (25-26 cm) reaching background ^{210}Pb levels (Figure 5.14, Table 5.1). Samples above 10 cm depth are therefore considered modern. The monotonically decreasing decay profile dictated the use of the CIC model (see Binford 1990).

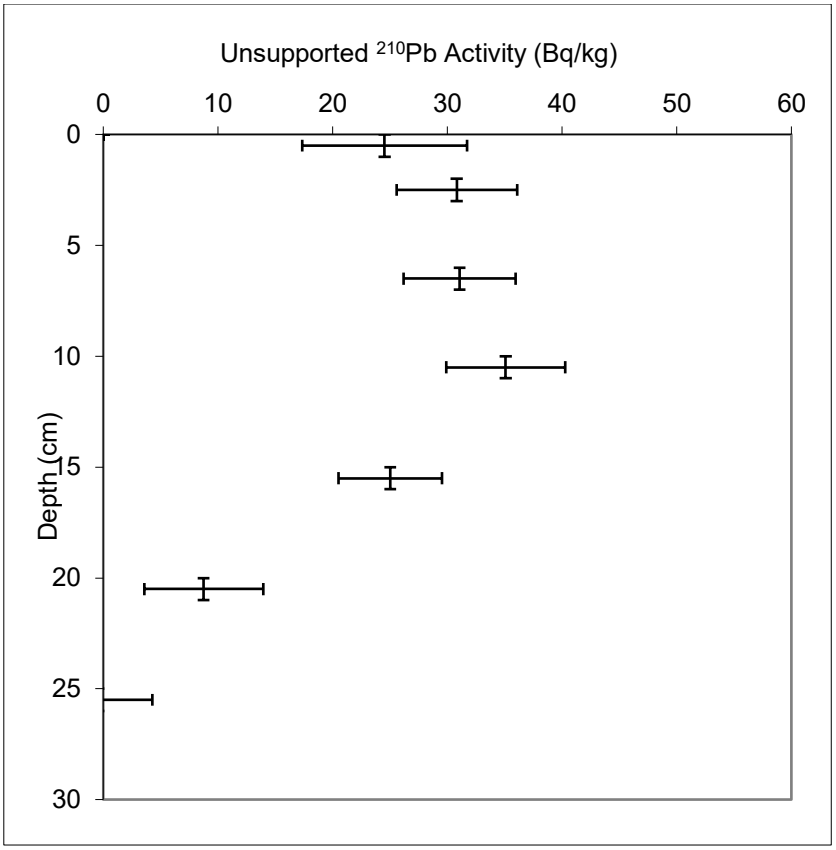

Figure 5.14: Unsupported ^{210}Pb activity for MAR2.

Table 5.1: ^{210}Pb by alpha spectrometry results for MAR2 samples; columns highlighted in red are mentioned in the text. Dates are presented as years prior to the collection date (2015).

ANSTO ID	Depth (cm)	Dry Bulk Density (g/cm^3)	Cumulative Dry Mass (g/cm^2)	Count Date	Total ^{210}Pb (Bq/kg)	Supported ^{210}Pb (Bq/kg)	Uncorrected Unsupported ^{210}Pb (Bq/kg)	Unsupported ^{210}Pb Decay corrected to 03-Oct-17 (Bq/kg)	Calculated CIC Ages (years)
U526	0 - 1	1.00	0.5 ± 0.5	02-May-18	64 ± 4	39 ± 6	24 ± 7	25 ± 7	
U527	2 - 3	1.00	2.5 ± 0.5	02-May-18	72 ± 3	42 ± 4	30 ± 5	31 ± 5	
U528	6 - 7	1.00	6.5 ± 0.5	02-May-18	69 ± 3	38 ± 3	31 ± 5	31 ± 5	
U087	10 - 11	1.00	10.5 ± 0.5	05-Oct-17	73 ± 4	38 ± 3	35 ± 5	35 ± 5	47 ± 14
U088	15 - 16	1.00	15.5 ± 0.5	05-Oct-17	64 ± 3	39 ± 3	25 ± 4	25 ± 4	69 ± 21
U089	20 - 21	1.00	20.5 ± 0.5	05-Oct-17	51 ± 3	42 ± 4	9 ± 5	9 ± 5	91 ± 28
U529	25 - 26	1.00	25.5 ± 0.5	02-May-18	45 ± 2	45 ± 4	Not detected	0 ± 5	

5.4.2.2 Carbon-14 (^{14}C) Dating

Samples analysed by accelerator mass spectrometry for ^{14}C dating display increasing age with depth, ranging from 1,105 ± 30 years BP at 44-45 cm to 4,155 ± 50 years BP at 279-280 cm depth with no reversals in age (uncalibrated radiocarbon ages; Table 5.2).

Table 5.2: ^{14}C by accelerator mass spectrometry dates for MAR2 samples.

ANSTO Code	Sample Type	ID	Average Depth	δ(^{13}C) ‰	% modern carbon	Conventional radiocarbon age
					pM C 1σ error	yrs BP
OZW494	Bulk sediment	MAR2 0-1m 44-45cm	44-45 cm	-23.7 ± 0.1	87.13 ± 0.31	1,105 ± 30
OZW495	Bulk sediment	MAR2 0-1m 72-73cm	72-73 cm	-21.0 ± 0.1	84.42 ± 0.36	1,360 ± 35
OZW496	Bulk sediment	MAR2 1-1.95m 44-45cm	120-121 cm	-24.0 ± 0.2	77.41 ± 0.30	2,055 ± 35
OZW497	Bulk sediment	MAR2 1-1.95m 84-85cm	160-161 cm	-24.1 ± 0.1	72.77 ± 0.36	2,555 ± 40
OZW498	Bulk sediment	MAR2 1.95-2.9m 44-45cm	208-209 cm	-25.2 ± 0.1	64.40 ± 0.26	3,535 ± 35
OZW499	Bulk sediment	MAR2 1.95-2.9m 84-85cm	248-249 cm	-25.8 ± 0.3	59.63 ± 0.36	4,155 ± 50

^{210}Pb dates (converted to years BP) and ^{14}C dates were combined to form a Bayesian age-depth model for MAR2 using the *Bacon* package within *R* (see Blaauw et al. 2019; R Development Core Team 2013) and using the Southern Hemisphere calibration curve SHCal13 (Hogg et al. 2013). Figure 5.15 shows a relatively steady sediment accumulation rate throughout the record. While samples above 10 cm depth (0-1, 4-5 and 8-9 cm) are assigned ages (-50, -35 and -20 cal BP, respectively) within the age-depth model, ^{210}Pb analysis suggests mixing across these depths with all three samples representing conditions since ~1950 CE.

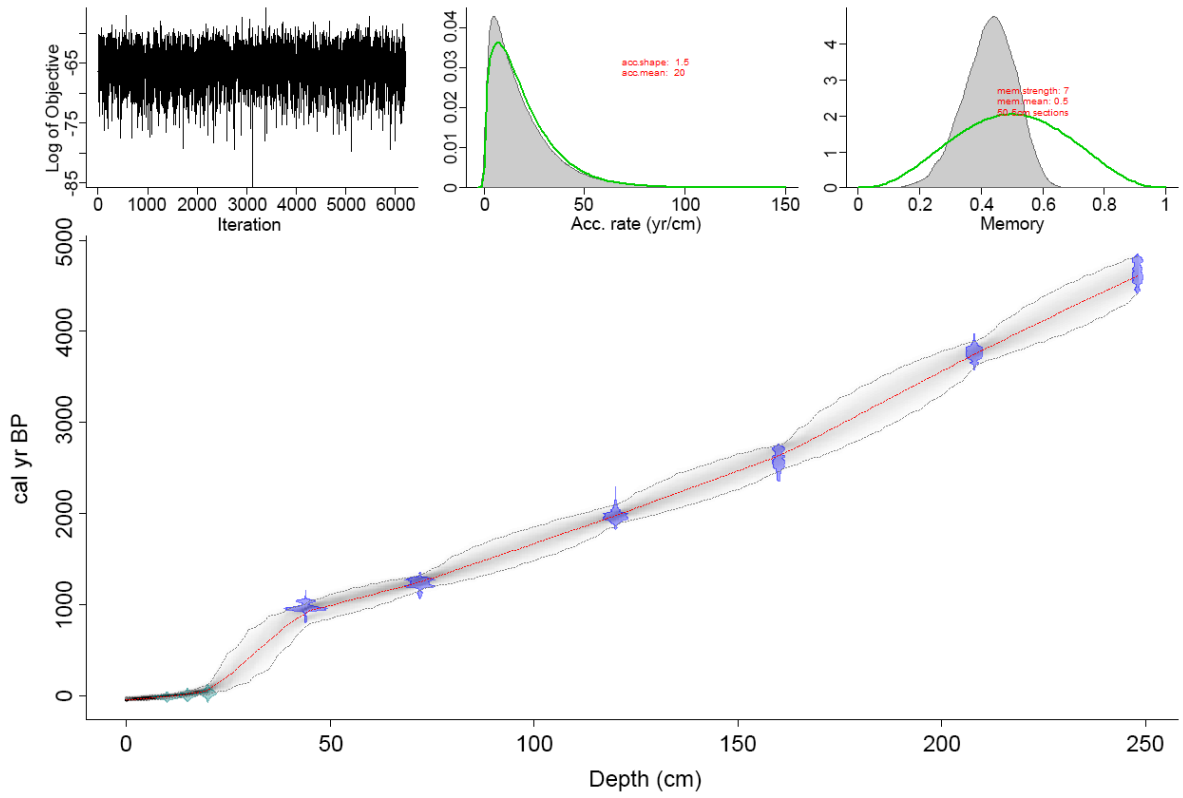

Figure 5.15: Age-depth model for MAR2 combining ^{210}Pb (green) and ^{14}C (blue) dates.

5.4.3 Itrax™ XRF Scanning

Sediment slices for all segments of MAR2 were analysed using an Itrax™ Elemental Core Scanner at ANSTO. Elemental counts were normalized by dividing each element count by the incoherent scattering (Mo inc) count for that depth (see Davies, Lamb & Roberts 2015, p.192) (Figure 5.16). Unlike cores BWIL2 (Chapter 6) and SANFC (Chapter 7), the MAR2 record presented in this chapter contains 3 metres of sediment, split into 6 segments for Itrax™ analysis, presented in Figure 5.17. The full record (0-5.85 m) for Marura contains 12 segments for Itrax™ analysis (Figure 5.16). The lower 5 cm of measurements for each core segment were removed from the elemental data prior to analysis to remove errors such as low total counts associated with transitions between segments. As stated in Chapter 4, elements of interest were selected from the list of interpreted elements by Davies, Lamb and Roberts (2015). Elements with consistently fewer than 100,000 counts per second were removed (P. Gadd pers. comm.).

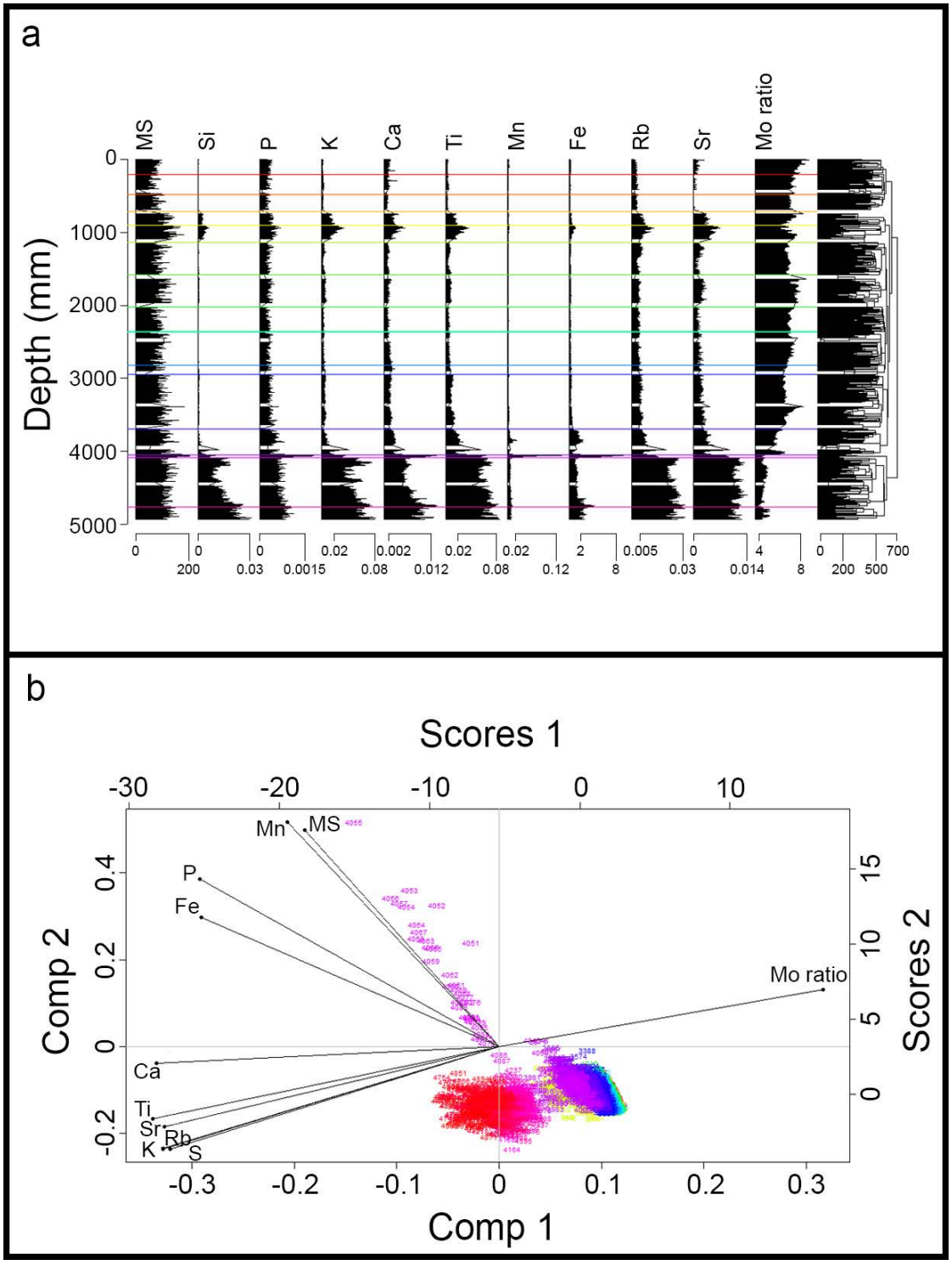

Figure 5.16: Selected Itrax™ normalized elemental and magnetic susceptibility (MS) data for MAR2 0-5.85 m: a) stratigraphic plot, and b) principal components analysis. Data are plotted by depth, and coloured numbers (sample depths) in plot b correspond to coloured depth zones identified by clustering in plot a.

The full 5.85 m record of Marura shows a distinct detrital phase in the lowermost core, transitioning to a dominant organic signal represented by Mo inc/Mo coh (Mo ratio; Woodward and Gadd 2019) at ~4 m depth. This organic signal is maintained for much of the record, except for a detrital phase between ~75 cm and 110 cm depth. This can be seen clearly in Figure 5.17 showing only 0-2.9 m, the depth covered for charcoal and pyrogenic carbon analysis.

Magnetic susceptibility (MS) shows a strong positive relationship with phosphorus ($r^2 = 0.87$) and positive correlations to all other elements except for Mo ratio. The remaining elements are all strongly positively correlated, aside from weak correlations between manganese (Mn) and all elements except iron (Fe) ($r^2 = 0.84$). The x axis in Figure 5.16 plot b represents detrital versus organic signals, and this principal component explains ~8 % of variance.

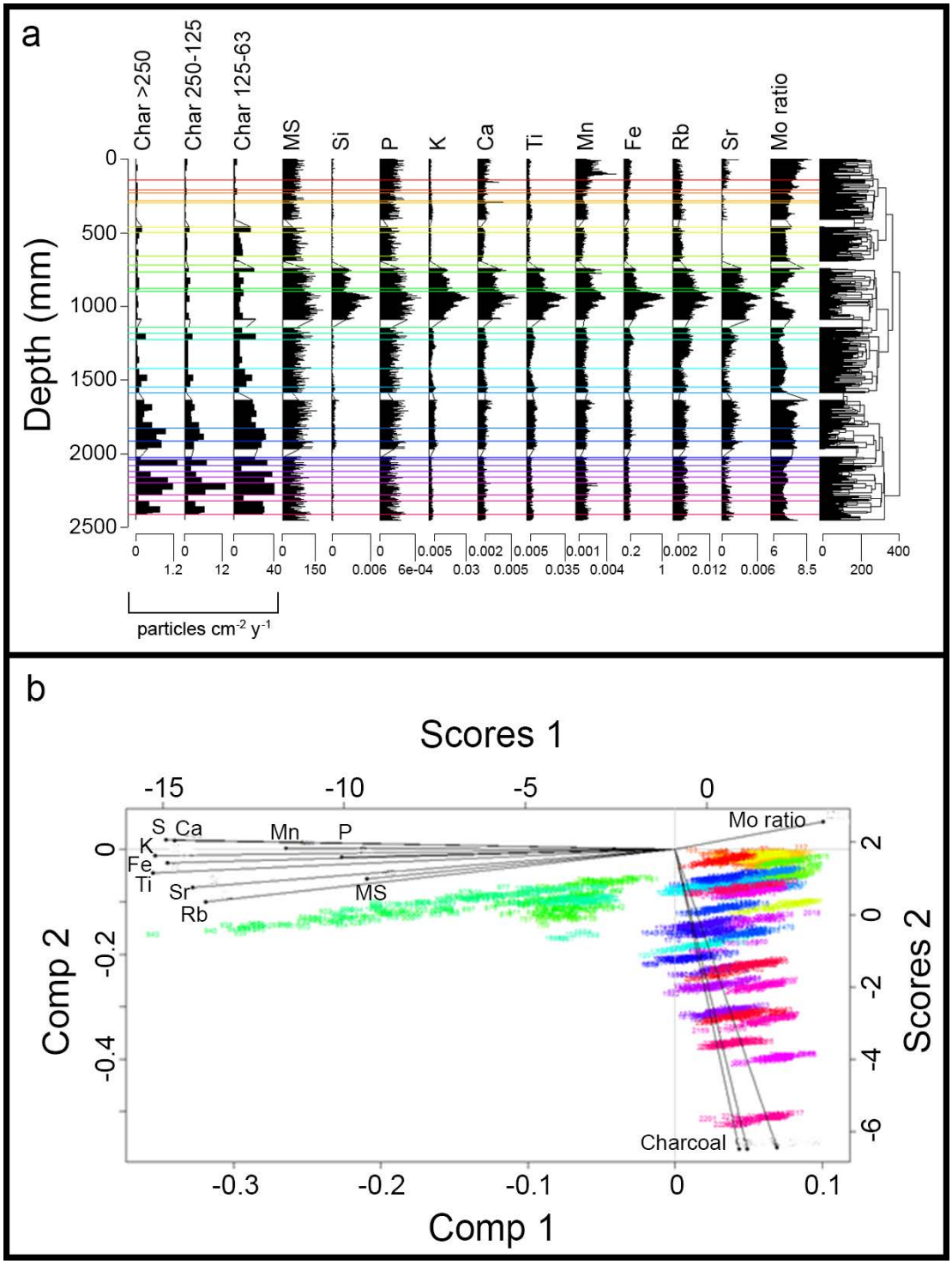

Figure 5.17: Selected Itrax™ normalized elemental data, magnetic susceptibility (MS) data and charcoal flux (particles/cm²/y divided into size fractions) for MAR2 0-2.9 m: a) stratigraphic plot, and b) principal components analysis. Data are plotted by depth, and coloured numbers (sample depths) in plot b correspond to coloured depth zones identified by clustering in plot a.

Strong positive correlations are present in MAR2 0-2.9 m between magnetic susceptibility (MS) and P ($r^2 > 0.95$), with weaker positive correlations between MS ($r^2 < 0.55$) and other elements, and P ($r^2 < 0.55$) and other elements. Strong positive correlations ($r^2 > 0.75$, except for correlations with Mn where $r^2 > 0.55$) are present between all other elements.

Despite weak ($r^2 < 0.55$) relationships between MS, P and these detrital elements, MS and P cluster with these elements along the x axis in Figure 5.17 plot b. This axis represents principal component 1 that explains ~54.1 % of variance and represents organic input (Mo ratio) versus detrital input (MS and all other elements). Visible linear clustering of samples in this plot is likely the result of resolution differences between charcoal flux values (every 4th centimetre) and Itrax^{TM} measurements (every millimetre).

Strong positive correlations ($r^2 > 0.86$) are present between the three charcoal flux size fractions, with weak correlations to all other variables ($r^2 < 0.2$). The charcoal flux measures cluster in the lower right quadrant of Figure 5.17 plot b, and are separated from all other variables along the y axis that represents principal component 2 (~19.7 % of variance). Charcoal flux variables are therefore influenced by factors beyond detrital versus organic input.

5.4.4 Sediment Core (MAR2) Charcoal

5.4.4.1 Charcoal Flux

Charcoal counts in all size fractions show a decreasing trend towards the top of the record (Figure 5.18). Smaller particles are consistently more abundant than larger particles throughout the record.

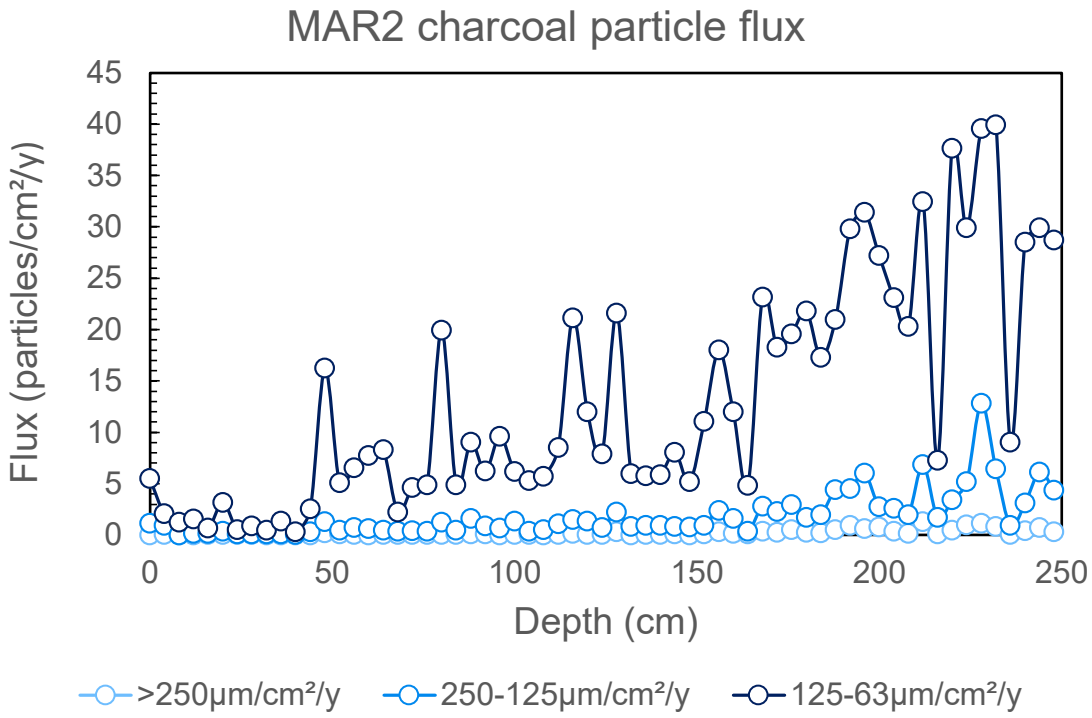

Figure 5.18: Charcoal particles by volume for MAR2, by depth.

Due to the relatively consistent mass accumulation rate throughout the record, charcoal flux for MAR2 is almost identical to charcoal particle counts by volume (Figure 5.19). Highest charcoal flux values occur between the earliest part of the record (~4600 cal BP) and ~2800 cal BP. The lowest charcoal flux values in the record occur in the most recent period, from ~800 cal BP to the present, with a slight increase in flux in the last century.

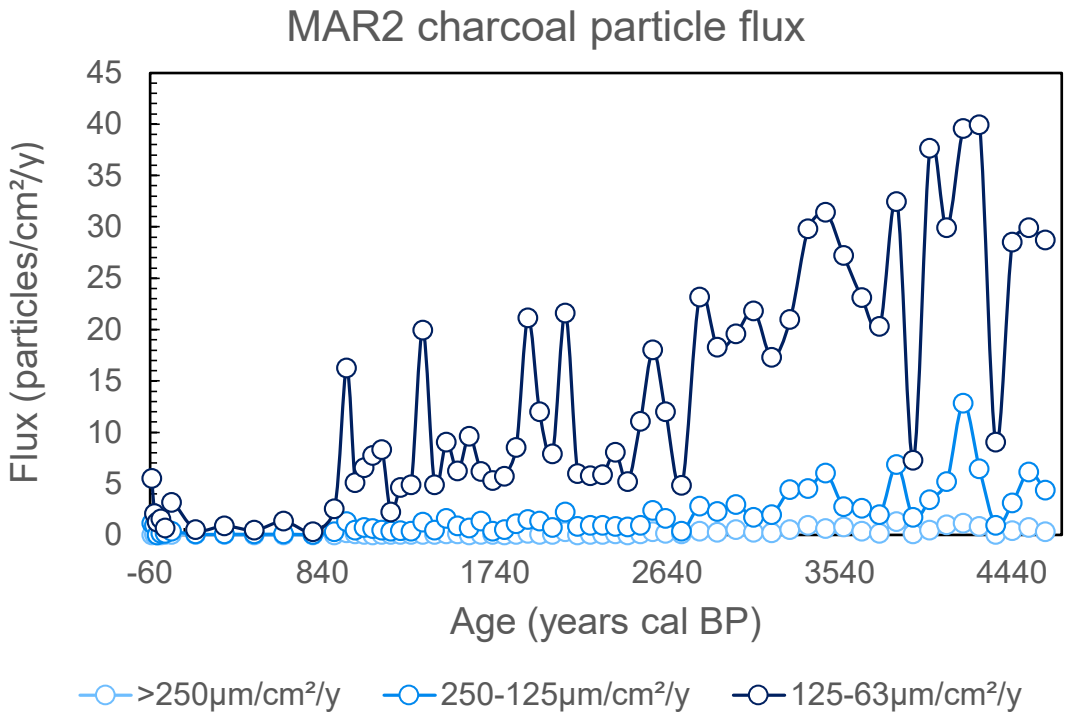

Figure 5.19: Charcoal flux for MAR2, by age.

5.4.4.2 Charcoal L:W Ratios

Elongate particles as determined from length-width ratios are present throughout the record, with high percentages of elongate particles in samples in the lower half of the record before increasing in variability in the upper half of the record into the present (Figure 5.20). This increasing variability (primarily visible as sharp peaks and troughs) coincides with decreasing total charcoal abundance and is therefore likely the result of low sample sizes.

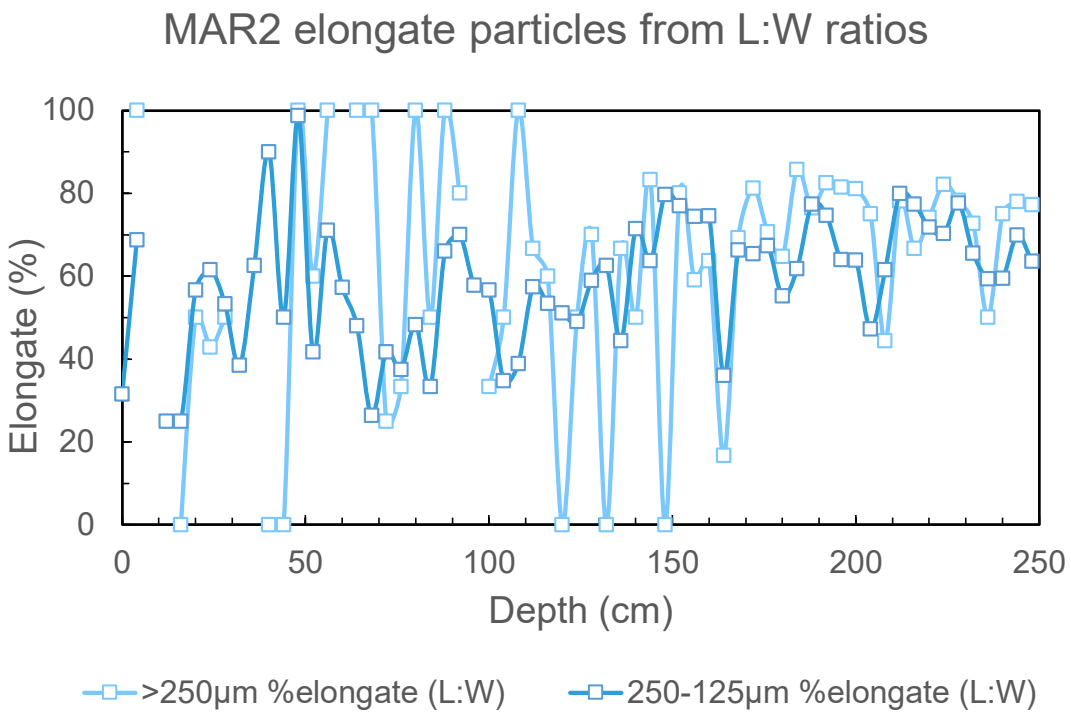

Figure 5.20: Percent elongate particles for MAR2, determined from length-width ratios, by depth.

The highest variability in percent elongate particles occurs in the >250 µm size fraction due to low particle counts, including reaching 100 % at 48-49 cm and dropping to 0 % in the next sample (44-45 cm, containing only one charcoal particle). Extreme values (0 or 100 %) of percent elongate particles in the 250 µm size fraction occur in samples with low (≤ 3) particle counts (excepting 48-49 cm, 11 particles measuring 100 % elongate).

5.4.4.3 Charcoal Morphotypes

Morphotypes in the 125-63 µm size fraction show a decrease in elongate types D and F through the MAR2 record (Figure 5.21). This coincides with an increase in geometric types C and S, and polygon types M and P.

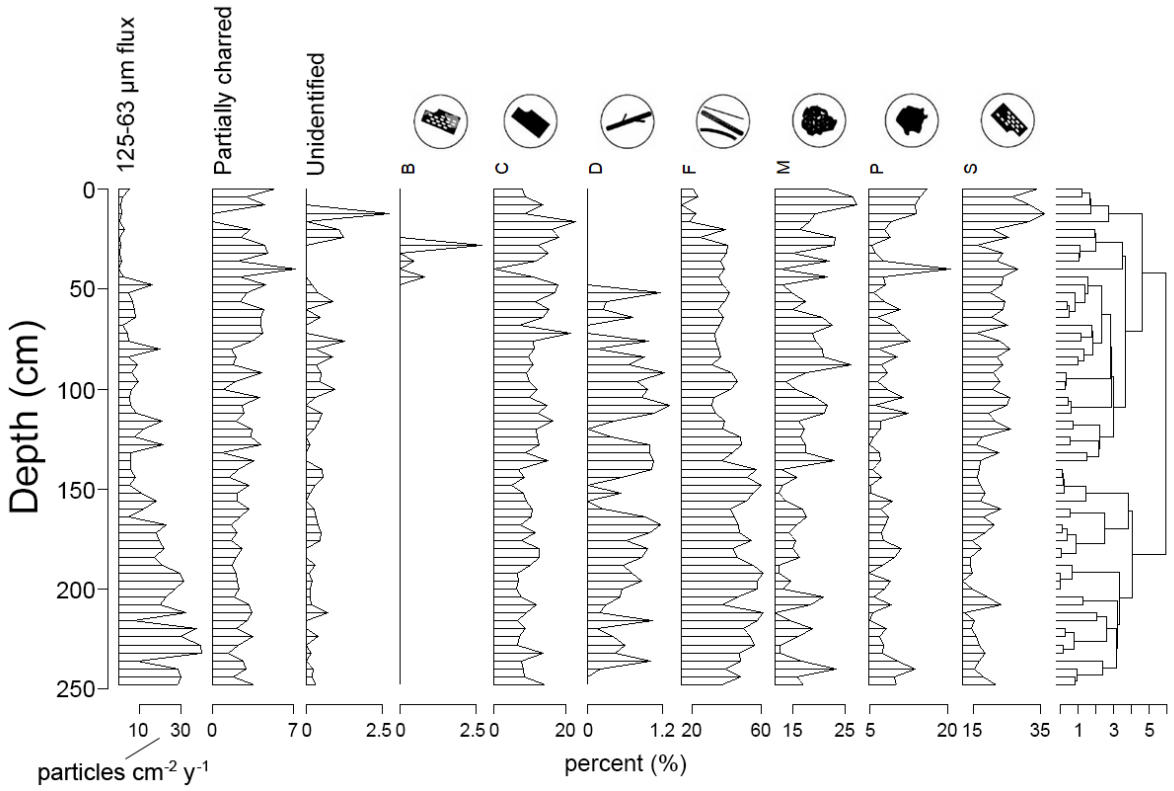

Figure 5.21: MAR2 125-63 µm morphotypes, by depth.

The complexity of morphotype data from the Courtney Mustaphi and Pisaric (2014) 27-type system for the macroscopic size classes was not useful for interpretation or analysis; full morphotype data is presented in Appendix 3. When simplified to the 7-type Enache and Cumming (2006) system, morphotypes in the 250-125 µm size fraction show similar trends to the microscopic fraction with decreasing type F and increasing types M, P and S (Figure 5.22).

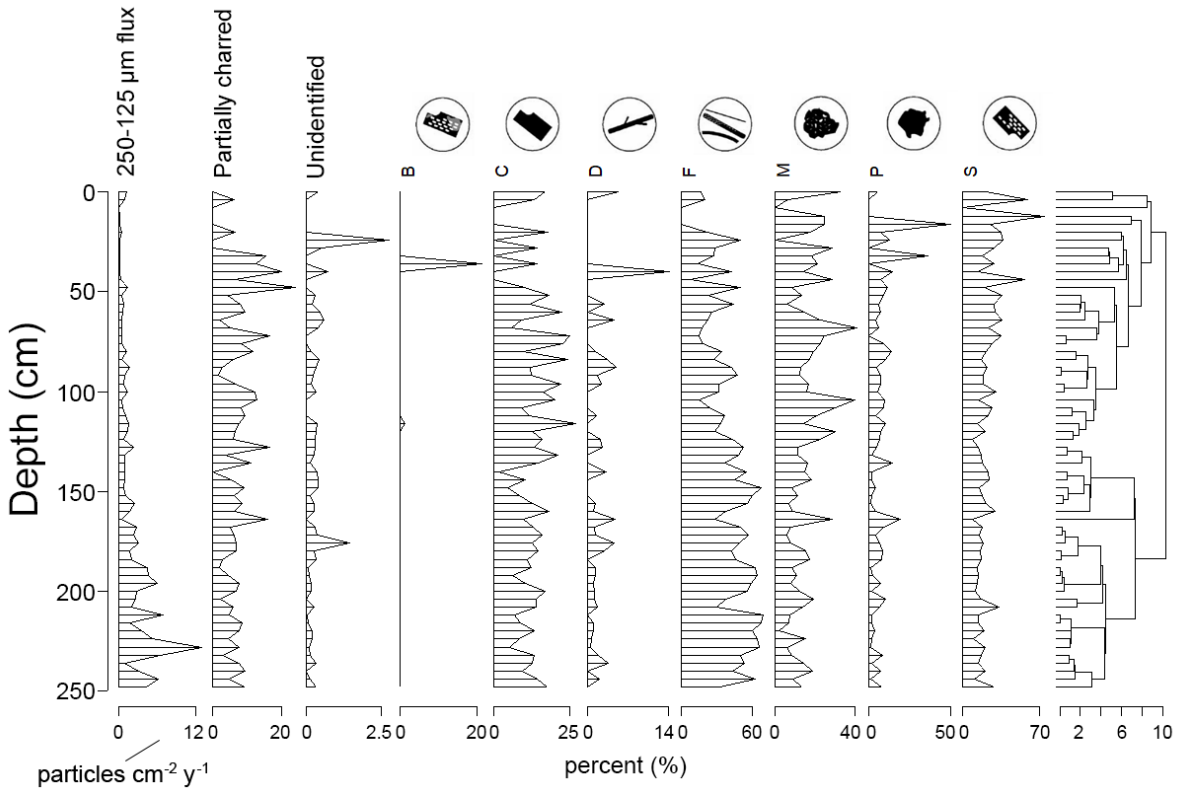

Figure 5.22: MAR2 250-125 µm morphotypes, by depth.

Limited trends are visible in morphotypes of the >250 µm size fraction, aside from potentially a decrease in type F through the record (Figure 5.23).

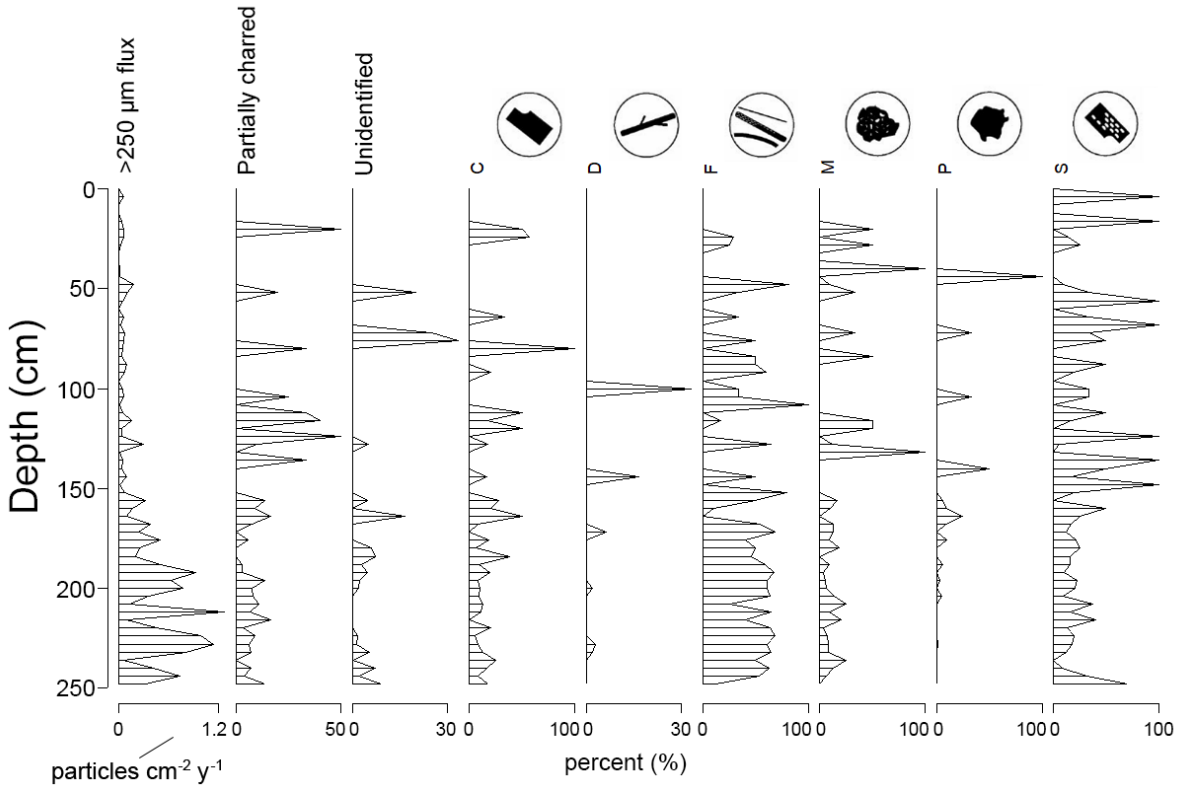

Figure 5.23: MAR2 >250 µm morphotypes, by depth. No particles of Type B were present in this size fraction.

The four uppermost samples (0-1, 4-5, 8-9 and 12-13 cm) in MAR2 represent recent conditions at the site since ~1950 CE. Morphotypes in this recent period in the 125-63 µm fraction contain similar contributions of all types except types B (partially burnt geometric with structure) and D (elongate with ramifications). The 250-125 µm is dominated in this period by types showing visible structure (M and S) although sample sizes are small, with one sample (8-9 cm) containing no charcoal in this size fraction (Figure 5.24). Only one charcoal particle in the >250 µm fraction is present within the three uppermost samples, of type S.

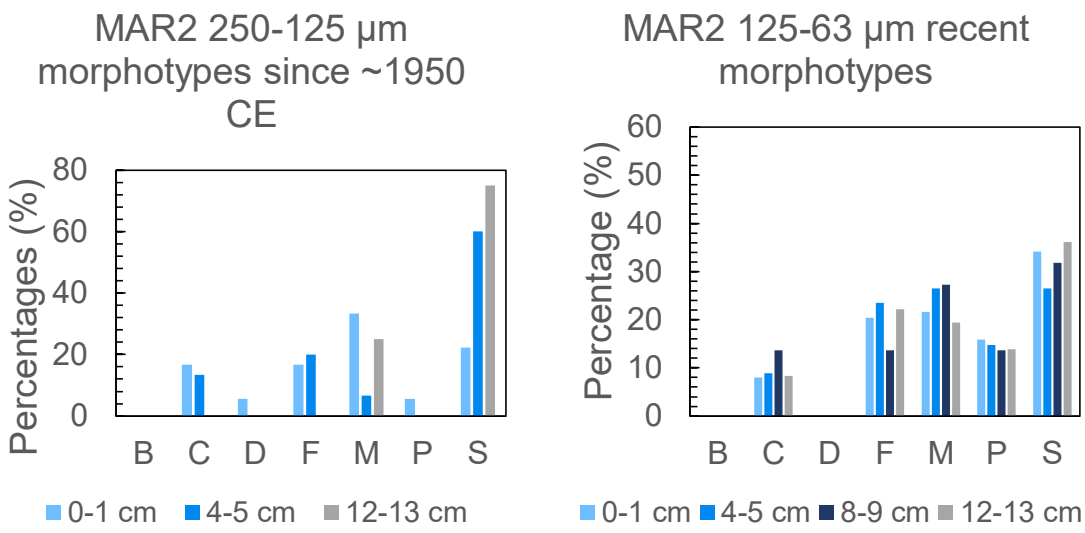

Figure 5.24: Morphotypes since ~1950 CE for MAR2, by size fraction. The >250 µm fraction contains a single charcoal particle (type S) in this period, not shown.

When simplified to elongate versus non-elongate morphotypes, percent elongate morphotypes display a decreasing trend from the oldest part of the record to the present (Figure 5.25). Percent elongate morphotypes for size fractions 250-125 µm and 125-63 µm show similar trends throughout the record, while >250 µm particles often deviate due to low particle counts.

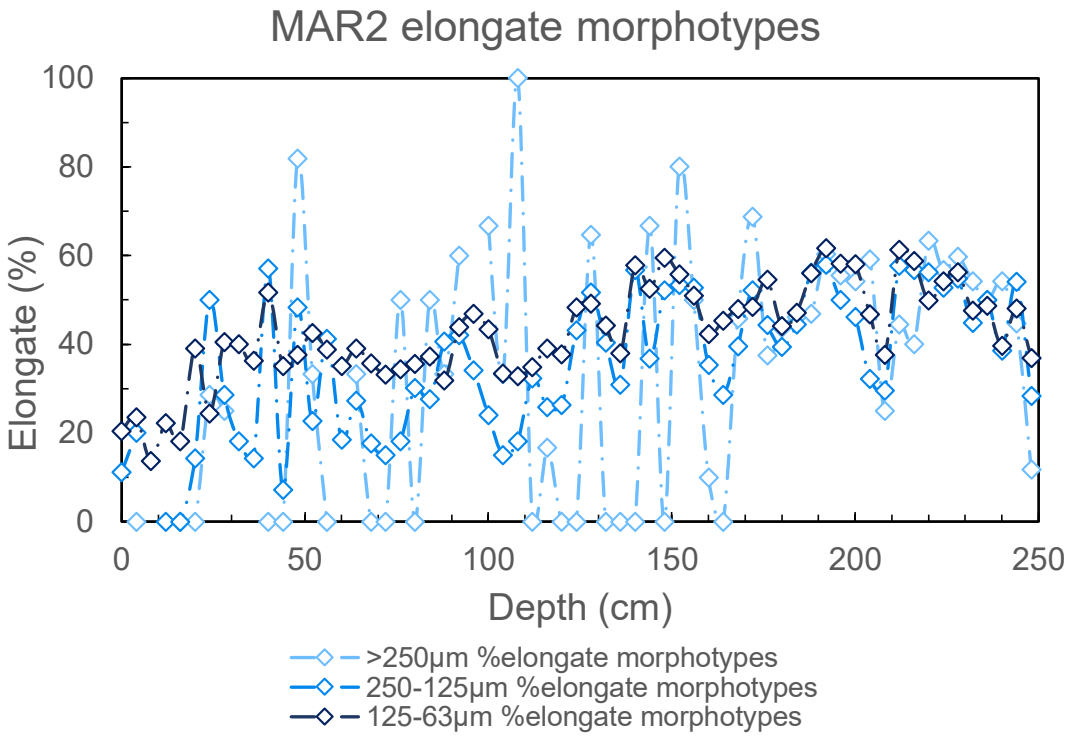

Figure 5.25: Percent elongate morphotypes for all charcoal size fractions for MAR2, by depth.

Percent elongate particles determined from length-width ratios and morphotypes show similar trends throughout the record (Figure 5.26, Figure 5.27). Elongate morphotypes consistently present slightly lower values than those given by length-width ratio determinations.

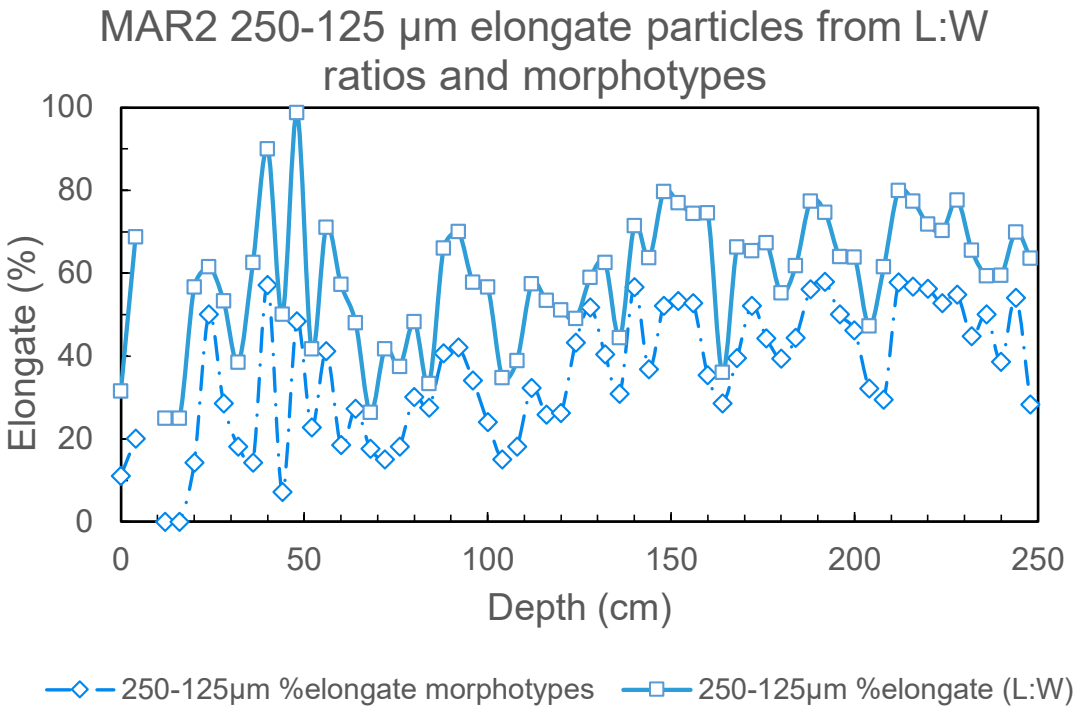

Figure 5.26: Percent elongate particles as determined by length-width ratios and morphotypes for MAR2 250-125 µm size fraction, by depth.

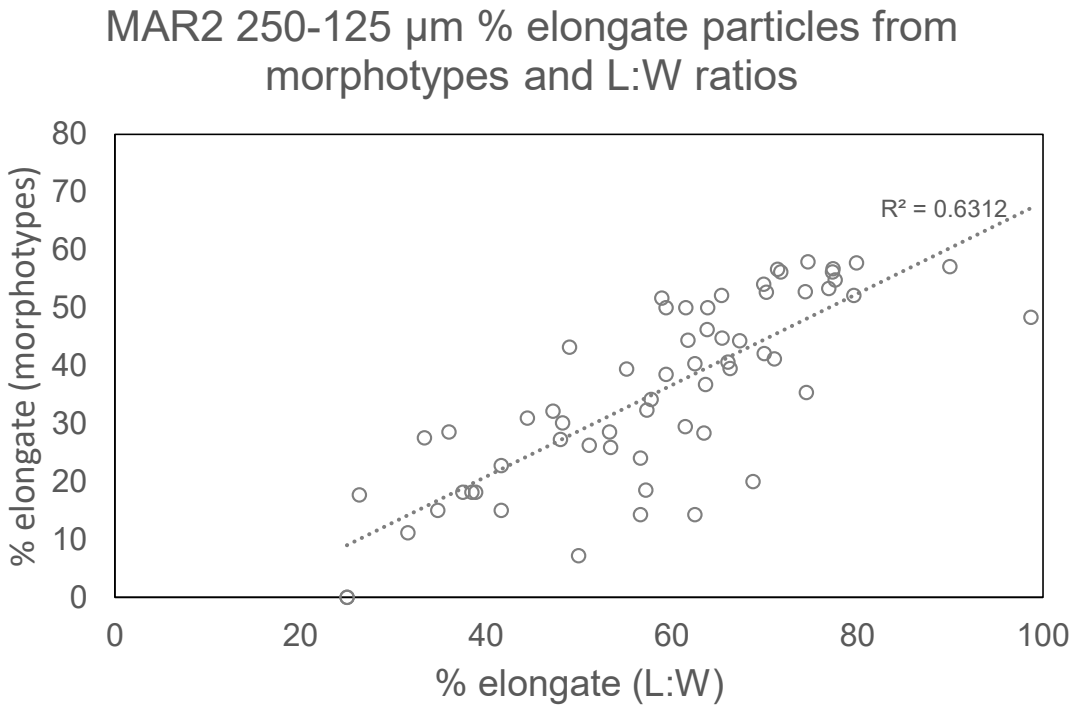

Figure 5.27: Elongate particles for MAR2 250-125 µm measured by length-width ratios and morphotypes.

5.4.5 Hydrogen Pyrolysis and Elemental Analysis

5.4.5.1 Pyrogenic Carbon Flux

Bulk and <63 µm total organic carbon and percent pyrogenic carbon show broadly similar trends but demonstrate that organic carbon content is not a major driver of pyrogenic carbon content (Figures 5.28 and 5.29). A decrease in total organic carbon in the bulk fraction between ~116 and 76 cm corresponds to a detrital phase identified via XRF (see 5.4.3 Itrax™ XRF Scanning).

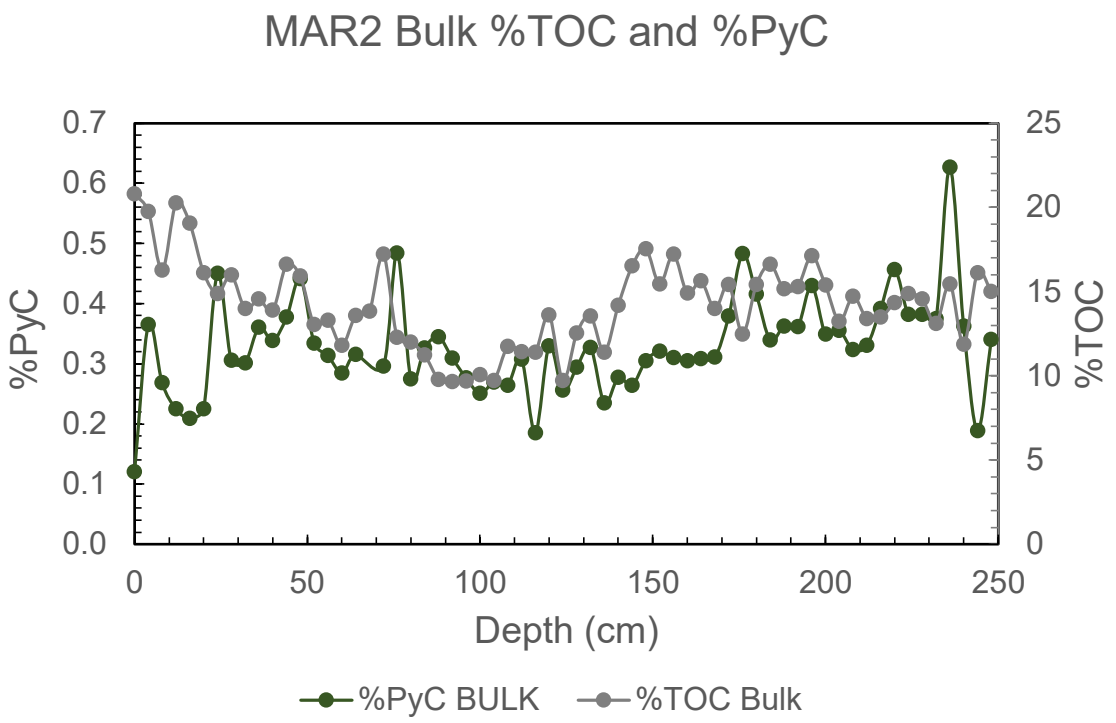

Figure 5.28: MAR2 bulk total organic carbon (%TOC) and percent pyrogenic carbon (large PyC peak at 68 cm removed), by depth.

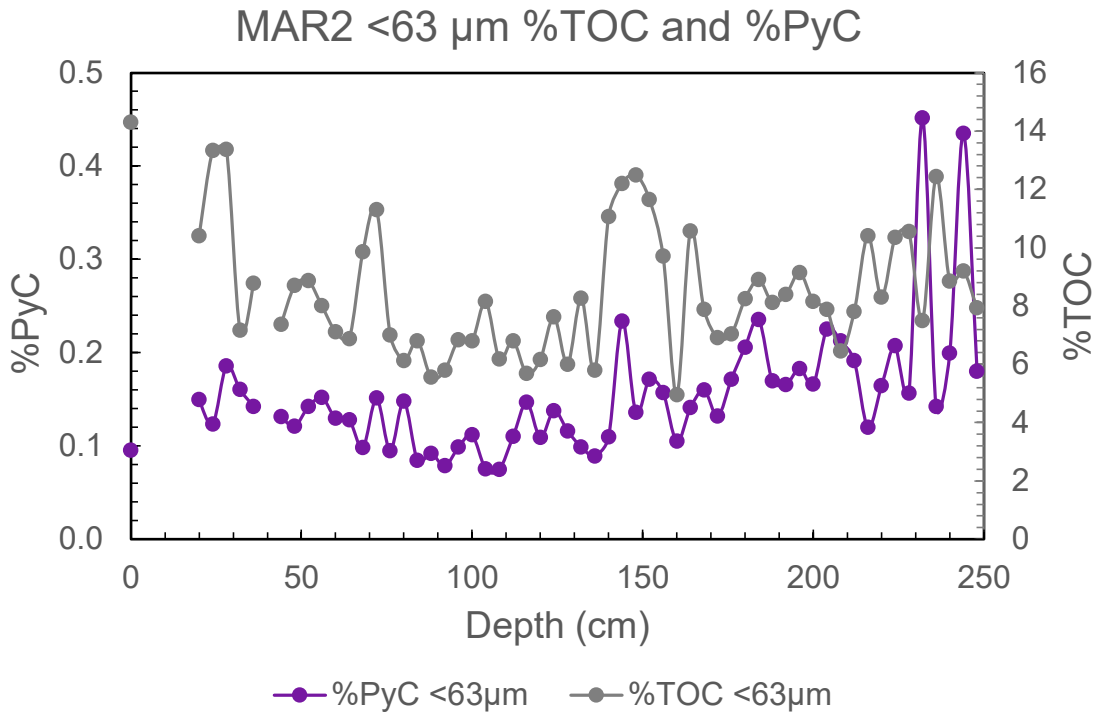

Figure 5.29: MAR2 <63 µm total organic carbon (%TOC) and percent pyrogenic carbon, by depth.

Pyrogenic carbon (PyC) flux (g/cm²/y) for bulk and <63 µm samples display similar patterns to charcoal flux, with a decreasing trend into the present (Figure 5.30).

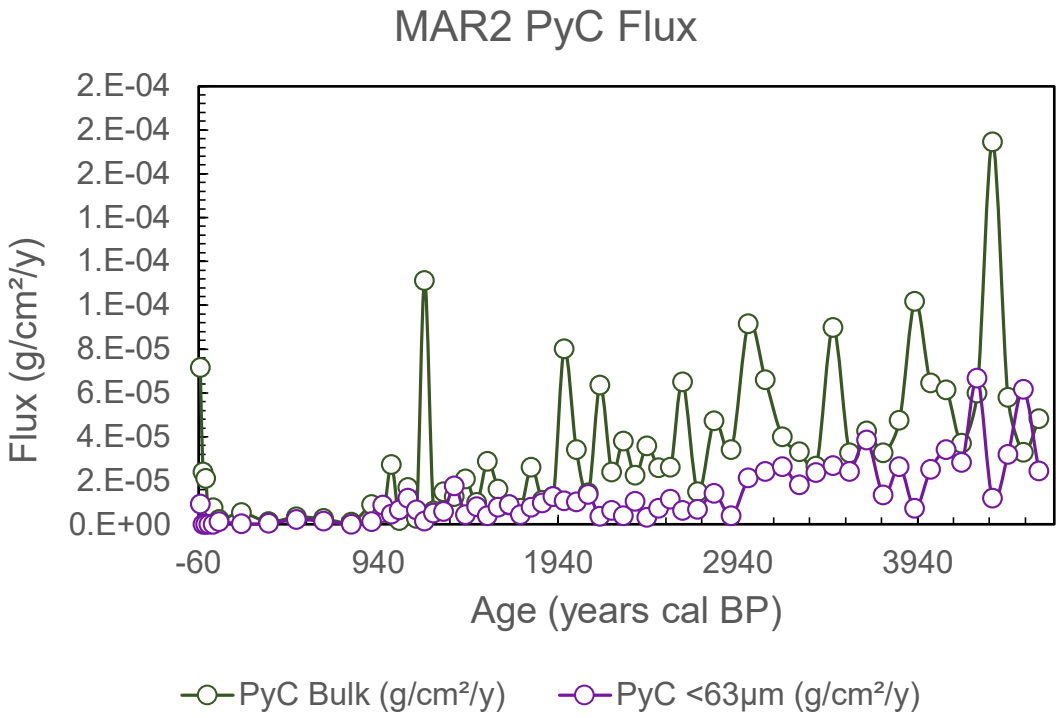

Figure 5.30: Bulk and <63 µm pyrogenic carbon (PyC) flux for MAR2, by age.

PyC flux for both size fractions displays similar trends to total charcoal flux (Figure 5.31).

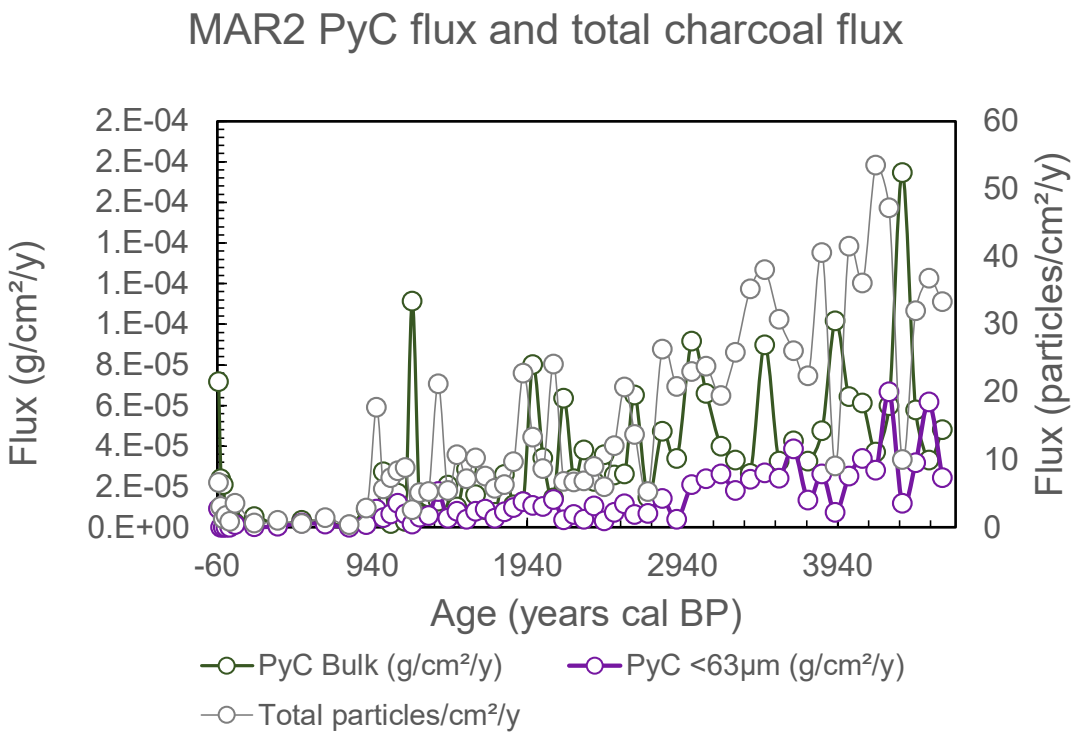

Figure 5.31: Pyrogenic carbon (PyC) flux and total charcoal flux for MAR2, by age.

PyC flux corresponds most closely to charcoal flux between the <63 µm PyC and 125-63 µm charcoal size fractions (Figure 5.32, Table 5.3).

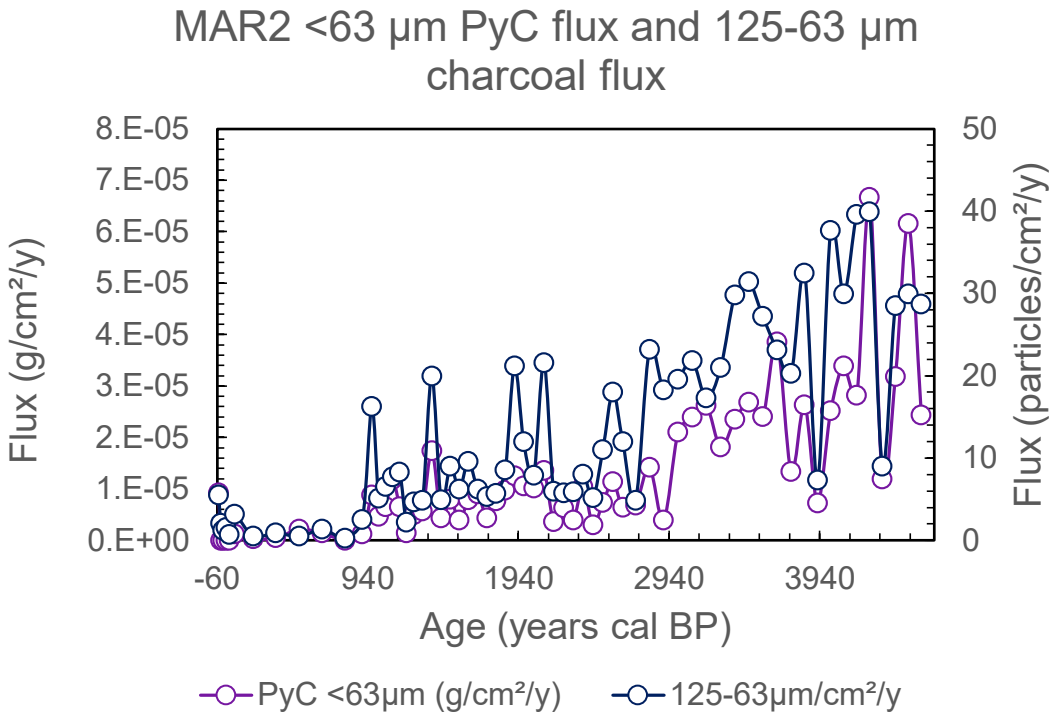

Figure 5.32: 125-63 µm charcoal flux and <63 µm pyrogenic carbon (PyC) flux for MAR2, by age.

Table 5.3: Charcoal and PyC flux variable r² values for MAR2.

	>250 µm	**250-125 µm**	**125-63 µm**	**<63 µm PyC**
Bulk PyC	0.0583	0.0782	0.1001	0.0945
>250 µm		0.8137	0.7381	0.5542
250-125 µm			0.737	0.5466
125-63 µm				0.7138

5.4.5.2 Pyrogenic Carbon $\delta^{13}C$

For both bulk and <63 µm size fractions, $\delta^{13}C$ values for total organics (pre-hydrogen pyrolysis) are more ^{13}C-depleted than $\delta^{13}C$ values for pyrogenic carbon (Figures 5.33 and 5.34). All stable carbon isotope results are reported relative to Vienna Peedee belemnite (VPDB), and precision (SD) with internal standards was better than ±0.1‰.

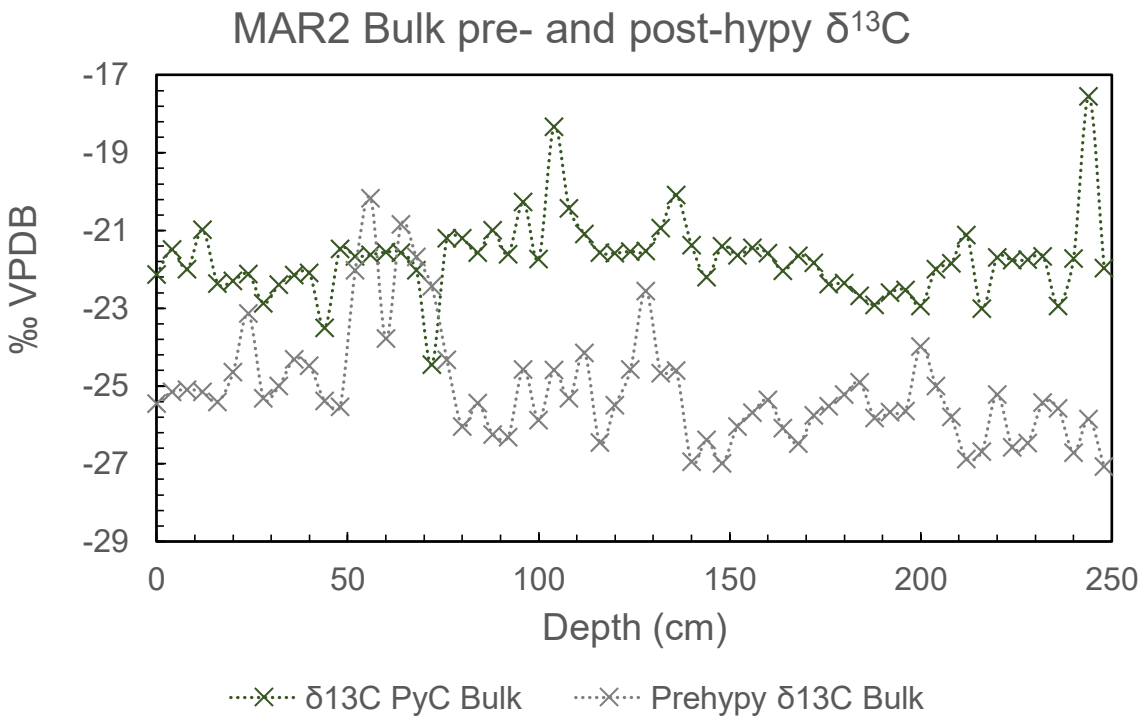

Figure 5.33: MAR2 $\delta^{13}C$ for bulk samples before (total organic carbon) and after (PyC) hydrogen pyrolysis, by depth.

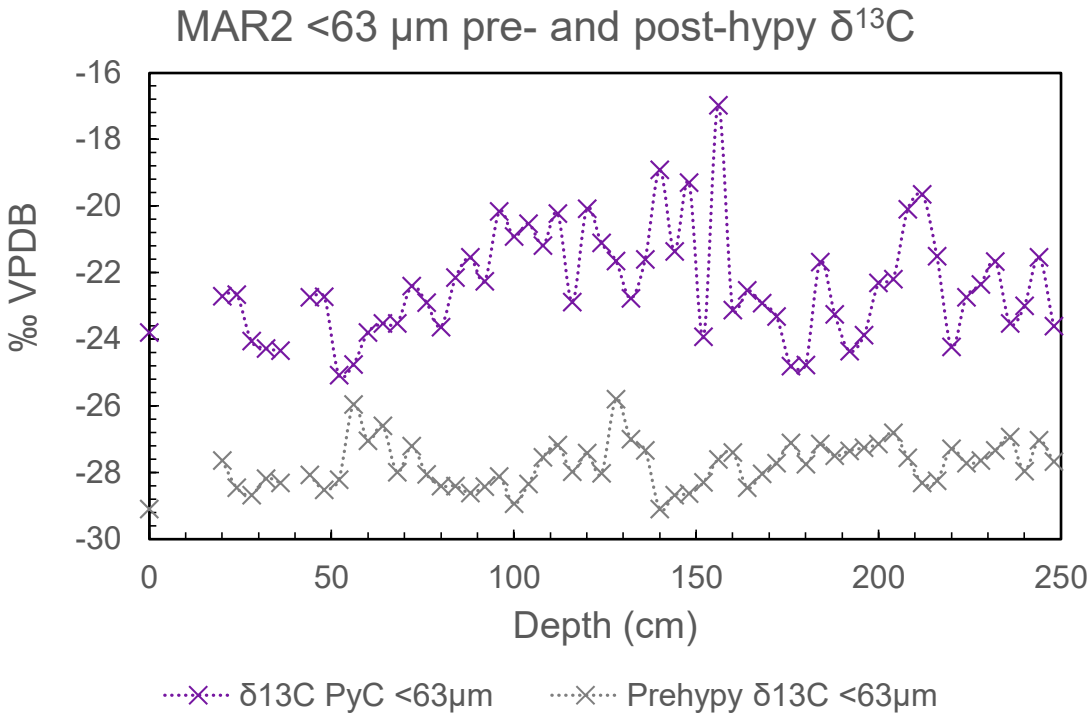

Figure 5.34: MAR2 $\delta^{13}C$ for <63 µm samples before (total organic carbon) and after (PyC) hydrogen pyrolysis, by depth.

MAR2 $\delta^{13}C$ values for pyrogenic carbon in the bulk fraction vary between -18 and -24 ‰, while values in the <63 µm size fraction vary between -17 and -25 ‰ (Figure 5.35). These values display a mix of those expected for C_4 (>-14 ‰) and C_3 (<-25 ‰) plants (O'Leary 1988, pp.330-331), reflecting the mixed woody and grassy vegetation surrounding Marura, although skewed in favour of C_3 biomass.

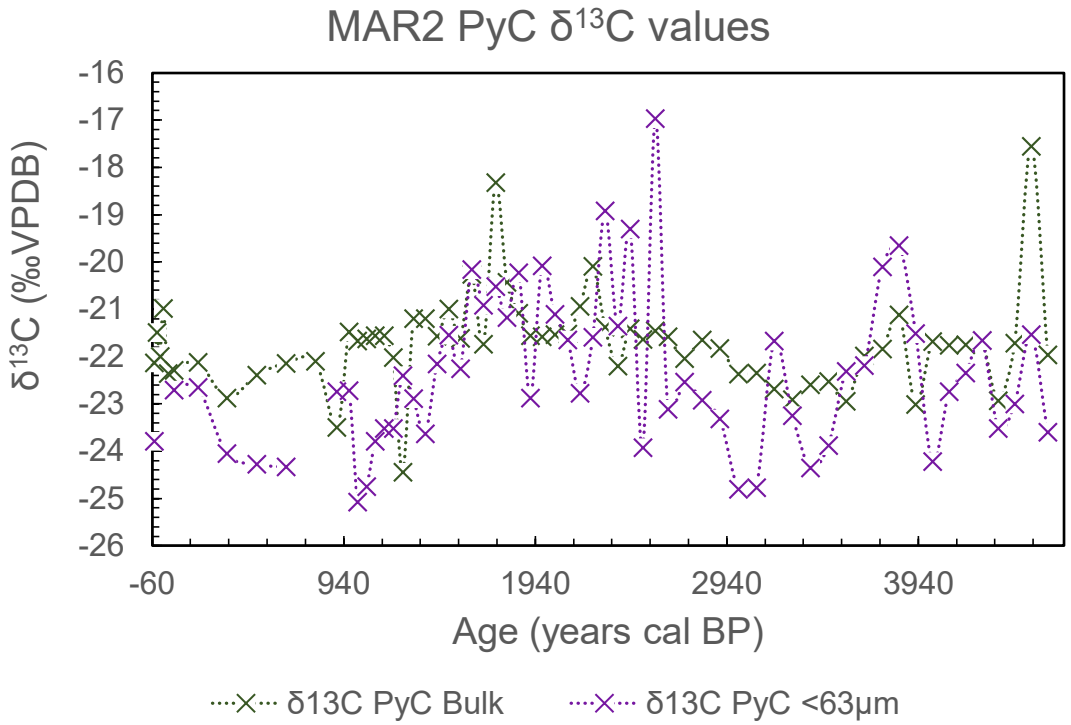

Figure 5.35: Bulk and <63 µm pyrogenic carbon (PyC) $\delta^{13}C$ for MAR2, by age.

While no overall trend is apparent for bulk PyC $\delta^{13}C$ values, trends may be present in the <63 µm size fraction. This is seen clearly when plotted as a 3 point running mean (Figure 5.36). Values are consistently higher (less ^{13}C-depleted) from ~2600-1500 cal BP, with periods of lower $\delta^{13}C$ values before and after this, excepting a brief increase from ~3900-3600 cal BP.

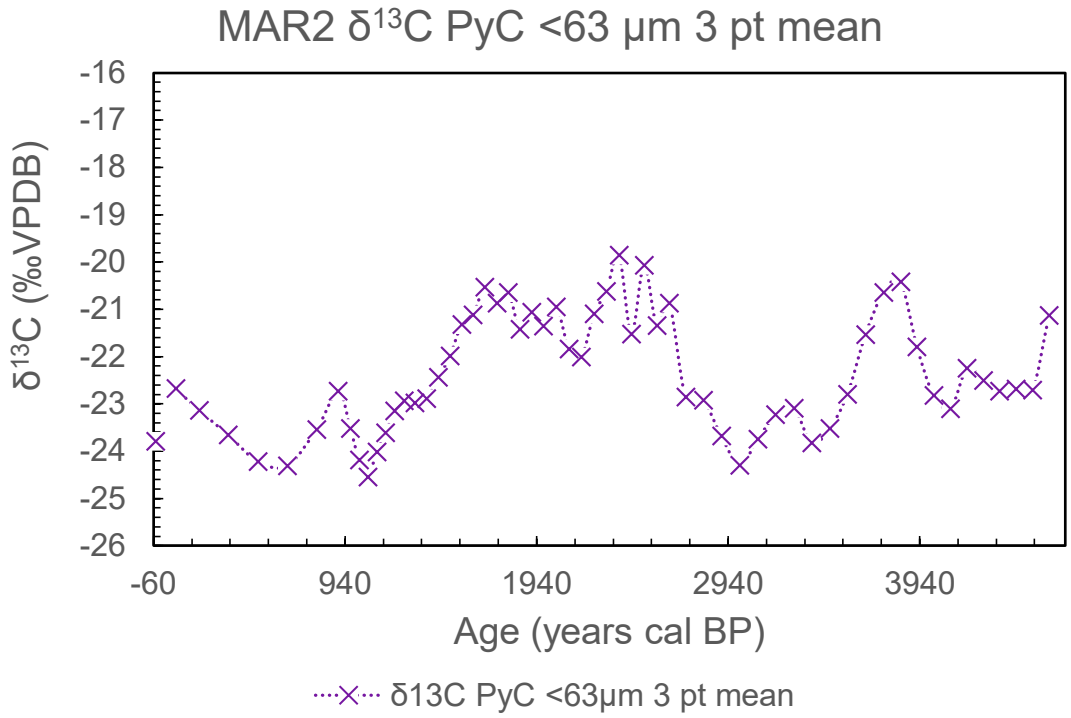

Figure 5.36: 3 point running mean of <63 µm PyC $\delta^{13}C$ for MAR2, by age.

5.5 Discussion

5.5.1 Elemental Composition

5.5.1.1 Mo Ratio and Detritus (MS, all elements)

Mo incoherent/coherent ratio is commonly interpreted as an indicator of organic content (see Davies, Lamb & Roberts 2015 for a summary and review; e.g. Sáez et al. 2009; Liu et al. 2013; Mackenzie et al. 2017) and is interpreted as such in this study. The Marura record shows fluctuations between organic-dominated and detrital-dominated signals; organic content (Mo ratio, as well as total organic carbon) is highest at the top (0 to ~50 cm) and towards the bottom (~160 to 210 cm) of the record, with detritus peaking between ~75 and 110 cm (1900 and ~1300 cal BP, segment U111 1-1.45 m). A change in colour from black to dark brown is visible

in the sediment of this segment and mottling is apparent in the radiograph of U111 coincident with the increased detrital signal (Figure 5.37).

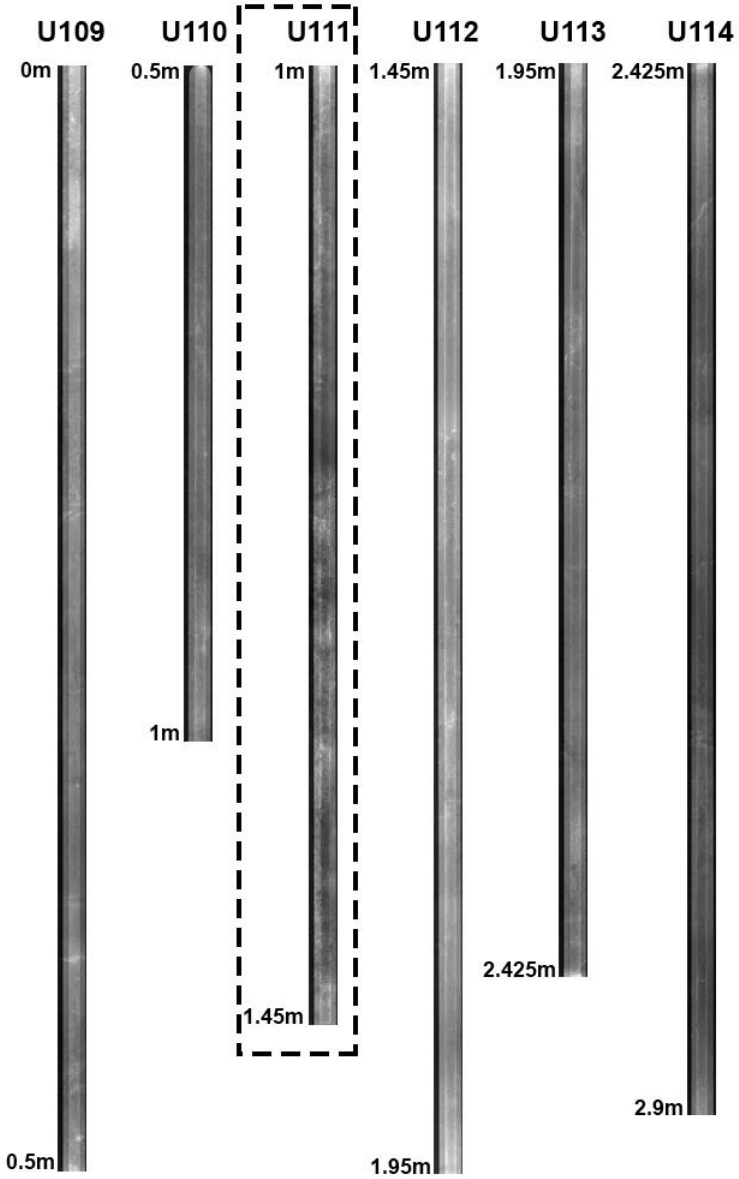

Figure 5.37: Radiographic scans of Marura core segments U109 (0-0.5 m) to U114 (2.425-2.9 m), recorded using Itrax™. Core depths are from measurements collected in the field and may vary from Itrax™ scan lengths. Mottling is visible in core U111 (1-1.45 m), indicated by a dashed box.

The detrital signal for Marura is comprised primarily of elements typically associated with detritus, increased run-off and erosion (see Davies, Lamb & Roberts 2015, pp.194-197); these elements are Si, K, Ca, Ti, Mn, Fe, Rb and Sr. While magnetic susceptibility (MS) and P are strongly positively correlated to each other in the top 3 m of the record ($r^2 = 0.98$) and cluster with the detrital elements in the principal components analysis (see Figure 5.18, plot b), both display weak positive correlations to the other detrital elements (maximum r^2 value of between 0.52 and 0.53 with Sr). This suggests that while increased magnetic susceptibility and P content occur during the identified detrital phase, these variables are not closely connected to the primary suite of detrital elements.

The primary detrital elements in this record are well documented as indicators of detrital input. K, Ti, Rb and Fe are associated with clays and detritus (Croudace et al. 2006; Davies, Lamb & Roberts 2015; Kylander et al. 2011; Mackenzie et al. 2017). Sr and Ca are indicative of silicate and carbonate weathering or authigenic precipitation (Cohen 2003; Lobb 2015; Mackenzie et al. 2017), and Ca/Ti and Sr/Ti are used to separate detrital Ca and Sr from biogenic/authigenic processes (Figure 5.39; Davies, Lamb & Roberts 2015; Fletcher et al. 2015; Kylander et al. 2011; Liu et al. 2013; Mackenzie et al. 2017). Similarly, Si may be detrital or the result of biogenic/authigenic processes and Si/Ti is commonly used to isolate the authigenic component (Cohen 2003; Croudace et al. 2006; Davies, Lamb & Roberts 2015; Liu et al. 2013; Mackenzie et al. 2017; Moreno et al. 2008; Sáez et al. 2009); analysis of this ratio is unnecessary in the Marura record as Si levels are negligible throughout the core excepting the detrital period at ~75-110 cm, indicating a detrital source of Si. Ca also appears primarily detrital during the ~75-110 cm section of the core, with biogenic/authigenic Ca elsewhere in the core and peaking in the upper ~75 cm (see Figure 5.38). Sr is predominantly biogenic/authigenic, with additional detrital Sr during the detrital phase.

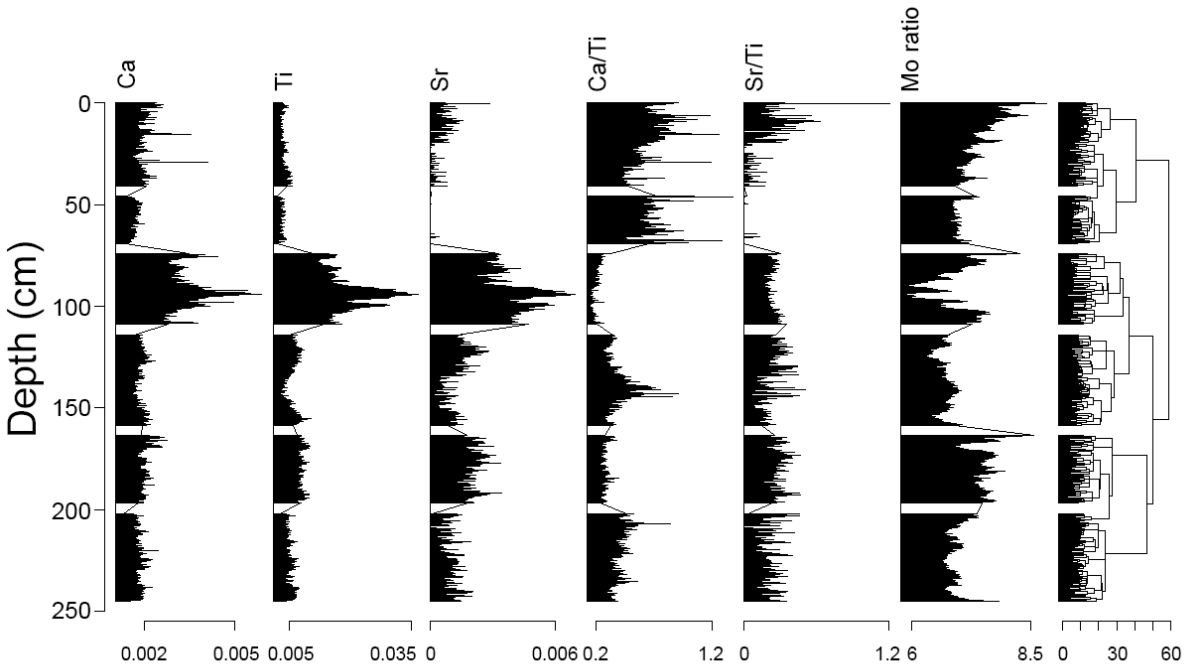

Figure 5.38: Selected normalized element counts and element ratios mentioned in the text from Itrax™ elemental data for MAR2 0-2.9 m, by depth.

Mn is commonly interpreted as an indicator of oxygenation of bottom waters, redox conditions and overall lake levels (Burn & Palmer 2014; Davies, Lamb & Roberts 2015; Kylander et al. 2011; Martin, Mooney & Goff 2014), but has also been used as an indicator of redox-sensitive detritus (Moreno et al. 2008) and wetland productivity (Mackenzie et al. 2017). Mn is identified by Plumb and Roberts (1967, p.18) as present in the soils of Blue Mud Bay, first recorded in 1803 by Matthew Flinders on Groote Eylandt. Mn appears in this record to be primarily derived from a detrital source, with strong positive correlations to many other detrital elements (maximum $r^2 = 0.757$ with Ca).

In summary, phases in the MAR2 record dominated by an organic signal occurred between ~4000 and ~2600 cal BP, concurrent with high charcoal flux, and from ~1000 cal BP to the present. Detrital input at Marura peaked between ~1900 and ~1300 cal BP.

5.5.2 Charcoal and Pyrogenic Carbon

Charcoal and PyC flux in all size fractions are highest in the earlier part of the MAR2 record (~4600 to ~1900 cal BP), decreasing progressively to 1000 cal BP followed by minimal flux until the last century. Trends are similar between the size fractions, particularly between the charcoal sizes (>250 µm, 250-125 µm and 125-63 µm) as well as between 125-63 µm charcoal flux and <63 µm PyC flux (see Figure 5.32). In detail, PyC flux values do not correspond closely with the equivalent charcoal flux values, with variation in the timing of peaks and troughs displaying an almost inverse relationship in some parts of the record. This is the result of different fire intensities as the proportion of pyrogenic carbon to charcoal increases with increasing intensity. This is supported by charcoal area measurements for the largest size fraction (>250 µm), which would correlate strongly with bulk PyC flux if these PyC peaks were the product of large charcoal pieces (Figure 5.39). These measures show similar trends between ~3700 and 2600 cal BP (shown in Figure 5.39 by a dashed grey bounding box) but display inverse trends for the rest of the record.

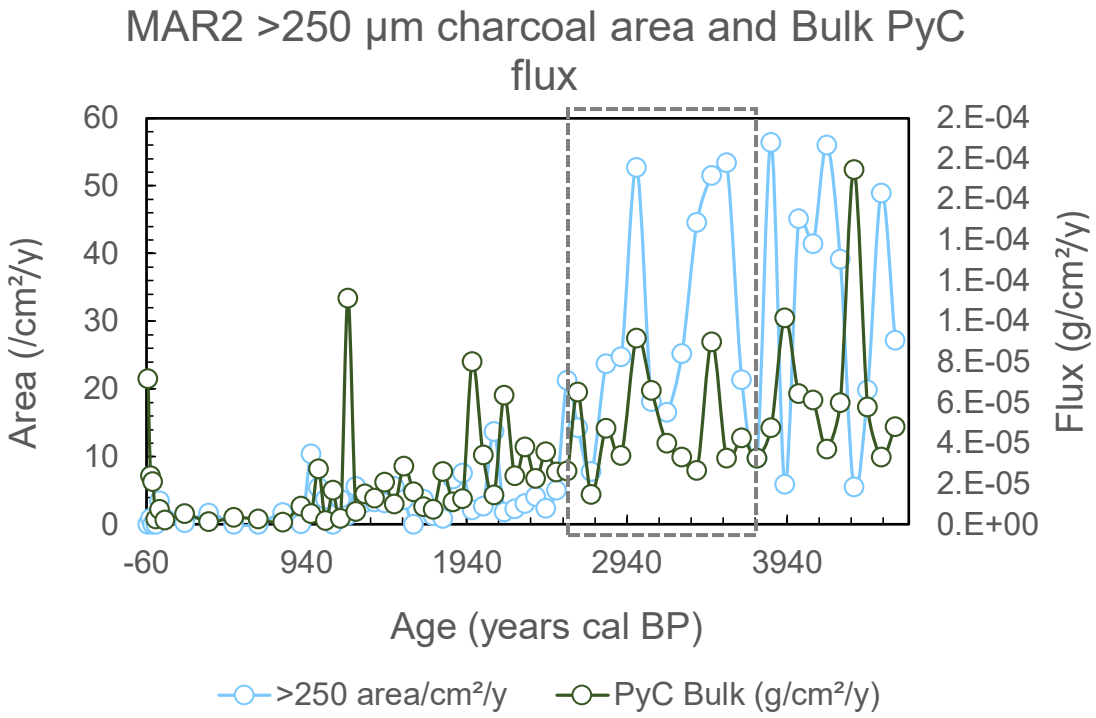

Figure 5.39: >250 µm charcoal area measurements and bulk PyC flux for MAR2, by age. Similar trends occur from ~3700-2600 cal BP, indicated by a dashed grey bounding box.

Marura has been less directly and extensively affected by European colonisation or land use than sites such as Big Willum Swamp (see Chapter 6) but has been influenced indirectly. Arnhem Land was under pastoral lease in the late 19th century, and this combined with missions established in the early 20th century reduced Indigenous populations in the region via genocide, displacement and relocations (see Chapter 3; Cole 1982). Therefore, it is expected that the MAR2 charcoal and PyC record reflects changes caused by European arrival, most likely in the form of Indigenous fire management practices being removed over the last century. This appears as a peak in charcoal and PyC fluxes from ~1950 CE.

5.5.2.1 Vegetation Burned

$\delta^{13}C$ depletion of PyC in "fine particle size fractions" is expected in grass-dominated environments as a result of the Stable Isotope Disequilibrium Effect (Saiz et al. 2015, p.1859); however, <63 µm PyC $\delta^{13}C$ is not consistently more or less ^{13}C-depleted than values for the bulk PyC fraction, therefore the Stable Isotope Disequilibrium Effect (SIDE) is not discernible in this record. The range of $\delta^{13}C$ values for both sizes (-17 to -25 ‰ for both, with bulk primarily falling between -20 and -23 ‰) reflect mixed C_3/C_4 vegetation signals (see O'Leary 1988). The variable relationship between values for the bulk and <63 µm fractions suggests changes to the type of vegetation burned through the record; however, the mechanisms behind this variation are unclear.

Elongate particle percentages from length-width ratios and morphotypes can help elucidate vegetation changes, but these measures are likely affected by sample sizes when charcoal abundance is low. The contribution of elongate particles to charcoal samples is higher at the bottom of the record, decreasing in quantity and increasing in variability through time. It is unclear if this reflects a decrease in grass/elongate vegetation over time or is an artefact of decreasing sample sizes, as charcoal flux similarly decreases towards the top of MAR2.

While all measures agree that mixed grass/wood (C_3/C_4) contribution is present throughout the record, elongate particle percentages from both measures show little correlation with PyC $\delta^{13}C$ values (r^2 values all below 0.1). This likely results from methodological differences, as different size fractions are being measured, a charcoal particle from a C_3 plant may break into elongate pieces, and the $\delta^{13}C$ value of a sample may be dominated by the largest (volume) particle in contains. Sudden changes in bulk PyC $\delta^{13}C$ values could therefore be the result of one or more large charcoal particles in the sample, such as a large piece of burned wood skewing a sample towards a lower value. However, for Marura, area measurements for >250 µm charcoal show no peaks in area corresponding with decreases in bulk PyC $\delta^{13}C$ (Figure 5.40).

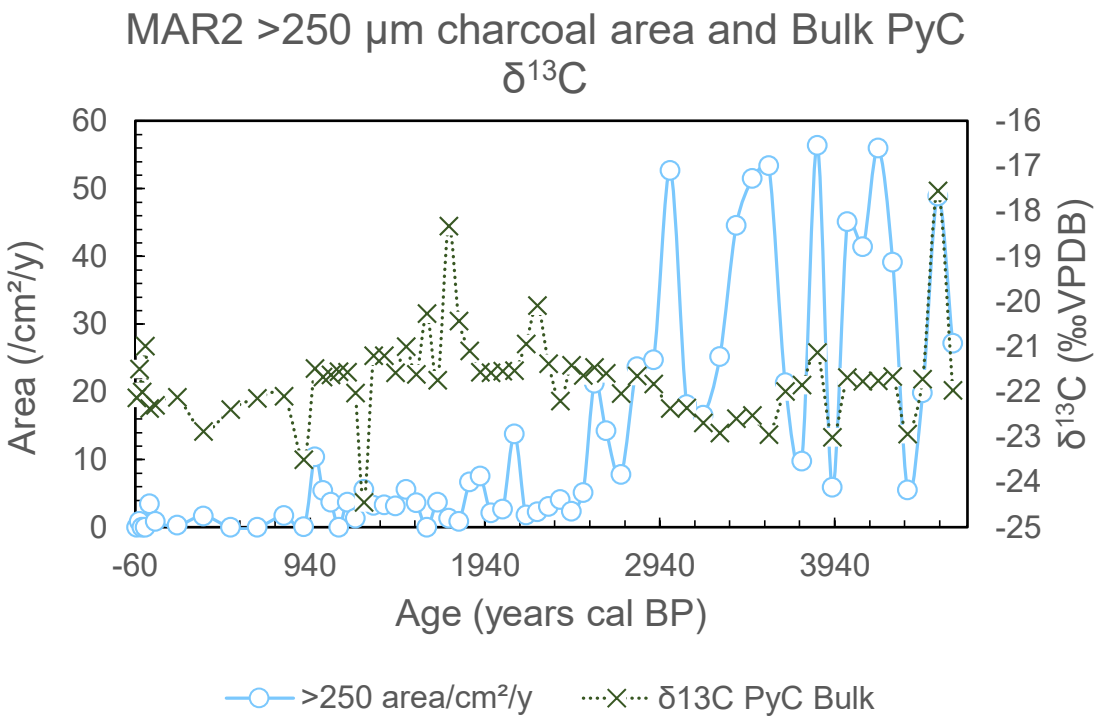

Figure 5.40: MAR2 >250 µm charcoal area and bulk PyC $\delta^{13}C$, by age.

5.6 Conclusion

Charcoal, PyC and elemental composition data for Marura (MAR2) presented in this chapter represent a late Holocene palaeofire record with mixed C_3/C_4 vegetation and decreasing charcoal flux over time. The highest values of charcoal flux and pyrogenic carbon occur between ~4600 and ~2800 cal BP, decreasing thereafter. A slight increase in charcoal and PyC flux values occurs after ~55 cal BP, potentially corresponding to European arrival and Indigenous depopulation in the region; however, this cannot be interpreted with confidence due to the likelihood of sediment mixing in the uppermost 10 cm.

Chapter 6 : Big Willum Swamp

6.1 Introduction

This chapter presents an overview of the land use history, geology, vegetation and current fire regime surrounding Big Willum Swamp, Weipa, Queensland. A methodological overview is provided, followed by results for sedimentary analyses, chronology and fire proxies. Objectives of analysis for this site, linked to the overall research aims of this study presented in Chapter 1, are as follows:

1) The creation of a high resolution multiproxy late Holocene palaeofire record for Big Willum Swamp
2) Characterisation of vegetation burned in the Big Willum Swamp record, and how it has or has not changed through time
3) Investigation of potential European influence, through Indigenous depopulation and establishment of a bauxite mine, on fire in the Big Willum Swamp record

Big Willum Swamp was selected for analysis as it is a perennially wet water body in a region (northern Cape York Peninsula) lacking in palaeoenvironmental records. Big Willum Swamp is the only site presented in this thesis that has previously been studied and thus may demonstrate the interpretive power and insights gained by a multiproxy approach compared directly to the existing record that utilises charcoal counts only.

6.2 Site Description

Big Willum Swamp (12.657°S, 141.998°E) (also known as Willem Swamp or Waandriipayn; Stevenson et al. 2015) is located within the active Rio Tinto bauxite mine in East Weipa, western Cape York Peninsula (Figure 6.1). The swamp is approximately 250 metres west-southwest to east-northeast by 600 metres north-northwest to south-southeast, and is classified as a palustrine system (Department of Environment & Science 2018a). The geophysics team was not present during fieldwork at this site, therefore resistivity data is not available for Big Willum Swamp.

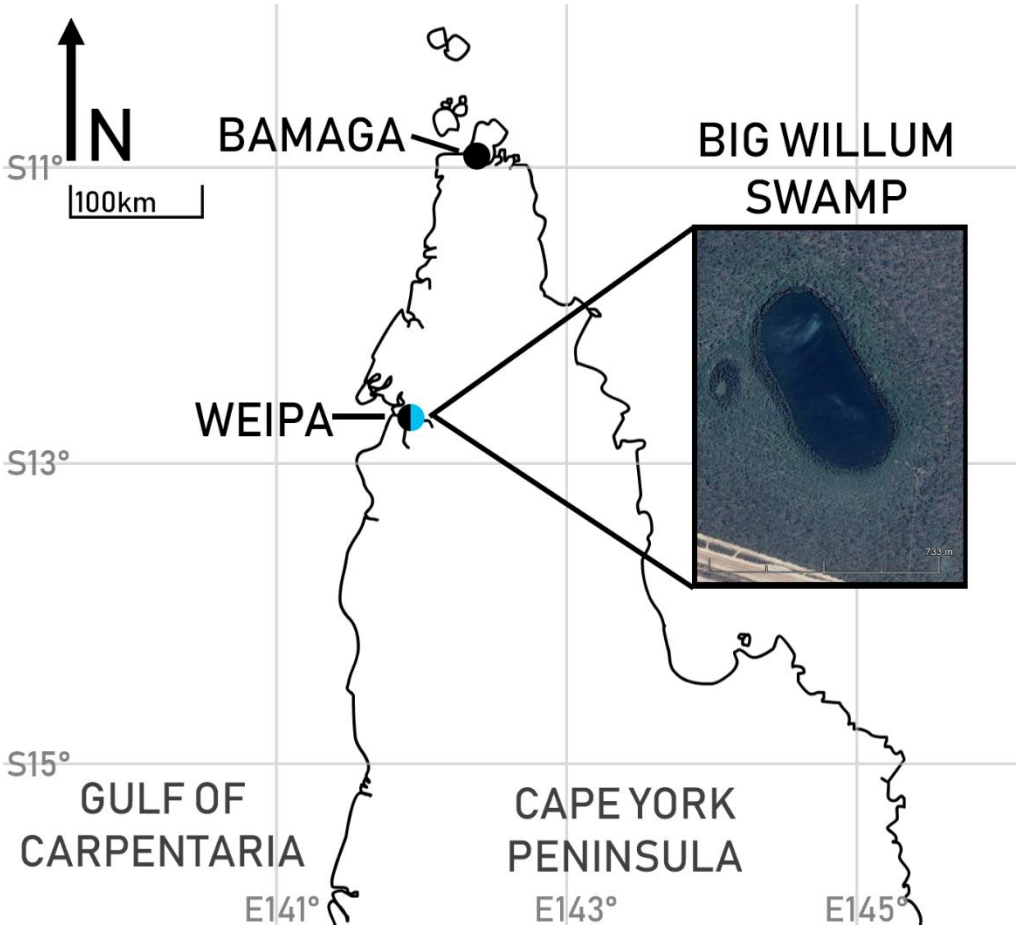

Figure 6.1: Location of Big Willum Swamp (inset after Google Earth 2018a).

Big Willum Swamp is the only site in this study that has been previously researched; Stevenson et al. (2015) present a palaeoenvironmental record for the site comprising pollen and charcoal (macro- and microscopic) data along with a radiocarbon chronology (Figure 6.2) while Proske et al. (2017) present a diatom record.

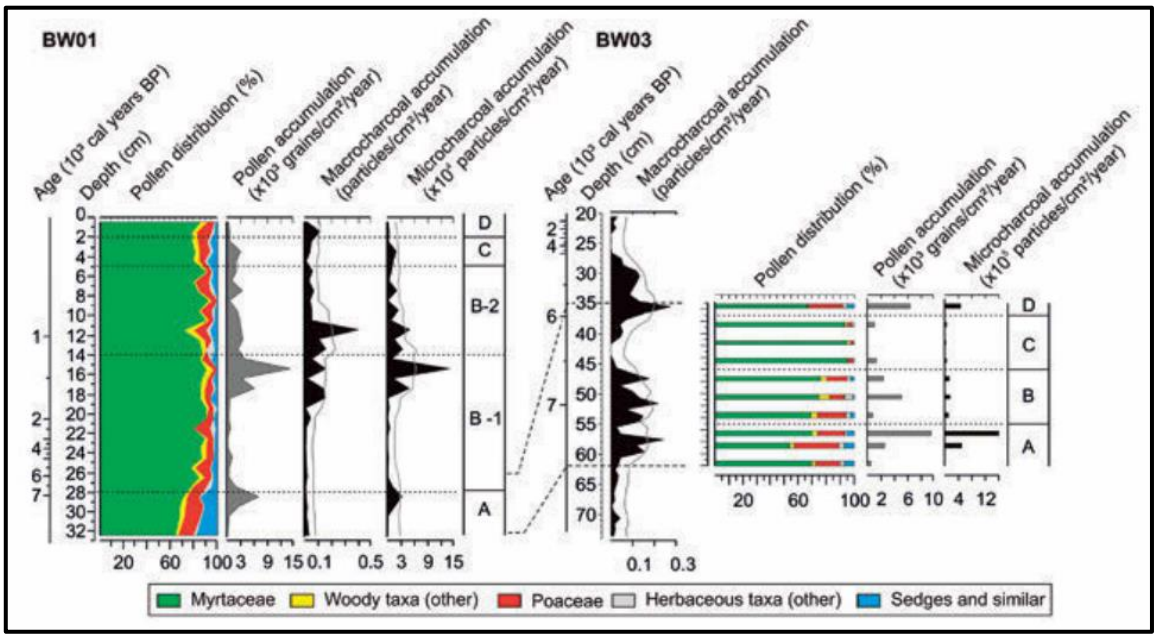

Figure 6.2: Charcoal and pollen diagram for Big Willum Swamp cores BW01 and BW03 from Stevenson et al. (2015).

Big Willum Swamp is at 28 m elevation, with a recorded maximum water depth of 3.5 m during fieldwork in July 2017. Most of the swamp is perennially wet (Figure 6.3).

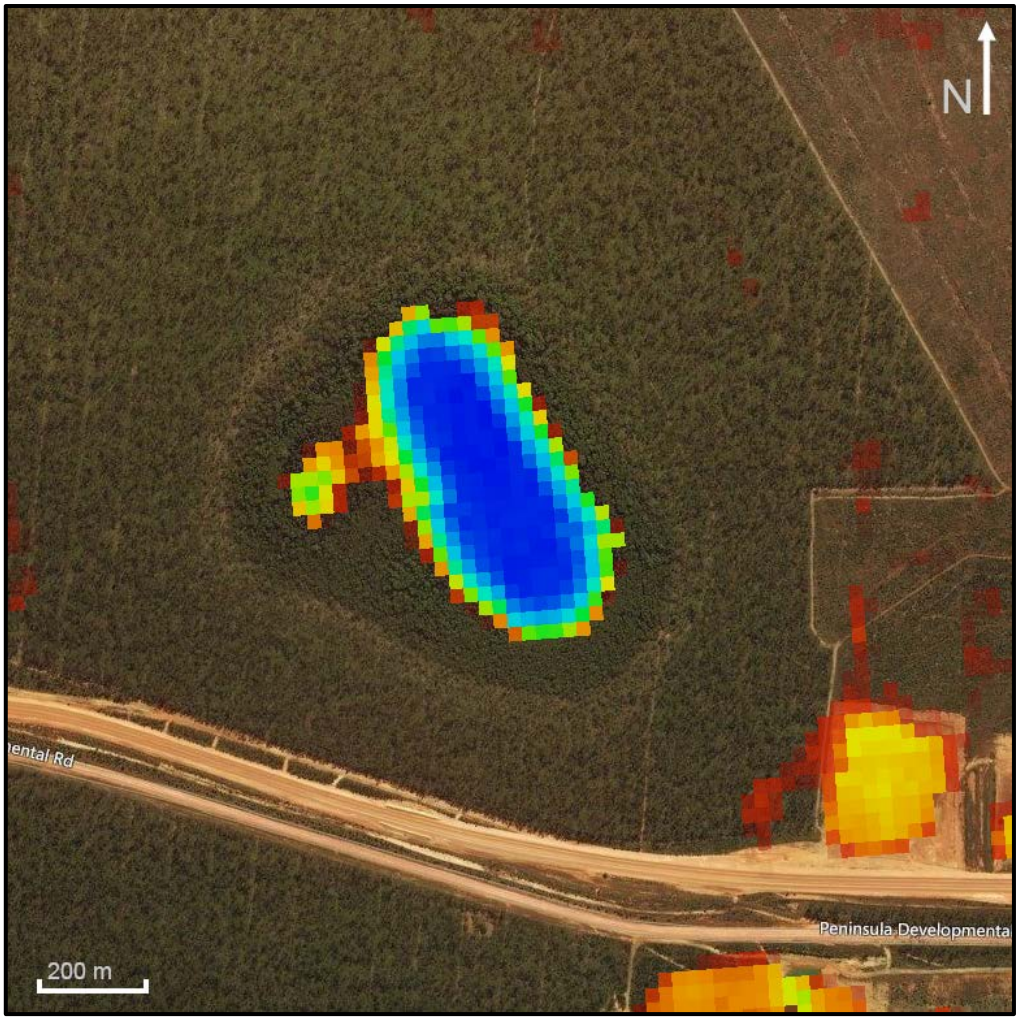

Figure 6.3: Big Willum Swamp water permanence derived from LANDSAT imagery for the period 1970-2018 (after Geoscience Australia 2018; Department of the Prime Minister & Cabinet 2019). Dark blue indicates >90 % water permanence over the observation period.

The swamp is surrounded by terrain with limited (~10 m) elevation changes and therefore the swamp has a small approximate catchment area of 0.75 km^2 (Figure 6.4).

Figure 6.4: Digital elevation map of Big Willum Swamp and surrounds, with the approximate catchment area of the swamp marked in orange (after Geoscience Australia 2015).

6.2.1 Land Use History

The Traditional Owners of the area including Big Willum Swamp are the Peppan people (Stevenson et al. 2015). Archaeological surveys and studies have identified stone surface scatters, earth mounds, scarred trees and shell mounds in the Weipa area and dating of these features suggests Indigenous occupation to have begun by ~2700 cal BP with intensification after ~1000 cal BP (Morrison 2014; Shiner & Morrison 2009; see Chapter 3). The archaeology includes "hundreds of archaeological and culturally important sites" surrounding the Wathayn

Outstation (Shiner et al. 2013, p.69) approximately four kilometres south of Big Willum Swamp. These sites incorporate numerous shell mounds, and a group of five identified earth mounds (Shiner et al. 2013; Shiner & Morrison 2009, p.53). The establishment of earth mounds near freshwater sources suggests "diversification of the economy away from the coast" beginning ~2200 cal BP (Brockwell et al. 2016, p.6), while the *Tegillarca* shell mounds represent episodic, seasonal gatherings of large groups of people during this period (Morrison 2003, pp.4-5). The varying height, shape, cluster size and location type of these shell mounds indicates that "significant variation existed in the nature of the *Tegillarca* gatherings over a long period" (Morrison 2003, p.5).

The European settlement of Weipa began with a Presbyterian mission on the Embley River, established in 1898 and officially named Weipa Mission in 1899 (Queensland Government 2017a; Weipa Town Authority 2014). Bauxite mining at Weipa began with the establishment of "Top Camp" at Munding in 1956 after the discovery of economic bauxite deposits the year prior (Weipa Town Authority 2014). Construction of the mining township of Weipa (known as Weipa North) was begun by Comalco (Commonwealth Aluminium Corporation) in 1964, with the township officially declared in 1967 (Weipa Town Authority 2014). The former Weipa Mission community, renamed Weipa South (1965) and later Napranum (1990), was transferred to the trusteeship of the Weipa South Aboriginal Council under a Deed of Grant in Trust in 1988 (Queensland Government 2017a). The Western Cape Communities Co-existence Agreement was signed in 2001 by Comalco, the communities of Aurukun, Mapoon, Napranum and New Mapoon, the Cape York Land Council, the Queensland Government and eleven Traditional Owner groups (Weipa Town Authority 2014). Comalco was renamed Rio Tinto Aluminium in 2006 (Weipa Town Authority 2014). Mining leases in the Weipa area span 3860 km^2, which includes currently active mining areas and land in various stages of rehabilitation (Rio Tinto 2017).

Aerial photographs combined with satellite imagery show minor changes to the overall size and shape of Big Willum Swamp since 1969, including a contraction of the swamp in 2005 to approximately 200 metres by 530 metres and subsequent re-expansion by 2013 (Figure 6.5). These images demonstrate that drying and shrinkage of the edges of Big Willum have occurred previously, while the centre of the swamp has remained perennially wet. This is demonstrated by water observations from space (see Figure 6.3 above).

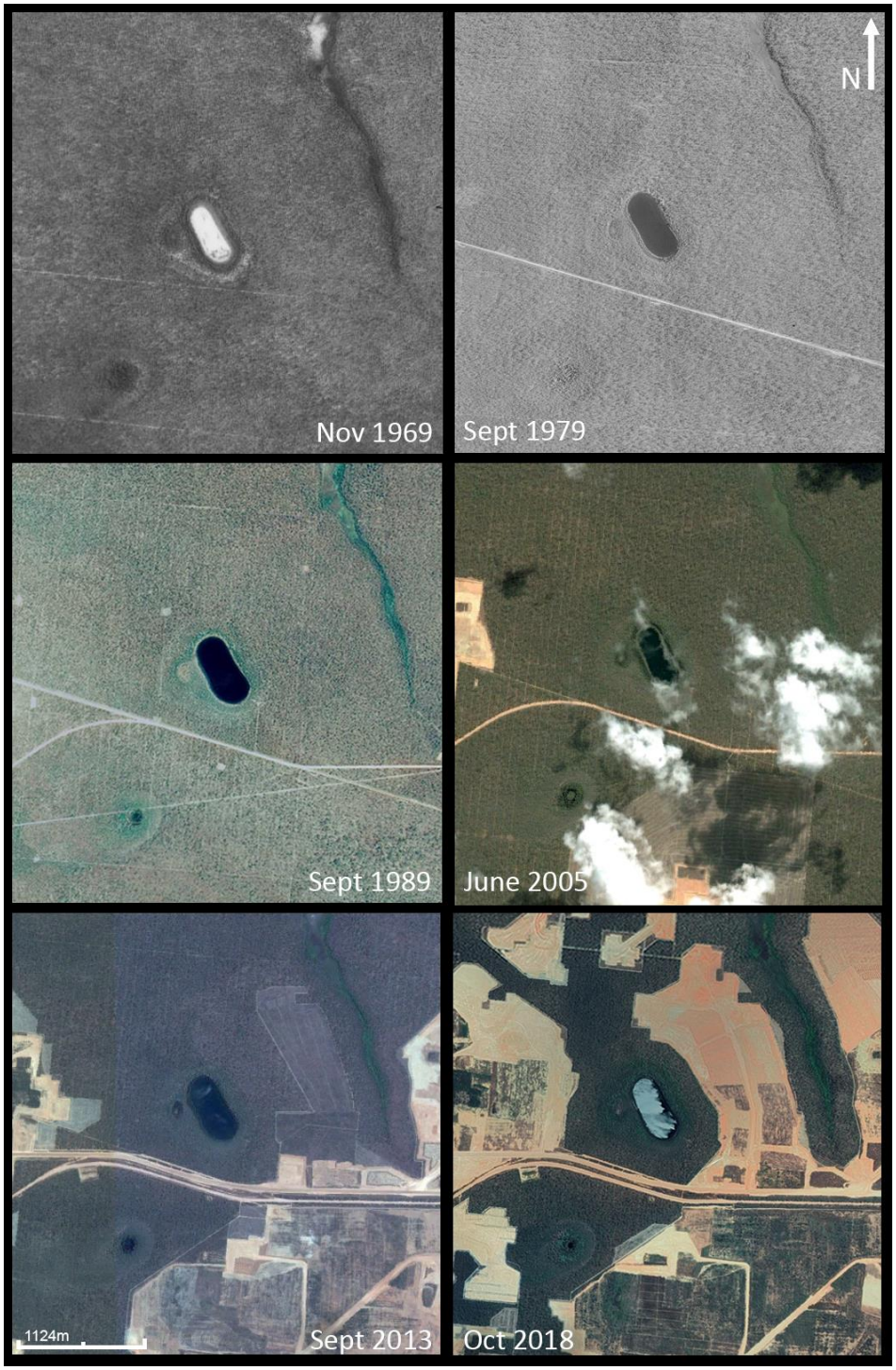

Figure 6.5: Aerial and satellite images of Big Willum Swamp (after Google Earth 2018a; Queensland Government 2019).

Aerial and satellite imagery also record the development of mining operations near Big Willum, beginning with small linear tracks across the 1969 image and proceeding to the creation of a road visible in the 1979 photograph, approximately 330 metres south of the water's edge (currently known as the Peninsula Developmental Road). Additional roads are visible in the 1989 image, and cleared vegetation associated with the active bauxite mine appears in the 2005 image. Vegetation clearing related to mining activities significantly expands in the 2013 and 2018 images.

6.2.2 Environment

6.2.2.1 Climate

The climate of Big Willum Swamp is classified as AW – Tropical/Equatorial Savanna with dry winter under the global Köppen-Geiger Climate Classification (Peel, Finlayson & McMahon 2007; Kottek et al. 2006). Mean annual rainfall is 1784.9 mm measured from the nearest weather station (Weipa Eastern Ave, approximately 13 km away), primarily (~95 %) occurring between November and April (BOM 2018d). Winds are low speed and multi-directional in January and predominantly from the southeast in July (BOM 2018d) (Figure 6.6). Average minimum and maximum daily temperature ranges from 18.8 °C and 34.8 °C, in August and October respectively (BOM 2018d). Mean relative humidity measured at 9 am varies between 66 % (October) and 87 % (February) (BOM 2018d).

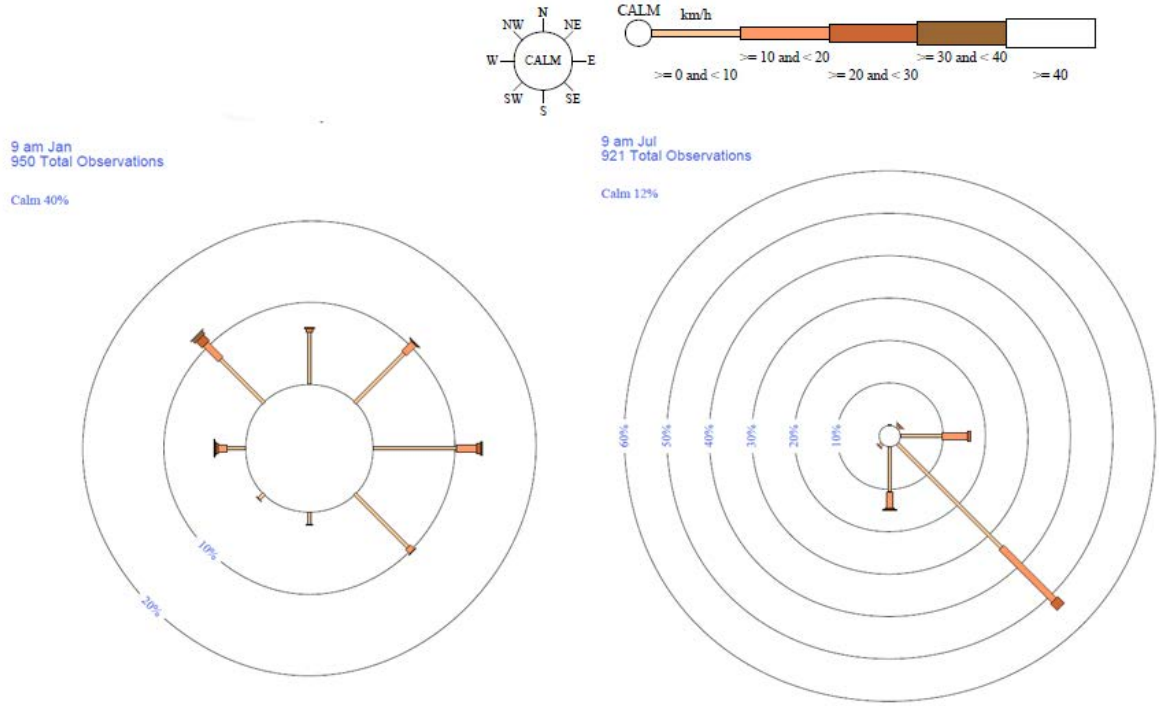

Figure 6.6: Average wind direction and speed 1959-1994, measured at 9am in January (left) and July (right), from Weipa Eastern Ave (after BOM 2018d).

In the period 1969-2016, 14 cyclones passed within 50 km of Big Willum and 22 passed within 100 km (BOM 2018a). Lightning cloud-to-ground flash density in Weipa and surrounds is between 2 to 3 flash/km^2/year, primarily occurring between November and April (BOM 2016a).

6.2.2.2 Geology and Vegetation

The Weipa region is comprised of three major physiographic units; from the ocean to inland these are the Mapoon Plain, the Weipa Plateau and the Merluna Plain (Cameron & Cogger 1992, p.5). Big Willum Swamp is located on the Weipa Plateau, which is overlain by "Quaternary and Tertiary aluminous laterite, including bauxite and the 'ironstone' below it"

(Bureau of Mineral Resources, Geology & Geophysics 1976). Biggs and Phillip (1995, p.14) identify this laterite as eroded remnants of the Bulimba sandstones, overlying the Rolling Downs Group. Big Willum Swamp in its current state was formed from the collapse of this underlying laterite karst (see Grimes & Spate 2008). Dominant soils in the surrounding area are "deep loamy yellowish red earths that are pisolitic (bauxitic)", with "neutral soils" as well as "acid forms" present (Mu17: Gn2.15, Gn2.14) (Northcote et al. 1960-1968).

The principal habitat on the Weipa Plateau is open woodland, occurring on "deep well-drained loamy or sandy soils" (Cameron & Cogger 1992, p.6). The vegetation surrounding Big Willum Swamp is clearly representative of this broader habitat type. The site is surrounded by open *Eucalyptus* woodland, dominated by *Eucalyptus tetrodonta* with *Corymbia nesophila* codominant, and low trees of *Grevillea glauca*, *G. parallela* and *Erythrophleum chlorostachys* (Figure 6.7; Neldner et al. 2017:108-9). There is a sparse, poorly developed shrub layer including *Coelospermum* and *Persoonia* (Cameron & Cogger 1992, p.6; Neldner et al. 2017, p.109), and a "mid-dense" ground layer of grasses dominated by *Heteropogon*, *Sarga* and *Alloteropsis* (Neldner et al. 2017, p.109; see also Figure 6.7).

Figure 6.7: *Eucalyptus* woodland vegetation at Big Willum Swamp. Left image from near the waterline of Big Willum Swamp (southern edge, looking west), showing the high water mark from the last wet season. Right image shows the grassy understorey on the southern side of Big Willum Swamp, beyond the most recent high water mark (photos taken July 2017).

Melaleuca (paperbark) woodland is present as a fringing community, dominated by *Melaleuca* species (e.g. *M. viridiflora*) with an undergrowth of sedges and grasses, merging landward into bare ground "covered by a layer of black-stained leaf litter" (Figure 6.8; Cameron & Cogger 1992, p.7).

Aquatic vegetation of Big Willum Swamp includes *Eleocharis* sedges and *Nymphaea* water lilies (see Figure 6.8). Submerged aquatic algae (unidentified) forms a thick covering of vegetation over the sediment (see Sample Collection below).

Figure 6.8: *Melaleuca* woodland at the southern waterline of Big Willum Swamp (left) and aquatic vegetation (right) of Big Willum Swamp (looking towards the southern shore).

6.2.2.3 Fire

In the 18 year period spanning 2000-2018 the area surrounding Big Willum burned on average every 2 to 6 years (every year at its most frequent) (Figure 6.9; NAFI 2019). However, some areas beyond the catchment of Big Willum were not burned at all during this period, likely due to mining activities and mining-related land clearance. Fires in the period 2000-2018 were primarily between July and October, with the earliest scar occurring in June 2016 on the southern margin of the swamp (NAFI 2019; see also Figure 6.7). Winds during these months are predominantly from the east to southeast; charcoal transported to Big Willum Swamp during these months would derive from land extensively modified by and cleared of vegetation for mining activities between 2005 and 2012 (as visible in satellite imagery).

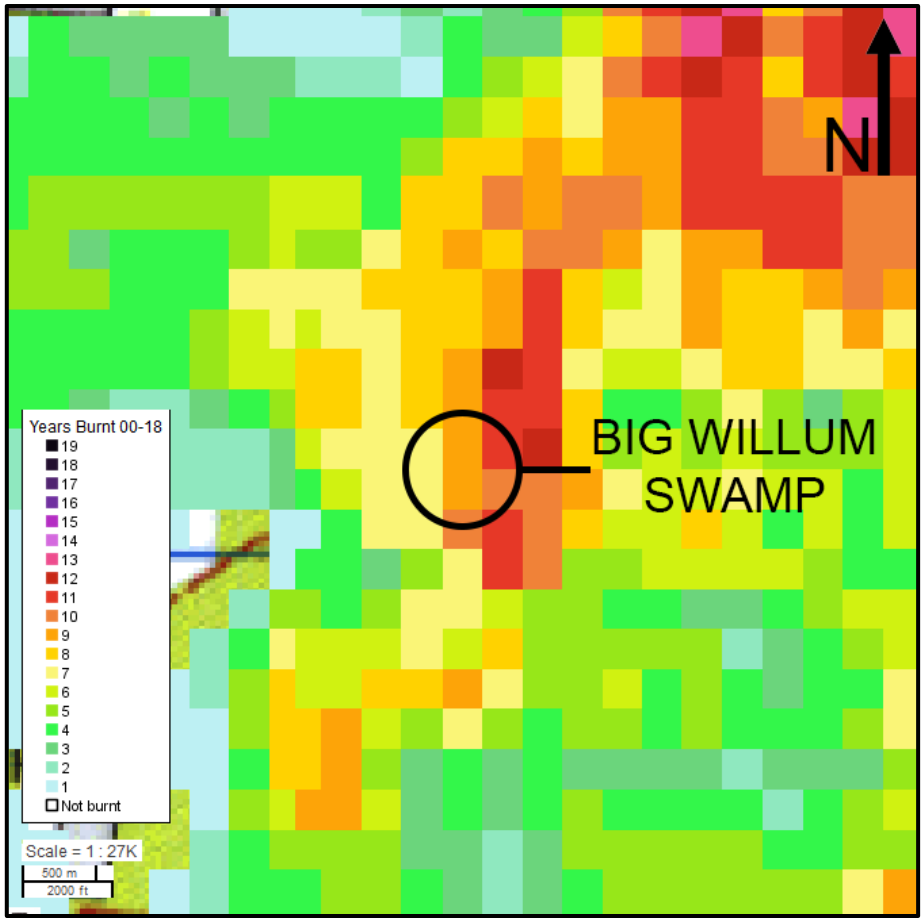

Figure 6.9: Number of years that areas around Big Willum Swamp burned 2000-2018 (after NAFI 2019).

6.3 Methods

6.3.1 Sample Collection

Samples were collected from Big Willum Swamp during fieldwork in July 2017. Sediment cores were collected using a raft-mounted hydraulic corer modified using Eijkelkamp equipment. Two cores were collected: BWIL1, a test core from 0-1 m, and BWIL2 covering 0-3 m. Surface samples were unable to be collected via grab sampler due to dense aquatic algae covering the water-sediment interface.

6.3.2 Laboratory Analyses

Laboratory methods and justification for the choice of methods are described in detail in Methods (Chapter 4). For Big Willum, core BWIL2 was selected for study as BWIL1 was a test core that covered only the top metre of sediment. As per Chapter 4, the core was divided for optical charcoal analysis (Courtney Mustaphi & Pisaric 2014; Enache & Cumming 2006; Stevenson and Haberle 2005) and chemical analysis (freeze-dried bulk and <63 μm samples; Wurster et al. 2012).

Sediment slices from the top metre of BWIL2 were analysed in an Itrax™ Elemental Core Scanner at the Australian Nuclear Science and Technology Organisation (ANSTO) Lucas Heights campus, as also detailed in Chapter 4. It was not possible to successfully remove slices of the 1-2 m or 2-3 m segments of BWIL2 for analysis by Itrax™ due to the dense, clay-rich texture of the sediment that crumbled during attempted sampling.

^{210}Pb sample preparation and analysis by alpha spectrometry and ^{14}C sample preparation and analysis by accelerator mass spectrometry were undertaken at ANSTO Lucas Heights on samples from BWIL2 as per the procedures outlined in Chapter 4.

6.4 Results

6.4.1 Sediment Descriptions

Munsell colour descriptions were determined using slices after ITRAX scanning and subsequently may have been affected by thawing, refreezing and drying. The top 7.5 cm was identified during core slicing and sampling to be composed primarily of moisture with minimal sediment, and subsequently sampling began at 7.5 cm (referred to thereafter as 0). BWIL2 0-0.5 m is 7.5YR – 3/1 Very dark grey with no discernible stratigraphy, before transitioning

abruptly in 0.5-1 m to 10YR – 5/2 Greyish brown (Figure 6.10). There is a second transition at ~0.585 m to 10YR – 7/1 Light grey denser, clay-rich sediment.

Figure 6.10: BWIL2 0-0.5 m (top) and 0.5-1 m (bottom) slice optical images captured by Itrax™ (top of cores on left, bottom on right).

BWIL2 sediments have the lowest moisture content of the three sites (Figure 6.11), measured as weight loss of a sample after drying as a percentage of wet sediment weight. Moisture content was only recorded for the top 13 cm of the core, corresponding with sampling for charcoal and hydrogen pyrolysis analysis. Moisture content decreases sharply at 12.5-13 cm where the sediment transitions to paler dense clay.

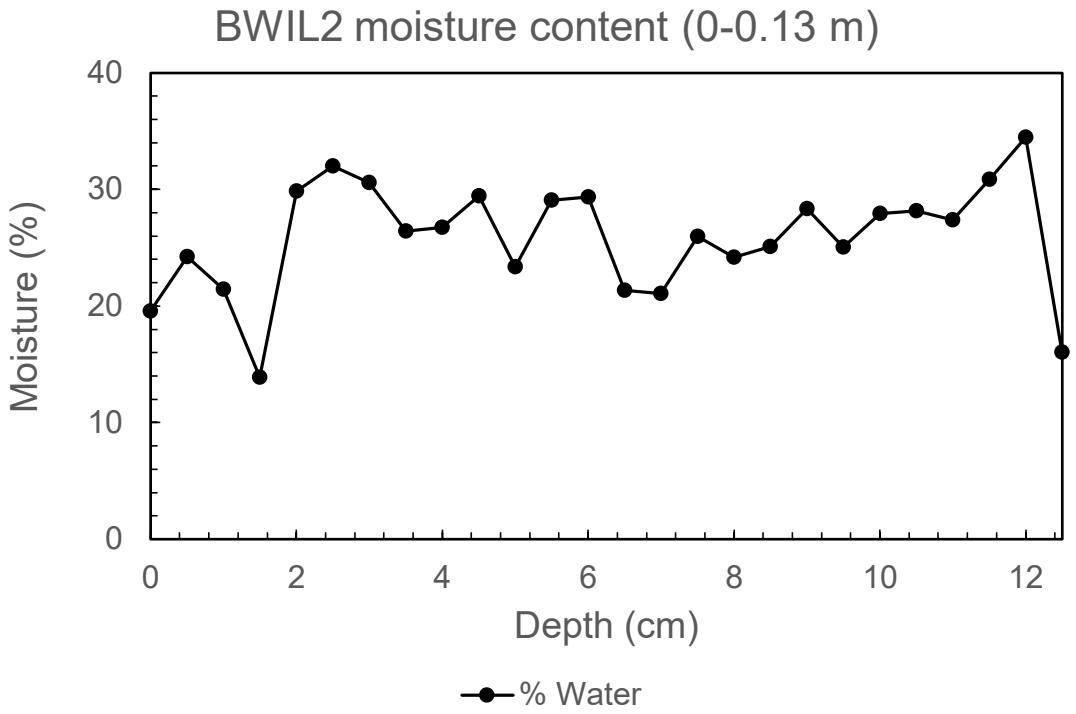

Figure 6.11: Moisture content for the top of BWIL2 (0-0.13 m).

6.4.2 Chronology

6.4.2.1 Lead-210 (^{210}Pb) Dating

Samples analysed by alpha spectrometry displayed a decreasing profile with depth of unsupported ^{210}Pb between 0 and 7 cm before reaching background levels (Table 6.1, Figure 6.12). Constant Initial Concentration (CIC) and Constant Rate of Supply (CRS) models are in close agreement, with sediment at 6.5-7 cm dated to 142 ± 11 or 164 ± 42 years.

Table 6.1: ^{210}Pb by alpha spectrometry results for BWIL2 samples; columns highlighted in red are mentioned in the text. Dates are presented as years prior to the collection date (2017)

ANSTO ID	Depth (cm)	Dry Bulk Density (g/cm^3)	Cumulative Dry Mass (g/cm^2)	Count Date	Total ^{210}Pb (Bq/kg)	Supported ^{210}Pb (Bq/kg)	Unsupported ^{210}Pb Decay corrected to 03-Oct-17 (Bq/kg)	Calculated CIC Ages (years)	Calculated CRS Ages (years)	CRS model Mass Accumulation Rates (g/cm^2/year)
U090	0.0 - 0.5	1.21	0.3 ± 0.3	06-Oct-17	193 ± 16	29 ± 6	164 ± 17	5 ± 5	4 ± 2	0.068 ± 0.005
U093	1.5 - 2.0	1.25	2.1 ± 0.3	06-Oct-17	99 ± 5	26 ± 3	73 ± 6	35 ± 6	32 ± 3	0.065 ± 0.007
U094	2.0 - 2.5	1.26	2.8 ± 0.3	06-Oct-17	83 ± 4	24 ± 3	59 ± 5	46 ± 6	42 ± 3	0.058 ± 0.007
U095	2.5 - 3.0	1.27	3.4 ± 0.3	06-Oct-17	91 ± 4	30 ± 4	61 ± 6	56 ± 6	56 ± 3	0.037 ± 0.005
U096	3.0 - 3.5	1.29	4.0 ± 0.3	06-Oct-17	42 ± 2	20 ± 2	22 ± 3	67 ± 7	69 ± 5	0.068 ± 0.012
U097	3.5 - 4.0	1.29	4.7 ± 0.3	06-Oct-17	39 ± 2	18 ± 2	21 ± 3	77 ± 7	80 ± 4	0.050 ± 0.009
U098	4.0 - 4.5	1.27	5.3 ± 0.3	06-Oct-17	51 ± 3	35 ± 4	16 ± 5	88 ± 8	93 ± 10	0.044 ± 0.013
U099	4.5 - 5.0	1.30	6.0 ± 0.3	06-Oct-17	44 ± 2	36 ± 4	8 ± 4	99 ± 9	106 ± 18	0.062 ± 0.029
U530	5.0 - 5.5	1.30	6.6 ± 0.3	02-May-18	42 ± 2	36 ± 3	6 ± 4	109 ± 9	116 ± 24	0.062 ± 0.021
U534	6.5 - 7.0	1.30	8.6 ± 0.3	10-May-18	41 ± 2	37 ± 4	3 ± 4	142 ± 11	164 ± 42	0.023 ± 0.015
U532	5.5 - 6.0	1.30	7.3 ± 0.3	10-May-18	41 ± 3	43 ± 4	Not detected			
U533	6.0 - 6.5	1.30	7.9 ± 0.3	10-May-18	43 ± 2	54 ± 5	Not detected			
U531	7.0 - 7.5	1.30	9.2 ± 0.3	02-May-18	40 ± 2	23 ± 2	17 ± 3			
U100	7.5 - 8.0	1.33	9.9 ± 0.3	06-Oct-17	34 ± 2	23 ± 2	11 ± 3			
U101	9.5 - 10.0	1.39	12.6 ± 0.3	06-Oct-17	33 ± 1	30 ± 3	4 ± 3			

.

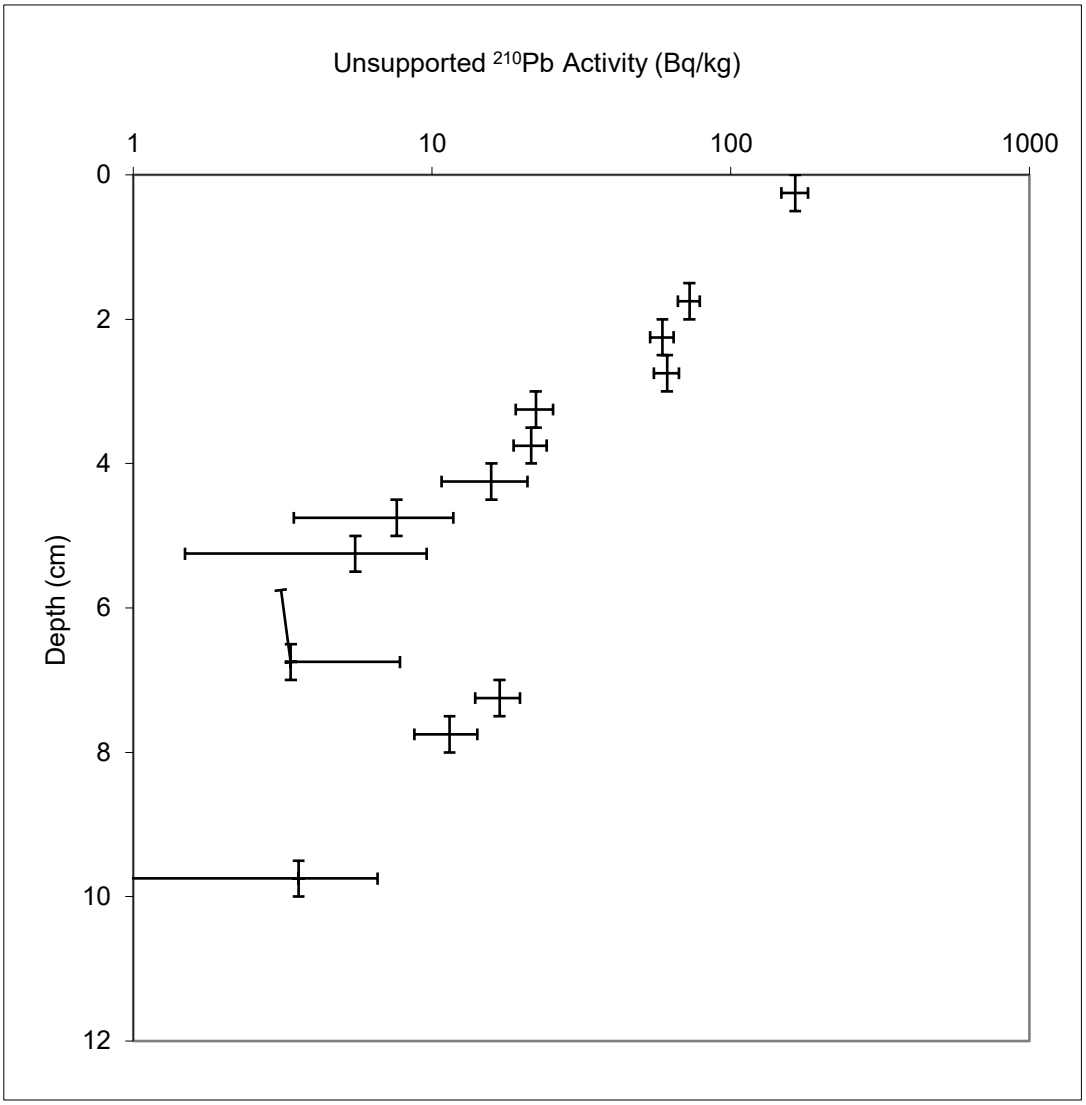

Figure 6.12: Unsupported ^{210}Pb activity by depth for BWIL2.

6.4.2.2 Carbon-14 (^{14}C) Dating

Samples analysed by accelerator mass spectrometry for ^{14}C dating display increasing age with depth, ranging from 760 ± 20 years BP at 5-5.5 cm to 3495 ± 30 years BP at 12-12.5 cm depth (uncalibrated radiocarbon ages) (Table 6.2).

Table 6.2: ^{14}C by accelerator mass spectrometry dates for BWIL2 samples.

ANSTO Code	Sample Type	ID	δ(^{13}C) ‰	% modern carbon	Conventional radiocarbon age
				pM C 1σ error	yrs BP
OZX211	Bulk sediment	BWIL2 5-5.5cm	-18.9 ± 0.1	90.95 ± 0.22	760 ± 20
OZW504	Bulk sediment	BWIL2 8-8.5cm	-20.5 ± 0.2	84.52 ± 0.21	1,350 ± 20
OZW505	Bulk sediment	BWIL2 9-9.5cm	-18.9 ± 0.1	82.30 ± 0.33	1,565 ± 35
OZW506	Bulk sediment	BWIL2 10-10.5cm	-18.6 ± 0.1	80.10 ± 0.28	1,780 ± 30
OZW507	Bulk sediment	BWIL2 11-11.5cm	-18.0 ± 0.1	67.33 ± 0.30	3,175 ± 40
OZW508	Bulk sediment	BWIL2 12-12.5cm	-18.8 ± 0.1	64.71 ± 0.24	3,495 ± 30

^{210}Pb dates (converted to years BP) and ^{14}C dates were combined to form a Bayesian age-depth model for BWIL2 using the *Bacon* package within *R* (see Blaauw et al. 2019; R Development Core Team 2013) and using the Southern Hemisphere calibration curve SHCal13 (Hogg et al. 2013). Figure 6.13 shows a period of low sediment accumulation between ~12 and 10 cm, covering approximately 2000 years. Low accumulation between 5.5 and 5 cm may be an artefact of the combination of (and transition between) ^{210}Pb and ^{14}C dates.

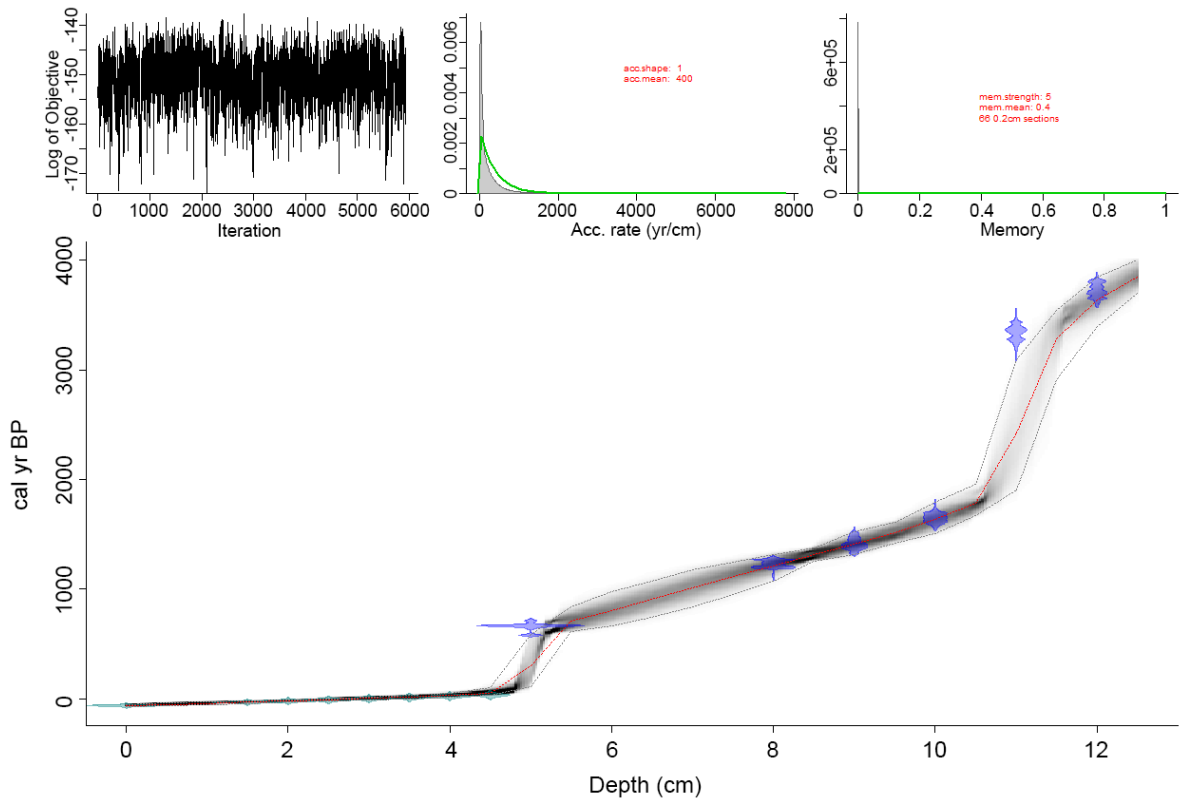

Figure 6.13: Age-depth model for BWIL2 combining ^{210}Pb (green) and ^{14}C (blue) dates.

6.4.3 Itrax™ XRF Scanning

Sediment slices from 0-1 m of BWIL2 were analysed using an Itrax™ Elemental Core Scanner. Elemental counts were normalized by dividing each element count by the incoherent scattering (Mo inc) count for that depth (see Davies, Lamb & Roberts 2015, p.192) (Figure 6.14). As stated in Chapter 4, elements of interest were selected from the list of interpreted elements by Davies, Lamb and Roberts (2015). Elements with consistently fewer than 100,000 counts per second were removed (P. Gadd pers. comm.).

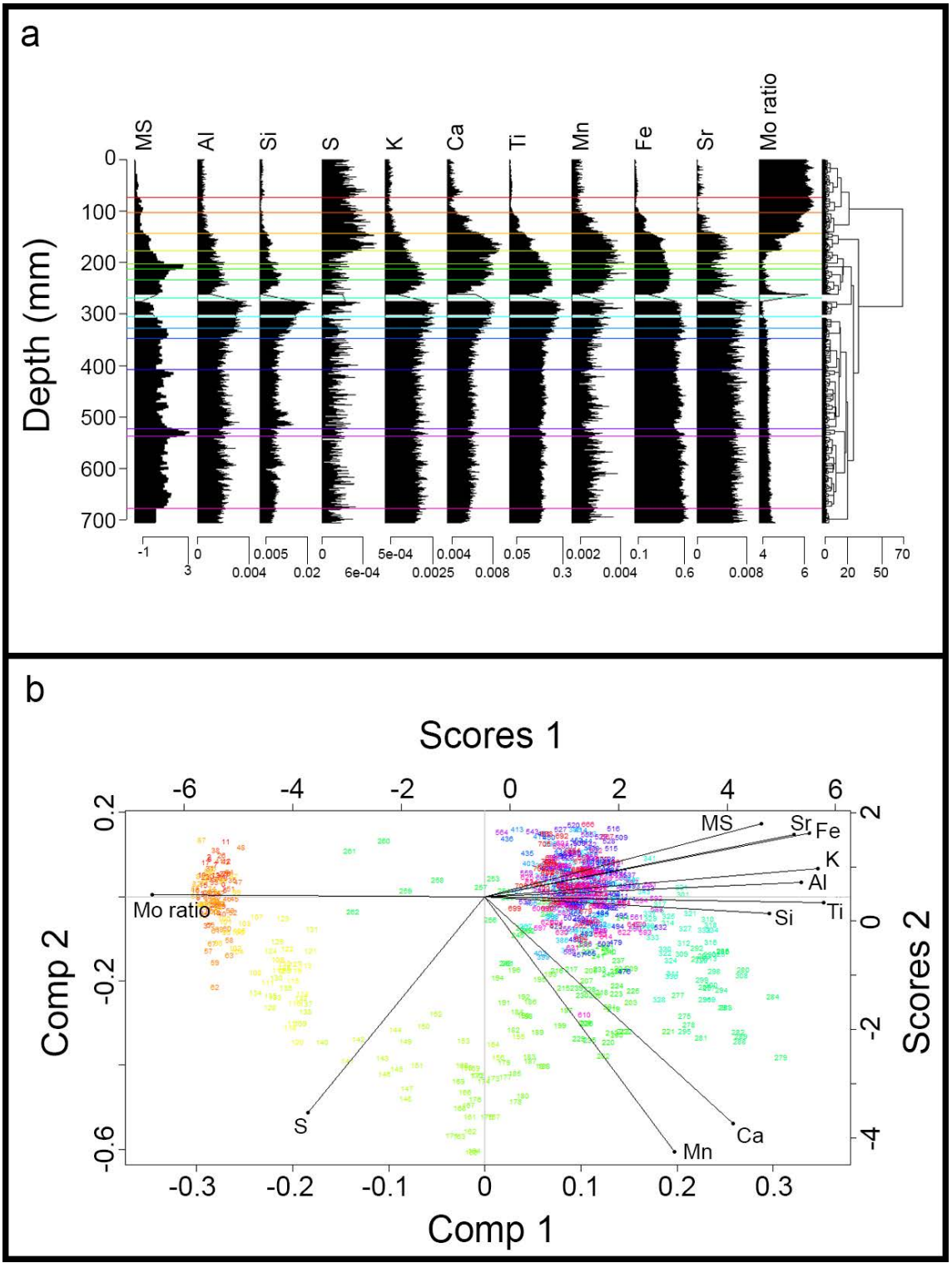

Figure 6.14: Selected Itrax™ normalized elemental and magnetic susceptibility (MS) data for BWIL2 0-1 m: a) stratigraphic plot, and b) principal components analysis. Data are plotted by depth.

The top metre of BWIL2 shows a dominant detrital signal, indicated by high magnetic susceptibility paired with high Al, Si, K, Ti, Fe and Sr, transitioning to an organic-rich phase in the top 20 cm, marked by a sharp increase in Mo inc/coh and high S (Figure 6.14 plot a).

These two primary signals are identified by principal component 1 (detrital versus organics) that explains 81.66 % of variation. This is visible in Figure 6.14 (plot b) as the grouping of magnetic susceptibility and these detrital elements in the upper right quadrant, with Mo ratio in the upper left. Elements Ca and Mn fall within the detrital signal (the right side of the x axis) while S falls within the organic signal (left side of the x axis) but these elements are also influenced by other factors (identified here as principal component 2, on the y axis) beyond the primary organic and detrital signals.

Itrax^{TM} data for the uppermost 13 cm of BWIL2 were combined with charcoal data to compare elemental and charcoal variations (Figure 6.15).

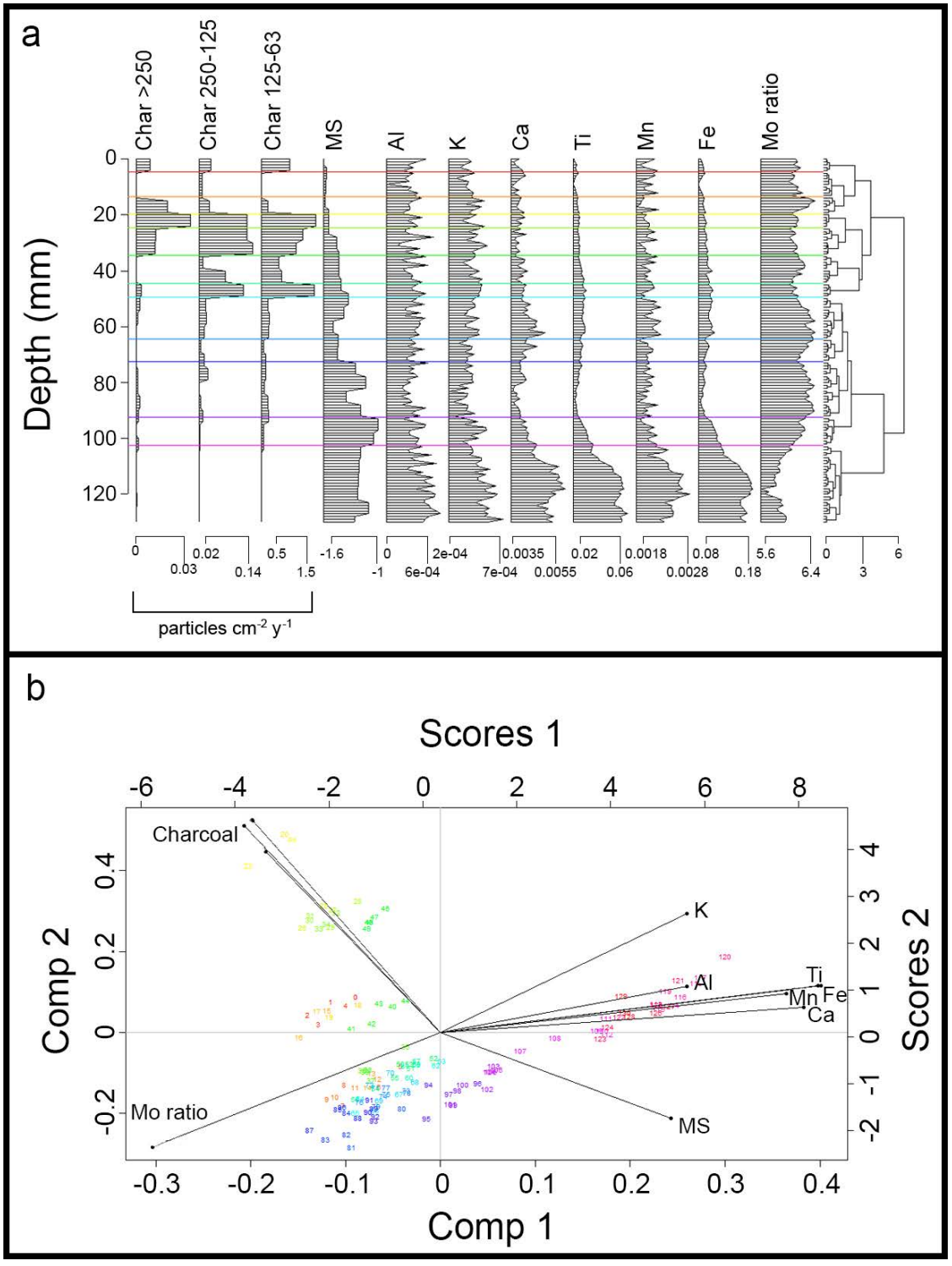

Figure 6.15: Selected Itrax™ normalized elemental and magnetic susceptibility (MS) data and charcoal flux (particles/cm²/y divided into size fractions) for BWIL2 0-0.13 m: a) stratigraphic plot, and b) principal components analysis. Data are plotted by depth.

Similar to the full 0-1 m of BWIL2, principal component 1 of the top 13 cm represents detrital versus organic input (explaining ~53 % of variation), represented in Figure 6.15 (plot b) by the x axis.

All charcoal size fractions, organic content (Mo ratio) and magnetic susceptibility (MS) are also influenced by principal component 2 (~22 % of variation), represented by the y axis. Unlike in the full top metre of BWIL2, elements Ca and Mn are grouped closely with the other detrital elements and both have strong positive correlations with Ti and Fe ($r^2 > 0.8$).

6.4.4 Sediment Core (BWIL2) Charcoal

The data presented in this section are described and plotted by a combination of depth (cm) and age (years cal BP). Flux values (units per cm^2 per year) are most suitably presented by age as these variables are rates of accumulation over time. However, the varied sediment accumulation rate of BWIL2 results in the majority of data points clustering closely together when plotted by age. Therefore, data are also presented by depth where appropriate and necessary to show variability and trends in the data.

6.4.4.1 Charcoal Flux

Charcoal counts in the macroscopic size fractions are low throughout the record, particularly in the >250 µm size fraction (12 of 26 samples contain no charcoal particles in this size) (Figure 6.16). Trends are consistent between the three size fractions where charcoal is present.

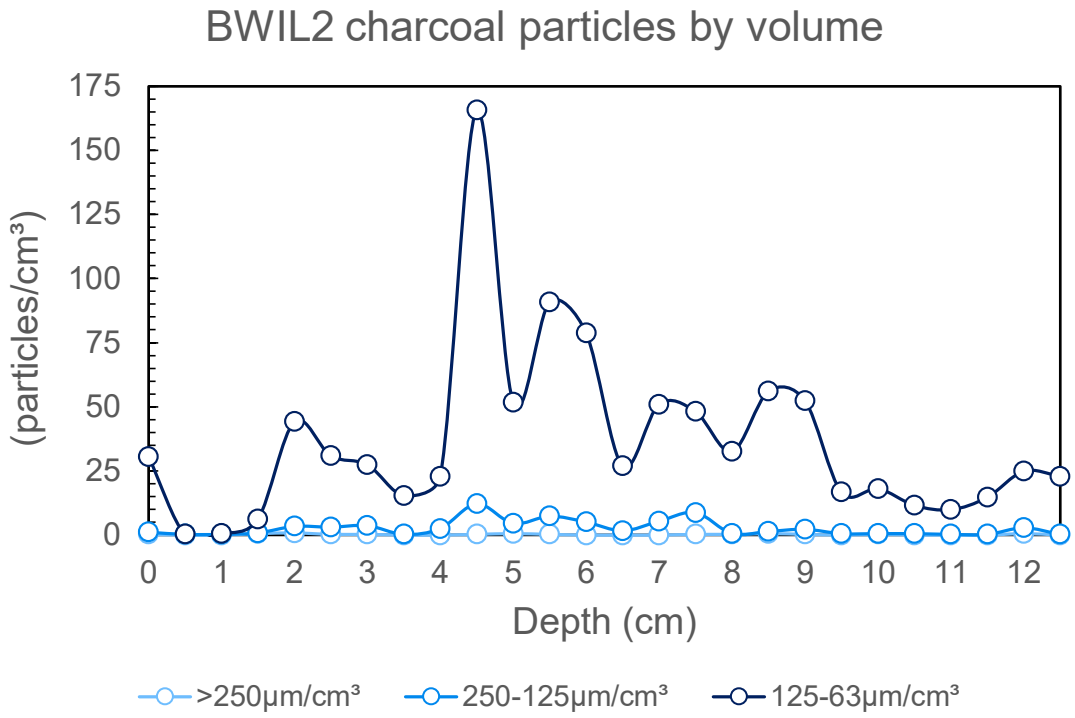

Figure 6.16: Charcoal particles by volume for BWIL2, by depth.

Charcoal in all size fractions in the BWIL2 record predominantly accumulated between ~1500 cal BP and the present, peaking after 304 cal BP (Figure 6.17, plot a). Peaks in charcoal flux occur around the year 1900 AD in the 250-125 µm and 125-63 µm fractions (4.5 cm depth), with no charcoal particles recorded in the >250 µm fraction (Figure 6.17, plot b). Peaks occur in the >250 µm and 125-63 µm fractions around 1970 AD, but this peak occurs earlier (~1947 AD) in the 250-125 µm fraction.

a)

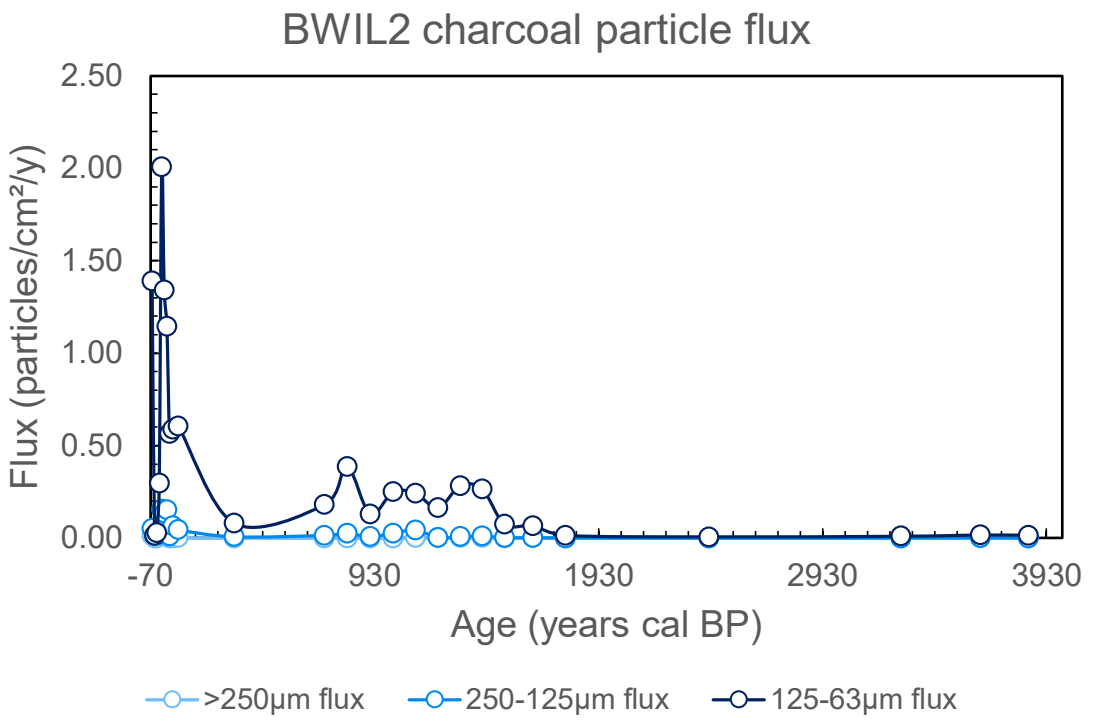

b)

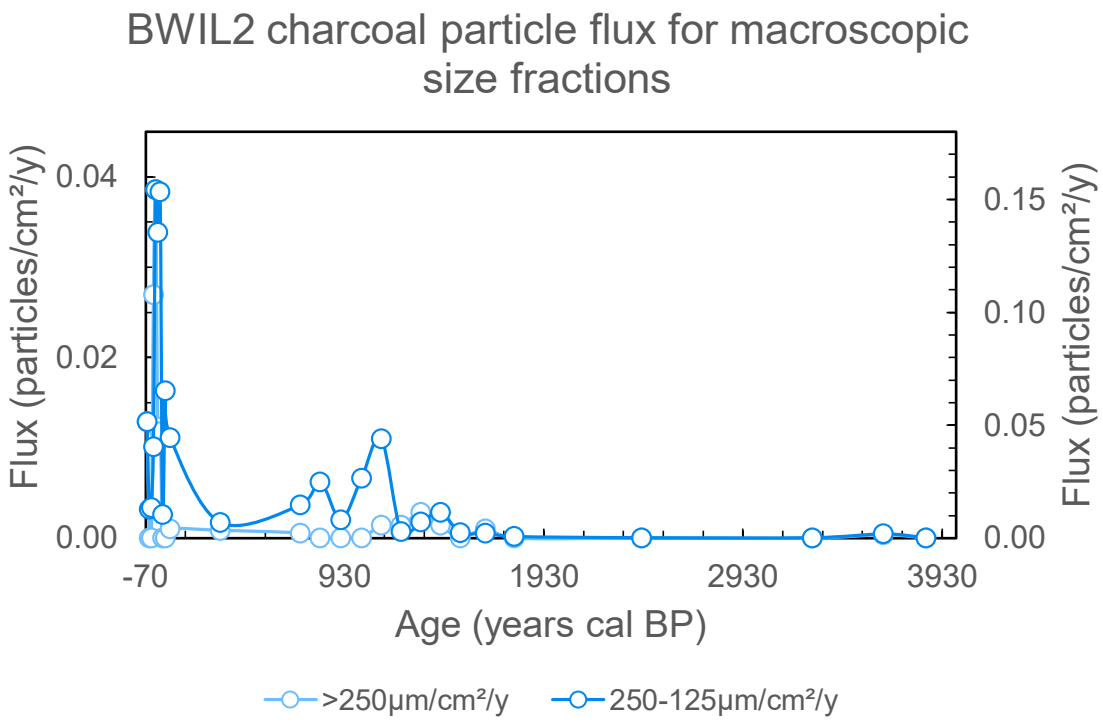

Figure 6.17: Charcoal flux for BWIL2, by age: a) all size fractions, and b) macroscopic size fractions only.

6.4.4.2 Charcoal L:W Ratios

Elongate particles as determined from length-width ratios are highly variable throughout the record due to many samples containing few (<13 particles per cubic cm) or no particles (Figure 6.18). Measurements for elongate particles vary between 0 and 100 % in both size fractions, with values between 20 and 85 % in the 250-125 µm fraction in samples with higher charcoal counts (2-3 cm and 4-7.5 cm).

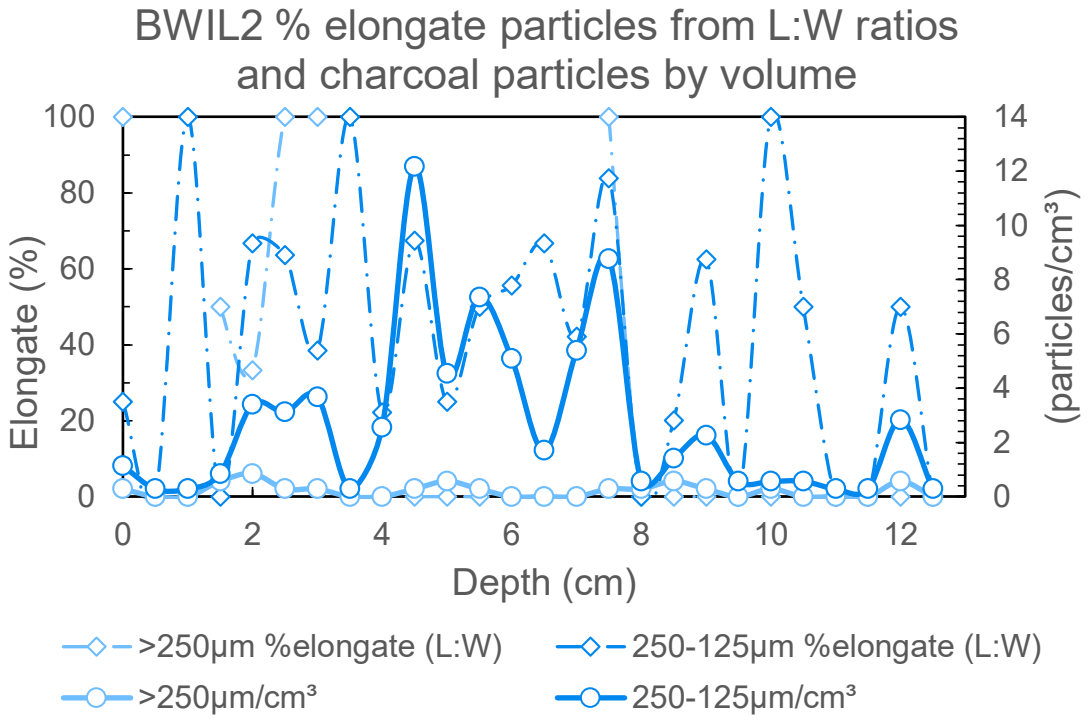

Figure 6.18: Percent elongate particles determined from length-width ratios and particle counts for BWIL2 macroscopic charcoal, by depth.

6.4.4.3 Charcoal Morphotypes

Morphotypes in the 125-63 µm size fraction are dominated by type F (elongate) followed by type S (structured geometric; Figure 6.19). No correlation between morphotype composition

and charcoal abundance is apparent, nor are there clear trends in morphotype composition over time.

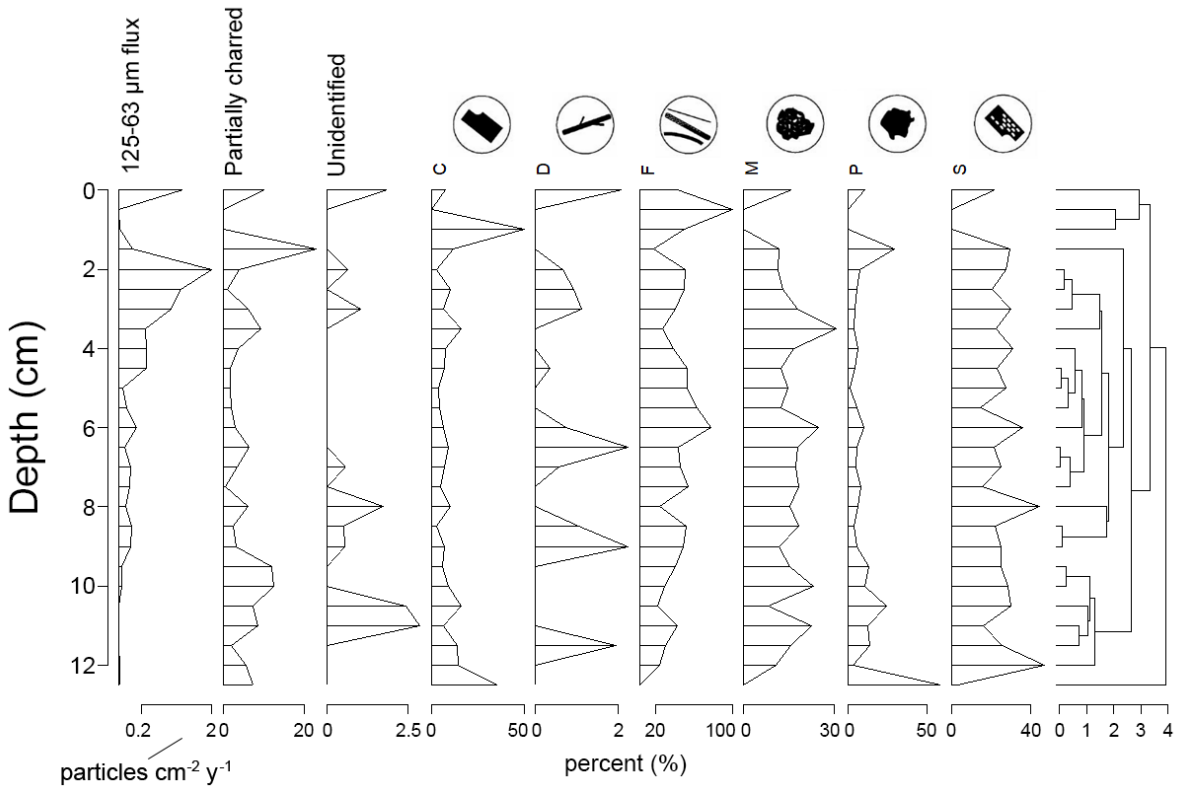

Figure 6.19: BWIL2 125-63 µm morphotypes, by depth.

When simplified to the 7-type Enache and Cumming (2006) system, morphotypes in the 250-125 µm size fraction are similarly dominated by type F, with declining type S over time into the present (Figure 6.20).

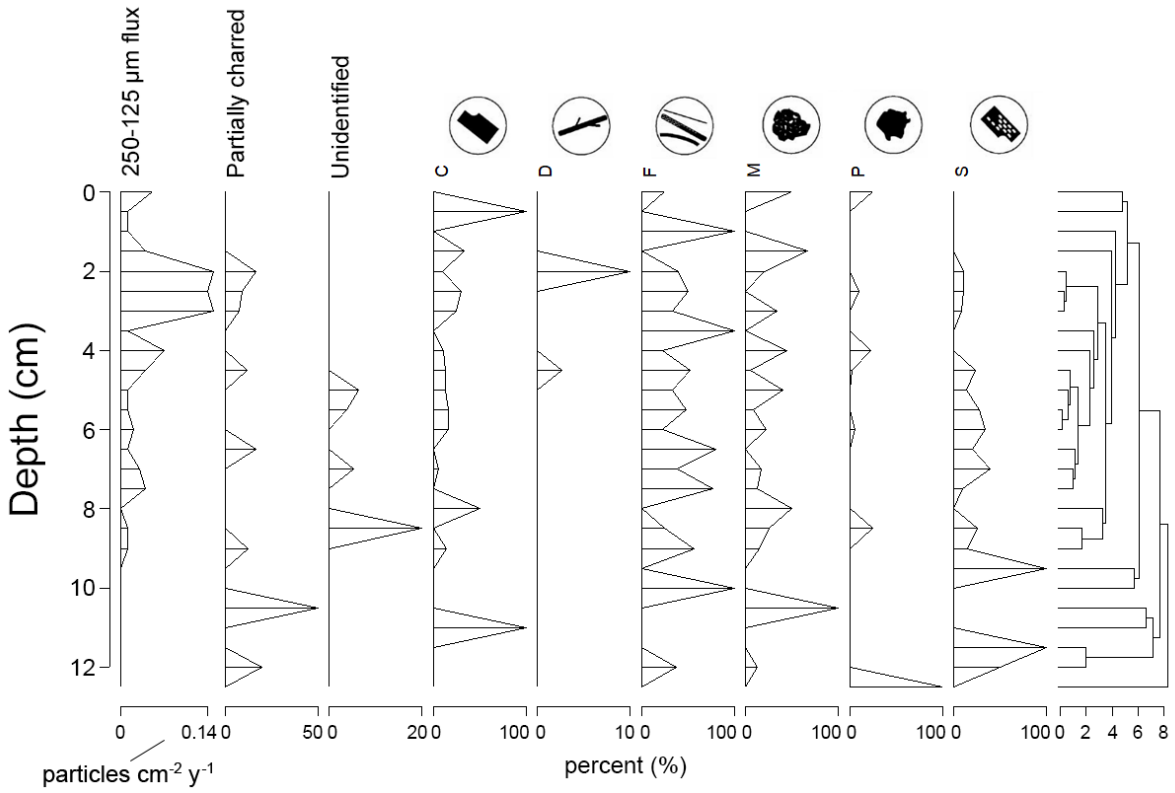

Figure 6.20: BWIL2 250-125 µm morphotypes, by depth.

Due to overall low charcoal counts, the >250 µm size fraction shows many sharp peaks with morphotypes comprising 50 to 100 % of each sample (Figure 6.21).

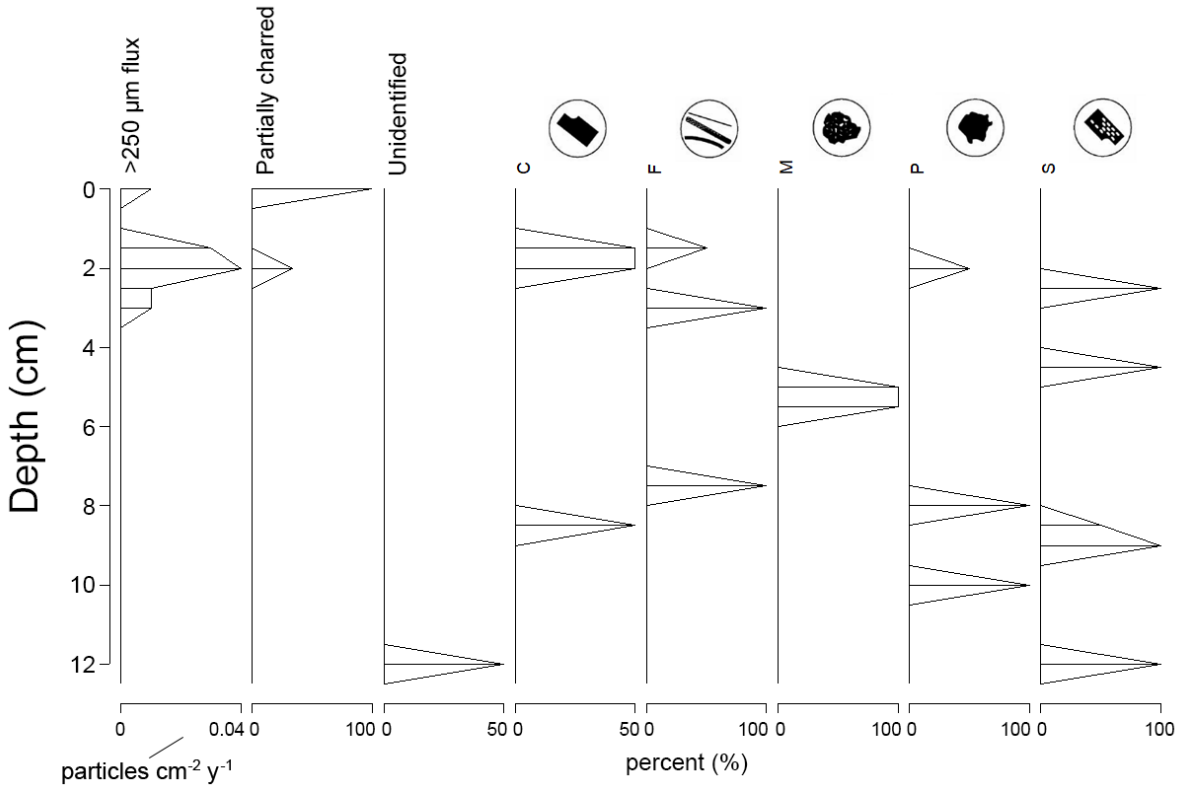

Figure 6.21: BWIL2 >250 µm morphotypes, by depth.

Morphotypes in the most recent period (since ~1950 CE) show varied composition across size fractions (Figure 6.22). While the 125-63 µm size fraction is dominated by type F (elongate), no clear patterns occur in the macroscopic sizes, potentially due to low particle counts.

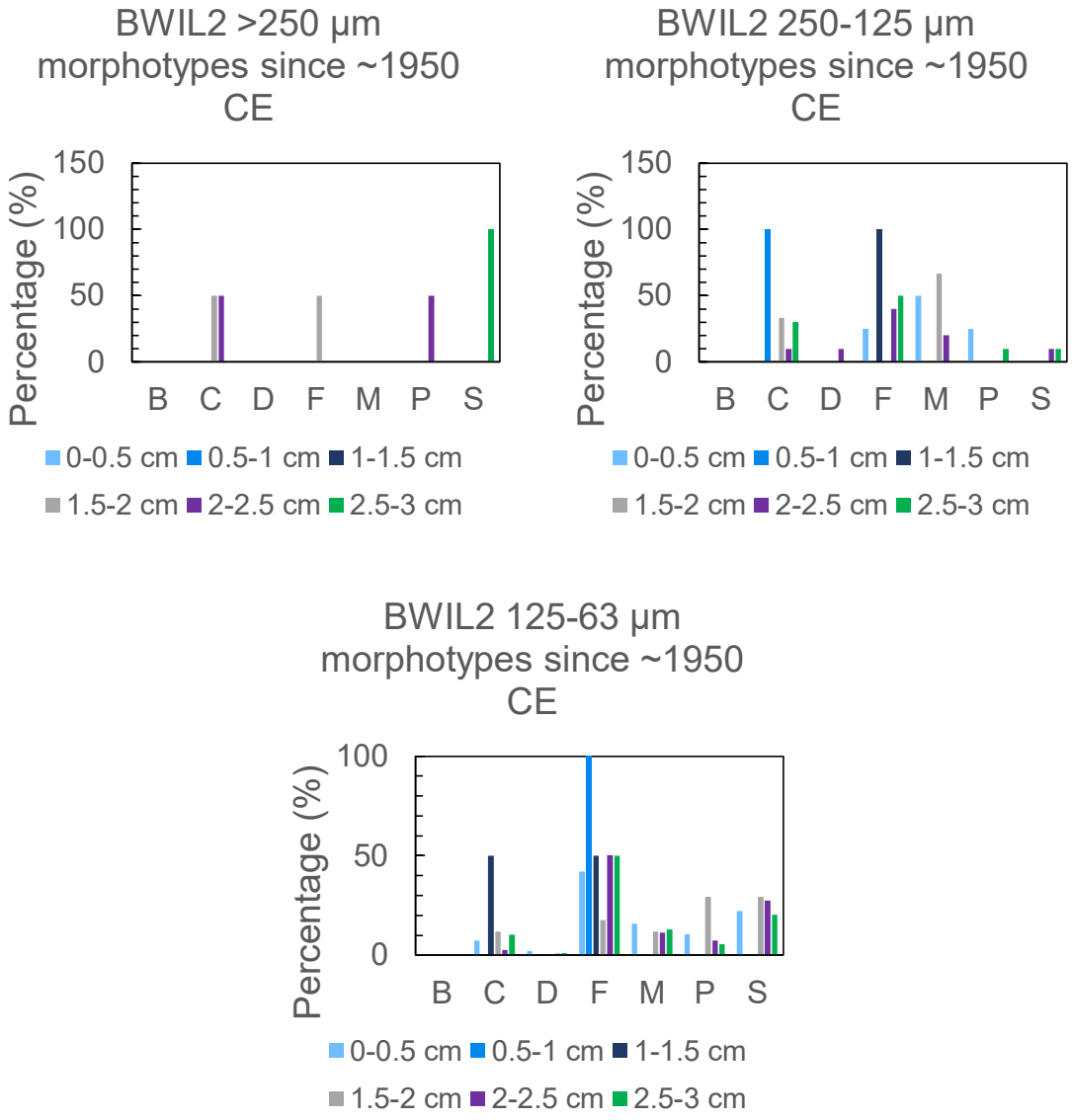

Figure 6.22: Morphotypes since ~1950 CE for BWIL2, by size fraction.

No consistent trends between the size classes are present in elongate morphotypes (Figure 6.23). Elongate morphotypes are consistently present in at least one size fraction throughout the record.

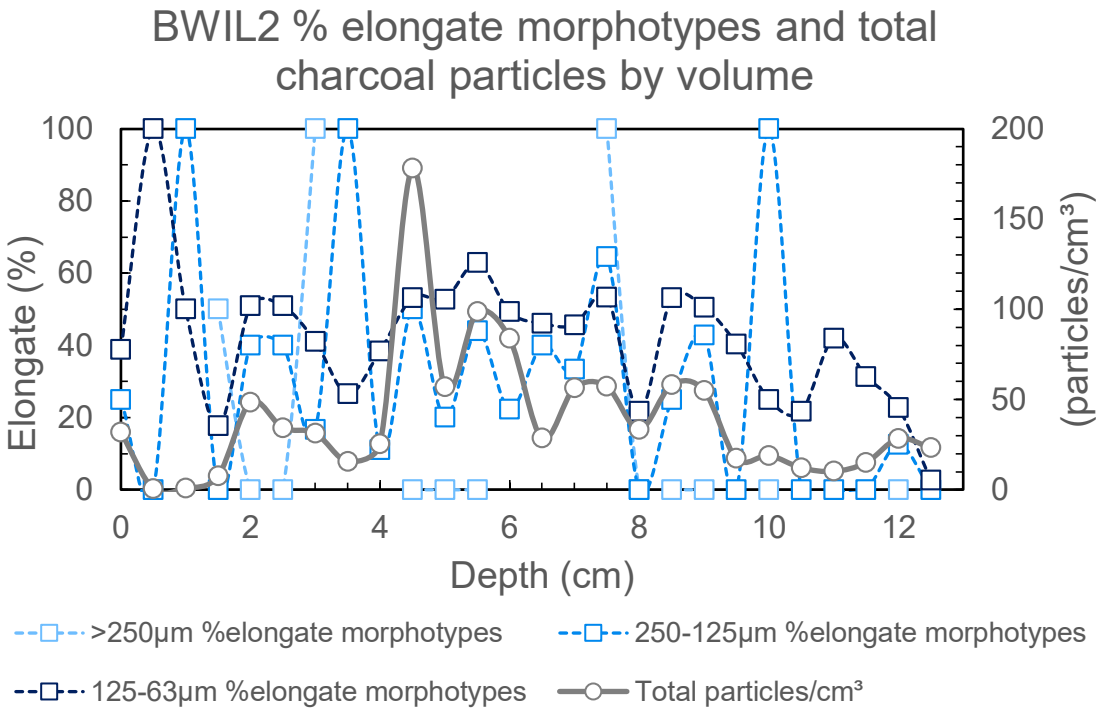

Figure 6.23: Percent elongate morphotypes for all charcoal size fractions, and total particle count, for BWIL2, by depth.

Percent elongate particles calculated from length-width ratios and morphotypes display similar trends throughout the record (Figure 6.24). Both measures estimate between 20 and 60 % elongate particles in the 250-125 µm and 125-63 µm size fractions in the period of highest charcoal counts (4 to 8 cm).

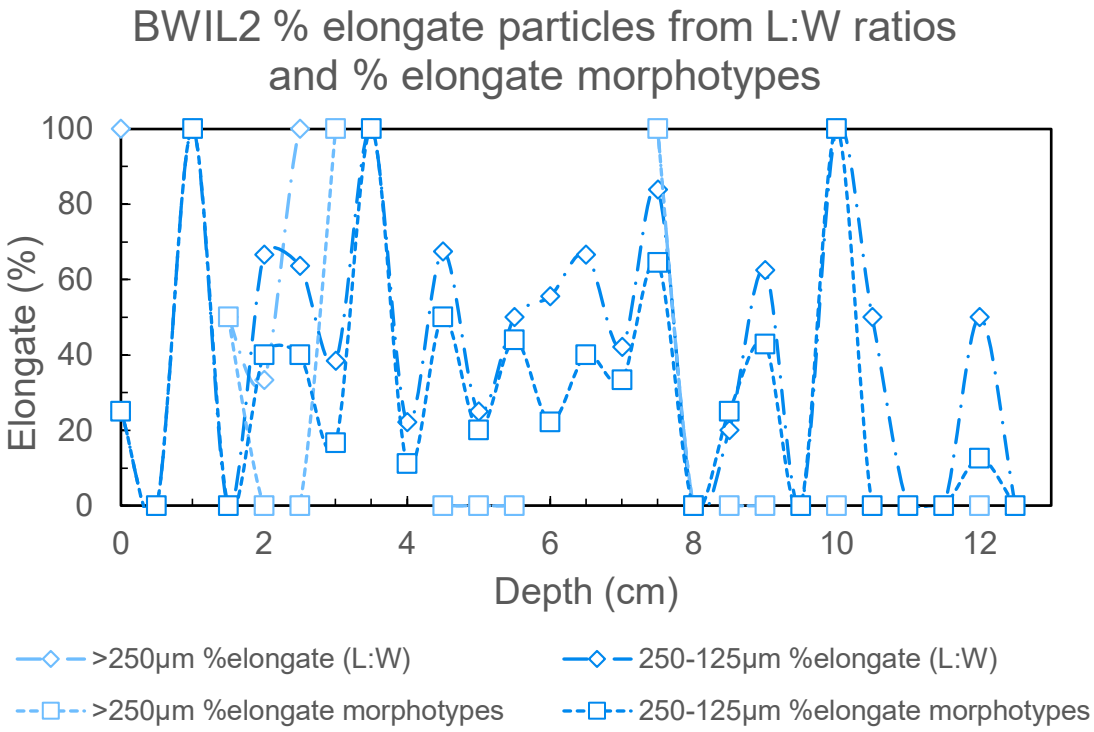

Figure 6.24: Percent elongate particles as determined by length-width ratios and morphotypes for BWIL2 by size fraction, by depth.

6.4.5 Hydrogen Pyrolysis and Elemental Analysis

6.4.5.1 Pyrogenic Carbon Flux

Total organic carbon and percent pyrogenic carbon show broadly similar trends in both bulk and <63 µm size fractions (Figures 6.25 and 6.26). Generally increasing total organic carbon content towards the uppermost core corresponds to a dominant organic signal at these depths identified via XRF (see Itrax™ XRF Scanning above).

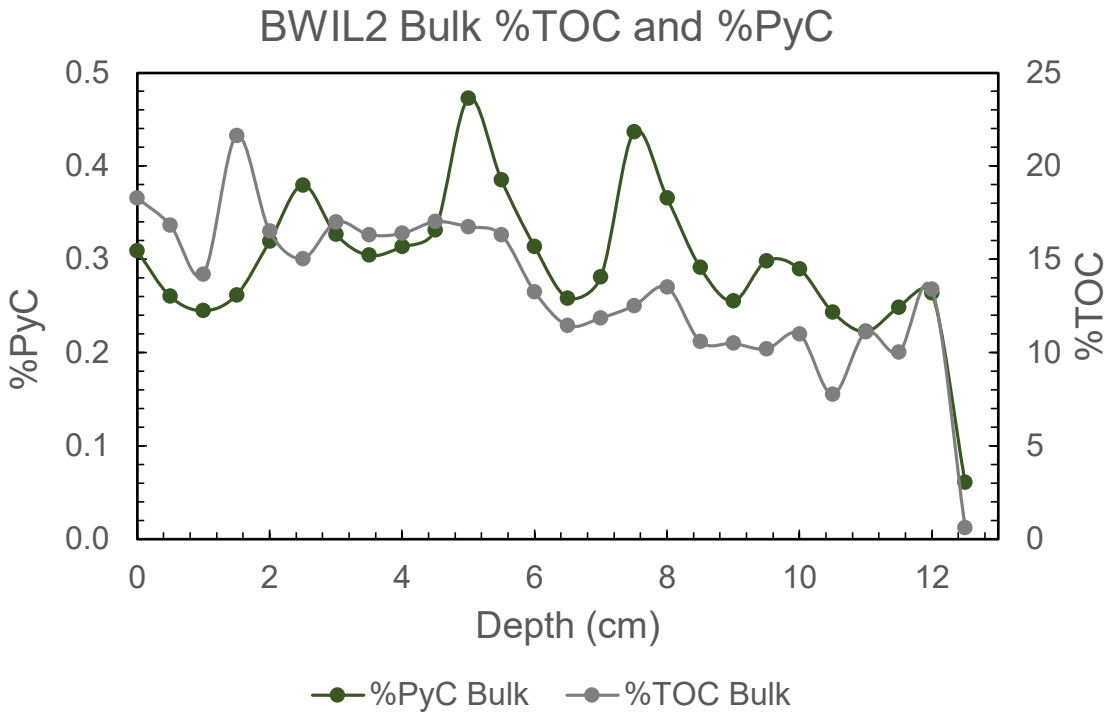

Figure 6.25: BWIL2 bulk total organic carbon (%TOC) and percent pyrogenic carbon, by depth.

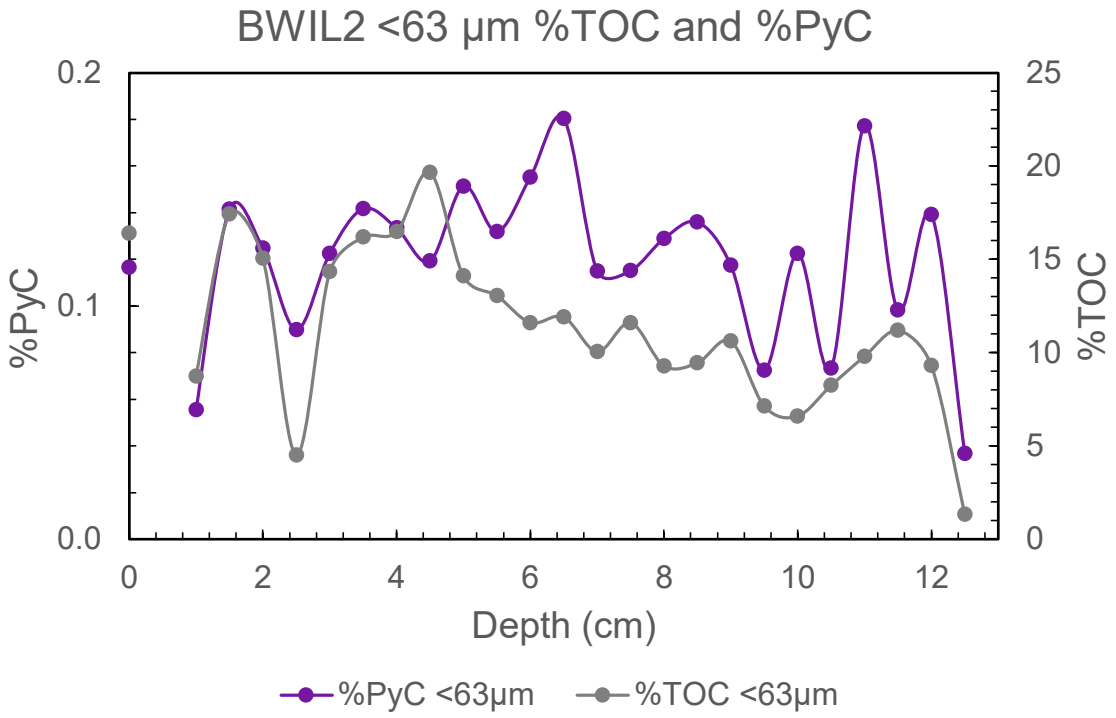

Figure 6.26: BWIL2 <63 µm total organic carbon (%TOC) and percent pyrogenic carbon, by depth.

Pyrogenic carbon (PyC) flux (g/cm²/y) for bulk and <63 µm samples of BWIL2 show similar trends to charcoal flux values, with values increasing at ~1630 cal BP and peak flux occurring in the most recent period (since ~1900 AD, Figure 6.27).

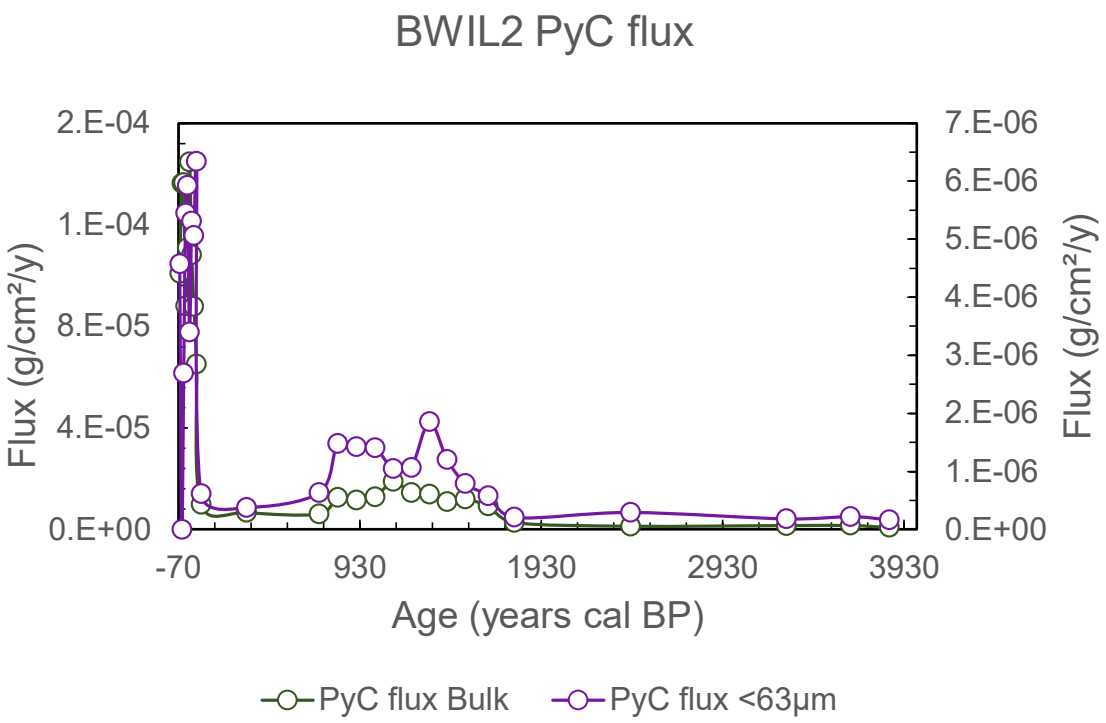

Figure 6.27: Bulk and <63 µm pyrogenic carbon (PyC) flux for BWIL2, by age.

Bulk PyC flux follows total charcoal flux closely, with the exception of very low charcoal counts from 0.5-1 cm (Figure 6.28).

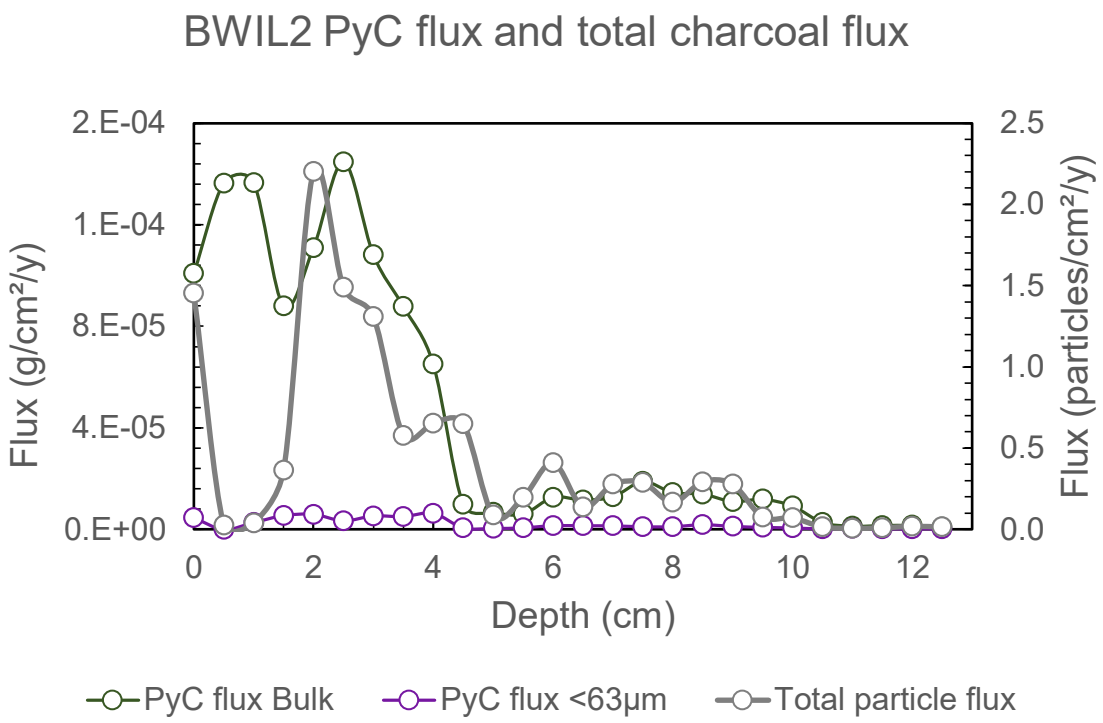

Figure 6.28: Bulk and <63 µm pyrogenic carbon (PyC) flux and total charcoal flux for BWIL2, by depth.

PyC for the <63 µm fraction is low throughout the record and corresponds well to charcoal flux for the 125-63 µm size fraction (Table 6.3), although a peak is present in <63 µm PyC flux at 4 cm that is not reflected in microscopic charcoal flux (Figure 6.29).

Table 6.3: Charcoal and PyC flux variable r² values for BWIL2.

	>250 µm	250-125 µm	125-63 µm	<63 µm PyC
Bulk PyC	0.2714	0.3949	0.3525	0.4483
>250 µm		0.5045	0.5682	0.4363
250-125 µm			0.7863	0.4799
125-63 µm				0.5323

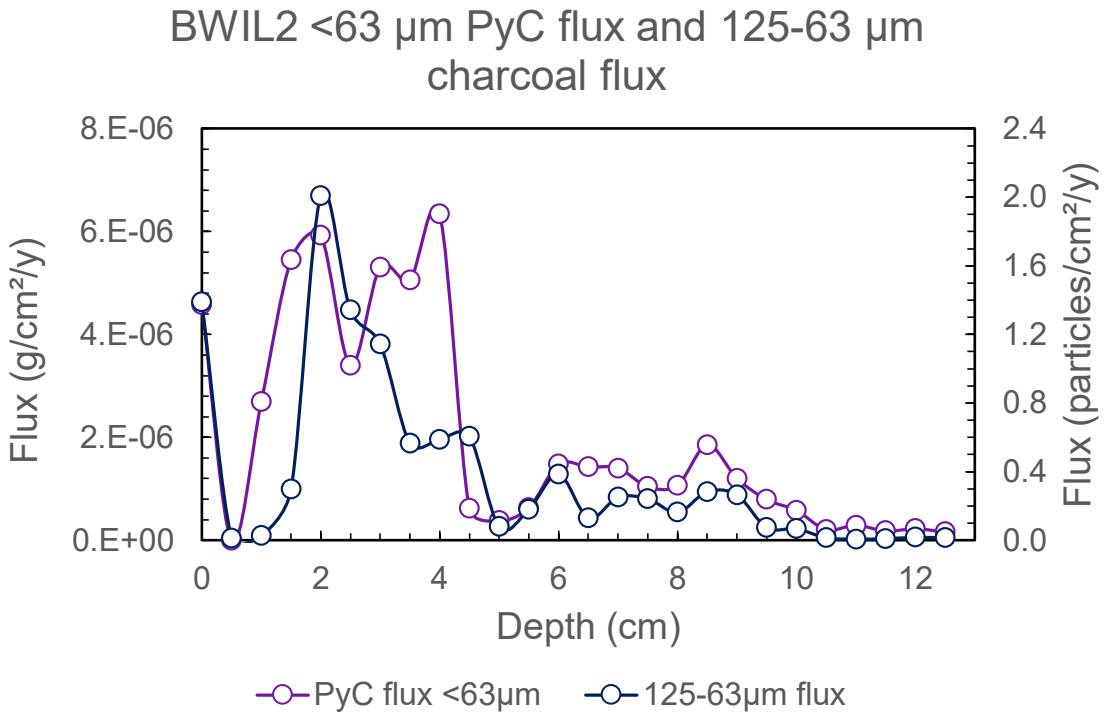

Figure 6.29: <63 µm pyrogenic carbon (PyC) flux and 125-63 µm charcoal flux for BWIL2, by depth.

6.4.5.2 Pyrogenic Carbon $\delta^{13}C$

Bulk $\delta^{13}C$ values for total organics (pre-hydrogen pyrolysis) are consistently more 13C-depleted than $\delta^{13}C$ values for pyrogenic carbon, while no clear relationship is present between total organic carbon and pyrogenic carbon $\delta^{13}C$ values in the <63 µm size fraction (Figures 6.30 and 6.31).

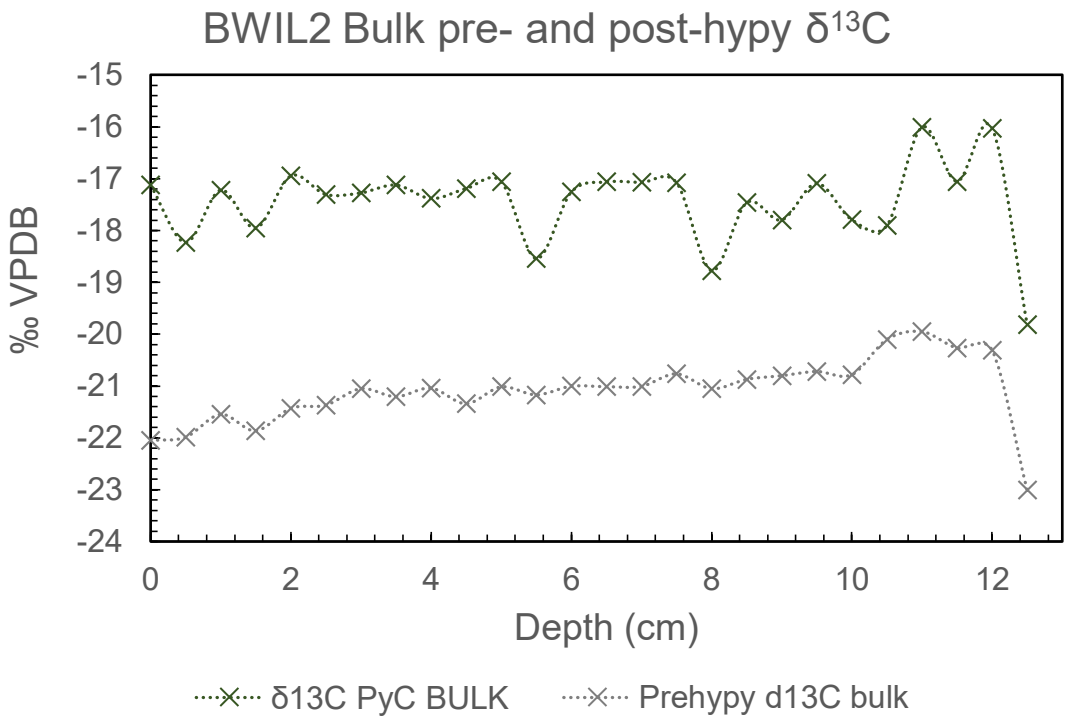

Figure 6.30: BWIL2 $\delta^{13}C$ for bulk samples before (total organic carbon) and after (PyC) hydrogen pyrolysis, by depth.

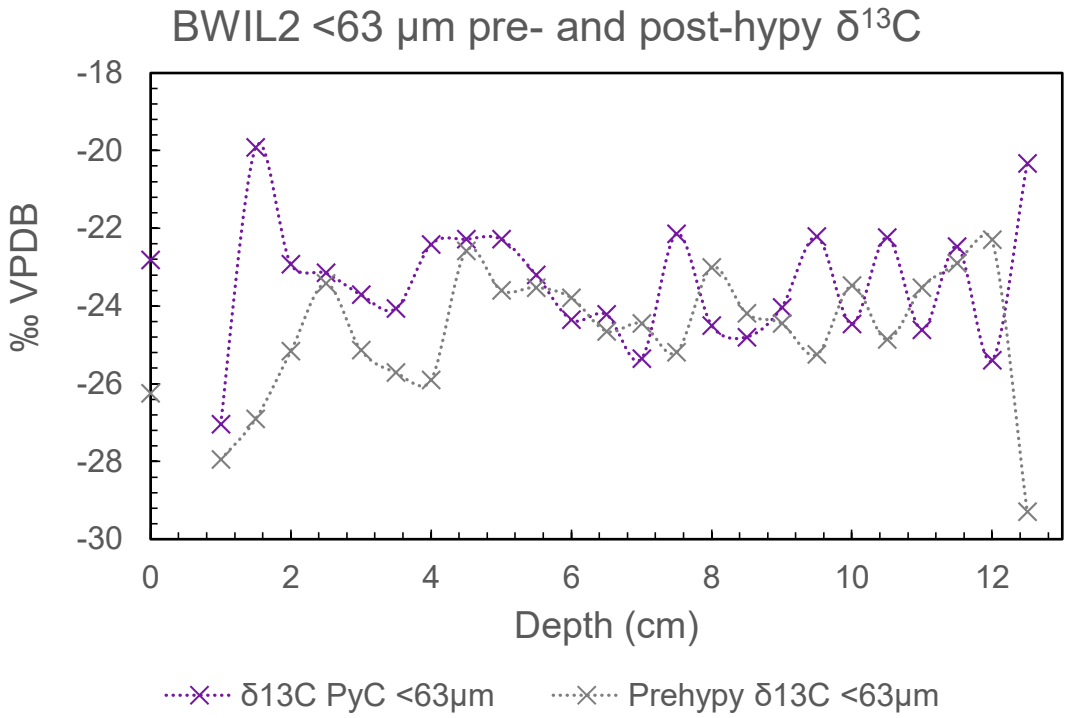

Figure 6.31: BWIL2 $\delta^{13}C$ for <63 µm samples before (total organic carbon) and after (PyC) hydrogen pyrolysis, by depth.

BWIL2 $\delta^{13}C$ values for pyrogenic carbon are consistent throughout the record, with some variation in the <63 µm fraction (Figure 6.32). Values for bulk samples fall between -16 and -20 ‰ and reflect the mixed C_3/C_4 vegetation surrounding the swamp, as values above -14‰ indicate C_4 plants and values below -25 ‰ C_3 plants (O'Leary 1988:330-1).

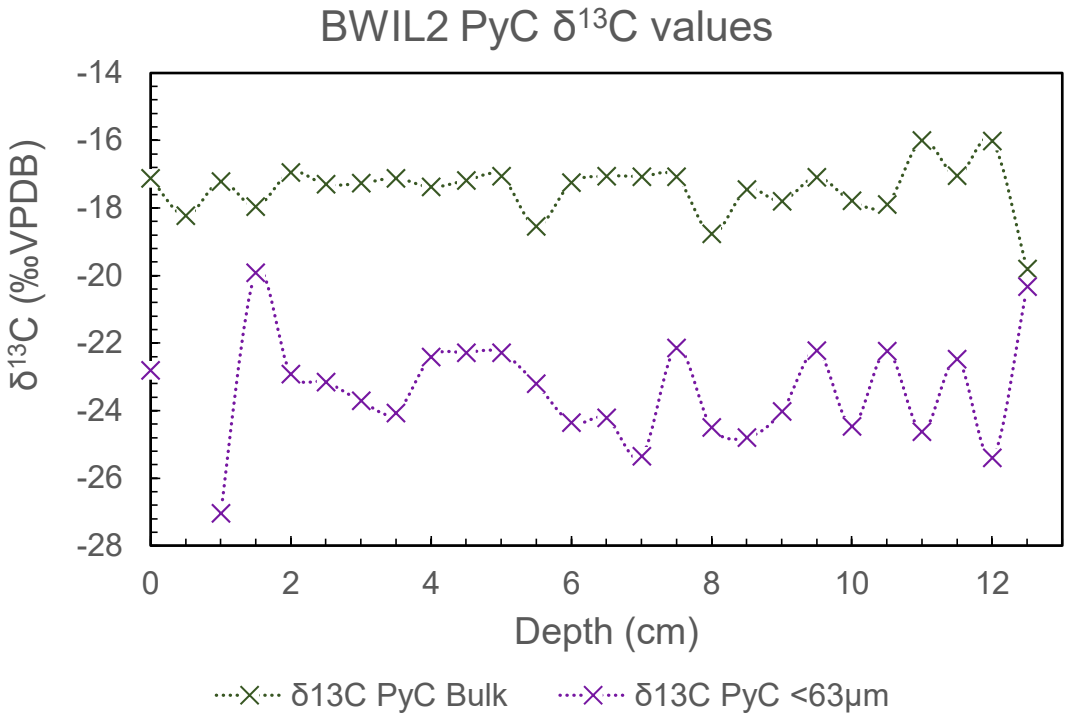

Figure 6.32: Bulk and <63 µm pyrogenic carbon (PyC) $\delta^{13}C$ for BWIL2, by depth.

Values for the <63 µm fraction are consistently more ^{13}C depleted than their associated bulk sample, reaching as low as -27 ‰ (1 cm) and no higher than -20 ‰ (12.5 cm).

6.5 Discussion

6.5.1 Elemental Composition

6.5.1.1 Mo Ratio, In-wash Detritus (Al, K, Ti, Fe) and Airborne Detritus (Ca, Mn)

Mo incoherent/coherent ratio is interpreted here as a proxy for organic content, as discussed in Chapter 5 (see also Davies, Lamb & Roberts 2015), alongside total organic carbon (%TOC). The soils of Big Willum Swamp and the surrounding East Weipa region contain Al, K, Ti and Fe in varying concentrations (Eggleton et al. 2018, p.S31) and these elements constitute the in-

wash (overland) detrital signal in the Big Willum record (see also Davies, Lamb & Roberts 2015, pp.193-199; Mackenzie et al. 2017).

Ca is typically interpreted as marine influence and not correlated to detrital elements (e.g. Croudace et al. 2006; Kylander et al. 2011; see also Chapter 7). While Ca and Mn show positive correlations with these detrital elements, particularly in the uppermost 13 cm of the Big Willum record ($0.5 < r^2 < 0.95$), they represent the airborne component of the detrital signal as neither Ca nor Mn are present in the soils at Big Willum Swamp (Eggleton et al. 2018).

A transition from this detrital signal, which dominates the majority of the top metre of BWIL2, to an organic signal begins at ~12 cm (~3600 cal BP) with all detrital elements reducing until ~9 cm depth (~1400 cal BP). This coincides with an increase in water content and visible decrease in clay content and sediment density (see Sediment Descriptions above). This transition may indicate that Big Willum Swamp became a permanent water body at this time after the collapse of the underlying porous bauxite laterite (see Grimes & Spate 2008; Twidale 1987; cf. Stevenson et al. 2015 who place the transition later, see Comparison to Stevenson et al. (2015) below).

6.5.1.2 Charcoal and Magnetic Susceptibility

The presence of charcoal occurs in the organic segment (12-0 cm, ~3600 cal BP to the present) and magnetic susceptibility greatly decreases after the detrital-to-organic transition. However, both charcoal and magnetic susceptibility display variation not captured within the detrital versus organic signal, identified in the Principal Components Analysis as principal component 2 (~22 % of variation). This indicates that these variables are affected by additional factors beyond detrital or organic input.

6.5.2 Charcoal and Pyrogenic Carbon

Charcoal flux in all size fractions and PyC flux (bulk and <63 μm) peak in the most recent period, between ~54 cal BP and the present, and this coincides broadly with an increase in sediment accumulation (Figure 6.33). However, this is not coupled with a detrital signal in sediment elemental composition and therefore does not indicate that increased charcoal abundance and sediment accumulation is the product of erosion.

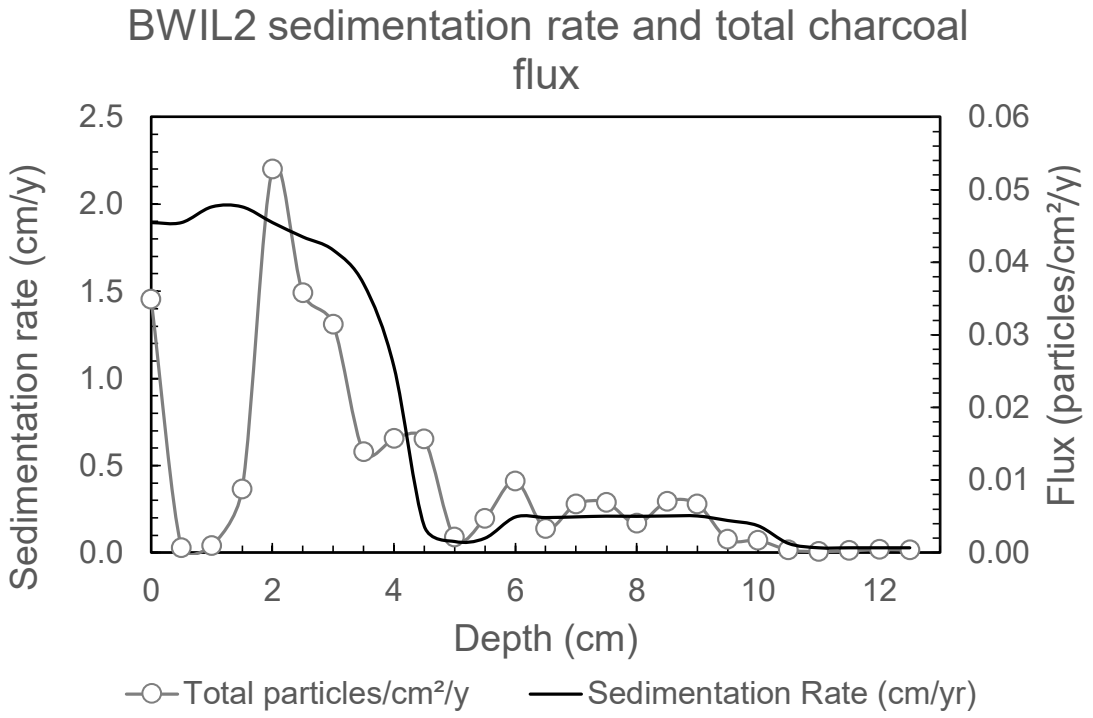

Figure 6.33: Sediment accumulation rate and total charcoal flux for BWIL2, by depth.

Increasing charcoal abundance since the early 19th century coincides broadly with increased European activity in Cape York Peninsula. The highest charcoal abundance in the record occurs between the years 1900 and 1970 AD (4.5-2 cm), corresponding with the establishment of

missions in the area and the creation of the currently active bauxite mine (Weipa Town Authority 2014; see Chapter 3).

Trends are similar between the size fractions for most of the record, with the exception of some peaks in the 250-125 μm size fraction and many samples containing no charcoal in the >250 μm fraction. General consistency between macroscopic charcoal flux, microscopic charcoal flux, bulk PyC flux and <63 μm PyC flux suggests that either a) the BWIL2 record represents a local fire signal or b) there is no distinction between local and regional fire events (any regional fire events also occur at a local scale) and the BWIL2 record represents a combined local-regional fire signal.

6.5.2.1 Vegetation Burned

Length-width measurements and morphotype data suggest mixed woody/grass contribution to charcoal throughout the record. This is supported by $\delta^{13}C$ values for bulk pyrogenic carbon which show combined C_3 ($\delta^{13}C < 25$ ‰) and C_4 ($\delta^{13}C > 14$ ‰) plant content (O'Leary 1988, pp.330-331). This suggests that while sedges may contribute to elongate particle counts (see Chapter 7), grasses are present in this record. Extreme values for elongate charcoal particles (e.g. 0 or 100 %) are likely the result of small sample sizes (low charcoal counts).

Pyrogenic carbon in the <63 μm fraction displays $\delta^{13}C$ values consistently lower than those of the bulk fraction. The Stable Isotope Disequilibrium Effect predicts $\delta^{13}C$ depletion of PyC in fine size fractions in grass-dominated environments (Saiz et al. 2015, p.1859); consistently lower $\delta^{13}C$ values for the <63 μm fraction than the bulk samples of BWIL2 indicate a constant contribution of grass throughout the record.

It is not possible to determine whether this charcoal record represents a local or combined local and regional signal using vegetation data, as open woodland with a grassy understorey is

present in both the local and regional environment (see Figure 6.5 and 6.2.2.2 Geology and Vegetation). However, this also allows for the Big Willum Swamp record to be considered representative of the broader landscape, and may reflect a landscape that behaves in a uniform way (cf. mosaic environments in the Jardine River region covered in Chapter 7). The consistently low volume of macroscopic charcoal throughout the record may indicate minimal local burning and a primarily regional signal.

6.5.3 Comparison to Stevenson et al. (2015)

Direct comparison to the results presented by Stevenson et al. (2015) for core BW01 is possible as both BW01 and BWIL2 from this study were collected centrally and contain late Holocene sediments (Figure 6.34). Stevenson et al. (2015) optically quantified charcoal in macroscopic (>125 μm) and microscopic (125-10 μm) size fractions, but were unable to produce a ^{210}Pb decay curve for BW01.

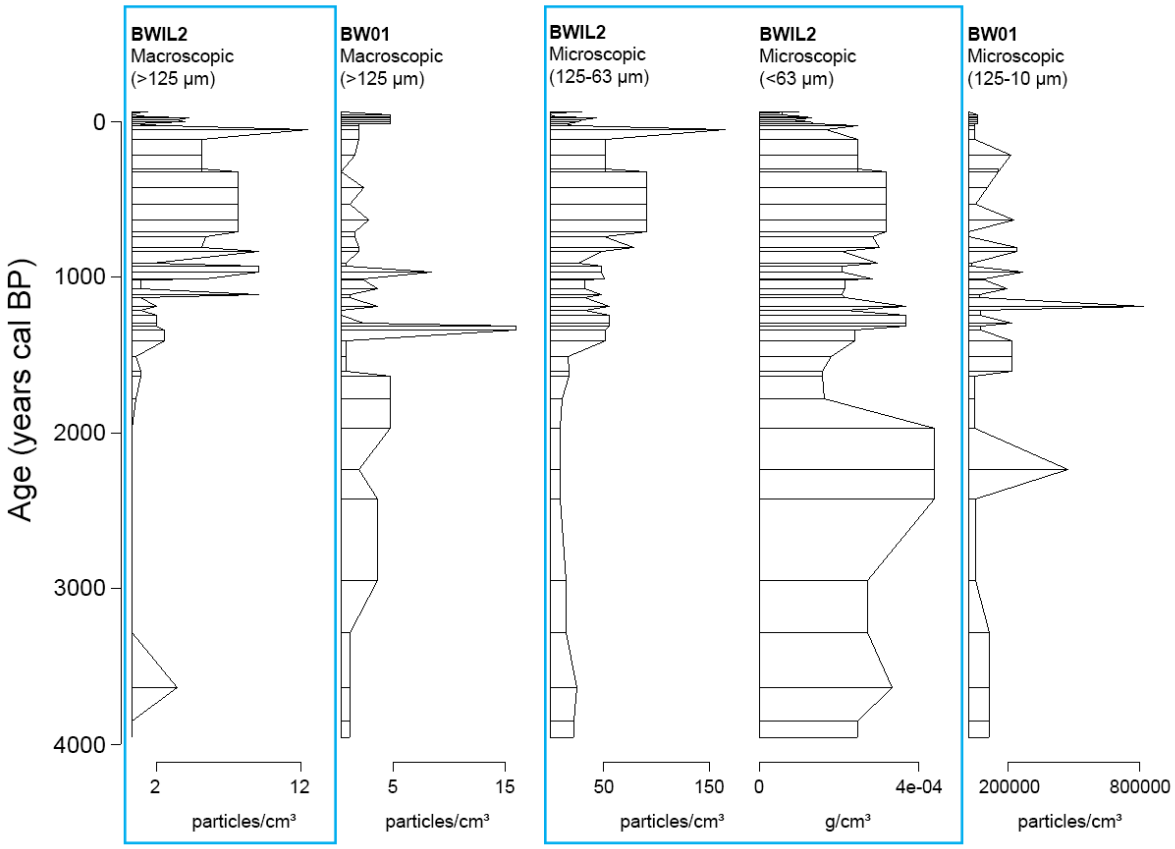

Figure 6.34: Comparison of charcoal and <63 µm PyC concentrations from BWIL2 (this study, outlined in blue) and BW01 (Stevenson et al. 2015).

Differences are apparent between the cores in the macroscopic size fraction. Concentrations are similar in the most recent period (since ~1940 AD) and at ~960 cal BP but diverge elsewhere. The large peak in BW01 at ~1300 cal BP is minor in BWIL2, and high concentrations from ~830 to 50 cal BP in BWIL2 are not reflected in BW01. The range of values is similar in magnitude between the two cores (maximum of 16 particles/cm³ in BW01 and ~12.5 in BWIL2).

Greater similarity is apparent between the microscopic size fractions of BW01 and BWIL2. Charcoal concentrations for the microscopic fraction of BW01 show similar trends to <63 µm

PyC concentration for BWIL2; this likely reflects the preparation method, as microscopic charcoal from BW01 was quantified on pollen slides which may have resulted in destruction of larger particles or preferential inclusion of smaller particles (C. Rowe pers. comm.). The significantly lower values for BWIL2 125-63 µm concentrations (maximum ~165 particles/cm^3) compared to the BW01 microscopic (125-10 µm) fraction (maximum ~8 million particles/cm^3) suggests the vast majority of particles within the BW01 microscopic fraction fall between 63 and 10 µm. The highest charcoal flux values in the 125-63 µm fraction of this study occur within the uppermost core which may not be present in BW01; this is demonstrated by the successful creation of a ^{210}Pb decay curve and subsequent chronology for BWIL2 that was not possible for BW01.

Itrax^{TM} elemental data in this study, combined with water content and visual changes in sediment texture and colour, suggest a shift from a predominantly detrital signal to more organic conditions at ~3600 cal BP. Stevenson et al. (2015) also identify a detrital-to-organic transition as Big Willum Swamp shifted from swamp conditions to a permanent deep water body, but place this transition at ~2200 cal BP in core BW01. However, elemental data is not available for BW01 making direct comparison difficult, and the detrital-to-organic elemental change identified in BWIL2 at ~3600 cal BP may represent only the beginning of a transition phase that later affected other proxies (e.g. pollen).

Pollen data from Stevenson et al. (2015) can also be broadly compared to vegetation data for this study. Stevenson et al. (2015:23) identify a "complete lack of any grass pollen" in BW01 at ~1100 cal BP (see Figure 6.2 earlier in this chapter). This does not correspond to elongate particles in BWIL2, which are present in all size fractions at ~1113 cal BP (7.5 cm depth). Little change is visible in δ^{13}C value for bulk PyC at this depth in BWIL2, although a slight increase is visible in the δ^{13}C value for <63 µm PyC (-22.14 ‰). Stevenson et al. (2015:24) also note a "greater representation of grass over other herbaceous taxa" in the zone spanning

400-100 cal BP. This is difficult to detect in the BWIL2 record, corresponding to ~304-54 cal BP (5-4.5 cm), with no elongate particles in the >250 µm size fraction, variable elongate particle percentages in the 250-125 µm size fraction, and little change in the 125-63 µm size fraction (to 63 % elongate particles).

The results of this study correspond broadly to those presented in Stevenson et al. (2015), including a period of low sedimentation before ~2200 cal BP, minimal or absent grass at ~1100 cal BP and an increase in burning over the last approximately 150 years. Interpretations of vegetation compositions vary, but comparisons are limited due to data in this study being constrained to grass versus non-grass content. Absence of large charcoal concentration peaks in the uppermost section of BW01 may be a result of the core not containing the most recent sediments and in this regard the results of this study are the more reliable. The comparability of results between this study and Stevenson et al. (2015) allows for interpretation of the Big Willum Swamp record in the context of both cores BWIL2 and BW01.

6.6 Conclusion

Charcoal, PyC and elemental composition data for Big Willum (BWIL2) presented in this chapter represent a late Holocene palaeofire record displaying contributions from mixed C_3/C_4 vegetation and increasing charcoal (and by implication fire) into the most recent period. Minimal charcoal is present prior to ~1700 cal BP, with the highest charcoal flux in all size fractions occurring after ~50 cal BP. This charcoal abundance coincides with intensified European activity in the Weipa region, including the establishment of Weipa Mission (1898 AD) and the creation (1956 AD) and ongoing operation of the currently active Weipa bauxite mine (Weipa Town Authority 2014).

Chapter 7 : Sanamere Lagoon

7.1 Introduction

This chapter provides an overview of the land use history, geology, vegetation and current fire regime surrounding Sanamere Lagoon, Cape York Peninsula, Queensland. An overview of the methods applied is provided, including details specific to Sanamere, followed by results for modern charcoal traps, sedimentary analyses, chronology, and fire proxies. Objectives of analysis for this site, linked to the overall research aims of this study presented in Chapter 1, are as follows:

1) The creation of a modern charcoal dataset from Cape York Peninsula for comparison to the sedimentary record of Sanamere Lagoon to investigate the efficacy of charcoal analysis methods for reconstructing fire incidence and fuel types
2) The creation of a new high resolution multiproxy Holocene palaeofire record for Cape York Peninsula
3) Characterisation of vegetation burned in the Sanamere Lagoon record, and how it has or has not changed through time

Sanamere Lagoon was selected for analysis as it is a perennially wet water body in a region (northern Cape York Peninsula) lacking in palaeoenvironmental records. This site was also selected for a modern comparison with open woodland locations elsewhere in Cape York Peninsula as the modern vegetation community immediately surrounding Sanamere Lagoon consists of dwarf heathland with an absence of grasses.

7.2 Site Description

Sanamere Lagoon (11.117°S, 142.35°E) is located approximately 20 kilometres south of Bamaga, close to the northern tip of Cape York Peninsula, far north Queensland (Figure 7.1, Figure 7.2). The lagoon is approximately 1.5 km north-south and 2km east-west and is part of the Jardine River Wetlands Aggregation in the Directory of Important Wetlands in Australia (Department of Environment & Science 2018a). Sanamere is classified as a palustrine system, also referred to as a "sub-coastal wet heath swamp" and is of value as a "wilderness wetland area" containing "wilderness heathland" as part of the Jardine River system (Department of Environment & Science 2018a; Abrahams et al. 1995, p.134). Palustrine systems are non-channel wetlands with "more than 30% emergent vegetation" (Department of Environment & Science 2018b).

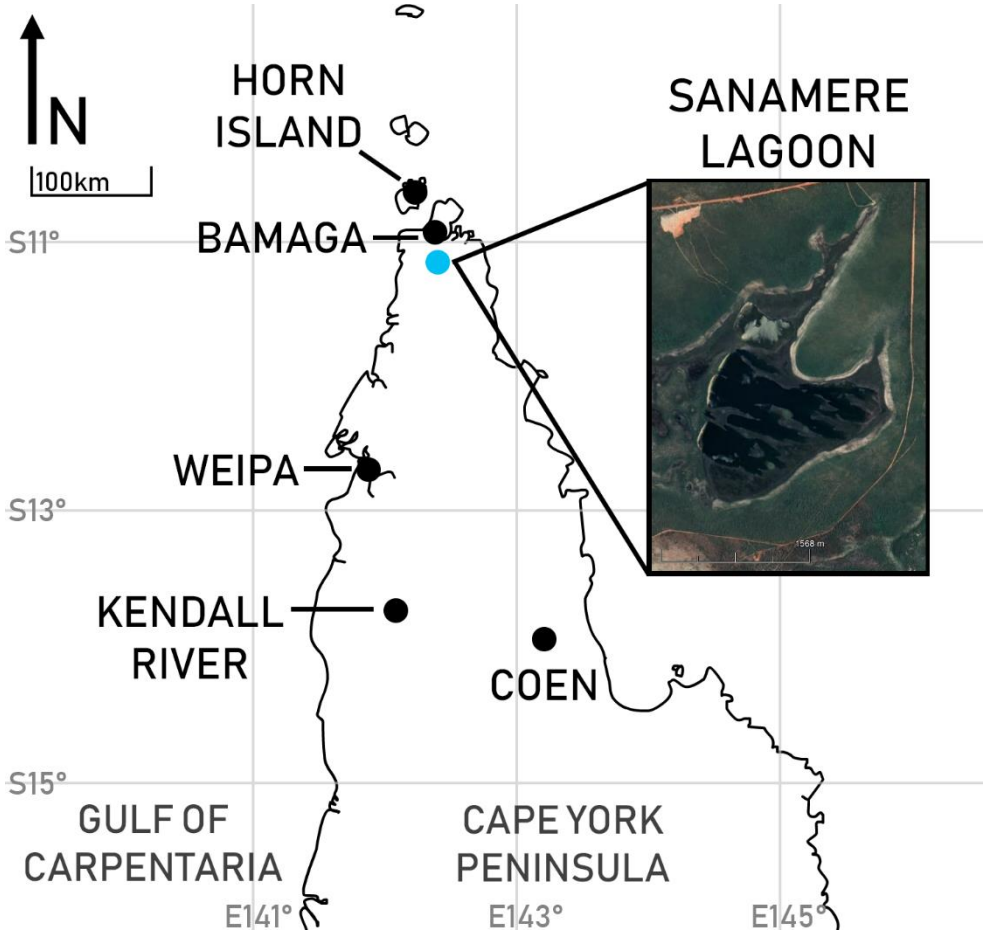

Figure 7.1: Location of Sanamere Lagoon and places mentioned in the text (inset after Google Earth 2018g).

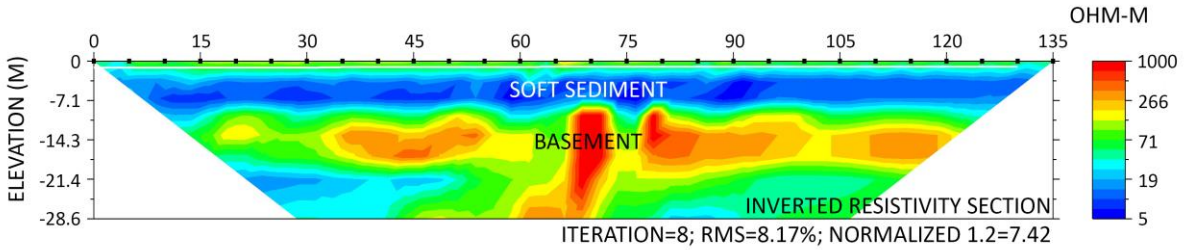

Figure 7.2: Sanamere Lagoon inverted resistivity section.

Sanamere Lagoon is at 15 m a.s.l. elevation, and maximum water depth measured in April 2016 was 1.25 m. The majority of the lagoon is perennially wet (Figure 7.3).

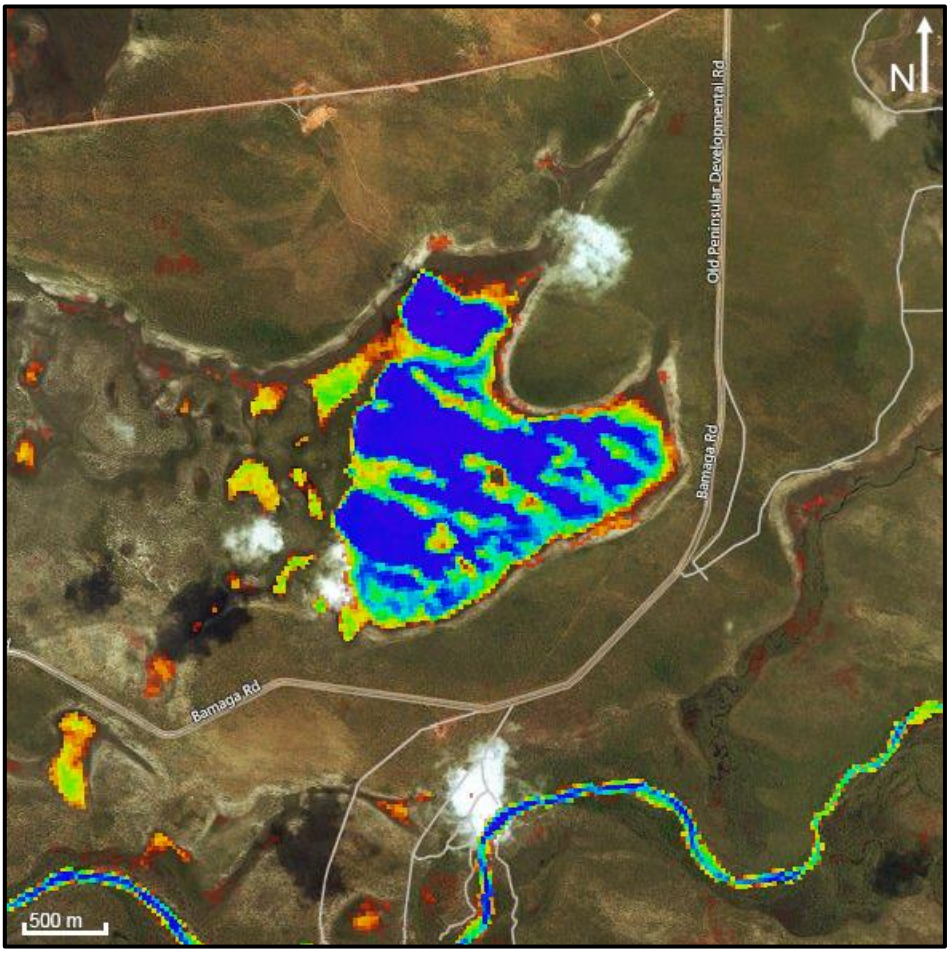

Figure 7.3: Sanamere Lagoon (and adjacent Jardine River) water permanence derived from LANDSAT imagery for the period 1970-2018 (after Geoscience Australia 2018; Department of the Prime Minister & Cabinet 2019). Dark blue indicates >90 % water permanence over the observation period.

Sanamere is an enclosed basin surrounded by higher elevation land, with the highest point (57 m a.s.l.) to the north-northeast of the lagoon, close to the current Bamaga Road (Department

of the Prime Minister & Cabinet 2019; Geoscience Australia 2015). Based on topography, Sanamere Lagoon has an approximate catchment area of 9 km^2, with the lowest point at ~17 m a.s.l. to the west of the lagoon (Figure 7.4). The original Northern Bypass of the Bamaga Road (described in Land Use History) as well as the Old Telegraph Track bisect the eastern side of the Sanamere catchment; at the time of fieldwork (2016-2017), the Old Telegraph Track, as the road was known, was becoming overgrown.

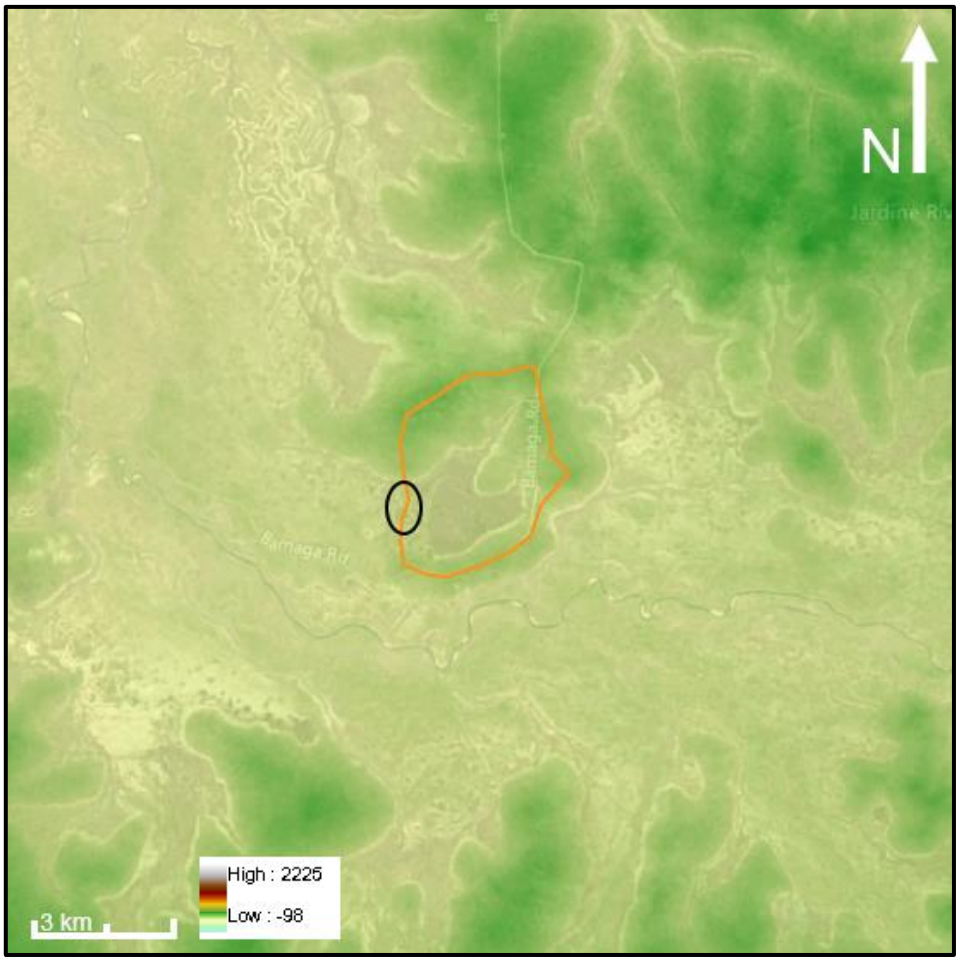

Figure 7.4: Digital elevation map of Sanamere Lagoon and surrounds, with the approximate catchment area of the lagoon marked in orange and western low point (outlet) circled in black. Darker green indicates higher elevation (after Geoscience Australia 2015).

7.2.1 Land Use History

Aerial photographs show minimal changes to the lagoon itself and immediate catchment since 1969, and also confirm that large areas of the lagoon are perennially wet (Figure 7.5).

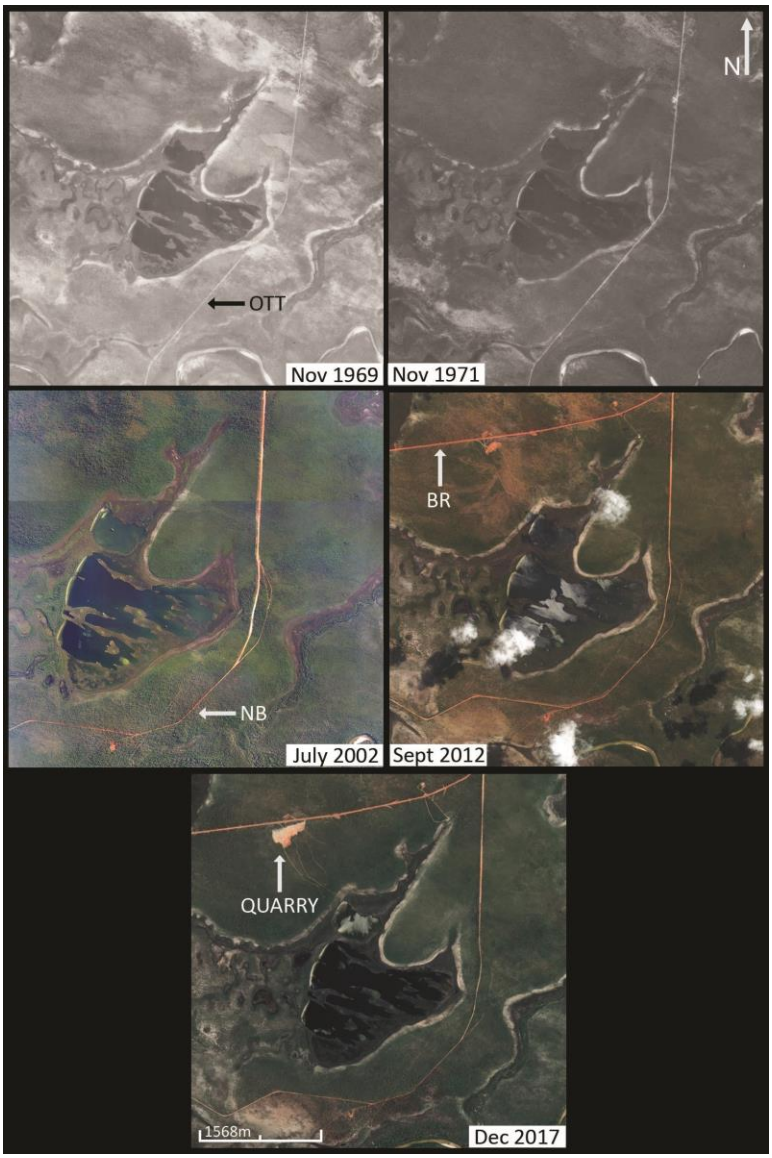

Figure 7.5: Aerial and satellite images of Sanamere Lagoon (after Google Earth 2018g; Queensland Government 2019). OTT: Old Telegraph Track, NB: Northern Bypass, BR: current Bamaga Road.

The Old Telegraph Track, completed in 1887 and operational until 1987 (Horsfall & Morrison 2010; Department of Environment & Science 2019a), is clearly visible in all aerial photographs running across the southeast edge of the lagoon (labelled OTT in the 1969 image, Figure 7.5). The largest settlement north of the Jardine River, Bamaga, was established between 1949 and 1952 and initially accessible from the south only via the Old Telegraph Track (Queensland Government 2015a, see Chapter 3). This track is located partly within the Sanamere catchment; however, based on direct field observations, it is the opinion of the author that this track had little impact in terms of erosion and vegetation disturbance. However, increased traffic near the site including use of the neighbouring Jardine River National Park may have affected recent fire regimes (see Fire section below).

The 2002 satellite image shows the addition of the Northern Bypass segment (labelled NB) of Bamaga Road, which diverts further east of Sanamere Lagoon than the Old Telegraph Track. The bypass uses the newer Jardine River crossing west of the former crossing used by the Old Telegraph Track. A subsequent addition to the Northern Bypass/Bamaga Road (labelled BR) is visible in the 2012 satellite image, diverting the majority of traffic to the west and north of Sanamere before recombining with the Old Telegraph Track. This recent diversion is the current main road north of the Jardine River, with the previous bypass referred to as Old Peninsular Development Road by the Australian Government National Map (Department of the Prime Minister & Cabinet 2019). Gravel quarrying for use on the main road is visible in the 2012 satellite image and enlarged in the 2017 image, as was observed at the time of fieldwork (see Department of National Parks, Sport & Racing 2013, p.6).

Sanamere Lagoon is located immediately west to the Jardine River National Park. This park was gazetted in 1977 and is used recreationally for camping, four-wheel driving, fishing, nature

walks and observing wildlife (Queensland National Parks & Wildlife Service 1996; Department of Environment & Science 2019a; Department of National Parks, Sport & Racing 2013). The Anggamudi (also known as Angkamuthi), Wuthahti (alternatively Wuthathi) and Yadhaigana (alternatively Yadhaykenu) people are the traditional owners of the Jardine River catchment (Wilderness Society 2018; Australian Institute of Aboriginal & Torres Strait Islander Studies [AIATSIS] 2014). Sanamere Lagoon is part of the Apudthama Land Trust Area, classified as Aboriginal Freehold land and managed under the Northern Peninsula Area Regional Council (Apudthama Land Trust 2018).

7.2.2 Environment

7.2.2.1 Climate

The climate of Sanamere Lagoon, as well as the majority of Cape York Peninsula, is classified as AW – Tropical/Equatorial Savanna with dry winter under the global Köppen-Geiger Climate Classification (Peel, Finlayson & McMahon 2007; Kottek et al. 2006). Mean annual rainfall is 1800 mm measured from the nearest weather station (Horn Island, approximately 55 km north of Sanamere), with rainfall primarily (~90 %) occurring between December and April (BOM 2018c). Winds are predominantly from the north-northwest and southeast in January and July, respectively (BOM 2018c) (Figure 7.6). Average minimum and maximum daily temperature ranges from 23 °C to 32 °C, in August and November-December respectively (Horn Island weather station, BOM 2018c). Mean relative humidity measured at 9 am varies between 69 % (October) and 83 % (February) (BOM 2018c).

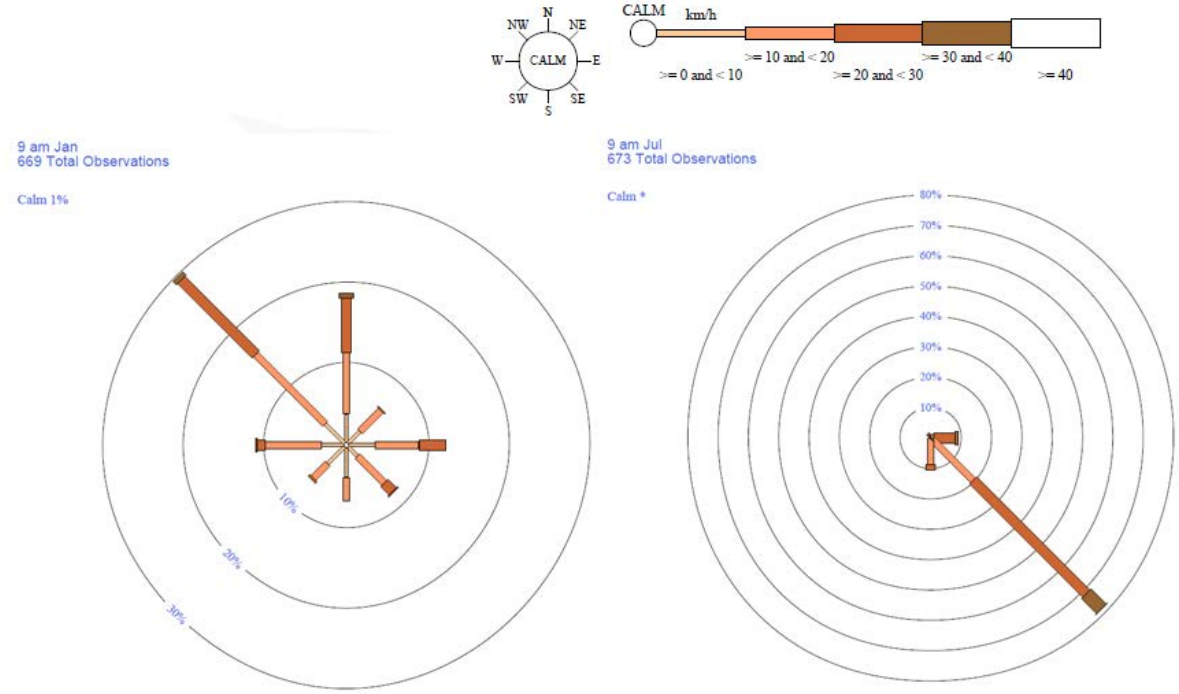

Figure 7.6: Average wind direction and speed 1995-2017, measured at 9 am in January (left) and July (right), from Horn Island weather station (BOM 2018c).

In the period 1969-2016, four cyclones passed within 50 km of Sanamere Lagoon, and 10 within 100 km (BOM 2018a). The far northern Cape York Peninsula region has an average annual lightning (cloud-to-ground) flash density of 1 flash/km^2/year, primarily occurring between November and April (BOM 2016a; Dowdy & Kuleshov 2014).

7.2.2.2 Geology and Vegetation

Sanamere Lagoon is underlain by Pleistocene sand with minor silt and clay, and is bordered by deeply weathered Middle Jurassic to Early Cretaceous quartzose sandstone and micaceous carbonaceous siltstone (Helby Beds; Bureau of Mineral Resources, Geology & Geophysics

1977). Dominant soils in the area are “deep bleached sands” (Ca43: Uc2.21) and “deep sandy mottled yellowish red earths” (Mt9: Gn2.64) (Northcote et al. 1960-1968).

The Jardine River is the largest perennial river system in Queensland, and the Jardine River Wetlands Aggregation crosses from the western coast of Cape York into the National Park in the east (Figure 7.7, Department of National Parks, Sport & Racing 2013:2). Both the Jardine-Heathlands Aggregation, adjacent to Sanamere Lagoon, and the Jardine River Wetlands Aggregation, containing Sanamere, have been identified as areas of high conservation and “wilderness value”, recognised for diverse vegetation and faunal assemblages (Department of Environment & Science 2019a, 2019b; Abrahams et al. 1995). The Jardine-Heathlands Aggregation protects 35 plant and animal species of conservation significance, while the Jardine River Wetlands Aggregation has been identified as an “essentially undisturbed catchment” (Department of National Parks, Sport & Racing 2013, p.3). The wetland communities of Cape York Peninsula are “amongst the largest, richest and most diverse in Australia” and contain a high species richness of rare and threatened plant taxa (Abrahams et al. 1995, pp.33-97). The Jardine River and associated wetlands have also been identified as an important habitat of the vulnerable Estuarine Crocodile (*Crocodylus porosus*), with the combined adult populations of the Jardine River and Jacky Jacky Creek systems being identified as “represent[ing] the largest breeding populations known in Queensland” (Abrahams et al. 1995, p.116).

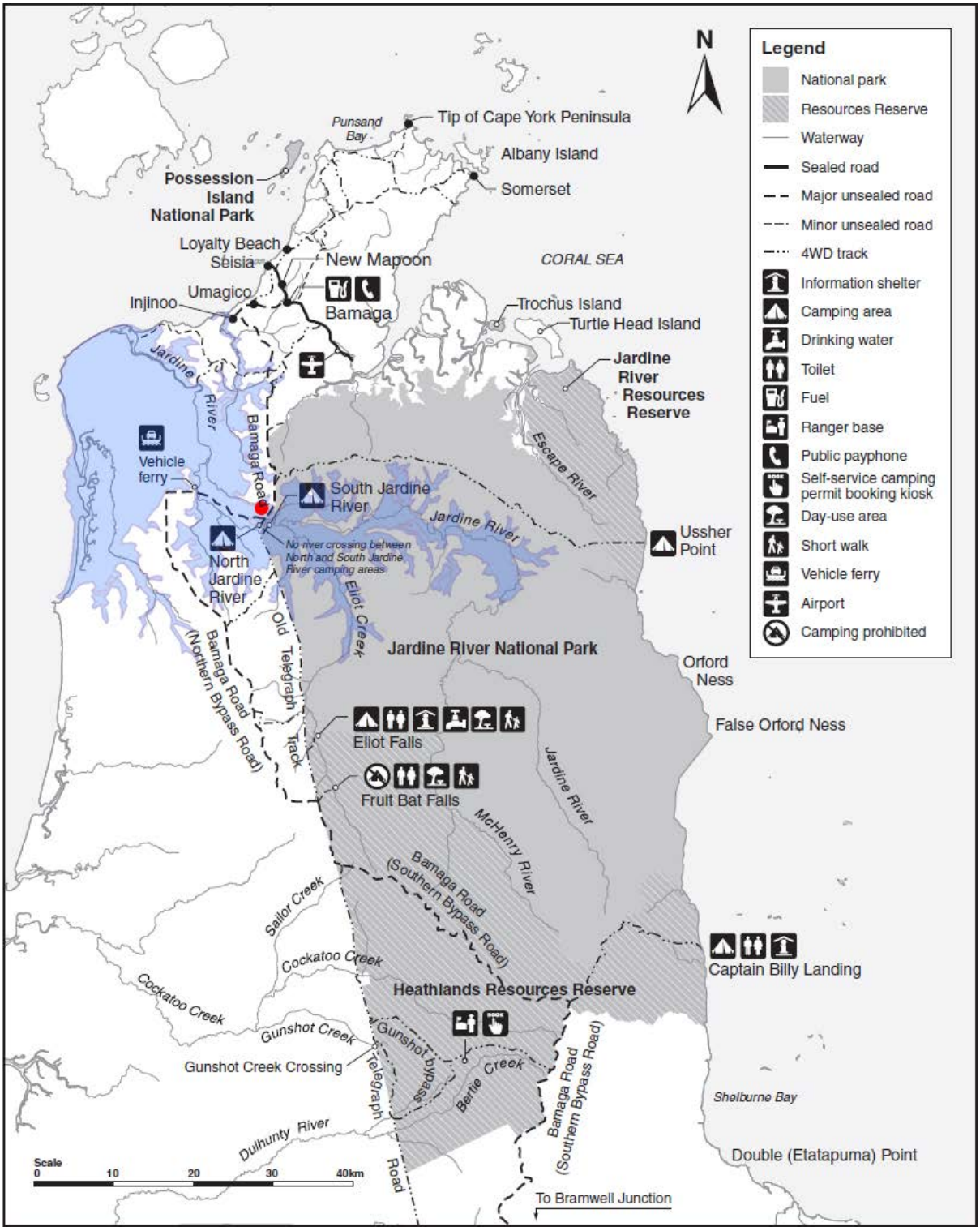

Figure 7.7: Map of the Jardine River National Park, Jardine River Resources Reserve and Heathland Resources Reserve, with Sanamere indicated in red and the Jardine River Wetlands Aggregation shaded blue (after Department of National Parks, Sport & Racing 2018).

Closed sedgeland with scattered Pandanus are found at the edge of Sanamere Lagoon (Figure 7.8), with sedges extending in bands into the water (structurally visible in satellite images, see Figure 7.5; also observed by Brass 1953, p.180). Waterlilies and other aquatic plants are absent with algae and sedges dominating in the water; sedges include dominant *Eleocharis* with *Schoenus* present. Also found on these wet sandy soils, predominantly close to the waterline, are insectivorous plants of *Nepenthes* (Pitcher Plants), adapted to source nutrients from insects due to the low nutrient content of the soil (Beasley 2009, p.178, 228).

Figure 7.8: Vegetation at the Sanamere Lagoon waterline, comprised of sedges and scattered *Pandanus*.

This sedgeland community transitions sharply to open heathland which dominates Sanamere Lagoon's broader catchment (Figure 7.9); heathland is commonly found on nutrient-poor "deep bleached sands" (Ca43: Uc2.21 mentioned previously, Northcote et al. 1960-1968; see Beasley 2009, p.178; Neldner et al. 2017, p.191). The heath forms a shrubland, dominated by *Neofabricia, Asteromytus*, *Baeckea*, *Jacksonia, Hibbertia, Thryptomene, Allocasuarina* and *Grevillea* (Department of Environment & Science 2019b; Neldner & Clarkson 1995, p.72). Trees are few, and when present, comprise *Grevillea pteridifolia* and *Banksia dentata*. Grasses are minor and ground cover consists of clumped sedges (*Schoenus*), notable across wetter soil areas and drainage lines. Bare sandy soils are visible and leaf litter is minimal. Open heathland vegetation extends approximately 300 metres from the water edge before transitioning into *Eucalyptus* woodlands.

Figure 7.9: Open heathland vegetation 50 metres from the waterline.

Beyond 300 metres from the waterline, vegetation changes in structure (particularly height) and composition (Figure 7.10). *Eucalyptus* woodlands occur, dominated by *Eucalyptus tetrodonta* with *Corymbia nesophila* codominant (Neldner & Clarkson 1995, p.116; Neldner et al. 2017, pp.108-109). Smaller sub-canopy trees are common and include *Acacia, Grevillea glauca* and *Grevillea pteridifolia* as well as *Livisonia* palm, with *Lomandra* and *Asteromyrtus* present as shrubs. *Casuarina* occurs in patches, and in wetter, low-lying areas *Banksia* is present. Grasses dominate ground cover in this area (*Poaceae*) and leaf litter is greater than that found in the heathland. Termite mounds were recorded in the field (2017) within the transition from heathland to woodland, along with indications of recent burning such as charcoal pieces and scorched woody debris.

Figure 7.10: Heathland to woodland transition at 300m (left) and *Eucalyptus* woodland at 400 m (right) from the waterline.

7.2.2.3 Fire

In the 18 year period spanning 2000-2018 the area immediately surrounding Sanamere Lagoon (both within the catchment and beyond) burned on average every 3 to 7 years (every year at its most frequent) (NAFI 2019). However, fire scars were recorded in this period over the surface of the lagoon (Figure 7.11) that are likely a result of error in the determination of fire scars (P. Jacklyn pers. comm.). Fire scars that extend substantially beyond the water surface may be assumed to represent real scars.

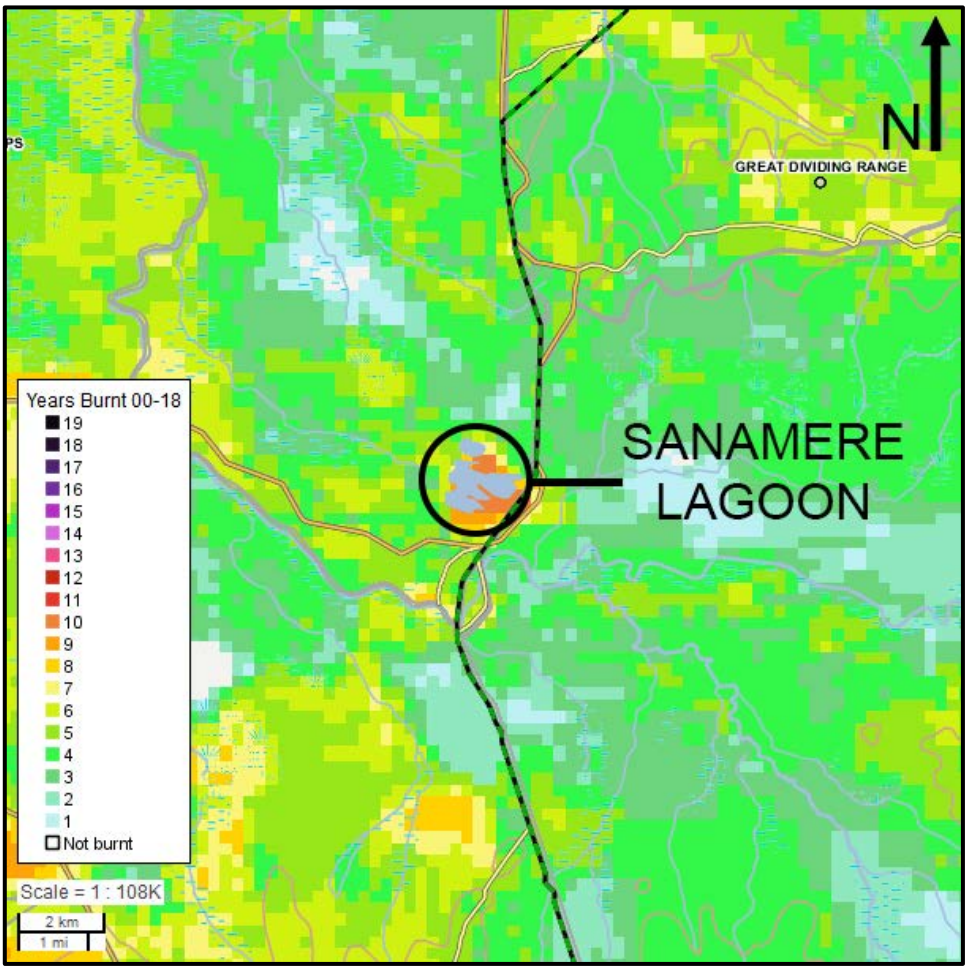

Figure 7.11: Number of years that areas around Sanamere Lagoon burned from 2000-2018 (NAFI 2019).

Fires in the period 2000-2018 were primarily between August and December. There was one July fire scar in 2003 including land surrounding and south of the lagoon as well as to the south-east extending into the Jardine River National Park (NAFI 2019). Fires occurring in May to July are frequently defined as "early dry season" fires (see Chapter 3 for a detailed discussion), while fires from August onwards (NAFI 2019; Russell-Smith et al. 1997; Russell-Smith & Edwards 2006) or from September to either October or November (Andersen, Cook & Williams 2003; Andersen et al. 2005) are defined as "late dry season" fires. The 2003 July fire scar at Sanamere is the only early dry season fire recorded in the period 2000-2018, with the remainder occurring during the late dry season or early wet season. Lightning-driven fire regimes have been associated with burns occurring in the late dry/early wet season (Veenendaal et al. 2018, p.9).

During the main burning months (August to December) recorded from 2000-2018 around Sanamere Lagoon, winds are predominantly from the east to southeast. Charcoal transported to the lagoon under these conditions is therefore most likely derived from the region that is now the Jardine River National Park. The Jardine-Heathlands Aggregation Management Statement released by the Department of National Parks, Sport and Racing (2013, pp.3-5) identifies "late season, hot fires" in the Jardine-Heathlands Aggregation as a result of a lack of fire management, and as typically originating from roadways including the Southern Bypass and the Old Telegraph Track. The document mentions that a lack of fire "may threaten" inland heath in the area (Department of National Parks, Sport & Racing 2013, p.3).

7.3 Methods

7.3.1 Sample Collection

Samples were collected from Sanamere Lagoon during two 2016 fieldwork trips (April and June) and one in July 2017. Sediment cores were collected by hand using a D-section corer from a boat and using a raft-mounted hydraulic corer modified from Eijkelkamp equipment (Figure 7.12).

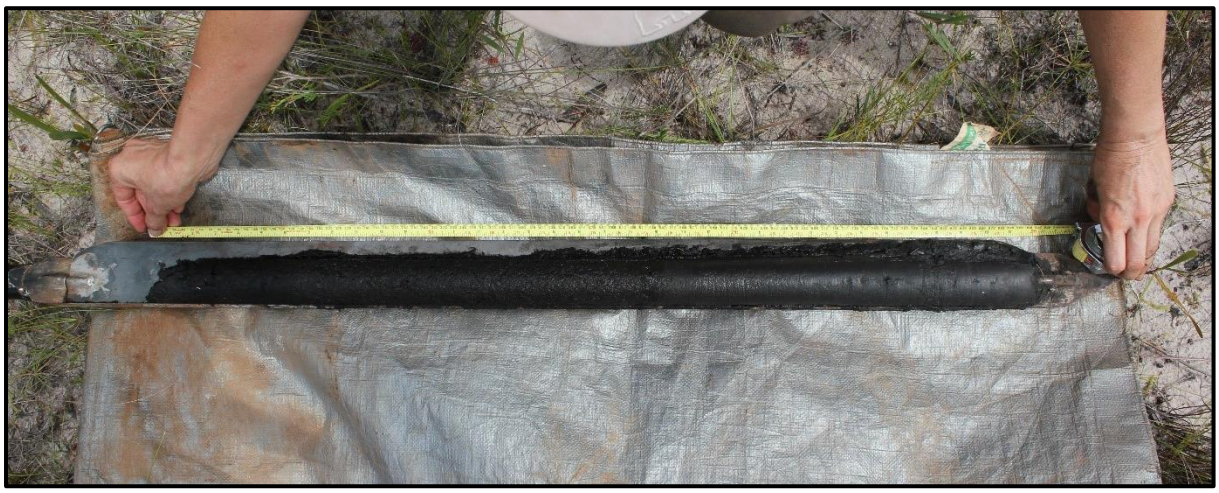

Figure 7.12: D-section SAN1 on site prior to sampling.

Multiple sediment cores were collected, with D-section core (SAN1) and a 15 cm diameter short core collected specifically to provide sufficient sample from the upper sediment layers to enable ^{210}Pb analysis, selected for analysis in this study (SANFC) (Figure 7.13). Cores were either sampled on-site (SAN1) or frozen for transport and storage before being sampled in the laboratory (SANFC). Cores were contiguously sampled at 0.5 cm intervals.

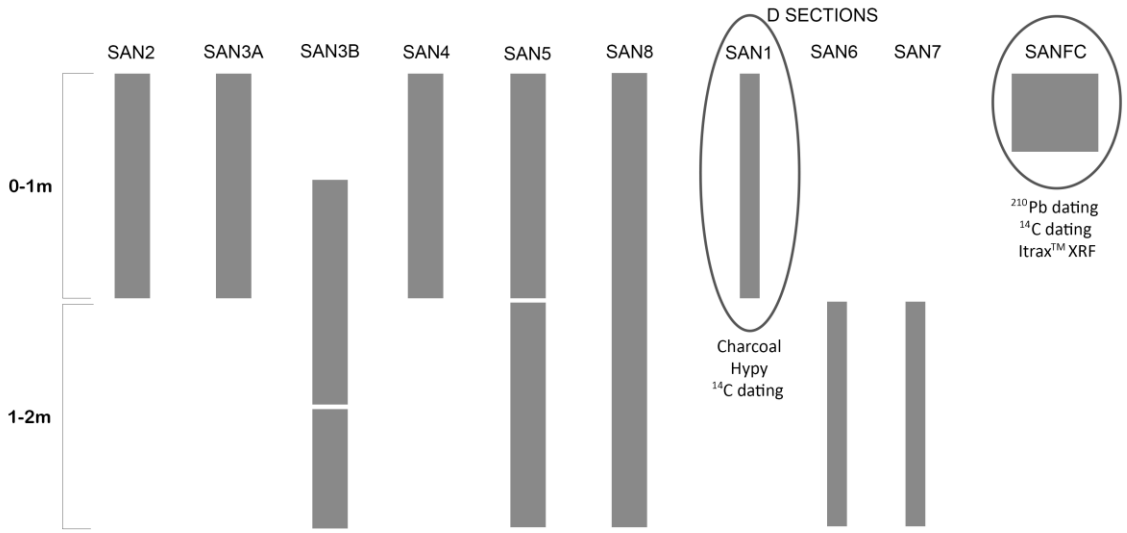

Figure 7.13: Visual representation of sediment cores collected from Sanamere Lagoon. Core numbers indicate the order samples were collected and are not related to coring location. Cores selected for study are circled, with analyses listed.

Ten surface samples were collected along a transect between the raft coring location in July 2017 and the shore of the lagoon using a grab sampler (Figure 7.14).

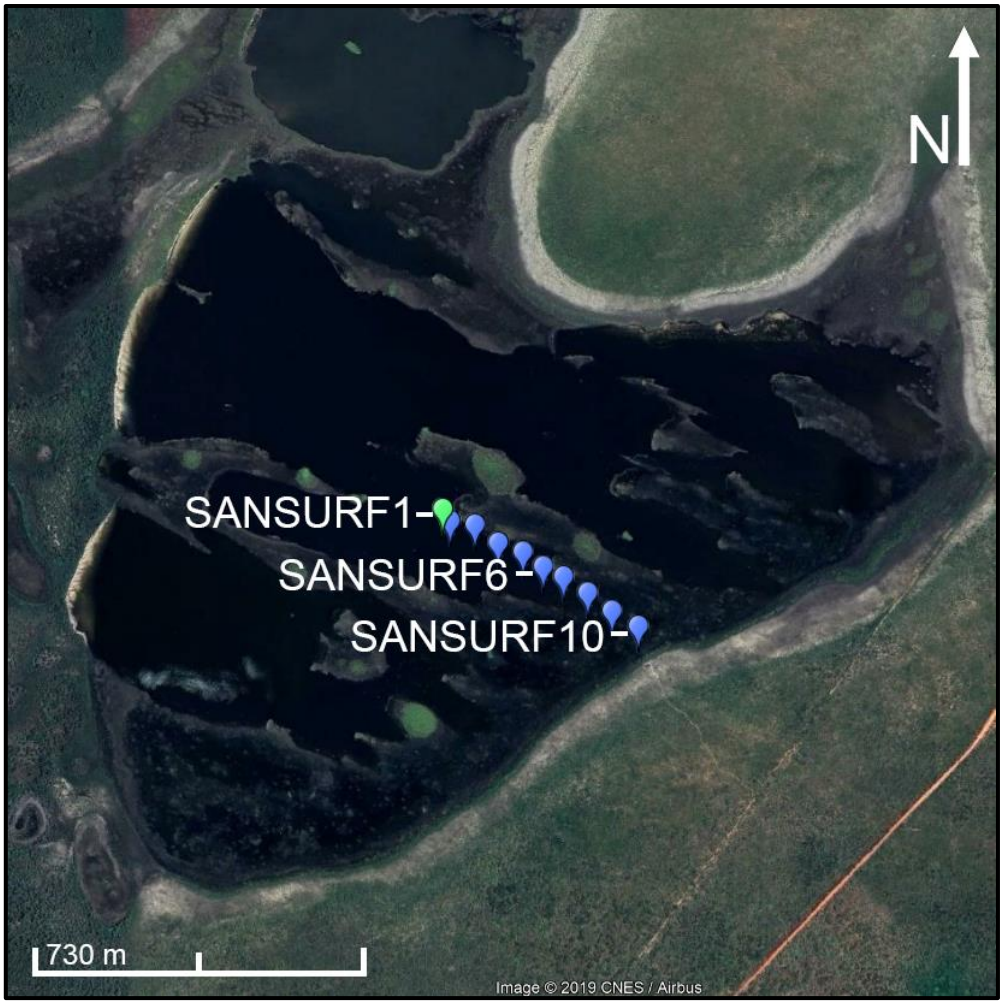

Figure 7.14: Map showing sample collection locations for Sanamere surface samples, with the raft coring position and first sample location marked in green (after Google Earth 2018g).

A charcoal trap was installed close to the lagoon to collect modern airborne charcoal, along with two charcoal traps installed at other locations on Cape York Peninsula (Coen and Kendall B) to create a comparative modern dataset (Figure 7.15, see Chapter 4 for detailed description).

Figure 7.15: Charcoal trap on site at Sanamere Lagoon after installation (April 2016).

7.3.2 Laboratory analyses

Laboratory methods and justification for the choice of methods are described in detail in Methods Chapter 4. For Sanamere, D-section core SAN1 was selected for study. SAN1 was deemed representative of uppermost (0-1 m) Sanamere sediments as it was collected centrally from the lagoon and removed intact. As per Chapter 4, the core was divided for optical charcoal analysis (Courtney Mustaphi & Pisaric 2014; Stevenson & Haberle 2005; Enache & Cumming

2006) and chemical analysis (freeze-dried bulk and <63 μm samples; Wurster et al. 2012). Charcoal trap samples were processed using the same method as sediment samples for optical charcoal analysis.

Two longitudinal sediment slices spanning the entire core length of SANFC were analysed using an Itrax^{TM} Elemental Core Scanner at the Australian Nuclear Science and Technology Organisation (ANSTO) Lucas Heights campus, as detailed in Chapter 4.

^{210}Pb sample preparation and analysis by alpha and gamma spectrometry was undertaken at ANSTO Lucas Heights on samples from the large-diameter (15 cm) core SANFC, as per the procedures outlined in Chapter 4. ^{14}C sample preparation and analysis by accelerator mass spectrometry was undertaken at ANSTO Lucas Heights on samples (hydrogen pyrolysis residue and bulk sediments) from D-section core SAN1 and large-diameter core SANFC, following the method described in Chapter 4. Hypy residue sample SAN1 15-15.5 cm (OZW501) prepared as part of the November 2017 batch failed to graphitise so was unable to be dated.

7.4 Results

7.4.1 Charcoal Traps

All collected charcoal trap samples contained charcoal particles (Figure 7.16). The charcoal trap installed at Sanamere Lagoon was emptied twice after installation in April 2016: once in June 2016 to ensure the trap was functioning and once in July 2017. SANFT1 therefore accumulated over two months only, while all other charcoal trap samples represent one year.

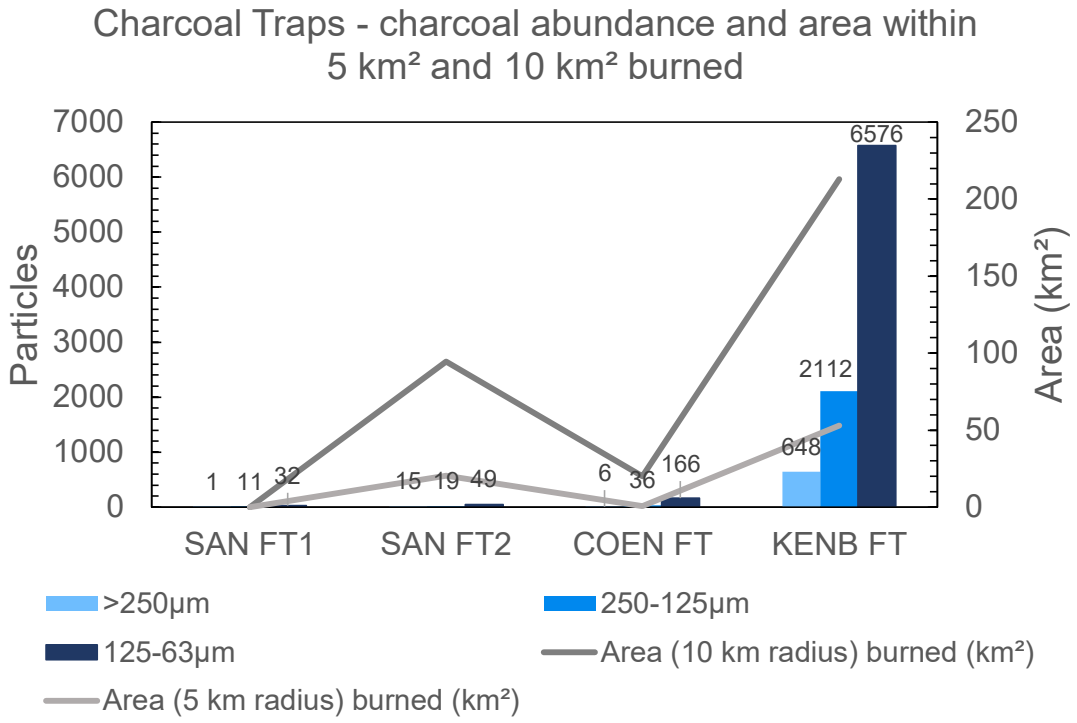

Figure 7.16: Charcoal particle counts for charcoal trap samples, and area burned within 5 km^2 and 10 km^2 (burn data from NAFI 2019). Area burn estimates for Sanamere Lagoon are likely to be overestimations.

While a larger area burned around Sanamere Lagoon than the Coen charcoal trap during the period of charcoal trap sample accumulation, COENFT contains more particles (208 total) than SANFT2 (83 total). This is likely due to an overestimation of area burned around Sanamere Lagoon due to the water surface of the lagoon being erroneously recorded as a fire scar in 2016 (see Fire section above). Kendall B charcoal trap contained significantly more charcoal than the other traps due to extensive burning during the collection period (213 km^2 of land within a 10 km^2 radius), visible in the landscape when the trap was retrieved (Figures 7.17 and 7.18).

Figure 7.17: Kendall B charcoal trap at installation (2016) and retrieval (2017) showing visible signs of recent burning.

Figure 7.18: Surrounding vegetation at Kendall B when the charcoal trap was installed and retrieved, showing obvious recent burning.

Limited elongate morphotypes were present in either of the Sanamere samples, with none recorded in the largest size fraction (>250 µm) of either SANFT1 or SANFT2 (Figure 7.19). Elongate morphotypes were well represented in both the Coen and Kendall B charcoal trap samples, with all COENFT size fractions displaying over 35 % elongate morphotypes and ~53 % of KENBFT 125-63 µm recorded as elongate (3288 particles of 6576) (for full comparison of morphotype data, see Chapter 8 Charcoal Traps and Surface Samples).

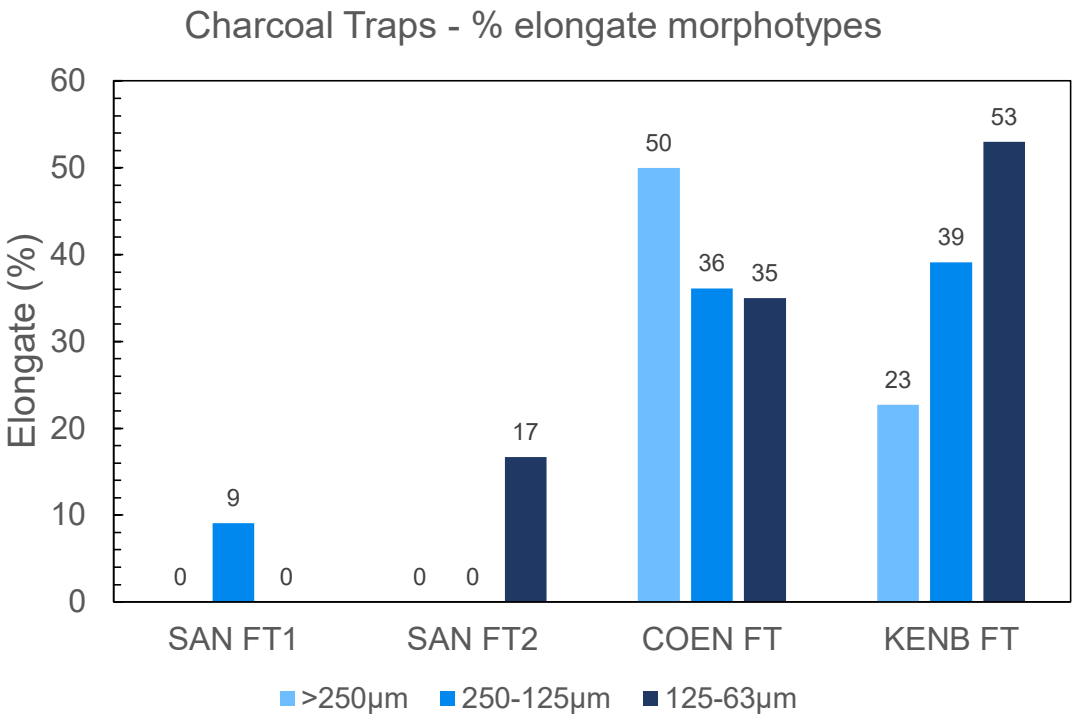

Figure 7.19: Percentage elongate morphotypes in charcoal particles from charcoal traps.

Charcoal from the Sanamere charcoal trap samples similarly displayed low percentage elongate particles determined from length-width ratios, with a maximum of 13.33 % in >250 µm of

SANFT2 (2 particles of 15, Figure 7.20). COENFT and KENBFT percentage elongate particles from length-width ratios show similar patterns as percentage elongate morphotypes.

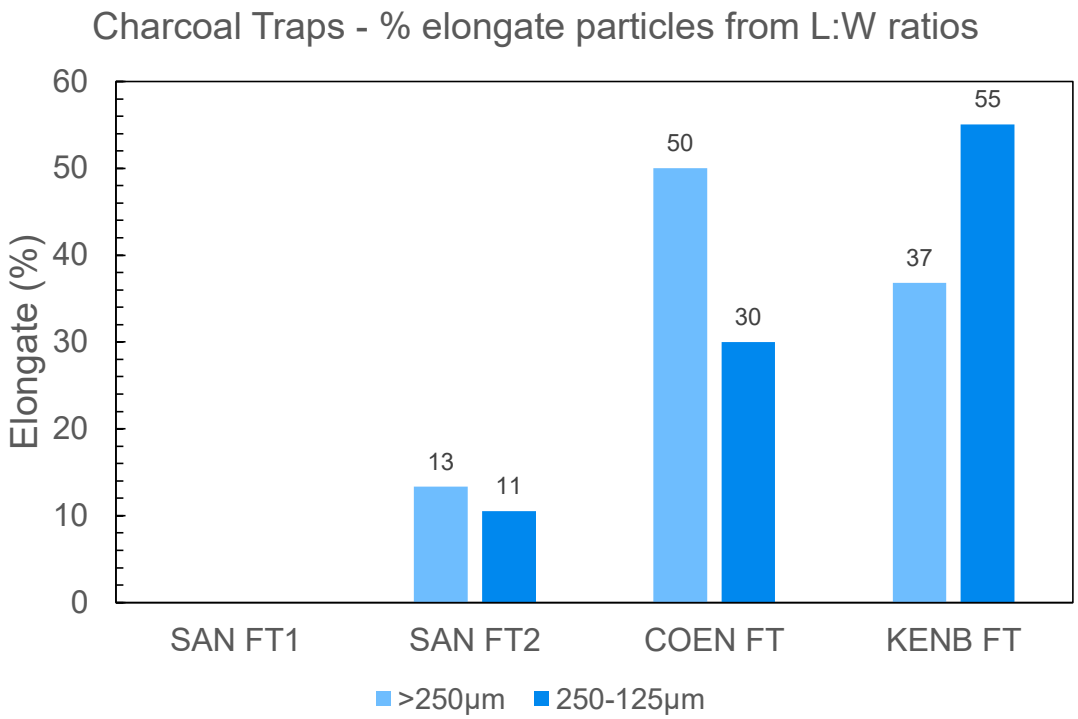

Figure 7.20: Percentage elongate charcoal particles from length-width ratios for charcoal particles from charcoal traps.

7.4.2 Surface Sample (SANSURF) Charcoal

Charcoal analysis was completed for three Sanamere surface covering the transect from the central coring position (SANSURF1) to the shore (SANSURF10), with one cubic centimetre of wet sediment collected from each sample for charcoal processing. Particle abundance varies greatly between the three samples (Figure 7.21), with the highest number of particles per cubic centimetre present in SANSURF1 (raft coring location at the centre of the lagoon). Lower abundances are shown in SANSURF6 (approximately halfway between the raft location and

the shore) and SANSURF10. A consistent relationship between the three size fractions is present in all surface samples, with particle counts increasing with decreasing particle size (also visible in the SAN1 samples, see below).

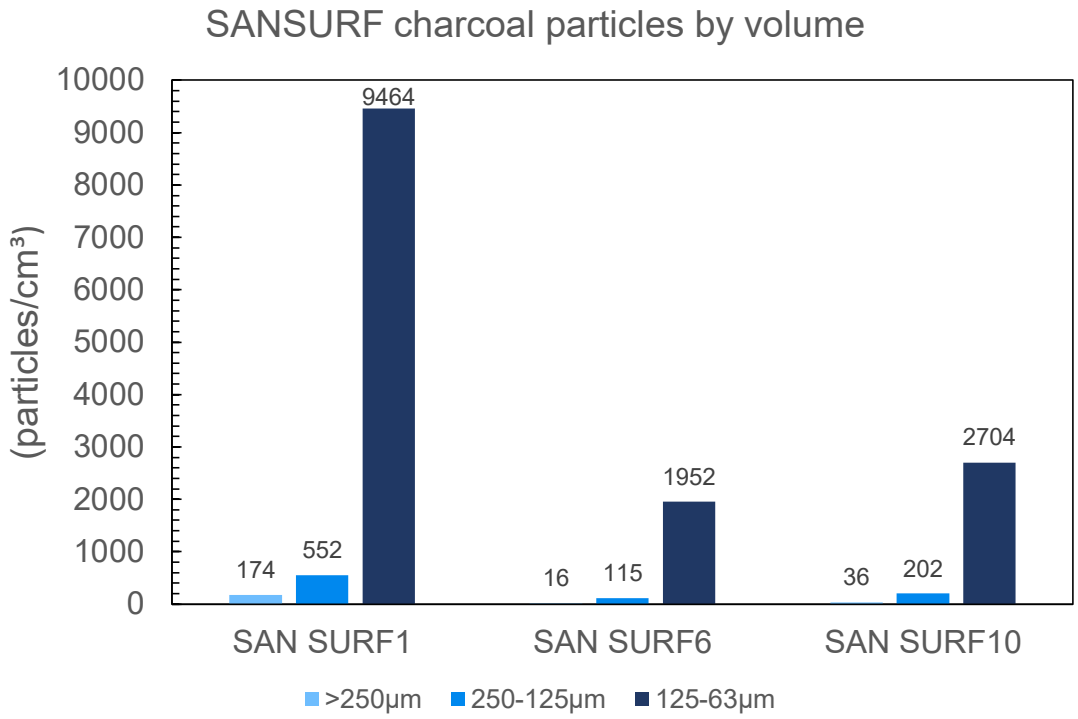

Figure 7.21: Charcoal particles by volume for Sanamere surface samples.

Morphotypes also vary between the three surface samples, with higher percentages of elongate types present in SANSURF6 (Figure 7.22).

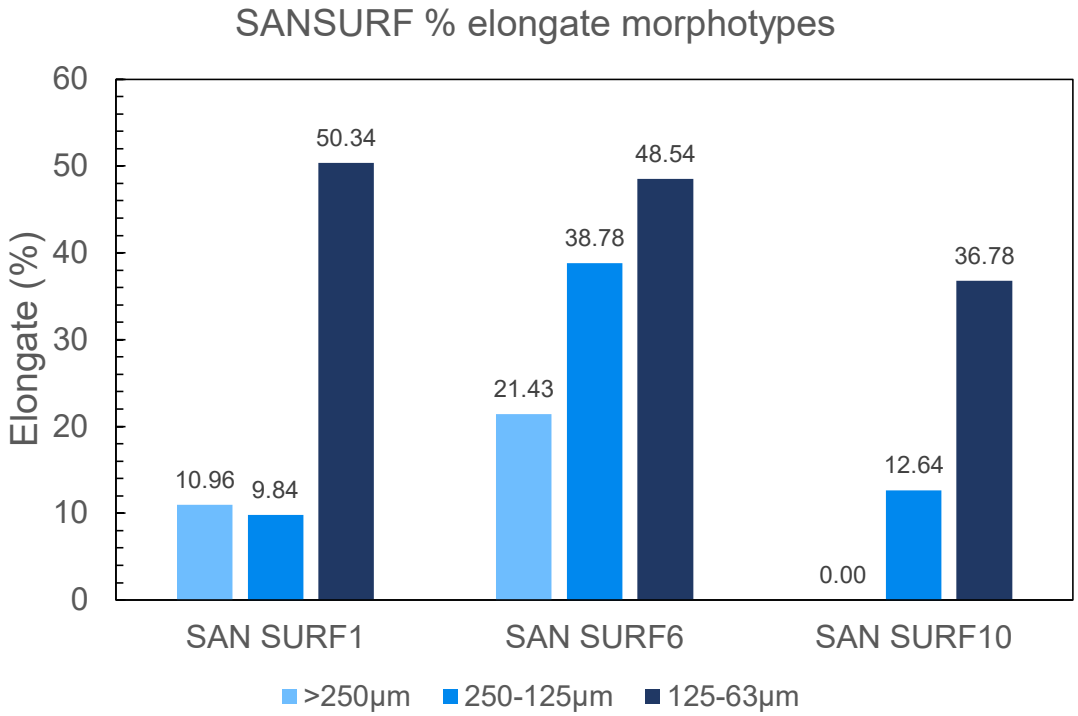

Figure 7.22: Percentage elongate morphotypes for Sanamere surface samples.

Length-width ratios for the surface samples present different patterns than those visible in elongate morphotypes (Figure 7.23). Length-width ratios show significantly higher contributions of elongate particles to the macroscopic (>250 µm and 250-125 µm) size fractions than shown in the morphotype data, exceeding 50% in SANSURF1 and SANSURF6. However, SANSURF6 consistently displays the highest proportion of elongate particles.

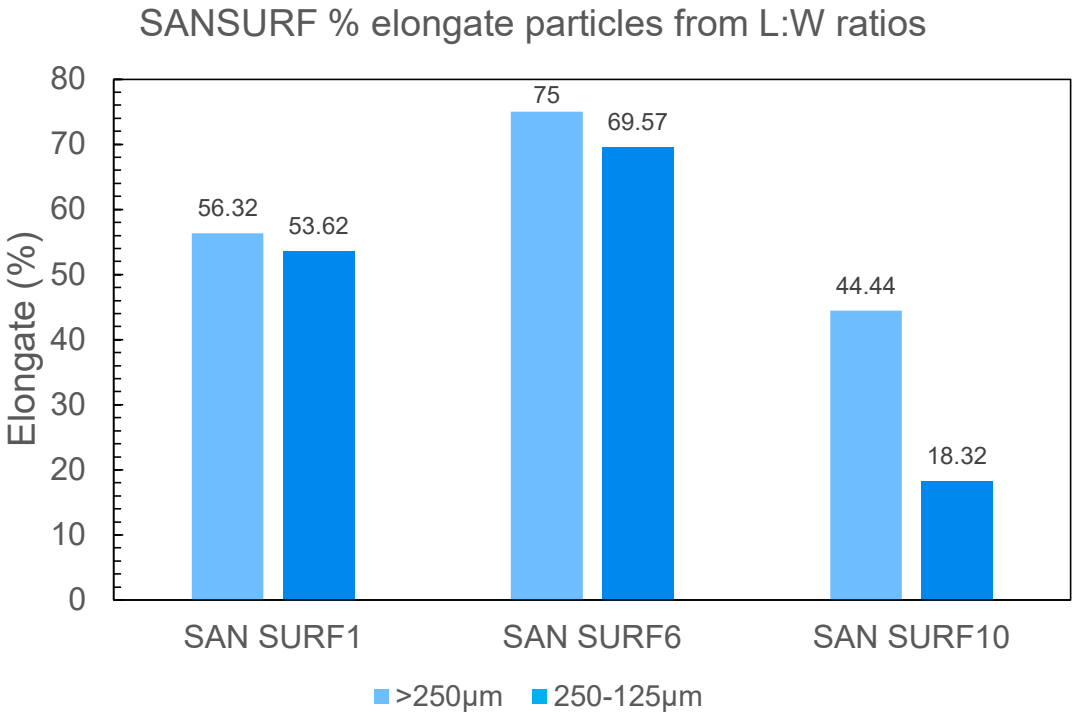

Figure 7.23: Percentage elongate particles from length-width ratios for Sanamere surface samples.

Morphotype composition is similar between samples, with high percentages of type S (structured geometric) in the >250 µm size fractions of all samples and similar proportions of morphotype varieties in the 125-63 µm size fractions (Figure 7.24).

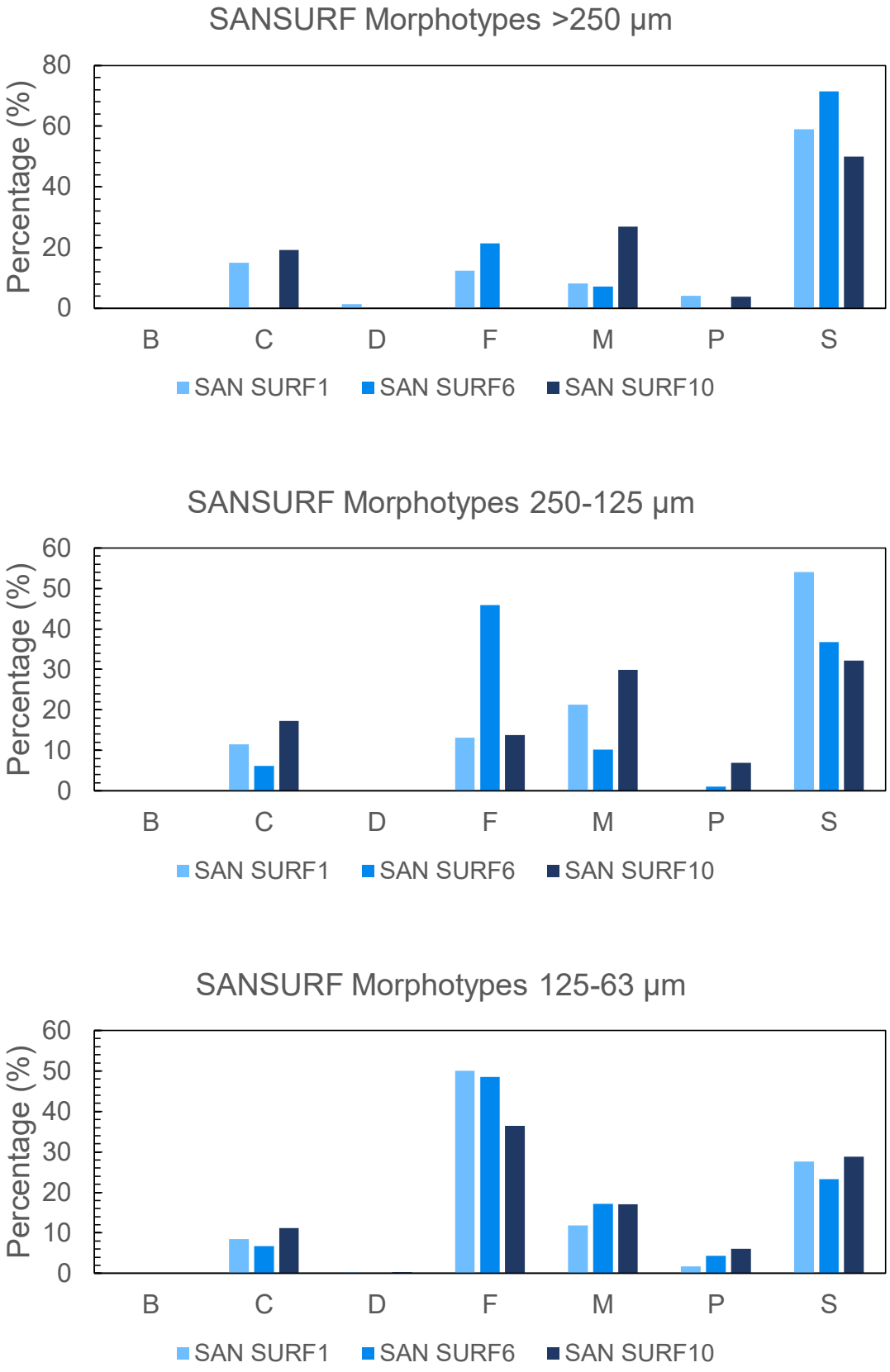

Figure 7.24: Morphotype composition of SANSURF samples.

7.4.3 Sediment Descriptions

Sediment from Sanamere is relatively consistent throughout the 2 m sediment depth with limited visually discernible stratigraphy. The sediment is peaty and primarily dark grey to black. Upper SAN1 is 10YR 2/1 Black, loose-packed peaty sediment, with a change in consistency and colour at approximately 55 cm to GLEY1 2.5/N Black smoother, more dense sediment which may indicate greater compression rather than a compositional change (Figure 7.25, see also moisture content below). Differences in colour classification are minimal as all recorded colours in the top metre are variants of black. Fine roots were noted in SAN1 between 52.5 and 54 cm during sampling.

Figure 7.25: SAN1 core on site showing characteristic peaty 10YR 2/1 Black sediment and consistency change (central) at approximately 55 cm depth to denser, smooth GLEY 2.5/N Black (bottom of core on the right).

Moisture content was calculated for SAN1 using samples freeze-dried prior to preparation for hydrogen pyrolysis, and was measured as weight loss of a sample after drying as a percentage

of wet sediment weight (Figure 7.26). Moisture content decreases sharply between 53 and 56.5 cm, visible in the intact core prior to sampling as a transition to denser, smooth sediment recorded at 55 cm (as seen in Figure 7.26).

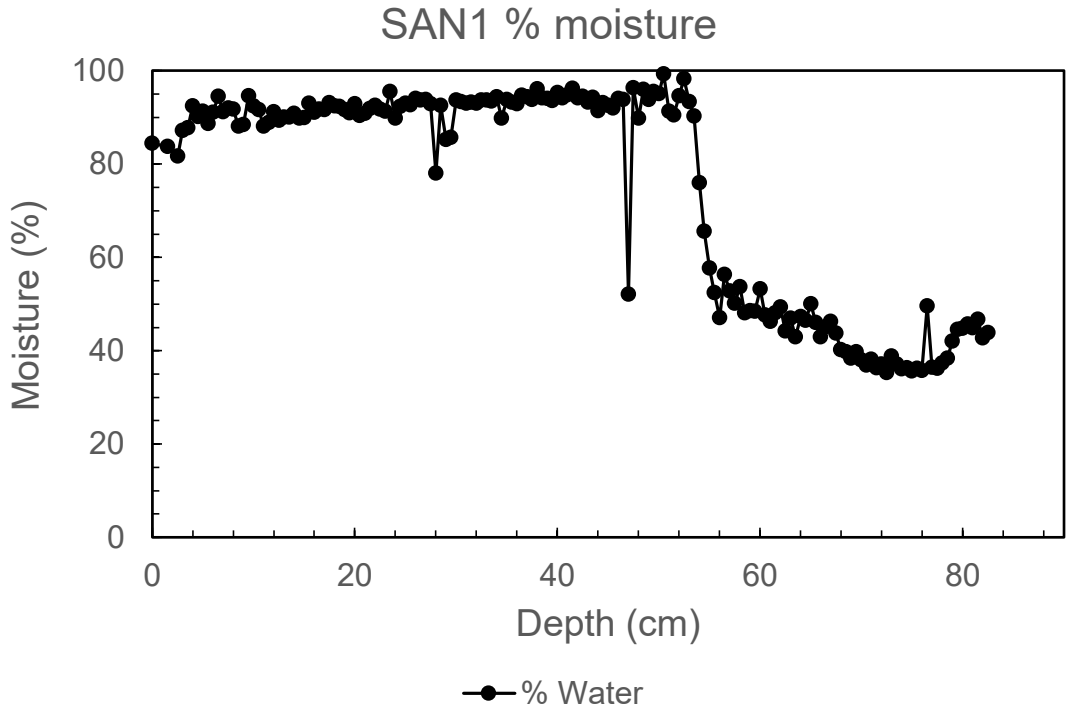

Figure 7.26: Moisture content for SAN1.

7.4.4 Chronology

7.4.4.1 Lead-210 (^{210}Pb) Dating

The ^{210}Pb activity profile derived from gamma spectrometry deviated from a monotonic decay profile for all SANFC samples except between 2 and 3 cm depth (Table 7.1). CIC (Constant Initial Concentration) and CRS (Constant Rate of Supply) age models were applied to samples above 3 cm and both models estimate that sediment at 2.5-3 cm dates to approximately 70 years ago. ^{137}Cs activities were low in all samples and could not be used to validate the ^{210}Pb

chronology. Samples analysed by alpha spectrometry displayed a decreasing profile in unsupported ^{210}Pb with depth, with lower uncertainties than the results from gamma spectrometry (Figure 7.27). CIC and CRS age models applied to the alpha spectrometry results are in agreement, with the deepest sample (4.5-5 cm) dated to either 157 ± 12 years BP (CIC) or 168 ± 57 years BP (CRS). Results from the CIC age model are used in subsequent data analyses as error margins are smaller and constant, and a monotonically decreasing decay profile dictates the use of the CIC model (see Binford 1990).

Table 7.1: ^{210}Pb by gamma (top) and alpha (bottom) spectrometry results for SANFC samples; columns highlighted in red are mentioned in the text. Dates are presented as years prior to the collection date (2017).

ANSTO ID	Depth (cm)	Dry Bulk Density (g/cm^3)	Cumulative Dry Mass (g/cm^2)	Count Date	Total ^{210}Pb (Bq/kg)	Supported ^{210}Pb (Bq/kg)	Unsupported ^{210}Pb Decay corrected to 01-Dec-17 (Bq/kg)	Calculated CIC Ages (years)	Calculated CRS Ages (years)	CRS model Mass Accumulation Rates (g/cm^2/year)
U076	0.0 - 0.1	0.12	0.01 ± 0.01	01-Nov-17	187 ± 8	24.7 ± 1.1	162 ± 8	1 ± 1	1 ± 1	0.012 ± 0.001
U077	0.1 - 0.5	0.12	0.04 ± 0.02	20-Nov-17	261 ± 12	26.0 ± 0.0	235 ± 12	5 ± 4	4 ± 2	0.007 ± 0.001
U078	0.5 - 1.0	0.12	0.09 ± 0.03	20-Nov-17	217 ± 8	26.3 ± 1.2	190 ± 9	13 ± 4	11 ± 3	0.007 ± 0.001
U080	1.5 - 2.0	0.27	0.29 ± 0.04	08-Nov-17	102 ± 15	27.1 ± 1.6	75 ± 15	42 ± 6	37 ± 6	0.008 ± 0.002
U082	2.5 - 3.0	0.19	0.52 ± 0.05	13-Nov-17	53 ± 0	26.7 ± 1.6	26 ± 2	76 ± 7	61 ± 9	0.011 ± 0.004
U083	3.0 - 3.5	0.12	0.60 ± 0.05	15-Nov-17	38 ± 4	13.4 ± 1.2	25 ± 4			
U084	3.5 - 4.0	0.15	0.66 ± 0.04	17-Nov-17	40 ± 3	19.2 ± 1.2	21 ± 4			
U085	4.0 - 4.5	0.08	0.72 ± 0.04	01-Dec-17	63 ± 4	25.3 ± 1.3	37 ± 4			
U086	4.5 - 5.0	0.14	0.78 ± 0.04	04-Dec-17	22 ± 4	19.9 ± 1.5	3 ± 4			
U081	2.0 - 2.5	0.27	0.26 ± 0.03	10-Nov-17	193 ± 34	24.0 ± 1.3	168 ± 34			
U079	1.0 - 1.5	0.12	0.07 ± 0.01	06-Nov-17	278 ± 34	33.4 ± 1.7	244 ± 34			

ANSTO ID	Depth (cm)	Dry Bulk Density (g/cm^3)	Cumulative Dry Mass (g/cm^2)	Count Date	Total ^{210}Pb (Bq/kg)	Supported ^{210}Pb (Bq/kg)	Unsupported ^{210}Pb Decay corrected to 01-Dec-17 (Bq/kg)	Calculated CIC Ages (years)	Calculated CRS Ages (years)	CRS model Mass Accumulation Rates (g/cm^2/year)
U076	0.0 - 0.1	0.12	0.01 ± 0.01	07-Feb-18	209 ± 10	23 ± 2	187 ± 10	1 ± 1	1 ± 1	0.010 ± 0.001
U077	0.1 - 0.5	0.12	0.04 ± 0.02	07-Feb-18	233 ± 12	23 ± 2	211 ± 13	7 ± 5	4 ± 2	0.008 ± 0.001
U078	0.5 - 1.0	0.12	0.09 ± 0.03	07-Feb-18	192 ± 8	24 ± 2	169 ± 8	18 ± 6	11 ± 3	0.008 ± 0.001
U079	1.0 - 1.5	0.12	0.15 ± 0.03	07-Feb-18	202 ± 8	22 ± 2	181 ± 9	30 ± 6	21 ± 5	0.005 ± 0.001
U080	1.5 - 2.0	0.27	0.25 ± 0.04	07-Feb-18	122 ± 6	16 ± 2	107 ± 6	50 ± 8	40 ± 6	0.005 ± 0.001
U081	2.0 - 2.5	0.27	0.39 ± 0.04	07-Feb-18	55 ± 2	16 ± 1	40 ± 3	77 ± 10	65 ± 10	0.006 ± 0.002
U082	2.5 - 3.0	0.19	0.50 ± 0.05	07-Feb-18	54 ± 3	22 ± 2	32 ± 3	100 ± 11	90 ± 16	0.004 ± 0.002
U083	3.0 - 3.5	0.12	0.58 ± 0.04	07-Feb-18	29 ± 2	17 ± 1	13 ± 2	115 ± 11	109 ± 22	0.005 ± 0.003
U084	3.5 - 4.0	0.15	0.65 ± 0.04	07-Feb-18	24 ± 1	14 ± 1	10 ± 2	128 ± 11	125 ± 29	0.004 ± 0.003
U086	4.5 - 5.0	0.14	0.79 ± 0.04	07-Feb-18	21 ± 1	18 ± 2	3 ± 2	157 ± 12	168 ± 57	0.003 ± 0.006
U085	4.0 - 4.5	0.08	0.74 ± 0.04	07-Feb-18	50 ± 2	19 ± 2	31 ± 3			

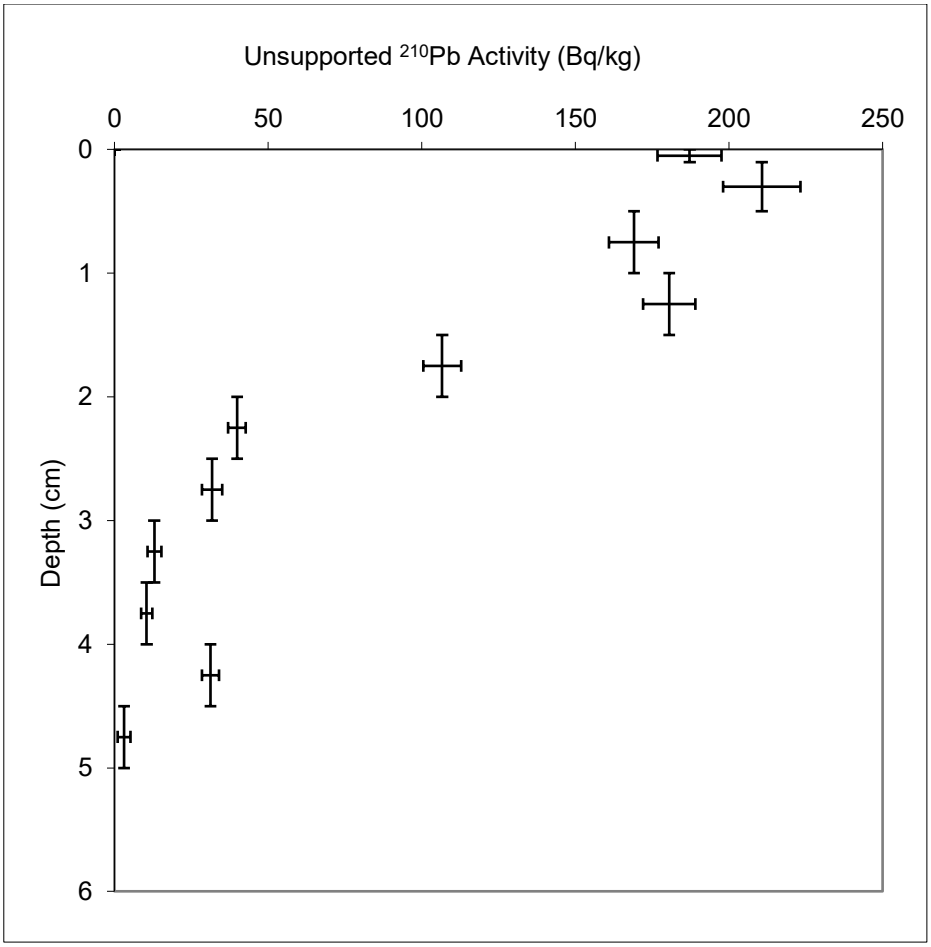

Figure 7.27: Unsupported ^{210}Pb activity by depth for SANFC.

7.4.4.2 Carbon-14 (^{14}C) Dating

Radiocarbon (^{14}C) dates indicate that core SAN1 contains sediment from the mid-Holocene, with late Holocene sediments either thin or absent (Table 7.2). Cores SAN1 and SANFC are offset by approximately 5 cm, with SANFC capturing (and potentially minimizing compression of) the uppermost sediment and water-sediment interface not present in SAN1. The combination of ^{210}Pb and ^{14}C dates identify an unconformity in SANFC between 5 and 10 cm depth, potentially indicated in the elemental record analysed by Itrax™ elemental scanning at approximately 7.5 cm depth (see below).

Variance is displayed between the bulk sediment and samples pretreated using hydrogen pyrolysis from SANFC (OZX215 and OZX216); both samples are from 10-10.5 cm depth and show a difference in conventional radiocarbon age of 750 years. This suggests that SAN1 10-10.5 cm may have produced a younger conventional radiocarbon age if bulk sediment was dated rather than hydrogen pyrolysis residue (OZW500).

Table 7.2: ^{14}C by accelerator mass spectrometry dates for SAN1 and SANFC samples.

ANSTO Code	Sample Type	ID	δ(^{13}C) ‰	% modern carbon	Conventional radiocarbon age
				pM C 1σ error	yrs BP
OZW500	Hypy residue	SAN1 10-10.5cm	-26.3	40.63 ± 0.33	7,230 ± 70
OZW502	Bulk sediment	SAN1 22-22.5cm	-27.5 ± 0.1	40.09 ± 0.14	7,345 ± 30
OZW503	Bulk sediment	SAN1 50-50.5cm	-26.4 ± 0.1	37.35 ± 0.11	7,910 ± 25
OZX213	Bulk sediment	SAN1 5-5.5cm	-26.1 ± 0.1	48.10 ± 0.19	5,880 ± 35
OZX214	Bulk sediment	SAN1 7-7.5cm	-25.0	44.34 ± 0.26	6,535 ± 50
OZX215	Bulk sediment	SANFC 10-10.5cm	-25.0 ± 0.1	49.31 ± 0.19	5,680 ± 35
OZX216	Hypy residue	SANFC 10-10.5cm	-23.6 ± 0.1	44.92 ± 0.19	6,430 ± 35

^{210}Pb dates (converted to years BP) and ^{14}C dates were combined to form a Bayesian age-depth model for SANFC, and ^{14}C dates to form a Bayesian age-depth model for SAN1, using the *Bacon* package within *R* (Blaauw et al. 2019; R Development Core Team 2013) (Figures 7.28 and 7.29) and using the Southern Hemisphere calibration curve SHCal13 (Hogg et al. 2013).

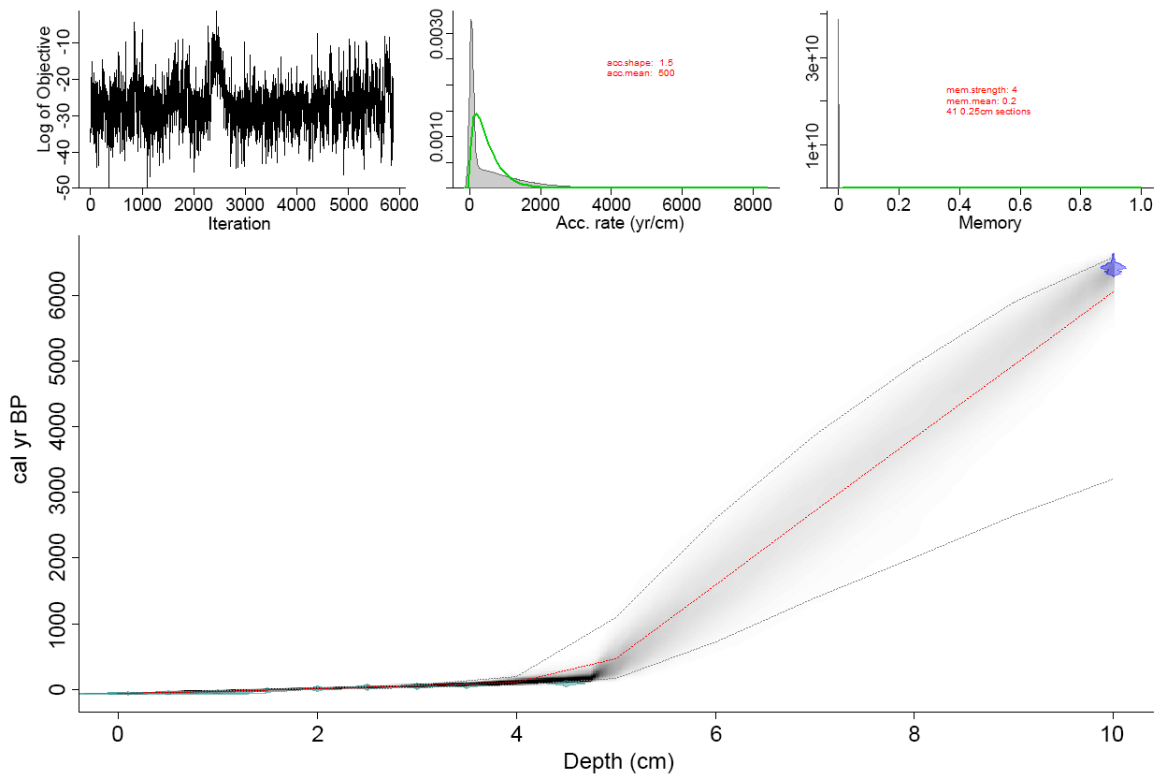

Figure 7.28: SANFC age-depth graph, combining ^{210}Pb (green) and ^{14}C (blue) dates. 14C date at 10-10.5 cm is OZX215 (bulk sediment).

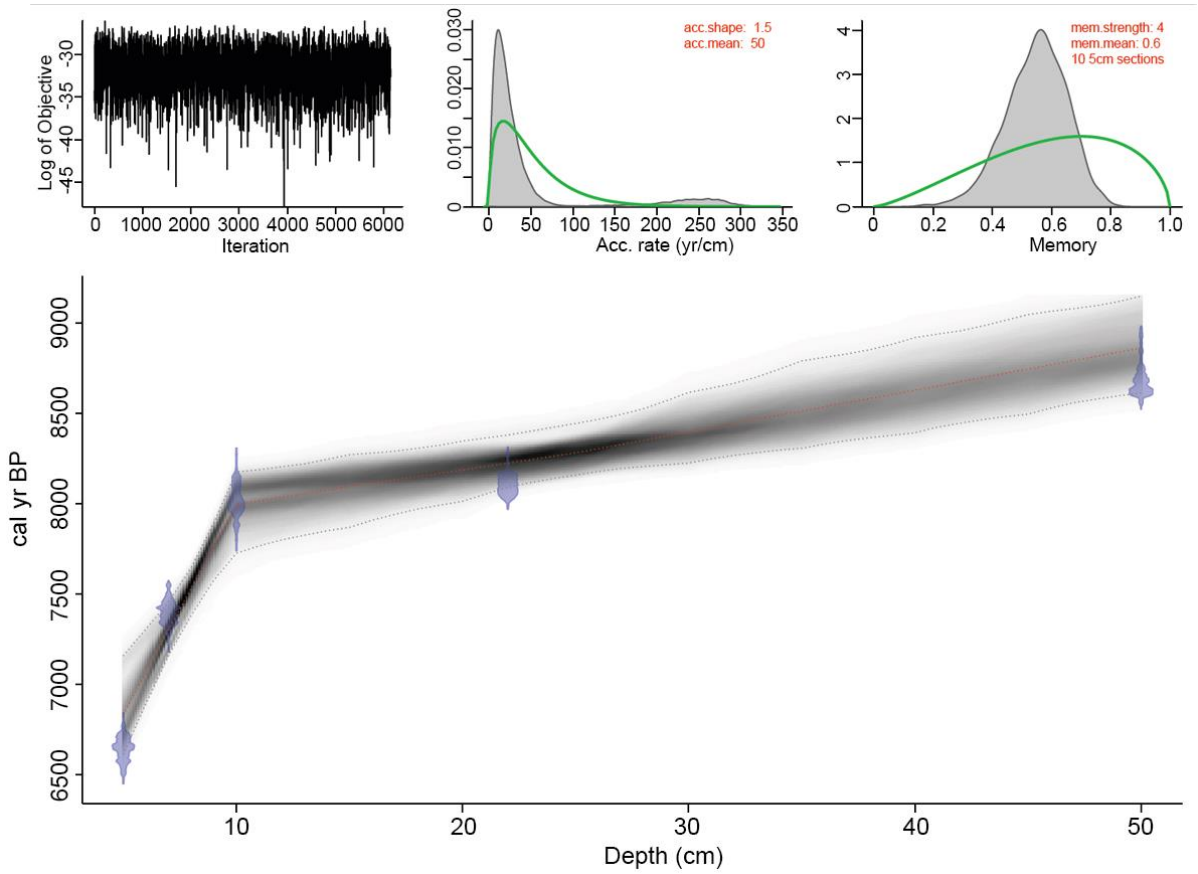

Figure 7.29: SAN1 age-depth graph, ^{14}C dates only.

7.4.3 Itrax™ XRF Scanning

Two adjacent slices from the wide-diameter SANFC core (0-0.3 m) were analysed using an Itrax™ Elemental Core Scanner. Slice 1 could not be scanned correctly due to changes in the width of the slice (as a result of thawing and refreezing, and an original narrow width), identified via high argon elemental counts as a proxy for the air gap between the sample and the detector; as a result only Slice 2 will be discussed. Elemental counts were normalized by dividing each element count by the incoherent scattering (Mo inc) count for that depth (see Davies, Lamb & Roberts 2015, p.192; Figure 7.30).

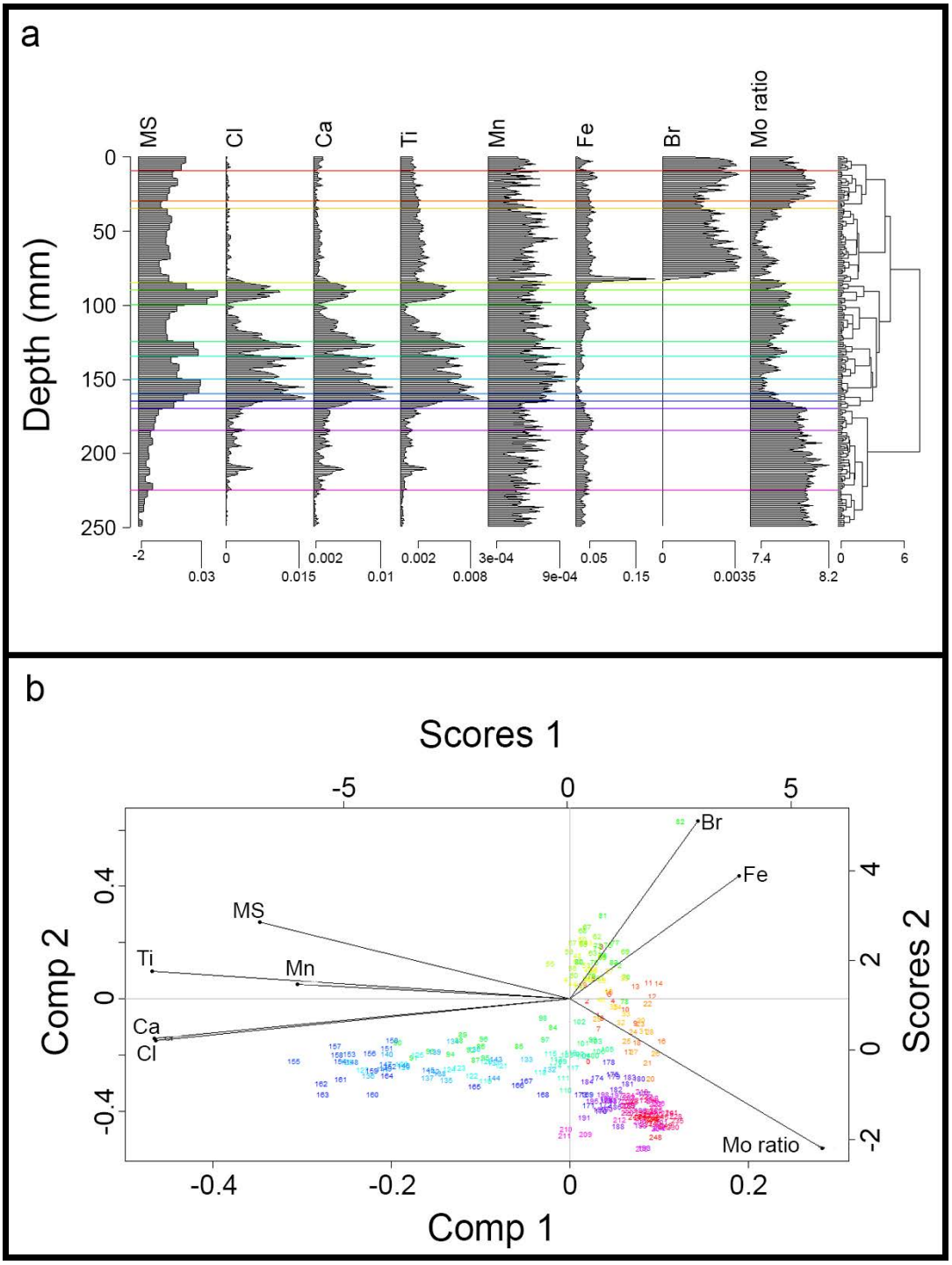

Figure 7.30: Selected Itrax™ normalized elemental and magnetic susceptibility (MS) data for SANFC Slice 2: a) stratigraphic plot, and b) principal components analysis. Data are plotted by depth.

The lower part of the core shows high Mo ratio (Mo inc/Mo coh) values, a proxy for organic content (Davies, Lamb & Roberts 2015). There is a decrease in Mo ratio coincident with increases in magnetic susceptibility (MS), chlorine (Cl), calcium (Ca) and titanium (Ti) in the middle section of the core (~17 cm to ~8 cm). The top of the core (~8cm and above) shows a return to increased organics along with the appearance of bromine (Br), and the transition to this zone is marked by a sharp peak in iron (Fe) and sharp decrease in manganese (Mn).

Strong positive correlations ($r > 0.9$) exist between Cl, Ca and Ti. A positive correlation is also present between Ti and magnetic susceptibility (MS) ($r = 0.67$). Component 1 identified by principal components analysis (Figure 7.30 plot b) explains ~51 % of variation and represents detrital input versus organic input. Component 2 explains ~20 % of variation and represents different sources of organic input (Mo ratio versus bromine).

7.4.4 Sediment Core (SAN1) Charcoal

7.4.4.1 Charcoal Flux

Charcoal counts are high in the upper (0-4.5 cm) and lower (17-24 cm) sections of the SAN1 record (Figure 7.31). Trends are consistent between the three size fractions throughout the record, with higher particle counts in smaller sizes except in low count samples between 14 and 16 cm.

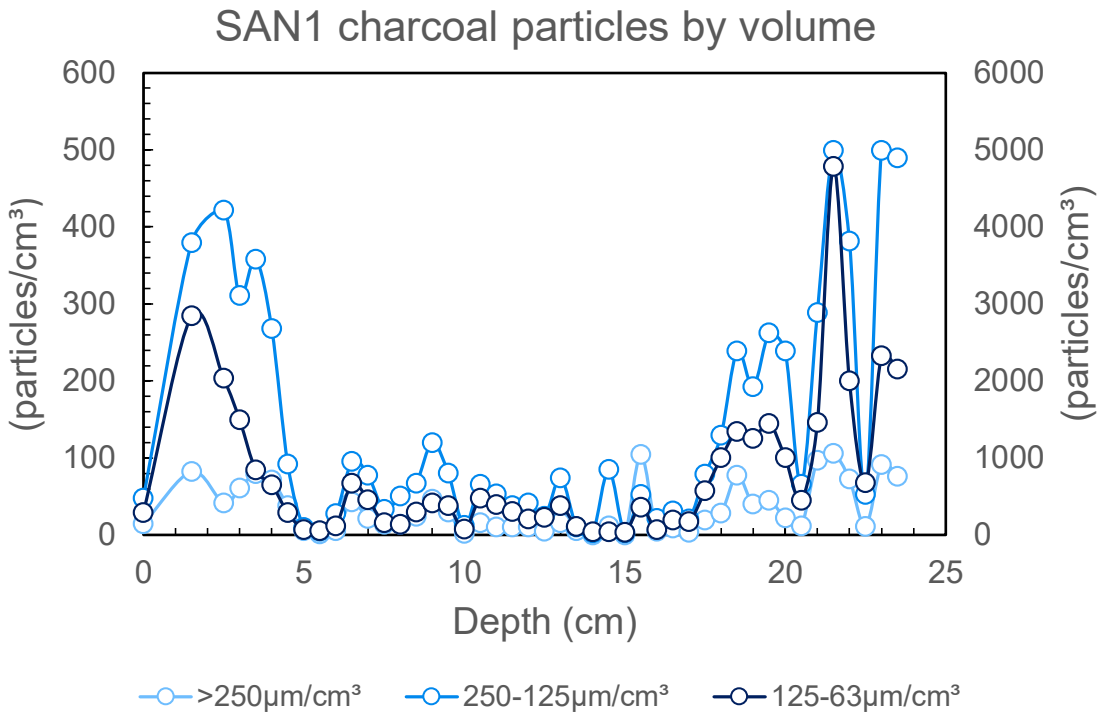

Figure 7.31: Charcoal particles by volume for SAN1, by depth.

Charcoal of all size fractions in core SAN1 predominantly accumulated between ~8200 and ~8000 cal BP (Figure 7.32). A lower amplitude sustained increase in charcoal flux occurs between ~6700 and 5500 cal BP in all size fractions.

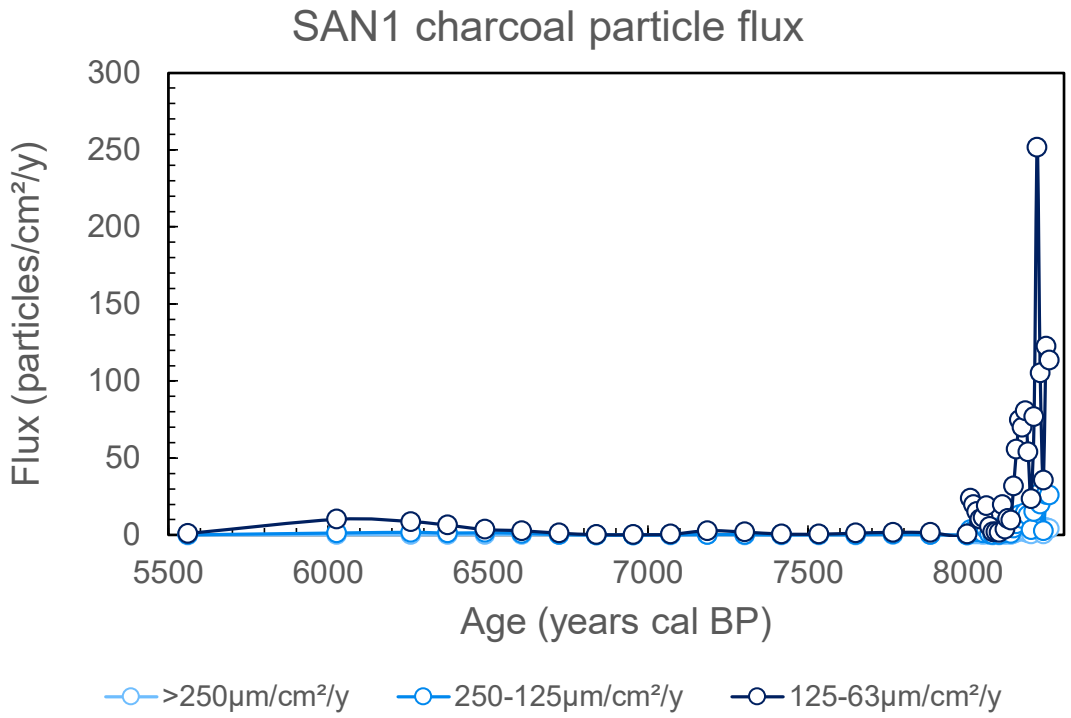

Figure 7.32: Charcoal flux for SAN1, by age.

7.4.4.2 Charcoal L:W Ratios

Elongate particles as determined from length-width ratios are consistently present in SAN1 macroscopic charcoal (Figure 7.33). Variability in elongate percentage is high between 10 and 18 cm, likely due to lower overall charcoal particle counts (including samples containing no >250 µm charcoal, at 14 and 15 cm).

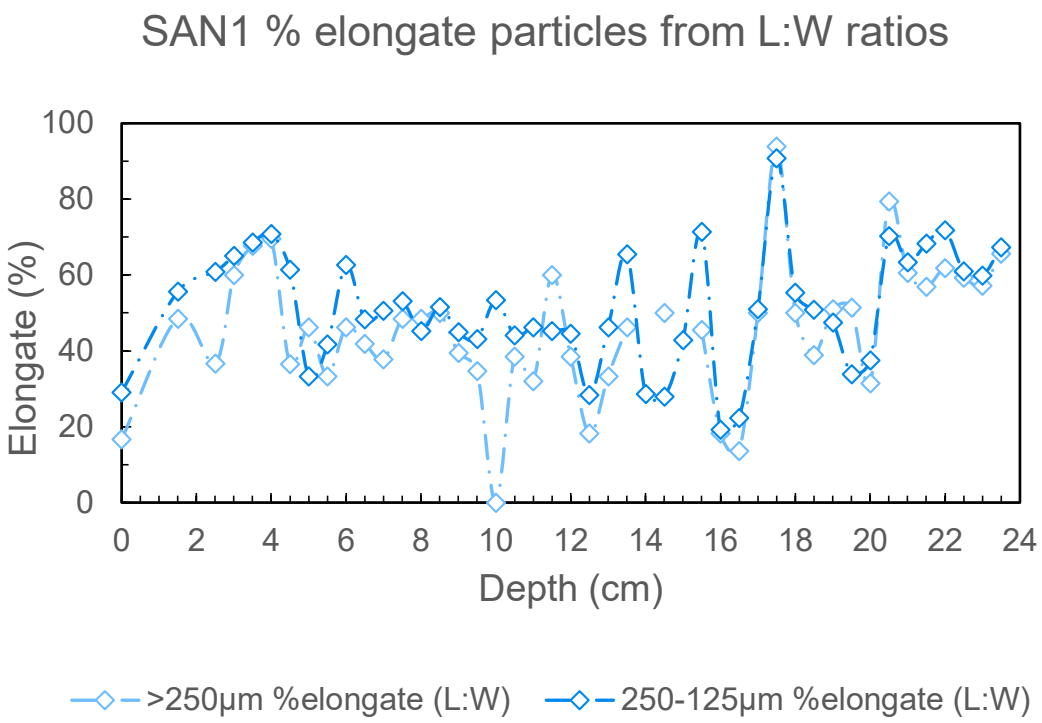

Figure 7.33: Percent elongate particles determined from length-width ratios for SAN1 macroscopic charcoal, by depth.

7.4.4.3 Charcoal Morphotypes

Morphotypes (when simplified to the 7-type Enache and Cumming (2006) system for comparison across macro- and microscopic charcoal sizes) show similar trends across all size fractions. Morphotype composition does not appear to be directly linked to charcoal abundance, except for samples with very low charcoal counts that sharply skew morphotype values.

In the 125-63 µm size fraction, type F (elongate) dominates throughout the record, followed by types S (structured geometric) and C (solid geometric) (Figure 7.34).

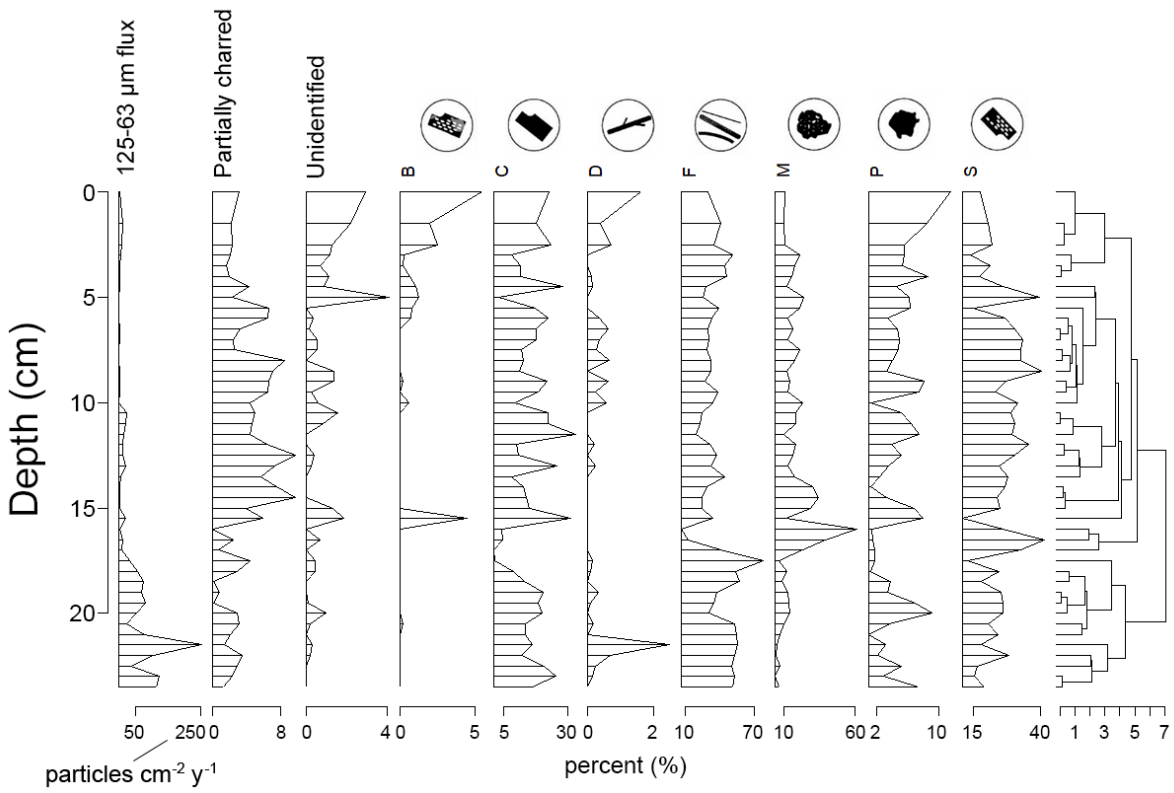

Figure 7.34: SAN1 125-63 µm morphotypes, by depth.

Type S constitutes most of the 250-125 µm size fraction, followed by type F (Figure 7.35).

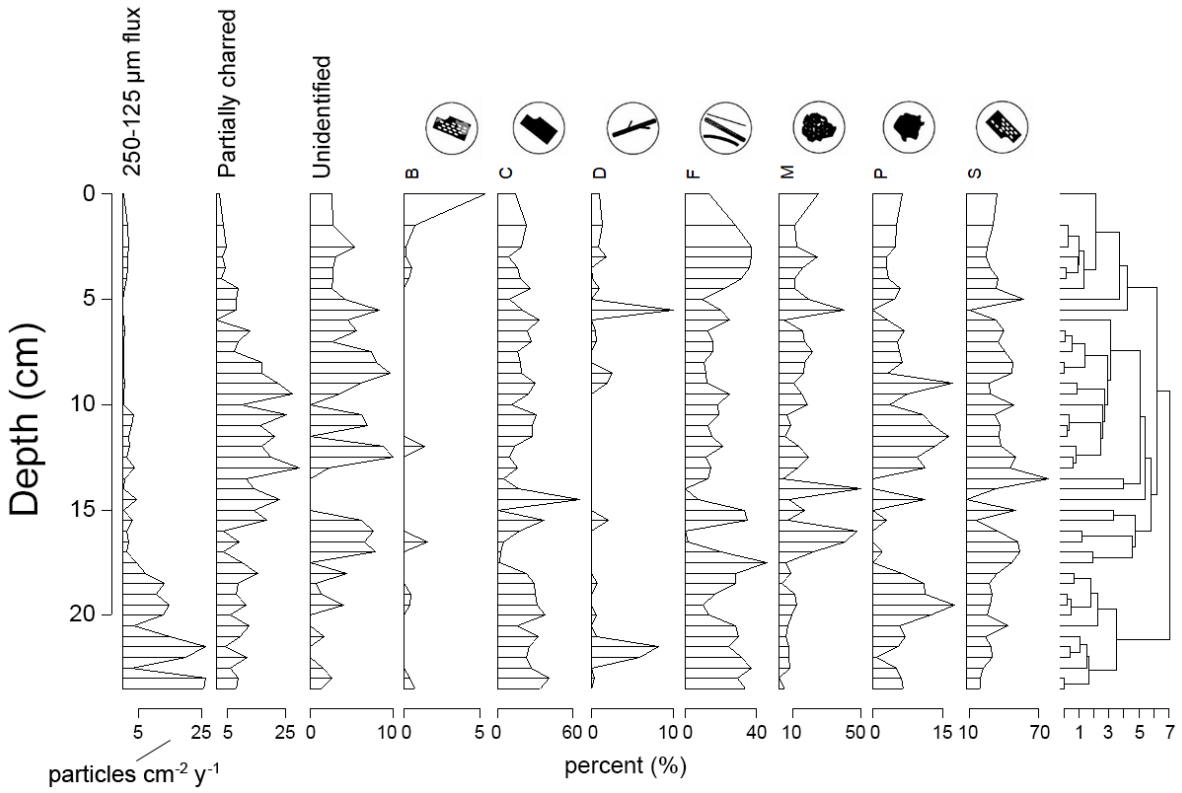

Figure 7.35: SAN1 250-125 µm morphotypes, by depth.

Type S is the dominant morphotype in the >250 µm size fraction, followed by type C (Figure 7.36).

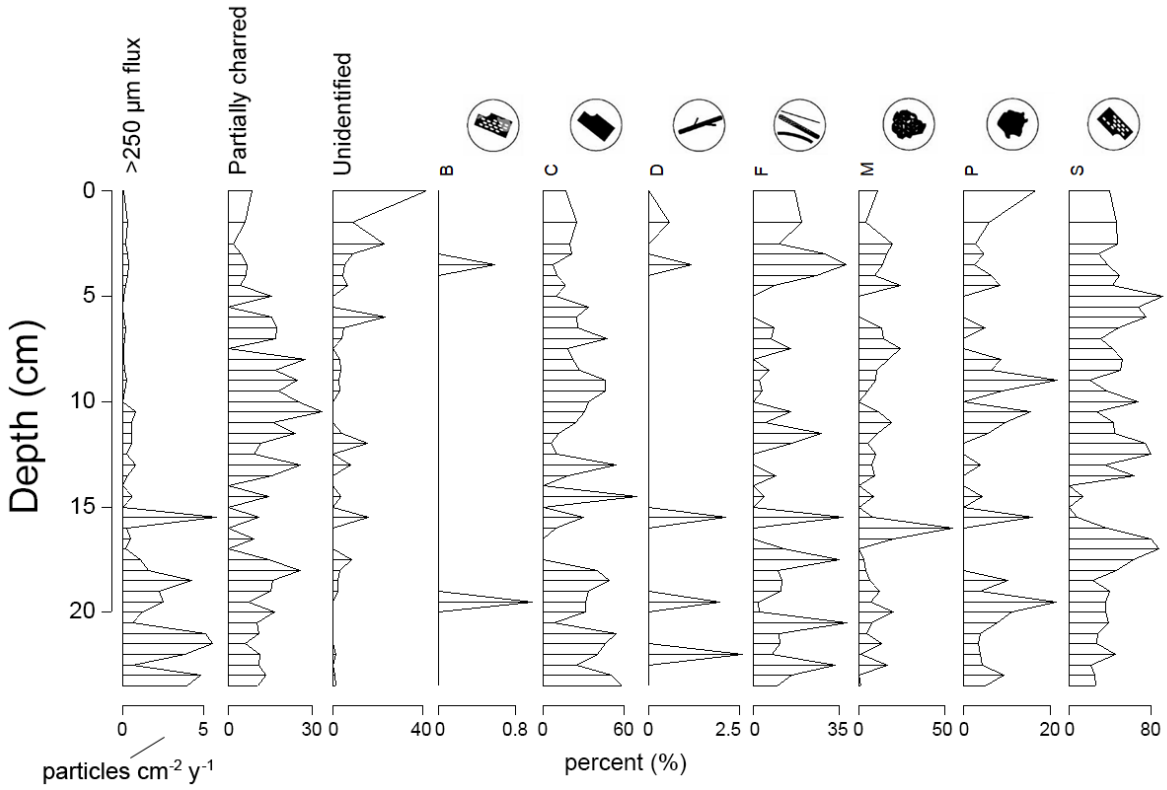

Figure 7.36: SAN1 >250 µm morphotypes, by depth.

Elongate morphotypes consistently form a higher percentage of particles in the 125-63 µm size fraction than the macroscopic fractions (only exceeded by other size fractions at 11.5 and 15.5 cm) (Figure 7.37). All three sizes display similar trends, with most deviations in the form of peaks in the >250 µm size fraction.

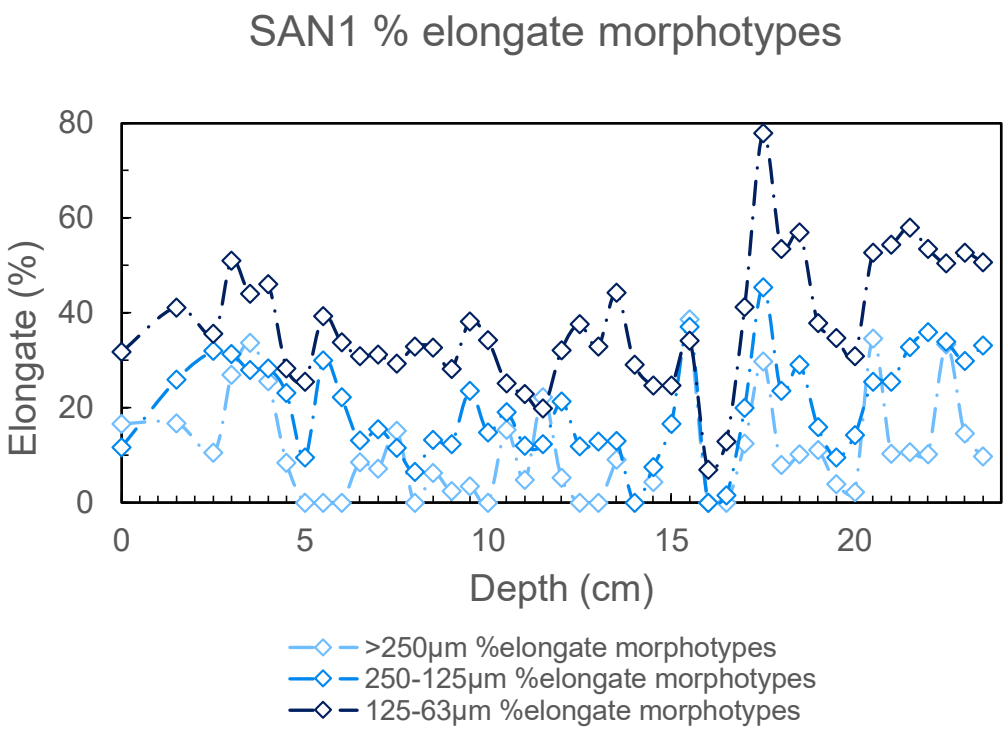

Figure 7.37: Percent elongate morphotypes for all charcoal size fractions for SAN1, by depth.

While percent elongate morphotypes are lower than percent elongate particles calculated from length-width ratios, both measures display similar trends throughout the record (Figure 7.38).

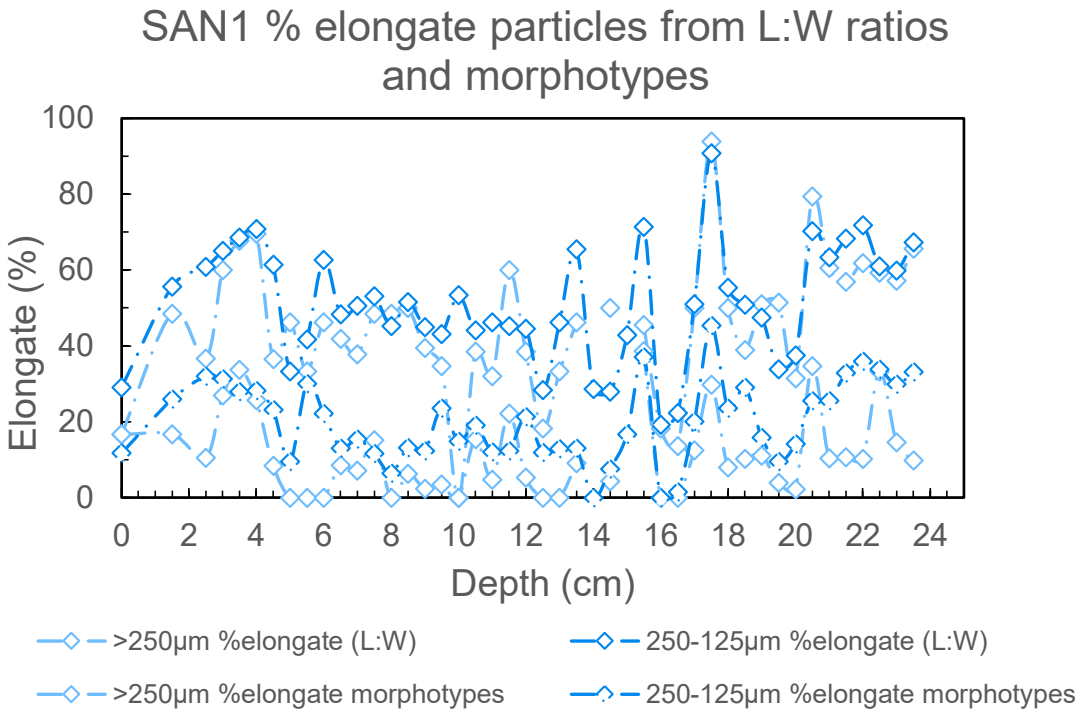

Figure 7.38: Percent elongate particles as determined by length-width ratios and morphotypes for SAN1 by size fraction, by depth.

7.4.5 Hydrogen Pyrolysis and Elemental Analysis

7.4.5.1 Pyrogenic Carbon Flux

Bulk and <63 µm size fractions show very different relationships between total organic carbon and percent pyrogenic carbon (Figures 7.39 and 7.40). Total organic carbon declines towards the top of the core in both size fractions, and bulk PyC varies independently of this aside from its decline from 3.5 to 0 cm. <63 µm percent pyrogenic carbon displays multiple sharp peaks independent of total organic carbon. A decrease in total organic carbon in the bulk fraction above 5 cm may correspond to the detrital phase identified via XRF in core SANFC between 17 and 8 cm depth (see Itrax™ XRF Scanning above).

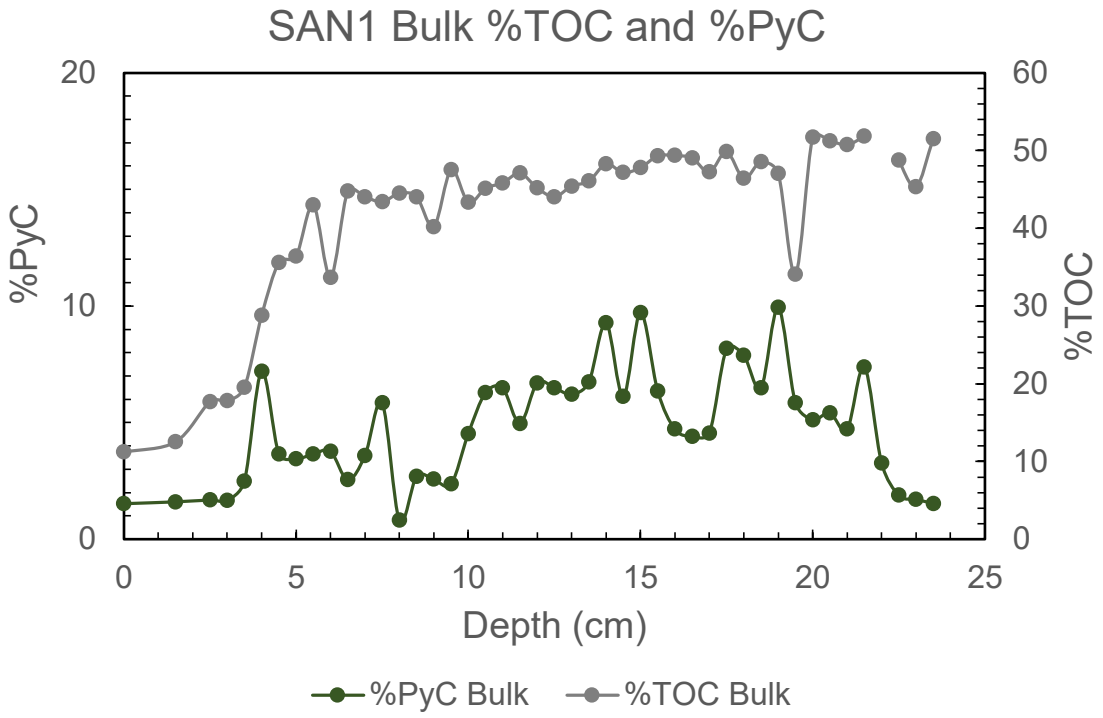

Figure 7.39: SAN1 bulk total organic carbon (%TOC) and percent pyrogenic carbon (large PyC peak at 68 cm removed), by depth.

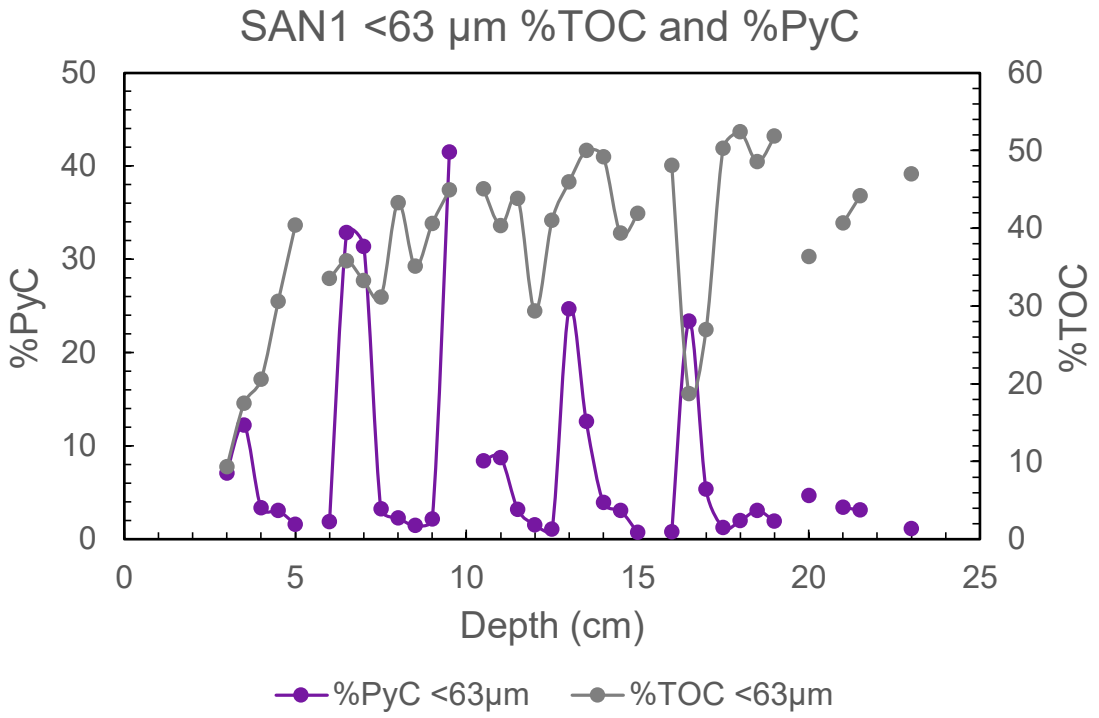

Figure 7.40: SAN1 <63 µm total organic carbon (%TOC) and percent pyrogenic carbon, by depth.

Pyrogenic carbon (PyC) flux (g/cm²/y) for bulk and <63 µm samples of SAN1 are similar to charcoal flux, with the highest PyC levels at the bottom of the record (~8000-8200 cal BP, Figure 7.41).

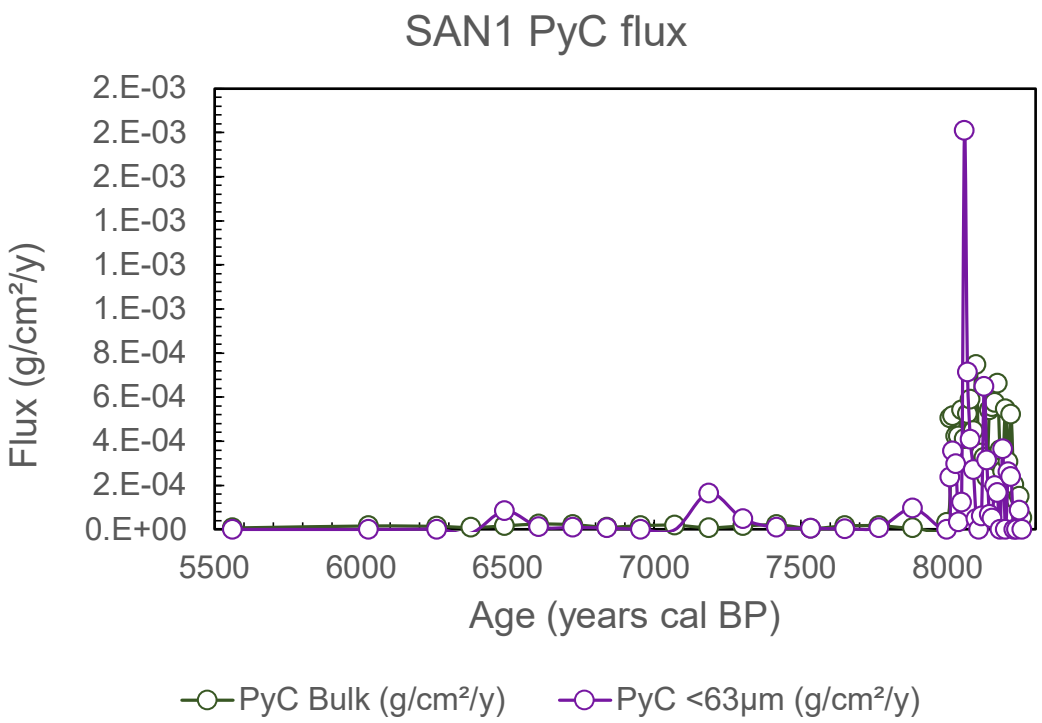

Figure 7.41: Bulk and <63 µm pyrogenic carbon (PyC) flux for SAN1, by age.

While the period of highest flux is broadly coincident between PyC and charcoal, differences are apparent between the two measures (Figure 7.42, Table 7.3). PyC flux in the <63 µm fraction peaks at ~8060 cal BP, a point where charcoal is present but does not peak in any size fraction. However, the size of this peak may be exaggerated as the value exceeds the PyC measured in the bulk fraction. Both bulk and <63 µm PyC flux also do not reflect the peak charcoal flux values at ~8200 cal BP, although PyC is present.

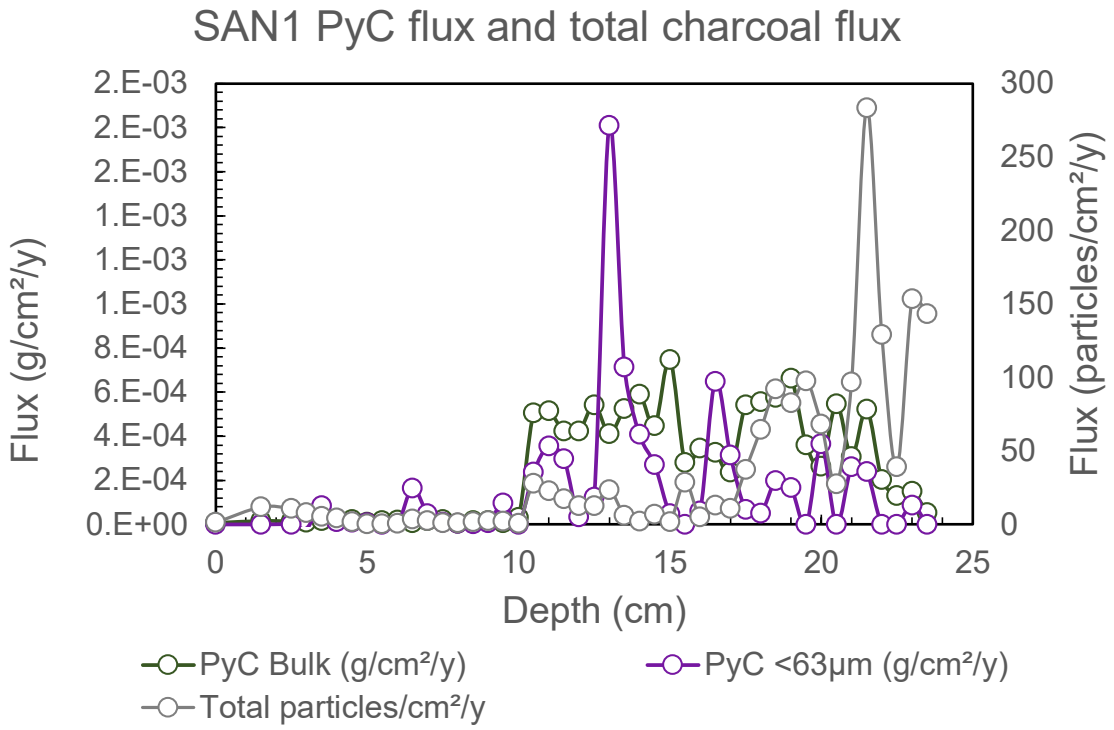

Figure 7.42: Bulk and <63 µm pyrogenic carbon (PyC) flux and total charcoal flux for SAN1, by depth.

Table 7.3: Charcoal and PyC flux variable r^2 values for SAN1.

	>250 µm	**250-125 µm**	**125-63 µm**	**<63 µm PyC**
Bulk PyC	0.0562	0.0379	0.0738	0.1218
>250 µm		0.7047	0.6578	0.0003
250-125 µm			0.8581	< 0.0001
125-63 µm				< 0.0001

7.4.5.2 Pyrogenic Carbon $\delta^{13}C$

In both bulk and <63 µm size fractions, $\delta^{13}C$ values for total organics (pre-hydrogen pyrolysis) are predominantly more 13C-depleted than $\delta^{13}C$ values for pyrogenic carbon (Figures 7.43 and 7.44). <63 µm PyC $\delta^{13}C$ values show higher variation than $\delta^{13}C$ values for total organic content in this size fraction.

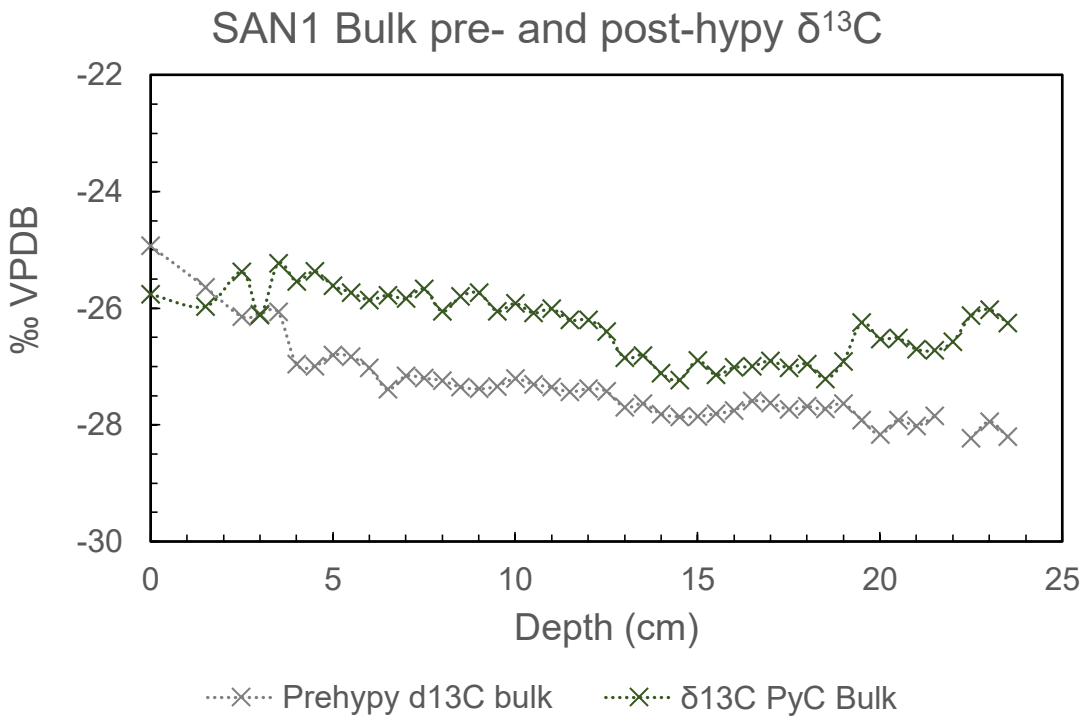

Figure 7.43: SAN1 $\delta^{13}C$ for bulk samples before (total organic carbon) and after (PyC) hydrogen pyrolysis, by depth.

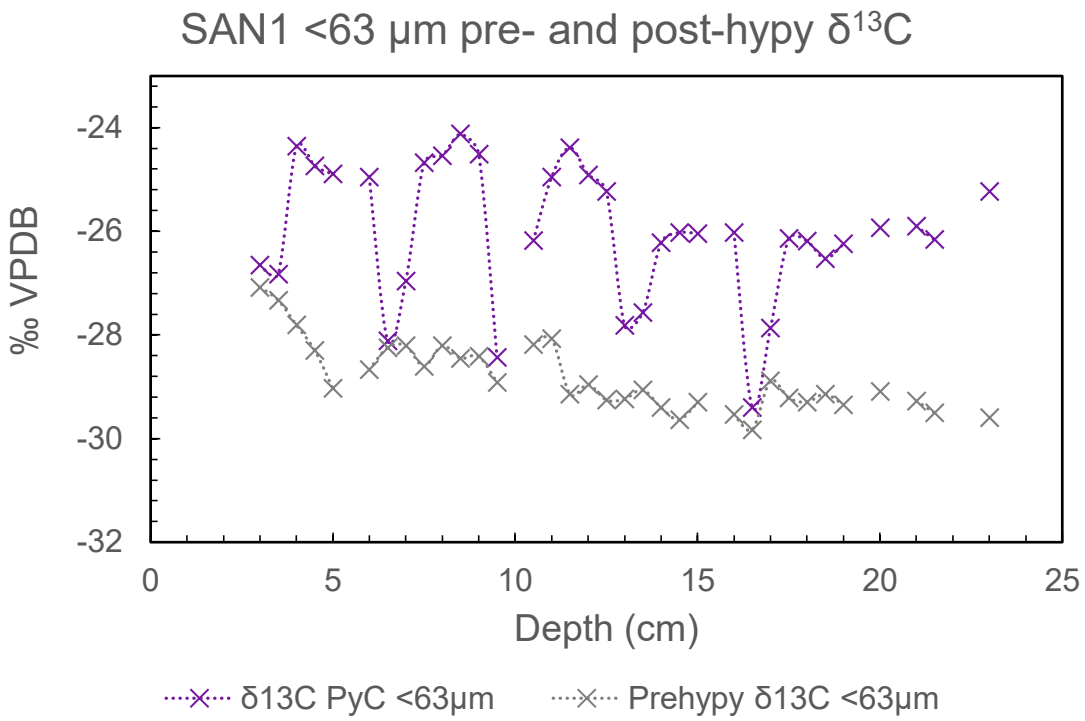

Figure 7.44: SAN1 $\delta^{13}C$ for <63 µm samples before (total organic carbon) and after (PyC) hydrogen pyrolysis, by depth.

SAN1 $\delta^{13}C$ values are consistently low (^{13}C depleted) for both bulk and <63 µm pyrogenic carbon (Figure 7.45), consistent with values associated with C_3 plants (-25 to -29 ‰; O'Leary 1988). Gaps in the <63 µm PyC $\delta^{13}C$ record are the result of samples that did not contain sufficient sample volume in the <63 µm size fraction for analysis.

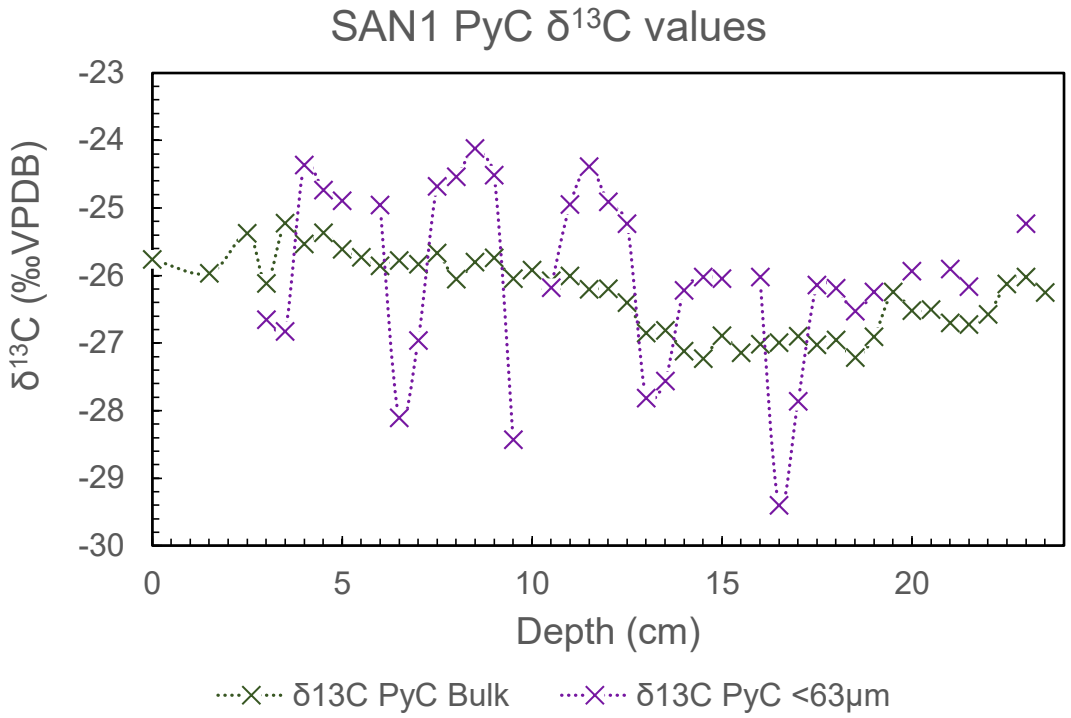

Figure 7.45: Bulk and <63 µm pyrogenic carbon (PyC) $\delta^{13}C$ for SAN1, by depth.

Values for the <63 µm fraction are more variable (between -24 and -29 ‰) than the bulk $\delta^{13}C$ but still within the range expected for C_3 plants. Troughs in <63 µm $\delta^{13}C$ value at 16.5, 13, 9.5 and 7-6.5 cm are coincident with peaks in percent PyC (Figure 7.46). However, these peaks exceed the PyC abundances for the bulk fraction at these depths and thus may not be accurate.

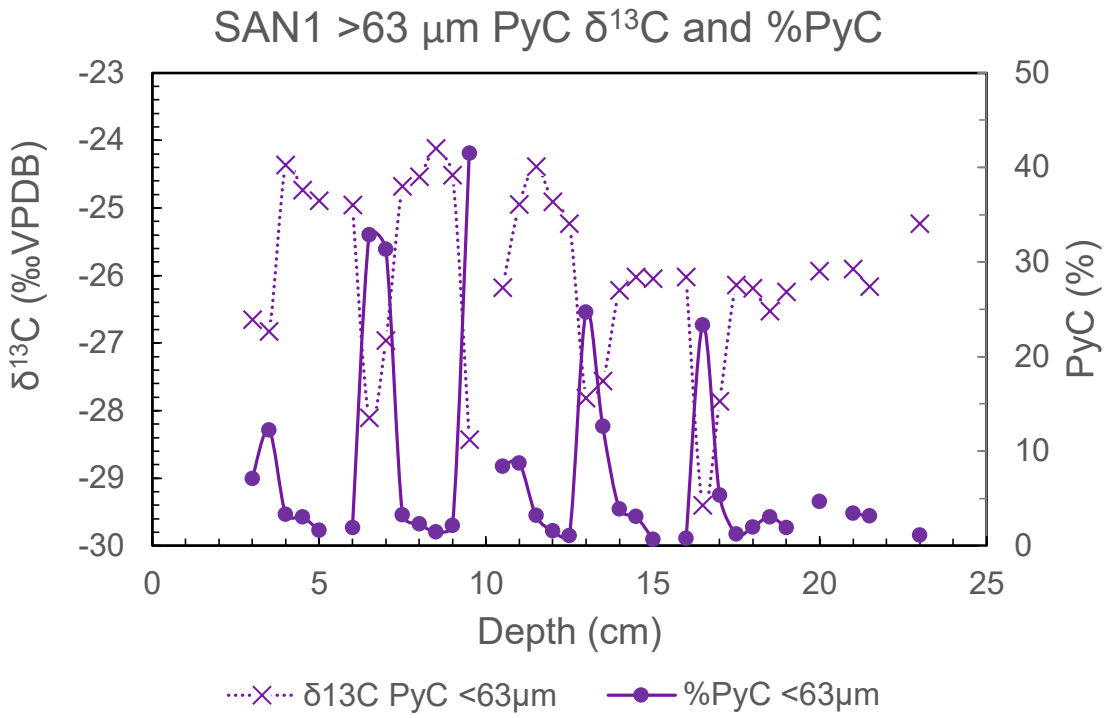

Figure 7.46: <63 µm pyrogenic carbon (PyC) $\delta^{13}C$ value and percentage PyC for SAN1, by depth.

7.5 Discussion

7.5.1 Charcoal Traps

No burning was recorded from April to June 2016 by satellite data within 10 km^2 of Sanamere (NAFI 2019); however, low numbers of charcoal particles were present in SANFT1 and most likely originate from one or more smaller fires not captured by satellite, such as fires of low intensity or campfires in the nearby Jardine River National Park designated campground that did not create a fire scar discernible by satellite imagery. Alternatively, charcoal particles in SANFT1 may have been generated in earlier fires and deposited on the ground, with wind making the particles airborne.

The inclusion of the Sanamere Lagoon water surface into the measurement of area burned during 2016 makes comparison of charcoal counts and burned area difficult. However, 74.3 km^2 of the total 94.6 km^2 burned area recorded was between the 5 km^2 and 10 km^2 radius (therefore not inclusive of the water surface), suggesting that minimal airborne charcoal is successfully transported to Sanamere Lagoon as charcoal counts in SANFT2 were low (covering a period of one year, less than double the counts of SANFT1 which collected for two months). This may suggest that this charcoal represents a local catchment signal. Elongate particle counts for SANFT1 and SANFT2 are low, which may represent minimal input from sedges burning within the catchment (see Vegetation Burned section below).

Coen and Kendall B charcoal traps display expected trends in abundance, e.g. low/high charcoal counts matching small/large area burned in each case. Both charcoal traps also display expected trends in percentage grass, with a higher contribution of elongate particles than at Sanamere, as both Coen and Kendall B charcoal trap sites are surrounded by eucalypt woodlands with a grassy understorey (Atlas of Living Australia 2018; Department of the Environment & Energy 2017). It is unclear whether Coen and Kendall B charcoal trap samples represent a local or combined local/regional signal. The COENFT charcoal is likely to have originated solely in the nearby (~250 m to the closest point of the recorded fire scar) August 2016 fire event but could be a combined accumulation from that event and more distant (2.8 km to fire scar) 2017 burns (Figure 7.47).

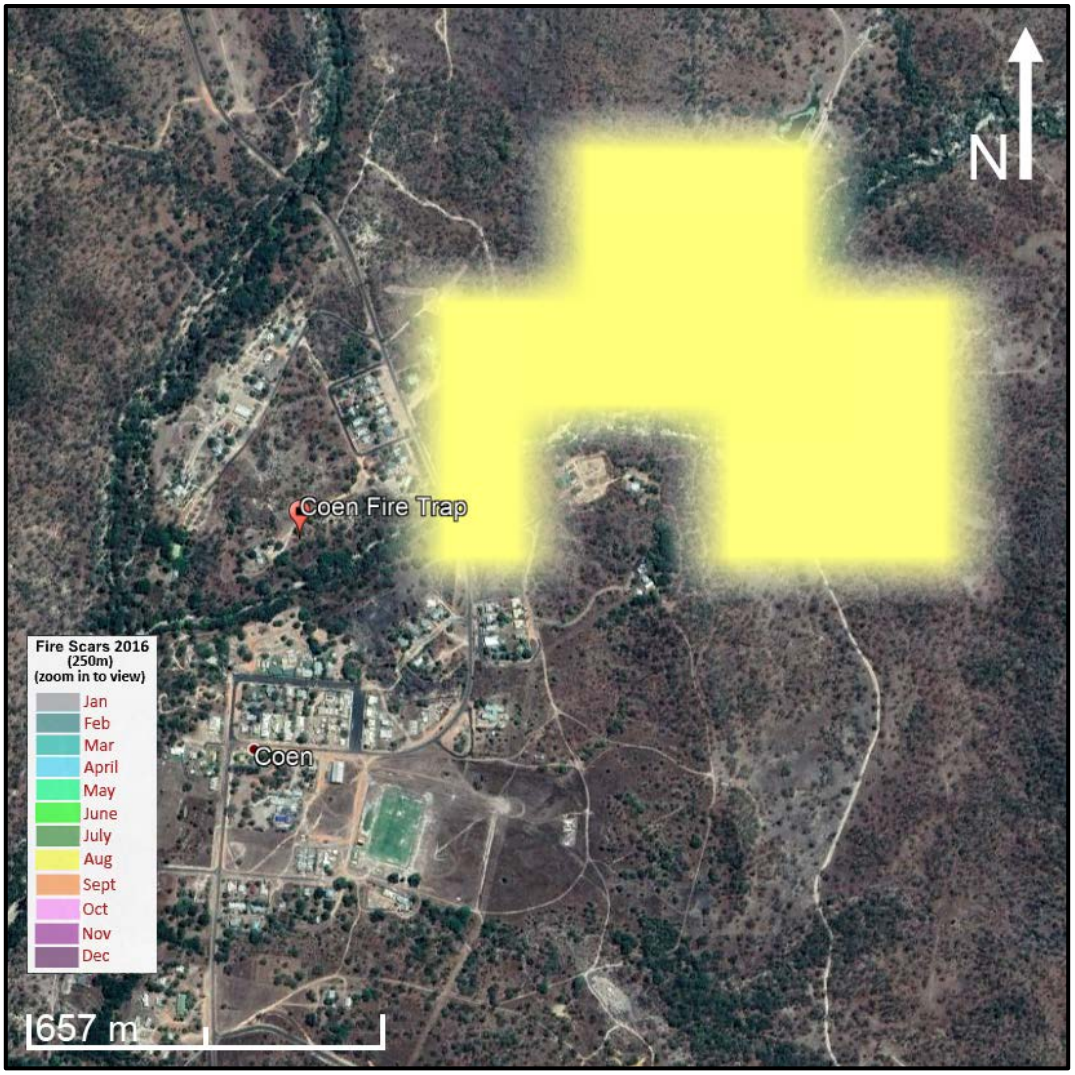

Figure 7.47: Fire scars around Coen in 2016 by month. A single fire scar from August (yellow) is within 10 km^2 of the Coen charcoal trap and was ~250 m distant at its closest point (after Google Earth 2018c; NAFI 2019).

Similarly, the large volume of KENBFT charcoal could be representative of the extensive burning within a 10 km^2 radius but is most likely representative of high volumes of charcoal created in closer proximity to the trap, as the July 2017 fire scar burned a 360 m radius around the charcoal trap (Figure 7.48).

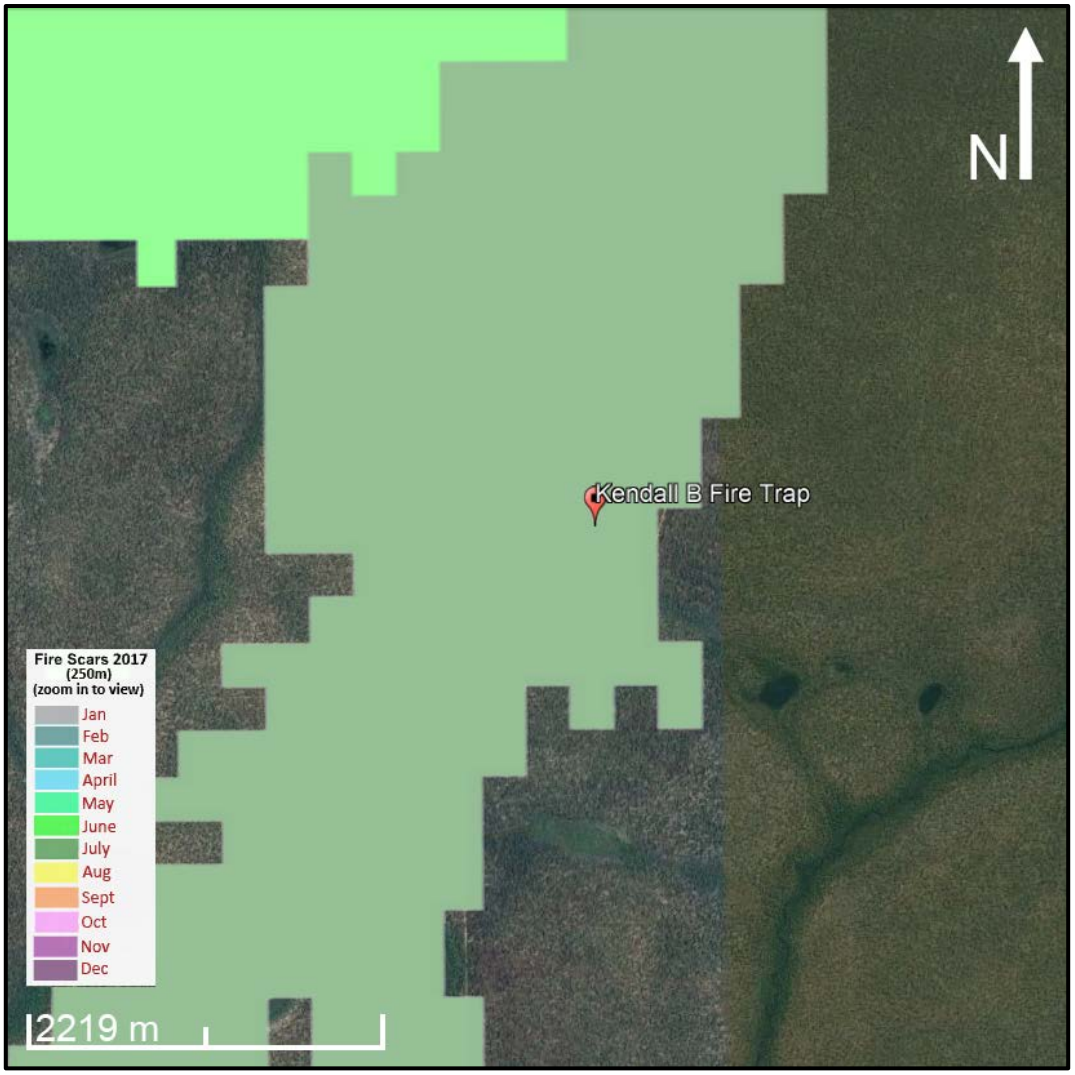

Figure 7.48: Fire scars around Kendall B charcoal trap in 2017 by month. The green July 2017 fire scar covers a 360 m radius around the charcoal trap (after Google Earth 2018e; NAFI 2019).

7.5.1.1 Charcoal Traps and Sediment Charcoal

Only one sediment sample (5.5-6 cm) contains a lower charcoal flux value than the values for samples SANFT1 and COENFT. 40 % of SAN1 charcoal flux values exceed the highest recorded charcoal trap flux (KENBFT, ~13 particles/cm²/y), with maximum values of ~283 particles/cm²/y (Table 7.4).

Table 7.4: Comparison of charcoal flux values for sediment core SAN1 and charcoal trap samples.

Sample	Total charcoal particles/cm²/y
SAN1 (sediment)	0.27 – 283.32
SANFT1	0.37342
SANFT2	0.117424
COENFT	0.294268
KENBFT	13.20813

Charcoal trap samples contain airborne charcoal only. The disparity between the highest charcoal flux in the charcoal traps, collected from a fire event that burned a 360 m radius around the trap, and the much higher recorded values in sedimentary charcoal potentially highlights the importance of ground-level, overland transport by water.

7.5.2 Elemental Composition

7.5.2.1 Organic Content: Mo Ratio and Br

Elemental data for core SANFC shows two transitions: the first from a more organic to a more detrital signal at ~17 cm, and the second from this detrital signal back to increased organics and the first appearance of bromine (Br) at ~8 cm. Mo incoherent/coherent ratio is interpreted in this study as a proxy for organic content, as discussed in Chapters 5 and 6 (see also Davies, Lamb & Roberts 2015). Similarly, Br is also interpreted as an organic indicator (Davies, Lamb

& Roberts 2015, p.202; Hahn et al. 2014; Mackenzie et al. 2017), and may indicate a change in type of organic matter from the earlier organic-rich period when Br was absent. Br has also been associated with warmer periods of climate (Pashkova et al. 2016, p.375).

7.5.2.2 Detrital Input: Calcium, Chlorine, Titanium and Magnetic Susceptibility

Ca, Cl and Ti represent a detrital signal in the Sanamere sediments. This is supported by a positive correlation with magnetic susceptibility, and negative correlation with organic input (Mo ratio). A consistently strong positive relationship between Ca and Ti is noteworthy as these elements are often negatively correlated (Kylander et al. 2011) and attributed to different sources, with Ti associated with detrital input and Ca attributed to carbonates and in-lake (authigenic) processes (e.g. Croudace et al. 2006; Sáez et al. 2009; Kylander et al. 2011; Liu et al. 2013; Fletcher et al. 2015; Hahn et al. 2014; Davies, Lamb & Roberts 2015; Lobb 2015; Mackenzie et al. 2017).

Positive correlation between Ca and Ti indicates an allochthonous (external) Ca source. Sanamere Lagoon is bordered on three sides by Helby Beds, described by Smart et al. (1980, p.16) as "shallow marine and paralic sediments". The Helby Beds formed from the Middle Jurassic to Early Cretaceous with the deposition of "fluvial, finally marine, deposition of quartzose sand, some silt and mud" (Smart et al. 1980, p.55). Weathering of this marine-sourced formation is likely the source of detrital Ca and Cl in Sanamere Lagoon. This detrital signal is dominant from ~8-17 cm and may indicate windy conditions or lower lake water levels.

7.5.2.3 Oxidation: Iron and Manganese

A sharp increase in Fe and decrease in Mn is present at ~8 cm, coincident with a decrease in Mo ratio and the appearance of Br. This increase in Fe/Mn around 8 cm may be coincident with the unconformity identified in the ^{14}C dates (between 5 and 10 cm).

Fe/Mn is associated with reducing conditions and may be used to identify oxidisation in a lake core (Davies, Lamb & Roberts 2015, p.195). However, high Mn and Mn/Fe have also been interpreted as a proxy for low lake levels and oxygenation of sediments (e.g. Burn & Palmer 2014; Kylander et al. 2011). The peak may also represent a natural redox boundary in the sediments (see Cohen 2003, p.246-247; Santschi et al. 1990). Applying known interpretations of Mn to Sanamere sediments is difficult as studies often discuss mechanisms in deep (>10 m water depth), temperate, seasonally anoxic lakes (e.g. Davison 1993).

Interpretation of isolated peaks in this record may also be problematic as the record is short (30 cm) and cannot currently be placed within the context of a full 2 m record for Sanamere Lagoon.

7.5.3 Chronological Gap

As determined from the combination of ^{210}Pb and ^{14}C dates, a chronological gap (or unconformity) in sediments at Sanamere Lagoon occurs between 5 and 10 cm in core SANFC. The peak in Fe/Mn in the elemental composition at ~8 cm in SANFC, as well as the first appearance of Br at this depth, may or may not be linked to this inferred unconformity. As the ^{14}C date obtained at 5 cm from SAN1 (mean age of 6838 cal BP from the age-depth model shown in Figure 7.29) corresponds most closely to the ^{14}C date from 10 cm in core SANFC (mean age of 6056 cal BP from the age-depth model shown in Figure 7.28), the chronological gap occurs within the top 5 cm of core SAN1, if captured at all. A conventional radiocarbon

age of 3840 ± 45 years BP (lab code OZX672) for pyrogenic carbon from a depth of 6 cm in core SAN8 (not analysed in this study; M. Rivera Araya pers. comm.) places this unconformity within the late Holocene.

This chronological gap potentially represents one or more events of sediment loss. Sediments (across all collected cores) do not show any visible changes in texture or colour to suggest drying or erosion accompanying this unconformity. During heavy rainfall events, Sanamere Lagoon has a potential outflow point on the western edge of the catchment, connecting the lagoon with the adjacent Jardine River. Periods of high rainfall or wind in the past, caused by a cyclone event or active monsoon, may have washed the upper layers of accumulated sediment from the coring location, either elsewhere in the lagoon or indeed over the sill into the Jardine River. One example of a high rainfall event in the recent past occurred in March 2005 when 100-150 mm rain fell in one week across northern Cape York Peninsula, caused by Tropical Cyclone Ingrid (BOM 2005). The likelihood of scouring events increases when water levels are lower, increasing over time as the depth of accumulated sediments has increased, and the lake has thus shallowed over time. The current elevation of the lagoon surface is ~15 m a.s.l. and the outlet point in the west of the Sanamere catchment is ~17 m a.s.l; water levels 2 m or more above the current level, raised by a combination of increased sediment depth and rainfall, would connect Sanamere Lagoon with the catchment outlet. As it is not known when in the late Holocene this sediment loss occurred, it is unknown whether this sediment loss event is linked in any way to the period beginning ~600-400 cal BP observed further south at Weipa by Stevenson et al. (2015, p.27) when conditions were “even wetter than in the preceding 1500 years”.

7.5.4 Charcoal and Pyrogenic Carbon

Charcoal flux, in all size fractions, peaks between ~8200 and 8000 cal BP, coincident with higher mass accumulation rates. A low sustained increase in charcoal flux indicates the consistent presence of fire between ~6500 and 5500 cal BP, not accompanied by an increase in mass accumulation.

These broad trends are also apparent in the pyrogenic carbon (PyC) record, where PyC flux is highest between ~8200 and 8000 cal BP. However, both PyC size fractions peak slightly later than charcoal flux, with peak PyC flux occurring at ~8000 cal BP. The lack of a peak in bulk PyC flux at ~8200 cal BP suggests that the peak charcoal flux recorded at this time contains charcoal from a low temperature fire event (or events) as charcoal created at temperatures lower than 550°C is removed during the hydrogen pyrolysis process (see Wurster et al. 2013).

A sharp peak in <63 μm PyC flux at ~8060 cal BP that coincides with a very low peak in charcoal flux may represent a more distant fire not reflected in the more local, larger size fractions or a high temperature local fire that produced a higher proportion of particles in the fine fraction (see Umbanhowar and McGrath 1998 for an experimental case study).

While elemental data is from a different core (SANFC) and thus comparisons to charcoal data from SAN1 should be made with caution, the high charcoal flux present towards the end of the SAN1 record likely coincides broadly with the organic signal present at the bottom of SANFC. If this is the case, increased sediment accumulation and high flux of charcoal between ~8200 and 8000 cal BP at Sanamere is linked to organic productivity rather than erosion (organic rather than detrital elemental signal).

7.5.4.1 Vegetation Burned

As discussed in Chapter 6, ^{13}C-depleted values in the smallest PyC size fraction are expected in grass-dominated environments (Stable Isotope Disequilibrium Effect; Saiz et al. 2015) and can thus be used to identify distant, non-local fire signals at Sanamere as grass is absent from the immediate (modern) environment. In the SAN1 record, $\delta^{13}C$ values are similar for both size fractions (between ~-25 and -27 ‰), falling within the expected range for C_3 plants (-25 to -29 ‰; O'Leary 1988) and implying the absence of grass in the record. This suggests that the record is a purely local fire signal, if vegetation during this period (~8300 to 5500 cal BP) was similar to the modern dwarf heathland in composition and extent. The record may represent a mixed local/extra-local signal if dwarf heathland surrounding Sanamere Lagoon covered a larger area during this period.

$\delta^{13}C$ values of -25 ‰ have also been identified for sedges such as *Eleocharis* (Bunn & Boon 1993, p.89; Boon & Bunn 1994, p.102). *Eleocharis*, with minor *Schoenus*, form extensive bands across shallower regions of Sanamere Lagoon and are also present as clumps within the dwarf heathland surrounding the lagoon (see Geology and Vegetation earlier in this chapter). Elongate charcoal particles, identified by both length-width ratio and morphotypes, are present in all size classes throughout the record. Rather than being grass-derived, elongate charcoal particles in the SAN1 record are primarily sedge-derived. This indicates that for periods during this record conditions were dry enough for sedges on the lake margin to burn.

It is worth noting that elongate particles are significantly less prevalent in both charcoal trap samples (SANFT1 and SANFT2) compared to surface sediment samples from within the lagoon (SANSURF1, SANSURF6 and SANSURF10) and samples from core SAN1. The lower percentages of elongate charcoal particles in both charcoal trap samples may indicate that sedge charcoal is primarily deposited via in-wash rather than aerial transport (charcoal traps only collected airborne particles) and/or that conditions in 2016-17 were not dry enough for sedges

to burn. While SAN1 has not been confirmed to contain sediments from the last ~160 years, surface grab samples contain the water-sediment interface and sediments captured within the uppermost SANFC and thus surface sample charcoal can be assumed to represent the most recent period of accumulation. Therefore, the presence of elongate charcoal particles in surface sediment samples indicates that sedges have burned during the most recent period of sediment accumulation.

7.6 Conclusion

Charcoal and PyC data from Sanamere (SAN1) presented in this chapter represent a mid-Holocene palaeofire record featuring the presence of burned sedges and C_3 woody vegetation and high charcoal and PyC flux between ~8200 and 8000 cal BP, with cooler fires prior to ~8100 cal BP and higher temperature fires between ~8100 and 8000 cal BP. A chronological gap in sediments of core SANFC was identified using absolute dating (^{14}C and ^{210}Pb), indicating one or more scour or washout events since ~5500 cal BP and prior to 160 years ago. Divergence between the charcoal and PyC records for SAN1 highlights the different factors affecting each measure including fire temperature, to be discussed further in the following chapters.

Chapter 8 : Methodological Synthesis

8.1 Introduction

This study applies a range of well-established palaeofire methods, such as optical charcoal analysis, charcoal size fractions and particle length-width ratios, along with some emerging methods and techniques that have not been applied in tropical Australian contexts, such as hydrogen pyrolysis, stable carbon isotope analysis and charcoal morphotype classification. This chapter evaluates and compares the data generated using these methods, addressing Research Aim 2 (evaluation of established and emerging palaeofire methods) outlined in Chapter 1, with the following specific objectives:

1) Evaluation of the applicability, utility and limitations of the techniques used in this study to Australian tropical savannas, including a comparison to modern samples
2) Development of a relative fire intensity measure, combining charcoal and pyrogenic carbon fluxes
3) Identification of how the techniques presented in this study may be used to identify anthropogenic influence in palaeofire records

Charcoal and pyrogenic carbon are directly compared as measures of fire incidence, and their combined results are analysed to determine fire intensities. Contrasting and complimentary data on fuel types from length-width ratios and morphotypes are discussed, including the applicability of existing classification systems to tropical northern Australian savannas. This morphological fuel type data is compared to $\delta^{13}C$ values for pyrogenic carbon, which provides a quantitative measure of C_3 versus C_4 fuel contribution. These techniques are then discussed for modern charcoal trap and surface sediment samples, including insights applicable to

sediment cores. Finally, the techniques evaluated in this chapter will be contextualised in terms of known fire regime characteristics to establish a framework for the interpretation of the fire records presented in the following chapter (Chapter 9).

8.2 Site Characteristics

While all three sites (each discussed in detail in Chapter 5, 6 and 7) are similar as they are located in tropical savannas under similar climatic conditions, the physical characteristics of each site are unique (summarised in Table 8.1). Sanamere Lagoon has the largest approximate catchment size and is the largest water body (by surface area) in this study. While the catchment of Sanamere Lagoon covers the largest elevation range of the three sites, this is spread over the largest, and relatively flat area while the Marura catchment is small and steep-sided.

Table 8.1: Physical characteristics of the sites in this study (data sources referenced in individual site chapters).

	Marura	Big Willum Swamp	Sanamere Lagoon
Water depth (at time of sample collection)	11 m	3.5 m	1.25 m
Sediment depth	5.75 m	≥ 3 m	2 m
Approximate catchment size	0.2 km²	0.75 km²	9 km²
Approximate water surface dimensions	210 x 230 m	250 x 600 m	1.5 x 2 km

Elevation range within catchment	43 to 69 m a.s.l.	27 to 39 m a.s.l.	15 to 56 m a.s.l.
Approximate distance to modern coastline	10 km	20 km	23 km
Mean annual rainfall (and primary months in which rainfall occurs)	1314.8 mm (Nov – Apr)	1784.9 mm (Nov – Apr)	1800 mm (Dec – Apr)
Average daily temperatures	15.1 – 34.5 °C	18.8 – 34.8 °C	23 – 32 °C
Annual cloud-to-ground lightning flash density	2 – 3 flash/km^2/y	2 – 3 flash/km^2/y	1 flash/km^2/y
Primary fire months (and wind direction)	Jul – Oct (SE to NE)	Jul – Oct (SE to E)	Aug – Dec (SE to E)

Marura is considerably closer to the modern coastline (~10 km) than the other sites; however, Big Willum Swamp is close (~5-10 km) to inlets of the Mission and Embley Rivers, environments which were densely occupied by Indigenous inhabitants during the late Holocene (e.g. Wathayn archaeological complex; see Chapter 3; Morrison 2013). The landscape around Sanamere Lagoon receives slightly fewer lightning strikes per year than Marura and Big Willum Swamp as well as higher rainfall, making lightning-triggered ignitions least likely at this site.

These differences in site characteristics have noticeable effects on the outcomes of methods applied in this study, outlined in the following sections.

8.3 Charcoal and Pyrogenic Carbon

8.3.1 Charcoal Size Fractions

As outlined in Chapter 4, different particle size fractions are associated with different source areas from local/within-catchment (>125 µm) to regional/beyond catchment (<125 µm) (see Clark 1988; Peters & Higuera 2007). In this study, the strength of relationships between different charcoal size fractions varies between sites.

At Big Willum Swamp, consistently low or nil flux values in the >250 µm size fraction indicate that the Big Willum record represents a primarily regional signal, beyond the catchment (>0.25 km from the water edge). This is supported by weak correlations between the >250 µm size fraction and all other measures, and a stronger correlation between bulk PyC and <63 µm PyC ($r^2 = 0.45$) than is present at the other sites in this study (Figure 8.1).

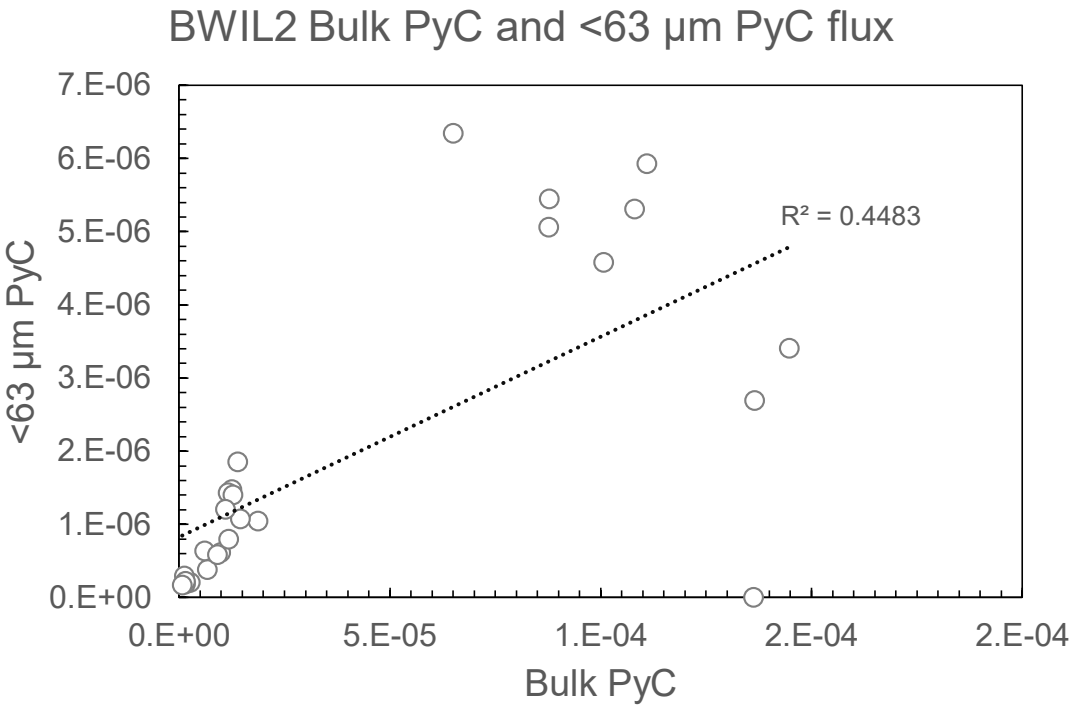

Figure 8.1: BWIL2 bulk and <63 µm PyC flux scatter plot.

In contrast, the $\delta^{13}C$ record for Sanamere Lagoon suggests a local within-catchment signal (<1.5 km from the water edge) for all measures except <63 µm PyC flux, due to the absence of a C_4 grass signal in the bulk PyC, when C_4 grasses are known to be abundant in the woodlands beyond the catchment (for more records with local-only signals, see also Carcaillet et al. 2001; Laird & Campbell 2000; Leys et al. 2015; Pitkänen, Lehtonen & Huttunen 1999). This is supported by strong positive correlations ($r^2 > 0.65$) between all charcoal size fractions and extremely weak correlations between <63 µm PyC flux and all other variables (Figure 8.2). This within-catchment signal is likely the product of multiple site dynamic effects, including a large catchment (compared to other sites in this study) and ineffective aerial particle transport to the lagoon (see Chapter 7 Charcoal Traps section). As the Sanamere Lagoon record does not primarily capture a beyond-catchment signal from the regionally widespread open eucalypt

woodland vegetation type, little comparative insight can be provided about the neighbouring Jardine River catchment from this record.

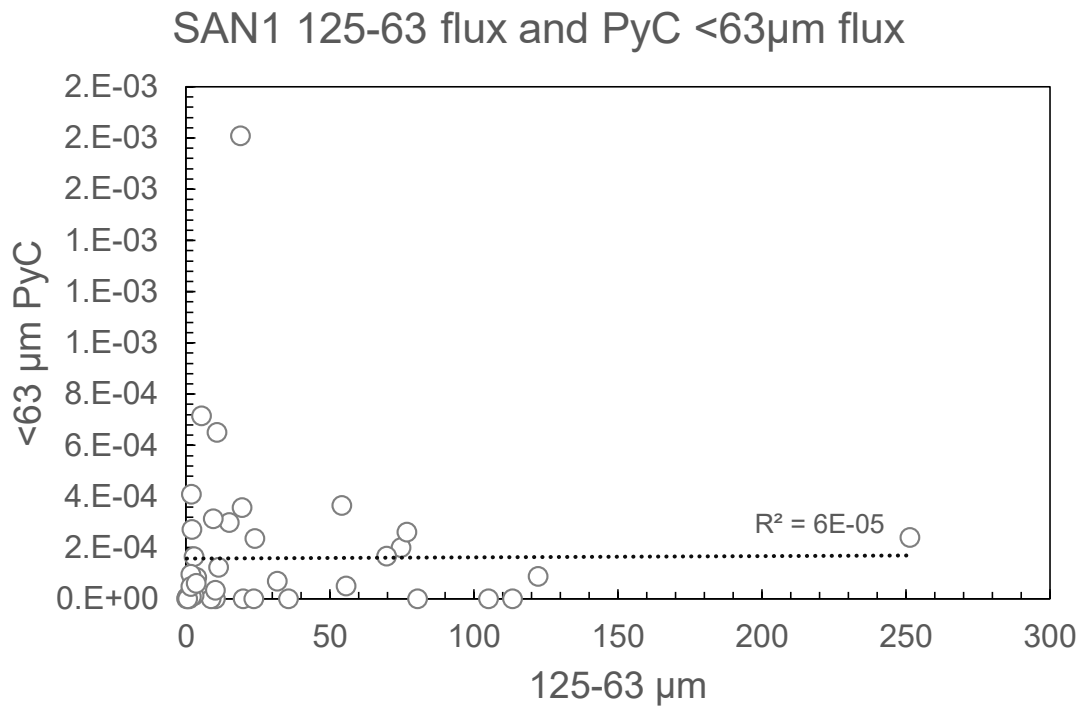

Figure 8.2: SAN1 125-63 µm charcoal flux and <63 µm PyC flux scatter plot.

Multiple strong positive correlations exist between charcoal variables for Marura. The Marura record does not appear skewed towards a local signal like the Sanamere record, as <63 µm PyC flux is strongly correlated ($r^2 = 0.71$) with 125-63 µm charcoal flux indicating the finest fraction is responding similarly to other fractions. Similarly, the Marura results do not appear skewed towards a regional signal like the Big Willum record, as >250 µm charcoal flux is abundant for much of the record, and strongly correlated with the other charcoal size fractions (Figure 8.3). The Marura record represents a blend of a local (<0.2 km from the water edge) and a regional (>0.2 km from the water edge) signal, which show similar trends for most of the record.

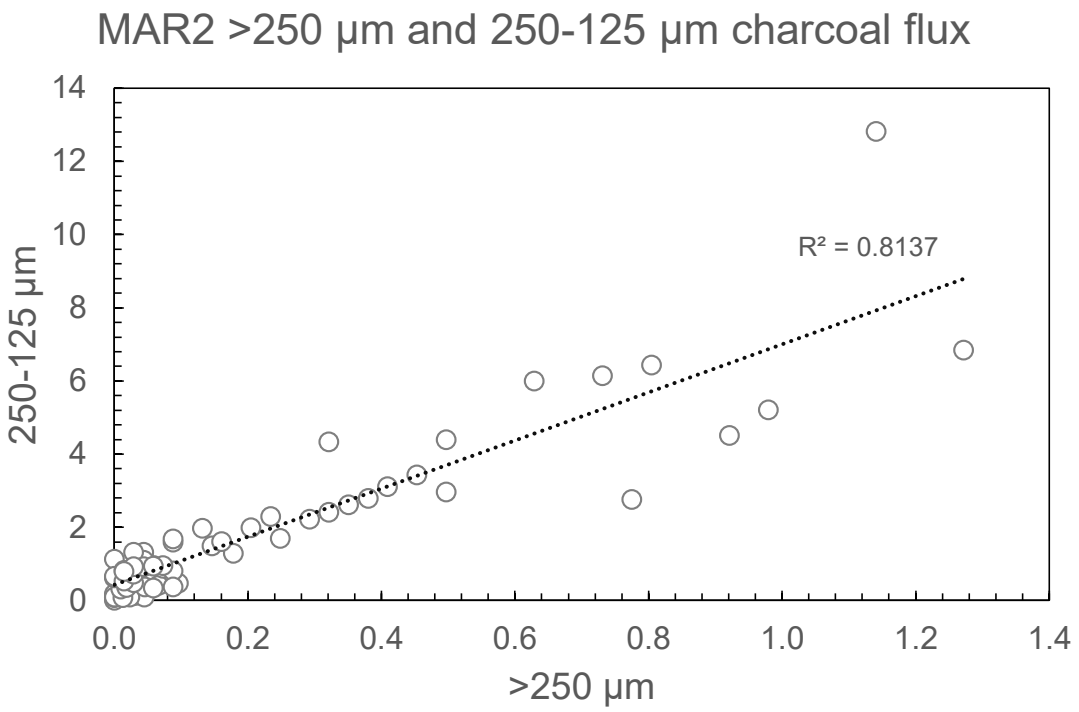

Figure 8.3: MAR2 >250 µm and 250-125 µm charcoal flux scatter plot.

8.3.2 Charcoal and Pyrogenic Carbon Flux

The chemical isolation of pyrogenic carbon using the hydrogen pyrolysis method is a relatively recent technique in palaeofire research (e.g. Ascough et al. 2009; Meredith et al. 2012; Wurster et al. 2012, 2013), with no existing studies combining pyrogenic carbon isolated using hydrogen pyrolysis with optical charcoal data published to date. Differences between charcoal and pyrogenic carbon measures are expected as they are distinctly separate, but related, fire proxies, and in this study have been analysed across different size fractions.

Across the three sites presented in this study, charcoal flux and pyrogenic carbon flux display comparable overall trends but with asynchronous peaks (see tables in Chapters 5, 6 and 7). Weak correlations between bulk PyC fluxes and charcoal fluxes is likely the product of small

sample sizes. A strong positive relationship ($r^2 = 0.71$) exists between 125-63 µm charcoal flux and <63 µm PyC flux at Marura, and the correlation between these variables at Big Willum Swamp ($r^2 = 0.53$) is of comparable strength to the relationships between the >250 µm size fraction and the other charcoal flux variables. The strength of these correlations indicates a link between the two microscopic size fractions and suggests some consistency of burn temperatures in the fine fraction; for Big Willum Swamp, this is explained by both of these size fractions being primarily derived from beyond the catchment, while at Marura this suggests comparable fire intensities (and therefore, fire regimes) at within-catchment and beyond catchment scales.

The absence of strong relationships between the measured PyC fluxes and charcoal variables in the Sanamere record indicates that these measures are capturing different trends and sources of variability at this site. The weakness of relationships between <63 µm PyC flux and all charcoal size fractions is due to the <63 µm PyC fraction deriving from beyond the Sanamere Lagoon catchment (as discussed further in Charcoal Morphology and $\delta^{13}C$ below), indicating a distinction between fire regimes at within-catchment and beyond catchment scales at this site. This demonstrates that these measures are not interchangeable but provide complementary data for a more nuanced palaeofire reconstruction.

8.3.2.1 Fire Intensity

Few palaeofire records are of high enough resolution to capture seasonal variations in burning, with individual data points for fire proxies representing an aggregate of the time segment they represent (e.g. 50 years). Charcoal fluxes/abundances cannot distinguish whether the particles within that time slice were created by small annual burns or in a single widespread fire event. Additionally, Preece (2002) identifies historical records of year-round burning by traditional

owners in Arnhem Land and Cape York Peninsula, indicating that the timing of burns may be of less importance than the frequency, intensity and severity.

Fire intensity can be broadly defined as the overall energy release of a fire, comprising multiple factors including temperature and residence times, and does not include ecosystem effects of fire (Keeley 2009). Trauernicht et al. (2015, p.1914) suggest that "fire intensity and heterogeneity" are affected by human fire management while the "total extent of landscape burnt" is primarily driven by climate, making traditional measures of biomass burning (e.g. charcoal flux) sensitive to climate signals but unable to detect an anthropogenic signal within a fire record.

As such, fire intensity data are critical in order to separate potential climatic and anthropogenic influences within a palaeofire record, and a fire intensity measure addresses Research Question ii (distinguishing anthropogenic and climate influences) outlined in Chapter 1. As the proportion of pyrogenic carbon to charcoal increases with increasing fire intensity (see Bird & Ascough 2012), the combination of charcoal and pyrogenic carbon flux data allows for the identification of peaks associated with different relative fire intensities. Peaks in fluxes can be separated into two dominant intensity types (Figure 8.4):

1) Low intensity, characterised by peak charcoal flux and low PyC flux (because large quantities of charcoal were produced with low pyrogenic carbon content)
2) High intensity, characterised by a peak in PyC and low charcoal flux (because charcoal that survived the fire was substantially converted to PyC measurable by hydrogen pyrolysis)

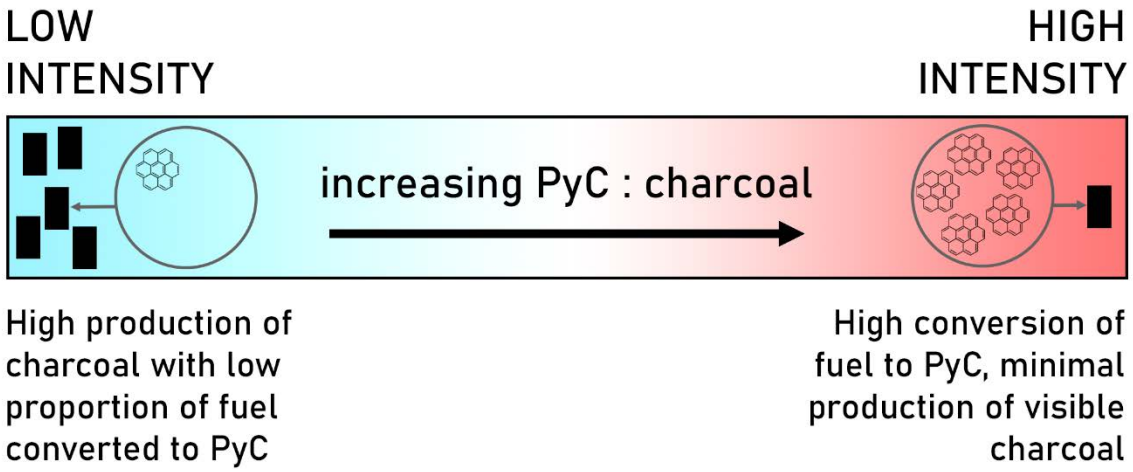

Figure 8.4: Graphical representation of intensity classifications of charcoal and pyrogenic carbon. Charcoal is represented by black rectangles. Pyrogenic carbon is represented by structural diagrams of coronene, as coronene contains the minimum number of polyaromatic rings for isolation by hydrogen pyrolysis.

Peaks in charcoal flux not reflected in PyC flux (as either the absence of a peak or the presence of a trough) are the product of cool, low intensity fire events generating minimal pyrogenic carbon (represented by blue bars in Figures 8.5, 8.6 and 8.7). A greater proportion of PyC flux relative to the charcoal flux indicate high intensity fires, either at severe intensities destroying larger particles (low or absent charcoal, coincident <63 µm PyC flux peak) or burning a smaller area or biomass volume (than comparable intensity fires that create both PyC and charcoal flux peaks) (represented by red bars in the figures below). Peaks in both charcoal flux and PyC flux occur under intermediate or indeterminate fire intensities, shown as the absence of low or high intensity bars on the following graphs; designations of low or high intensity bars have only been made where a clear determination is apparent. Ideally, charcoal and pyrogenic carbon would be measured within one sample, allowing low, intermediate and high intensity

designations to be made with greater certainty; this would be difficult to achieve due to practical considerations such as division of charcoal into multiple size fractions and potentially low sample volumes as a result.

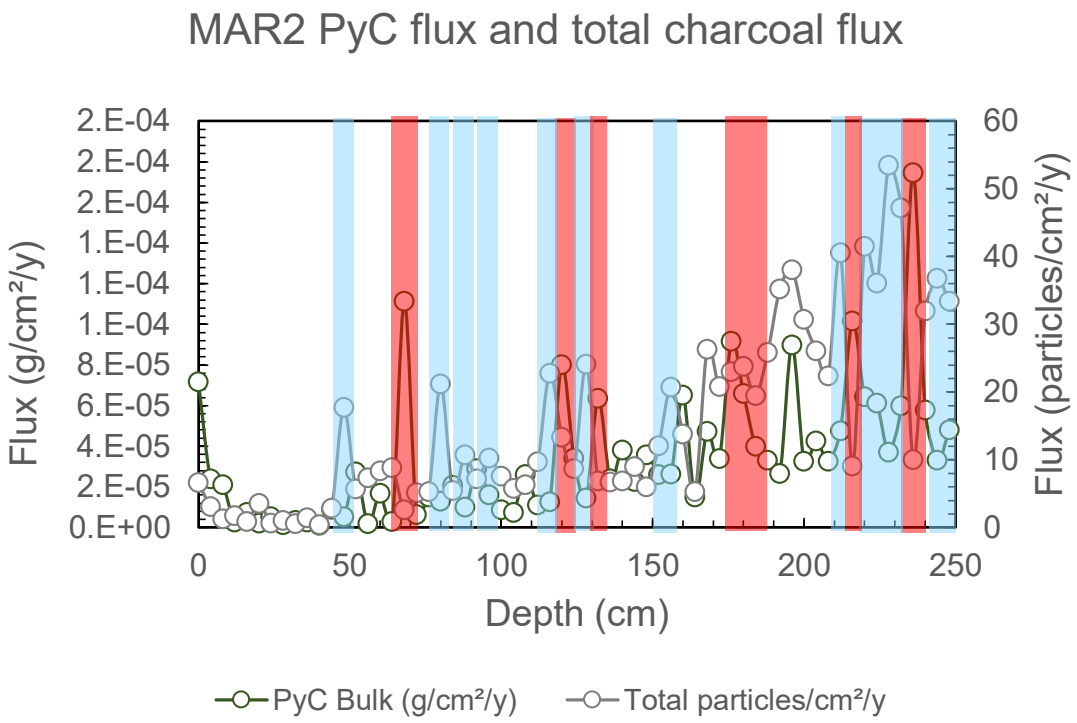

Figure 8.5: MAR2 bulk PyC flux and total charcoal flux, by depth. Blue bands indicate cool, low intensity fire (high charcoal, low PyC), and red bands indicate hot, high intensity fire (high PyC, low charcoal).

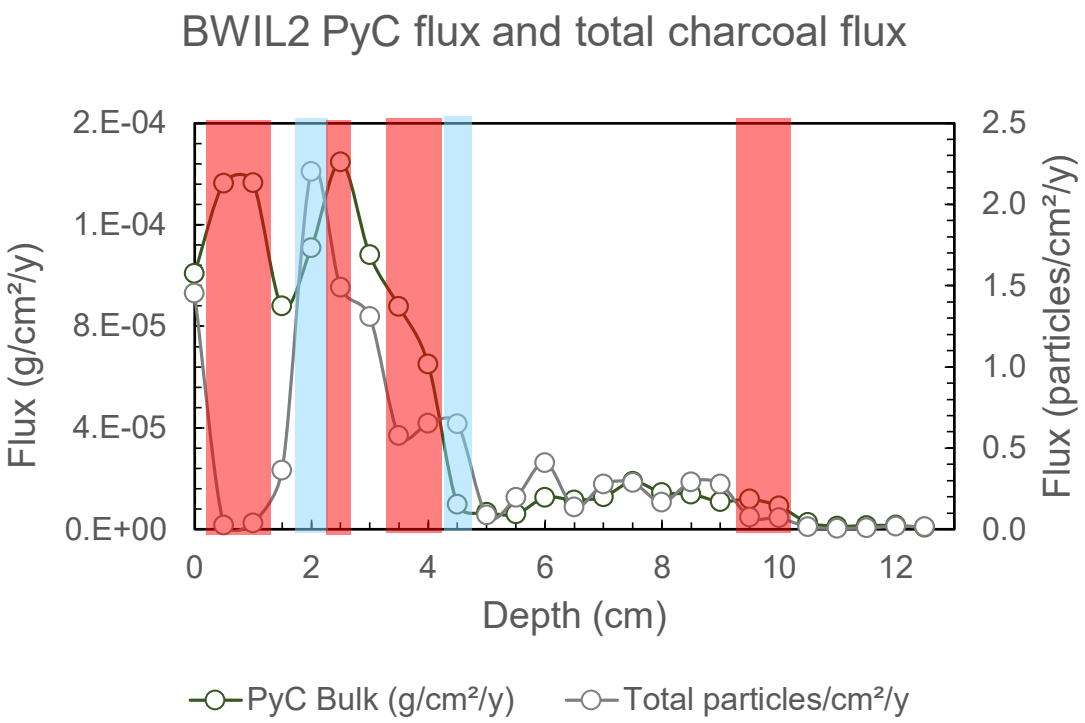

Figure 8.6: BWIL2 bulk PyC flux and total charcoal flux, by depth. Blue bands indicate cool, low intensity fire (high charcoal, low PyC), and red bands indicate hot, high intensity fire (high PyC, low charcoal).

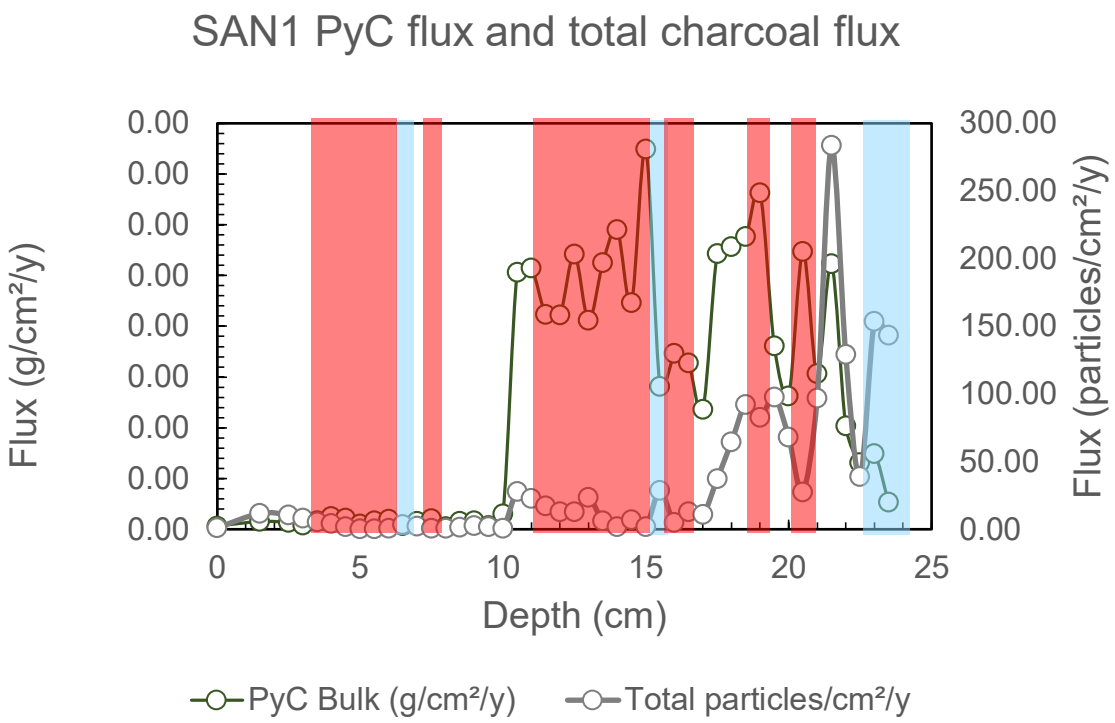

Figure 8.7: SAN1 bulk PyC flux and total charcoal flux, by depth. Blue bands indicate cool, low intensity fire (high charcoal, low PyC), and red bands indicate hot, high intensity fire (high PyC, low charcoal).

All three records show varying fire intensities through time. Marura shows the highest variability, with numerous shifts between low, high and indeterminate intensities, and no one intensity type remaining dominant for more than ~300 years. While the charcoal flux peak at 2 cm depth at Big Willum Swamp may be classified as a cool burn due to charcoal flux peaking and PyC flux decreasing (relative to the previous sample), both fluxes are still high and thus this may reasonably be considered intermediate or indeterminate intensity. In that case, the uppermost 4 cm (~30 cal BP to present) of the Big Willum record contains only high intensity fire events.

The Sanamere Lagoon record is dominated by high intensity fire events, with the exception of a significant low intensity charcoal flux peak at the beginning of the record (~8260-8240 cal BP). This data will be further discussed in the context of each site history in Chapter 9.

If variation in fire intensity is taken as an indicator of anthropogenic influence (following Trauernicht et al. 2015), the Marura record indicates the highest levels of human influence on landscape fire of the sites in this study, while the Sanamere Lagoon record shows the least human influence. Overall low charcoal and pyrogenic carbon abundances combined with low resolution make assessing human influence on fire at Big Willum Swamp difficult. The absence of anthropogenic burning in the tropical savannas of northern Australia has been associated with large scale, high intensity "wildfires" in the late dry season, with a fire return interval of 1-3 years (Yibarbuk et al. 2001, p.329, 337); the presence of substantial periods of cool, low intensity fires in a palaeofire record therefore also suggests human intervention.

It is not certain that overall charcoal or pyrogenic carbon abundance, as measures of total biomass burned, capture a purely climatic signal as proposed by Trauernicht et al. (2015). The overall decline in flux values at Marura through the late Holocene may indicate a buffer effect created by human fire management, as the climate of this period is known to be increasingly variable with intensifying ENSO conditions compared to the mid-Holocene (e.g. Diaz & Markgraf 1992; Field et al. 2017; Fletcher et al. 2015; Walker et al. 2018); this will be discussed further in Chapter 9.

8.3.3 Pyrogenic Carbon and Total Organic Carbon

The relationship between total organic carbon and percent pyrogenic carbon varies between sites, and to a lesser extent between size fractions (Figure 8.8). Clustering is apparent for each

site, with Marura and Big Willum Swamp overlapping in tight clusters and Sanamere Lagoon separated and scattered more broadly.

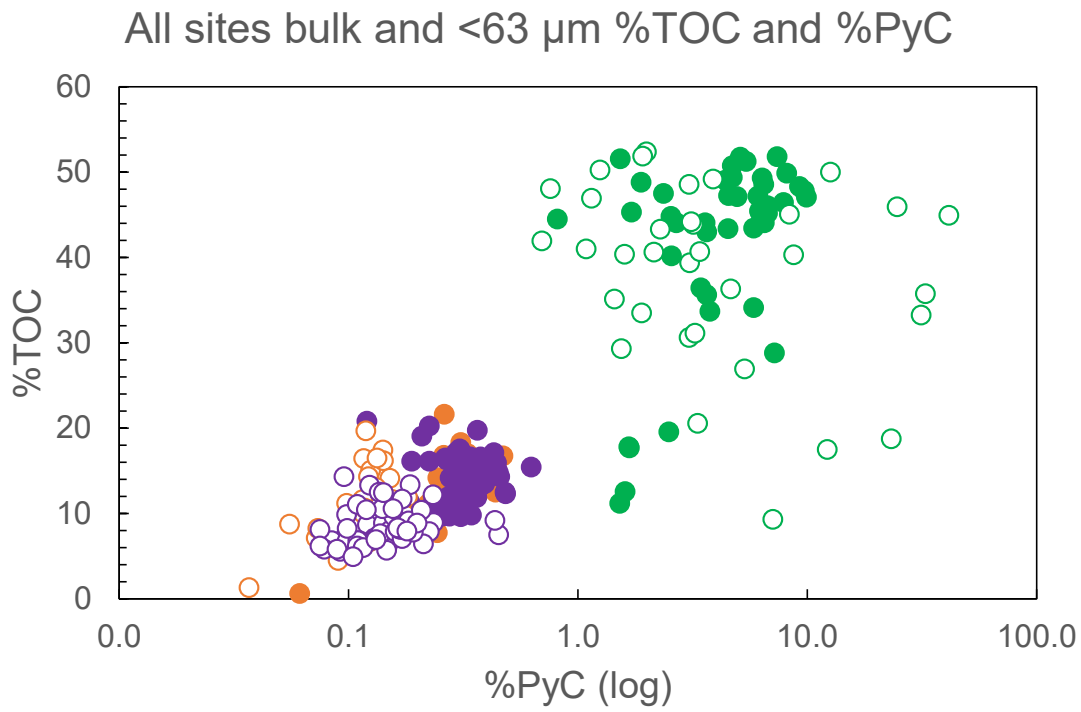

Figure 8.8: Total organic carbon (%TOC) and percent pyrogenic carbon (log scale) for bulk (closed circles) and <63 µm (open circles) size fractions. Purple: Marura, orange: Big Willum Swamp, green: Sanamere Lagoon.

This indicates that pyrogenic carbon percentage is more closely linked to total organic content at Marura and Big Willum Swamp, where vegetation is mixed tree-grass. Pyrogenic carbon percentages are not consistently connected to total organic carbon at Sanamere Lagoon. Sanamere Lagoon also has a higher average total organic carbon content throughout the record (~40 %) than peak %TOC values at Marura or Big Willum Swamp (both ~20 %). The scatter

within the Sanamere <63 µm size fraction is likely the result of various inputs from within and beyond the catchment influencing this fraction (see Chapter 7 Discussion).

8.4 Length-Width Ratios and Morphotypes

8.4.1 Length-Width Ratios

Different studies suggest different thresholds equal to or above which a particle is considered elongate or elongated (Figure 8.9); a length-width ratio of 3.6 was selected for this study. Length-width ratios offer a simple, easily replicable method for identifying potentially grass-derived particles. The combination of length-width ratios and other methods for identifying fuel type, such as morphology and $\delta^{13}C$ values, allows for the identification of grass and non-grass elongate fuels.

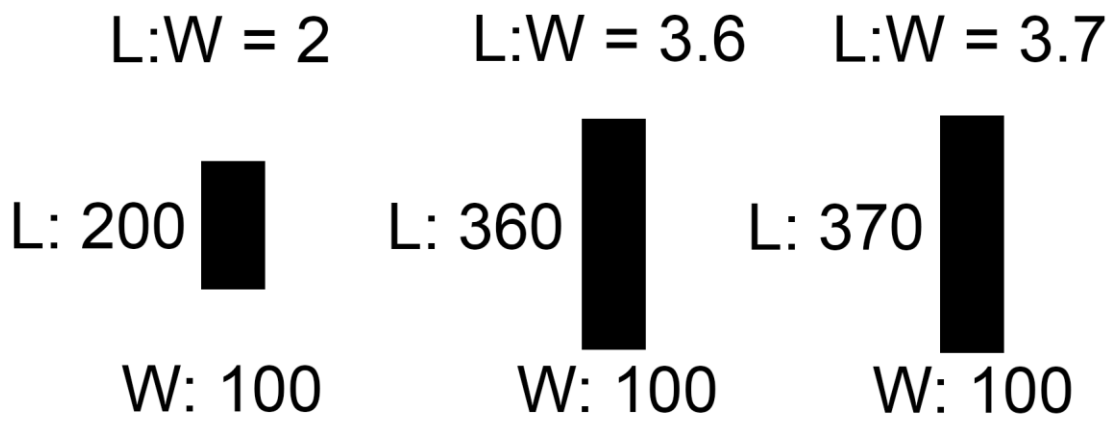

Figure 8.9: Visualisation of length-width ratios suggested as the threshold for particles to be considered "elongate(d)": a) 2 (Aleman et al. 2013), b) 3.6 (Umbanhowar & McGrath 1998), and c) 3.7 (Crawford & Belcher 2014).

8.4.2 Morphotypes

As stated in Chapter 4, both morphotype classification systems applied in this study were developed using samples from British Columbia, in temperate forests. Both systems, particularly the detailed 27-type Courtney Mustaphi and Pisaric (2014) system, therefore contain details specific to temperate forest environments (e.g. the presence of conifer needle morphotypes) and may overlook or not capture details specific to savannas. For example, the association of certain particle morphologies (e.g. type M; Enache & Cumming 2006) with high fire intensities due to their creation during crown fires likely does not apply in environments such as dwarf heathlands that do not have a distinct crown layer that only burns under severe fire conditions.

8.4.2.1 Courtney Mustaphi and Pisaric (2014): 27-Type Morphotype Classification

The extensive detail within Courtney Mustaphi & Pisaric's (2014) morphotype system, applied to the macroscopic size fractions, was not useful to this study for a number of reasons. Firstly, some types were specific to fuel types not found in tropical Australian savanna environments, namely types C1 (charred conifer needles) and C2 (needle fragments) (Courtney Mustaphi & Pisaric 2014, p.741). Secondly, distinctions which are applicable to these environments did not necessarily provide diagnostic data applicable to interpretation in this study. For example, A1 (foliated polygon) is associated with wood as a fuel, while A3 (solid, closed polygon) is associated with "punky wood" or leaves as fuel (Courtney Mustaphi & Pisaric 2014, p.739). If both of these particles are taken to originate from wood, the distinction between these two types does not provide any additional data to assist in the reconstruction of landscape vegetation.

Some types were also identified by Courtney Mustaphi & Pisaric (2014) as potentially the product of numerous fuel types, thus preventing the attribution of a distinctive fuel type; for

example, type B2 is identified as either wood or *Poaceae* leaf-derived, B4 as either leaves or *Poaceae* leaves, and B5 as conifer needles, grass or leaves (Courtney Mustaphi & Pisaric 2014, p.740). Therefore, classifying a particle as B2, B4 or B5 cannot distinguish whether the particle is tree, shrub or grass-derived and subsequently these types provide no interpretable data for this study. Type A6 (framework-supported polygon), identified in samples from all three sites in this study, is not attributed to any fuel source by Courtney Mustaphi & Pisaric (2014:739).

Finally, the volume of data generated by applying Courtney Mustaphi & Pisaric's (2014) 27-type system is difficult to manage and must be simplified for analysis, thus removing the additional detail that it provides. Morphotype data for the macroscopic size fractions in this study were subsequently simplified to Enache and Cumming's (2006) 7-type system, allowing comparison to the microscopic (125-63 μm) size fraction, as well as simplified further into elongate versus non-elongate morphotypes for comparison to length-width ratio data.

8.4.2.2 Enache and Cumming (2006): 7-Type Morphotype Classification

The 7-type system presented by Enache and Cumming (2006) is a less detailed and potentially more widely applicable morphotype system (see Figure 8.10). However, due to the system being derived from fossil charcoal data rather than burning under laboratory conditions, Enache and Cumming (2006) do not attribute fuel sources to all morphotypes, specifically types B (partial burn), P (irregular, powdery) and D (elongate with ramifications). Therefore, classification of particles as these types does not provide fuel type data for interpretation in the context of this study.

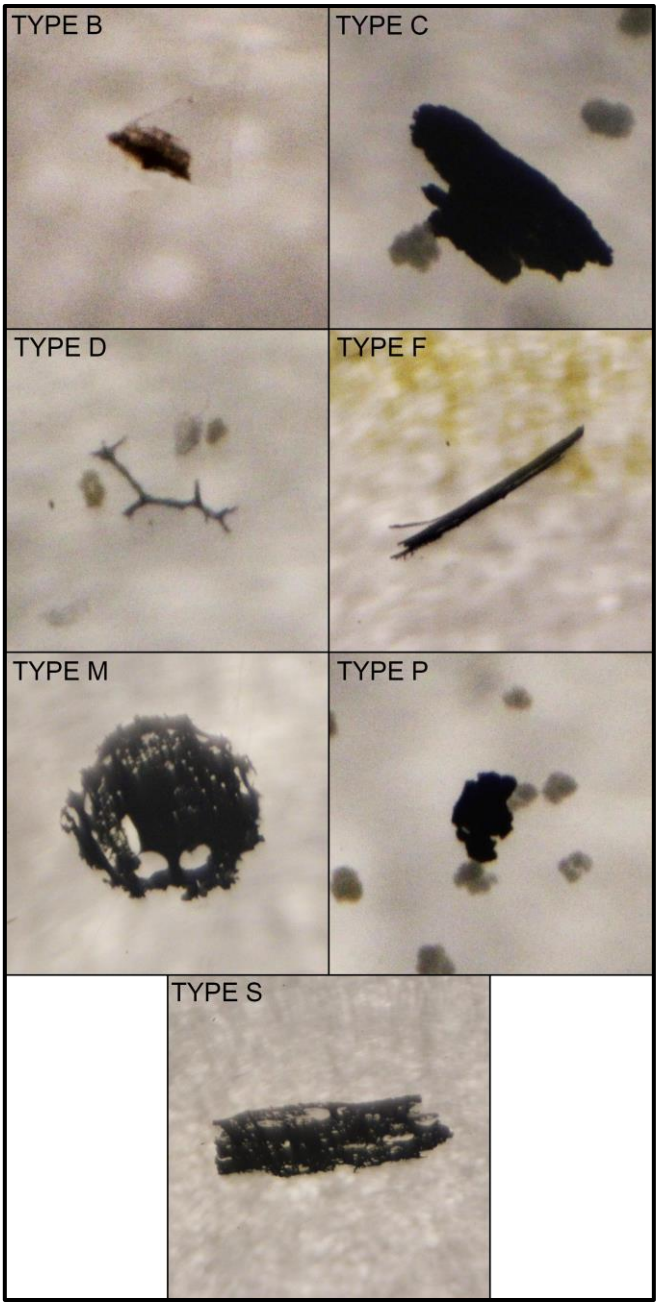

Figure 8.10: Example particles from this study for each type in Enache and Cumming's (2006) morphotype classification.

Charcoal particles were also found in this study that may not be accurately classified under these existing morphotype systems and were thus recorded either as "Unidentified" or as the closest corresponding morphotype available. While Enache and Cumming (2006, p.285)

describe type M particles as irregular, highly porous, and “thin”, particles were found in this study that were irregular, highly porous, and thick (three-dimensional) (Figure 8.11). These particles, when encountered in the 125-63 µm size fraction, were recorded as type M as this is the closest corresponding morphotype within the Enache and Cumming (2006) system.

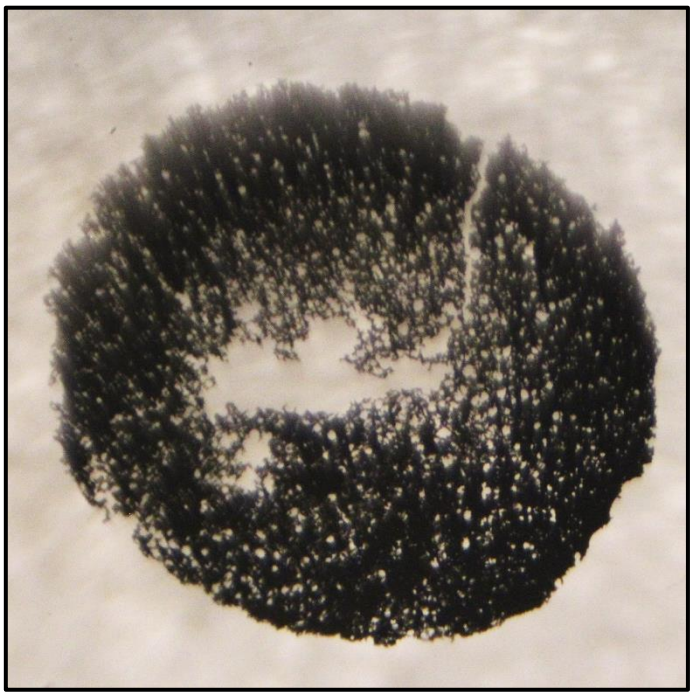

Figure 8.11: Particle from SAN1 7.5-8cm >250 µm displaying irregular shape, high porosity, and depth (three-dimensionality), classified as type M under the Enache and Cumming (2006) system.

Discrepancies in vegetation/fire dynamics when comparing temperate forests with tropical savannas as well as particles being classified as the closest available type make applying interpretations by Enache and Cumming (2006) to the results of this study difficult. This may explain why an increase in type M particles is not observed during high intensity fire events identified in the SAN1 record (see Fire Intensity above, and Chapter 7 Results), as Enache and

Cumming (2006) describe this particle type as being generated under high temperature, high intensity conditions; however, this is likely also a product of vegetation structure differences as the dwarf heathland currently surrounding Sanamere Lagoon does not include a canopy layer to be affected by crown fires (see Enache & Cumming 2006, p.288). Similarly, particles classified as type P in this study were irregular with no visible structure, but were not necessarily "powdery" in texture or thin ("sheets") as described by Enache and Cumming (2006, p.285).

However, the simplicity of Enache and Cumming's (2006) seven-type system does allow for an overview of particle morphological changes through a charcoal record, even if this cannot be confidently linked to specific fuel types. Charcoal morphology in all size fractions at Marura, for example, show a decline in elongated type F over time while geometric type S with visible structure increases (see Chapter 5 Results). While Enache and Cumming (2006) describe type F as most abundant in samples with low charcoal counts at their British Columbian site, the opposite trend is apparent in the Marura record.

No studies to date have demonstrated what morphologies are present in savanna environments. Leys et al. (2015) investigate morphotypes within a North American tallgrass prairie, and describe very specific "cell" and "fibrous" types associated with herbaceous fuels and "dark", "lattice", "branched" and "sponge" with woody fuels (see Leys et al. 2015 Appendix 1, p.2). The array of particle morphologies encountered at sites in this study suggests that the small selection of morphotypes presented by Ley et al. (2015) applicable to temperate prairies do not cover the full range of fuels present in Australia's savannas.

Morphological changes within a record may also be significant to estimating the source area of charcoal in conjunction with particle size, with different particle shapes and densities within a size fraction dispersing differently. Enache and Cumming (2006, p.290) suggest that porous

particles (e.g. types M and S) may be more effectively aerially transported than dense (e.g. types C and P) morphologies. Vachula and Richter (2018) model the settling velocity of particles and demonstrate that porous, non-spherical particles take longer to settle, and may therefore travel further before settling, compared to denser, spherical particles. These studies do not discuss the overland (e.g. in-wash) transport efficiency of these particles.

8.4.3 Length-Width Ratios and Morphotypes Comparison

Leys et al. (2015, p.11) notes the potential of combining aspect ratio measurements with morphotype analysis to better identify fuel types. Aspect ratio and morphotypes provide comparable data when analysing elongate versus non-elongate particles, with length-width measurements being more consistent and less reliant on analyst discretion. As discussed in Chapters 5-7, length-width ratios and elongate morphotypes produced similar estimates of elongate particle percentages in this study, with slightly higher values estimated by ratio measurements. Either method is therefore applicable if the desired data is an elongate/non-elongate binary, with aspect ratio ideal for precision, and morphotypes for speed of analysis. This binary is taken to be representative of grass versus non-grass (woody) content (e.g. Aleman et al. 2013; Umbanhowar & McGrath 1998), although must be interpreted with caution as high incidence of breakage (e.g. in high energy depositional environments or during laboratory processing) as well as non-grass elongate plants (e.g. sedges, see Chapter 7 as well as discussion below) can also influence this measure. Elongate particles with ramifications may also affect this, as ramified elongates have been identified as deriving from leaf stems (see Courtney Mustaphi & Pisaric 2014, p.741).

Morphotypes allow for the identification of fuels beyond an elongate/non-elongate measure. The applicability of morphotype analysis to a site or record depends on (i) whether the

chosen/available morphotype classification system is appropriate to that environment, and (ii) whether differentiating between various fuel types is meaningful in relation to vegetation structure and dynamics. The identification of wood versus leaf charcoal may be used to determine fire temperature or severity in an environment where wood only burns under high severity fires such as crown fires (e.g. temperate and montane forests; Feurdean & Vasiliev 2019). The distinction between such types may not be useful or interpretable in an environment where no link is known between fuel source and fire conditions (e.g. tropical dwarf heathland; see Chapter 7).

8.5 Charcoal Morphology and $\delta^{13}C$

Similar to charcoal and pyrogenic carbon fluxes, charcoal morphology and pyrogenic carbon $\delta^{13}C$ values provide complementary data. Morphological data can provide detail beyond a grass/non-grass binary, although the utility and interpretability of this data may depend on existing reference collections of fuel types (see Morphotypes above). Contrastingly, $\delta^{13}C$ values can quantitatively determine the contribution of C_3 versus C_4 fuels. The combination of these two types of measures in this study reveals the nuances of each analysis and the benefits of combining them.

The Sanamere Lagoon record provides an ideal example due to its local C_3-only vegetation within-catchment and mixed C_3-C_4 vegetation communities beyond the catchment. Elongate charcoal particles identified by length-width ratios and morphotypes are present throughout the Sanamere record, which would typically be interpreted as the presence of grasses (e.g. Aleman et al. 2013; Umbanhowar & McGrath 1998). Consistently low ^{13}C values in pyrogenic carbon in this record, however, identifies an absence of C_4 grass contributing to the fuel. Elongate particles in the Sanamere record are therefore likely the product of C_3 plants such as sedges

(see Bunn & Boon 1993, p.89; Boon & Bunn 1994, p.102), which are abundant in the modern vegetation at the site. This demonstrates the benefits of combining these methods; analysis of elongate particles only would result in the erroneous interpretation that grasses are present throughout the record, while analysis of $\delta^{13}C$ values only would not allow for the identification of sedges distinct from the contribution of other C_3 fuels. This is valuable information as sedges at Sanamere Lagoon currently grow in waterlogged sediments fringing the lagoon, thus the presence of sedge charcoal in the record indicates potentially arid conditions and fire events close to the water edge.

Elongate particles sourced from non-grass fuels are also suggested by the morphotype systems used in this study (as discussed in Morphotypes above). Ramified (branching) morphotypes are typically elongate in aspect ratio but are not necessarily identified as grasses, such as C5, C6 and C7 (Courtney Mustaphi & Pisaric 2014, p.741) which are associated with leaf stem fuels, and Type D (Enache & Cumming 2006) where no fuel type is specified. This demonstrates the importance of developing new morphotype systems for different regions or climate zones (e.g. the tropics) and the combination of measures such as morphotypes, aspect ratio and $\delta^{13}C$ values.

These demonstrated differences between elongate particle measures and $\delta^{13}C$ values unsurprisingly result in only very weak correlations between these measures in this study ($r^2 < 0.2$; Figures 8.12, 8.13 and 8.14). It is noteworthy that these poor correlations occur at all sites including Big Willum Swamp and Marura where elongate particle percentages and $\delta^{13}C$ values both suggest mixed grass and woody contributions throughout these records (see Figures 8.12 and 8.13). Some of these differences may result from dissimilarities across size fractions; elongate particle percentages were recorded for distinct size classes while $\delta^{13}C$ values were analysed for bulk PyC and the <63 μm size fraction only.

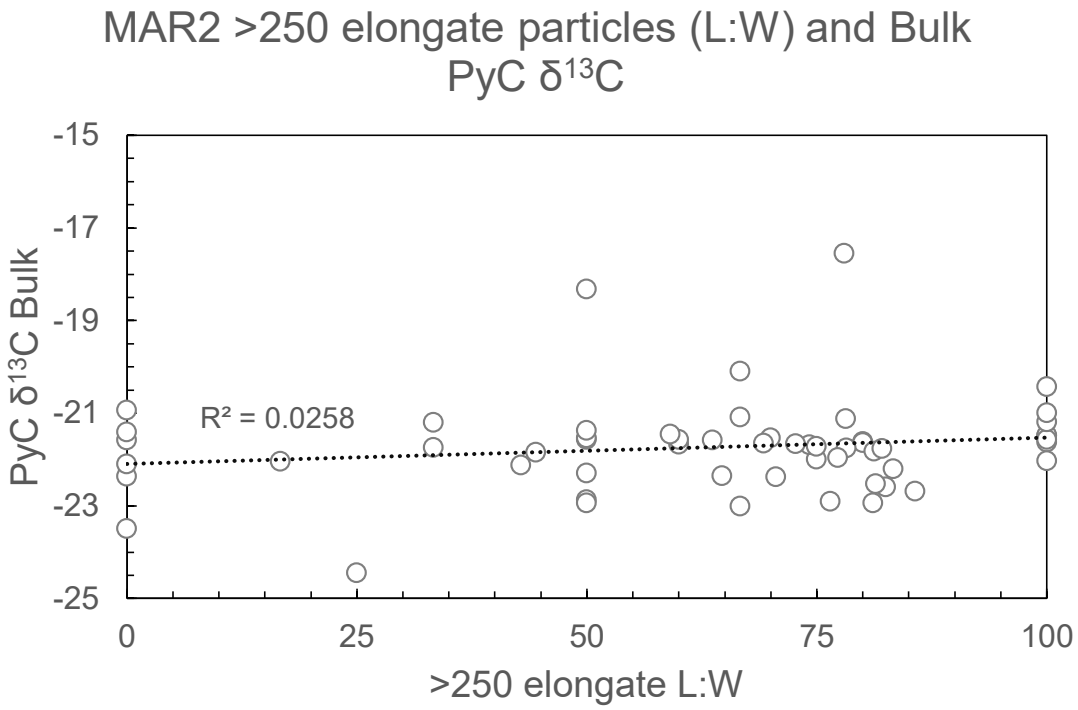

Figure 8.12: MAR2 >250 µm percent elongate particles from length-width ratios and bulk PyC $\delta^{13}C$ scatter plot.

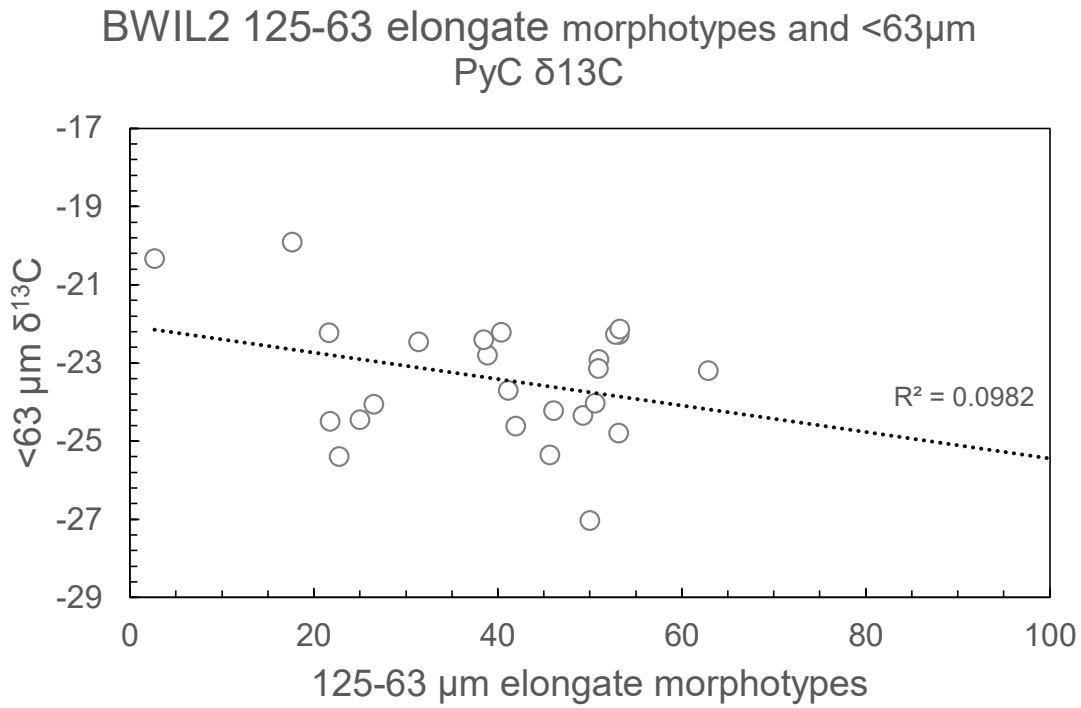

Figure 8.13: BWIL2 125-63 µm percent elongate morphotypes and <63 µm PyC $\delta^{13}C$ scatter plot.

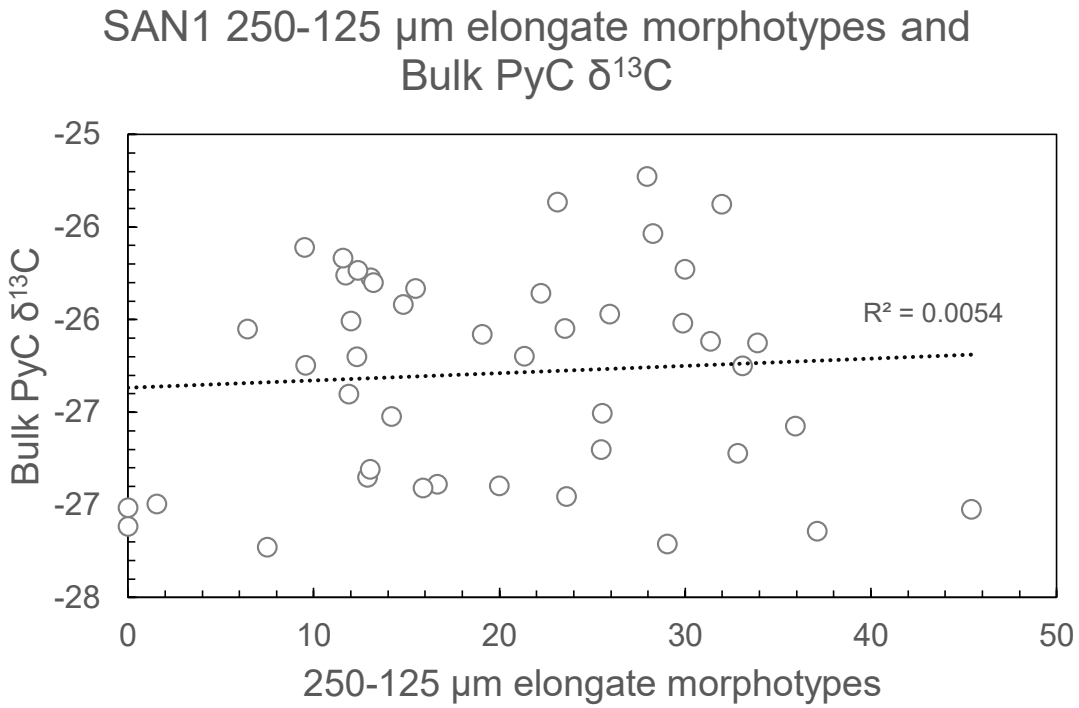

Figure 8.14: SAN1 250-125 µm percent elongate morphotypes and bulk PyC $\delta^{13}C$ scatter plot.

8.5.1 Pyrogenic Carbon and Total Organic Carbon $\delta^{13}C$

Clustering by site is apparent in $\delta^{13}C$ values pre-hydrogen pyrolysis (total organic carbon) and post-hydrogen pyrolysis (PyC) for the bulk fraction (Figure 8.15), with Big Willum and Sanamere clustering tightly and Marura showing a greater scatter. Less distinct clustering occurs in the <63 µm size fraction for all sites; Marura and Sanamere vary most in pyrogenic carbon <63 µm $\delta^{13}C$ values and less in total organic carbon, while Big Willum varies across both total organic carbon and PyC.

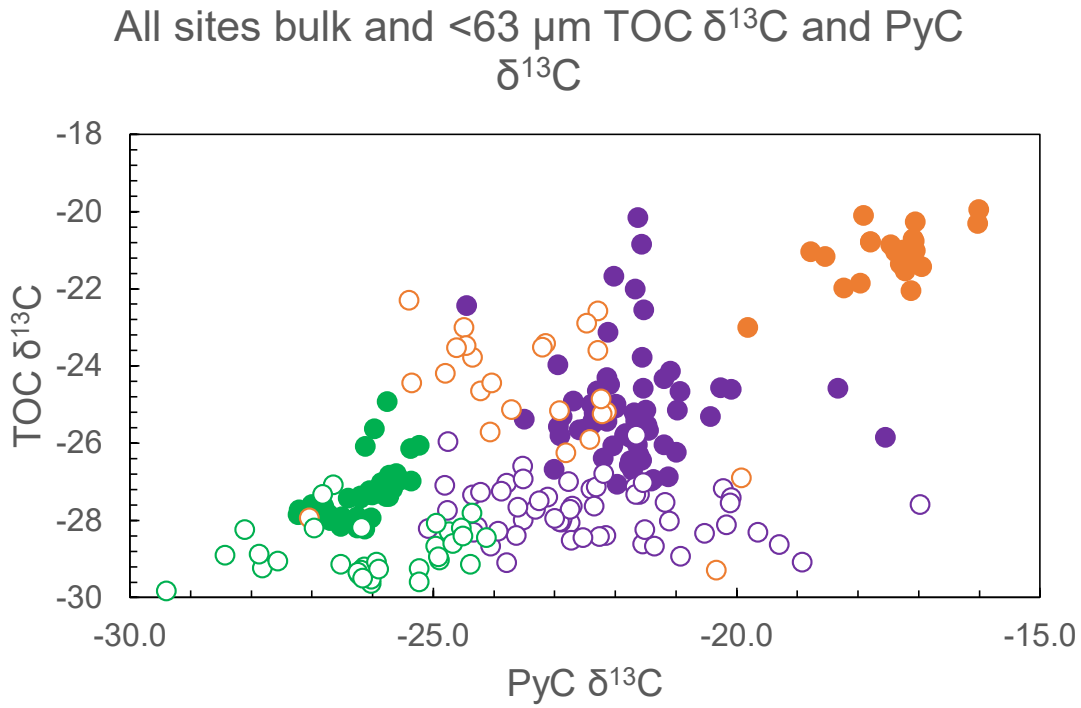

Figure 8.15: Total organic carbon (TOC) and pyrogenic carbon $\delta^{13}C$ values for bulk (closed circles) and <63 µm (open circles) size fractions. Purple: Marura, orange: Big Willum Swamp, green: Sanamere Lagoon.

Consistently more ^{13}C-depleted values in the PyC <63 µm fraction are predicted by the Stable Isotope Disequilibrium Effect for grass-dominated environments (see Saiz et al. 2015; Chapter 6); this is most clearly visible for Big Willum Swamp, where <63 µm PyC $\delta^{13}C$ values are significantly lower than their bulk equivalents as well as being predominantly lower than pre-hydrogen pyrolysis (total organic carbon) <63 µm $\delta^{13}C$. Only a small subset of samples for Sanamere Lagoon show this relationship, as these points (6.5, 9.5, 13-13.5 and 16.5 cm) are coincident with peaks in pyrogenic carbon percentage and represent input from distant fire events beyond the C_3-dominated catchment. Some samples for Marura show this effect, suggesting a mix of grass-dominated and more woody-fuelled fires through the record.

It is unclear why most samples across all sites show ^{13}C enrichment for PyC, excepting those demonstrating the Stable Isotope Disequilibrium Effect (^{13}C depletion). Previous studies have shown that pyrogenic carbon (e.g. Bird & Ascough 1997; Saiz et al. 2015) and even charred wood (Czimczik et al. 2002) are typically ^{13}C-depleted compared to the original biomass.

8.6 Charcoal Traps, Recent Sediments and Surface Samples

Charcoal trap samples serve as a modern test of the charcoal methods applied in this study, as well as a modern calibration for data in the Sanamere record (see Chapter 7). Charcoal abundance in the Coen (COENFT) and Kendall B (KENBFT) samples reflects the total area burned within a 5 km^2 radius around each trap, with high charcoal abundances in KENBFT linked to extensive burning around the Kendall B trap. While a substantial area burned between the 5 km^2 and 10 km^2 radii around Sanamere, SANFT2 charcoal abundances are low suggesting minimal regional aerial transport of charcoal to Sanamere Lagoon from beyond the catchment (burn estimates within 5 km^2 likely contain erroneous data, see Chapter 7). Charcoal flux for charcoal trap samples also demonstrates the importance of overland transport of charcoal into a site, as the immediate area around the Kendall B charcoal trap was burned directly and yet contained substantially less charcoal (as measured by particles/cm^2/y) than found in the SAN1 record. Elongate particles (from length-width ratios and morphotypes) in the COENFT and KENBFT samples demonstrate that elongate particle contributions reflect the mixed tree-grass environments surrounding both traps. Morphotypes also reflect the distinction between open woodland with a grassy understorey (COENFT and KENBFT) and dwarf heathland (SANFT1 and SANFT2), with the former dominated by type F (elongate) and the latter by either type C (solid geometric; SANFT1) or types M and S (structured polygon and structured geometric; SANFT2) (Figure 8.16).

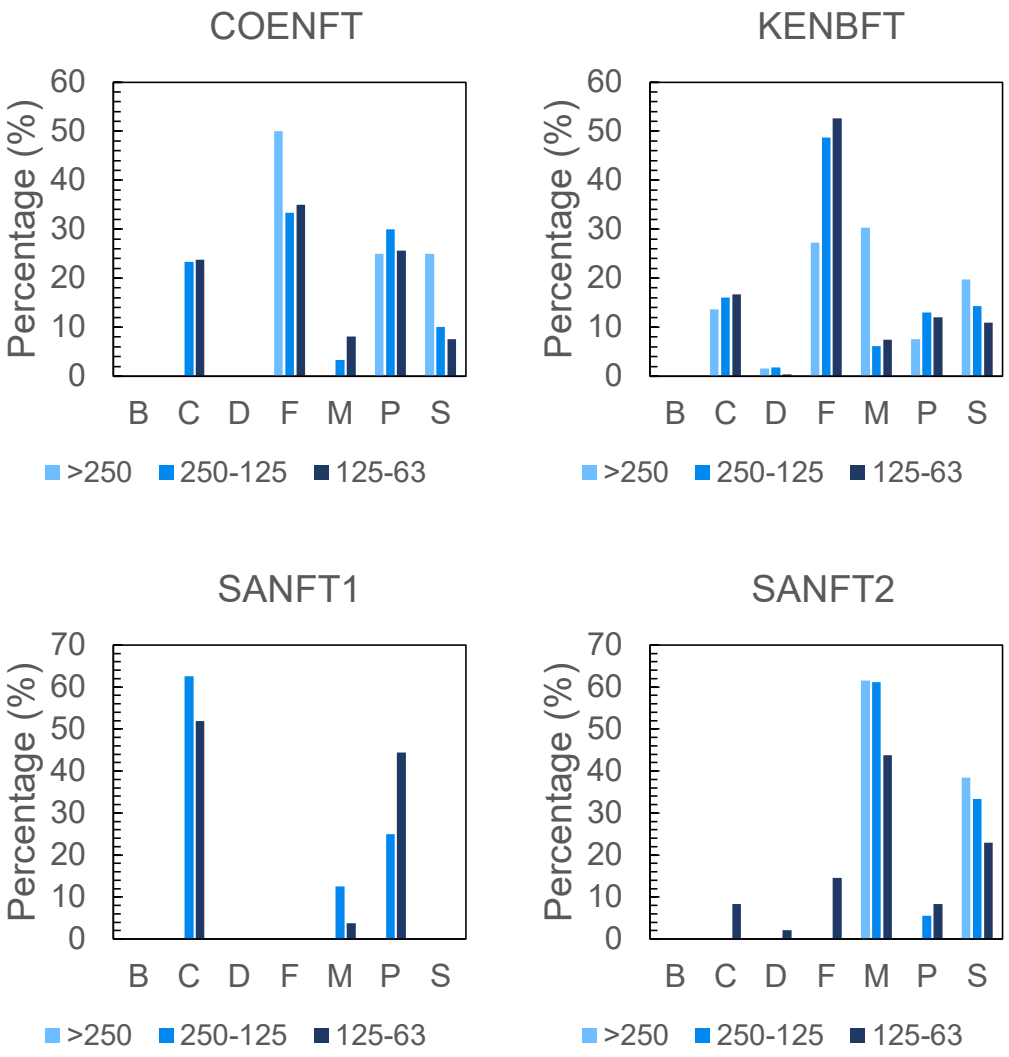

Figure 8.16: Charcoal trap sample charcoal morphotypes.

It is noteworthy that type D (elongate with ramifications) is absent from all samples except for low percentages (<2 %) in KENBFT and a single type D particle in SANFT2. While Enache and Cumming (2006) do not attribute a specific fuel to type D particles, Courtney Mustaphi and Pisaric (2014, p.741) associate morphologies broadly classified within this type to leaf veins. The near-absence of this morphotype from both mixed tree-grass and heathland environments suggests this morphology is not produced in equal proportions to others derived

from woody vegetation, potentially dependent on fire characteristics. The lack of type B (partially burned structured geometric) particles is expected as this type was poorly represented in all samples of this study, with partially blackened particles primarily recorded as "partial char" or not classified as charcoal.

Morphologies from charcoal trap samples can also be compared to recent sediments from the MAR2 (see Chapter 5: Charcoal Morphotypes) and BWIL2 (see Chapter 6: Charcoal Morphotypes) records and compared to modern vegetation. Similar to the charcoal trap samples, morphotypes B (partially burned structured geometric) and D (elongate with ramifications) are mostly absent in the most recent period (~1950 CE onwards) at Marura and Big Willum Swamp. Type F (elongate) dominates the COENFT and KENBFT samples as well as the 125-63 μm fraction in the most recent period at Big Willum Swamp. While type F is present at Marura in this period, types M (irregular, structured) and S (structured geometric) dominate. These results suggest vegetation at Big Willum Swamp since ~1950 CE is most comparable to modern vegetation at Coen and Kendall River Station, while Marura shows similarities but is less dominated by grasses.

Surface samples analysed from Sanamere Lagoon represent the variability present within a sedimentary environment. The relationship between charcoal abundance and collection location (distance from lake edge) is not straightforward, as demonstrated across SANSURF1 (centrally collected, highest abundances), SANSURF6 (collected halfway to shore, lowest abundances) and SANSURF10 (collected close to the water edge). The significantly higher charcoal abundances recorded in SANSURF1 for all size fractions (see Chapter 7) support sampling from the centre of a water body. Each surface sample also varies somewhat in morphotype and elongate versus non-elongate particle composition; this is likely the result of small sample sizes, as 125-63 μm charcoal abundances are significantly higher than the macroscopic sizes and morphologies in this size fraction are very similar across the three

samples. Differences in charcoal abundance as well as morphology demonstrate that interpretation of minor changes in a record should take into account possible within-site variability.

8.7 Fire Proxies and Fire Regimes

Data from every proxy presented in this chapter can be combined to better understand the palaeofire records in this study. Interpretation of this data depends strongly on the known characteristics of fire regimes in the northern Australian tropics, as introduced in Chapter 3.

Ethnographically recorded Indigenous fire regimes are primarily characterised by low intensity fires over small areas, with spatial and temporal heterogeneity creating a "patch mosaic" (Bliege Bird et al. 2013). An established patch mosaic allows for low intensity fires to be lit without fear of excessive spread under "late dry season climatic conditions" (e.g. low fuel moisture, high winds, high temperature) that would result in a widespread, high intensity fire in a homogenous unburned landscape (Yibarbuk et al. 2001, p.337). The timing of traditional Indigenous burning regimes are therefore limited only by when fuels are dry enough for ignition, with historical accounts from Cape York Peninsula and Arnhem Land recording fires being lit throughout the dry season and sometimes in the middle of the wet season (Crowley 1995, p.40; Preece 2002, 2013).

However, Indigenous burning was likely not limited to low intensity fires. Crowley (1995, p.12) notes that low intensity fires and low fire frequencies are associated with canopy dominance, while high fire intensities and frequencies shift dominance to the ground layer; the required fire intensity and frequency is highly dependent on the intended outcome/s of burning (for examples of Indigenous uses for fire, see Chapter 3). The heathland communities of Cape York Peninsula appear adapted to hot fires:

> Fires occur in these [heathland] communities despite the fact that some are found on extremely wet soils. Cool fires lead to very little regeneration; hotter fires release seed dormancy in a range of species that disappear from the vegetation as time since last fire increases (Stanton 1992)… Such communities thus appear to be adapted to hot, relatively infrequent fires (Dunlop and Webb 1991), and a fire strategy whereby small areas are burnt at intervals of 5 to 10 years has been proposed (Stanton 1992) (Crowley 1995, pp.17-18).

High intensity fires, as well as low intensity fires, are therefore likely to be a component of Indigenous fire management, dependent on the purpose/s of burning and characteristics of the vegetation community being managed.

Fire regime transitions in northern Australia with European invasion may appear as the replacement of Indigenous land management with European land management (e.g. pastoralism or mining) or the removal of Indigenous management without replacement by another management system. Removal of Indigenous fire management without the introduction of another fire management system has been associated with widespread, high intensity late dry season fires (e.g. Yates, Edwards & Russell-Smith 2008; Yibarbuk et al. 2001). Crowley (1995, p.48, 50, 52) describes European and other contemporary fire regimes in northern Australia as less "diverse" than Indigenous fire management systems that preceded them, with fires for pastoral management primarily lit in the early dry season (see also Crowley & Garnett 2000).

The relationship between fire regimes and total area burned is less clear. Multiple studies argue that total area burned is closely linked to climatic conditions, with anthropogenic fire regimes affecting the spatial and temporal distribution of fire, including intensity and fire frequency, but not reducing the overall area burned (Bliege Bird et al. 2008; Head 1994; Trauernicht et al.

2015). However, anthropogenic burning may also act as a buffer for increasing climatic variability that would otherwise increase fire sizes and overall fire risk (Bliege Bird et al. 2012).

Vegetation composition is another aspect affecting, and affected by, fire regimes. The type of vegetation present at a site initially dictates the type of fire that the environment can carry (based on fuel availability) while maintenance of certain fire regimes can protect fire-sensitive plants (e.g. *Callitris intratropica*; Trauernicht et al. 2013) or patches of fire-prone vegetation communities (e.g. rainforests; Bowman 2000; Hill, Griggs & Bamanga Bubu Ngadimunku Incorporated 2000). However, there is debate around long-term drivers of vegetation change, with arguments for climate as a primary driver (Black & Mooney 2006; Mooney et al. 2011; Sakaguchi et al. 2013), human influence as a primary driver (Gammage 2012; Trauernicht et al. 2013; Veenendaal et al. 2018), and a mix of both (McWethy et al. 2017; Power et al. 2008; Rull et al. 2015). Shifts in fuel types in isolation cannot be simply categorised as a climatic or anthropogenic signal.

To summarise, Indigenous fire regimes can therefore be expected to appear in the palaeofire record as variable fire intensities (measured by comparing charcoal and PyC fluxes) across space and time (measured by comparing size fractions and changes through the record). Climatic shifts may be considered the primary driver of overall fire incidence (overall charcoal and PyC flux), although anthropogenic buffer effects must also be considered. Vegetation changes (measured by particle morphology and $\delta^{13}C$ values) must be considered in the context of fire incidence and intensity.

The cessation of Indigenous fire management is likely marked by a sudden shift to less variable fire intensities (e.g. low or indeterminate for European pastoral management or high intensity for unmanaged regions), although this occurs over a relatively short period (~100-150 years) compared to the total time span of each palaeofire record which may make variability difficult

to assess. However, the constrained timeframe for European influence will assist in identifying this transition.

8.8 Conclusion

All of the palaeofire techniques evaluated in this chapter have been demonstrated to provide useful interpretive data for the sites in this study. The combination of charcoal and pyrogenic carbon measures allows for the identification of fire intensities along with overall fire abundance. Intensity data can then be interpreted in terms of fire seasonality and anthropogenic influence. Size fraction divisions within both charcoal and pyrogenic carbon allow for this analysis to occur across space as well as time. Aspect ratio, morphology and pyrogenic carbon $\delta^{13}C$ values combined allow for the identification of C_3-C_4 fuel contributions as well as elongate C_3 fuels. Future work will ideally combine this suite of fire proxies with molecular markers such as levoglucosan (e.g. Schüpbach et al. 2015) and vegetation measures such as pollen (e.g. Daniau et al. 2019). All of the methods evaluated in this chapter will be applied in the following chapter to interpret the fire records of Marura, Big Willum Swamp and Sanamere Lagoon.

Chapter 9 : Fire Histories and Interpretation

9.1 Introduction

This chapter applies the parameters established in Chapter 8 to interpret the results for each site in this study. Individual site records are presented, contextualised by existing palaeoenvironmental and archaeological data to create comprehensive interpretations of palaeofire for Marura, Big Willum Swamp and Sanamere Lagoon. Each record is divided into main palaeofire phases, identifying major changes in charcoal and pyrogenic carbon measures determined using CONISS cluster analysis. These records address Research Aim 1 (creation of new palaeofire records) outlined in Chapter 1 along with all Research Questions, to meet the following objectives:

1) Creation of new palaeofire records for regions previously lacking fire proxy data
2) Characterisation of changes in fire incidence, fire intensity, and vegetation (fuel types) in these fire histories
3) Identification of anthropogenic influence distinct from climate in these fire histories
4) Identification and characterisation of European influence on fire at Marura and Big Willum Swamp

The chapter concludes with an overview of fire regimes in northern Australia during the late Holocene in light of the new records presented here for Marura and Big Willum Swamp.

9.2 Fire Histories by Site

9.2.1 Marura

Marura has the smallest water surface area of the sites in this study, as well as a small and steep-sided catchment (see Chapter 8, Table 8.1). Marura is also closer to the modern coastline (~10 km) than the other sites and surrounded by open *Eucalyptus* woodland comparable to Big Willum Swamp.

The Marura palaeofire record can be separated into three main phases: 4600-2800 cal BP (Phase I), 2800-900 cal BP (Phase II) and 900 cal BP to present (Phase III). While these phases are primarily determined from trends in charcoal and PyC fluxes, they also broadly correspond to known changes in the regional archaeological and palaeoenvironmental records, as discussed below.

9.2.1.1 Marura Phase I – 4600 to 2800 cal BP

Phase I is characterised by high charcoal and pyrogenic carbon fluxes, the highest across the Marura record, with peak charcoal and pyrogenic carbon fluxes occurring around 4300-4000 cal BP. An organic rich phase in the Marura sedimentary record (identified via XRF and total organic carbon percentages) also begins at ~4000 cal BP, lasting until ~2600 cal BP (see Chapter 5, Figure 5.17). Pyrogenic carbon $\delta^{13}C$ values in this phase show mixed C_3-C_4 contribution, and elongate particle contributions show very similar trends across all size fractions (averaging between 40 and 60 %) suggesting similarities in tree-grass ratio across spatial scales within and beyond the catchment of Marura.

Two significant shifts occur in bulk PyC $\delta^{13}C$ values at the start of this phase: a peak at ~4500 cal BP (-18 ‰) indicating high grass content, and a trough shortly after at ~4350 cal BP (-24 ‰, indicating high woody content), with coincident but less dramatic changes evident in the

<63 µm PyC $\delta^{13}C$ values. The <63 µm PyC $\delta^{13}C$ values show very little correspondence with the bulk fraction after this point in the record, suggesting that at the beginning of this phase the similar C_3/C_4 vegetation compositions in the Marura catchment and greater region diverged after this point. The grassy sample at ~4500 cal BP occurred under low fire intensities, while the woodier (^{13}C-depleted) sample at ~4350 cal BP along with a later similar trough at ~4000 cal BP occurred under high fire intensities (Figure 9.1).

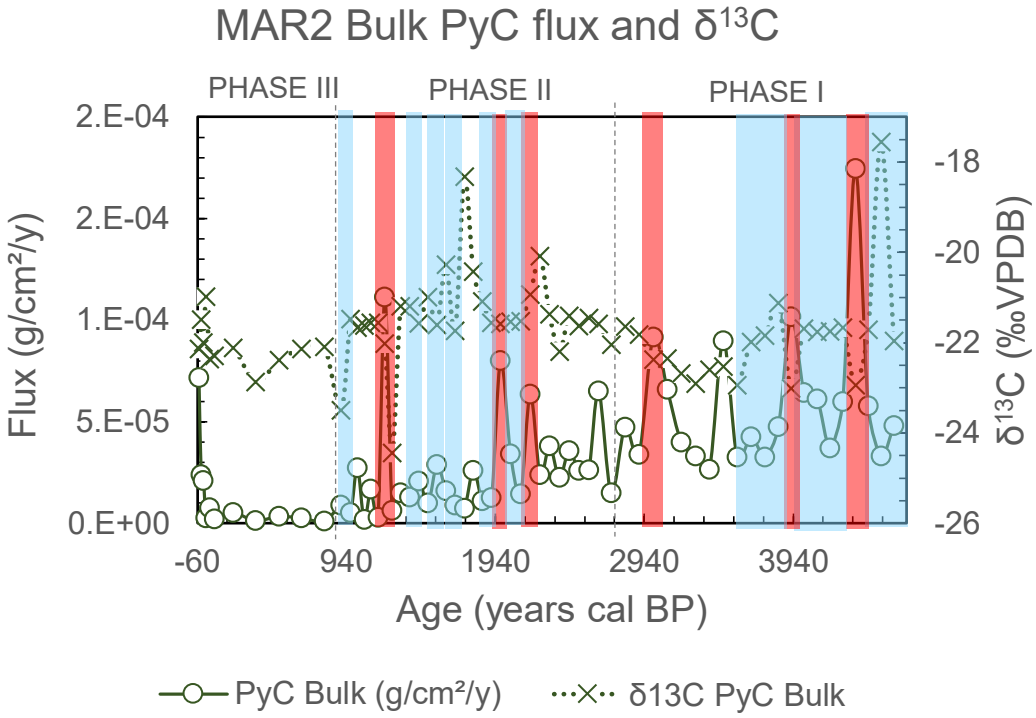

Figure 9.1: MAR2 bulk pyrogenic carbon (PyC) flux and $\delta^{13}C$ values. Blue bars: low intensity, red bars: high intensity (see Chapter 8).

As detailed in Chapter 2, some palaeoenvironmental records from central and western northern Australia show a drying trend into the late Holocene coinciding with Marura Phase I, with onset ranging from ~4 ka (Kapalga South Billabong; Shulmeister & Lees 1995) to ~3 ka (Black

Springs; McGowan et al. 2012). Shulmeister (1992) identifies a precipitation maximum at ~4 ka for Four Mile Billabong on Groote Eylandt followed by a precipitation decline from ~3.8 ka. Biomass promoted by the mid-Holocene precipitation maximum likely provided fuel for increased fire incidence during the transition to increasingly dry and variable conditions in the late Holocene (e.g. Prebble et al. 2005). Peak charcoal and pyrogenic carbon fluxes at Marura (~4000 cal BP) coincide with this potentially regional transition from higher effective precipitation in the mid-Holocene to drier and/or more variable conditions into the late Holocene suggesting a climatic control on fire incidence and mixed composition burning in this phase. More records in this region with precipitation proxies are needed to better understand regional precipitation trends throughout the Holocene.

High charcoal abundance also occurs at Walala on Vanderlin Island during this phase (~4500-3000 cal BP), corresponding to high values at Marura, although data points between 3000 BP and the present for Walala are limited (Prebble et al. 2005). While Prebble et al. (2005, p.368) do not attempt to ascribe a cause to this high fire incidence, they identify vegetation change at Walala responding less directly to climate after ~5500 cal BP, "instead mediated through changing fire regimes". Microscopic charcoal abundance at Girraween Lagoon peaks around 3000 cal BP and decreases thereafter into the present, comparable to Marura (Rowe et al. 2019). This may suggest that climate was a significant driver of fire incidence at this time, with peak fire incidence at the onset of the late Holocene as effective precipitation decreased, and followed by fire incidence declining towards the present.

9.2.1.2 Marura Phase II – 2800 to 900 cal BP

While charcoal and PyC fluxes show a decreasing trend throughout the Marura record, the most pronounced change in flux occurs around 2800 cal BP, after which time values across all sizes

never again reach peak levels seen prior to ~2800 cal BP (excepting one peak in bulk pyrogenic carbon flux indicating a high intensity fire event at ~1200 cal BP). This decrease in flux is most apparent in the macroscopic charcoal size fractions. Additionally, elongate particle contributions to the largest macroscopic charcoal size fraction (>250 µm) increase in variability at this time and no longer show similar trends to elongate particles in the other size fractions. Despite this, charcoal fluxes for all size fractions are most strongly correlated during this phase (Table 9.1). In Phase II (~2600 cal BP), the Marura XRF record ceases to be dominated by an organic elemental signal. A minor peak in detrital elements occurs in this phase from ~1900 to ~1300 cal BP, along with a trough in total organic carbon percentages; this does not appear to correspond to any other proxies measured in this study.

Table 9.1: Correlations (r^2 values) for Marura charcoal flux variables divided by phase. ** denotes correlations at a significance level of 0.01.

Phase I	**250-125 µm**	**125-63 µm**
>250 µm	0.8010**	0.7502**
250-125 µm		0.7455**
Phase II	**250-125 µm**	**125-63 µm**
>250 µm	0.8285**	0.7562**
250-125 µm		0.8350**
Phase III	**250-125 µm**	**125-63 µm**
>250 µm	0.2360	-0.0341

250-125 µm		0.8141**

This period is difficult to classify at a regional scale as many sites show increasing climate variability, often linked to intensification of ENSO (e.g. Shulmeister & Lees 1995; Prebble et al. 2005; McGowan et al. 2012; Denniston et al. 2013; Field et al. 2017), expressed in different ways. For example, Field et al. (2017, p.14) describe short alternating wet and dry periods from 5000-2600 cal BP at Black Springs (in the northern Kimberley) followed by "pronounced" aridity until ~1300 cal BP then a transition to "modern conditions". Head and Fullager (1992, p.29) describe "less fluctuation in water levels in the last 1 – 2,000 years than previously" at swamp sites in the west of the Northern Territory and contrast this to concurrent periods of aridity inferred from dune instability. Shulmeister and Lees (1995, p.12) also note three phases of dune activation during this period, as well as a "sharp decline" in effective precipitation at Groote Eylandt from 3700-1000 BP with increasing precipitation thereafter.

During this period, archaeological data becomes available in the Blue Mud Bay area. Marura Phase II corresponds broadly to the first occupation phase of Point Blane Peninsula outlined by Faulkner (2013, p.141, 165, 169) from 3000-1000 BP with sites characterised by "intense and focussed" sand and mudflat shellfish exploitation (Figure 9.2). Initial occupation of Groote Eylandt also falls within this phase (~2500 BP), with sporadic site use at Malmudinga rockshelter including the "collection primarily of rock/coral shellfish species" (Clarke 1994, p.159, 470) and intensive use of Angwurrkburna rockshelter (Clarke 1994, p.287).

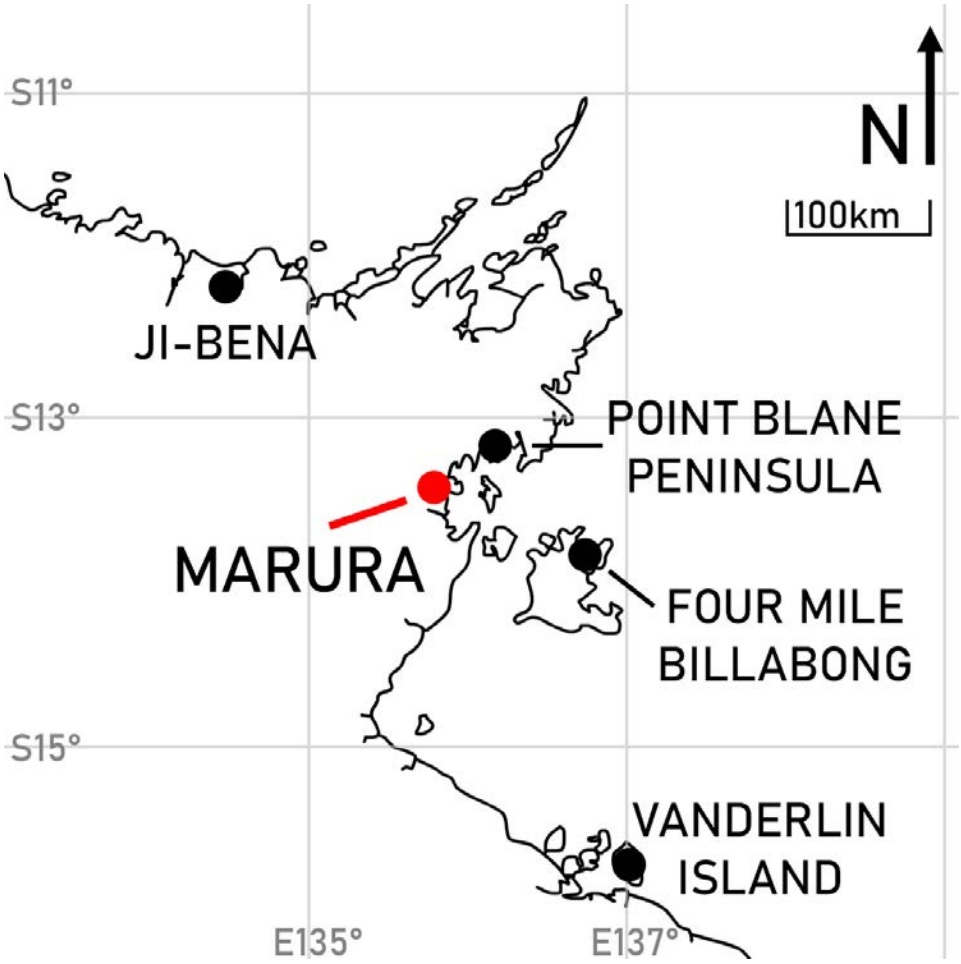

Figure 9.2: Marura and nearby palaeoenvironmental and archaeological sites mentioned in the text.

While climate is likely the dominant driver of fire during Phase I, anthropogenic burning becomes increasingly important from this phase onwards. Lower overall fire incidence compared to Phase I is likely due to continuing dry conditions producing less tree-grass biomass than during the mid-Holocene precipitation maximum. Alternating low/high intensity burns, a declining trend in fire incidence throughout Phase II and consistently low levels of macroscopic charcoal flux suggest Marura was actively managed during this time (Figure 9.3). This is particularly evident after ~1900 cal BP, with the reduction of high intensity burns (and a reduction of bulk PyC flux overall) with the exception of a high intensity event at ~1200 cal

BP. This high intensity fire event (or period) centred on ~1200 cal BP coincides with peak ENSO event frequency as described by Moy et al. (2002, p.164) for a record from Ecuador, suggesting this climate extreme briefly re-established climate as the dominant driver of fire at Marura. However, coral records by McGregor and Gagan (2004) and Toth et al. (2012) do not identify peak ENSO event frequency at this time, although it does fall within the period (~2000 cal BP to present) of increased El Niño events described by Toth et al. (2012).

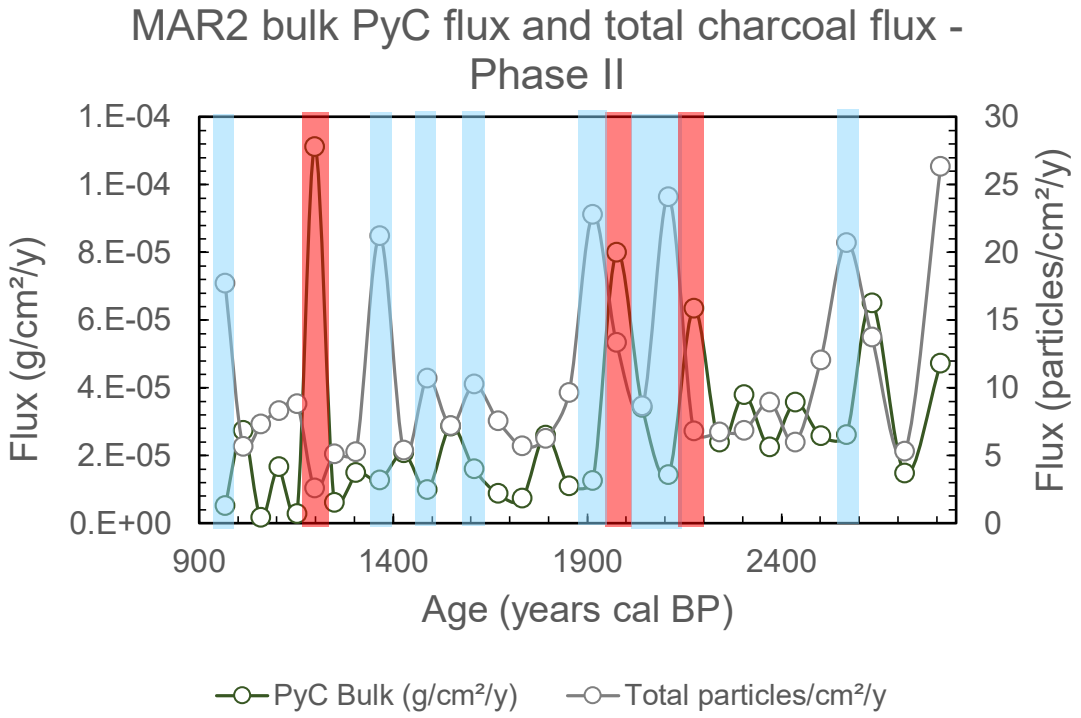

Figure 9.3: Total charcoal flux and bulk PyC flux for Marura Phase II. Blue bars: low intensity, red bars: high intensity (see Chapter 8).

While both bulk and <63 µm PyC $\delta^{13}C$ values show mixed C_3-C_4 contribution throughout the Marura record, these size fractions behave differently, with much higher variability in the <63 µm size fraction particularly noticeable during this phase and indicating changes beyond the

Marura catchment but not affecting the catchment itself. Phase II also shows more variability in bulk PyC $\delta^{13}C$ values than the preceding phase (not including dramatic deviations near the beginning of Phase I, discussed above); however, low and high intensity phases of burning do not affect bulk PyC $\delta^{13}C$ values as directly or noticeably as in the previous phase (see Figure 9.1).

Through indications such as short, alternating fire intensity phases and decoupling of bulk PyC $\delta^{13}C$ values from fire intensity changes, the fire record at this time has been established as human-driven. This style of burning, as active fire management, is well documented; multiple studies by Bliege Bird et al. (2008, 2012, 2013) describe Martu mosaic burning for subsistence in the Western Desert creating landscape patchiness, functioning as a buffer to climate-driven large scale fires and promoting species such as varanid lizards that require both burnt and unburnt habitat patches. Trauernicht et al. (2015, p.1912) demonstrate this for the savannas of Arnhem Land by mapping the modern distribution of the fire-sensitive conifer *Callitris intratropica*, concluding that small fires increase patch ages, patch age diversity and fire-return intervals compared to "fewer, larger fires burning the same proportion of the landscape". The mixed C_3-C_4 contribution in Phase II is therefore suggested to reflect a reorganised spatial arrangement of tree-grass vegetation within the Marura catchment. The reduction of elongate charcoal particles after ~2300 cal BP may reflect anthropogenic burning aimed to increase woody plant diversity at the expense of grasses, as described by Rowe et al. (2019, p.27) at Girraween Lagoon near Darwin, with peak *Eucalyptus* contribution at Girraween Lagoon from 2850-600 cal BP.

The $\delta^{13}C$ values for <63 μm PyC drop to their lowest level in the record (-25 ‰) at the start and end of this phase indicating a dominantly woody source, coinciding with troughs in elongate particles (from aspect ratios and morphotypes) in the macroscopic charcoal size fractions (>125 μm). A dominant organic signal (measured via XRF and total organic carbon)

returns at ~1000 cal BP, and charcoal flux (all size fractions) and <63 μm pyrogenic carbon flux show a minor peak at the end of this phase (~960 cal BP) before decreasing into Phase III.

The return to a dominant organic signal at Marura corresponds to the effective precipitation "recovery" at ~1000 BP described by Shulmeister (1992, p.113) for Four Mile Billabong (Groote Eylandt). This suggests the latest peaks in flux at the end of Phase II may have been fuelled by an increase in biomass enabled by increased effective precipitation, under low intensities similar to the increase in "'cool' fires" after ~1000 cal BP at Four Mile Billabong (Shulmeister 1992, p.112). However, this transition at Four Mile Billabong is represented by one radiocarbon date (980 ± 170 yr BP) with no analytical details given (Shulmeister 1992).

9.2.1.3 Marura Phase III – 900 cal BP to Present

Charcoal and pyrogenic carbon fluxes drop to their lowest levels for all sizes in the Marura record after ~900 cal BP, and total organic carbon percentages and the XRF elemental record reflect high organics for the remainder of the record. This implies that the decrease in fluxes into Phase III are not the result of relatively low effective precipitation reducing available biomass. This phase contains the weakest correlations between the >250 μm charcoal size fraction and other sizes, with many samples containing no charcoal measuring >250 μm, while the relationship between the 250-125 μm and 125-63 μm fractions remains strong ($r^2 = 0.81$; see Table 9.1 above). Minimal variation in $\delta^{13}C$ values for both bulk (-21 to -23 ‰) and <63 μm (-23 to -24 ‰) pyrogenic carbon occurs after this point in the record.

At this time, human activity on Groote Eylandt shifts away from inland sandstone rockshelters to coastal sites as part of "increas[ing] intensity of coastal occupation" (Clarke 1994, p.470). Clarke (1994, p.470) has suggested that this may have coincided with early sporadic and small-scale contact with Macassans, although archaeological evidence supporting this early date is

limited. Marura Phase III also corresponds to the second main occupation phase of Point Blane Peninsula, associated with a decline in the exploitation of sand and mudflat shellfish at ~1000 BP and increase in the exploitation of mangrove species after ~500 BP at Myaoola Bay (Faulkner 2013, p.141, 170). Humans were therefore mobile around the Blue Mud Bay region during this period, actively adapting to changing resource availability. From this, it is proposed that human use of Marura and the surrounding landscape continued through this period with a possible decrease in intensity as mobility increased. Declining charcoal and PyC fluxes during this phase likely reflect a decrease in the effective transport of these fire products into the site due to fine scale landscape patchiness developed and maintained by anthropogenic burning.

Charcoal and PyC fluxes show an increase at the very end of this phase, after 55 cal BP (Figures 9.4 and 9.5). Fluxes for every size fraction (except for >250 μm) peak in the uppermost sample (MAR2 0-1 m 0-1 cm) to values not seen since the end of Phase II. As this occurs within the potentially mixed uppermost 10 cm of sediment, the exact date of this peak is uncertain. <63 μm PyC flux also displays a minor peak between ~650 and ~450 cal BP, reflected in a peak at ~640 cal BP in 125-63 μm charcoal flux but otherwise not discernible in other size fractions suggesting a strictly regional increase of intermediate intensity fire not visible in the local signal.

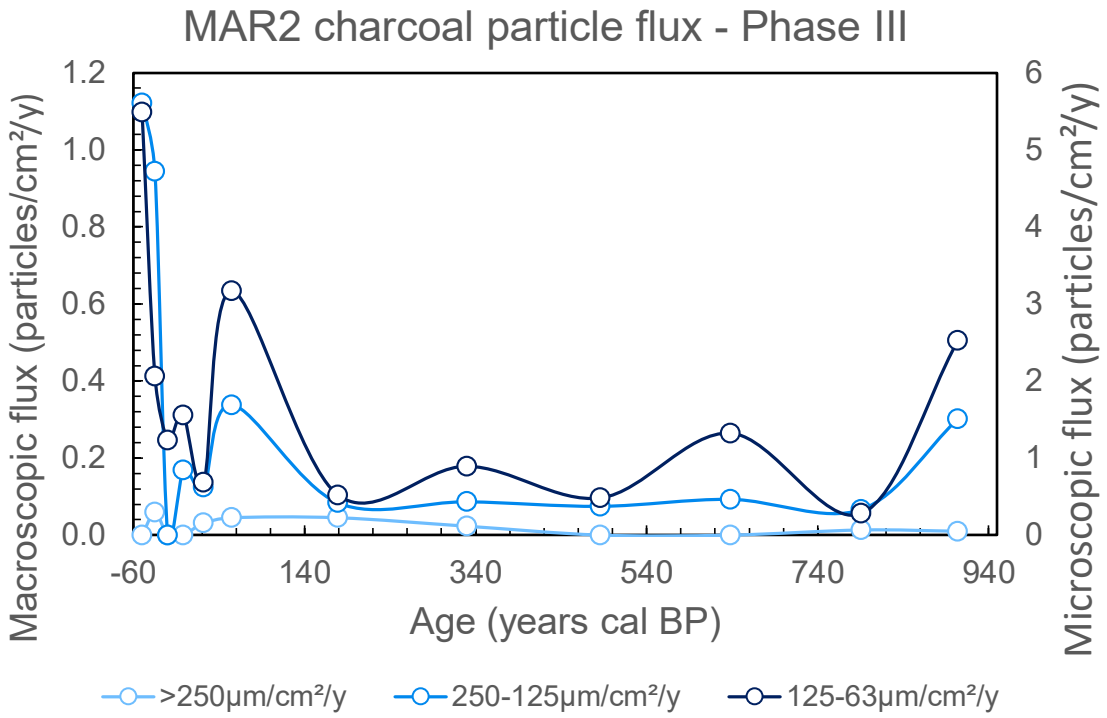

Figure 9.4: Charcoal flux for Phase III of MAR2, by age.

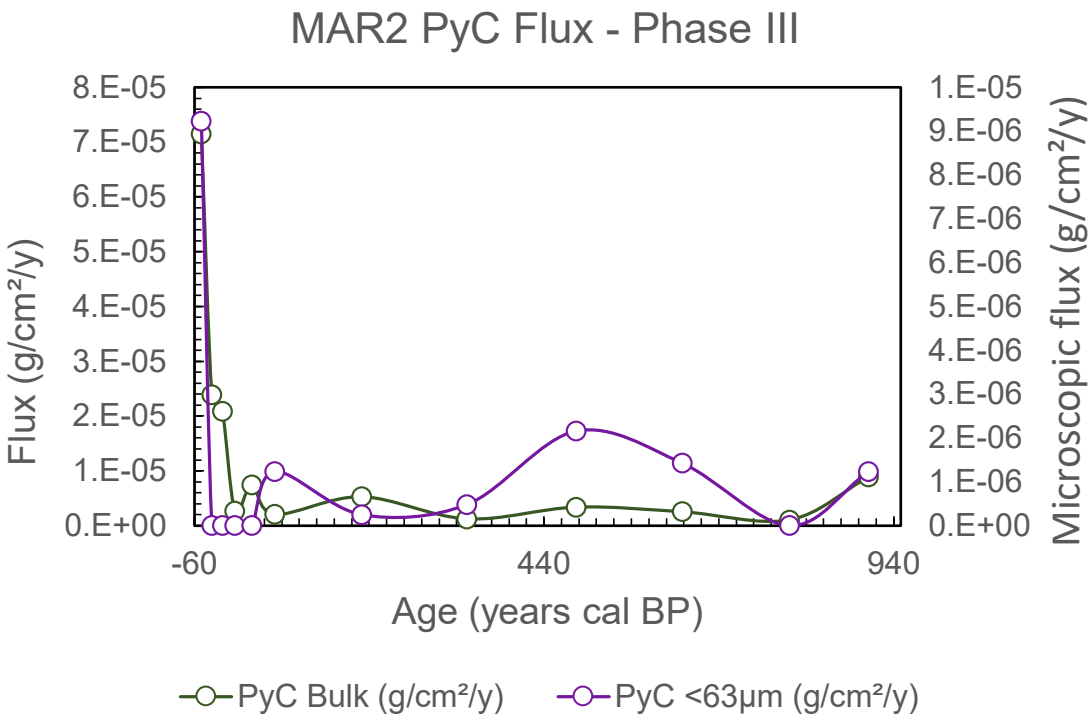

Figure 9.5: PyC flux for Phase III of MAR2, by age.

Arnhem Land was under pastoral lease from the late 19th to early 20th centuries before the establishment of the Arnhem Land Aboriginal Reserve in 1931 (Barrier Miner 1931; Cole 1982; see Chapter 3). Russell-Smith et al. (1997, p.180) note the prevalence of intense late dry season fires in western Arnhem Land beginning in the last century with the "collapse of traditional management practice", with such fires becoming commonplace after the 1940s. Changes in settlement patterns also lead to altered fire management in areas such as Arnhem Land even after management has been returned to traditional owners (see Head 1994, p.177). It is therefore not surprising that fire proxies peak at Marura over the last century, including high bulk PyC flux suggesting intermediate fire intensities as associated with European-influenced or unmanaged late dry season burns.

The Marura palaeofire record displays a combination of climate and anthropogenic effects on fire, with the role of human-driven fire regimes becoming increasingly dominant over time. It is well established that ENSO periodicity intensified in the late Holocene across northern Australia to conditions comparable to the present (e.g. Diaz & Markgraf 1992; Donders et al. 2007; Field et al. 2017). Prebble et al. (2005, p.368) note the difficulty of disentangling the effects of ENSO (for example drought leading to increased fire) and human-driven increases in landscape burning (see also Fletcher et al. 2015 linking ENSO to shifts in biomass burning). In the Marura record, however, fire incidence (across all measures) decreases significantly into this period known for ENSO-driven variability, and human activity in the region is apparent from archaeological data (see Clarke 1994; Faulkner 2013).

High fire incidence in Phase I was fuelled by tree-grass biomass produced under relatively high effective precipitation conditions at the mid-to-late Holocene transition, and while cool (low

intensity) burns in this period may have been the result of anthropogenic burning it is difficult to conclusively separate human influence on fire from climate change in this phase. Human-driven fire in the landscape containing Marura during Phases II and III resulted in minimal charcoal and pyrogenic carbon input into the sinkhole and may have operated as a buffer to potential ENSO-driven effects on fire through the increasingly variable late Holocene. While climate-driven fire in Phase I supported regional homogeneity of vegetation structures linked to dominant fire intensities, anthropogenic burning in Phases II and III established mixed and spatially variable C_3-C_4 vegetation. Decreasing charcoal through these phases likely resulted from the establishment of patch-scale burning (see Chapter 3, also Bliege Bird 2008, 2016; Gammage 2012) across the Blue Mud Bay landscape, leading to an overall decrease in charcoal and PyC abundance as well as potentially acting as a barrier to the transport of charcoal and PyC into the sinkhole from more distant fires. Peaks across charcoal and PyC fluxes over the last 100 years to levels not seen since ~900 cal BP coincide with the cessation of traditional Indigenous burning practices in the area (e.g. Haberle 2005; Moss et al. 2015).

9.2.2 Big Willum Swamp

Big Willum Swamp has a slightly larger catchment size (~0.75 km^2) than Marura and is distant from the modern coastline (~20 km) but close to inlets of the Embley and Mission Rivers (see Chapter 8, Table 8.1). The Big Willum Swamp catchment is of low relief.

The Big Willum palaeofire record can be classified into three main phases: 3900-1700 cal BP (Phase I), 1700-~500 cal BP (Phase II) and ~500 cal BP to present (Phase III).

9.2.2.1 Big Willum Phase 1: 3900-1700 cal BP

The earliest phase in the Big Willum record is characterised by minimal or absent charcoal in all size fractions, including PyC abundances, and a low sedimentation rate. An elemental transition in the Itrax™ XRF data occurs in sediments in this phase with an increase in organics beginning at ~3600 cal BP corresponding to increasing total organic carbon percentages, with detrital elements reducing through this phase (see Chapter 6, Figure 6.17). Bulk and <63 µm PyC $\delta^{13}C$ values are inversely related during this period ($r^2 = 0.9$) (Figure 9.6). Sedimentation rates are lowest during this phase; as a result, this phase is represented by 2.5 cm of sediment in BWIL2.

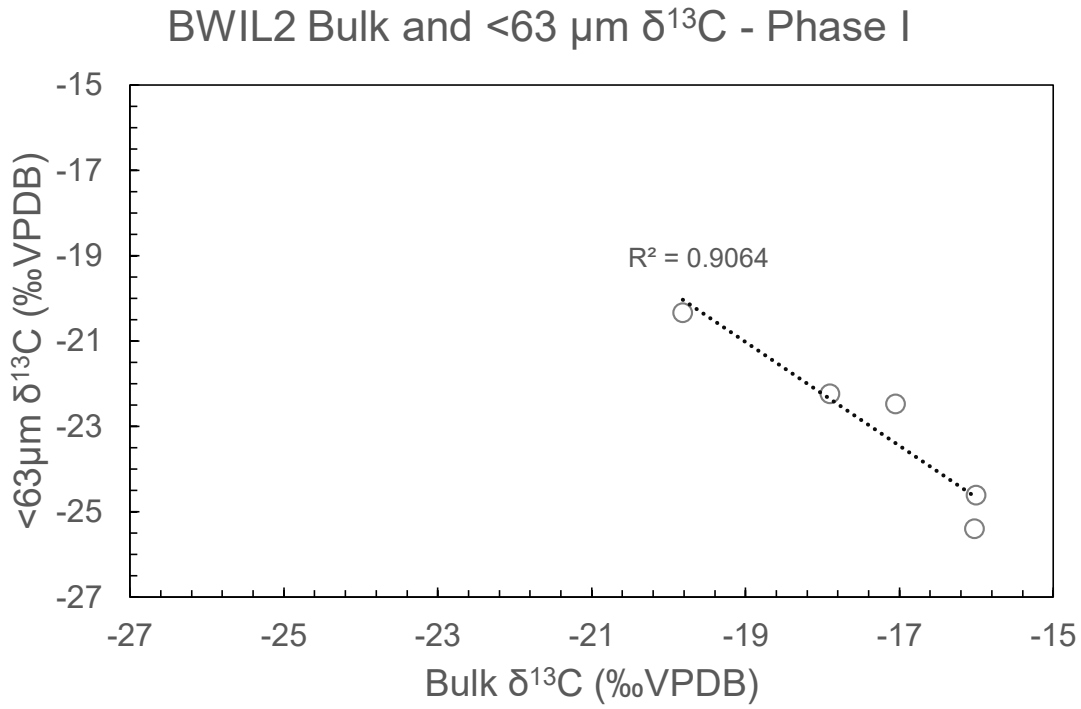

Figure 9.6: BWIL2 bulk and <63 µm PyC $\delta^{13}C$ values scatter plot.

Phase I represents the shift from earlier swamp conditions to Big Willum Swamp becoming a deep water body, as identified by Stevenson et al. (2015) at ~2200 cal BP in core BW01. This was likely due to the collapse of the underlying porous bauxite laterite (see Grimes & Spate 2008; Twidale 1987); changing conditions in this phase, therefore, do not represent a regional climate or fire signal but rather site-specific changes in swamp/lake conditions. Accumulation of earth mounds in the nearby Wathayn region (Weipa) fall within this phase at ~2200 cal BP, coinciding with the establishment of new nearby freshwater sources including Big Willum Swamp (Brockwell et al. 2016). Peak shell mound accumulation also occurred in the Wathayn region around this time, from 2700-2100 cal BP, with depositional concentrations decreasing with the establishment of earth mounds (Petchey et al. 2013, in Stevenson et al. 2015, p.28). Brockwell et al. (2016, p.6) suggest that an increase in permanent water sources from ~2200 cal BP, such as Big Willum Swamp after becoming a deep water body, allowed for "diversification of the economy away from the coast". From this statement by Brockwell et al. (2016), it is expected that human use of the Big Willum Swamp catchment increased at this time.

Comparison to other palaeoenvironmental records for this phase is difficult as changes in the Big Willum record reflect shifts in the hydrology of the site. Similarly, low charcoal and PyC fluxes in this phase may be the result of depositional processes, and are not likely to be indicative of an absence of fire in the region.

9.2.2.2 Big Willum Phase II: 1700-~500 cal BP

Charcoal and PyC fluxes in all size fractions increase slightly in this phase, along with a minor increase in sedimentation rate. The phase begins with a high fire intensity period (~1650-1500 cal BP; Figure 9.7) followed by intermediate/indeterminate intensities for the remainder of this

phase, with minimal local impact within the catchment (very low flux for >250 µm). Organics, represented by Mo ratio, dominate the Itrax™ elemental signal from this phase onwards after the establishment of Big Willum Swamp as a permanent deep water body in the previous phase, with detrital elements continuing to reduce until ~1400 cal BP. This is also reflected in increasing total organic carbon content through this phase and into Phase III.

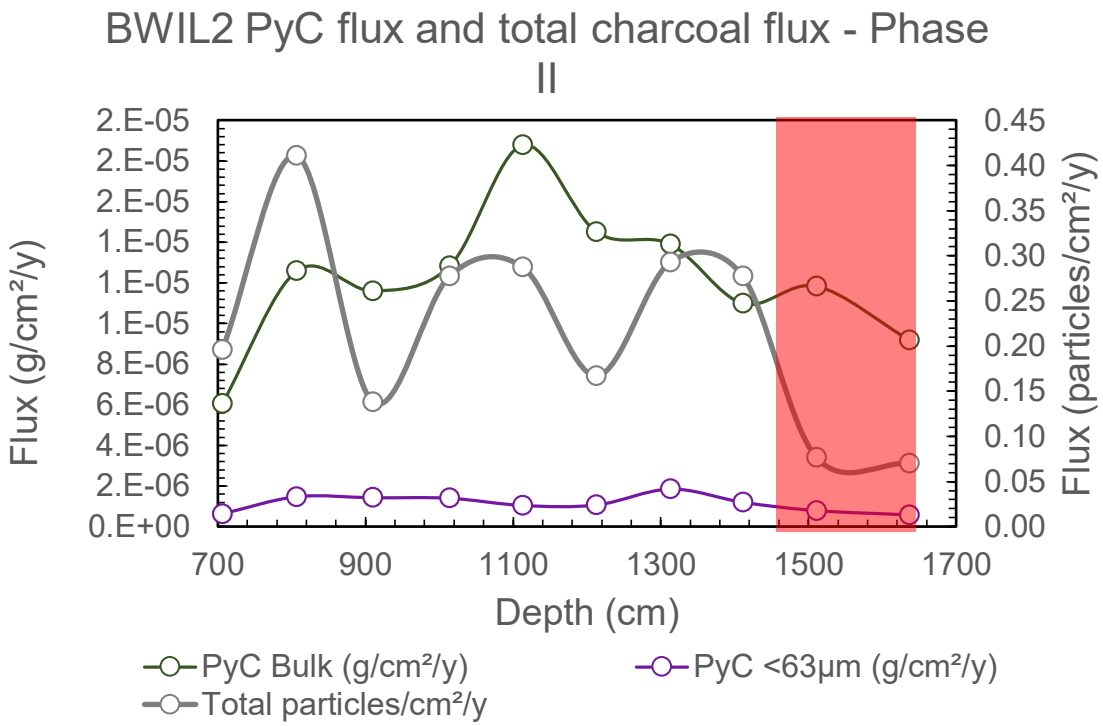

Figure 9.7: BWIL2 bulk and <63 µm PyC flux and total charcoal flux for Phase II. Red bars: high intensity.

This phase coincides with the initiation of the main phase of shell mound accumulation around Albatross Bay (~1600 cal BP; Morrison 2013). This shift in resource use has been compared to other models of economic intensification "in the context of higher climatic variability after the onset of the El Niño Southern Oscillation" (Morrison 2013, p.89), indicating both changes

in human activity and climatic variability in the Weipa region at this time. Morrison (2013, p.89) notes that this may also have been accompanied by "greater degrees of familiarity with local environments and more localised land-use patterns"; increased fire incidence during this phase in the Big Willum record indicates that this localised land-use included the application of fire to the landscape. This fire application appears to have had minimal impact on vegetation composition within and beyond the Big Willum Swamp catchment.

Bulk PyC flux increases to a peak at ~1100 cal BP in this phase before decreasing through the rest of the phase; this is matched by a peak in 250-125 µm charcoal flux and suggests an intermediate intensity fire (or fires), corresponding to the large burning event/s identified by Stevenson et al. (2015) at ~1000 BP in BW01. Stevenson et al. (2015, p.24-25, 28) describe this fire event as the only one in the BW01 record that is in any way "landscape altering" as it coincides with a "subtle shift in the pollen taxa", and suggest that the cause may have been the initiation of a more permanent expansion of human populations to inland regions. This subtle vegetation shift corresponds to a minor increase in <63 µm PyC $\delta^{13}C$ value (-22‰ VPDB, suggesting a slight decrease in grass content due to the Stable Isotope Disequilibrium Effect; see Saiz et al. 2015 and Chapter 6) with no change in bulk PyC $\delta^{13}C$ value.

While fire intensities during Phase II are intermediate/indeterminate or high, overall fluxes are low compared to the next phase (Phase III) suggesting low overall fire incidence.

9.2.2.3 Big Willum Phase III: ~500 cal BP to Present

The most recent phase in the Big Willum record is characterised by high charcoal and PyC fluxes and increased sedimentation rates. The exact timing of termination of Phase II and onset of Phase III is unclear due to the low resolution of BWIL2; the transition occurs between 5.5 and 6 cm, identified by the age-depth model (see Chapter 6) as between 706 and 304 cal BP. It

is reasonable to assume from this age range and pre-existing archaeological (Brockwell et al. 2016) and palaeoenvironmental (Stevenson et al. 2015) evidence that this transition occurred at ~500 cal BP. Brockwell et al. (2016, p.5) show that the majority of Weipa earth mounds were occupied in the last 500 years, in regions close to Big Willum Swamp (Wathayn and Diingwulung). The BW03 record of Stevenson et al. (2015, p.27), collected from near Big Willum Swamp's periphery, suggests increased sedimentation after ~600-400 cal BP indicating higher water levels, along with dominance of *Corymbia* pollen (seasonal inundation of low-lying areas around the swamp) and peak levels of *Leptospermum* pollen (found in gallery forests alongside permanent fresh water). This transition is therefore believed to represent a climatic shift to wetter conditions and a corresponding change in human activities such as reduced mobility enabled by "greater freshwater and resource security" (Stevenson et al. 2015, p.28; see also Brockwell et al. 2016, p.7).

Stevenson et al. (2015, p.26) note that Big Willum Swamp may have reached its present extent around the onset this phase (~600-400 cal BP). Occupation of earth mounds at Wathayn "trebled" in the last 500 years (Brockwell et al. 2016, p.6), concurrent with the wettest phase inferred from BW01 (Stevenson et al. 2015). This increase in occupational intensity does not correspond to an increase in fire abundance and may in fact coincide with an overall decrease in charcoal and PyC. This is similar to the Marura palaeofire record (see above); it is possible that this is the result of a combination of wet conditions and continuing fire management, although it is worth noting that the resolution for this period is low (1 cm).

Peak fire activity across all measures occurs in the last century, constrained by ^{210}Pb dates (see Chapter 6), coinciding with the establishment of Weipa Mission in 1896 and increasing European activity into the 20th century (see Chapter 3). This is in agreement with a peak in macroscopic charcoal in the last century identified by Stevenson et al. (2015) in BW01.

High-temperature burning on the regional scale peaks at ~30 cal BP (1920 CE) (Figure 9.8).

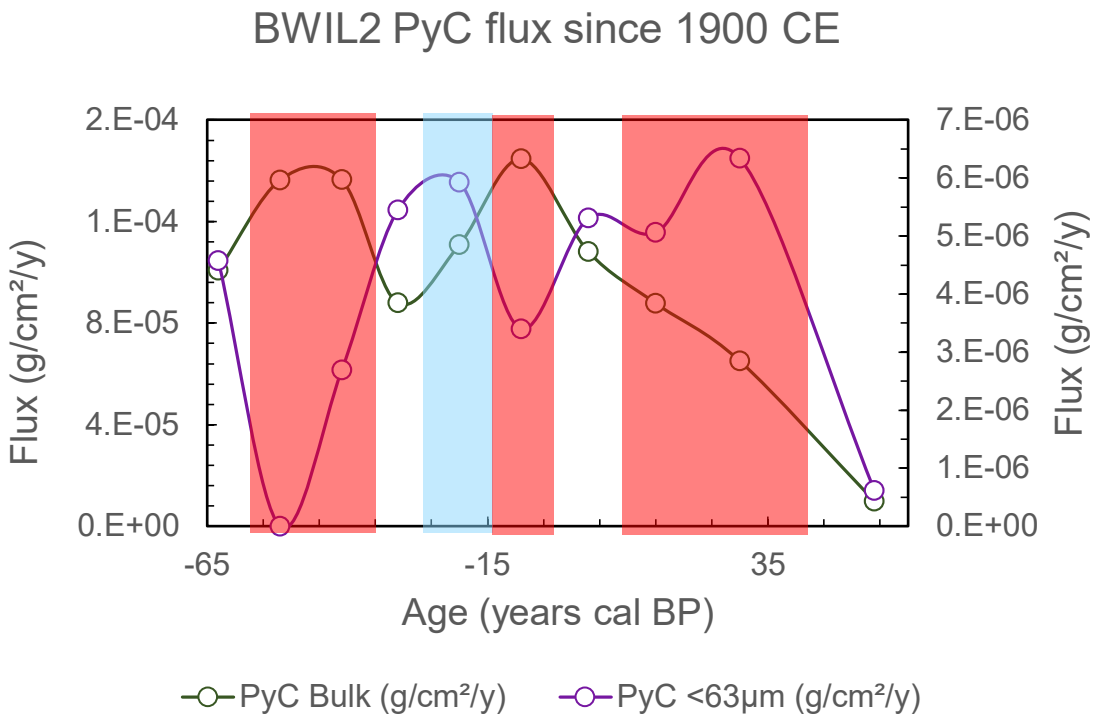

Figure 9.8: Pyrogenic carbon (PyC) flux from ~50 cal BP (1900 CE) to present for BWIL2. Blue bars: low intensity, red bars: high intensity.

Charcoal flux in BWIL2 increases from 15 cal BP (1935 CE) to peak at ~-20 cal BP (1970 CE). This peak in fire incidence coincides with the commencement of commercial bauxite shipments from Weipa (1963) and the official opening of the Weipa township (1967; see Chapter 3) and likely represents woody and grassy burns related to the establishment of the mine and township.

A similar recent increase in charcoal is described by Moss et al. (2015, p.143) at Marralda Swamp in the South Wellesley Islands following the removal of the Indigenous population after a cyclone in 1948. Similarly, the Big Willum record captures not only the removal of traditional fire management practices but also the introduction of European land management

in its stead. Charcoal peaks in the most recent period attributed to European influence also occur at Lake Euramoo (~250 BP to present; Haberle 2005) and records in the Torres Strait (~1000 BP to present at Badu 15, late Holocene increasing to the present at Tiam Point, ~500 BP to present at Zurath Swamp; Rowe 2005, 2007). This demonstrates the significant impact that European invasion had on fire incidence across the broader Cape York Peninsula region. While fire intensity data is not available for the sites not included in this study, historical and modern observations (e.g. Evans & Russell-Smith 2019; Moura et al. 2019) combined with the Marura and Big Willum records presented here show that this impact included a shift to higher fire intensities.

The Big Willum Swamp palaeofire record captures changes in human activity in the landscape, linked to shifts in climate. This record also likely captures a regional signal (>0.25 km from the water edge) with little local input, representative of fire regimes of both the Big Willum Swamp catchment and beyond due to the relatively homogeneous vegetation composition across the Weipa Plateau (see Chapter 6). Low charcoal and PyC fluxes early in the record are likely due to hydrological changes at the site affecting preservation and transport, as Big Willum transitioned from an ephemeral swamp to a permanent deep water body. This new availability of freshwater sources also led to the initiation of earth mound occupation at nearby Wathayn (Brockwell et al. 2016). Increasing fire abundance in Phase II coincides with Indigenous occupation seen in the establishment of shell mounds across Albatross Bay, with these low charcoal and PyC fluxes likely resulting from controlled burns. These controlled burns appear to have been of neither low nor high intensity with minimal effect on vegetation composition. Ethnographic evidence of burning by the Wik traditional owner group to the south of the Embley River (Perry et al. 2018, p.27) suggests that these burns may have been to protect important plant food resources within this mixed vegetation base. Stable carbon isotopes

demonstrate that vegetation burned around Big Willum Swamp was consistently a mix of C_3 woody plants and C_4 grasses throughout the record, comparable to modern vegetation at the site. The last century saw a considerable increase in fire incidence at Big Willum Swamp coinciding with permanent European settlement in the area and the establishment of a bauxite mine, with fire peaking around 1970 CE at high intensities.

9.2.3 Sanamere Lagoon

Sanamere Lagoon has the largest water surface area and catchment size of the sites in this study (see Chapter 8, Table 8.1). Unlike Marura and Big Willum Swamp, Sanamere Lagoon is surrounded by dwarf heathland vegetation to ~300 m from the waterline, where vegetation transitions to open woodland.

The palaeofire record for Sanamere Lagoon can be divided into two main phases: Phase I (8300-8000 cal BP) and Phase II (8000-5500 cal BP). ^{210}Pb dating of core SANFC suggests a third phase could exist covering the last ~170 years or more, but these sediments were not captured in the core SAN1 analysed for palaeofire reconstruction.

9.2.3.1 Sanamere Phase I: 8300-8000 cal BP

This phase is characterised by high charcoal and PyC flux, and a high sedimentation rate. Bulk PyC δ^{13}C values in this phase are ^{13}C-depleted (range of -26 to -27 ‰), displaying a largely or exclusively C_3 signal and an absence or near absence of C_4 grasses. The persistent contribution of elongate charcoal particles to the record, coupled with low δ^{13}C values, implies a large and constant input of C_3 sedge-derived charcoal to the record.

Phase I dominates the record, covering 24-10 cm depth in SAN1 and representing a period of rapid sediment accumulation. A radiocarbon date at 50 cm (~8800 cal BP) in core SAN1

suggests that this phase of high sediment accumulation may extend further than the 24 cm depth covered in this analysis. As a result of this high sedimentation rate, this phase is better resolved than Phase II. Local cool (low intensity) fires, identified by high charcoal flux and low PyC flux, dominate the beginning of this phase around ~8250 cal BP followed by an indeterminate intensity phase, centred on ~8220 cal BP resulting in the highest charcoal fluxes in the Sanamere record. Charcoal fluxes decrease thereafter while PyC fluxes increase, indicating persistently high fire intensities. Flux for the largest charcoal size fraction, >250 µm, peaks again sharply at ~8110 cal BP with little effect in the smaller size fractions, suggesting a localised fire event.

Peaks in <63 µm PyC flux at 8125 cal BP and ~8060 cal BP correspond to declines in $\delta^{13}C$ values for that fraction, and appear only as very minor peaks in charcoal flux. These peaks likely represent fine-grained input from more distant grassy fires beyond the C_3-dominated catchment, with ^{13}C-depleted $\delta^{13}C$ values resulting from the Stable Isotope Disequilibrium Effect (see Saiz et al. 2015 and Chapter 6 Discussion).

Luly, Grindrod and Penny (2006, p.1092) describes northern Australian lowland sites as having "shallow and variable lake levels early in the Holocene" due to arid conditions, followed by increasing effective precipitation into the mid-Holocene. This suggests the high fire incidence during Sanamere Phase I may have been due to, or enabled by, relatively low effective precipitation coinciding with low lake levels; this also suggests an increased likelihood of sedges close to the lagoon being vulnerable to burning, resulting in the sedge charcoal observed in the record.

Similar to the Sanamere record, macroscopic charcoal at Lake Euramoo peaks around 8000 cal BP and decreases thereafter, while microscopic charcoal peaks earlier (Haberle 2005, p.348). An increase in charcoal at Three-Quarter Mile Lake on Cape York Peninsula also begins at

~8000 cal BP but continues to increase into the late Holocene (Luly, Grindrod & Penny 2006). However, both Lake Euramoo and Three-Quarter Mile Lake are located in regions that currently support rainforest, making direct comparison of charcoal from these sites to the Sanamere palaeofire record problematic as the site is surrounded by dwarf heathland.

The end of this early to mid-Holocene phase also includes the first evidence of "sustained human presence" on Badu Island (Torres Strait) and the onset of sea-level rise severing the land bridge between Cape York Peninsula and Papua New Guinea (David et al. 2004, p.72). Human activity on Cape York Peninsula in the late Pleistocene to early Holocene is also known from rock art and rockshelter sites in the southeast (David & Lourandos 1998; Haberle & David 2004). This indicates increasing human presence to the north and southeast of Sanamere Lagoon during this phase; unfortunately no archaeological data is available for the Jardine River region. While humans are therefore known to have been in the greater region during this time, the low productivity of Sanamere Lagoon and the surrounding dwarf heathland makes human use of the lagoon unlikely except as a source of freshwater.

This period covers the 8.2 ka arid event identified in Northern Hemisphere palaeoclimate records, although it is unclear if and how this impacted the Southern Hemisphere (see Haberle & David 2004 for discussion).

9.2.3.2 Sanamere Phase II: 8000-5500 cal BP

The transition from Phase I to Phase II is marked by sharp declines in charcoal flux, PyC flux and sedimentation rate. This phase is represented by the uppermost 10 cm of sediment in core SAN1. Despite the significant shift (decrease) in fire incidence into this phase, bulk PyC $\delta^{13}C$ values do not reflect any significant change, showing the continuation of C_3 plant contribution (range of -25 to -26 ‰) with an absence of grasses similar to the previous phase. Elongate

particles continue to contribute in all charcoal size fractions in this phase, representing the input of sedges close to the lake edge.

While charcoal fluxes are low in this phase when compared to Phase I, peaks in charcoal abundance remain apparent. Minor peaks occur in charcoal flux around ~7750 cal BP and ~7180 cal BP before flux increases after ~6800 cal BP, decreasing only in the uppermost sample (~5560 cal BP) (Figure 9.9). The increased fire abundance between ~6800 and ~6000 cal BP includes a period of higher fire intensities from ~7200-6500 cal BP and intermediate or indeterminate intensities thereafter.

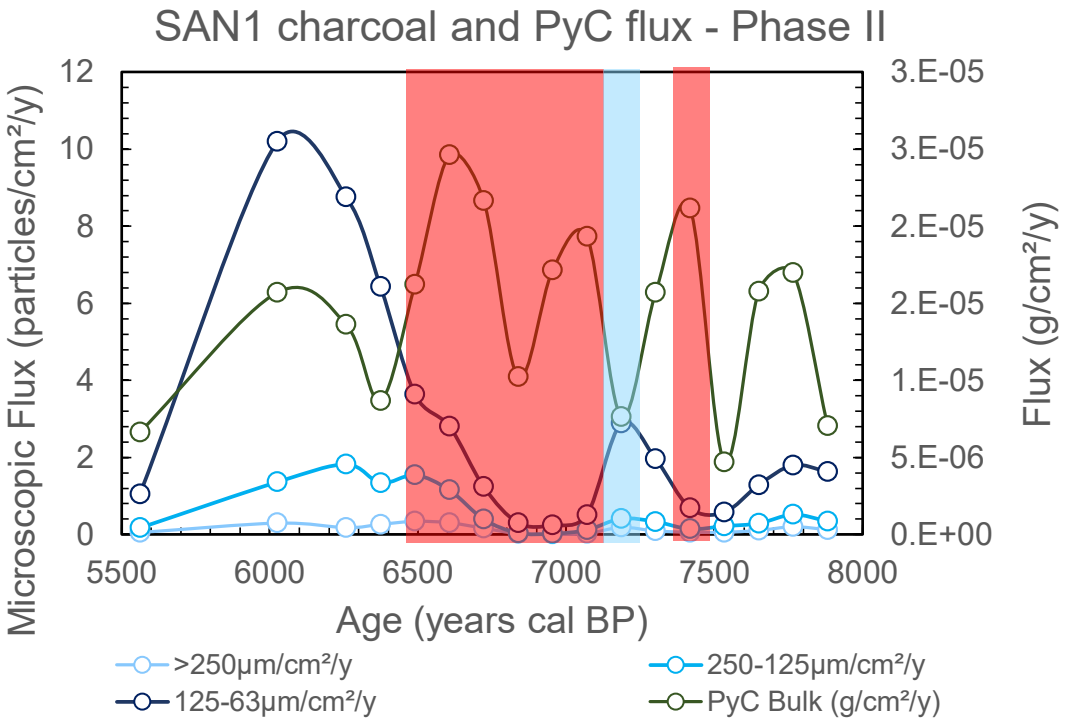

Figure 9.9: Charcoal and PyC flux for SAN1 Phase II by size fraction. Blue bars: low intensity, red bars: high intensity.

Comparison with Itrax^{TM} elemental data must be done with caution as scanning was undertaken on core SANFC while all other proxies were analysed from SAN1. However, the ^{14}C date on bulk sediment from 10 cm in core SANFC was calibrated to ~6000 cal BP allowing comparison for this depth; this places the end of Phase II within the detrital-dominated phase of the elemental record (see Chapter 7, Figure 7.30). This phase likely begins at the transition (approximately 17 cm depth) from an organic- to detrital-dominated elemental signal, with dominant organics corresponding to the period of highest charcoal and PyC accumulation seen at Big Willum Swamp and Marura, but obtaining additional dates for SANFC would be necessary to confirm this. Contrastingly, total organic carbon percentages suggest gradually declining organic content throughout Phases I and II before decreasing sharply at ~4.5 cm (~6700 cal BP), indicating that high fire incidence at the end of Phase II corresponds to low rather than high organic content.

This phase coincides with increasing effective precipitation into the mid-Holocene across northern Queensland and the Northern Territory, marked by deepening, stable lake levels (see summary by Luly, Grindrod, & Penny 2006, p.1092). Sanamere Lagoon likely deepened during this phase, increasing the distance between the centre of the lake (where core SAN1 was collected) and the shoreline as well as decreasing the volume of sediment deposited in the centre.

The end of this phase coincides with an increase in occupation sites in southeast Cape York Peninsula, associated with increasing population densities (after 5500 cal BP; Haberle & David 2004). At a similar time (~6000 BP), permanent human occupation of Badu ceased as it was separated from the mainland by rising sea-levels, with occupation shifting to "transient visits from overseas (likely ultimately from the Australian mainland)" over the next ~3500 years (David et al. 2004). This increase in population and mobility across Cape York Peninsula

makes human impact or influence on, or possibly the use of, Sanamere Lagoon more likely at the end of Phase II.

At some point after this phase, one or more sediment scouring events occurred that removed the upper sediment from the Sanamere core site, likely resulting from tropical cyclone activity (e.g. Nott et al. 2007, 2009). Nott et al. (2009) present a record from south-eastern Cape York Peninsula of intense tropical cyclone events over the last 6000 years, with a recurrence interval of approximately 200 years between events. This demonstrates multiple active, intense tropical cyclones making landfall on Cape York Peninsula during the period of sediment loss at Sanamere Lagoon. This sediment loss is evident in the uppermost 5 cm of core SANFC containing sediments from the last ~170 years only and a ^{14}C determination for SANFC 10 cm bulk sediments returning a date of ~6000 cal BP. Additional ^{14}C determinations from core SAN8, not analysed in this study, reduce the maximum age of the chronological gap to ~4000 cal BP (M. Rivera Araya, pers. comm.).

This event, or events, shifted the uppermost layers of accumulated sediments either to the edges of the lagoon or through the westerly output point into the Jardine River (see Chapter 7 Figure 7.4). Such scouring would be made possible by the shallow water depth of Sanamere Lagoon (modern water depth of ~1.25 m).

The palaeofire record for Sanamere Lagoon is dominated by a period of rapid sediment accumulation from ~8300-8000 cal BP with all measures indicating high fire incidence of variable intensity. The record shows the consistent contribution of C_3 plants including sedges with minimal or absent C_4 grass input, suggesting the modern dwarf heathland vegetation or a similar vegetation community was present from at least 8300-5500 cal BP at Sanamere Lagoon.

This also indicates that the Sanamere Lagoon palaeofire record represents a dominantly local fire signal.

Lower than present sea-levels during Phase I, and continuing into Phase II, placed Sanamere Lagoon a significant distance from the coastline (see Figure 2.9 in Faulkner 2013, p.22); this combined with the low productivity of dwarf heathland due to low nutrient sandy soils and the absence of archaeological data makes it uncertain whether Sanamere Lagoon was utilised by Indigenous inhabitants of Cape York Peninsula during the early to mid-Holocene. The predominance of high fire intensities throughout the record may be the product, or possibly partly the cause, of heathland plants of Cape York Peninsula being adapted to hot fires (Crowley 1995, pp.17-18). Fire intensity, therefore, cannot be easily interpreted as a proxy for anthropogenic influence at this site and it is uncertain whether climate, human activity or a combination of both were drivers of the fire regimes captured in the Sanamere Lagoon palaeofire record.

9.3 Site Comparisons

9.3.1 Fire Proxies

The palaeofire record for each of these sites represents three very different fire histories, captured in sedimentary environments that have very different characteristics. The Marura record captures high fire incidence and variable fire temperatures at the beginning of the late Holocene with overall fire incidence decreasing over time, sedimentation rate remaining steady (likely the result of Marura's small catchment size providing minimal material to erode under significant rainfall variability), and an increase in fire incidence in the last century. The Big Willum record shows a transition from ephemeral swamp conditions to a permanent deep water body followed by a slight increase in fire incidence for ~1000 years before a sharp increase in

fire incidence coinciding with European arrival in the region. The Sanamere Lagoon record captures a short period (~300 years; 8300-8000 cal BP) of high fire incidence, increasing fire temperatures and rapid sediment deposition before a shift from an active to a stable catchment as effective precipitation increased and the lake deepened, marked by a sharp decline in fire incidence and sedimentation over a longer period (~2500 years; 8000-5500 cal BP).

Despite Marura being the smallest site by water surface area and catchment size, the lowest charcoal abundances are within the Big Willum record. This is likely the result of the small elevation range within the Big Willum catchment, hence lower likelihood of deposition from overland flow, and minimal local burning.

9.3.2 Vegetation Burned

A similarity between the sites in this study is the consistency of vegetation structure throughout each record, as indicated by the carbon isotope composition of vegetation burnt.

Marura shows consistently mixed C_3-C_4 contribution; however, variations are apparent in the fine fraction with changing trends over time. This indicates that while C_3 and C_4 vegetation are consistently present at Marura, the balance between these vegetation types has not remained constant on temporal or spatial scales, as bulk PyC and <63 µm PyC $\delta^{13}C$ values are not strongly correlated. As described above, this is considered to be the result of anthropogenic patch burning, established during Marura Phase II (2800-900 cal BP), creating heterogeneity within the Marura catchment and between catchments across the greater Blue Mud Bay region.

Big Willum Swamp shows the least variation in vegetation type, with mixed C_3-C_4 contribution throughout the record. This consistency is expected as Big Willum Swamp is located on the Weipa Plateau, a region with widespread open woodlands dominated by *Eucalyptus tetrodonta* (Cameron & Cogger 1992, p.5; Stevenson et al. 2015, p.19). The homogeneity of this

vegetation community across local (Big Willum Swamp's catchment) and regional (the Weipa Plateau) scales leads to consistent $\delta^{13}C$ values for both PyC measures, with no temporal trend in $\delta^{13}C$ apparent that coincides with changes in climate.

Sanamere Lagoon indicates the continuous presence of C_3 vegetation burning in all size fractions over ~3000 years within the catchment, and the finest fraction delivering irregular pulses of more ^{13}C-depleted material from distant fires to the site.

It is worth noting that $\delta^{13}C$ measurements capture changes in overall vegetation structure at a coarse scale; the absence of significant changes in $\delta^{13}C$ values does not preclude the possibility of finer scale vegetation changes. This structural level data is ideal for detecting major shifts in the vegetation burning at a site.

9.3.3 Itrax™ Elemental Composition

High charcoal fluxes at Big Willum and Marura are broadly associated with organic-rich phases identified using Itrax™ elemental scanning, matched by total organic carbon percentages; this may also be the case for Sanamere but would require additional dating to confirm the relationship between cores SAN1 and SANFC. This relationship may be the result of taphonomic processes, as organic-rich sediments may preserve charcoal better than other sediments such as clays. Detrital elements in the lower portion of the Big Willum record are also associated with ephemeral swamp conditions before the site transitioned to being a deep water body, suggesting that low charcoal and pyrogenic carbon fluxes in this phase likely represent differences in the depositional environment.

9.3.4 Fire Regimes in the Late Holocene

Direct chronological comparison of palaeofire records is only possible between Big Willum Swamp and Marura, as the Sanamere Lagoon record does not contain late Holocene sediments.

Marura shows high prevalence of fire in the Blue Mud Bay region at the onset of the late Holocene (~4200 cal BP; Walker et al. 2018), coinciding with a regionally identified shift from wet to dry conditions (Shulmeister 1992). A substantial decline in fire incidence occurs at ~2800 cal BP, with only short periods of dominance of any one fire intensity (low or high) compared to earlier in the record (Marura Phase I). This is coincident with the occupation of archaeological sites in the region (see Faulkner 2013), and shows the establishment of anthropogenic heterogeneous patch burning and a shift from climate to humans as the main driver of fire at Marura. Low abundance or absence of charcoal in Phase I (3900-1700 cal BP) of the Big Willum record is the result hydrological changes at the site during this early period and therefore fluxes in this phase are not directly comparable. Fluxes at Big Willum Swamp increase after ~1700 cal BP, shortly before initiation of the main phase of shell mound construction at nearby Albatross Bay (Morrison 2013). This burning is predominantly at the regional scale and is likely the product of anthropogenic burning to protect important food resources (see Perry et al. 2018, p.27).

Fluxes at Marura drop sharply at ~900 cal BP, with minimal charcoal and pyrogenic carbon deposited in the sinkhole over the next ~750 years. Burning around Big Willum Swamp declines slightly later, at ~500 cal BP, when the site is estimated to have reached its current extent between ~600 and 400 cal BP when effective precipitation increased (Stevenson et al. 2015).

Both sites show dramatic fire regime changes resulting from European arrival. A regional shift to increasing fire incidence occurs at Marura at 55 cal BP (1895 CE), not associated with

notably high fire intensities but likely marking the beginning of depopulation and subsequent removal of established Indigenous fire regimes; around this time, Arnhem Land was under pastoral lease held by the Eastern and African Cold Storage Company, whose employees were known to kill Indigenous inhabitants (Cole 1982). Fire incidence at Marura peaks in the uppermost samples after ~1950 CE onwards (coincident with a "very strong" El Niño event in 1980 CE; BOM n.d.) to fluxes not seen in the preceding 900 years, indicating a significant increase in fire incidence (local and regional) associated with intermediate/indeterminate fire intensities. Similarly, an initial increase in high intensity regional burning at Big Willum occurs at 30 cal BP (1920 CE); multiple droughts were historically recorded around this time, affecting fishing and hunting by inhabitants of the Weipa Mission (Queensland Government 2017a). This is followed by increasing high intensity burns close to Big Willum Swamp after ~1955 CE and peaking around 1970 CE, depositing greater amounts of charcoal and pyrogenic carbon into the site than at any other period in the record. This increase in fire incidence coincides with initial discovery of economic bauxite deposits in the Weipa region, and the establishment of a bauxite mine and the Weipa township (Weipa Town Authority 2014). These recent fire regime shifts are not accompanied by noticeable changes in overall vegetation structure (as inferred from PyC $\delta^{13}C$ values) at either site.

These two records show contrasting late Holocene fire histories for environmentally comparable sites separated by the Gulf of Carpentaria. Despite significant differences in fire regimes across more than 2000 years, both Big Willum Swamp and Marura display sudden increases in fire incidence, with high intensities at Big Willum, in the last century producing charcoal and pyrogenic carbon fluxes unmatched in either the last 900 years (Marura) or the entirety of the record (Big Willum Swamp). European arrival, Indigenous depopulation and associated changes in land management significantly impacted fire regimes in the Blue Mud

Bay and Weipa regions. However, these changes did not alter the gross vegetation community structure at either Big Willum Swamp or Marura.

9.4 Conclusion

The three palaeofire records presented in this chapter represent three very different site histories. Fire incidence was at its peak at Marura at the onset of the late Holocene (~4600-2800 cal BP) when effective precipitation began to decline. Humans replaced climate as the main driver of fire at Marura after ~2800 cal BP, applying varying fire intensities to create heterogeneous patches of mixed C_3-C_4 vegetation while overall fire incidence decreased.

Minimal charcoal or pyrogenic carbon is present early in the Big Willum Swamp record (~3900-1700 cal BP), increasing only after the site deepened into a permanent freshwater body. Fire incidence remained low for most of the record, with indeterminate intensity fires beyond the Big Willum Swamp catchment likely produced by an anthropogenic fire regime. Fire incidence and intensities increased with European arrival at both Marura and Big Willum Swamp, as the Blue Mud Bay and Weipa regions were depopulated, and a bauxite mine was established at Weipa.

Fire incidence as well as sedimentation rate was highest at Sanamere Lagoon from ~8300-8000 cal BP, coincident with arid conditions recorded in south-eastern Cape York Peninsula. While charcoal and pyrogenic carbon flux declined sharply after ~8000 cal BP, fire intensities remained high for the majority of the record, likely due to the dwarf heathland vegetation surrounding the site being adapted to such high intensity fires.

Identified gaps in these new datasets include limited data for Big Willum Swamp in the period prior to ~1700 cal BP prior to sedimentation increase and the chronological gap in sediments at Sanamere Lagoon spanning the late Holocene.

These palaeofire records contribute new knowledge of fire regimes and vegetation change at two previously unstudied sites, as well as an expanded dataset for Big Willum Swamp. Collectively, these records demonstrate the variability between sites throughout northern Australian tropical savannas, indicating that no individual site or dataset can be assumed to be representative of the greater region. Additionally, Indigenous fire management does not uniformly appear in Australian palaeofire records as a single consistent signal. Determining fire intensity is critical to distinguishing anthropogenic effects on fire from the influence of climate, achieved in this study through the novel combination of charcoal and pyrogenic carbon analyses.

Chapter 10 : Conclusion

> *"There are different types of country on the one area of land, places that want to burn and areas on that same land we don't burn, let the country rest too. Fire is all year round, when we apply fire it's fire management, when we're not applying fire it's still fire management." Victor Steffensen (in George et al. 2013, p.19)*

Fire has existed on Earth for over 400 million years (Bowman et al. 2009; Scott 2000) and is both universal and context-specific, determined by a multitude of ecological, climatic and anthropogenic factors. Landscape fire is an ever-present element in many environments across the globe and is a force potentially of both widespread destruction (e.g. Chafer, Noonan & Macnaught 2004; Moore 2015; Siegert et al. 2001) and regeneration that supports biodiversity (e.g. He, Lamont & Pausas 2019; Scott et al. 2012; Veenendaal et al. 2018). Relationships between humans and fire are complex and highly variable across space and time (e.g. Archibald, Staver & Levin 2012; Bowman et al. 2011; Moura et al. 2019).

While fire has long been an ecological, social and potentially even mythical "pervasive presence" in human lives (Pyne 2016; see also Pyne 1997), it now plays an increasingly economic role with the rise of carbon credits and carbon abatement programs (e.g. Holden & Dixon 2018; Johnston 2016; Murphy 2013) including prescribed burning strategies in northern Australia (e.g. Russell-Smith et al. 2013). Climate change is predicted to lengthen fire seasons and increase fire severity, but the full effects of these changes are not known (CSIRO 2009);

modelling suggests increased frequency and severity of fire weather due to anthropogenic climate change is already underway in some parts of the world (particularly the Amazon and the Mediterranean), with up to ~60 % of global "burnable lands" potentially affected by the mid-twenty-first century (Abatzoglou, Williams & Barbero 2019). Recent increases in the frequency of "catastrophic" fire conditions in eastern Australia have resulted in extensive damage, injury, and deaths (e.g. Bradstock & Nolan 2019; Cox 2019; Kellett, Visontay & Gair 2019). A greater understanding of fire in different environmental and climatic contexts is urgently needed.

In Australia, the observational record is short, making palaeofire research critical to understanding fire, vegetation, human and climate dynamics over long timescales. Whether to inform future fire planning for management purposes, or simply to better understand characteristics of fire in the past, methods must be rigorous for the creation of robust palaeofire data. Unfortunately, the palaeofire discipline has continually lagged behind other palaeoecological areas such as palynology in regards to improving techniques (e.g. France et al. 2000; see Figueiral & Mosbrugger 2000 for discussion). Critical examination of palaeofire techniques is required to determine their applicability to savanna contexts in particular, and determine new multiproxy methodologies for improved palaeofire studies into the future.

The late Holocene is a period worthy of detailed study as it is most climatically comparable to modern conditions (e.g. Shulmeister & Lees 1995; Donders et al. 2007, 2008; Reeves et al. 2013a). During the late Holocene in the region, the El Niño-Southern Oscillation developed (Diaz & Markgraf 1992; Toth et al. 2012), sea-levels stabilised after a high-stand in the mid-Holocene (Chappell 1983; Yu & Zhao 2010), and the Indonesian-Australian Summer Monsoon weakened (Wyrwoll & Miller 2001). Multiple sites across northern Australia show indicators of rainforest disturbance during the late Holocene, attributed to ENSO-driven changes in climate (e.g. storms and drought) and/or human activity (e.g. increased application of fire)

(Haberle 2005; Prebble et al. 2005; Proske & Haberle 2012; Rowe 2007). Indigenous population growth beginning in the early Holocene reached its peak in the late Holocene (Williams 2013). The late Holocene also contains the transition from palaeoenvironmental to historical timescales, a period that is critical for any attempts to compare palaeofire with, or extrapolate it to, modern and future fire planning and modelling (e.g. Aleman et al. 2013; Ekblom & Gillson 2010; Higuera, Sprugel & Brubaker 2005; Perry, Wilmshurst & McGlone 2014). However, the historical record can often be overlooked in favour of reconstructions focused on deeper time periods. Existing palaeoenvironmental reconstructions suggest increasing climatic variability throughout the late Holocene in northern Australia, with this variability expressed in different region-specific ways. However, data remain limited for northern Australia compared to the relatively well-studied southeast, with many key regions lacking palaeoenvironmental records of any kind (e.g. Arnhem Land). As discussed in Chapter 2, few available records in northern Australia include fire proxies such as charcoal, limiting our understanding of the characteristics of fire in the past and how fire regimes have changed over long timescales relative to changing human activity (described in Chapter 3) and climate. A more detailed understanding of the long-term interactions between fire, climate and humans in northern Australian savannas requires additional sites with proxy palaeofire records as well as the introduction of techniques developed elsewhere to expand the ability to interpret palaeofire data beyond simple charcoal abundance information.

This study has provided a way forward for future work through the creation of three new multiproxy fire records from northern Australia that incorporate and test the ability of new techniques to enable a more nuanced interpretation of palaeofire records. These records demonstrate the similarities, and differences, within and between sites across the tropical savannas of northern Australia by investigating temporal and spatial variations within and beyond site catchments. This study went beyond analysing fire occurrence – as is the standard

for most palaeofire studies utilising a single proxy such as charcoal abundance – to also identify fire characteristics. The result is an improved multiproxy palaeofire methodology applicable across varied vegetation and environment types, to create a nuanced fire history beyond fire abundance or occurrence.

Chapter 4 outlined the methodology applied in this study. This included the description of multiple fire proxies established in previous studies, but not previously combined as is the case here. Optical analysis of charcoal particles included division into size fractions to separate fire signals from within and beyond site catchments, and also the recording of particle aspect ratios and classification into morphotypes to identify fuel type. Chemical analysis utilised the hydrogen pyrolysis method to isolate pyrogenic carbon, with pyrogenic carbon $\delta^{13}C$ values measured to determine C_3-C_4 plant contributions. Site chronologies were created using ^{210}Pb and ^{14}C dating, and sediment elemental composition determined using Itrax™ X-ray fluorescence scanning.

Chapter 5 presented background data, site characteristics and results for Marura sinkhole, in eastern Arnhem Land (Northern Territory). The Marura palaeofire record covers ~4600 cal BP to present, with high fire incidence early in the record declining through time. Mixed C_3-C_4 (woody/grassy) vegetation is present throughout, with most variability in the <63 μm PyC fraction thought to be a signal derived largely from beyond the catchment, therefore reflecting regional rather than local environmental change.

Chapter 6 presented background data, site characteristics and results for Big Willum Swamp in Weipa, Cape York Peninsula (Queensland). The Big Willum Swamp palaeofire record covers ~3900 cal BP to present, with highest fire incidence occurring over the last century. Consistent mixed C_3-C_4 (woody/grassy) vegetation is present through the record, reflecting the persistence of open Eucalypt woodland with a grassy understorey in the region for at least 4000

years. Low or absent charcoal in the >250 µm size fraction indicates minimal burning close to the swamp edge.

Chapter 7 presented background data, site characteristics and results for Sanamere Lagoon on Cape York Peninsula (Queensland). The Sanamere Lagoon palaeofire record covers ~8300-5500 cal BP, with high fire incidence and sedimentation early in the record followed by an abrupt decline at ~8000 cal BP. Elongate charcoal particle contributions combined with consistently ^{13}C-depleted $\delta^{13}C$ values demonstrate that sedges (common within 300 m of the lake edge) burned throughout the record. Changes in $\delta^{13}C$ values isolated to the <63 µm fraction show the contribution of distant grass-dominated fires from outside the catchment.

Evaluation of the range of palaeofire techniques utilized in this study, discussed in Chapter 8, demonstrated the interpretive power of combining traditional and emerging methods. Charcoal and pyrogenic carbon data were successfully combined in this study to determine relative fire intensities, critical for distinguishing anthropogenic from climatic drivers affecting fire (see Trauernicht et al. 2015). Pyrogenic carbon $\delta^{13}C$ values alongside charcoal particle aspect ratios determined the contribution of non-grass elongates (sedges) at Sanamere Lagoon.

Size fractions across charcoal and pyrogenic carbon measures demonstrated the importance of dividing and analysing different size classes; these size divisions capture potentially distinct signals from within a catchment and beyond. For example, minimal local burning (identified by >250 µm charcoal) occurred close to Big Willum Swamp throughout the palaeofire record presented here until a significant increase over the last century (Phase III). Different fractions in this study also showed that site characteristics can affect which sizes represent a regional signal (e.g. Laird and Campbell 2000; Pitkänen, Lehtonen & Huttunen 1999). For example, 125-63 µm charcoal at Sanamere Lagoon originated from within the C_3-dominated catchment but this fraction is classified as microscopic and often considered to be regionally sourced. This

suggests factors such as catchment size and landscape relief may influence the extent of the source area represented by these size fractions.

This methodological examination also demonstrated the issues associated with applying morphotype methods developed specifically for temperate environments of the northern hemisphere to tropical savanna contexts. The application of morphotype classifications from other bioregions to savannas raises issues when interpreting fuel types in terms of fire characteristics, but does reveal greater diversity and broad trends than data captured by aspect ratios alone. Full implementation of morphotypes will require considerably more work on linking fuel type to morphology, which falls beyond the scope of this study.

Chapter 9 interpreted the results for each site in this study, presenting complete palaeofire records divided into phases and contextualized by existing palaeoenvironmental, archaeological and historical data.

10.1 Fire Records by Site

The Marura palaeofire record can be summarised as follows:

- Phase I (4600-2700 cal BP): High fire incidence occurs in this phase, displaying homogeneity in fire and vegetation signals across the catchment and the greater Blue Mud Bay region. Fire incidence in this phase is primarily climate-driven as effective precipitation declined from the mid- into late Holocene.
- Phase II (2700-900 cal BP): Declining fire incidence characterises this phase, with increasing patch heterogeneity with the establishment of patch burning and human fire management increasingly influential.
- Phase III (900 cal BP to present): Minimal charcoal and pyrogenic carbon enter the site in this phase due to small-scale patch burning minimizing transport to the site. Fire

incidence resurges after ~1950 CE from European-driven Indigenous depopulation of the region and subsequent removal of Indigenous fire management.

The Big Willum Swamp palaeofire record can be summarised as follows:

- Phase I (3900-1700 cal BP): This phase is characterised by low or absent charcoal and pyrogenic carbon due to ephemeral swamp conditions, with Big Willum Swamp becoming a permanent deep water body at ~2200 cal BP (see Stevenson et al. 2015), through collapse of the underlying bauxitic laterite.
- Phase II (1700-~500 cal BP): Increasing fire incidence of indeterminate intensity occurs in this phase, associated with increasing intensity of human use of the landscape. Local burning remains minimal at the site.
- Phase III (~500 cal BP to present): Peak fire incidence in the record occurs over the last century with the establishment of Weipa Mission followed by a bauxite mine.

The Sanamere Lagoon palaeofire record can be summarised as follows:

- Phase I (8300-8000 cal BP): Peak fire incidence and high sedimentation rates characterise this phase, with low lake levels and relatively dry conditions (low effective precipitation; see Luly, Grindrod & Penny 2006).
- Phase II (8000-5500 cal BP): Charcoal and pyrogenic carbon decline sharply at the onset of this phase along with sedimentation as the lake deepened in response to increasing effective precipitation (see Luly, Grindrod & Penny 2006).

The absence of late Holocene sediments in the Sanamere Lagoon record indicates one or more scouring events occurred between ~100-4000 cal BP, as the result of cyclones (e.g. Nott et al. 2009) or active monsoon conditions combined with shallowing water due to the progressive build-up of sediment on the lake bottom. The consistent presence of elongate charcoal particles

and bulk pyrogenic carbon $\delta^{13}C$ values consistent with strictly C_3 plants indicate the contribution of burned sedges throughout the record.

Marura and Big Willum Swamp present contrasting records for palaeofire activity in the late Holocene. Highest fire incidence in the Marura record occurs at the onset of the late Holocene, while Big Willum Swamp does not accurately record this period due to ephemeral swamp conditions at the site (see Stevenson et al. 2015). At both Marura and Big Willum Swamp fire incidence increases after European arrival; however, this post-contact fire peak is much higher than any preceding fire incidences at Big Willum Swamp while the increase at Marura is comparable to fire incidence levels ~900 years ago at the site. These sites capture the diversity of fire histories and vegetation changes in the savanna region during the late Holocene, despite comparable modern vegetation compositions at Marura and Big Willum Swamp. These records demonstrate that no one site may be considered representative of northern Australian savannas in the late Holocene.

10.2 Methodological Considerations

The combination of palaeofire techniques in this study generated data not obtainable by any of these methods used in isolation and this combination provided additional interpretive power. The combination of charcoal and pyrogenic carbon fluxes allowed for inferences relating to fire intensity, with implications for teasing apart human versus climate signals in the palaeofire record (see Trauernicht et al. 2015). Elongate charcoal, measured by aspect ratio or morphotype, alongside pyrogenic carbon $\delta^{13}C$ values allowed for the identification of the significant and sustained contribution of burned sedges to the Sanamere Lagoon record, where these would have been identified as grass-derived without the stable isotope data. The division of both charcoal and pyrogenic carbon into size fractions allowed for the separation of different

spatial signals within the record, including distant fires not affecting the catchment of a particular site, and burning different vegetation to that present within the catchment (e.g. Marura and Sanamere Lagoon).

Much of the detail provided by morphotype systems from temperate environments, such as Courtney Mustaphi and Pisaric's (2014) 27-type morphotype classification system, does not appear applicable to savanna contexts. However, the overall morphological changes captured by simpler morphotype systems such as Enache and Cumming's (2006) 7-type system do show more general trends in vegetation burned throughout each record. These changes combined with other techniques may provide interpretable data on shifts in vegetation composition in palaeofire records. This would be assisted by conducting experimental studies in tropical savannas, similar to those of Jensen et al. (2007) and Wragg, Mielke and Tilman (2018), to investigate the morphotypes generated by fires in these environments. Morphotypes recorded in modern charcoal traps and recent (since ~1950 CE) sediment samples from Marura and Big Willum Swamp suggest broadly similar morphologies across the open woodland environments in this study, with grasses (elongate particles) less dominant at Marura. Development of a savanna-specific morphotype classification system may draw out more subtle distinctions than those captured by Enache and Cumming's (2006) generalised system.

The identification of a chronological gap in the sediments of Sanamere Lagoon was unexpected as the disconformity was not visible in the sediments. This prevented the reconstruction of a full late Holocene palaeofire record for the site but demonstrates the effects of one or more cyclone events between ~4000 and ~100 cal BP. Similarly, ephemeral conditions at Big Willum Swamp prevented the reconstruction of a palaeofire record prior to ~2200 cal BP at the site (see Stevenson et al. 2015), while the deepening of Big Willum after this point likely led to increased human use of the site as a freshwater source. In both cases, these breaks in continuity of the data shed light on changing conditions at each site. High sedimentation at

Marura required discontinuous sampling of the uppermost 3 m of sediment for analysis, unlike continuous 0.5 cm sampling for Big Willum Swamp (13 cm overall) and Sanamere Lagoon (24 cm overall). Discontinuous sampling does not allow for analyses separating a primary (local) signal from noise (background) (e.g. Higuera et al. 2009; Kelly et al. 2011). However, the signal detection method was designed for environments with low fire return intervals (e.g. temperate and boreal forests; see Fletcher et al. 2015; Hawthorne & Mitchell 2016; Moos & Cumming 2012) while northern Australian savannas may have fire return intervals as short as 1-3 years (Cremer 2004, p.13). As most sites do not have annual resolution, continuous sampling of a site in the savanna region is unlikely to distinguish signal peaks from an underlying background/noise. Palaeofire records for savannas are subsequently examined for overall trends in fire incidence rather than distinct fire events, making discontinuous sampling suitable for savanna sites.

Were this study to be done over again, obtaining a single core from Sanamere Lagoon that captured the water-sediment interface and sufficient sediment depth (e.g. 0.5 m or more) to be sampled for all analyses would have improved the interpretation of results. Installation and analysis of samples from charcoal traps at Marura and Big Willum Swamp, had circumstances permitted this, would also have created a more robust modern comparison dataset. Additional techniques or proxies such as reflectance (e.g. Constantine et al. 2019) or biomarkers (e.g. Argiriadis et al. 2018) may have improved the interpretation of results, although the choice to analyse multiple sites rather than perform more analyses on one or two sites provides a more valuable regional and inter-site comparisons.

10.3 Areas for Future Work

Future work will likely further develop techniques to automate the analyses undertaken here, including the application of neural networks (see Bassis, Esposito & Morabito 2014) for charcoal identification and classification as an expansion of the pilot study outlined here in Appendix 4. Charcoal morphotype analysis in savanna contexts would benefit greatly from experimental burning of savanna vegetation under laboratory conditions (similar in approach to studies such as Jensen et al. 2007; Lynch, Clark & Stocks 2004; Saiz et al. 2018; Umbanhowar & McGrath 1998; Wragg, Mielke & Tilman 2018) and collection of modern samples from landscape fires (e.g. charcoal traps in this study; Leys et al. 2015; Pisaric 2002) to investigate savanna-specific charcoal morphologies, preferably with samples from sites where palaeofire records can also be created that apply the understanding of these morphologies.

Future work will ideally include comparison of fire intensities derived from charcoal and pyrogenic carbon to other emerging intensity measures such as reflectance (e.g. Ascough et al. 2010; Constantine et al. 2019). Development and further refinement of techniques for fire intensity estimation is of high priority for palaeofire research to better characterise fire regimes and distinguish climate and human drivers of change (see Trauernicht et al. 2015, p.1914). Development of spectral analysis techniques similar to or extending from existing analytical programs such as CharAnalysis (Higuera et al. 2009) that are more appropriate for savanna environments rather than temperate forests would also benefit savanna palaeofire studies.

Palaeofire research would also benefit from the increased use of open access databases such as the Global Charcoal Database (Power et al. 2010) as standard practice for data sharing and to improve modelling of past and future fire conditions (e.g. Flannigan et al. 2009; Sánchez Goñi et al. 2017; Williams et al. 2015a).

Fire is ubiquitous across much of Australia and the globe, with anthropogenic climate change presenting challenges in the management of fire into the future (e.g. Abatzoglou, Williams & Barbero 2019). Tackling these challenges requires a detailed understanding of the context from which these fire regimes arise, namely fire-climate-human-vegetation dynamics across long timescales as described by palaeofire research. This study presents three new palaeofire records for tropical savannas in northern Australia and will ideally be followed by further research into the long history of interactions between fire, vegetation, climate and humans in this significant region. Continued development of palaeofire techniques building on this thesis will ensure the rigour of palaeofire data creation to improve our knowledge of the nuances of fire regimes from the past into the future.

References

Abatzoglou, JT, Williams, AP & Barbero, R 2019, 'Global emergence of anthropogenic climate change in fire weather indices', *Geophysical Research Letters*, vol. 46, pp. 326-336, DOI:10.1029/2018GL080959.

Abrahams, H, Mulvaney, M, Glasco, D & Bugg, A 1995, *Areas of Conservation Significance on Cape York Peninsula*, Australian Heritage Commission, Canberra.

Aleman, JC, Blarquez, O, Bentaleb, I, Bonté, P, Brossier, B, Carcaillet, C, Gond, V, Gourlet-Fleury, S, Kpolita, A, Lefèvre, I, Oslisly, R, Power, MJ, Yongo, O, Bremond L & Favier, C 2013, 'Tracking land-cover changes with sedimentary charcoal in the Afrotropics', *The Holocene*, vol. 23, no. 12, pp. 1853-1862, DOI:10.1177/0959683613508159.

Andersen, AN, Cook, GD & Williams, RJ 2003, *Fire in Tropical Savannas*, Springer-Verlag, New York.

Andersen, AN, Cook, GD, Corbett, LK, Douglas, MM, Eager, RW, Russell-Smith, J, Setterfield, SA, Williams, RJ & Woinarski, JCZ 2005, 'Fire frequency and biodiversity conservation in Australian tropical savannas: Implications from the Kapalga fire experiment', *Austral Ecology*, vol. 30, pp. 155-167, DOI:10.1111/j.1442-9993.2005.01441.x.

Anindilyakwa Land Council 2016, *Anindilyakwa Indigenous Protected Area Plan of Management 2016*, Anindilyakwa Land Council, viewed 20 September 2018, <https://www.anindilyakwa.com.au/uploads/images/Anindilyakwa-IPA-Management-Plan.pdf>.

Apudthama Land Trust 2018, *Map of Land Trust Area*, Apudthama Land Trust, viewed 3 April 2018, <http://www.apudthamalandtrust.com.au/about/map-of-land-trust-area/>.

Archibald, S, Staer, C & Levin, SA 2012, 'Evolution of human-driven fire regimes in Africa', *Proceedings of the National Academy of Sciences of the United States of America*, vol. 109, no. 3, pp. 847-852, DOI:10.1073/pnas.1118648109.

Argiriadis, E, Battistel, D, McWethy, DB, Vecchiato, M, Kirchgeorg, T, Kehrwald, NM, Whitlock, C, Wilmshurst, JM & Barbante, C 2018, 'Lake sediment fecal and biomass burning biomarkers provide direct evidence for prehistoric human-lit fires in New Zealand', *Scientific Reports*, vol. 8, article no. 12113, DOI:10.1038/s41598-018-30606-3.

Ascough, PL, Bird, MI, Brock, F, Higham, TFG, Meredith, W, Snape SE & Vane, CH 2009, 'Hydropyrolysis as a new tool for radiocarbon pre-treatment and the quantification of black carbon', *Quaternary Geochronology*, vol. 4, pp. 140-147, DOI:10.1016/j.quageo.2008.11.001.

Ascough, PL, Bird, MI, Scott, AC, Collinson, ME, Cohen-Ofri, I, Snape, CE & Le Manquais, K 2010, 'Charcoal reflectance measurements: Implications for structural characterization and assessment of diagenetic alteration', *Journal of Archaeological Science*, vol. 37, pp. 1590-1599, DOI:10.1016/j.jas.2010.01.020.

Atlas of Living Australia 2018, *Spatial Portal – Layer NVIS 4.1 Major Vegetation Groups*, Commonwealth Scientific & Industrial Research Organisation, viewed 12 June 2017, <https://spatial.ala.org.au/>.

Australia On the Map 2006, *Landings List: A Timeline of Unveiling Australia to the World*, viewed 1 March 2018, <http://www.australiaonthemap.org.au/landings-list/>.

Australian Dictionary of Biography 2018, *Thomson, Donald Finlay Fergusson (1901-1970)*, viewed 20 September 2018, < http://adb.anu.edu.au/biography/thomson-donald-finlay-fergusson-11851/text21213>.

Australian Institute of Aboriginal and Torres Strait Islander Studies [AIATSIS] 2014, *AUSTLANG*, Australian Institute of Aboriginal and Torres Strait Islander Studies, viewed 1 June 2018, <https://collection.aiatsis.gov.au/austlang/search>.

Bailey, G 1993, 'Shell mounds in 1972 and 1992: Reflections on recent controversies at Ballina and Weipa', *Australian Archaeology*, no. 37, pp. 1-18, DOI:10.1080/03122417.1993.11681491.

Bailey, G, Chappell, J & Cribb, R 1994, 'The origin of *Anadara* shell mounds at Weipa, north Queensland, Australia', *Archaeology in Oceania*, vol. 29, no. 2, pp. 69-80, DOI:10.1002/arco.1994.29.2.69.

Baker, R 1988, 'Traditional Aboriginal land use in the Borroloola region', in NM Williams & G Baines (eds), *Traditional Ecological Knowledge*, Australian National University, Canberra, pp. 126-143.

Barham, AJ, Rowland, MJ & Hitchcock, G 2004, 'Torres Strait *bepotaim*: An overview of archaeological and ethnoarchaeological investigations and research', *Memoirs of the Queensland Museum*, vol. 3, no. 1, pp. 1-72.

Barrier Miner 1931, 'Arnhem Land: Proposal to Declare Aboriginal Reserve', *Barrier Miner*, 4 September, p. 1.

Bassis, S, Esposito, A & Morabito, FC 2014, *Recent Advances of Neural Network Models and Applications*, Proceedings of the 23rd Workshop of the Italian Neural Networks Society (SIREN), 23-25 May, Vietri sul Mare, Salerno, Italy, Springer, Switzerland.

Bayon, G, De Deckker, P, Magee, JW, Germain, Y, Bermell, S, Tachikawa, K & Norman, MD 2017, 'Extensive wet episodes in Late Glacial Australia resulting from high-latitude forcings', *Scientific Reports*, vol. 7, article no. 44054, DOI:10.1038/srep44054.

Beasley, J 2009, *Plants of Cape York Peninsula: The Compact Guide*, John Beasley, Kuranda, Queensland.

Beaton, JM 1985, 'Evidence for a coastal occupation time-lag at Princess Charlotte Bay (north Queensland) and implications for coastal colonization and population growth theories for Aboriginal Australia', *Archaeology in Oceania*, vol. 20, no. 1, pp. 1-20, DOI:10.1002/j.1834-4453.1985.tb00096.x.

Beringer, J, Hutley, LB, Abramson, D, Arndt, SK, Briggs, P, Bristow, M, Canadell, JG, Cernusak, LA, Eamus, D, Edwards, AC, Evans, BJ, Fest, B, Goergen, K, Grover, SP, Hacker, J, Haverd, V, Kanniah, K, Livesley, SJ, Lynch, A, Maier, S, Moore, C, Raupach, M, Russell-Smith, J, Scheiter, S, Tapper, NJ & Uotila, P 2015, 'Fire in Australian savannas: From leaf to landscape', *Global Change Biology*, vol. 21, pp. 62-81, DOI:10.1111/gcb.12686.

Biggs, AJW & Phillip, SR 1995, *Soils of Cape York Peninsula*, Queensland Department of Primary Industries, Mareeba, Queensland.

Binford, MW 1990, 'Calculation and uncertainty analysis of ^{210}Pb dates for PIRLA project lake sediment cores', *Journal of Paleolimnology*, vol. 3, pp. 253-267, DOI:10.1007/BF00219461.

Bird, DW, Bliege Bird, R & Parker, CH 2004, 'Women who hunt with fire: Aboriginal resource use and fire regimes in Australia's Western Desert', *Australian Aboriginal Studies*, no. 1, pp. 90-96.

Bird, MI & Ascough, PL 2012, 'Isotopes in pyrogenic carbon: A review', *Organic Geochemistry*, vol. 42, pp. 1529-1539, DOI:10.1016/j.orggeochem.2010.09.005.

Bird, MI & Cali, JA 1996, 'A revised high-resolution oxygen-isotope chronology for ODP-668B: Implications for Quaternary biomass burning in Africa', *Global & Planetary Change*, vol. 33, pp. 73-76, DOI:10.1016/S0921-8181(02)00062-0.

Bird, MI & Grōcke, DR 1997, 'Determination of the abundance and carbon isotope composition of elemental carbon in sediments', *Geochemica et Cosmochimica Acta*, vol. 61, no. 16, pp. 3413-3423.

Blaauw, M, Andres Christen, J, Esuivel Vazquez, J, Belding, T, Theiler, J, Gough, B & Karney, C 2019, Package 'rbacon', viewed 1 June 2018, <https://cran.r-project.org/web/packages/rbacon/rbacon.pdf>.

Black, MP & Mooney, SD 2006, 'Holocene fire history from the Greater Blue Mountains World Heritage Area, New South Wales, Australia: The climate, humans and fire nexus', *Regional Environmental Change*, vol. 6, pp. 41-51, DOI:10.1007/s10113-005-0003-8.

Black, MP, Mooney, SD & Haberle, SG 2007, 'The fire, human and climate nexus in the Sydney Basin, eastern Australia', *The Holocene*, vol. 17, no. 4, pp. 469-480, DOI:10.1177/0959683607077024.

Blake, T 1998, 'Deported… at the sweet will of the government: The removal of Aborigines to reserves in Queensland 1897-1939', *Aboriginal History*, vol. 22, pp. 51-61, DOI:10.22459/AH.22.2011.04.

Bliege Bird, R, Bird, DW & Codding, BF 2016, 'People, El Niño southern oscillation and fire in Australia: Fire regimes and climate controls in hummock grasslands', *Philosophical*

Transactions of the Royal Society B, vol. 371, article no. 20150343, DOI:10.1098/rstb.2015.0343.

Bliege Bird, R, Bird, DW, Codding, BF, Parker, CH & Jones, JH 2008, 'The "fire stick farming" hypothesis: Australian Aboriginal foraging strategies, biodiversity, and anthropogenic fire mosaics', *Proceedings of the National Academy of Sciences of the United States of America*, vol. 105, no. 39, pp. 14796-14801, DOI:10.1073/pnas.0804757105.

Bliege Bird, R, Codding, BF, Kauhanen, PG & Bird, DW 2012, 'Aboriginal hunting buffers climate-driven fire-size variability in Australia's spinifex grasslands', *Proceedings of the National Academy of Sciences of the United States of America*, vol. 109, no. 26, pp. 10287-10292, DOI:10.1073/pnas.1204585109.

Bliege Bird, R, Tayor, N, Codding, BF & Bird, DW 2013, 'Niche construction and Dreaming logic: Aboriginal patch mosaic burning and varanid lizards (*Varanus gouldii*) in Australia', *Proceedings of the Royal Society B*, vol. 280, p. 20132297, DOI:10.1098/rspb.2013.2297.

Boon, PI & Bunn, SE 1994, 'Variations in the stable isotope composition of aquatic plants and their implications for food web analysis', *Aquatic Botany*, vol. 48, pp. 99-108, DOI:10.1016/0304-3770(94)90077-9.

Bourke, PM 2004, 'Three Aboriginal shell mounds at Hope Inlet: Evidence for coastal, not maritime late Holocene economies on the Beagle Gulf mainland, northern Australia', *Australian Archaeology*, vol. 59, pp. 10-22, DOI:10.1080/03122417.2004.11681787.

Bourke, P, Brockwell, S, Faulkner, P & Meehan, B 2007, 'Climate variability in the mid to late Holocene Arnhem Land region, north Australia: Archaeological archives of

environmental and cultural change', *Archaeology in Oceania*, vol. 42, no. 3, pp. 91-101, DOI:10.1002/j.1834-4453.2007.tb00022.x.

Bowman, DM 2000, *Australian Rainforests: Islands of Green in a Land of Fire*, Cambridge University Press, Cambridge.

Bowman, D 2019, 'The causes of unprecedented bushfires are complex but climate change is part of the puzzle', *ABC News*, viewed 15 November 2019, <https://www.abc.net.au/news/2019-11-12/cause-of-bushfires-is-complex-but-climate-change-is-part-of-it/11692176>.

Bowman, DMJS, Balch, JK, Artaxo, P, Bond, WJ, Carlson, JM, Cochrane, MA, D'Antonio, CM, DeFries, RS, Doyle, JC, Harrison, SP, Johnston, FH, Keeley, JE, Krawchuk, MA, Kull, CA, Marston, JB, Moritz, MA, Prentice, IC, Roos, CI, Scott, AC, Swetnam, TW, van der Werf, GR & Pyne, SJ 2009, 'Fire in the Earth system', *Science*, vol. 324, no. 5926, pp. 481-484, DOI:10.1126/science.1163886.

Bowman, DMJS, Balch, J, Artaxo, P, Bond, WJ, Cochrane, MA, D'Antonio, CM, DeFries, R, Johnston, RH, Keeley, JE, Krawchuk, MA, Kull, CA, Mack, M, Moritz, MA, Pyne, S, Roos, CI, Scott, AC, Sodhi, NS & Swetnam, TW 2011, 'The human dimension of fire regimes on Earth', *Journal of Biogeography*, vol. 38, pp. 2223-2236, DOI:10.1111/j.1365-2699.2011.02595.x.

Bowman, DMJS & Panton, WJ 1993, 'Decline of *Callitris intratropica* R.T. Baker & H.G. Smith in the Northern Territory: Implications for pre-and post-European colonization fire regimes', *Journal of Biogeography*, vol. 20, pp. 373-381, DOI:10.1111/j.1442-9993.1988.tb00964.x.

Bradstock, R & Nolan, RH 2019, 'Drought and climate change were the kindling, and now the east coast is ablaze', *The Conversation*, viewed 12 November 2019

<https://theconversation.com/drought-and-climate-change-were-the-kindling-and-now-the-east-coast-is-ablaze-126750>.

Brass, LJ 1953, *Results of the Archbold Expeditions No. 68: Summary of the 1948 Cape York (Australia) Expedition – with Notes on the Mammals of Cape York Peninsula by G.H.H. Tate*, Bulletin of the American Museum of Natural History, vol. 102, no. 2, New York.

Breman, E, Gillson, L & Willis, K 2011, 'How fire and climate shaped grass-dominated vegetation and forest mosaics in northern South Africa during past millennia', *The Holocene*, vol. 22, no. 12, pp. 1427-1439, DOI:10.1177/0959683611400196.

Brockwell, S 2006, 'Earth mounds in northern Australia: A review', *Australian Archaeology*, vol. 63, pp. 47-56, DOI:10.1080/03122417.2006.11681837.

Brockwell, S, Bourke, P, Clarke, A, Crassweller, C, Faulkner, P, Meehan, B, O'Connor, S, Sim, R & Wesley, D 2011, 'Holocene settlement of the northern coastal plains, Northern Territory, Australia', *The Beagle: Records of the Museums and Art Galleries of the Northern Territory*, vol. 27, pp. 1-22.

Brockwell, S, Faulkner, P, Bourke, P, Clarke, A, Crassweller, C, Guse, D, Meehan, B & Sim, R 2009, 'Radiocarbon dates from the Top End: A cultural chronology for the Northern Territory coastal plains', *Australian Aboriginal Studies*, no. 1, pp. 54-76.

Brockwell, S, Meehan, B & Ngurrabangurraba, B 2005, 'An-barra Archaeological Project: A progress report', *Australian Aboriginal Studies*, no. 1, pp. 84-89.

Brockwell, S., Ó Foghlú, B, Fenner, JN, Stevenson, J, Proske, U & Shiner, J 2017, 'New dates for earth mounds at Weipa, north Queensland, Australia', *Archaeology in Oceania*, vol. 52, no. 2, pp. 127-134, DOI:10.1002/arco.5118.

Buckman, S, Brownlie, KC, Bourman, RP, Murray-Wallace, CV, Morris, RH, Lachlan, TJ, Roberts, RG, Arnold, LJ & Cann, JH 2009, 'Holocene palaeofire records in a high-level, proximal valley-fill (Wilson Bog), Mount Lofty Ranges, South Australia', *The Holocene*, vol. 19, no. 7, pp. 1017-1029, DOI:10.1177/0959683609340998.

Bunn, SE & Boon, PI 1993, 'What sources of organic carbon drive food webs in billabongs? A study based on stable isotope analysis', *Oecologia*, vol. 96, pp. 85-94, DOI:10.1007/BF00318034.

Bureau of Meteorology [BOM] 2005, *Tropical Cyclone Ingrid*, Australian Government, viewed 3 August 2020, <http://www.bom.gov.au/cyclone/history/pdf/ingrid.pdf>.

Bureau of Meteorology [BOM] 2008, *The Australian Monsoon*, Australian Government, viewed 1 September 2016, <http://www.bom.gov.au/climate/about/australian-climate-influences.shtml?bookmark=monsoon>.

Bureau of Meteorology [BOM] 2010, *Australian Climate Influences*, Australian Government, viewed 1 September 2016, <http://www.bom.gov.au/climate/about/australian-climate-influences.shtml?bookmark=introduction>.

Bureau of Meteorology [BOM] 2016a, *Average Annual Thunder-Day and Lightning Flash Density*, Australian Government, viewed 1 March 2018, <http://www.bom.gov.au/jsp/ncc/climate_averages/thunder-lightning/index.jsp?maptype=otdg#maps>.

Bureau of Meteorology [BOM] 2016b, *Indigenous Weather Knowledge: Yirrganydji Season: Kurraminya – Dry Season*, Australian Government, viewed 1 October 2018, <http://www.bom.gov.au/iwk/calendars/yirrganydji/yirrganydji_dry_season.shtml>.

Bureau of Meteorology [BOM] 2018a, *Cyclone Tracks – Southern Hemisphere*, Australian Government, viewed 13 June 2018, <http://www.bom.gov.au/cyclone/history/tracks/beta/>.

Bureau of Meteorology [BOM] 2018b, *Monthly Climate Statistics: Groote Eylandt Airport*, Australian Government, viewed 13 June 2018, <http://www.bom.gov.au/climate/averages/tables/cw_014518.shtml>.

Bureau of Meteorology [BOM] 2018c, *Monthly Climate Statistics: Horn Island*, Australian Government, viewed 13 June 2018, <http://www.bom.gov.au/climate/averages/tables/cw_027058.shtml>.

Bureau of Meteorology [BOM] 2018d, *Monthly Climate Statistics: Weipa Eastern Ave*, Australian Government, viewed 13 June 2018, <http://www.bom.gov.au/climate/averages/tables/cw_027042.shtml>.

Bureau of Meteorology [BOM] 2019, *ENSO Outlook*, Australian Government, viewed 1 March 2019, <http://www.bom.gov.au/climate/enso/outlook/#tabs=Criteria>.

Bureau of Meteorology [BOM] n.d. *El Niño – Detailed Australian Analysis*, Australian Government, viewed 3 October 2019, <http://www.bom.gov.au/climate/enso/enlist/>.

Bureau of Mineral Resources, Geology & Geophysics 1976, *Weipa Sheet SD 54-3,* Map, Australian Government, Canberra.

Bureau of Mineral Resources, Geology & Geophysics, 1977, *Jardine River Sheet SC 54-15*, Map, Australian Government, Canberra.

Burn, MJ & Palmer, SE 2014, 'Solar forcing of Caribbean drought events during the last millennium', *Journal of Quaternary Science*, vol. 29, no. 8, pp. 827-836, DOI:10.1002/jqs.2660.

Burrows, MA, Fenner, J & Haberle, SG 2014, 'Humification in northeast Australia: Dating millennial and centennial scale climate variability in the late Holocene', *The Holocene*, vol. 24, no. 12, pp. 1707-1718, DOI:10.1177/0959683614551216.

Burrows, ND, Burbidge, AA, Fuller, PJ & Behn, G 2006, 'Evidence of altered fire regimes in the Western Desert region of Australia', *Conservation Science Western Australia*, vol. 3, no. 3, pp. 272-284.

Cameron, EE & Cogger, HG 1992, 'The herpetofauna of the Weipa region, Cape York Peninsula', *Technical Reports of the Australian Museum*, vol. 7, pp. 1-200, DOI:10.3853/j.1031-8062.7.1992.72.

Carbonell, E, Bermúdez de Castro, JM & Sala, R 2018, '"Homo Sapiens": Who are we? Essential traits of our species', *Mètode Science Studies Journal*, vol. 8, pp. 107-113, DOI:10.7203/metode.8.9481.

Carcaillet, C, Bouvier, M, Fréchette, B, Larouche, AC & Richard, PJH 2001, 'Comparison of pollen-slide and sieving methods in lacustrine charcoal analyses for local and regional fire history', *The Holocene*, vol. 11, no. 4, pp. 467-476, DOI:10.1191/095968301678302904.

Carron, W 1849, *Narrative of an Expedition Undertaken under the Direction of the Late Mr. Assistant Surveyor E.B. Kennedy*, Project Gutenberg, viewed 12 August 2016, <http://gutenberg.net.au/ebooks02/0201121.txt>.

Chafer, CJ, Noonan, M & Macnaught, E 2004, 'The post-fire measurement of fire severity and intensity in the Christmas 2001 Sydney wildfires', *International Journal of Wildland Fire*, vol. 13, no. 2, pp. 227-240, DOI:10.1071/WF03041.

Chappell, J 1983, 'Evidence for smoothly falling sea level relative to north Queensland, Australia, during the past 6,000 yr', *Nature*, vol. 302, no. 31, pp. 406-408, DOI:10.1038/302406a0.

Clark, JS 1988, 'Particle motion and the theory of charcoal analysis: Source area, transport, deposition, and sampling', *Quaternary Research*, vol. 30, pp. 67-80, DOI:10.1016/0033-5894(88)90088-9.

Clark, RL 1983, 'Pollen and charcoal evidence for the effects of Aboriginal burning on the vegetation of Australia', *Archaeology in Oceania*, vol. 18, no. 1, pp. 32-37, DOI:10.1002/arco.1983.18.1.32.

Clarke, AF 1994, 'Winds of Change: An Archaeology of Contact in the Groote Eylandt Archipelago, Northern Australia', PhD thesis, Australian National University, Canberra.

Clarkson, C 2007, *Lithics in the Land of the Lightning Brothers: The Archaeology of Wardaman Country, Northern Territory*, Terra Australis 25, ANU E Press, Canberra.

Clarkson, C, Jacobs, Z, Marwick, B, Fullagar, R, Wallis, L, Smith, M, Roberts, RG, Hayes, E, Lowe, K, Carah, X, Florin, SA, McNeil, J, Cox, D, Arnold, LJ, Hua, Q, Huntley, J, Brand, HEA, Manne, T, Fairbairn, A, Shulmeister, J, Lyle, L, Salinas, M, Page, M, Connell, K, Park, G, Norman, K, Murphy, T & Pardoe, C 2017, 'Human occupation of northern Australia by 65,000 years ago', *Nature*, vol. 547, pp. 306-310, DOI:10.1038/nature22968.

Cohen, AS 2003, *Paleolimnology: The History and Evolution of Lake Systems*, Oxford University Press, Oxford.

Cole, K 1982, *A History of Numbulwar*, Keith Cole Publications, Victoria.

Commonwealth Scientific & Industrial Research Organisation [CSIRO] 2009, *Bushfires in Australia*, Commonwealth Scientific & Industrial Research Organisation, viewed 28 November 2018, <https://www.aph.gov.au/DocumentStore.ashx?id=3d4e5dd5-9374-48e9-b3f4-4e6e96da27f5>.

Commonwealth Scientific & Industrial Research Organisation [CSIRO] 2016, *Kunwinjku seasonal calendar*, Commonwealth Scientific & Industrial Research Organisation, vewied 20 September 2018, <https://www.csiro.au/en/Research/Environment/Land-management/Indigenous/Indigenous-calendars/Kunwinjku>.

Constantine, M, Baker, P, Bird, M, Cohen, T, Hibert, B, Majo, C, McBreath, A, Rich, A, Zheng, X & Mooney, S 2019, 'Using ATR-FTIR to quantify pyrolysis intensity as a proxy for fire severity in eastern Australia', paper presented at the *20th Congress of the International Union for Quaternary Research (INQUA)*, Dublin, Ireland, 25-31 July 2019.

Courtney Mustaphi, CJ & Pisaric, MF 2013, 'Varying influence of climate and aspect as controls of montane forest fire regimes during the late Holocene, south-eastern British Columbia, Canada', *Journal of Biogeography*, vol. 40, pp. 1983-1996, DOI:10.1111/jbi.12143.

Courtney Mustaphi, CJ & Pisaric, MF 2014, 'A classification for macroscopic charcoal morphologies found in Holocene lacustrine sediments', *Progress in Physical Geography*, vol. 38, no. 6, pp. 734-754, DOI:10.1177/0309133314548886.

Cox, L 2019, 'Catastrophic fire danger: What does it mean and what should we do in these conditions?', *The Guardian*, viewed 12 November 2019, <https://www.theguardian.com/australia-news/2019/nov/11/catastrophic-fire-danger-what-does-it-mean-and-and-what-should-we-do-in-these-conditions>.

Crawford, AJ & Belcher, CM 2014, 'Charcoal morphometry for palaeoecological analysis: The effects of fuel type and transportation on morphological parameters', *Applications in Plant Sciences*, vol. 2, no. 8, article no. 1400004, DOI:10.3732/apps.1400004.

Cremer, KW 2004, 'Biodiversity protection: Effects of fire regime on vegetation in Australia', *Biodiversity*, vol. 5, no. 4, pp. 13-21, DOI:10.1080/14888386.2004.9712744.

Croudace, IW, Rindby, A & Rothwell, RG 2006, 'ITRAX: Description and evaluation of a new multi-function X-ray core scanner', in RG Rothwell (ed.), *New Techniques in Sediment Core Analysis*, Geological Society, London, pp. 51-63.

Crowley, GM 1995, *Fire on Cape York Peninsula*, Cape York Peninsula Land Use Strategy Program, Office of the Coordinator General of Queensland, Brisbane & Department of the Environment, Sport and Territories, Canberra.

Crowley, GM & Garnett, ST 2000, 'Changing fire management in the pastoral lands of Cape York Peninsula of northeast Australia, 1623 to 1996', *Australian Geographical Studies*, vol. 38, no. 1, pp. 10-26, DOI:10.1111/1467-8470.00097.

Czimczik, CI, Preston, CM, Schmidt, MWI, Werner, RA & Schulze, E-D 2002, 'Effects of charring on mass, organic carbon, and stable carbon isotope composition of wood', *Organic Geochemistry*, vol. 33, pp. 1207-1223, DOI:10.1016/S0146-6380(02)00137-7.

Daniau, A-L, Desprat, S, Aleman, JC, Bremond, L, Davis, B, Fletcher, W, Marlon, JR, Marquer, L, Montade, V, Morales-Molino, C, Naughton, F, Rius, D & Urrego, DH 2019, 'Terrestrial plant microfossils in palaeoenvironmental studies, pollen, microcharcoal and phytolith: Towards a comprehensive understanding of vegetation, fire and climate changes over the past one million years', *Revue de micropaléontologie*, vol. 63, pp. 1-35, DOI:10.1016/j.revmic.2019.02.001.

David, B & Lourandos, H 1998, 'Rock art and socio-demography in northeastern Australian prehistory', *World Archaeology*, vol. 30, no. 2, pp. 193-219, DOI:10.1080/00438243.1998.9980407.

David, B, McNiven, I, Mitchell, R, Orr, M, Haberle, S, Brady, L & Crouch, J 2004, 'Badu 15 and the Papuan-Austronesian settlement of Torres Strait', *Archaeology in Oceania*, vol. 39, no. 2, pp. 65-78, DOI:10.1002/j.1834-4453.2004.tb00564.x.

Davies, SJ, Lamb, HF & Roberts, SJ 2015, 'Micro-XRF core scanning in palaeolimnology: Recent developments', in IW Croudace & RG Rothwell (eds), *Micro-XRF Studies of Sediment Cores: Applications of a Non-Destructive Tool for the Environmental Sciences*, Developments in Paleoenvironmental Research 17, Springer, New York, pp. 189-226.

Davison, W 1993, 'Iron and manganese in lakes', *Earth-Science Reviews*, vol. 34, pp. 119-163, DOI:10.1016/0012-8252(93)90029-7.

Denniston, RF, Wyrwoll, K-H, Polyak, VJ, Brown, JR, Asmerom, Y, Wanamaker Jr, AD, LaPointe, Z, Ellerbroek, R, Barthelmes, M, Cleary, D, Cugley, J, Woods, D & Humphreys, WF 2013, 'A stalagmite record of Holocene Indonesian-Australian summer monsoon variability from the Australian tropics', *Quaternary Science Reviews*, vol. 78, pp. 155-168, DOI:10.1016/j.quascirev.2013.08.004.

De Oliceria Goday, JM 1983, 'Development of an analytical method for the determination of ^{238}U, ^{234}U, ^{232}Th, ^{230}Th, ^{228}Th, ^{228}Ra, ^{226}Ra, ^{210}Pb and ^{210}Po and its applications to environmental samples', *KFK 3502, Kernforschangszentrum,* Karlsruhe, p. 144.

Department of the Environment & Energy 2013 *Dhimurru Indigenous Protected Area (IPA)*, Australian Government, viewed 20 September 2018, <https://www.environment.gov.au/indigenous/ipa/declared/dhimurru.html>.

Department of the Environment & Energy 2017 *NVIS Fact Sheet: MVG 5 – Eucalypt woodlands*, Australian Government, Canberra.

Department of Environment & Science 2018a, *WetlandInfo*, Queensland Government, viewed 7 March 2018, <https://wetlandinfo.des.qld.gov.au/wetlands/>.

Department of Environment & Science 2018b, *WetlandInfo: Wetland systems*, Queensland Government, viewed 3 December 2018, <https://wetlandinfo.des.qld.gov.au/wetlands/what-are-wetlands/definitions-classification/system-definitions.html>.

Department of Environment & Science 2019a, *Jardine River National Park, Heathlands Resources Reserve and Jardine River Resources Reserve: Nature, Culture and History*, Queensland Government, viewed 21 November 2019, <https://parks.des.qld.gov.au/parks/jardine-river/culture.html>.

Department of Environment & Science 2019b, *Jardine River Wetlands Aggregation DIWA Nationally Important Wetland – Facts and Maps*, Queensland Government, viewed 22 November 2019, <https://wetlandinfo.des.qld.gov.au/wetlands/facts-maps/diwa-wetland-jardine-river-wetlands-aggregation/>.

Department of the Environment, Water, Heritage and the Arts 2008, *Laynhapuy, Arnhem Land, Northern Territory*, Australian Government, viewed 21 September 2018, <http://www.environment.gov.au/indigenous/publications/pubs/fs-laynhapuy.pdf>.

Department of National Parks, Sport & Racing 2013, *Jardine-Heathlands Aggregation Management Statement 2013*, Queensland Government, Brisbane.

Department of National Parks, Sport & Racing 2018, *Jardine River National Park, Heathlands Resources Reserve and Jardine River Resources Reserve Map*, Queensland Government, Brisbane.

Department of the Prime Minister & Cabinet 2019, *NationalMap*, Australian Government, viewed 1 March 2019, <https://nationalmap.gov.au/>.

Department of Science, Information Technology & Innovation 2015, *Severe Tropical Cyclone Lam Fact Sheet*, Queensland Government, viewed 21 October 2019, < https://www.publications.qld.gov.au/dataset/tropical-cyclone-wave-and-storm-tide-reports/resource/2810c335-0827-4464-9aaf-ffe74d1cbcd4>.

Department of Sustainability, Environment, Water, Population & Communities 2011, *The Feral Water Buffalo (*Bubalus bubalis*)*, Australian Government, viewed 1 October 2018, <https://www.environment.gov.au/system/files/resources/b4a187ba-7a72-4ed2-ab06-7a8b8a1b87a0/files/buffalo.pdf>.

Diaz, HF & Markgraf, V 1992, *El Niño: Historical and Paleoclimatic Aspects of the Southern Oscillation*, Cambridge University Press, Cambridge.

Donders, TH, Haberle, SG, Hope, G, Wagner, F & Visscher, H 2007, 'Pollen evidence for the transition of the eastern Australian climate system from the post-glacial to the present-day ENSO mode', *Quaternary Science Reviews*, vol. 26, pp. 1623-1637, DOI:10.1016/j.quascirev.2006.11.018.

Donders, TH, Wagner-Cremer, F & Visscher, H 2008, 'Integration of proxy data and model scenarios for the mid-Holocene onset of modern ENSO variability', *Quaternary Science Reviews*, vol. 27, pp. 571-579, DOI:10.1016/j.quascirev.2007.11.010.

Dowdy, AJ & Kuleshov, Y 2014, 'Climatology of lightning activity in Australia: Spatial and seasonal variability', *Australian Meteorological and Oceanographic Journal*, vol. 64, pp. 103-108, DOI:10.22499/2.6402.002.

Doyle, K 2019, *Monsoon: The Complex Weather Phenomenon that Comes and Goes*, ABC News, viewed 1 February 2019, <https://www.abc.net.au/news/2019-01-18/monsoon-explaining-the-complex-weather-phenomenon/10722716>.

Duyfken Replica Foundation 2016, *Carstenzoon 1623*, Duyfken Replica Foundation, viewed 1 March 2018, <http://www.duyfken.com/Dutch%20mariners/carstenszoon-1623>.

Eakins, JD & Morrison, RT 1978, 'A new procedure for the determination of lead-210 in lake and marine sediments', *International Journal of Applied Radiation and Isotopes*, vol. 29, pp. 531-536, DOI:10.1016/0020-708X(78)90161-8.

Eggleton, RA, Taylor, G, Le Gleuher, M, Foster, LD, Tilley, DB & Morgan, CM 2018, 'Regolith profile, mineralogy and geochemistry of the Weipa Bauxite, northern Australia', *Australian Journal of Earth Sciences*, vol. 55, pp. S17-43, DOI:10.1080/08120090802438233.

Ekblom, A & Gillson, L 2010, 'Fire history and fire ecology of Northern Kruger (KNP) and Limpopo National Park (PNL), southern Africa', *The Holocene*, vol. 20, no. 7, pp. 1063-1077, DOI:10.1177/0959683610369499.

Enache, MD & Cumming BF 2006, 'Tracking recorded fires using charcoal morphology from the sedimentary sequence of Prosser Lake, British Columbia (Canada)', *Quaternary Research*, vol. 65, pp. 282-292, DOI:10.1016/j.yqres.2005.09.003.

Enfield, DB 1989, 'El Niño, past and present', *Reviews of Geophysics*, vol. 27, no. 1, pp. 159-187, DOI:10.1029/RG027i001p00159.

Enright, NJ & Thomas, I 2008, 'Pre-European fire regimes in Australian ecosystems', *Geography Compass*, vol. 2, no. 4, pp. 979-1011, DOI:10.1111/j.1749-8198.2008.00126.x.

Evans, J & Russell-Smith, J 2019, 'Delivering effective savanna fire management for defined biodiversity conservation outcomes: An Arnhem land case study', *International Journal of Wildland Fire*, Preprint, DOI:10.1071/WF18126.

Faulkner, P 2013, *Life on the Margins: An Archaeological Investigation of Late Holocene Economic Variability, Blue Mud Bay, Northern Australia,* Terra Australis 38, ANU E Press, Canberra.

Faulkner, P & Clarke, A 2004, 'Late-Holocene occupation and coastal economy in Blue Mud Bay, northeast Arnhem Land: Preliminary archaeological findings', *Australian Archaeology*, no. 59, pp. 23-30, DOI:10.1080/03122417.2004.11681788.

Feurdean, A & Vasiliev, J 2019, 'The contribution of fire to the late Miocene spread of grasslands in eastern Eurasia (Black Sea region)', *Scientific Reports*, vol. 9, article no. 6750, DOI:10.1038/s41598-019-43094-w.

Field, E, McGowan, HA, Moss, PT & Marx, SK 2017, 'A late Quaternary record of monsoon variability in the northwest Kimberley, Australia', *Quaternary International*, vol. 449, pp. 119-135, DOI:10.1016/j.quaint.2017.02.019.

Figueiral, I & Mosbrugger, V 2000, 'A review of charcoal analysis as a tool for assessing Quaternary and Tertiary environments: Achievements and limits', *Palaeogeography, Palaeoclimatology, Palaeoecology*, vol. 164, pp. 397-407, DOI:10.1016/S0031-0182(00)00195-4.

Fink, D, Hotchkis, M, Hua, Q, Jacobsen, G, Smith, AM, Zoppi, U, Child, D, Mifsud, C, van der Gaast, H, Williams, A & Williams, M 2004, 'The ANTARES AMS facility at ANSTO', *Nuclear Instruments & Methods in Physics Research Section B*, vol. 223-224, pp. 109-115, DOI:10.1016/j.nimb.2004.04.025.

Finsinger, W, Kelly, R, Fevre, J & Magyari, EK 2014, 'A guide to screening charcoal peaks in macrocharcoal-area records for fire-episode reconstructions', *The Holocene*, vol. 24, no. 8, pp. 1002-1008, DOI:10.1177/0959683614534737.

Fitzsimons, J, Russell-Smith, J, James, G, Vigilante, T, Lipsett-Moore, G, Morrison J & Looker, M 2012, 'Insights into the biodiversity and social benchmarking components of the northern Australian fire management and carbon abatement programmes', *Ecological Management & Restoration*, vol. 13, no. 1, pp. 51-57, DOI:10.1111/j.1442-8903.2011.00624.x.

Flannigan, MD, Krawchuk, MA, de Groot, WJ, Wotton, BM & Gowman, LM 2009, 'Implications of changing climate for global wildland fire', *International Journal of Wildland Fire*, vol. 18, pp. 483-507, DOI:10.1071/WF08187.

Fletcher, M-S, Benson, A, Heijnis, H, Gadd, PS, Cwynar, LC & Rees, ABH 2015, 'Changes in biomass burning mark the onset of an ENSO-influenced climate regime at 42°S in southwest Tasmania, Australia', *Quaternary Science Reviews*, vol. 122, pp. 222-232, DOI:10.1016/j.quascirev.2015.05.002.

Flinders, M 1814, *A Voyage to Terra Australis*, G. & W. Nicol, London.

Fox, ID, Neldner, VJ, Wilson, GW & Bannink, PJ 2001, *The Vegetation of the Australian Tropical Savannas*, Queensland Government, Brisbane.

France, I, Duller, AWG, Duller, GAT & Lamb, HF 2000, 'A new approach to automated pollen analysis', *Quaternary Science Reviews*, vol. 19, pp. 537-546, DOI:10.1016/S0277-3791(99)00021-9.

Gammage, B 2012, *The Biggest Estate on Earth*, Allen & Unwin, New South Wales.

Genever, M, Grindrod, J & Barker, B 2003, 'Holocene palynology of Whitehaven Swamp, Whitsunday Island, Queensland, and implications for the regional archaeological record', *Palaeogeography, Palaeoclimatology, Palaeoecology*, vol. 201, pp. 141-156, DOI:10.1016/S0031-0182(03)00542-X.

George, T 2013, *Fire: and the Story of Burning Country*, Cyclops Press, Avalon, NSW.

Geoscience Australia 2015, *SRTM 1 sec DEM Image*, Dataset, Australian Government, Canberra.

Geoscience Australia 2018, *Water Observations from Space (WOfS) Filtered Statistics*, Dataset, Australian Government, Canberra.

Glasspool, IJ, Edwards, D & Axe, L 2004, 'Charcoal in the Silurian as evidence for the earliest wildfire', *Geology*, vol. 32, no. 5, pp. 381-383, DOI:10.1130/G20363.1.

Golding, AS 1961, 'Determination of dissolved radium', *Analytical Chemistry*, vol. 33, p. 406, DOI:10.1021/ac60171a030.

Google Earth 2018a, *Big Willum Swamp, Weipa, Queensland, 12°39'22"S, 141°59'54"E, elevation 31m*, viewed 13 June 2018, <http://www.google.com/earth/index.html>.

Google Earth 2018b, *Cape York Peninsula, Queensland, 12°27'00"S, 144°31'11"E*, viewed 22 August 2018, <http://www.google.com/earth/index.html>.

Google Earth 2018c, *Coen, Queensland, 13°56'50"S, 143°12'32"E, elevation 203m*, viewed 9 September 2019, <http://www.google.com/earth/index.html >.

Google Earth 2018d, *Gulf of Carpentaria, 13°48'19"S, 139°56'12"E*, viewed 5 October 2018, <http://www.google.com/earth/index.html>.

Google Earth 2018e, *Kendall River Station, Queensland, 13°50'50"S, 142°07'01"E, elevation 63m*, viewed 9 September 2019, <http://www.google.com/earth/index.html >.

Google Earth 2018f, *Marura sinkhole, Arnhem Land, Northern Territory, 13°24'34"S, 135°46'29"E, elevation 50m*, viewed 19 October 2016, <http://www.google.com/earth/index.html>.

Google Earth 2018g, *Sanamere Lagoon, Cape York Peninsula, Queensland, 11°07'19'S, 142°21'32"E, elevation 16m*, viewed 19 February 2018, <http://www.google.com/earth/index.html>.

Grimes, K & Spate, A 2008, 'Laterite karst', *Australasian Cave & Karst Management Association Journal*, vol. 73, pp. 49-52.

Haberle, SG 2005, 'A 23,000-yr pollen record from Lake Euramoo, Wet Tropics of NE Queensland, Australia', *Quaternary Research*, vol. 64, pp. 343-356, DOI:10.1016/j.yqres.2005.08.013.

Haberle, SG & David, B 2004, 'Climates of change: Human dimensions of Holocene environmental change in low latitudes of the PEPII transect', *Quaternary International*, vol. 118-119, pp. 165-179, DOI:10.1016/S1040-6182(03)00136-8.

Haberle, SG, Hope, GS & van der Kaars, S 2001, 'Biomass burning in Indonesia and Papua New Guinea: Natural and human induced fire events in the fossil record',

Palaeogeography, Palaeoclimatology, Palaeoecology, vol. 171, pp. 259-268, DOI:10.1016/S0031-0182(01)00248-6.

Haberle, SG, Rule, S, Roberts, P, Heijnis, H, Jacobsen, G, Turney, C, Cosgrove, R, Ferrier, A, Moss, P, Mooney, S & Kershaw, P 2010, 'Paleofire in the wet tropics of northeast Queensland, Australia', *PAGES News*, vol. 18, no. 2, pp. 78-80, DOI:10.22498/pages.18.2.78.

Hahn, A, Kliem, P, Oehlerich, M, Ohlendorf, C, Zolitschka, B & the PASADO Science Team 2014, 'Elemental composition of the Laguna Potrok Aike sediment sequence reveals paleoclimatic changes over the past 51 ka in southern Patagonia, Argentina', *Journal of Paleolimnology*, vol. 52, pp. 349-366, DOI:10.1007/s10933-014-9798-y.

Haines, PW, Rawlings, D, Sweet, I, Pietsch, B, Plumb, K, Madigan, T & Krassay, A 1999, *Blue Mud Bay, Northern Territory: 1:250 000 Scale Geological Series, Explanatory Notes*, Northern Territory Geological Survey, Darwin.

Hardy, M, Nelson, R & Holmes, JH 1995, *Land Tenure Systems and Issues in Cape York Peninsula. (Cape York Peninsula Land Use Strategy),* Office of the Co-Ordinator General of Queensland, Brisbane, Department of the Environment, Sport and Territories, Canberra, Queensland Department of Lands, Brisbane & University of Queensland, Brisbane.

Hart, CW & Pilling, AR 1960, *The Tiwi of North Australia*, Henry Holt & Company, New York.

Haug, GH, Hughen, KA, Sigman, DM, Peterson, LC & Röhl, U 2001, 'Southward migration of the Intertropical Convergence Zone through the Holocene', *Science*, vol. 293, no. 5533, pp. 1304-1308, DOI:10.1126/science.1059725.

Hawthorne, D & Mitchell, FJG 2016, 'Identifying past fire regimes throughout the Holocene in Ireland using new and established methods of charcoal analysis', *Quaternary Science Reviews*, vol. 137, pp. 45-53, DOI:10.1016/j.quascirev.2016.01.027.

He, T, Lamont, BB & Pausas, JG 2019, 'Fire as a key driver of Earth's biodiversity', *Biological Reviews*, vol. 94, no. 6, pp. 1983-2010, DOI:10.1111/brv.12544.

Head, L 1994, 'Landscapes socialised by fire: Post-contact changes in Aboriginal fire use in northern Australia, and implications for prehistory', *Archaeology in Oceania*, vol. 29, no. 3, pp. 172-181, DOI:10.1002/arco.1994.29.3.172.

Head, L & Fullager, R 1992, 'Palaeoecology and archaeology in the east Kimberley', *Quaternary Australasia*, vol. 10, no. 1, pp. 27-31.

Heeres, JE 1899, *The Part Borne by the Dutch in the Discovery of Australia 1606-1765*, Luzac, London.

Hesse, PP, Magee, JW & van der Kaars, S 2004, 'Late Quaternary climates of the Australian arid zone: A review', *Quaternary International*, vol. 118-119, pp. 87-102, DOI:10.1016/S1040-6182(03)00132-0.

Higuera, PE, Brubaker, LB, Anderson, PM, Hu, FS & Brown, TA 2009, 'Vegetation mediated the impacts of postglacial climate change on fire regimes in the south-central Brooks Range, Alaska', *Ecological Monographs*, vol. 79, no. 2, pp. 201-219, DOI:10.1890/07-2019.1.

Higuera, PE, Sprugel, DG & Brubaker, LB 2005, 'Reconstructing fire regimes with charcoal from small-hollow sediments: A calibration with tree-ring records of fire', *The Holocene*, vol. 15, no. 2, pp. 238-251, DOI:10.1191/0959683605hl789rp.

Hill, R, Griggs, P & Bamanga Bubu Ngadimunku Incorporated 2000, 'Rainforests, agriculture and Aboriginal fire-regimes in wet tropical Queensland, Australia', *Australian Geographical Studies*, vol. 38, no. 2, pp. 138-157, DOI:10.1111/1467-8470.00108.

Hiscock, P 1994, 'Technological responses to risk in Holocene Australia', *Journal of World Prehistory*, vol. 8, no. 3, pp. 267-292, DOI:10.1007/BF02221051.

Hiscock, P 1997, 'Archaeological evidence for environmental change in Darwin Harbour', in JR Hanley, G Caswell, D Megirian & HK Larson (eds), *Proceedings of the Sixth International Marine Biological Workshop: The Marine Flora and Fauna of Darwin Harbour, Northern Territory, Australia*, Museums and Art Galleries of the Northern Territory & the Australian Marine Sciences Association, Darwin, pp. 445-449.

Hiscock, P & Faulkner, P 2006, 'Dating the Dreaming? Creation of myths and rituals for mounds along the northern Australian coastline', *Cambridge Archaeological Journal*, vol. 16, no. 2, pp. 209-222, DOI:10.1017/S0959774306000126.

Hiscock, P & Hughes, P 2001, 'Prehistoric and World War II use of shell mounds in Darwin Harbour', *Australian Archaeology*, vol. 52, pp. 41-45, DOI:10.1080/03122417.2001.11681701.

Hogg, AG, Hua, Q, Blackwell, PG, Niu, M, Buck, CE, Guilderson, TP, Heaton, TJ, Palmer, JG, Reimer, PJ, Reimer, RW, Turney, CSM & Zimmerman, SRH 2013, 'SHCal13 Southern Hemisphere calibration, 0-50,000 years cal BP', *Radiocarbon* vol. 55, no. 4, pp. 1889-1903, DOI:10.2458/azu_js_rc.55.16783.

Holdaway, SJ, Fanning, PC, Petchey, F, Allely, K, Shiner, KI & Bailey, G 2017, 'Temporal variability in shell mound formation at Albatross Bay, northern Australia', *PLoS ONE*, vol. 12, no. 18, article no. e0183863, DOI:10.1371/journal.pone.0183863.

Holden & Dixon 2018 *A Climate Dividend for Australians*, University of New South Wales, viewed 12 November 2019, <https://www.grandchallenges.unsw.edu.au/sites/default/files/2019-03/Australian%20Climate%20Dividend%20Plan_0.pdf>.

Horsfall, N & Morrison, M 2010, *Cape York Peninsula Cultural Story: Non-Indigenous and Shared History*, Australian Government, Canberra.

Hua, Q, Jacobsen, GE, Zoopi, U, Lawson, EM, Williams, AA, Smith, AM & McGann, MJ 2001, 'Progress in radiocarbon target preparation at the ANTARES AMS Centre', *Proceedings of the 17th International Radiocarbon Conference Part 1*, vol. 43, no. 2A, pp. 275-282, DOI:10.1017/S003382220003811X.

International Commission on Stratigraphy 2019, *ICS v2019/05*, International Commission on Stratigraphy, viewed 7 October 2019, <http://stratigraphy.org/ICSchart/ChronostratChart2019-05.pdf>.

Iversen, J 1941, 'Landnam i Danmarks stenalder (Land occupation in Denmark's Stone Age)', *Danmarks Geologiske Undersogelse*, vol. 66, pp. 1-68.

Jardine, F & Jardine, A 1867, *Narrative of the Overland Expedition of the Messrs. Jardine, from Rockhampton to Cape York, Northern Queensland*, J.W. Buxton, Brisbane.

Jensen, K, Lynch, EA, Calcote, R & Hotchkiss, SC 2007, 'Interpretation of charcoal morphotypes in sediments from Ferry Lake, Wisconsin, USA: Do different plant fuel sources produce distinctive charcoal morphotypes?', *The Holocene*, vol. 17, no. 7, pp. 907-915, DOI:10.1177/0959683607082405.

Johnston, S 2016, 'Indigenous innovation could save a billion tonnes of greenhouse gases', *The Conversation*, viewed 31 October 2019, <https://theconversation.com/indigenous-innovation-could-save-a-billion-tonnes-of-greenhouse-gases-57720>.

Keeley, JE 2009, 'Fire intensity, fire severity and burn severity: A brief review and suggested usage', *International Journal of Wildland Fire*, vol. 18, pp. 116-126, DOI:10.1071/WF07049.

Kellett, C, Visontay, E & Gair, K 2019, 'NSW, Queensland fires emergency: Homes lost as bushfires ravage two states', *The Australian*, viewed 12 November 2019, <https://www.theaustralian.com.au/nation/nsw-fires-emergency-warnings-issued-for-fires-in-forster-port-macquarie-hillville/news-story/5e60f35550fb35c3477ae7dedcb9cc8a>.

Kelly, RF, Higuera, PE, Barrett, CM & Hu, FS 2011, 'A signal-to-noise index to quantify the potential for peak detection in sediment-charcoal records', *Quaternary Research*, vol. 75, pp. 11-17, DOI:10.1016/j.yqres.2010.07.011.

Kershaw, AP 1971, 'A pollen diagram from Quincan Crater, north-east Queensland, Australia', *The New Phytologist*, vol. 70, no. 4, pp. 669-681, DOI:10.1111/j.1469-8137.1971.tb02567.x.

Kershaw, AP 1976, 'A late Pleistocene and Holocene pollen diagram from Lynch's Crater, north-eastern Queensland, Australia', *The New Phytologist*, vol. 77, no. 2, pp. 469-498, DOI:10.1111/j.1469-8137.1976.tb01534.x.

Kershaw, AP 1983, 'A Holocene pollen diagram from Lynch's Crater, north-eastern Queensland, Australia', *The New Phytologist*, vol. 94, no. 4, pp. 669-682, DOI:10.1111/j.1469-8137.1983.tb04875.x.

Kershaw, AP, Bretherton, SC & van der Kaars, S 2007, 'A complete pollen record of the last 230 ka from Lynch's Crater, north-eastern Australia', *Palaeogeography, Palaeoclimatology, Palaeoecology*, vol. 251, pp. 23-45, DOI:10.1016/j.palaeo.2007.02.015.

Kimber, RG 1998, 'Learning about fire: Western Desert Aborigines', in NM Williams & G Baines (eds), *Traditional Ecological Knowledge*, Australian National University, Canberra, pp. 121-125.

Kottek, M, Grieser, J, Beck, C, Rudolf, B & Rubel, F 2006 'World map of the Köppen-Geiger climate classification updated', *Meteorologische Zeitschrift*, vol. 15, no. 3, pp. 259-263, DOI:10.1127/0941-2948/2006/0130.

Kylander, ME, Ampel, L, Wohlfarth, B & Veres, D 2011, 'High-resolution X-ray fluorescence core scanning analysis of Les Echets (France) sedimentary sequence: New insights from chemical proxies', *Journal of Quaternary Science*, vol. 26, no. 1, pp. 109-117, DOI:10.1002/jqs.1438.

Laird, LD & Campbell, ID 2000, 'High resolution palaeofire signals from Christina Lake, Alberta: A comparison of the charcoal signals extracted by two different methods', *Palaeogeography, Palaeoclimatology, Palaeoecology*, vol. 164, pp. 111-123, DOI:10.1016/S0031-0182(00)00179-6.

Laynhapuy Homelands Aboriginal Corporation 2017a, *Balma*, Laynhapuy Homelands Aboriginal Corporation, viewed 20 September 2018, <https://www.laynhapuy.com.au/our-homelands/balma/>.

Laynhapuy Homelands Aboriginal Corporation 2017b, *Yirralka Rangers*, Laynhapuy Homelands Aboriginal Corporation, Nhulunbuy, Northern Territory, viewed 20

September 2018, <https://www.laynhapuy.com.au/services/yirralka-rangers-land-sea-management/>.

Lees, BG 1992, 'Geomorphological evidence for late Holocene climatic change in northern Australia', *Australian Geographer*, vol. 23, no. 1, pp. 1-10, DOI:10.1080/00049189208703048.

Lentfer, CJ, Felgate, MW, Mills, RA & Specht, J 2013, 'Human history and palaeoenvironmental change at Site 17, Freshwater Beach, Lizard Island, northeast Queensland, Australia', *Queensland Archaeological Research*, vol. 16, pp.141-164, DOI:10.25120/qar.16.2013.227.

Leys, B, Brewer, SC, McConaghy, S, Mueller, J & McLauchlan, KK 2015, 'Fire history reconstruction in grassland ecosystems: Amount of charcoal reflects local area burned', *Environmental Research Letters*, vol. 10, article no. 114009, DOI:10.1088/1748-9326/10/11/114009.

Leys, BA, Commerford, JL & McLauchlan, KK 2017, 'Reconstructing grassland fire history using sedimentary charcoal: Considering count, size and shape', *PLoS ONE*, vol. 12, no. 4, article no. e0176445, DOI:10.1371/journal.pone.0176445.

Lim, TP & Dave, NK 1981, 'A rapid method of ^{226}Ra analysis in water samples using an alpha-spectrometric technique', *CIM Bulletin*, vol. 74, p. 97, DOI:10.1016/s0969-8043(03)00172-6.

Lim, TP, Dave, NK & Cloutier, NR 1989, 'High resolution alpha spectrometry for radium analysis – The effects of sample thickness and filter pore size', *International Journal of Applied Radiation and Isotopes*, vol. 40, no. 1 Part A: Applied Radiation and Isotopes, pp. 63-71, DOI:10.1016/0883-2889(89)90175-5.

Liu, X, Colman, SM, Brown, ET, Minor, EC & Li, H 2013, 'Estimation of carbonate, total organic carbon, and biogenic silica content by FTIR and XRF techniques in lacustrine sediments', *Journal of Paleolimnology*, vol. 50, pp. 387-398, DOI:10.1007/s10933-013-9733-7.

Lobb, J 2015, 'A Palaeoenvironmental and Palaeofire Record from Dunphy Lake, Warrumbungle Mountains, South-Eastern Australia', Master of Research thesis, Macquarie University.

Loos, N 1974, 'Aboriginal-Dutch relations in north Queensland, 1606-1756', *Queensland Heritage*, vol. 3, pp. 3-8.

Loos, N 1982, *Invasion and Resistance: Aboriginal-European Relations on the North Queensland Frontier 1861-1897,* Australian National University Press, Canberra.

Lourandos, H & Ross, A 1994, 'The great 'Intensification Debate': Its history and place in Australian archaeology', *Australian Archaeology*, vol. 39, pp. 54-63, DOI:10.1080/03122417.1994.11681528.

Luly, JG, Grindrod, JF & Penny, D 2006, 'Holocene palaeoenvironments and change at Three-Quarter Mile Lake, Silver Plains Station, Cape York Peninsula, Australia', *The Holocene*, vol. 16, no. 8, pp. 1085-1094, DOI:10.1177/0959683606069398.

Lynch, JA, Clark, JS & Stocks, BJ 2004, 'Charcoal production, dispersal and deposition from the Fort Providence experimental fire: Interpreting fire regimes from charcoal records in boreal forests', *Canadian Journal of Forest Research*, vol. 34, pp. 1642-1656, DOI:10.1139/x04-071.

MacDonald, GM, Larsen, CPS, Szeicz, JM & Moser, KA 1991, 'The reconstruction of boreal forest fire history from lake sediments: A comparison of charcoal, pollen,

sedimentological, and geochemical indices', *Quaternary Science Reviews*, vol. 10, pp. 53-71, DOI:10.1016/0277-3791(91)90030-X.

Mackenzie, L, Heijnis, H, Gadd, P, Moss, P & Shulmeister, J 2017, 'Geochemical investigation of the South Wellesley Island wetlands: Insight into wetland development during the Holocene in tropical northern Australia', *The Holocene*, vol. 27, no. 4, pp. 566-578, DOI:10.1177/0959683616670219.

Martin, L, Mooney, S & Goff, J 2014, 'Coastal wetlands reveal a non-synchronous island response to sea-level change and a palaeostorm record from 5.5 kyr to present', *The Holocene*, vol. 24, no. 5, pp. 569-580, DOI:10.1177/0959683614522306.

Maruyama, TM, Oliveira, LS, Britto Jr, AS & Nisgoski, S 2018, 'Automatic classification of native wood charcoal', *Ecological Informatics*, vol. 46, pp. 1-7, DOI:10.1016/j.ecoinf.2018.05.008.

Masiello, CA 2004, 'New directions in black carbon organic geochemistry', *Marine Chemistry*, vol. 92, pp. 201-213, DOI:10.1016/j.marchem.2004.06.043.

May, SM, Brill, D, Leopold, M, Callow, JN, Engel, M, Scheffers, A, Opitz, S, Norpoth, M & Brückner, H 2017, 'Chronostratigraphy and geomorphology of washover fans in the Exmouth Gulf (NW Australia) – A record of tropical cyclone activity during the late Holocene', *Quaternary Science Reviews*, vol. 169, pp. 65-84, DOI:10.1016/j.quascirev.2017.05.023.

McGowan, H, Marx, S, Moss, P & Hammond, A 2012, 'Evidence of ENSO mega-drought triggered collapse of prehistory Aboriginal society in northwest Australia', *Geophysical Research Letters*, vol. 39, p. L22702, DOI:10.1029/2012GL053916.

McGregor, HV & Gagan, MK 2004, 'Western Pacific coral $\delta^{18}O$ records of anomalous Holocene variability in the El Niño-Southern Oscillation', *Geophysical Research letters*, vol. 31, article no. L11204, DOI:10.1029/2004GL019972.

McMillan, A 2008, *An Intruder's Guide to East Arnhem Land*, Niblock Publishing, Northern Territory.

McWethy, DB, Haberle, SG, Hopf, F & Bowman, DMJS 2017, 'Aboriginal impacts on fire and vegetation on a Tasmanian island', *Journal of Biogeography*, vol. 44, pp. 1319-1330, DOI:10.1111/jbi.12935.

Meredith, W, Ascough, PL, Bird, MI, Large, DJ, Snape, CE, Sun, Y & Tilston, EL 2012, 'Assessment of hydropyrolysis as a method for the quantification of black carbon using standard reference materials', *Geochimica et Cosmochimica Acta*, vol. 97, pp. 131-147, DOI:10.1016/j.gca.2012.08.037.

Miller, G, Mangan, J, Pollard, D, Thompson, S, Fetzer, B & Magee, J 2005, 'Sensitivity of the Australian Monsoon to insolation and vegetation: Implications for human impact on continental moisture balance', *Geology*, vol. 33, no. 1, pp. 65-68, DOI:10.1130/G21033.1.

Millspaugh, SH & Whitlock, C 1995, 'A 750-year fire history based on lake sediment records in central Yellowstone National Park, USA', *The Holocene*, vol. 5, no. 3, pp. 283-292, DOI:10.1177/095968369500500303.

Mitchell, S 1993, 'Shell mound formation in northern Australia: A case study from Croker Island, northwestern Arnhem Land', *The Beagle: Records of the Northern Territory Museum of Arts and Sciences*, vol. 10, no. 1, pp.179-192.

Mooney, SD & Tinner, W 2011, 'The analysis of charcoal in peat and organic sediments', *Mires and* Peat, vol. 7, pp. 1-18.

Mooney, SD, Harrison, SP, Bartlein, PJ, Daniau, A-L, Stevenson, J, Brownlie, KC, Buckman, S, Cupper, M, Luly, J, Black, M, Colhoun, E, D'Costa, D, Dodson, J, Haberle, S, Hope, GS, Kershaw, P, Kenyon, C, McKenzie, M & Williams, N 2011, 'Late Quaternary fire regimes of Australasia', *Quaternary Science Reviews*, vol. 30, pp. 28-46, DOI:10.1016/j.quascirev.2010.10.010.

Moore, DR 1979, *Islanders and Aborigines at Cape York*, Australian Institute of Aboriginal Studies, Canberra.

Moore, G 2015, 'Home was where the hearth is: Fire, destruction, and displacement in nineteenth-century settler narratives', *Antipodes*, vol. 29, no. 1, pp. 29-42, DOI:10.13110/antipodes.29.1.0029.

Moos, MT & Cumming, BF 2012, 'Climate-fire interactions during the Holocene: A test of the utility of charcoal morphotypes in a sediment core from the boreal region of north-western Ontario (Canada)', *International Journal of Wildland Fire*, vol. 21, pp. 640-652, DOI:10.1071/WF10117.

Moreno, A, Valero-Garcés, BL, Gonazález-Sampériz, P & Rico, M 2008, 'Flood response to rainfall variability during the last 2000 years inferred from Taravilla Lake record (Central Iberian Range, Spain)', *Journal of Paleolimnology*, vol. 40, pp. 943-961, DOI:10.1007/s10933-008-9209-3.

Morrison, M 2003, 'Old boundaries and new horizons: The Weipa shell mounds reconsidered', *Archaeology in Oceania*, vol. 38, no. 1, pp. 1-8, DOI:10.1002/j.1834-4453.2003.tb00516.x.

Morrison, M 2013, 'Niche production strategies and shell matrix site variability at Albatross Bay, Cape York Peninsula', *Archaeology in Oceania*, vol. 48, no. 2, pp. 78-91, DOI:10.1002/arco.5002.

Morrison, M 2014, 'Chronological trends in late Holocene shell mound construction across northern Australia: Insights from Albatross Bay, Cape York Peninsula', *Australian Archaeology*, vol. 79, pp.1-13, DOI:10.1080/03122417.2014.11682014.

Moss, PT, Cosgrove, R, Ferrier, Å & Haberle, SG 2012, 'Holocene environments of the sclerophyll woodlands of the Wet Tropics of northeastern Australia', in SG Haberle & B David (eds), *Peopled Landscapes: Archaeological and Biogeographic Approaches to Landscapes*, Terra Australis 34, ANU E Press, Canberra, pp. 329-341.

Moss, PT & Kershaw, AP 2000, 'The last glacial cycle from the humid tropics of northeastern Australia: Comparison of a terrestrial and a marine record', *Palaeogeography, Palaeoclimatology, Palaeoecology*, vol. 155, pp. 155-176, DOI:10.1016/S0031-0182(99)00099-1.

Moss, P, Mackenzie, L, Ulm, S, Sloss, C, Rosendahl, D, Petherick, L, Steinberger, L, Wallis, L, Heijnis, H, Petchey, F & Jacobsen, G 2015, 'Environmental context for late Holocene human occupation of the South Wellesley Archipelago, Gulf of Carpentaria, northern Australia', *Quaternary International*, vol. 385, pp. 136-144: DOI:10.1016/j.quaint.2015.02.051.

Moss, PT, Ulm, S, Mackenzie, L, Wallis, LA, Rosendahl, D & Steinberger, L 2019, 'Robust local vegetation records from dense archaeological shell matrixes: A palynological analysis of the Thundiy shell deposit, Bentinck Island, Gulf of Carpentaria, Australia', *Archaeological and Anthropological Sciences*, vol. 11, pp. 511-520, DOI:10.1007/s12520-016-0394-0.

Moura, LC, Scariot, AO, Schmidt, IB, Beatty, R & Russell-Smith, J 2019, 'The legacy of colonial fire management policies on traditional livelihoods and ecological sustainability in savannas: Impacts, consequences, new directions', *Journal of Environmental Management*, vol. 232, pp. 600-606, DOI:10.1016/j.jenvman.2018.11.057.

Moy, CM, Seltzer, GO, Rodbell, DT & Anderson, DM 2002, 'Variability of El Niño/Southern Oscillation activity at millennial timescales during the Holocene epoch', *Nature*, vol. 420, pp. 162-165, DOI:10.1038/nature01194.

Mullins, CE 1977, 'Magnetic susceptibility of the soil and its significance in soil science – A review', *Journal of Soil Science*, vol. 28, pp. 223-246, DOI:10.1111/j.1365-2389.1977.tb02232.x.

Murphy, B 2013, 'Savanna burning: Carbon pays for conservation in northern Australia', *The Conversation*, viewed 31 October 2019, <https://theconversation.com/savanna-burning-carbon-pays-for-conservation-in-northern-australia-12185>.

Nanson, GC, Price, DM, Jones, BG, Maroulis, JC, Coleman, M, Bowman, H, Cohen, TJ, Pietsch, TJ & Larsen, JR 2008, 'Alluvial evidence for major climate and flow regime changes during the middle and late Quaternary in eastern central Australia', *Geomorphology*, vol. 101, pp. 109-129, DOI:10.1016/j.geomorph.2008.05.032.

National Archives of Australia 2018a, *Commonwealth Government Records about the Northern Territory Part 1: 1.4 Establishment of the Pastoral Industry*, Australian Government, viewed 20 September 2018, <http://guides.naa.gov.au/records-about-northern-territory/part1/chapter1/1.4.aspx>.

National Archives of Australia 2018b, *Commonwealth Government Records about the Northern Territory Part 2: 8.4 Establishment of Patrol Officers*, Australian

Government, viewed 20 September 2018, <http://guides.naa.gov.au/records-about-northern-territory/part2/chapter8/8.4.aspx>.

National Library of Australia 1950-1952, *Blue Mud Bay [Cartographic Material] SVY 1424 – Run 5A Frame 5115*, MAP D 53 7.

National Museum of Australia 2018, 'Old Masters: Arnhem Land', National Museum of Australia, viewed 1 June 2018, <http://www.nma.gov.au/exhibitions/old_masters/arnhem_land>.

Neldner, VJ & Clarkson, JR 1995, *Vegetation Survey and Mapping of Cape York Peninsula*, Queensland Department of Environment and Heritage, Brisbane.

Neldner, VJ, Niehus, RE, Wilson, BA, McDonald, WJF, Ford, AJ & Accad, A 2017, *The Vegetation of Queensland: Descriptions of Broad Vegetation Groups*, Department of Science, Information Technology & Innovation, Brisbane.

Nhulunbuy Corporation n.d. *Local History*, Nhulunbuy Corporation, viewed 20 September 2018, <https://www.ncl.net.au/welcome-to-nhulunbuy/local-history/>.

Norris, RP & Hamacher, DW 2009, 'The astronomy of Aboriginal Australia', *Proceedings of the International Astronomical Union*, vol. 5, article no. S260, pp. 39-47, DOI:10.1017/S1743921311002122.

Northcote, KH, Beckmann, GG, Bettenay, E, Churchward, HM, Van Dijk, DC, Dimmock, GM, Hubble, GD, Isbell, RF, McArthur, WM, Murtha, GG, Nicolls, KD, Paton, TR, Thompson, CH, Webb, AA & Wright, MJ 1960-1968, *Atlas of Australian Soils, Sheets 1 to 10 with Explanatory Data*, Commonwealth Scientific & Industrial Research Organisation & Melbourne University Press, Melbourne.

Northern Australian Fire Information [NAFI] 2019, *Fire History – North Australia & Rangelands Fire Information*, Charles Darwin University & Department of the Environment & Energy, Darwin, viewed 28 August 2019, <https://www.firenorth.org.au/nafi3/>.

Northern Land Council 2019, *Indigenous Protected Areas*, Northern Land Council, viewed 1 June 2018, <https://www.nlc.org.au/our-land-sea/caring-for-country/indigenous-protected-areas>.

Northern Territory Government 1982, *NTRS 3862/P2 1982 Arnhem Highway NTc773 Frame 110*, Aerial photograph.

Notaro, M, Wyrwoll, K-H & Chen, G 2011, 'Did Aboriginal vegetation burning impact on the Australian summer monsoon?', *Geophysical Research Letters*, vol. 38, article no. L11704, DOI:10.1029/2011GL047774.

Nott, J, Haig, J, Neil, H & Gillieson, D 2007, 'Greater frequency variability of landfalling tropical cyclones at centennial compared to seasonal and decadal scales', *Earth & Planetary Science Letters*, vol. 255, pp. 367-372, DOI:10.1016/j.epsl.2006.12.023.

Nott, J & Price, D 1999, 'Waterfalls, floods and climate change: Evidence from tropical Australia', *Earth & Planetary Science Letters*, vol. 171, pp. 267-276, DOI:10.1016/S0012-821X(99)00152-1.

Nott, JF, Price, DM & Bryant, EA 1996, 'A 30,000 year record of extreme floods in tropical Australia from relict plunge-pool deposits: Implications for future climate change', *Geophysical Research Letters*, vol. 23, no. 4, pp. 379-382, DOI:10.1029/96GL00262.

Nott, J, Smithers, S, Walsh, K & Rhodes, R 2009, 'Sand beach ridges record 6000 year history of extreme tropical cyclone activity in northeastern Australia', *Quaternary Science Reviews*, vol. 28, pp. 1511-1520, DOI:10.1016/j.quascirev.2009.02.014.

Ó Foghlú, B, Wesley, D, Brockwell, S & Cooke, H 2016, 'Implications for culture contact history from a glass artefact on a Giingwulung earth mound in Weipa', *Queensland Archaeological Research*, vol. 19, pp. 1-22, DOI:10.25120/qar.19.2016.3499.

O'Leary, MH 1988, 'Carbon isotopes in photosynthesis', *BioScience*, vol. 38, no. 5, pp. 328-336, DOI:10.2307/1310735.

OpenStreetMap Contributors 2019, *OpenStreetMap*, OpenStreetMap Foundation, viewed 27 June 2019, <https://www.openstreetmap.org/>.

Palmer, E 1903, *Early Days in North Queensland*, Angus & Robertson, Sydney.

Parr, CL & Andersen, AN 2006, 'Patch mosaic burning for biodiversity conservation: A critique of the pyrodiversity paradigm', *Conservation Biology*, vol. 20, no. 6, pp. 1610-1619, DOI:10.1111/j.1523-1739.2006.00492.x.

Pashkova, GV, Aisueva, TS, Finkelshtein, AL, Ivanov, EV & Shchetnikov, AA 2016, 'Analytical approaches for determination of bromine in sediment core samples by X-ray fluorescence spectrometry', *Talanta*, vol. 160, pp. 375-380, DOI:10.1016/j.talanta.2016.07.059.

Peel, MC, Finlayson, BL & McMahon, TA 2007, 'Updated world map of the Köppen-Geiger climate classification', *Hydrology and Earth System Sciences Discussions*, vol. 4, no. 2, pp. 439-473, DOI:10.5194/hess-11-1633-2007.

Perry, GLW, Wilmshurst, JM & McGlone, MS 2014, 'Ecology and long-term history of fire in New Zealand', *New Zealand Journal of Ecology*, vol. 38, no. 2, pp. 157-176.

Perry, JJ, Sinclair, M, Wikmunea, H, Wolmby, S, Martin, D & Martin, B 2018, 'The divergence of traditional Aboriginal and contemporary fire management practices on Wik traditional lands, Cape York Peninsula, northern Australia', *Ecological Management & Restoration*, vol. 19, no. 1, pp. 24-31, DOI:10.1111/emr.12301.

Petchey, F, Ulm, S, David, B, McNiven, IJ, Asmussen, B, Tomkins, H, Dolby, N, Aplin, K, Richards, T, Rowe, C, Leavesley, M & Mandui, H 2013, 'High-resolution radiocarbon dating of marine materials in archaeological contexts: Radiocarbon marine reservoir variability between *Anadara, Gafrarium, Batissa, Polymesoda* spp. and Echinoidea at Caution Bay, southern coastal Papua New Guinea', *Archaeological & Anthropological Sciences*, vol. 5, no. 1, pp. 69-80, DOI:10.1007/s12520-012-0108-1.

Peters, ME & Higuera, PE 2007, 'Quantifying the source area of macroscopic charcoal with a particle dispersal model', *Quaternary Research*, vol. 67, pp. 304-310, DOI:10.1016/j.yqres.2006.10.004.

Pisaric, MFJ 2002, Long-distance transport of terrestrial plant material by convection resulting from forest fires, *Journal of Paleolimnology*, vol. 28, pp. 348-354, DOI:10.1023/A:1021630017078.

Pitkänen, A, Lehtonen, H & Huttunen, P 1999, 'Comparison of sedimentary microscopic charcoal particle records in a small lake with dendrochronological data: Evidence for the local origin of microscopic charcoal produced by forest fires of low intensity in eastern Finland', *The Holocene*, vol. 9, no. 5, pp. 559-567, DOI:10.1191/095968399670319510.

Plumb, KA & Roberts, HG 1967, *Explanatory Notes on the Blue Mud Bay – Port Langdon 1:250,000 Geological Series Sheet SD53-7/8: Records 1964/67*, Bureau of Mineral

Resources, Geology & Geophysics, Commonwealth Government of Australia, Canberra.

Power, MJ, Marlon, JR, Bartlein, PJ & Harrison, SP 2010, 'Fire history and the Global Charcoal Database: A new tool for hypothesis testing and data exploration', *Palaeogeography, Palaeoclimatology, Palaeoecology*, vol. 291, pp. 52-59, DOI:10.1016/j.palaeo.2009.09.014.

Power, MJ, Marlon, J, Ortiz, N, Bartlein, PJ, Harrison, SP, Mayle, FE, Ballouche, A, Bradshaw, RHW, Carcaillet, C, Cordova, C, Mooney, S, Moreno, PI, Prentice, IC, Thonicke, K, Tinner, W, Whitlock, C, Zhang, Y, Zhao, Y, Ali, AA, Anderson, RS, Beer, R, Behling, H, Briles, C, Brown, KJ, Brunelle, A, Bush, M, Camill, P, Chu, GQ, Clark, J, Colombaroli, D, Connor, S, Daniau, A-L, Daniels, M, Dodson, J, Doughty, E, Edwards, ME, Finsinger, W, Foster, D, Frechette, J, Gaillard, M-J, Gavin, DG, Gobet, E, Haberle, S, Hallett, DJ, Higuera, P, Hope, G, Horn, S, Inoue, J, Kaltenrieder, P, Kennedy, L, Kong, ZC, Larsen, C, Long, CJ, Lynch, J, Lynch, EA, McGlone, M, Meeks, S, Mensing, S, Meyer, G, Minckley, T, Mohr, J, Nelson, DM, New, J, Newnham, R, Noti, R, Oswald, W, Pierce, J, Richard, PJH, Rowe, C, Sanchez Goñi, MF, Shuman, BN, Takahara, H, Toney, J, Turney, C, Urrego-Sanchez, DH, Umbanhowar, C, Vandergoes, M, Vanniere, B, Vescovi, E, Walsh, M, Wang, X, Williams, N, Wilmshurst, J & Zhang, JH 2008 'Changes in fire regimes since the Last Glacial Maximum: An assessment based on a global synthesis and analysis of charcoal data', *Climate Dynamics*, vol. 30, pp. 887-907, DOI:10.1007/s00382-007-0334-x.

Prajapati, S 2017, *Making Sense of Conductivity, TDS, and Concentration in Water Treatment, Sensorex*, viewed 21 October 2019, <https://sensorex.com/blog/2017/11/09/electrical-conductivity-of-water/>.

Prebble, M, Sim, R, Finn, J & Fink, D 2005, 'A Holocene pollen and diatom record from Vanderlin Island, Gulf of Carpentaria, lowland tropical Australia', *Quaternary Research*, vol. 64, pp. 357-371, DOI:10.1016/j.yqres.2005.08.005.

Preece, N 2002, 'Aboriginal fires in monsoonal Australia from historical accounts', *Journal of Biogeography*, vol. 29, pp. 321-336, DOI:10.1046/j.1365-2699.2002.00677.x.

Preece, ND 2013, 'Tangible evidence of historic Australian indigenous savanna management', *Austral Ecology*, vol. 38, pp. 241-250, DOI:10.1111/j.1442-9993.2012.02415.x.

Proske, U 2016, 'Holocene freshwater wetland and mangrove dynamics in the eastern Kimberley, Australia', *Journal of Quaternary Science*, vol. 31, no. 1, pp. 1-11, DOI:10.1002/jqs.2827.

Proske, U & Haberle, SG 2012, 'Island ecosystem and biodiversity dynamics in northeastern Australia during the Holocene: Unravelling short-term impacts and long-term drivers', *The Holocene*, vol. 22, no. 10, pp. 1097-1111, DOI:10.1177/0959683612441840.

Proske, U, Stevenson, J, Seddon, AWR & Taffs, K 2017, 'Holocene diatom records of wetland development near Weipa, Cape York, Australia', *Quaternary International*, vol. 440, pp. 42-54, DOI:10.1016/j.quaint.2016.09.014.

Pyne, SJ 1991, *Burning Bush*, Henry Holt & Company, New York.

Pyne, SJ 1997, *Vestal Fire: An Environmental History, Told Through Fire, of Europe and Europe's Encounter with the World*, University of Washington Press, Washington, USA.

Pyne, SJ 2016, 'Fire in the mind: Changing understandings of fire in Western civilization', *Philosophical Transactions of the Royal Society B*, vol. 371, p. 20150166, DOI:10.1098/rstb.2015.0166.

Queensland Government 2015a *Bamaga*, Queensland Government, viewed 1 March 2018, <https://www.qld.gov.au/atsi/cultural-awareness-heritage-arts/community-histories-bamaga>.

Queensland Government 2015b, *Mapoon*, Queensland Government, viewed 1 March 2018, <https://www.qld.gov.au/atsi/cultural-awareness-heritage-arts/community-histories-mapoon>.

Queensland Government 2015c, *Seisia*, Queensland Government, viewed 1 March 2018, <https://www.qld.gov.au/atsi/cultural-awareness-heritage-arts/community-histories-seisia>.

Queensland Government 2016, *Injinoo*, Queensland Government, viewed 1 March 2018, <https://www.qld.gov.au/atsi/cultural-awareness-heritage-arts/community-histories-injinoo>.

Queensland Government 2017a, *Napranum*, Queensland Government, viewed 1 March 2018, <https://www.qld.gov.au/atsi/cultural-awareness-heritage-arts/community-histories-napranum>.

Queensland Government 2017b, *New Mapoon*, Queensland Government, viewed 1 March 2018, <https://www.qld.gov.au/atsi/cultural-awareness-heritage-arts/community-histories-new-mapoon>.

Queensland Government 2019, *QImagery*, Queensland Government, viewed 13 June 2017, <https://qimagery.information.qld.gov.au/>.

Queensland National Parks & Wildlife Service 1996, *Visitor Information: Jardine River National Park*, Information brochure, Queensland Department of Environment, Cairns.

Quigley, MC, Horton, T, Hellstrom, JC, Cupper, ML & Sandiford, M 2010, 'Holocene climate change in arid Australia from speleothem and alluvial records', *The Holocene*, vol. 20, no. 7, pp. 1093-1104, DOI:10.1177/0959683610369508.

Raggio, O 1958, 'The myth of Prometheus: Its survival and metamorphoses up to the eighteenth century', *Journal of the Warburg & Courtauld Institutes*, vol. 21, no. 1/2, pp. 44-62, DOI:10.2307/750486.

R Development Core Team 2013, *R: A Language and Environment for Statistical Computing*, R Foundation for Statistical Computing, Vienna, Austria.

Reeves, JM, Barrows, TT, Cohen, TJ, Kiem, AS, Bostock, HC, Fitzsimmons, KE, Jansen, JD, Kemp, J, Krause, C, Petherick, L, Phipps, SJ & OZ-Intimate Members 2013a, 'Climate variability over the last 35,000 years recorded in marine and terrestrial archives in the Australian region: An OZ-INTIMATE compilation', *Quaternary Science Reviews*, vol. 74, pp. 21-34, DOI:10.1016/j.quascirev.2013.01.001.

Reeves, JM, Bostock, HC, Ayliffe, LK, Barrows, TT, De Deckker, P, Devriendt, LS, Dunbar, GB, Drysdale, RN, Fitzsimmons, KE, Gagan, MK, Griffiths, ML, Haberle, SG, Jansen, JD, Krause, C, Lewis, S, McGregor, HV, Mooney, SD, Moss, P, Nanson, GC, Purcell, A & van der Kaars, S 2013b, 'Palaeoenvironmental change in tropical Australasia over the last 30,000 years – A synthesis by the OZ-INTIMATE group', *Quaternary Science Reviews*, vol. 74, pp. 97-114, DOI:10.1016/j.quascirev.2012.11.027.

Rio Tinto 2017, *Weipa Operations Sustainable Development Report*, Rio Tinto, Weipa.

RMIT ABC Fact Check 2019, 'Were Queensland fire danger indices historically high for early September?', *ABC News*, viewed 15 November 2019, <https://www.abc.net.au/news/2019-11-14/fact-check-did-high-fire-danger-indices-come-earlier-this-year/11506082>.

Robins, RP, Stock, EC & Trigger, DS 1998, 'Saltwater people, saltwater country: Geomorphological, anthropological and archaeological investigations of the coastal lands in the southern gulf country of Queensland', *Memoirs of the Queensland Museum*, vol. 1, no. 1, pp. 75-125.

Rosendahl, D, Lowe, KM, Wallis, LA & Ulm, S 2014, 'Integrating geoarchaeology and magnetic susceptibility at three shell mounds: A pilot study from Mornington Island, Gulf of Carpentaria, Australia', *Journal of Archaeological Science*, vol. 49, pp. 21-32, DOI:10.1016/j.jas.2014.04.017.

Rowe, C 2005, 'A Holocene History of Vegetation Change in the Western Torres Strait Region, Queensland, Australia', PhD thesis, Monash University, Clayton.

Rowe, C 2006, 'Landscapes in western Torres Strait history', in B David, B Barker & IJ McNiven (eds), *Social Archaeology of Australian Indigenous Societies*, Aboriginal Studies Press, Canberra, pp. 270-286.

Rowe, C 2007, 'A palynological investigation of Holocene vegetation change in Torres Strait, seasonal tropics of northern Australia', *Palaeogeography, Palaeoclimatology, Palaeoecology*, vol. 251, pp. 83-103, DOI:10.1016/j.palaeo.2007.02.019.

Rowe, C, Brand, M, Hutley, LB, Wurster, C, Zwart, C, Levchenko, V & Bird, M 2019, 'Holocene savanna dynamics in the seasonal tropics of northern Australia', *Review of Palaeobotany & Palynology*, vol. 267, pp. 17-31, DOI:10.1016/j.revpalbo.2019.05.004.

Rull, V, Montoya, E, Vegas-Vilarrúbia, T & Ballesteros, T 2015, 'New insights on palaeofires and savannisation in northern South America', *Quaternary Science Reviews*, vol. 122, pp. 158-165, DOI:10.1016/j.quascirev.2015.05.032.

Russell-Smith, J 1985, 'A record of change: Studies of Holocene vegetation history in the South Alligator River Region, Northern Territory', *Proceedings of the Ecological Society of Australia*, vol. 13, pp. 191-202.

Russell-Smith, J 2001, 'Pre-contact Aboriginal and contemporary fire regimes of the savanna landscapes of northern Australia: Patterns, changes and ecological responses', *Ngoonjook*, pp. 6-32.

Russell-Smith, J, Cook, GD, Cooke, PM, Edwards, AC, Lendrum, M, Meyer, CP & Whitehead, PJ 2013, 'Managing fire regimes in north Australian savannas: Applying Aboriginal approaches to contemporary global problems', *Frontiers in Ecology & the Environment*, vol. 11, no. 1, pp. e55-e63, DOI:10.1890/120251.

Russell-Smith, J & Edwards, AC 2006, 'Seasonality and fire severity in savanna landscapes of monsoonal northern Australia', *International Journal of Wildland Fire*, vol. 15, pp. 541-550, DOI:10.1071/WF05111.

Russell-Smith, J, Lucas, D, Gapindi, M, Gunbunuka, B, Kapirigi, N, Namingum, G, Lucas, K, Giuliani, P & Chaloupka, G 1997, 'Aboriginal resource utilization and fire management practice in western Arnhem Land, monsoonal northern Australia', *Human Ecology*, vol. 25, no. 2, pp. 159-195, DOI:10.1023/A:1021970021670.

Sáez, A, Valero-Garcés, BL, Giralt, S, Moreno, A, Bao, R, Pueyo, JJ, Hernández, A & Casas, D 2009, 'Glacial to Holocene climate changes in the SE Pacific: The Raraku Lake sedimentary record (Easter Island, 27°S)', *Quaternary Science Reviews*, vol. 28, pp. 2743-2759, DOI:10.1016/j.quascirev.2009.06.018.

Saiz, G, Goodrick, I, Wurster, C, Nelson, PN, Wynn, J & Bird, M 2018, 'Preferential production and transport of grass-derived pyrogenic carbon in NE-Australian savanna

ecosystems', *Frontiers in Earth Science*, vol. 5, pp. 1-13, DOI:10.3389/feart.2017.00115.

Saiz, G, Wynn, JG, Wurster, CM, Goodrick, I, Nelson, PN & Bird, MI 2015, 'Pyrogenic carbon from tropical savanna burning: Production and stable isotope composition', *Biogeosciences*, vol. 12, pp. 1849-1863, DOI:10.5194/bg-12-1849-2015.

Sakaguchi, S, Bowman, DMJS, Prior, LD, Crisp, MD, Linde, CC, Tsumura, Y & Isagi, Y 2013, 'Climate, not Aboriginal landscape burning, controlled the historical demography and distribution of fire-sensitive conifer populations across Australia', *Proceedings of the Royal Society B*, vol. 280, p. 20132182, DOI:10.1098/rspb.2013.2182.

Sánchez Goñi, MF, Desprat, S, Daniau, A-L, Bassinot, FC, Polanco-Martínez, JM, Harrison, SP, Allen, JRM, Anderson, RS, Behling, H, Bonnefille, R, Burjachs, F, Carrión, JS, Cheddadi, R, Clark, JS, Combourieu-Nebout, N, Courtney Mustaphi, CJ, Debusk, GH, Dupont, LM, Finch, JM, Fletcher, WJ, Giardini, M, González, C, Gosling, WD, Grigg, LD, Grimm, EC, Hayashi, R, Helmens, K, Heusser, LE, Hill, T, Hope, G, Huntley, B, Igarashi, Y, Irino, T, Jacobs, B, Jiménez-Moreno, G, Kawai, S, Kershaw, P, Kumon, F, Lawson, IT, Ledru, M-P, Lézine, A-M, Liew, PM, Magri, D, Marchant, R, Margari, V, Mayle, FE, McKenzie, M, Moss, P, Müller, S, Müller, UC, Naughton, F, Newnham, RM, Oba, T, Pérez-Obiol, R, Pini, R, Ravazzi, C, Roucoux, KH, Rucina, SM, Scott, L, Takahara, H, Tzedakis, PC, Urrego, DH, van Geel, B, Valenzia, BG, Vandergoes, MJ, Vincens, A, Whitlock, CL, Willard, DA & Tamamoto, M 2017, 'The ACER pollen and charcoal database: A global resource to document vegetation and fire response to abrupt climate changes during the last glacial period', *Earth System Science Data*, vol. 9, pp. 679-695, DOI:10.5194/essd-9-679-2017.

Santschi, P, Höhener, P, Benoit, G & Buchholtz-ten Brink, M 1990, 'Chemical processes at the sediment-water interface', *Marine Chemistry*, vol. 30, pp. 269-315, DOI:10.1016/0304-4203(90)90076-O.

Schüpbach, S, Kirchgeorg, T, Colombaroli, D, Beffa, G, Radaelli, M, Kehrwald, NM & Barbante, C 2015, 'Combining charcoal sediment and molecular markers to infer a Holocene fire history in the Maya Lowlands of Petén, Guatemala', *Quaternary Science Reviews*, vol. 115, pp. 123-131, DOI:10.1016/j.quascirev.2015.03.004.

Scott, AC 2000, 'The pre-Quaternary history of fire', *Palaeogeography, Palaeoclimatology, Palaeoecology*, vol. 164, pp. 281-329, DOI:10.1016/S0031-0182(00)00192-9.

Scott, K, Setterfield, SA, Douglas, MM, Parr, CL, Schatz, J & Andersen, AN 2012, 'Does long-term fire exclusion in an Australian tropical savanna result in a biome shift? A test using the reintroduction of fire', *Austral Ecology*, vol. 37, pp. 693-711, DOI:10.1111/j.1442-9993.2012.02379.x.

Shine, D, Wright, D, Denham, T, Aplin, K, Hiscock, P, Parker, K & Walton, R 2013, 'Birriwilk rockshelter: A mid- to late Holocene site in Manilikarr Country, southwest Arnhem Land, Northern Territory', *Australian Archaeology*, vol. 76, no. 1, pp. 69-78, DOI:10.1080/03122417.2013.11681967.

Shine, D, Marshall, M, Wright, D, Denham, T, Hiscock, P, Jacobsen, G & Stephens, S-P 2015, 'The archaeology of Bindjarran rockshelter in Manilikarr Country, Kakadu National Park, Northern Territory', *Australian Archaeology*, vol. 80, no. 1, pp. 104-111, DOI:10.1080/03122417.2015.11682050.

Shine, D, Hiscock, P & Denham, T 2016, 'The archaeology of Ingaanjalwurr rockshelter in Manilikarr Country, western Arnhem Land', *Australian Archaeology*, vol. 82, no. 1, pp. 67-75, DOI:10.1080/03122417.2016.1163941.

Shiner, JS, Fanning, PC, Holdaway, SJ, Petchey, F, Beresford, C, Hoffman, E & Larsen B 2013, 'Shell mounds as the basis for understanding human-environment interaction in far north Queensland, Australia', *Queensland Archaeological Research*, vol. 16, pp. 65-91, DOI:10.25120/qar.16.2013.224.

Shiner, J & Morrison, M 2009, 'The contribution of heritage surveys towards understanding the cultural landscape of the Weipa bauxite plateau', *Australian Archaeology*, vol. 68, no. 1, pp. 52-55, DOI:10.1080/03122417.2009.11681890.

Shlisky, A, Waugh, J, Gonzalez, P, Gonzalez, M, Manta, M, Santoso, H, Alvarado, E, Ainuddin Nuruddin, A, Rodriguez-Trejo, DA, Swaty, R, Schmidt, D, Kaufmann, M, Myers, R, Alencar, A, Kearns, F, Johnson, D, Smith J & Zollner, D 2007, 'Fire, ecosystems and people: Threats and strategies for global biodiversity conservation', *GFI Technical Report 2007-2*, The Nature Conservancy.

Shulmeister, J 1992, 'A Holocene pollen record from lowland tropical Australia', *The Holocene*, vol. 2, no. 2, pp. 107-116, DOI:10.1177/095968369200200202.

Shulmeister, J 1999, 'Australasian evidence for mid-Holocene climate change implies precessional control of Walker Circulation in the Pacific', *Quaternary International*, vol. 57-58, pp. 81-91, DOI:10.1016/S1040-6182(98)00052-4.

Shulmeister, J & Lees, BG 1995, 'Pollen evidence from tropical Australia for the onset of an ENSO-dominated climate at c. 4000 BP', *The Holocene*, vol. 5, no. 1, pp. 10-18, DOI:10.1177/095968369500500102.

Siegert, F, Ruecker, G, Hinrichs, A & Hoffmann, AA 2001, 'Increased damage from fires in logged forests during droughts caused by El Niño', *Nature*, vol. 414, pp. 437-440, DOI:10.1038/35106547.

Sim, R & Wallis, L 2008, 'Northern Australian offshore island use during the Holocene: The archaeology of Vanderlin Island, Sir Edward Pellew Group, Gulf of Carpentaria', *Australian Archaeology*, vol. 67, pp. 95-106, DOI:10.1080/03122417.2008.11681882.

Smart, J, Grimes, KG, Doutch, HF & Pinchin, J 1980, *The Carpentaria and Karumba Basins, North Queensland*, Australian Government Printing Service, South Australia.

South Australian History 2018, *Northern Territory History: Early Settlements*, Flinders Ranges Research, viewed 20 September 2018, <https://www.southaustralianhistory.com.au/nthistory1.htm>.

South Australian Register 1885, 'Government Gazette: Proclamation of the Town of Borroloola, Northern Territory', *South Australian Register*, 11 September, p. 5.

State Library of South Australia 2007, *Taking it to the Edge: Land: David Lindsay*, Government of South Australia, viewed 20 September 2018, <http://www.samemory.sa.gov.au/site/page.cfm?u=207>.

Steinke, S, Mohtadi, M, Prange, M, Varma, V, Pittauerova, D & Fischer, HW 2014, 'Mid- to late-Holocene Australian-Indonesian summer monsoon variability', *Quaternary Science Reviews*, vol. 93, pp. 142-154, DOI:10.1016/j.quascirev.2014.04.006.

Stephens, K & Head, L 1995, 'Palaeoecology of archaeological and swamp sites in SE Cape York Peninsula', in MJ Morwood & DR Hobbs (eds), *Quinkan Prehistory: The Archaeology of Aboriginal Art in Southeast Cape York Peninsula, Australia,* Tempus 3, University of Queensland, St Lucia, pp. 18-32.

Stevenson, J, Brockwell, S, Rowe, C, Proske, U & Shiner, J 2015, 'The palaeoenvironmental history of Big Willum Swamp, Weipa: An environmental context for the archaeological

record', *Australian Archaeology*, vol. 80, pp. 17-31, DOI:10.1080/03122417.2015.11682041.

Stevenson, J & Haberle, S 2005, *Macro charcoal analysis: A modified technique used by the Department of Archaeology and Natural History,* Palaeoworks Technical Papers 5, Australian National University, Canberra.

Stone, T 1989, 'Origins and environmental significance of shell and earth mounds in northern Australia', *Archaeology in Oceania*, vol. 24, no. 2, pp. 59-64, DOI:10.1002/j.1834-4453.1989.tb00212.x.

Sydney Morning Herald 2004, *Arnhem Land*, Sydney Morning Herald, viewed 20 September 2018, <https://www.smh.com.au/lifestyle/arnhem-land-20040208-gdkqam.html>.

Taçon, PSC, May, SK, Fallon, SJ, Travers, M, Wesley, D & Lamilami, R 2010, 'A minimum age for early depictions of Southeast Asian praus', *Australian Archaeology*, vol. 71, pp. 1-10, DOI:10.1080/03122417.2010.11689379.

Toth, LT, Aronson, RB, Vollmer, SV, Hobbs, JW, Urrego, DH, Cheng, H, Enochs, IC, Combosch, DJ, van Woesik, R & Macintyre, IG 2012, 'ENSO drove 2500-year collapse of eastern Pacific coral reefs', *Science*, vol. 337, no. 6090, pp. 81-84, DOI:10.1126/science.1221168.

Trauernicht, C, Brook, BW, Murphy, BP, Williamson, GJ & Bowman, DMJS 2015, 'Local and global pyrogeographic evidence that indigenous fire management creates pyrodiversity', *Ecology & Evolution*, vol. 5, no. 9, pp. 1908-1918, DOI:10.1002/ece3.1494.

Trauernicht, C, Murphy, BP, Tangalin, N & Bowman, DMJS 2013, 'Cultural legacies, fire ecology, and environmental change in the Stone Country of Arnhem Land and Kakadu

National Park, Australia', *Ecology & Evolution*, vol. 3, no. 2, pp. 286-297, DOI:10.1002/ece3.460.

Turney, CSM & Hobbs, D 2006, 'ENSO influence on Holocene Aboriginal populations in Queensland, Australia', *Journal of Archaeological Science*, vol. 33, pp. 1744-1748, DOI:10.1016/j.jas.2006.03.007.

Twidale, CR 1987, 'Sinkholes (dolines) in lateritised sediments, Western Sturt Plateau, Northern Territory, Australia', *Geomorphology*, vol. 1, pp. 33-52, DOI:10.1016/0169-555X(87)90005-5.

Ulm, S 2011, 'Coastal foragers on southern shores: Marine resource use in northeast Australia since the late Pleistocene', in NF Bicho, JA Haws & LG Davis (eds), *Trekking the Shore: Changing Coastlines and the Antiquity of Coastal Settlement*, Springer Science & Business Media, Germany, pp. 441-461.

Umbanhowar, CE & McGrath, MJ 1998, 'Experimental production and analysis of microscopic charcoal from wood, leaves and grasses', *The Holocene*, vol. 8, no. 3, pp. 341-346, DOI:10.1191/095968398666496051.

Vachula, RS & Richter, N 2018, 'Informing sedimentary charcoal-based fire reconstructions with a kinematic transport model', *The Holocene*, vol. 28, no. 1, pp. 173-178, DOI:10.1177/0959683617715624.

Vandeputte, K, Moens, L & Dams, R 1996, 'Improved sealed-tube combustion of organic samples for stable isotope analysis, radiocarbon dating and percent carbon determinations', *Analytical Letters*, vol. 29, no. 15, pp. 2761-2773, DOI:10.1080/00032719608002279.

van der Kaars, S & De Deckker, P 2002, 'A late Quaternary pollen record from deep-sea core Fr10/95, GC17 offshore Cape Range Peninsula, northwestern Western Australia', *Review of Palaeobotany and Palynology*, vol. 120, pp. 17-39, DOI:10.1016/S0034-6667(02)00075-1.

Veenendaal, EM, Torello-Raventos, M, Miranda, HS, Margarete Sato, N, Oliveras, I, van Langvelde, F, Asner, GP & Lloyd, J 2018, 'On the relationship between fire regime and vegetation structure in the tropics', *New Phytologist*, vol. 218, no. 1, pp. 153-166, DOI:10.1111/nph.14940.

Veth, P, Hiscock, P & Williams, A 2011, 'Are tulas and ENSO linked in Australia?', *Australian Archaeology*, vol. 72, pp. 7-14, DOI:10.1080/03122417.2011.11690526.

Walker, M, Head, MJ, Berkelhammer, M, Björck, S, Cheng, H, Cwynar, L, Fisher, D, Gkinis, V, Long, A, Lowe, J, Newnham, R, Olander Rasmussen, S & Weiss, H 2018, 'Formal ratification of the subdivision of the Holocene Series/Epoch (Quaternary System/Period): Two new Global Boundary Stratotype Sections and Points (GSSPs) and three new stages/subseries', *Episodes*, vol. 41, no. 4, p. 213, DOI:10.18814/epiiugs/2018/018016.

Weipa Town Authority 2014, *Western Cape History*, Weipa Town Authority, viewed 18 July 2018, <http://www.weipatownauthority.com.au/western-cape-history>.

Weltje, GJ, Bloemsma, MR, Tjallingii, R, Heslop, D, Röhl, U & Croudace, IW 2015, 'Prediction of geochemical composition from XRF core scanner data: A new multivariate approach including automatic selection of calibration samples and quantification uncertainties', in IW Croudace & RG Rothwell (eds), *Micro-XRF Studies of Sediment Cores: Applications of a Non-Destructive Tool for the Environmental Sciences*, Developments in Paleoenvironmental Research 17, Springer, New York.

Wende, R, Nanson, GC & Price, DM 1997, 'Aeolian and fluvial evidence for late Quaternary environmental change in the east Kimberley of Western Australia', *Australian Journal of Earth Sciences*, vol. 44, no. 4, pp. 519-526, DOI:10.1080/08120099708728331.

Whitehead, PJ, Purdon, P, Russell-Smith, J, Cooke, PM & Sutton, S 2008, 'The management of climate change through prescribed savanna burning: Emerging contributions of Indigenous people in northern Australia', *Public Administration and Development*, vol. 28, pp. 374-385, DOI:10.1002/pad.512.

Whitlock, C, Higuera, PE, McWethy, DB & Briles, CE 2010, 'Paleoecological perspectives on fire ecology: Revisiting the fire-regime concept', *The Open Ecology Journal*, vol. 3, pp. 6-23, DOI:10.2174/1874213001003020006.

Wilderness Society 2018, *Jardine River*, Wilderness Society, viewed 1 March 2018, <https://www.wilderness.org.au/jardine-river>.

Williams, AN 2013, 'A new population curve for prehistoric Australia', *Proceedings of the Royal Society B*, vol. 280, p. 20130486, DOI:10.1098/rspb.2013.0486.

Williams, AN, Mooney, SD, Sisson, SA & Marlon, J 2015a, 'Exploring the relationship between Aboriginal population indices and fire in Australia over the last 20,000 years', *Palaeogeography, Palaeoclimatology, Palaeoecology*, vol. 432, pp. 49-57, DOI:10.1016/j.palaeo.2015.04.030.

Williams, AN, Ulm, S, Turney, CSM, Rohde, D & White, G 2015b, 'Holocene demographic changes and the emergence of complex societies in prehistoric Australia', *PLoS One*, vol. 10, no. 6, article no. e0128661, DOI:10.1371/journal.pone.0128661.

Woodroffe, CD, Thom, BG & Chappell, J 1985, 'Development of widespread mangrove swamps in mid-Holocene times in northern Australia', *Nature*, vol. 317, pp. 711-713, DOI:10.1038/317711a0.

Woodward, CA & Gadd, PS 2019, 'The potential power and pitfalls of using the X-ray fluorescence molybdenum incoherent: Coherent scattering ratio as a proxy for sediment organic content', *Quaternary International*, vol. 514, pp. 30-43, DOI:10.1016/j.quaint.2018.11.031.

Wragg, PD, Mielke, T & Tilman, D 2018, 'Forbs, grasses and grassland fire behaviour', *Journal of Ecology*, vol. 105, no. 6, pp. 1983-2001, DOI:10.1111/1365-2745.12980.

Wurster, CM, Lloyd, J, Goodrick, I, Saiz, G & Bird, MI 2012, 'Quantifying the abundance and stable isotope composition of pyrogenic carbon using hydrogen pyrolysis', *Rapid Communications in Mass Spectrometry*, vol. 26, pp. 2690-2696, DOI:10.1002/rcm.6397.

Wurster, CM, Saiz, G, Schneider, MPW, Schmidt, MWI & Bird, MI 2013, 'Quantifying pyrogenic carbon from thermosequences of wood and grass using hydrogen pyrolysis', *Organic Geochemistry*, vol. 62, pp. 28-32, DOI:10.1016/j.orggeochem.2013.06.009.

Wyrwoll, K-H & Miller, GH 2001, 'Initiation of the Australian summer monsoon 14,000 years ago', *Quaternary International*, vol. 83-85, pp. 119-128, DOI:10.1016/S1040-6182(01)00034-9.

Yates, CP, Edwards, AC & Russell-Smith, J 2008, 'Big fires and their ecological impacts in Australian savannas: Size and frequency matters', *International Journal of Wildland Fire*, vol. 17, pp. 768-781, DOI:10.1071/WF07150.

Yibarbuk, D, Whitehead, PJ, Russell-Smith, J, Jackson, D, Godjuwa, C, Fisher, A, Cooke, P, Choquenot, D & Bowman, DMJS 2001, 'Fire ecology and Aboriginal land management in central Arnhem Land, northern Australia: A tradition of ecosystem management', *Journal of Biogeography*, vol. 28, pp. 325-343, DOI:10.1046/j.1365-2699.2001.00555.x.

Yu, K-F & Zhao, J-X 2010, 'U-series dates of Great Barrier Reef corals suggest at least +0.7 m sea level ~7000 years ago', *The Holocene*, vol. 20, no. 2, pp. 161-168, DOI:10.1177/0959683609350387.

Appendix 1: Lead-210 (^{210}Pb) Dating Pretreatment Method

Samples were prepared for analysis by alpha spectrometry in October 2017 and May 2018 following the ANSTO Environmental Radioactivity Measurement Centre (ERMC) Lead-210 dating sample preparation method (see also Eakins and Morrison 1978). Approximately 2g of dried sediment was weighed into a beaker, and approximately 0.2g of ^{209}Po tracer was added to each sample. 2M HNO_3 was added (enough to wet the sample) and beakers were placed on a hot plate at approximately 60°C to test reactivity. 25mL of concentrated HNO_3 was added slowly (rate determined by sample reactivity) while samples were on the hot plate to digest organics (Figure A1.1). One to two drops of n-octanol were added to samples which reacted vigorously (excessive foaming). Samples were left on the hot plate to evaporate close to dryness.

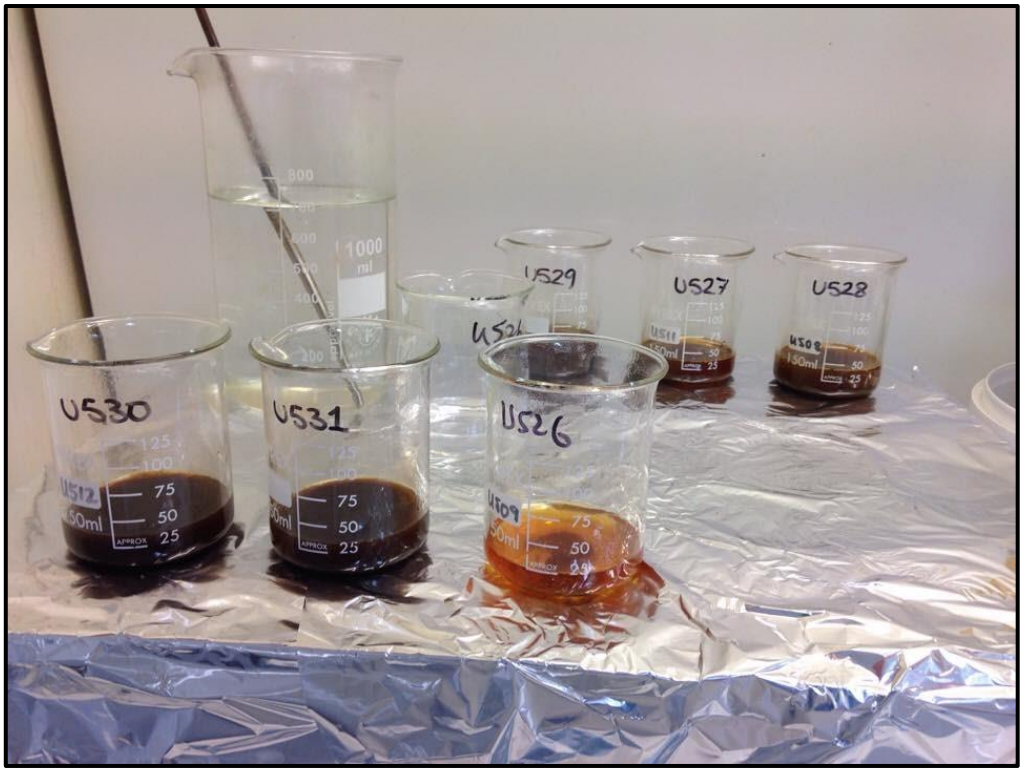

Figure A1.1: Samples on hot plate after the addition of 25mL HNO_3.

Approximately 20mL 30% H_2O_2 was added slowly before each sample again evaporated close to dryness. Samples were removed from the hot plate to cool and 40mL aqua-regia (10mL conc. HNO_3 and 30mL conc. HCl) added. Samples were returned to the hot plate, covered with a labelled watch glass and left to reflux overnight at approximately 60°C (Figure A1.2).

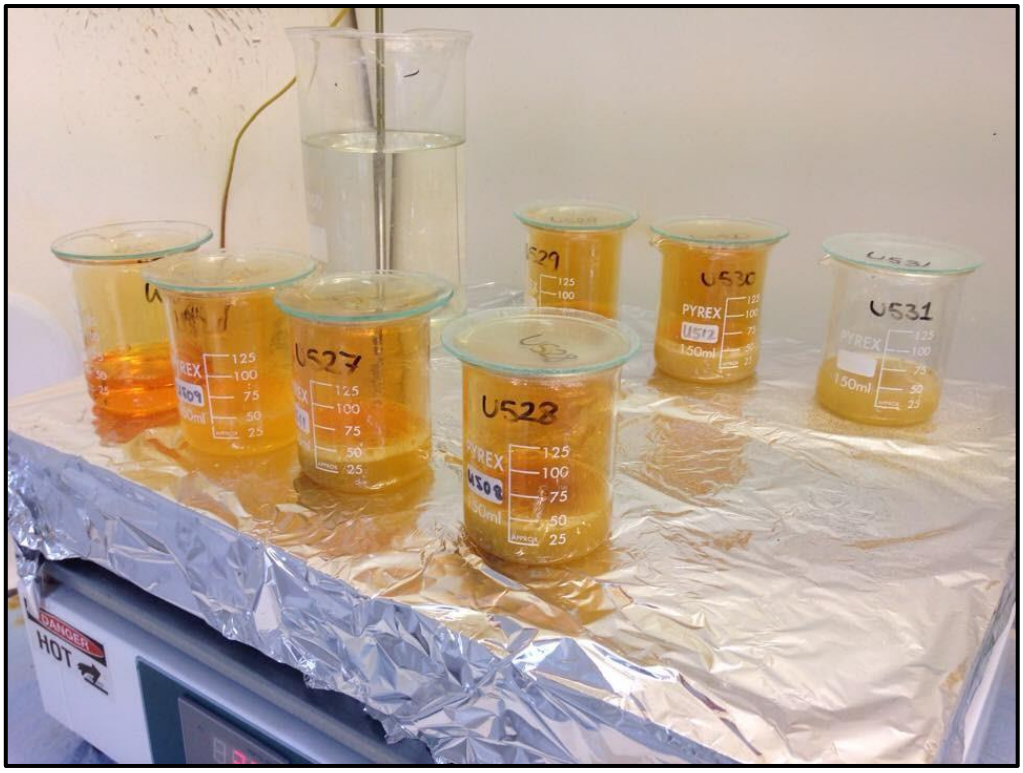

Figure A1.2: Samples on hot plate after addition of 40mL aqua-regia, prior to overnight reflux.

All samples successfully digested overnight and contained residue. Samples were transferred to 50mL centrifuge tubes using 6M HCl to rinse then centrifuged at 4000RPM for five minutes. Supernatant was poured back into the original beakers, while ~15mL 6M HCl was added to the residue and placed on a vortex mixer before being centrifuged again. Supernatant was poured off a second time and the residue discarded. Samples in beakers were returned to the hot plate to evaporate. ~10mL 6M HCl was added to rinse beaker walls before samples were left to evaporate again. ~5mL conc. HCl was added to each beaker and samples were left to evaporate close to dryness, thereby completing the digestion phase (Figure A1.3).

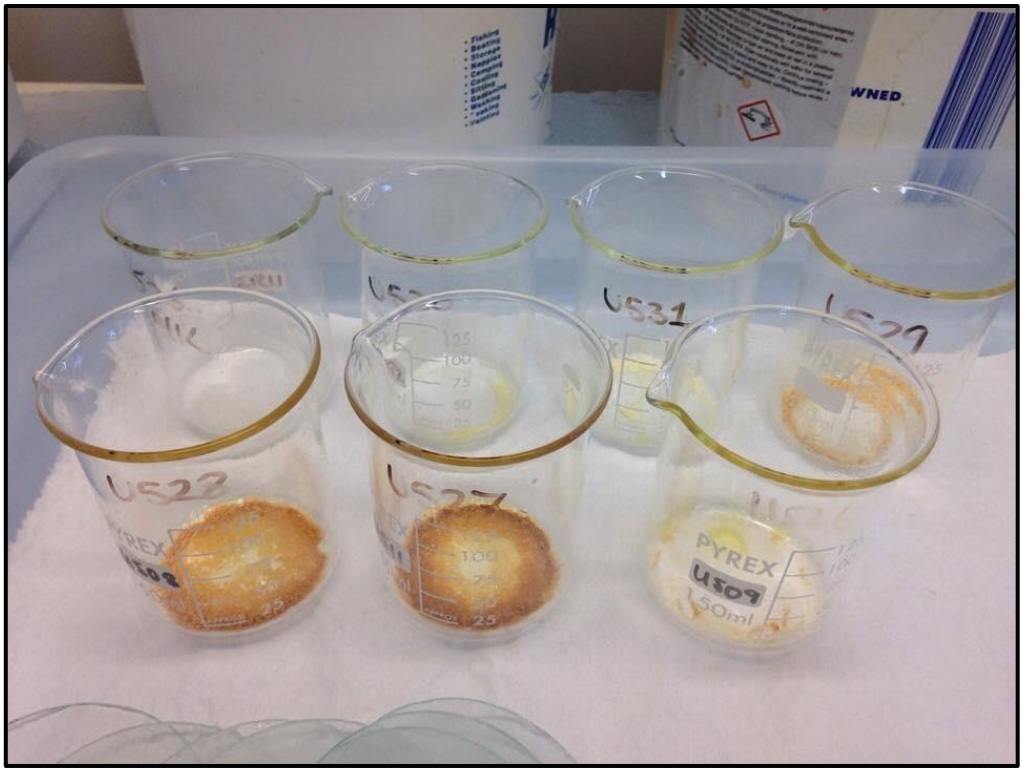

Figure A1.3: Samples after final evaporation completing the digestion phase.

This procedure was followed by the ERMC Polonium chemical isolation method (see also De Oliceria Goday 1983). 80mL 0.04M HCl was added to each sample while on a stirring hot plate. 1mL of 20% ascorbic acid was added to each sample to reduce Fe(III) to Fe(II) as Fe(II) will not deposit on the silver disk during polonium deposition. This was followed by 100µL 1M citric acid to complex trace iron and chromium and prevent later co-deposition. 10mg of Bi^{3+} holdback carrier was added to inhibit autodeposition of bismuth. The pH of each sample was adjusted to 1.5 with the addition of cresol red indicator and NH_4OH, and this was verified using a narrow range pH paper (Figure A1.4).

Figure A1.4: Samples at 1.5 pH ready for polonium deposition.

1g of hydroxylammonium chloride was added to each sample and a silver disk holder immediately floated in the solution to begin polonium deposition. Samples were left on the hot place (~60°C) for at least four hours for deposition to occur, with the silver disk holders checked for bubbles every ~30 minutes (bubbles inhibit deposition) (Figure A1.5).

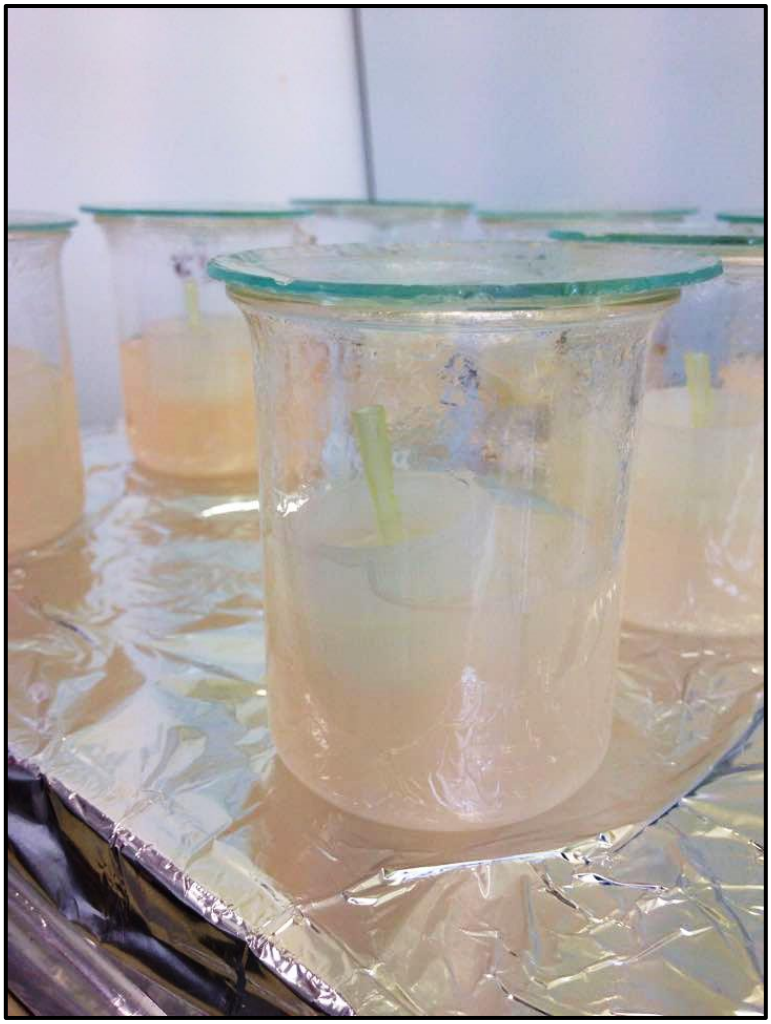

Figure A1.5: Silver disk holders floating in samples during polonium deposition.

Upon completion of deposition, beakers were removed from the hot plate. The silver disk holders were removed from each sample, disassembled to remove the silver disk, and disks rinsed with distilled water and ethanol before being placed in labelled petri dishes. Dry disks were labelled (opposite to the deposition side), for polonium counting by alpha spectrometry.

This was followed by the ERMC Radium chemical isolation (see also Golding 1961; Lim and Dave 1981; Lim *et al.* 1989) procedure. Magnetic stirring rods were removed from each beaker. Samples were rinsed using distilled water from beakers to larger 1L beakers containing 800mL molecular filtered water and a stirring rod. 20mL conc. H_2SO_4 was added to each beaker,

samples were placed on a stirring hot plate (not heating) and 100mL 20% Na_2SO_4 was added. 10mL 10mg/mL Pb^{2+} carrier was dripped gradually into each sample via burette (Figure A1.6).

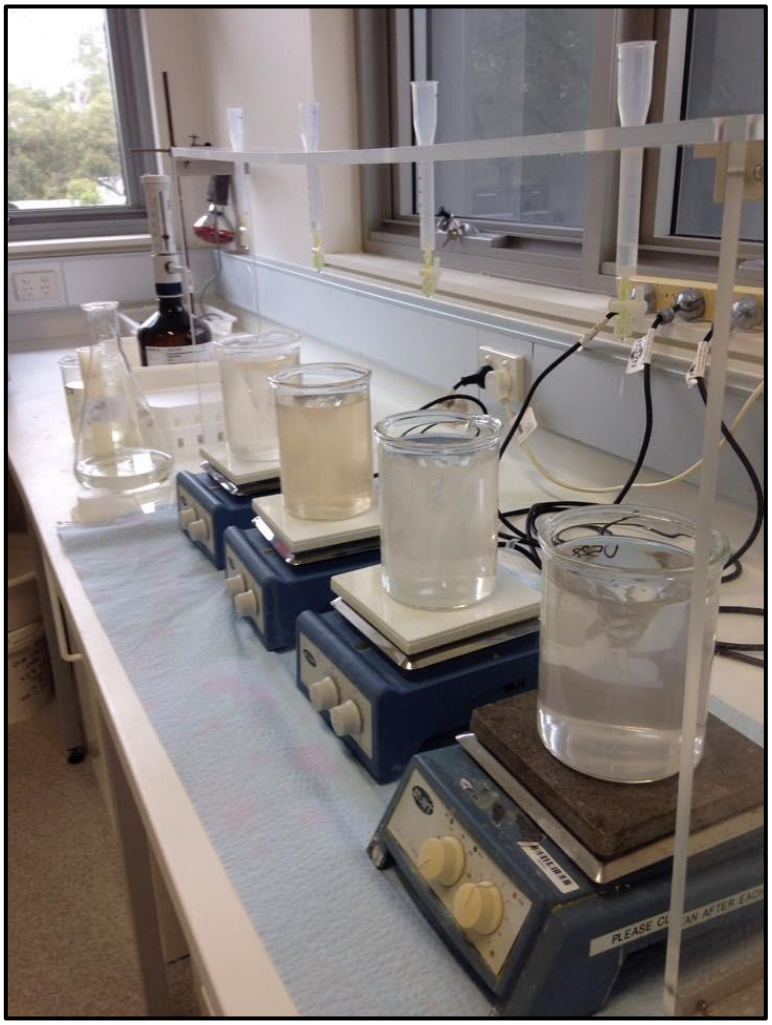

Figure A1.6: Samples on stirring hot plate with 10mL 10mg/mL Pb^{2+} carrier being added via burette.

Samples were removed from the hot plate, stirring rods removed, and left covered overnight to allow Pb/Ba/Ra sulphate precipitate to flocculate. Supernatant was discarded and residue rinsed into centrifuge tubes using 50% ethanol, centrifuged and decanted. 5mL 0.2M Na_5DTPA was added along with one drop of thymol blue indicator to verify that samples had a sufficiently

high (>9) pH. Samples were mixed using a vortex mixer and placed in a sonicator bath for 30 minutes.

2 drops of methyl red indicator were added. Using a 0.45µm disposable membrane filter, samples were transferred into 70mL polycarbonate vials. 5mL 4% Na_2SO_4 was used to rinse the centrifuge tube and passed through the filter. 2mL of 1:1 acetic acid/water and 1mL $BaSO_4$ seeding suspension (sonicated for 15 minutes prior) were simultaneously added to each sample (Figure A1.7) before samples were placed in refrigeration for at least 30 minutes.

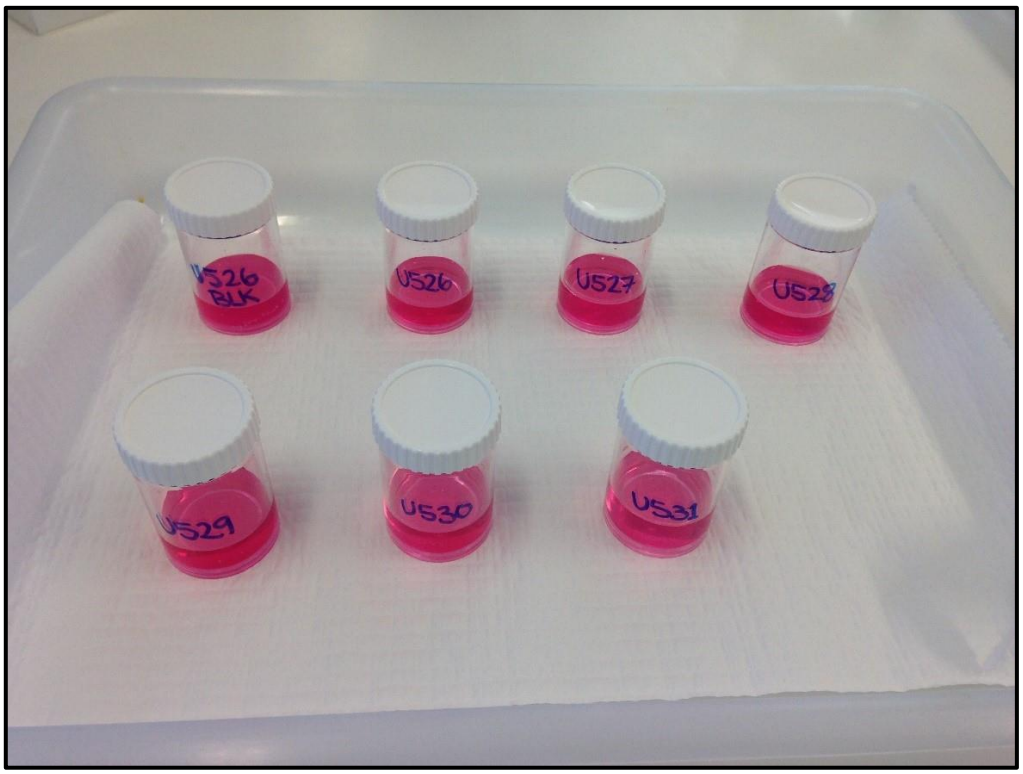

Figure A1.7: Samples after simultaneous addition of 2mL 1:1 acetic acid/water and 1mL $BaSO_4$ seeding suspension.

Cooled samples were poured through a smooth-surfaced Millipore "VV" membrane filter in a lock-seal Gelman filter apparatus and allowed to drain (Figure A1.8). Vials were rinsed with

50% ethanol, which was then also passed through the filter apparatus. Membrane filters were removed and placed in labelled petri dishes for radium counting by alpha spectrometry.

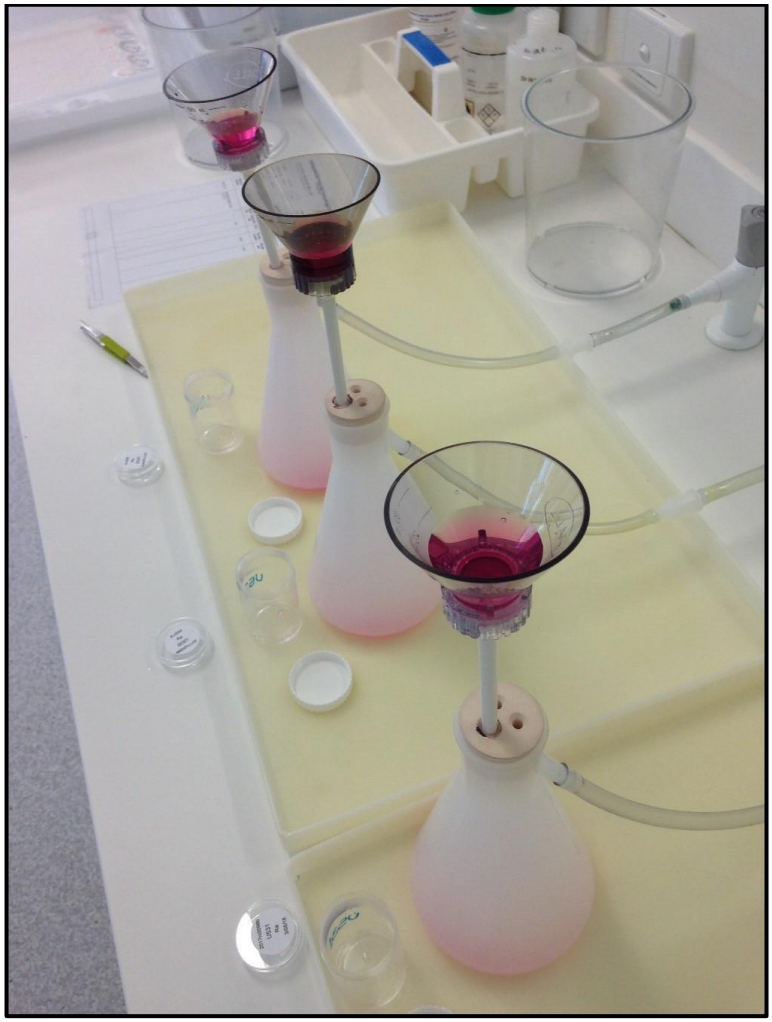

Figure A1.8: Samples draining through the "VV" membrane filters in a lock-seal Gelman filter apparatus.

Appendix 2: Carbon-14 (^{14}C) Dating Pretreatment Method

Dried samples were transferred into 50mL centrifuge tubes and their weights were recorded. ~10-15mL 2M HCl was added, and samples were placed in a waterbath at 60°C for one hour, to remove carbonates and infiltrated fulvic acids. Supernatants were poured off and samples were rinsed with molecular filter water and centrifuged, repeated three times. Samples then underwent alkali (NaOH) rinses of increasing concentration from 1% to 10%, placed in a waterbath at 60°C for one hour (Figure A2.1) and rinsed/centrifuged repeatedly until supernatant was clear after each alkali repetition. Alkali rinses were repeated until supernatants were clear after removal from the waterbath. ~10-15mL 2M HCl was added and samples were left overnight before being rinsed/centrifuged three times.

Figure A2.1: Samples during the alkali phase in a waterbath, ANSTO AMS pretreatment laboratory, November 2017.

Low volume samples were transferred directly into combustion tubes using a pipette. Samples of higher volume were transferred into small beakers using a pipette (Figure A2.2). Excess water was pipetted off and samples were placed in a drying oven at 60°C over the weekend.

Figure A2.2: Samples in the ANSTO AMS pretreatment laboratory prior to drying, November 2017.

Appendix 3: Morphotype Data

A3.1 Marura

Morphotype data for >250 µm and 250-125 µm size fractions of Marura using Courtney Mustaphi and Pisaric's (2014) 27-type system are shown in Figures A3.1 and A3.2.

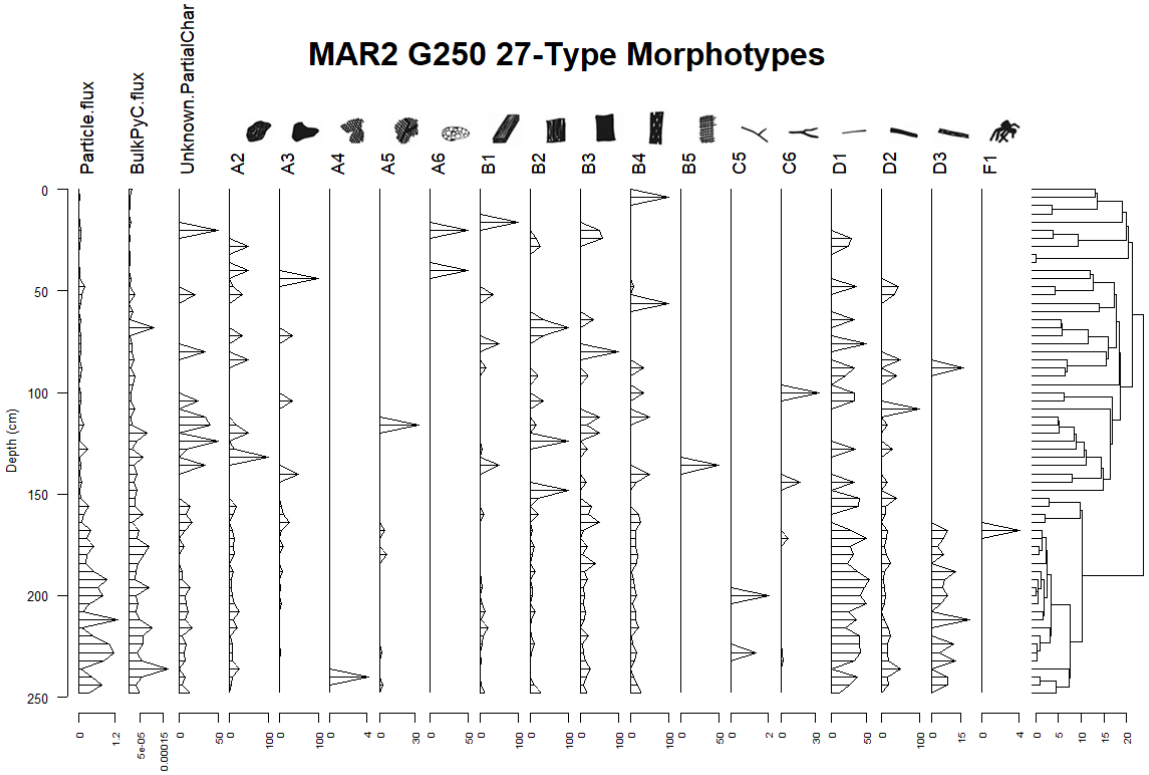

Figure A3.1: Morphotype data for MAR2 >250 µm charcoal (morphotype images from Courtney Mustaphi & Pisaric 2014).

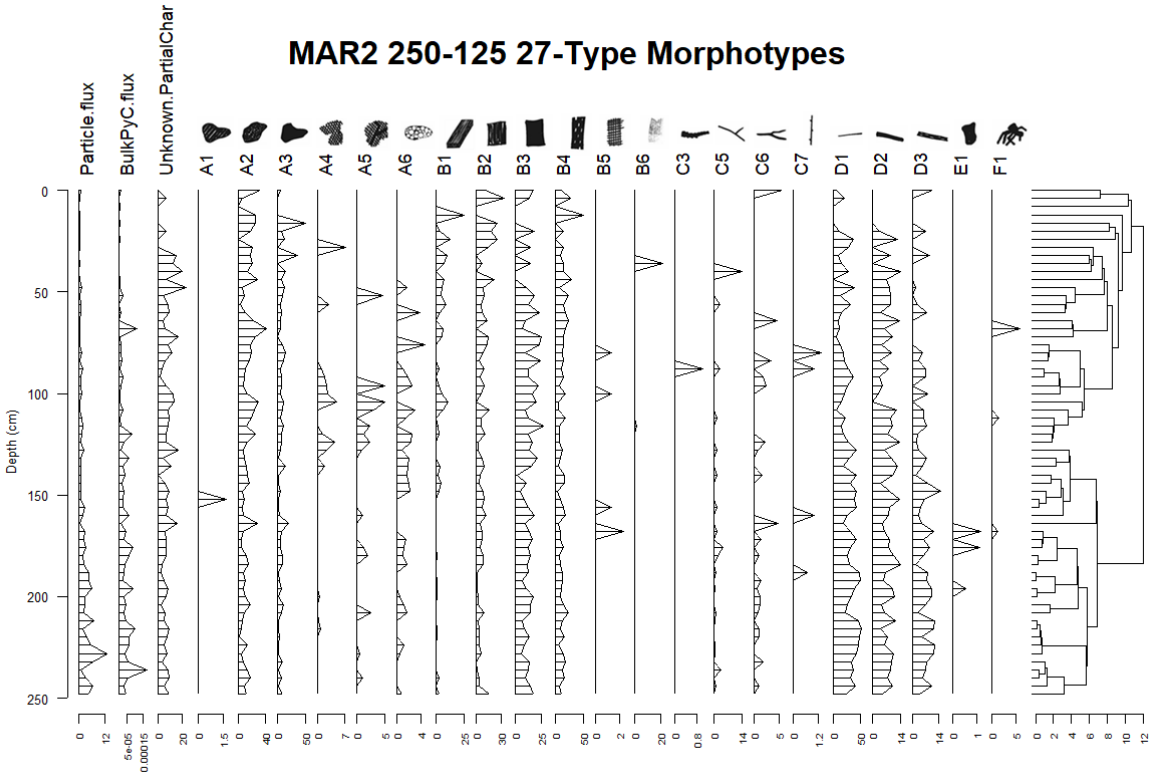

Figure A3.1: Morphotype data for MAR2 >250 µm charcoal (morphotype images from Courtney Mustaphi & Pisaric 2014).

A3.2 Big Willum Swamp

Morphotype data for >250 µm and 250-125 µm size fractions of Big Willum Swamp using Courtney Mustaphi and Pisaric's (2014) 27-type system are shown in Figures A3.3 and A3.4.

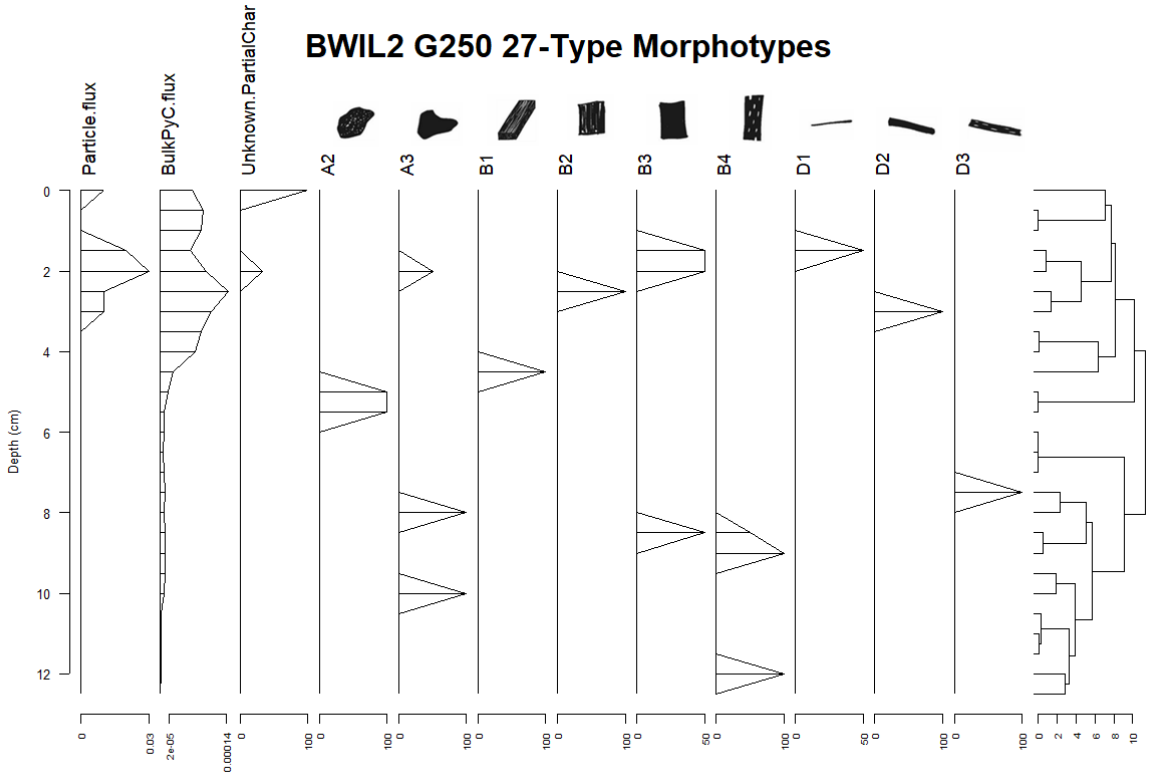

Figure A3.3: Morphotype data for BWIL2 >250 µm charcoal (morphotype images from Courtney Mustaphi & Pisaric 2014).

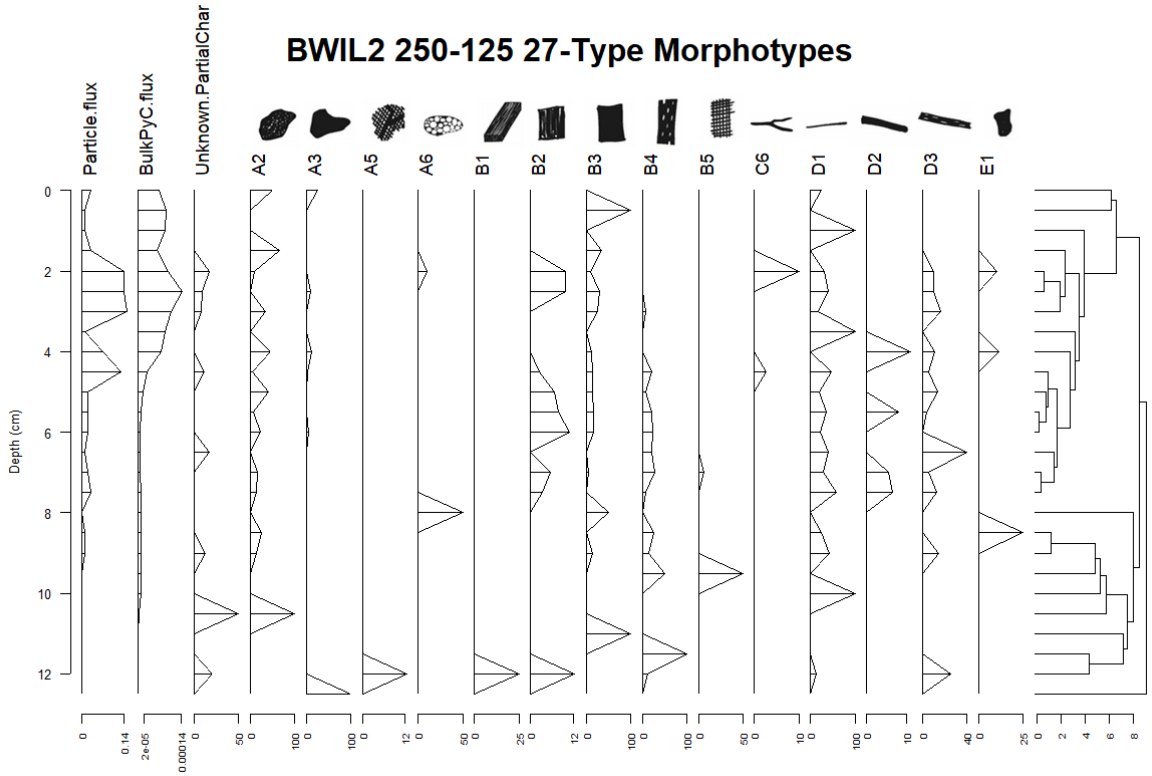

Figure A3.3: Morphotype data for BWIL2 250-125 µm charcoal (morphotype images from Courtney Mustaphi & Pisaric 2014).

A3.3 Sanamere Lagoon

Morphotype data for >250 µm and 250-125 µm size fractions of Sanamere Lagoon using Courtney Mustaphi and Pisaric's (2014) 27-type system are shown in Figures A3.5 and A3.6.

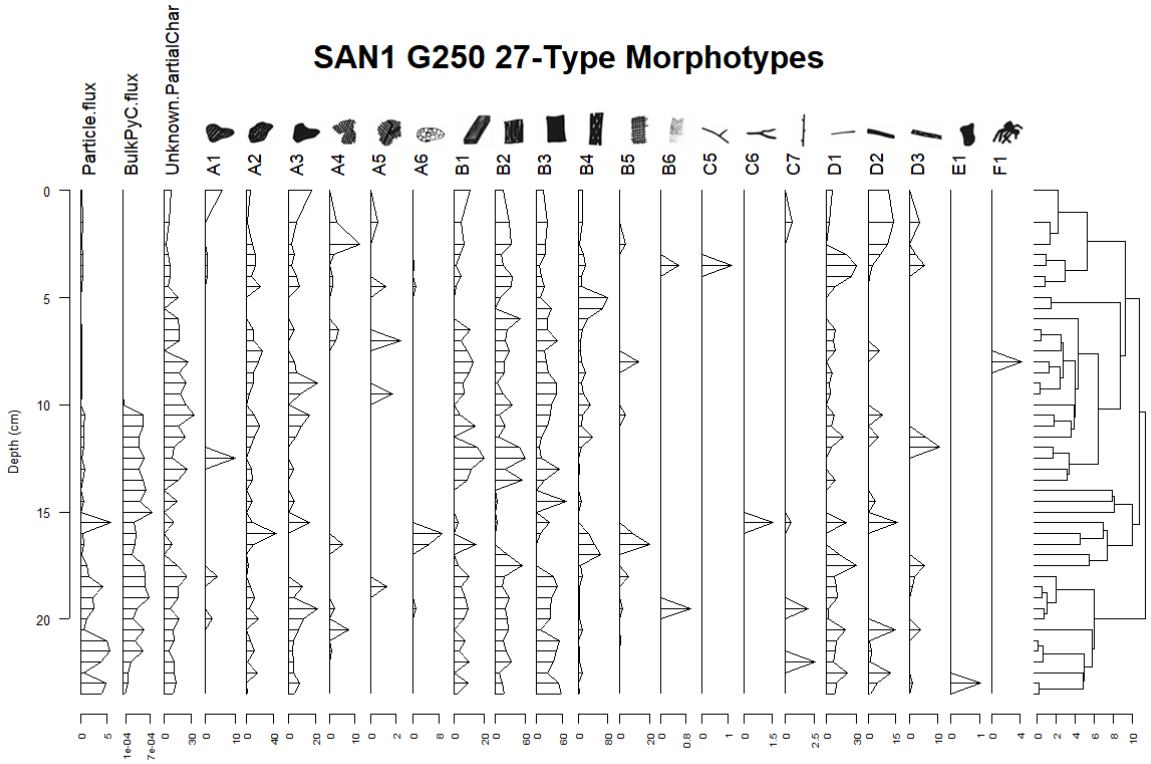

Figure A3.5: Morphotype data for SAN1 >250 µm charcoal (morphotype images from Courtney Mustaphi & Pisaric 2014).

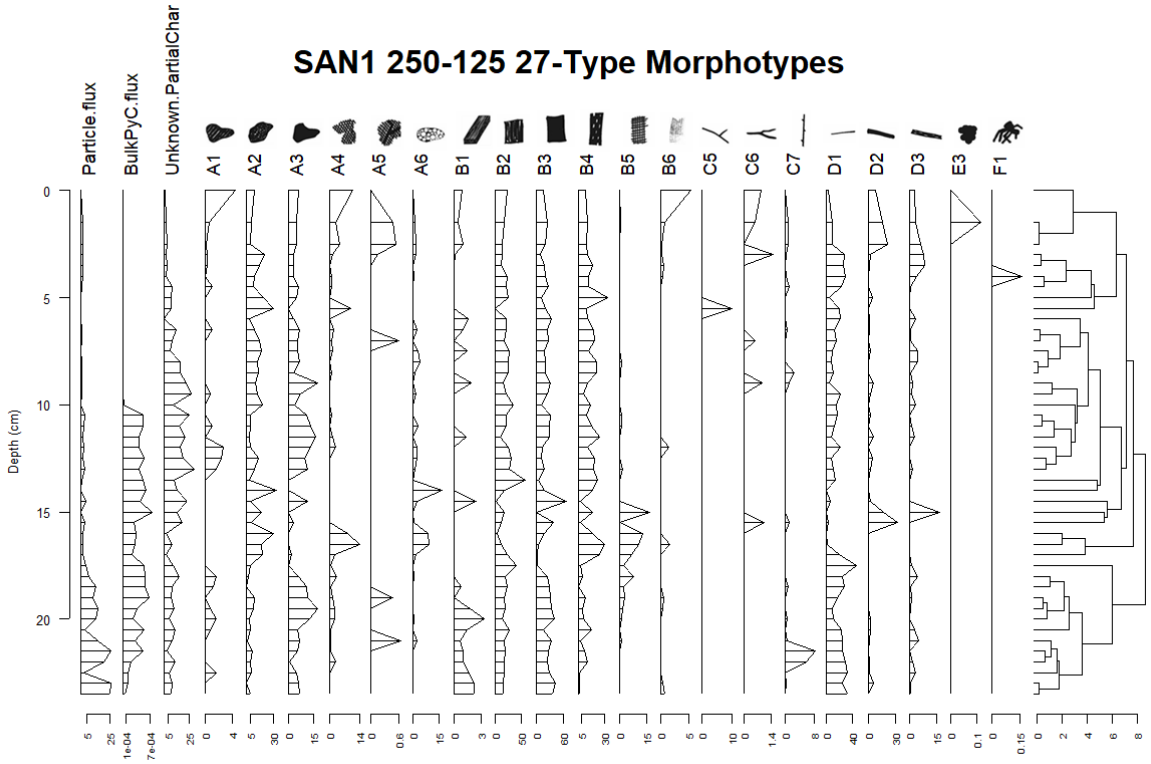

Figure A3.6: Morphotype data for SAN1 250-125 µm charcoal (morphotype images from Courtney Mustaphi & Pisaric 2014).

Appendix 4: Fossil Charcoal Particle Identification and Classification by Two Convolutional Neural Networks

This appendix is a reproduction of the following publication:

Rehn, E, Rehn, A & Possemiers, A 2019, 'Fossil charcoal particle identification and classification by two convolutional neural networks', *Quaternary Science Reviews*, vol. 226, p. 106038, DOI:10.1016/j.quascirev.2019.106038.

Quaternary Science Reviews 226 (2019) 106038

Contents lists available at ScienceDirect

Quaternary Science Reviews

journal homepage: www.elsevier.com/locate/quascirev

Fossil charcoal particle identification and classification by two convolutional neural networks

E. Rehn [a, b, *], A. Rehn [c], A. Possemiers [c]

[a] College of Science and Engineering, James Cook University, PO Box 6811, Cairns QLD 4870, Australia
[b] ARC Centre of Excellence for Australian Biodiversity and Heritage, James Cook University, PO Box 6811, Cairns QLD 4870, Australia
[c] College of Business, Law and Governance, James Cook University, PO Box 6811, Cairns QLD, 4870, Australia

ARTICLE INFO

Article history:
Received 12 June 2019
Received in revised form
15 October 2019
Accepted 23 October 2019
Available online xxx

Keywords:
Fossil charcoal analysis
Palaeolimnology
Palaeofire
Artificial neural networks
Quaternary
Global
Sedimentology
Lakes
Lagoons & swamps

ABSTRACT

Fire is a significant natural and cultural phenomenon, affecting spatial scales from local to global, and is represented in most palaeoenvironmental records by fossil charcoal. Analysis is resource-intensive and requires high-level expert knowledge. This study is a preliminary investigation of the application of artificial neural networks to fossil charcoal particle analysis, utilizing a U-Net variant for charcoal particle identification and VGG for particle classification by morphology. Both neural networks performed well, reaching ~96% accuracy for particle identification and ~75% accuracy for classification. Future work will include expansion of the training dataset, including total number of particles and number of sites. The development and application of this automated system will increase the efficiency of fossil charcoal analysis.

1. Introduction

Fire has existed on Earth for over 400 million years (Bowman et al., 2009:481) and is an important environmental process interconnected to climate, vegetation structure, and carbon cycling (Beringer et al., 2015; Bowman et al., 2009; Veenendaal et al., 2017). Fire occurrence is also linked to people; humans have had a long and complex history with fire (Bowman et al., 2011; Scott et al., 2016), including the widespread use of fire as a landscape management tool (e.g. Anderson, 1994; Archibald et al., 2012; Montiel and Kraus, 2010; Rolland, 2004; Rull et al., 2015). Moss and Kershaw (2000), for example, suggest the impacts of Australian indigenous use of fire in the landscape can be seen over 38,000 years ago in the palaeoenvironmental record. Both natural and anthropogenic fire are connected to significant issues for asset management, conservation and cultural practice.

Fossil charcoal is an important palaeofire proxy. It has high preservation potential (Conedera et al., 2009; Mooney and Tinner, 2011; Whitlock and Larsen, 2001), and charcoal records are available worldwide (see Global Paleofire Working Group 2017 as well as Power et al., 2010, for depictions of the spatial and temporal scope of global charcoal records). Analysis of fossil charcoal, including identification of the type of vegetation that burned to create it, allows for the creation of long term fire records contextualised by fuel type (e.g. Aleman et al., 2013; Crawford and Belcher, 2014; Jensen et al., 2007). Such information allows for a greater understanding of fire and vegetation dynamics across time and space. However, traditional (optical) charcoal analysis is a time-intensive process; fossil charcoal is commonly quantified on pollen slides (particles <125 μm diameter) or wet sieved and suspended in water, with charcoal abundance measurements taken via microscope as either particle counts or area measurements (see Mooney and Tinner, 2011; Stevenson and Haberle, 2005). Increasing the speed of charcoal analysis will enable researchers to process a larger volume of samples in a given time frame, allowing for higher resolution records.

Recent developments in artificial neural networks have led to

* Corresponding author. College of Science and Engineering, James Cook University, PO Box 6811, Cairns, QLD, 4870, Australia.
E-mail address: emma.rehn@my.jcu.edu.au (E. Rehn).

https://doi.org/10.1016/j.quascirev.2019.106038
0277-3791/

their successful application to problems across a diverse range of disciplines (e.g. review of developments and applications including finance, bioinformatics and environmental risk, Bassis et al., 2014; engineering, Mehrjoo et al., 2008; medical imaging, Wu et al., 2017). Drawing from these developments and using them as a framework for this study, the identification and classification process of fossil charcoal particles is an ideal candidate for automation using neural networks.

2. Background and related work

While volumes of preserved charcoal (number of fossil charcoal particles) help indicate the amount of fire in past landscape, the fuel source (vegetation type) of a fossil charcoal particle is significant as this reflects the composition of the surrounding environment. The aspect ratio of a macroscopic (>125 μm) charcoal particle provides this data, with more elongated particles identified as grass-derived and blockier particles as wood- or leaf-derived (e.g. Umbanhowar and McGrath, 1998; Aleman et al., 2013; Crawford and Belcher, 2014; Leys et al., 2017). The threshold ratio for a particle to be considered elongate is a matter of debate, ranging from a length-width ratio of 2 or greater (Aleman et al., 2013) through to 3.7 (Crawford and Belcher, 2014).

An alternative method of fuel identification is classification by morphology (morphotypes) (e.g. Jensen et al., 2007). Enache and Cumming (2006) present a 7-type classification scheme based on morphological differences such as elongate versus blocky, geometric versus irregular, and the presence of internal structure such as voids. Courtney Mustaphi and Pisaric (2014) expand this to 27 different morphotypes including types specific to a temperate biome, such as type C1 (charred conifer needles). Enache and Cumming (2006) morphotype classifications are a simpler system applicable to a broader range of environments.

The current standard for automated quantification of charcoal particles is ImageJ, originally developed by the US National Institutes of Health (Schneider et al., 2012; for examples of its application see Barr et al., 2017; Crawford and Belcher, 2016; Halsall et al., 2018; Hawthorne and Mitchell, 2016; Stevenson and Haberle, 2005). The input image is a petri dish containing charcoal, and potentially other non-black particles; ImageJ output contains the total number of dark particles and particle area based on a user-defined threshold (Abramoff et al., 2004; Ferreira and Rasband, 2011; see Mooney and Tinner, 2011:11 for instructions on charcoal analysis using one of ImageJ's predecessors, Scion Image). Image classification, as is required for identifying morphotypes, is currently beyond the capabilities of ImageJ.

Few studies have applied neural networks to palaeoenvironmental problems. In palaeolimnology, Racca et al. (2003) use a multi-layer perceptron neural network to reduce diatom taxa for calibration purposes. Maruyama et al. (2018) use a convolutional neural network as a feature extractor to identify the species of native wood charcoal pieces, created from samples of modern trees. Weller et al. (2007) apply a supervised neural network to identification of sedimentary organic matter within pollen slides. A preliminary study automating pollen analysis by a neural network is presented by France et al. (2000). To date, no published studies have utilized neural networks for charcoal particle identification or classification.

In this study, two Convolutional Neural Networks (CNN) are used to identify and categorise charcoal particles: a variant of U-Net, and VGG, implemented in Keras with a Tensorflow backend (Abadi et al., 2015).

The U-Net variant is used to first mask, per pixel, charcoal particles so as to eliminate image artifacts or non-charcoal particles that made it through the filtering process. U-Net is an autoencoder network that uses multiple alternating layers of convolutions followed by max pooling to "encode" features from an image input. In our case, strided subimages of 512x512x3 pixels are encoded down to a feature space of 16x16x256. Once encoded into the feature space the network then "decodes" using alternating layers of upsampling, deconvolution (Zeiler et al., 2010) followed by the copy and crop of encoder layer outputs, sometimes referred to as skip connections, found in the U-Net architecture (Ronneberger et al., 2015). Training the network with binary images, representing "charcoal particle" and "not charcoal particle", the network learns how to encode and decode information in images to generate the binary masks itself and generalises to images that are outside the training data.

Due to the nature of charcoal particles being of high contrast, and the lack of similar looking distractors in the dataset, we deviated from the default U-Net architecture by removing the use of multiple layers of convolution and deconvolution between up-samples and down-samples. This drastically reduces the number of operations that the network needs to perform and still provided adequate results for the purposes of segmenting out individual particles for VGG to classify.

VGG is a very deep convolutional network for image recognition and is considered a staple for image based classification (Simonyan and Zisserman, 2014). To accelerate the training process we used the pre-trained version of VGG16 that comes with Keras and locked the first 25 layers. Referred to in the literature as transfer learning (Weiss et al., 2016), the initial layers of VGG encode simple shapes such as lines, gradients and basic textures, hence avoiding spending time relearning those features from scratch while also reducing the amount of training data needed. Transfer learning does have a limitation in that the input images must conform to the same size that VGG16 was originally trained on; therefore, cropped individual particles are scaled to fit the 221x221 image size that VGG expects.

3. Implementation

3.1. Sample Collection and Preparation

Samples were taken from Holocene sediment cores collected from three wetlands in tropical northern Australia: Sanamere Lagoon (11.117°S, 142.35°E), Big Willum Swamp (12.657°S, 141.998°E) and Marura Sinkhole (13.409°S, 135.774°E). Sediment samples were prepared for fossil charcoal analysis following the method outlined by Stevenson and Haberle (2005); samples were placed in mid-strength (~5% concentration) bleach for 72 h before wet sieving to isolate the >63 μm fraction. Samples were suspended in water and photographed through a dissecting microscope using a DSLR and lens adapter.

The morphotype classification system devised by Enache and Cumming (2006) was selected for charcoal classification in this study (Fig. 1). Two of the seven morphotypes (types B and D) were excluded from this study as they were insufficiently represented in the training dataset.

3.2. Network training

To prepare the input dataset for the U-Net network, each photograph of suspended samples was manually labelled with binary masks indicating the locations of any present charcoal particles. These masks were then used to segment the training data and extract images of each individual charcoal particle, in the same manner that the final system segments images based on masks generated by the trained U-Net network. The individual charcoal particle images were then manually classified by morphotype to form the input dataset for VGG.

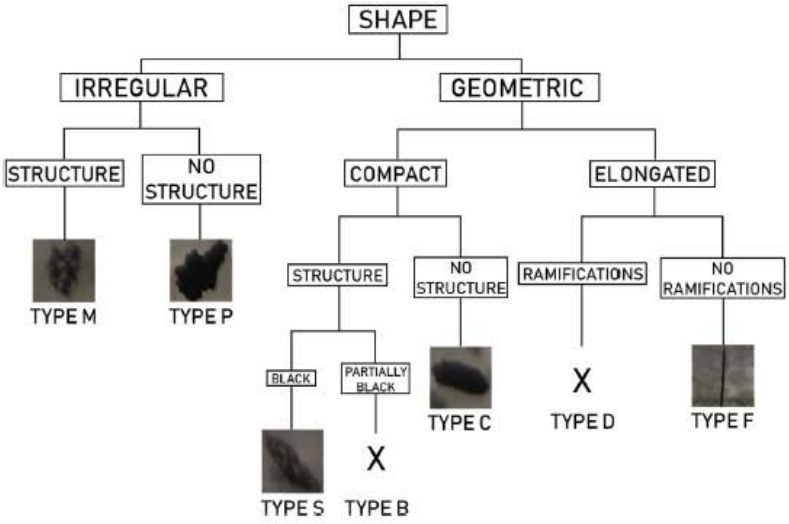

Fig. 1. Morphotype classification system of Enache and Cumming (2006) used in this study with example particle photographs from the validation dataset (adapted from Enache and Cumming, 2006:285).

The overall dataset for each network - 976 images for the U-Net network divided into 1714 individual particle images for VGG - was then separated into training and validation datasets, with 90% of images allocated to the training dataset (Table 1) and the remaining 10% of images allocated to the validation dataset. The selection of the individual images in each allocation was randomly computed in order to prevent biases in the trained networks due to over- or under-representation of any given classification label.

Both the U-Net network and VGG were trained using the popular RMSProp optimiser (Tieleman and Hinton, 2012), selected due to its ability to adaptively control the learning rate during training without the need to manually adjust this parameter. The U-Net network was trained from a blank state, whereas VGG was trained using transfer learning to accelerate the process, as stated previously. Each network was trained until the point at which its accuracy in predicting the classification labels of the validation dataset ceased to improve, as is standard practice for preventing overfitting and ensuring the generalisability of the trained networks (see Prechelt, 1998).

4. Results

The trained U-Net network achieved 96.06% accuracy, while the trained VGG network achieved 75.15% accuracy (Fig. 2).

The U-Net network results were sliced by using a connected components algorithm (Grana et al., 2010) to isolate individual particles, shown in Fig. 2 as a red bounding box. Identified particles measuring less than 63 × 63 μm were discarded, as samples were processed to only contain particles >63 μm (described in Sample Collection and Preparation above).

Table 1
Number of particle images of each morphotype classification in the network training dataset.

Morphotype	Images
Type C	403
Type F	465
Type M	196
Type P	167
Type S	483

5. Discussion and areas for future work

This study is a proof of concept for the application of neural networks to charcoal particle analysis. Our initial results demonstrate the feasibility of this methodology, with high accuracy achieved by U-Net for charcoal identification and VGG for morphotype classification. In combination with an appropriate mechanical apparatus for particle photography such as an automated stage, this methodology has the potential to significantly accelerate particle analysis workflows, reducing the number of hours that human experts must spend on labour-intensive visual inspection and providing a foundation for more complex and comprehensive analysis tasks.

As a proof of concept, the scope of this initial study is limited with respect to available image data. Training dataset images in this study are relatively clean with minimal non-charcoal particles and dark organics present. While this is the ideal result of sample preparation for charcoal analysis, the robustness of charcoal identification by U-Net could be improved by the inclusion in the training dataset of images containing more non-charcoal particles. Our training dataset also excludes morphotypes B (partially black, structured geometric) and D (elongate with ramifications) due to a lack of sufficient training images for these morphotypes.

Future work could include an expansion of the training dataset to include a greater number of images from more sites, covering a larger geographic area and more diverse particle assemblages. With the increase of images, the reliance on transfer learning to detect simple features could potentially be mitigated and a more specialized network could be used in the place of VGG. A larger dataset would also likely provide sufficient samples to encompass the morphologies not present in the dataset for this study. To improve the scalability and accessibility of this expanded dataset, an online charcoal image library could also be created, facilitating contributions by international researchers and providing a central

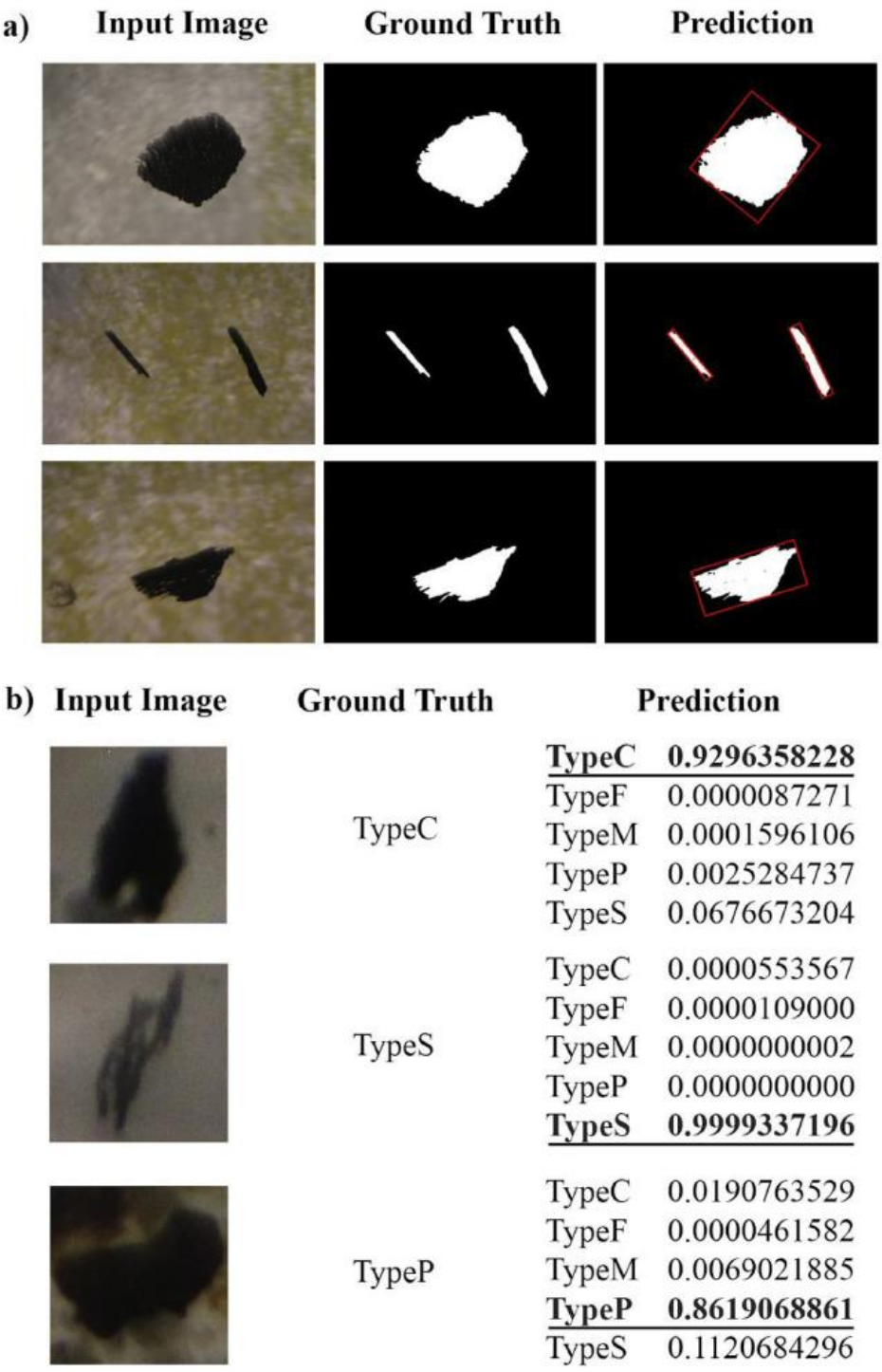

Fig. 2. Example results from the validation datasets: a) U-Net network, with red bounding boxes around identified particles for segmentation, and b) VGG, with the highest probability classification underlined. (For interpretation of the references to colour in this figure legend, the reader is referred to the Web version of this article.)

repository for researchers wishing to utilise the dataset to train neural networks. As a first step towards this goal, we have made the source code and training data for this study available online, accompanied by comprehensive instructions for reproducing our results. These resources can be found at: https://github.com/adamrehn/charcoal-morphotypes.

6. Conclusion

The automated classification presented in this experimental study provides a fast and flexible method of charcoal analysis. This two-stage pre-trained network utilizing a broadly applicable morphotype classification system can be applied to samples from any site without requiring the creation of additional training datasets. Alternatively, these neural networks can be trained using any morphotype system, including classifications that may be more region- or biome-specific.

Automated charcoal identification and classification using neural networks will increase the efficiency of charcoal analysis, enabling higher sampling resolutions and/or the analysis of more sites and sediment cores. This study presents a promising preliminary investigation into the application of neural networks to the automation of charcoal particle analysis, ultimately feeding into a broad shift to utilizing artificial neural networks to address increasingly complex analytical problems.

Data availability

The training dataset of processed charcoal particle images used in this paper is available via the following:

Rehn, E.; Rehn, A. (2019): Fossil charcoal particle training data for neural networks. James Cook University. (dataset). http://doi.org/10.25903/5d006c1494cf9.

CRediT authorship contribution statement

E. Rehn: Conceptualization, Investigation, Writing - original draft, Writing - review & editing. **A. Rehn:** Methodology, Software, Writing - original draft, Writing - review & editing. **A. Possemiers:** Software, Writing - original draft.

Acknowledgements

This study forms one part of author ER's PhD degree within the College of Science and Engineering, James Cook University. Sample collection was undertaken as part of an Australian Research Council Laureate Fellowship ID:FL140100044 (CI: M. Bird). ER acknowledges financial support from the Australian Institute of Nuclear Science and Engineering (Postgraduate Research Award 12143) and an Australian Government Research Training Program Scholarship. The authors would like to thank Cassandra Rowe and Sean Ulm for editorial feedback on the manuscript. This research was conducted by the Australian Research Council Centre of Excellence for Australian Biodiversity and Heritage (project number CE170100015).

Appendix A. Supplementary data

Supplementary data to this article can be found online at https://doi.org/10.1016/j.quascirev.2019.106038.

References

Abadi, M., Agarwal, A., Barham, P., Brevdo, E., Chen, Z., Citro, C., Corrado, G.S., Davis, A., Dean, J., Devin, M., Ghemawat, S., Goodfellow, I., Harp, A., Irving, G., Isard, M., Jia, Y., Jozefowicz, R., Kaiser, L., Kudlur, M., Levenberg, J., Mané, D., Monga, R., Moore, S., Murray, D., Olah, C., Schuster, M., Shlens, J., Steiner, B., Sutskever, I., Talwar, K., Tucker, P., Vanhoucke, V., Vasudevan, V., Viégas, F., Vinyals, O., Warden, P., Wattenberg, M., Wicke, M., Yu, Y., Zheng, X., 2015. TensorFlow: Large-Scale Machine Learning on Heterogeneous Systems. Retrieved 20 May 2019 from. https://tensorflow.org.

Abramoff, M.D., Magalhães, P.J., Ram, S.J., 2004. Image processing with ImageJ. Biophot. Int. 36–42.

Aleman, J.C., Blarquez, O., Bentaleb, I., Bonté, P., Brossier, B., Carcaillet, C., Gond, V., Gourlet-Fleury, S., Kpolita, A., Lefèvre, I., Oslisly, R., Power, M.J., Yongo, O., Bremond, L., Favier, C., 2013. Tracking land-cover changes with sedimentary charcoal in the Afrotropics. Holocene 23 (12), 1853–1862.

Anderson, M.K., 1994. Prehistoric anthropogenic wildland burning by hunter-gatherer societies in the temperate regions: a net source, sink, or neutral to the global carbon budget? Chemosphere 29 (5), 913–934.

Archibald, S., Staver, A.C., Levin, S.A., 2012. Evolution of human-driven fire regimes in Africa. PNAS 109 (3), 847–852.

Bart, C., Tibby, J., Moss, P.T., Halverson, G.P., Marshall, J.C., McGregor, G.B., Stirling, E., 2017. A 25,000-year record of environmental change from Welsby Lagoon, North Stradbroke Island, in the Australian subtropics. Quat. Int. 449, 106–118. https://doi.org/10.1016/j.quaint.2017.04.011.

Bassis, S., Esposito, A., Morabito, F.C., 2014. Recent advances of neural network models and applications. In: Proceedings of the 23rd Workshop of the Italian Neural Networks Society (SIREN), May 23-25, Vietri Sul Mare, Salerno, Italy. Springer, Switzerland.

Beringer, J., Hutley, L.B., Abramson, D., Arndt, S.K., Briggs, P., Bristow, M., Canadell, J.G., Cernusak, L.A., Eamus, D., Edwards, A.C., Evans, B.J., Fest, B., Goergen, K., Grover, S.P., Hacker, J., Haverd, V., Kanniah, K., Livesley, S.J., Lynch, A., Maier, S., Moore, C., Raupach, M., Russell-Smith, J., Scheiter, S., Tapper, N.J., Uotila, P., 2015. Fire in Australian savannas: from leaf to landscape. Glob. Chang. Biol. 21, 62–81. https://doi.org/10.1111/gcb.12686.

Bowman, D.M., Balch, J.K., Artaxo, P., Bond, W.J., Carlson, J.M., Cochrane, M.A., D'Antonio, C.M., DeFries, R.S., Doyle, J.C., Harrison, S.P., Johnston, F.H., Keeley, J.E., Krawchuk, M.A., Kull, C.A., Marston, J.B., Moritz, M.A., Prentice, I.C., Roos, C.I., Scott, A.C., Swetnam, T.W., van der Werf, G.R., Pyne, S.J., 2009. Fire in the Earth system. Science 324 (5926), 481–484.

Bowman, D.M., Balch, J.K., Artaxo, P., Bond, W.J., Cochrane, M.A., D'Antonio, C.M., DeFries, R.S., Johnston, F.H., Keeley, J.E., Krawchuk, M.A., Kull, C.A., Mack, M., Moritz, M.A., Pyne, S., Roos, C.I., Scott, A.C., Sodhi, N.S., Swetnam, T.W., 2011. The human dimension of fire regimes on Earth. J. Biogeogr 38, 2223–2236.

Conedera, M., Tinner, W., Neff, C., Meurer, M., Dickens, A.F., Krebs, P., 2009. Reconstructing past fire regimes: methods, applications, and relevance to fire management and conservation. Quat. Sci. Rev. 28, 555–576.

Crawford, A.J., Belcher, C.M., 2014. Charcoal morphometry for paleoecological analysis: the effects of fuel type and transportation on morphological parameters. Appl. Plant Sci. 2 (8), 1400004. https://doi.org/10.3732/apps.1400004.

Crawford, A.J., Belcher, C.M., 2016. Area-volume relationships for fossil charcoal and their relevance for fire history reconstruction. Holocene 26 (5), 822–826. https://doi.org/10.1177/0959683615618264.

Enache, M.D., Cumming, B.F., 2006. Tracking recorded fires using charcoal morphology from the sedimentary sequence of Prosser Lake, British Columbia (Canada). Quat. Res. 65, 282–292. https://doi.org/10.1016/j.yqres.2005.09.003.

Ferreira, T., Rasband, W., 2011. The ImageJ User Guide 1.44. Retrieved 17 September 2018 from. https://imagej.nih.gov/ik/docs/user-guide.pdf.

France, I., Duller, A.W., Duller, G.A., Lamb, H.F., 2000. A new approach to automated pollen analysis. Quat. Sci. Rev. 19, 537–546.

Global Paleofire Working Group, 2017. Global Charcoal Database. Retrieved 20 May 2019 from. https://www.paleofire.org/.

Grana, C., Borghesani, D., Cucchiara, R., 2010. Optimized block-based connected components labeling with decision trees. IEEE Trans. Image Process. 19 (6), 1596–1609.

Halsall, K.M., Ellingsen, V.M., Asplund, J., Bradshaw, R.H., Ohlson, M., 2018. Fossil charcoal quantification using manual and image analysis approaches. Holocene 28 (8), 1345–1353. https://doi.org/10.1177/0959683618771488.

Hawthorne, D., Mitchell, F.J., 2016. Identifying past fire regimes throughout the Holocene in Ireland using new and established methods of charcoal analysis. Quat. Sci. Rev. 137, 45–53. https://doi.org/10.1016/j.quascirev.2016.01.027.

Jensen, K., Lynch, E.A., Calcote, R., Hotchkiss, S.C., 2007. Interpretation of charcoal morphotypes in sediments from Ferry Lake, Wisconsin, USA: do different plant fuel sources produce distinctive charcoal morphotypes? Holocene 17 (7), 907–915. https://doi.org/10.1177/0959683607082405.

Leys, B.A., Commerford, J.L., McLauchlan, K.K., 2017. Reconstructing grassland fire history using sedimentary charcoal: considering count, size and shape. PLoS One 12 (4), e0176445. https://doi.org/10.1371/journal.pone.0176445.

Maruyama, T.M., Oliveira, L.S., Britto, A.S., Nisgoski, S., 2018. Automatic classification of native wood charcoal. Ecol. Inf. 26, 1–7. https://doi.org/10.1016/j.ecoinf.2018.05.008.

Mehrjoo, M., Khaji, N., Moharrami, H., Bahreininejad, A., 2008. Damage detection of truss bridge joints using artificial neural networks. Expert Syst. Appl. 35, 1122–1131. https://doi.org/10.1016/j.eswa.2007.08.008.

Montiel, C., Kraus, D. (Eds.), 2010. Best Practices of Fire Use - Prescribed Burning and Suppression Fire Programmes in Selected Case-Study Regions in Europe. European Forest Institute, Joensuu, Finland.

Mooney, S.D., Tinner, W., 2011. The analysis of charcoal in peat and organic sediments. Mires Peat 7, 1–18.

Moss, P.T., Kershaw, A.P., 2000. The last glacial cycle from the humid tropics of northeastern Australia: comparison of a terrestrial and a marine record. Palaeogeogr. Palaeoclimatol. Palaeoecol. 155, 155–176.
Courtney Mustaphi, C.J., Pisaric, M.F., 2014. A classification for macroscopic charcoal morphologies found in Holocene lacustrine sediments. Prog. Phys. Geogr. 38 (6), 734–754. https://doi.org/10.1177/0309133314548886.
Power, M.J., Marlon, J.R., Bartlein, P.J., Harrison, S.P., 2010. Fire history and the Global Charcoal Database: a new tool for hypothesis testing and data exploration. Palaeogeogr. Palaeoclimatol. Palaeoecol. 291, 52–59. https://doi.org/10.1016/j.palaeo.2009.09.014.
Prechelt, L., 1998. Early stopping - but when?. In: Orr, G.B., Müller, K.R. (Eds.), Neural Networks: Tricks of the Trade, vol. 1524. Springer, Berlin, pp. 55–69. Lecture Notes in Computer Science.
Racca, J.M., Wild, M., Birks, H.J., Prairie, Y.T., 2003. Separating the wheat from chaff: diatom taxon selection using an artificial neural network pruning algorithm. J. Palaeolimnol. 29, 123–133.
Rolland, N., 2004. Was the emergence of home bases and domestic fire a punctuated event? A review of the Middle Pleistocene record in Eurasia. Asian Perspect. 43 (2), 248–280.
Ronneberger, O., Fischer, P., Brox, T., 2015. U-net: convolutional networks for biomedical image segmentation. CoRR abs/1505.04597.
Rull, V., Montoya, E., Vegas-Vilarrúbia, T., Ballesteros, T., 2015. New insights on palaeofires and savannisation in northern South America. Quat. Sci. Rev. 122, 158–165. https://doi.org/10.1016/j.quascirev.2015.05.032.
Schneider, C.A., Rasband, W.S., Eliceiri, K.W., 2012. NIH Image to ImageJ: 25 years of image analysis. Nat. Methods 9, 671–675.
Scott, A.C., Chaloner, W.G., Belcher, C.M., Roos, C.I., 2016. The interaction of fire and mankind: Introduction. Philos. Trans. Royal Soc. B 371, 20150162.
Simonyan, K., Zisserman, A., 2014. Very deep convolutional networks for large-scale image recognition. CoRR abs/1409.1556.
Stevenson, J., Haberle, S., 2005. Macro Charcoal Analysis: A Modified Technique Used by the Department of Archaeology and Natural History. Palaeoworks Technical Papers 5. The Australian National University, Canberra, Australia.
Tieleman, T., Hinton, G., 2012. Lecture 6.5-rmsprop: divide the gradient by a running average of its recent magnitude. COURSERA Neural Netw. Mach. Learn. 4 (2), 26–31.
Umbanhowar, C.E., McGrath, M.J., 1998. Experimental production and analysis of microscopic charcoal from wood, leaves and grasses. Holocene 8 (3), 341–346.
Veenendaal, E.M., Torello-Raventos, M., Miranda, H.S., Sato, N.M., Oliveras, I., van Langvelde, F., Asner, G.P., Lloyd, J., 2017. On the relationship between fire regime and vegetation structure in the tropics. New Phytol. 218 (1), 153–166. https://doi.org/10.1111/nph.14940.
Weiss, K., Khoshgoftaar, T.M., Wang, D., 2016. A survey of transfer learning. J. Big Data 3 (1), 9.
Weller, A.F., Harris, A.J., Ware, J.A., 2007. Two supervised neural networks for classification of sedimentary organic matter images from palynological preparations. Math. Geol. 39, 657–671. https://doi.org/10.1007/s11004-007-9120-x.
Whitlock, C., Larsen, C., 2001. Charcoal as a fire proxy. In: Smol, J.P., Birks, H.J.B., Last, W.M., Bradley, R.S., Alverson, K. (Eds.), *Tracking Environmental Change Using Lake Sediments*. Developments in Paleoenvironmental Research, vol. 3. Springer, Dordrecht, Netherlands.
Wu, D., Kim, K., El Fakhri, G., Li, Q., 2017. Iterative low-dose CT reconstruction with priors trained by artificial neural network. IEEE Trans. Med. Imaging 36 (12), 2479–2486.
Zeiler, M.D., Krishnan, D., Taylor, G.W., Fergus, R., 2010. Deconvolutional networks. In: *2010* IEEE Computer Society Conference on Computer Vision and Pattern Recognition, pp. 2528–2535.

Appendix 5: Copyright Permissions

This administrative form
has been removed

This administrative form
has been removed